

DESIGN AND ANALYSIS OF SHELL STRUCTURES

@Seismicisolation

SOLID MECHANICS AND ITS APPLICATIONS

Volume 16

Series Editor:

G.M.L. GLADWELL

Solid Mechanics Division, Faculty of Engineering

University of Waterloo

Waterloo, Ontario, Canada N2L 3G1

Aims and Scope of the Series

The fundamental questions arising in mechanics are: *Why?*, *How?*, and *How much?*

The aim of this series is to provide lucid accounts written by authoritative researchers giving vision and insight in answering these questions on the subject of mechanics as it relates to solids.

The scope of the series covers the entire spectrum of solid mechanics. Thus it includes the foundation of mechanics; variational formulations; computational mechanics; statics, kinematics and dynamics of rigid and elastic bodies; vibrations of solids and structures; dynamical systems and chaos; the theories of elasticity, plasticity and viscoelasticity; composite materials; rods, beams, shells and membranes; structural control and stability; soils, rocks and geomechanics; fracture; tribology; experimental mechanics; biomechanics and machine design.

The median level of presentation is the first year graduate student. Some texts are monographs defining the current state of the field; others are accessible to final year undergraduates; but essentially the emphasis is on readability and clarity.

For a list of related mechanics titles, see final pages.

@Seismicisolation

Design and Analysis of Shell Structures

by

M. FARSHAD

*EMPA,
Switzerland*



Springer-Science+Business Media, B.V.

@Seismicisolation

Library of Congress Cataloging-in-Publication Data

Farshad, Mehdi.

Design and analysis of shell structures / Mehdi Farshad.
p. cm. -- (Solid mechanics and its applications ; 16)

Includes index.

ISBN 978-90-481-4200-2 ISBN 978-94-017-1227-9 (eBook)

DOI 10.1007/978-94-017-1227-9

1. Shells (Engineering)--Design and construction. 2. Structural analysis (Engineering) I. Title. II. Title: Shell structures.

III. Series.

TA660.S5F42 1992

624.1'7762--dc20

92-18175

ISBN 978-90-481-4200-2

Printed on acid-free paper

All Rights Reserved

© 1992 Springer Science+Business Media Dordrecht

Originally published by Kluwer Academic Publishers in 1992

No part of the material protected by this copyright notice may be reproduced or utilized in any form or by any means, electronic or mechanical, including photocopying, recording or by any information storage and retrieval system, without written permission from the copyright owner.

@Seismicisolation

Contents

Preface

xi

Chapter 1 - Introduction to Shells

1.1 - Introduction	1
1.2 - Uses of Shell Structures	2
1.3 - Geometry of Shells	3
1.4 - Classification of Shell Surfaces	4
1.5 - Summary of Classification of Shell Surfaces	8
1.6 - Outline of General Structural Features of Shells	8
References for Chapter One	9

Chapter 2 - Preliminaries of Shell Analysis and Design

2.1 - Introduction	11
2.2 - Thin Shells	12
2.3 - Internal Force System in a Shell	12
2.4 - Qualitative Description of Shell Behavior	15
2.5 - An Overview of Shell Theories	19
2.6 - Assumptions of Classical Shell Theories	19
2.7 - Force Method of Shell Analysis	20
2.8 - General Shell Design Considerations	21
2.9 - Stability Considerations in Shell Design	22
2.10 - Codes of Practice	23
References for Chapter Two	24

Chapter 3 - Membrane Behavior of Cylindrical Shells

3.1 - Introduction	25
3.2 - Geometrical Description	25
3.3 - Membrane Equations of Cylindrical Shells	26
3.4 - Cylindrical Vaults	28
3.5 - Containment Vessels	30
3.5.1-Fluid Tanks	30
3.5.2-Pipes under Internal Pressure	30
3.6 - Membrane Deformation of Cylindrical Shells	31
3.7 - Displacements of Cylindrical Vaults	33

Numerical Example 3.1	33
3.8 - Qualitative Description of Cylindrical Shells Behavior	34
Problems	38
References for Chapter Three	42
Chapter 4 - Bending Analysis of Circular Cylindrical Shells	43
4.1 - Introduction	43
4.2 - General Governing Equations	44
4.2.1-Equilibrium Equations	44
4.2.2-Kinematic Relations	45
4.2.3-Constitutive Relations	47
4.3 - Displacement Equations of Circular Cylindrical Shells	50
4.4 - Circular Cylinders with Axisymmetric Loading	51
4.5 - Some Axisymmetric Problems of Circular Cylinders	53
4.5.1-General Solution to Axisymmetric Problems	53
4.5.2-A Fundamental Problem	54
4.5.3-Thin Circular Cylinders under Internal Pressure	55
4.5.4-Analysis of Liquid Retaining Cylindrical Shells	56
Numerical Example 4.1	58
Problems	60
References for Chapter Four	61
Chapter 5 - Design of Concrete Cylindrical Shell Roofs	63
5.1 - Introduction	63
5.2 - Geometric Design of Cylindrical Shell Roofs	64
5.2.1-Overall Dimensioning of the Shell	64
5.2.2-Dimensions of Edge Beams	67
5.2.3-Profile, Central Angle, and Curvature of the Shell	67
5.2.4 -Rise of the Shell	67
5.2.5-Shell Thickness	67
5.3 - Reinforcement of Concrete Cylindrical Roofs	68
5.4 - "Beam-Arch" Method of Vaulted Roof Analysis	72
Numerical Example 5.1	78
5.5 - Analysis of Cylindrical Vaults by ASCE Tables	87
5.6 - Design Examples of Reinforced Concrete Cylindrical Shell Roofs	89
5.6.1-Design of A Single Shell without Edge Beams	89
5.6.2-Design of an Inner Shell in a Shell Group	92
5.6.3-Design of a Single Simply Supported Shell with Edge Beams	95
5.6.4-Design of an Inner Shell in a Shell Group with Edge Beams	97
Problems	100
References for Chapter Five	101
Chapter 6 - Membrane Analysis of Shells of Revolution	103
6.1 - Introduction	103
6.2 - Geometrical Description	104
6.3 - Governing Membrane Equations	106
6.4 - Rotational Shells with Axisymmetric Loading	108

6.5 - Spherical Domes	111
6.5.1-Membrane Forces	111
6.5.2-Domes with Skylight	112
Numerical Example 6.1	113
6.6 - Fluid Storage Tanks	115
6.6.1-Spherical Liquid Storage Tank	115
6.6.2-Cylindrical Tanks with Spherical Ends	116
6.6.3-Pressure Vessels	120
6.7 - Shells of Revolution with Nonsymmetric Loading	121
6.8 - Wind-Induced Stresses in Domes	122
6.9 - Displacements of Axisymmetric Shells	125
6.10 - Membrane Deformation of Spherical Domes	128
Numerical Example 6.2	129
6.11 - Qualitative Description of Dome Behavior	130
6.12 - Conical Shells	133
Problems	137
References for Chapter Six	139
 Chapter 7 - Bending Analysis of Axisymmetric Shells	 141
7.1 - Introduction	141
7.2 - Governing Equations of Axisymmetric Shells	142
7.2.1-Equilibrium Equations	142
7.2.2-Kinematical Relations	144
7.2.3-Constitutive Relations	148
7.3 - Reduction of Shell Equations	149
7.4 - Edge Effects in Axisymmetric Shells	153
7.5 - Analysis of Axisymmetric Shells for Edge Effects	155
7.6 - Influence Coefficients for Axisymmetric Shells	158
7.7 - Force Method of Axisymmetric Shells Analysis	160
7.8 - Sample Analysis of a Dome	160
Problems	166
References for Chapter Seven	167
 Chapter 8 - Design of Reinforced Concrete Domes	 169
8.1 - Introduction	169
8.2 - Domes with Rings	170
8.3 - Force Method of "Dome-Ring" Analysis	171
8.3.1-General Methodology	171
8.3.2-Analysis of the Ring	174
8.3.3- Analysis of Dome under Edge and Distributed Forces	177
8.3.4-"Dome-Ring" Interaction	177
8.3.5-Summary of "Dome-Ring" Analysis Relations	181
8.3.6-Application of the Force Method	183
8.4 - Buckling Considerations in Concrete Domes Design	184
8.5 - Design Guides for Dome Geometry	184
8.6 - Design of a Reinforced Concrete "Dome-Ring" Roof	186
Problems	193
References for Chapter Eight	194

Chapter 9 - Analysis of Shells with Arbitrary Geometry	195
9.1 - Introduction	195
9.2 - Membrane Theory of General Shells	197
9.2.1-Geometrical Description of Arbitrary Surfaces	197
9.2.2-Methodology of Membrane Analysis of General Shells	199
9.2.3-Equilibrium Equations of General Shells	202
9.2.4-Solution of Membrane Equations by Stress Function	205
9.3 - Bending Theory of Shallow Shells	205
Problems	212
References for Chapter Nine	214
Chapter 10 - Design of Hyperbolic Paraboloid Shells	215
10.1 - Introduction	215
10.2 - Geometrical Description	217
10.3 - Membrane Analysis of HP Shells	222
Numerical Example 10.1	225
10.4 - Description of Membrane Behavior of HP Shells	227
10.5 - Bending Filed in Hyperbolic Paraboloid Shells	232
10.6 - General Design Considerations of HP Shells	234
10.7 - Design of a Reinforced Concrete HP Shell Roof	239
Problems	245
References for Chapter Ten	247
Chapter 11 - Analysis and Design of Folded Plates	249
11.1 - Introduction	249
11.2 - General Features of Folded Plates	250
11.3 - General Design Considerations of Prismatic Folded Plates	254
11.4 - Methodology of Analysis of Folded Plates	256
11.4.1-Preliminary Analysis	257
11.4.2-Corrective Analysis	258
11.4.3-Compatibility Analysis and Superposition of Results	258
11.5 - Basic Steps in the Folded Plates Analysis	259
11.5.1-Schematics of Analysis	259
11.5.2-Shear Stresses at Plates Junctions	260
11.5.3-Distribution of Junctional Shear Forces	262
11.5.4-Summary of Analysis Procedure	265
11.6 -Analysis of a RC Folded Plate Roof	265
Problems	288
References for Chapter Eleven	289
Chapter 12 - Design of Liquid Retaining Shells	291
12.1 - Introduction	291
12.2 - Classifications of Liquid Containers	292
12.3 - General Design Considerations	292
12.3.1-Shape Design	292

12.3.2-Serviceability Design	296
12.4 - Loading Conditions	297
12.5 - Axisymmetric Behavior of Circular Containers	299
12.6 - Force Method of Container Shells Analysis	304
12.6.1-Influence Coefficients	304
12.6.2-Analysis of "Wall-Base" Interaction	305
12.6.3-Analysis of "Wall to Roof" Connection	311
12.7 - An Example of Cylindrical Container Analysis	319
12.8 - Design of a Reinforced Concrete Container	326
12.9 - Some Considerations on Reinforcements Detail	329
12.10 - Cylindrical Walls with Domical Roofs	331
12.11 - Design of a Cylindrical "Wall-Dome" Container Problems	333
References for Chapter Twelve	340
	341
 Chapter 13 - Buckling of Shells	343
13.1 - Introduction	343
13.2 - Concepts of Stability and Instability	344
13.3 - Types of Loss of Stability	345
13.3.1-Bifurcation of Equilibrium	345
13.3.2-Limitation of Equilibrium	349
13.4 - An Overview of Shell Buckling	349
13.5 - Methodology of Linear Stability Analysis of Shells	352
13.6 - Buckling of Circular Cylindrical Shells	353
13.7 - Buckling of Circular Cylinders under Axial Force	360
13.7.1-General Modes of Cylinders Buckling under Axial force	360
13.7.2-Buckling of Axially Loaded Cylindrical Shells	362
13.7.3-Buckling of Cylindrical Shells under External Pressure	366
13.8 - Buckling of Concrete Cylindrical Roofs	367
13.9 - Buckling Formulas for the Shells of Revolution	368
13.10 - Buckling of Domes	368
13.10.1-Buckling Modes of Domes	368
13.10.2-Buckling of Concrete Domes	369
13.11 - Buckling of Hyperbolic Paraboloid Shells	370
13.11.1-General Buckling Behavior of HP Shells	370
13.11.2-Buckling Formulas for Hyperbolic Paraboloid Shells	371
Problems	372
References for Chapter Thirteen	374
	374
 Appendices	375
Appendix A - Formulas for the Membrane Field in Shells	
Appendix B -Tables For Analysis of Circular Cylindrical Shell Roofs	
 Subject Index	

Preface

Shell Structures present immense structural and architectural potential in various fields of civil, mechanical, architectural, aeronautical, and marine engineering. Examples of shell structures in civil and architectural engineering are: varieties of concrete shell roofs, liquid retaining structures and water tanks, concrete silos, cooling towers, containment shells of nuclear power plants, and concrete arch dams. In mechanical engineering, shell forms are used in piping systems, curved panels, and in pressure vessel technology. Aircrafts, space crafts, missiles, ships, and submarines are examples of shells used in aeronautical and marine engineering. Shells are found in various biological forms such as the eye and the skull, plants, and animal shapes. Thus, another application of shell engineering would be the field of Biomechanics.

Shell structures developed since ancient times and now are being increasingly used in various industries. Shells are used in the covering of large spans, liquid retaining installations, silos, and containment structures. They are also used in the construction of light-weight vehicles, pressure vessels, and space structures. Advent of such materials as ferro-cement, fiber-reinforced concrete, composite materials, and reinforced polymers have all enhanced the domain of shell technology. With the development of new prefabrication schemes as well as the need for recycling of materials, the potential of shell applications has further increased. In addition to mechanical advantages, such as durability, high strength and stability, shell structures enjoy the unique position of having extremely high aesthetic value in various architectural designs.

In spite of all these features and potential applications, many engineers and architects are unacquainted with shells as well as the aspects of shell behavior and design. The purpose of this book is to familiarize the engineering and architectural students, as well as practicing engineers and architects, with the behavior and design aspects of shell structures. The goal of this book is to present three aspects: the physical behavior, the structural analysis, and the

design of shells in a simple, integrated, and yet concise fashion. Thus, the book contains three major aspects of shell engineering. These are: (1) physical understanding of shell behavior, (2) use of applied shell theories, (3) development of design methodologies together with shell design examples.

To achieve these goals, simplified shell theories have been discussed in this book and have been immediately applied to actual problems. In this sense, the book bridges the gap between the elaborate theoretical treatments of shells, on the one hand, and, the practical aspects of the analysis and design of shells, on the other hand. Being aware of a wide variety of existing numerical routines for shells analysis, we have, nevertheless, made use of simple analytical schemes of shell analysis so that the designer can understand the analysis procedure and to perform parametric studies. The theoretical tools required for rational analysis of shells are kept at a modest level so that engineering and architectural students, as well as practicing engineers and architects, can grasp the fundamentals of shell behavior and, at the same time, understand the related theory and be able to apply it to actual design problems. To achieve a physical understanding of complex shell behavior, quantitative presentations are supplemented by *qualitative* discussions so that the reader can grasp a "physical feeling" of shell behavior. To make the book useful as a reference manual, a number of analysis and detailed design examples are also worked out in various chapters.

The actual design of shells, involves the use of appropriate codes of practice. Thus, while making use of some existing codes on shells, in order to provide a text that could be used in various countries, we have attempted to present the designs apart from the existing codes. In some cases, the common guidelines provided by several standards, including ACI, BS, DIN, and IS, have been used.

This book can be used as a text book, and / or a reference book in undergraduate as well as graduate university courses in the fields of civil, mechanical, architectural, aeronautical, and materials engineering. It can also be used as a reference and design-analysis manual for the practicing engineers and architects. To make the book useful to design engineers and architects, the text is supplemented by a number of appendices containing tables of shell analysis and design charts and tables. Metric system is used throughout this book.

The material of this book have been developed through many years of teaching at the Universities of Shiraz and Tehran, University of Toronto, and the Swiss Federal Institute of Technology (ETHZ) as well as through research and practical design experience by the author. Thus, in the development of this text, various viewpoints and experiences have been extremely constructive.

The author would like to thank the Swiss Federal Laboratories for Materials Testing and Research (**EMPA**, Dübendorf) and, in particular, Professor F. Eggimann and Professor U. Meier and Hr. H. Fritz for supporting this project. Special thanks are due to Hr. P. Flüeler who has given great encouragement and support in bringing this book to its present publication. The author would also like to thank professor Gladwell for his useful comments on the manuscript. This book is dedicated to my family (Gowhar, Anahita, and Mazda) who have shown great patience during the long period of manuscript preparation.

M. Farshad

Switzerland

Chapter 1

Introduction to Shells

1.1 - Introduction

Generally speaking, shells are spatially curved surface structures which support external applied loads. Shells are found in a variety of natural structures such as eggs, plants, leaves, skeletal bones, and geological forms. Shell structures have also been built by man since the most ancient times. Many shell domes built of masonry and stone in ancient times, are still in existence in some parts of the world.

In this introductory chapter, first some references will be made to a number of important and well-known fields of applications of shell structures. Then, engineering classifications of the surfaces, as the main geometrical feature of shells, will be presented. In the forthcoming chapters, these classifications will be extensively used. They also prove to be very useful in understanding shell properties and behavior as well as being helpful in the design of varieties of shell structures.

1.2 - Uses of Shell Structures

Shell structures can be efficiently and economically used in various fields of engineering and architecture. A great variety of shell roofs have been designed and constructed in many parts of the world. Large spans have been easily covered by reinforced concrete shells. Water retaining shells have been constructed of steel, concrete and even precast and /or prestressed concrete. Tall silos (up to 60 meters high) and other containment structures of high efficiency have been built using shell forms. Structurally efficient doubly curved high arch dams (up to 300 meters high) have been constructed to resist high intensity hydrodynamic as well as earthquake loadings. The containment shells of nuclear power plants, requiring high degree of safety, have always been made of reinforced concrete shells. Tall chimneys and also huge cooling towers (as high as 200 meters) have been built of steel or reinforced concrete shells. The set of figures (1-1) show some of these applications of shell structures .

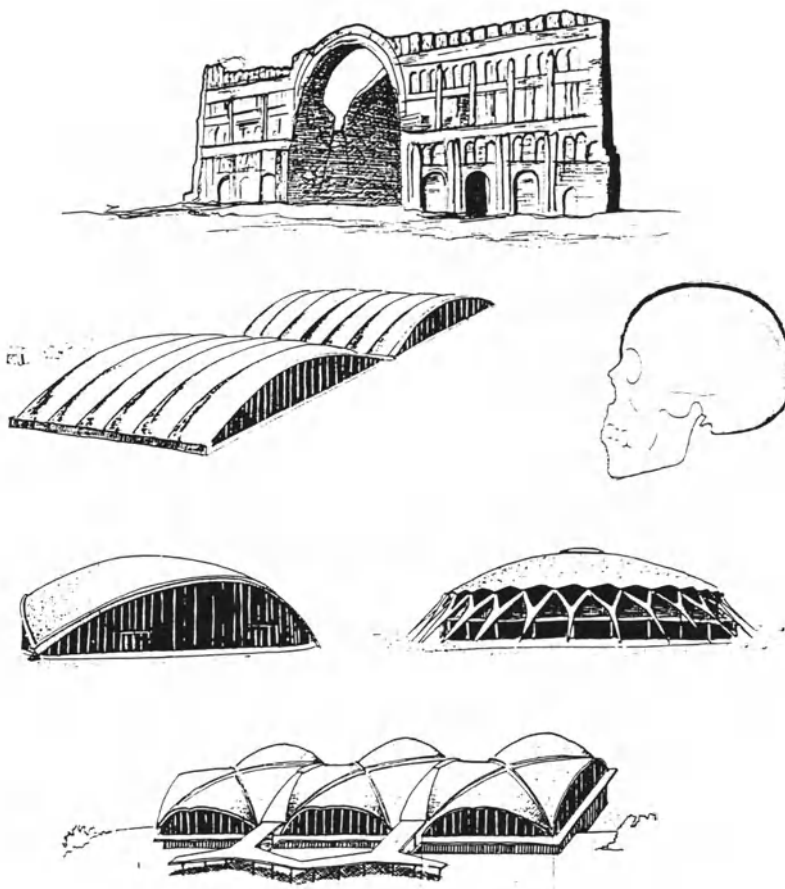


Figure (1-1) Examples of shell structures

Recently, with the advent of various fiber-reinforced and laminated composite materials, the domain of application and range of structural efficiency of shell forms has immensely increased. Ground, as well as space vehicles, having shell forms, have been designed and successfully built of high strength temperature resistant composite materials. The skin of aircraft structures and also ship hulls are composed of shell forms, built of stiffened shells and / or composite material bodies.

These applications are several important cases of shell technology as applied to various fields of engineering and architecture. One may also conceive of other applications in which the structurally efficient, economically promising, and aesthetically appealing shell forms could be conveniently designed and constructed.

1.3 - Geometry of Shells

The geometry of a shell is defined by the prescription of its middle surface and its thickness at all points. Suppose that we have a general surface in space. At any point, A, on this surface, a plane tangent to the shell can be imagined, figure (1-2). A normal to the tangent plane, at this point, would be considered to be the normal to the surface at that point. Obviously, an infinite number of planes intersecting the surface could be passed through point A. Some of these intersecting planes contain the normal to the surface at A. Such planes are normal to the tangent plane at that point and thus could also be considered to be normal to the shell middle surface.

The plane curves formed by the intersecting planes containing normals to the surface are called *normal sections* of the surface at a point. Obviously, every one of these curves would have a local curvature and a corresponding radius of curvature (quantitatively, an inverse of curvature) at that point. Out of these infinitely many plane curves, formed by intersection, there will be one curve having a maximum value of curvature (K_1) and another having a minimum value of curvature (K_2).

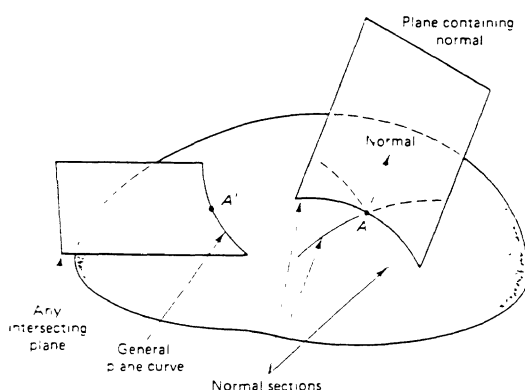


Figure 1-2: Intersections of planes with a surface

The two plane curves, formed by the normal plane sections, are called the *principal sections*, and their curvatures, denoted by K_1 and K_2 , are called the *principal curvatures* of the surface at A. It can be proved, by differential geometry, that these two intersecting principal sections are always *orthogonal* to each other.

The product of the two principal curvatures, $K = K_1 \times K_2$ is an algebraic quantity which, by definition, called the *Gaussian curvature* of the surface a point A. If $K_2 = 0$, $K_1 \neq 0$, then the surface is said to have a single or zero Gaussian curvature. If $K > 0$, the surface is said to have a *positive Gaussian curvature*; if $K < 0$, the surface has a *negative Gaussian curvature*. Knowing the parametric equations of a surface, we can readily obtain the expressions for the principal curvatures, K_1 and K_2 .

1.4 - Classifications of Shell Surfaces

Using the definition of Gaussian curvature, we may make a useful classification of surfaces. Depending on whether the quantity $K = K_1 \times K_2$ is positive, negative, or zero at a point, the surface is, respectively, called a *synclastic surface*, an *anticlastic surface*, or a surface with *zero Gaussian curvature* at that point. This type of classification is demonstrated in figure (1-3).

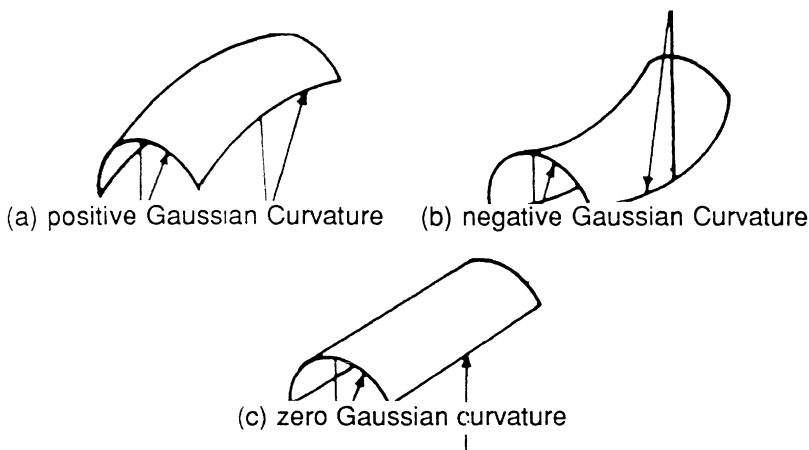


figure (1-3) Surfaces with positive, negative, and zero Gaussian curvature

Another delineation of surfaces can be made on the bases of their geometrical developability. According to this distinction, shell surfaces are either *developable* or *nondevelopable*. Developable surfaces are, by definition, the ones which can be "developed" into a plane form without cutting and/or stretching their middle surface. A nondevelopable surface, on the other hand, is a surface which has to be cut and / or stretched in order to be developed into a planar form.

Surfaces with double curvature are usually nondevelopable, whereas surfaces with single curvature are always developable. Surfaces with positive and negative Gaussian curvature (i.e., synclastic and anticlastic surfaces) are *developable*, while those with zero Gaussian curvature are *nondevelopable*, figure(1-4).

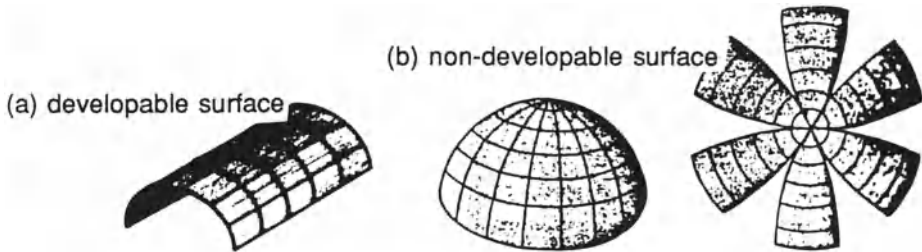


Figure (1-4) Examples of developable and nondevelopable surfaces

The classification of shell surfaces into developable and non-developable has some structural significance. From physical point of view, shells with nondevelopable surface require more external energy, than do developable shells, to be "stretched out", i.e., to collapse into a plane form. Hence, one may conclude that nondevelopable shells are, in general, stronger and more stable than the corresponding developable shells having the same overall dimensions.

A third type of classification of surfaces, which is very useful in shell analysis and design, is the categorization of various surfaces into *surfaces of revolution*, *translational surfaces*, and *ruled surfaces*.

Surfaces of revolution

Surfaces of revolution are generated by the revolution of a plane curve, called *the meridional curve*, about an axis, called *the axis of revolution*. The axis of revolution, does not always have to intersect the meridional curve. In the special case of conical surfaces, the meridional curve consists of a line segment. Examples of surfaces of revolution are shown in figures (1-5).

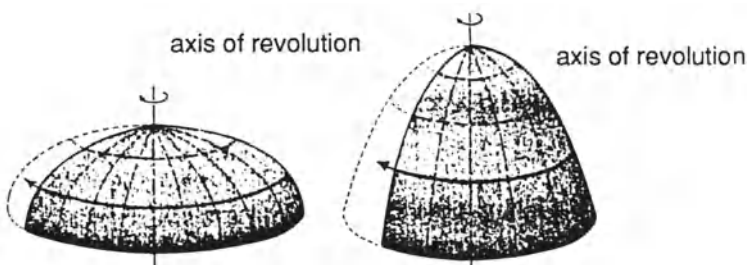
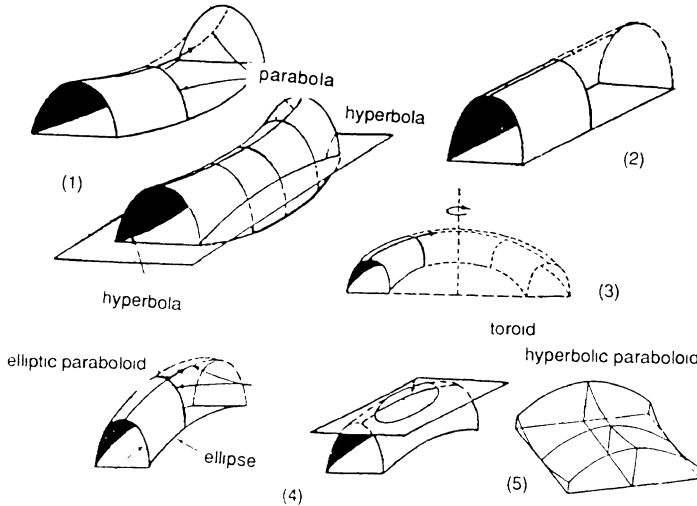


Figure (1-5) Some examples of surfaces of revolution

Surfaces of translation

Surfaces of translation are defined as the surfaces generated by sliding a plane curve along another plane curve, while keeping the orientation of the sliding curve constant. The second curve on which the original plane curve slides, is called the *generator* of the surface. In the special case in which the generator is a straight line, the resulting translational surface is called a *cylindrical surface*. Examples of translational surfaces are shown in figure (1-6).



Figure(1-6) Some examples of translational surfaces

Ruled surfaces

Ruled surfaces are obtained by sliding a straight line, two ends of which remain on two generating curves, in such a fashion that it remains parallel to a prescribed direction or plane. The generating straight line is not necessarily at right angles to the planes containing the director curves. Some examples of ruled surfaces are shown in figure (1-7). From a practical viewpoint, molding of in-situ cast concrete shells, having ruled surface forms, can be more easily and economically made by the rectilinear forming elements, thus reducing the forming expenses.

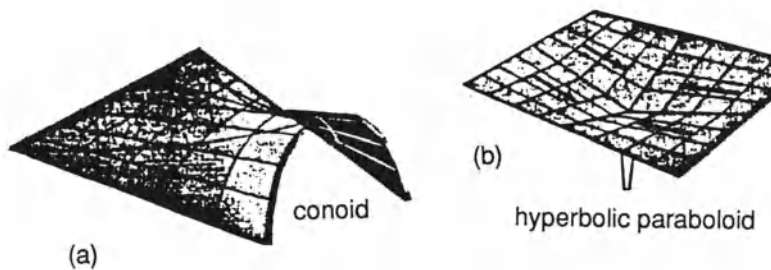


Figure (1-7) Some examples of ruled surfaces.

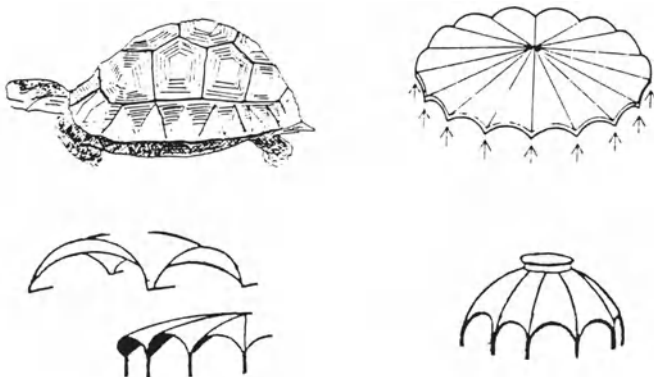


Figure (1-8) Examples of combined shells

1.5 - Summary of Classifications of Shell Surfaces

Based on our foregoing discussion, we can now summarize and broadly classify the shell surfaces which are commonly used in engineering practice. It may be noted that the same type of shell may very well appear in more than one category.

- 1) Singly curved, or shells of zero Gaussian curvature. In some cases, developable
 - Shells of revolution: circular cylinders; cones
 - Shells of translation and ruled surfaces: circular or non-circular cylinders; cones
- 2) Doubly curved shells having positive Gaussian curvature (synclastic shells); non-developable shells
 - Shells of revolution: Spherical domes. ellipsoids of revolution; paraboloids of revolution
 - Shells of translation and ruled surfaces: elliptic paraboloids; paraboloids of revolution
- 3) Doubly curved shells with negative Gaussian curvature (anticlastic shells), non-developable
 - Shells of revolution : Hyperboloids of revolution of one sheet
 - Shells of revolution and ruled surfaces: hyperbolic paraboloids; conoids; hyperboloids of revolution of one sheet
- 4) Combined shells, partly synclastic and partly anticlastic shells; shells composed of simpler shell forms, figure(1-8).
- 5) Shells with discontinuous curvature; folded plates

1.6 - Outline of General Structural Features of Shells

In the course of the chapters that follow, various unique structural features of shells will be qualitatively and quantitatively introduced and used in design. In this introductory chapter, only a reference is made to some of the characteristics of shell structures. The salient features of shells, as compared with other structural forms such as beams, frames, and plates can be outlined as follows:

- (a) Efficiency of load carrying behavior
- (b) High degree of reserved strength and structural integrity
- (c) High strength to weight ratio
- (d) Very small thickness ratio to other dimensions (span, radius of curvature)
- (e) Very high stiffness
- (f) Containment of space

In the forthcoming chapters these aspects of shells behavior will be described in detail.

References for Chapter One

- 1.1 - M. Farshad, *Structural Forms*, (in Farsi), Vol. I, 1986, Vol. II, 1987, University of Shiraz Publications, Shiraz, 1973
- 1.2 - M. Farshad, *Principles of Structures*, (in Farsi), Dehkhoda Publishers, Teheran, 1983
- 1.3 - M. Salvadori and R. Heller, *Structure in Architecture*, Prentice-Hall, Inc., N.J., 1963
- 1.5 - A. Hodkinson, (ed), *A J Handbook of Building Structure*, The Architectural Press, London, 1974
- 1.6 - D. P. Billington, *Thin Shell Concrete Structures*, McGraw Hill Book Co. N.Y., 1965, revised edition 1982
- 1.7 - G.S. Ramaswamy, *Design and construction of Concrete Shell Roofs*, McGraw-Hill Book Co., N.Y., 1968
- 1.8 - V.S. Kelkar and R.T. Sewell, *Fundamentals of the Analysis and Design of Shell Structures*, Prentice-Hall, INC., N.J., 1987

Chapter 2

Preliminaries of Shell Analysis and Design

2.1 - Introduction

The behavior of shell structures is, in various aspects, different from that of so-called "framed structures". This feature originates mainly from the geometrical features of shells which make the internal force system in shells differ from those in other types of structural forms. The internal force distribution in shells is, in general, three dimensional, i.e., spatial. Moreover, shell structures carry the applied forces mostly by the so-called *membrane forces*, whereas other structural forms carry the applied loads by bending mechanisms. These unique features of shells are also reflected in their design as well as in their method of construction.

In this chapter, we will first define the internal stress and force system in thin shells. Then, to achieve an overall understanding, a qualitative discussion of structural behavior of shells will be presented. Later on in the chapter, theories of shell analysis will be placed in perspective and the bases of shell analysis methodologies will be presented. Finally, a number of general shells design considerations will be outlined.

2.2 - Thin Shells

The surface passing through the mid thickness of the shell at each point is, by definition, called the *middle-surface* of the shell, figure (2-1). If the thickness of the shell is very small compared with the radii of curvature of the shell mid-surface, then the shell is considered as a *thin shell*. The thickness to radii ratio, or sometimes the thickness to span ratio, of about 1/200, occurring in reinforced concrete shells, puts the actual shells well in the range of being "thin shell" structures. For metallic and composite shells, this ratio is in practice much smaller, of the order of 1/300.

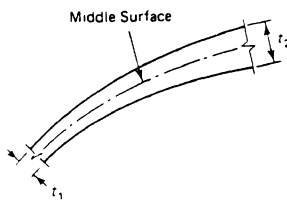


Figure (2-1) Middle surface of a thin shell

2.3 - Internal Force System in a Shell

Consider a shell with a general geometry. An infinitesimal element of this shell can be cut out by intersecting it with two pairs of principal plane sections which are located at arc lengths ds_x and ds_y apart. Two intersecting planes, are from each pair the normal to the shell at the common corner point. The resulting plane curves of intersection are principal sections and are thus perpendicular to each other, figure(2-2). The principal plane curves have principal radii of curvature which, in this figure, are designated by r_x and r_y .

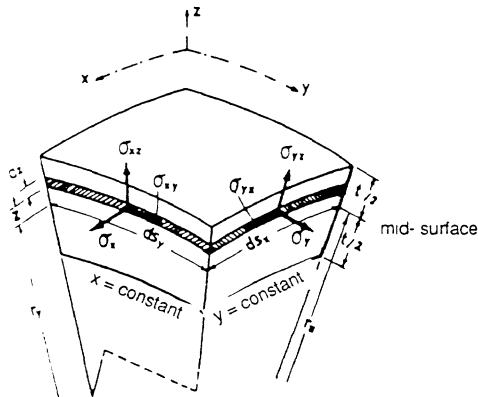


Figure (2-2) A shell element demonstrating the principal radii of curvature and the internal stresses

In a shell structure subjected to applied external loading, temperature changes, support settlements, and deformation constraints, some internal stresses may develop. These internal stresses are shown on the shell element of figure(2-3). As we see, the general state of stress in a shell element consists of membrane normal and shear stresses lying in the shell surface, as well as the transverse shear stresses. In thin shells, the component of stress normal to the shell surface, compared with other components of the internal stresses, is very small and is neglected in the classical shell theories.

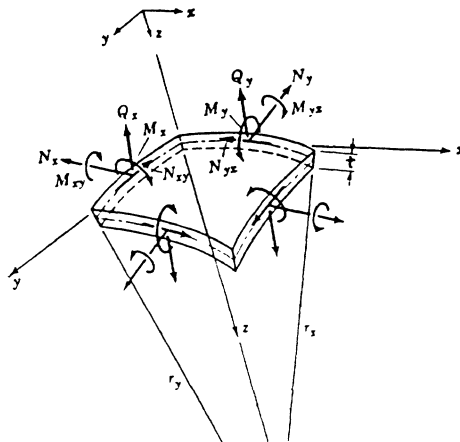


Figure (2-3) Components of internal force resultants in a shell element

The internal stresses acting on an infinitesimal element of the shell may be properly integrated across the shell thickness to give the so-called *resultant internal forces*. From a statical point of view, the resultant force system at any section consists of a force and a moment vector. These internal force vectors can be resolved into components which altogether constitute the internal force system in the shell. Figure (2-3), shows the components of resultant internal forces in a shell element.

Referring to figure (2-2), we can readily derive the relations between stress components and components of internal force resultant in a shell element. The desired relations (2-2) have been obtained using the requirement of statical equivalency between the internal stresses and their resultant forces. In these relations, t is the thickness of the shell.

The internal forces at each point of the shell may be placed in one of two groups of force fields: *membrane forces*; *bending forces*. Figure (2-4a) shows the membrane force system in an infinitesimal shell element. Figures (2-4b) and (2-4c) show the bending force system in the same shell element. The overall force field in a point of a shell consists of the forces shown in figures (2-4a), (2-4b), and (2-4c).

$$N_x = \begin{cases} + \frac{t}{2} \\ - \frac{t}{2} \end{cases} \sigma_x (1 + \frac{z}{r_y}) dz , \quad N_y = \begin{cases} + \frac{t}{2} \\ - \frac{t}{2} \end{cases} \sigma_y (1 + \frac{z}{r_x}) dz$$

$$N_{xy} = \begin{cases} + \frac{t}{2} \\ - \frac{t}{2} \end{cases} \sigma_{xy} (1 + \frac{z}{r_y}) dz , \quad N_{yx} = \begin{cases} + \frac{t}{2} \\ - \frac{t}{2} \end{cases} \sigma_{yx} (1 + \frac{z}{r_x}) dz$$

(2-1)

$$Q_x = \begin{cases} + \frac{t}{2} \\ - \frac{t}{2} \end{cases} \sigma_{xz} (1 + \frac{z}{r_y}) dz , \quad Q_y = \begin{cases} + \frac{t}{2} \\ - \frac{t}{2} \end{cases} \sigma_{yz} (1 + \frac{z}{r_x}) dz$$

$$M_x = \begin{cases} + \frac{t}{2} \\ - \frac{t}{2} \end{cases} z \sigma_x (1 + \frac{z}{r_y}) dz , \quad M_y = \begin{cases} + \frac{t}{2} \\ - \frac{t}{2} \end{cases} z \sigma_y (1 + \frac{z}{r_x}) dz$$

$$M_{xy} = - \begin{cases} + \frac{t}{2} \\ - \frac{t}{2} \end{cases} z \sigma_{xy} (1 + \frac{z}{r_y}) dz , \quad M_{yx} = \begin{cases} + \frac{t}{2} \\ - \frac{t}{2} \end{cases} z \sigma_{yx} (1 + \frac{z}{r_x}) dz$$

The *membrane forces*, as the name implies, are the resultant internal forces which lie "inside" the mid-surface of the shell. The membrane force field causes the stretching or contraction of the shell, as a **membrane**, without producing any bending and / or local curvature changes. The membrane force field consists of two membrane normal resultant forces and a membrane shear force.

The second group of internal forces are called the *bending forces*, since they cause bending and twisting of the shell cross-sections. The bending force field consists of bending moments, twisting couples, and transverse shear forces.

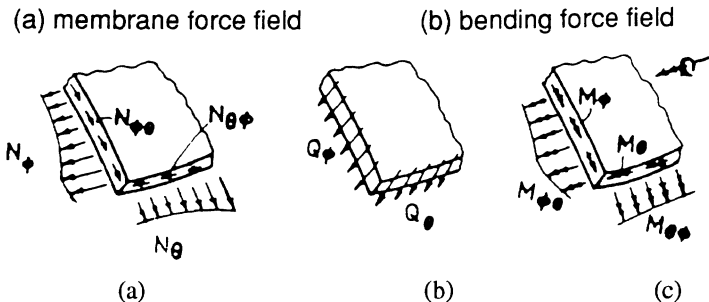
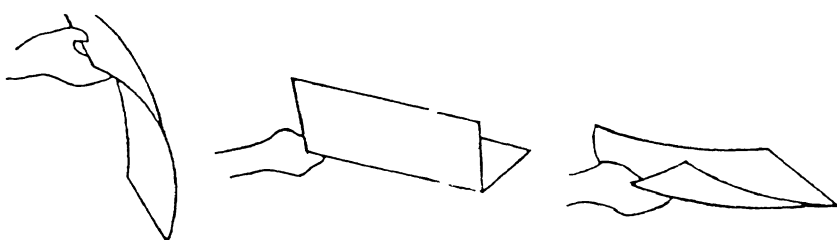


Figure (2-4) Membrane and bending resultant force fields in a shell element

2.4 - Qualitative Description of Shell Behavior

Shell structures support applied external forces efficiently by virtue of their geometrical forms. Shells, having their spatial curvature, are much stronger and stiffer than other structural forms. For this reason shells are sometimes referred to as **form resistant** structures. The strength to weight ratio of a shell structure is usually much smaller than that of other structural systems having the same span and overall dimensions. A simple experiment, demonstrated in figure (2-5), shows the structural efficiency of a shell and also a folded plate as compared with a flat plate of the same material and dimensions.



Figure(2-5) A simple paper-sheet experiment showing the structural efficiency of shell and folded plate form

As we have seen before, the load-carrying mechanism, i.e., the internal forces at any point of a shell, consist of ten component internal force resultants (N_x , N_y , N_{xy} , N_{yx} , M_x , M_y , M_{xy} , M_{yx} , Q_x , Q_y). These components, can be separated into two groups, entitled membrane and bending internal force field, as follows :

Membrane field: N_x , N_y , N_{xy} , N_{yx}

Bending field: M_x , M_y , M_{xy} , M_{yx} , Q_x , Q_y

In this terminology, M_x and M_y stand for bending moments while M_{xy} and M_{yx} represent the twisting couples. Q_x and Q_y represent the out-of-plane shear forces.

For a material body in spatial equilibrium there are six governing equilibrium equations. Since there are more than six force resultants, we conclude that a shell is, in general, an *internally statically indeterminate* structure.

The internal force redundancy, although it is an indication of additional load carrying mechanisms, is not always required for shell equilibrium. Let us imagine a shell subjected to applied loading in which only the membrane force field has been produced and the bending field is absent. By writing the moment equation of equilibrium about the normal to the shell element (z axis) we can conclude that $N_{xy} = N_{yx}$. Therefore, the membrane force field will consist of the forces N_x , N_y , and $N_{xy} = N_{yx}$.

In a shell in which only the membrane field exists, three of the six equilibrium moment equations ($M_x = 0$, $M_y = 0$, $M_z = 0$) are identically satisfied. We are then left with three remaining force equilibrium equations and three internal membrane forces to be determined. Since the number of equilibrium equations and the number of unknown forces are equal, the membrane shell is statically determinate and its internal force system can be determined by the use of the equilibrium equations alone, without the need of any auxiliary relations.

The membrane force field is, of course, associated with the membrane normal and shear forces, which are assumed to be uniformly distributed through the thickness of the shell. A shell in which only the membrane force field exists is said to have a *membrane behavior*. The resultant theory which is called the **membrane theory** of shells.

A shell will have a pure membrane behavior provided certain boundary requirements, loading conditions, and geometrical configurations are satisfied. In order that a membrane theory be totally applicable, the forces and the displacements at the shell boundaries must be force-compatible and deformation-compatible with the true membrane behavior of the shell.

There may be some conditions in which the pure membrane action of a given shell could be disturbed and thus the premises of a membrane theory would be violated. The most prominent of these conditions are the following:

- (a) Deformation constraints and some boundary conditions which are incompatible with the requirements of a pure membrane field.
- (b) Application of concentrated forces, and change in the shell geometry and / or sudden change of curvature.

In figure (2-6a), the shell support and its boundary conditions are such that, assuming a pure membrane field in the shell, all equations of equilibrium are satisfied. On the other hand, the membrane forces alone can not satisfy the equilibrium at the boundary of figure

(2-6b). Also, the fixed boundary condition of figure (2-6c) is incompatible with the requirements of a pure membrane field.

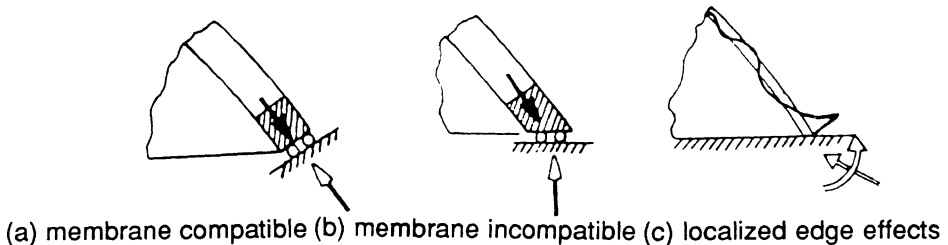


Figure (2-6) Membrane compatible and membrane incompatible boundary conditions in a shell

For a pure membrane field to exist in a shell, displacement requirements dictated by the membrane behavior at the shell boundary must also be fulfilled. Figure (2-7) shows two examples in which the requirements of a pure membrane behavior are not completely fulfilled. In this case, pure membrane action requires that the domes subjected to applied loading or temperature variations have free boundary displacements, whereas the actual support displacement conditions impose some constraints to such freedom of membrane action and hence disturb the pure membrane field in the shell.

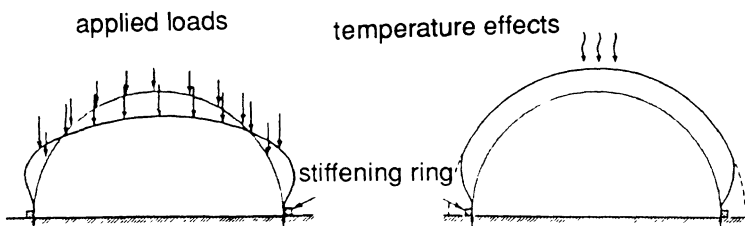


Figure (2-7) A dome shell with edge constraints

The loading and the shell geometrical conditions must also conform to a pure membrane field. For example, kinks and other discontinuities in shell geometry and also concentrated loadings as demonstrated in figure (2-8), would disturb the membrane mode of shell behavior.

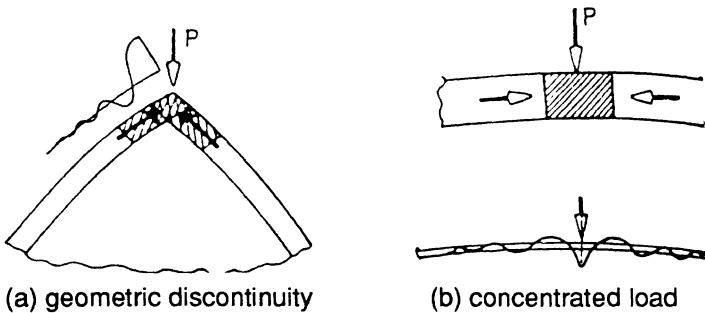


Figure (2-8) Geometrical and loading discontinuities in shells

In the foregoing situations, exemplified by figures (2-6), (2-7), and (2-8), the membrane behavior of the shells is, to some extent, disturbed. In other words, the membrane field of forces and deformations will not, by themselves, be sufficient to satisfy all equilibrium and/or displacement requirements in the regions of *equilibrium unconformity*, *geometrical incompatibility*, *loading discontinuity* and *geometrical nonuniformity*. Therefore, the so-called membrane theory would not hold throughout such shells. In these circumstances, some (or all) of the bending force field components are produced and, by being activated in those regions, compensate for the shortcomings of the membrane field in the disturbed zone.

If it is developed in some region of a shell, the bending field usually has a local range of influence. Laboratory and field experiments, as well as elaborate theoretical calculations, show that the bending field produced in any one of the above-mentioned situations would mostly remain confined to the region in which the membrane conditions are violated. This feature is shown in figures (2-5) and (2-7) by a bending field that "decays out" from the source of membrane nonconformity.

The bending forces, being confined to a small region, leave the rest of the shell virtually free of bending actions. Therefore, in most cases, the major part of a shell structure behaves as a true membrane. This very interesting and unique character of shells is the result of the inherent curvature in the spatial shell form. It is this salient feature of shells that is responsible for the most profound and efficient structural performance of shells observed in nature, as well as in the shells designed and constructed in engineering practice.

To summarize, shell structures carry the applied external forces mostly by the mechanism of membrane action. In some regions of the shell a bending force field may develop to satisfy specific equilibrium or deformation requirements. The range of influence of the bending field is local and is confined to the vicinity of loading and geometrical discontinuities and/or the deformation incompatibilities. The rest of the shell is virtually free from bending actions and can be analyzed and designed as a membrane. Depending on the nature of the applied forces, this membrane shell may be in tension or compression or partly both. The extent of the domain of influence of bending depends on the particular shell geometry and its edge and loading conditions.

2.5 - An Overview of Shell Theories

Many shell theories have been established to analyze the structural shell behavior. The factors influencing the assumptions and domains of applications of the individual shell theories have been the material type and behavior; the shell geometry; the loading conditions; the deformation ranges; the particular shell behavior desired, and the computational means. Accordingly, there are linear and nonlinear theories, membrane and bending theories of shells. The nonlinearity can be material and / or geometrical. Shell analysis computer programs are based on these theories and thus enjoy the capabilities of their theoretical foundation or suffer from the shortcomings of their theoretical modeling.

Any shell theory, is, as any other theory in continuum mechanics, founded on three set of relations. These relations are the ***equilibrium equations***, ***kinematical relations***, and ***constitutive relations***. To be complete, these three sets of field equations must be accompanied by the appropriate boundary conditions of the particular shell problem.

The membrane theory of shells, based on the assumption of membrane behavior of shells, is a simple but useful analytical tool for shell analysis and design. Earlier, it was pointed out in some detail that a shell structure depicts an overall membrane behavior and that the bending actions may, in most cases, be neglected, or at most be taken into account as "corrections" to the membrane field. The **membrane theory** can certainly be used in the initial designs and analyses. It could also be used as a tool to understand the structural behavior of a shell without elaborate formulations or numerical computations. Calculations based on membrane theory, can also serve as guidelines by which the order-of magnitude of the expected results and / or the computer outputs can be interpreted and checked.

2.6 - Assumptions of Classical Shell Theories

The so-called ***classical theories*** of shells are based on the following assumptions:

- 1) The shell is assumed to be *thin*, i.e., its thickness is small compared with its representative minimum radius of curvature, or lateral dimensions.
- 2) Plane sections originally normal to the shell mid-surface remain plane and perpendicular to the deformed mid-surface. The latter assumption is equivalent to ignoring the shear deformations.
- 3) The stress component normal to the shell mid-surface is very small compared with other stress components, and can be neglected.
- 4) The displacements and strains are so small that their higher powers can be neglected.

These assumptions are valid for most engineering shell structures. Therefore, the classical theories based on these assumptions can be used for analysis and design of a variety of shell structures, including reinforced concrete and metallic shells. For composite shells, refinements in these assumptions are sometimes necessary.

2.7 - Force Method of Shell Analysis

To perform a shell structural analysis , one of the two general well known methods of structural analysis may be used. These are: ***the force method*** (or *compatibility method*); ***the displacement method*** (or *the stiffness method*). Many Finite Element shell computer programs are based on the stiffness method. However, for manual calculations, the compatibility method offers certain advantages over the stiffness method.

The analysis of a given shell, according to the force method exemplified by figure (2-9a), includes the following stages :

- (1) First, a **membrane analysis** of the given shell subjected to applied distributed external loading, figure(2-9b), is carried out. In this stage, the boundary conditions are assumed to be compatible with the requirements of the membrane action of the shell. The internal forces as well as the edge displacements and rotations are to be determined from this membrane analysis. At this stage, the shell is statically determinate.

(2) The unknown corrective redundant bending forces are applied to the shell from which the distributed loading is now removed, figure(2-9c). The shell is analyzed with the help of an appropriate **bending theory**. The internal forces as well as the edge displacements and rotations are obtained. This stage of analysis yields the corrections, i.e., the redundant forces, due to the bending field which exist at the shell boundaries. The internal forces and edge deformations of the shell are obviously expressed in terms of unknown bending forces.

(3) The results of analyses performed in stages(1) and (2) are combined to satisfy the **compatibility requirements** at the shell boundaries. The compatibility requirements, expressed in terms of known membrane displacements and unknown edge forces, yield a set of simultaneous algebraic equations from which the redundant edge forces can be determined.

(4) Having performed the membrane analysis and having obtained the corrective boundary bending effects, one can now **superimpose** these two fields to determine the complete force and deformation field in the shell. This completes the force method analysis of the shell.

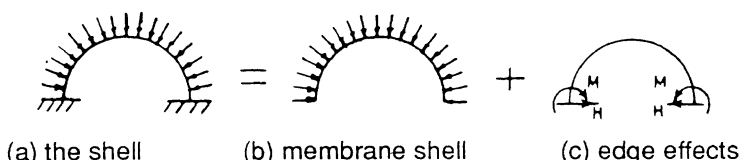


Figure 2-9 An example of shell analysis procedure according to the force method.

The force method of analysis can also be applied to the analysis of a shell structure composed of several shell segments. It is also applicable in the analysis of the shells having flexural edge members. It can be automatized as computer software.

2.8 - General Shell Design Considerations

A structural design shell design normally involves the following activities:

- (1) Choice of a **shell geometry** which meets the overall architectural requirements.
- (2) An trial choice of the **dimensions** of the shell and its **supporting members**, based on previous experience and / or observation of similar shell structures.
- (3) A **preliminary design** and analysis of the shell. For this purpose we can use the membrane theory as well as other simplified shell analysis schemes, such as, the beam theory of cylindrical shells.

In this stage we obtain the initial dimensions of the shell system including the shell thickness, the pattern of shell reinforcements, and the tentative values of required materials and reinforcements. These results are useful for a more comprehensive analysis and also for the initial material and cost estimates.

The preliminary analysis and design of a shell also provides an insight into the general behavior of that shell. Therefore, having performed an initial design-analysis, the designer would have a free hand in changing its design or refining it without having to go into extensive calculations and / or unwanted expenses.

- (4) A more **comprehensive analysis** and detailed design of the shell using bending theory and / or the available computer programs. In many cases, this stage is only required for a final check of the design. A logically based preliminary design usually remains valid, except for some local modifications or perturbations.

Determination of the form, dimensions, and reinforcements of some shells can also be obtained through experiments on physical models of the shell. This is particularly so for the complicated shell geometries and / or cases in which there are no reliable analytical tools. Many arch domes and shell roofs have been designed by the help of experiments performed on scaled models of the actual structure. The experimental and theoretical tools can also complement one another to achieve a sound engineering design of the shell structures.

- (5) The shell designer should always bear in mind that the shell body, in a shell structure, is only an *element* of the whole **structural system**. The shell elements, in a shell structure, are usually accompanied by the strengthening members such as stiffeners, edge and / or ridge beams, and end diaphragms. The structural unity of these various elements, specially under dynamic loadings, is of prime importance. Therefore, design - construction precautions must be taken to assure the **integrity** of the structure as a whole.

An integrated structural shell design, as any other sound structural design, is one which takes into consideration a complete pattern of force flow, figure (2-10). Also, a good design should always involve considerations related to construction, shell manufacturing processes, and shell aesthetics.

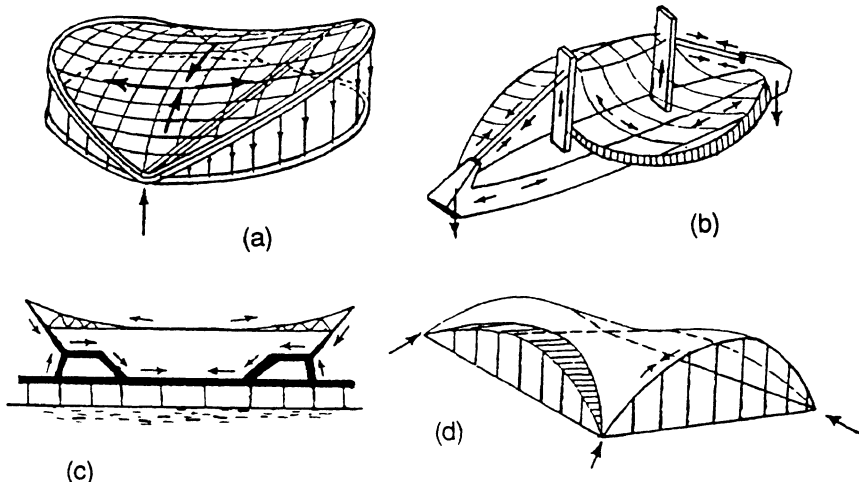


Figure (2-10) Force flow in some shell structural systems

2.9 - Stability Considerations in Shell Design

Metallic, composite and concrete shells are truly thin-walled structures. For example, the thickness to span ratio of reinforced concrete roofs usually falls below 1/200. This ratio is still smaller for metallic and composite shells. On the other hand, there exist situations in which, due to applied loading and / or thermal effects compressive internal stresses may be produced in the shell. These effects could make the shell elastically unstable and thus cause buckling failure of the shell structure.

The buckling strength of shells can be several order of magnitudes lower than the material strength of the shell. Furthermore, thin shells have been shown to be among the so-called *imperfection-sensitive* structures. This means that the buckling load of a shell is highly dependent on imperfections in shell geometry and loading. As a consequence, the true buckling load of an actual shell could be several times smaller than the buckling strength of a corresponding ideal perfect shell.

Premature failure of shells, due to the buckling, makes the stability design of shells important. In fact, dimensioning of shell thickness is usually based on buckling considerations rather than material strength criteria. For in-situ reinforced concrete shells, constructional processes also play a major role in dimensioning the shell thicknesses.

Chapter 13 of this book, will treat the buckling instability of shells. That chapter will present some simplified and practical formulas for the design of shells. These formulas may be used in the actual design of shell structures.

2.10 - Codes of Practice

The practical design of shell structures are based on *Codes of Practice*. Codes of practice, offer general design guidelines specifying limiting design parameters, such as the minimum reinforcement, maximum stress and strain, and minimum thickness.

There are many codes and standards: American Concrete Institute (ACI) codes on shells; German Norm (DIN), the British Standards (BS); and the Indian Standards (IS). These codes help the designer to carry-out a practical design of shells. These standards can be used as guidelines and as official criteria in the design process. In this text, we will use some of these standards in working out the detailed design examples.

References for Chapter Two

- 2.1 - M. Farshad, *Shell Structures*, (in Farsi) Shiraz University Press, Vol. I, 1986, Vol. II, 1987, Shiraz
- 2.2 - M. Farshad, *Principles of Structures*, (In Farsi), Dehkhoda Publications, Tehran, 1983
- 2.3 - M. Salvadori and R. Heller, *Structure in Architecture*, Prentice-Hall,INC.,N.J.,1963
- 2.4 - W. Flügge, *Stresses in Shells*, Springer Verlag, Berlin, 1962
- 2.5 - E. H. Baker, L. Kovalevsky, and F.L. Rish, *Structural Analysis of Shells*, McGraw-Hill Book Co.,N.Y.,1972

Chapter 3

Membrane Behavior of Cylindrical Shells

3.1 - Introduction

Cylindrical shell forms are used in water and gas retaining structures, circular silos, pipes, pressure vessels, and cylindrical vaulted shell roofs of various kinds. This chapter studies the membrane behavior of cylindrical shells. First, we derive the governing membrane equations. Then, we apply these equations to the analysis of various types of cylindrical shells, including vessels, pipes, and vaults. The results of the present chapter will also be used in more comprehensive analysis and design of cylindrical shells treated in future chapters. Some basic design considerations related to such shells will also be presented.

3.2 - Geometrical Description

A cylindrical surface is generated by sliding a plane *generating curve* (the plane of which remains parallel to a fixed plane) along a straight line called the *directrix* of the cylinder. The generating curve of a cylindrical shell may be a closed profile (pipes) or open (vaults). In the particular case of a circular (i.e., constant curvature) profile, the resulting shell is called a *circular cylindrical shell*.

The mid-surface of a cylindrical shell is a surface with single curvature. The curvature of a generating curve may vary along the profile curve. Any point on the mid-surface of a cylindrical shell can be identified by two coordinate parameters. These two parameters are the longitudinal distance from some arbitrarily chosen origin, x , and the angle ϕ between the normal to the shell at that point and a reference normal at some chosen origin, figure (3-1).

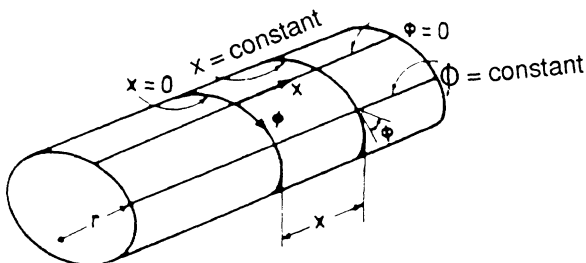


Figure (3-1) Geometrical description of a cylindrical shell

3.3 - Membrane Equations of Cylindrical Shells

Consider an element of a cylindrical shell, such as the one shown in figure(3-1). Let (x, ϕ) designate the coordinates of a corner point of this element. The free body diagram of this element is shown in figure (3-2). In this figure, the r direction identifies the normal to the shell surface at the point (x, ϕ) . The symbols N_x , N_ϕ , $N_{\phi x}$, and $N_{x\phi}$ denote the unknown membrane forces in the shell; these have units of force per length. The known quantities p_x , p_ϕ , and p_r , having units of force per area, represent the intensity of the applied distributed forces in the x , ϕ , and r directions, respectively. All these parameters are functions of the position coordinates x and ϕ .

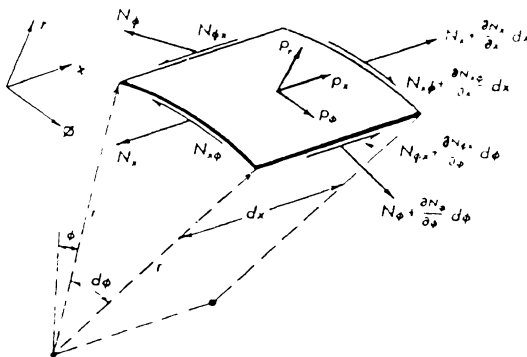


Figure (3-2) Free body diagram of a cylindrical membrane

It is convenient to write the governing membrane equations of equilibrium for the cylindrical shell element in the x , ϕ , and r directions. The moment equation of equilibrium yields $N_{x\phi} = N_{\phi x}$. Hence, the three remaining equilibrium relations are sufficient to determine the three unknown membrane forces N_x , N_ϕ and $N_{x\phi} = N_{\phi x}$.

The equilibrium of forces in the x -direction gives:

$$\sum F_x = 0$$

$$\frac{\partial N_x}{\partial x} dx \cdot r d\phi - \frac{\partial N_{\phi x}}{\partial \phi} d\phi \cdot dx + p_x \cdot dx \cdot r d\phi = 0$$

Equilibrium along the tangent to the shell, the ϕ direction, yields:

$$\sum F_\phi = 0$$

$$\frac{\partial N_\phi}{\partial \phi} d\phi \cdot dx + \frac{\partial N_{x\phi}}{\partial x} dx \cdot r d\phi + p_\phi \cdot dx \cdot r d\phi = 0$$

Finally, by writing the equilibrium relation in the r -direction, i.e., along the normal to the shell, we obtain:

$$\sum F_r = 0$$

$$N_\phi dx \cdot d\phi - p_r \cdot dx \cdot r d\phi = 0$$

Dividing both sides of these equations by the arbitrarily small, but nonzero, length parameters ds and $r d\phi$, we finally obtain the following membrane equations of equilibrium for cylindrical shells.

$$N_\phi = P_r r \quad (5-1)$$

$$\frac{\partial N_{x\phi}}{\partial x} = -P_\phi - \frac{1}{r} \frac{\partial N_\phi}{\partial \phi} \quad (5-2)$$

$$\frac{\partial N_x}{\partial x} = -P_x - \frac{1}{r} \frac{\partial N_{x\phi}}{\partial \phi} \quad (5-3)$$

These equations can be integrated in a sequential manner to yield the membrane force field functions N_ϕ , $N_{\phi x}$, and N_x . The general integral expressions are,

$$N_\phi = r P_r \quad (5-4a)$$

$$N_{\phi x} = - \int (P_\phi + \frac{1}{r} \frac{\partial N_\phi}{\partial \phi}) dx + f_1(\phi) \quad (5-4b)$$

$$N_x = - \int (P_x + \frac{1}{r} \frac{\partial N_{\phi x}}{\partial \phi}) dx + f_2(\phi) \quad (5-4c)$$

The functions $f_1(\phi)$ and $f_2(\phi)$, resulting from integration, depend on the boundary conditions of the particular shell. They can be uniquely obtained for each individual shell problem. In the following sections, we will apply these expressions to some shell analysis problems.

3.4 - Cylindrical Vaults

Consider a semi-circular cylindrical roof loaded by its own weight, having an intensity p . Assume that the shell has two end diaphragms and is supported at its four corners, figure(3-3). A diaphragm can well resist the forces in its own plane but it is practically incapable of supporting out-of-plane forces. Therefore, at each end of the shell we may assume that $N_x=0$. The components of dead weight loading are

$$P_\phi = p \sin \phi \quad , \quad P_r = -p \cos \phi$$

Hence, using the expressions (3-4), and using the condition of $N_x = 0$ at the ends we find the following membrane field:

$$\begin{aligned} N_\phi &= -p a \cos \phi \\ N_{\phi x} &= -2p x \sin \phi \\ N_x &= -\frac{p}{4a} (l^2 - 4x^2) \cos \phi \end{aligned} \quad (3-5)$$

Figure (3-3) shows the variations of internal membrane forces in an arbitrary section, located at a distance x .

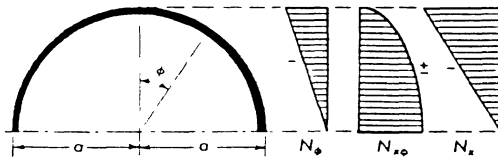


Figure (3-3) Variations of membrane forces in a section of a cylindrical vault

Referring to these graphs, and expressions, we can make the following observations:

- (a) At the longitudinal edges of the shell, i.e., at $\phi = \pm \pi / 2$, we have: $N_\phi=0$. This means that this shell has no need of longitudinal normal support.
- (b) At the longitudinal edges ($\phi = \pm \pi / 2$), the membrane shear force in the shell is $N_{x\phi} = 2px$. This means that there is a need for a longitudinal edge member to absorb this force and to transfer it to the end diaphragms. This edge member is shown in figure (3-4).

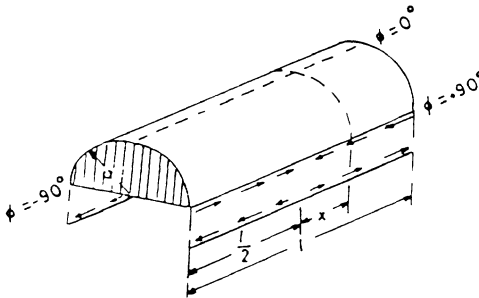


Figure (3-4) Transfer of edge shear forces to the edge beam

The longitudinal edge member required by the membrane theory is called an **edge beam**. Figure (3-3) shows the mechanism of shear load transfer from the shell to the edge beam. The shear force in the shell, upon its transfer to the edge beam, becomes an **axial tension** in the beam. The magnitude of axial tension force in the edge beam at any section is obtained by integration of edge shears along the edge. Its expression is:

$$N = \int_{\frac{l}{2}}^x N_{x\phi} dx = - 2P \int_{\frac{l}{2}}^x x dx = \frac{1}{4} P(l^2 - 4x^2) \quad (3-6)$$

At the ends of the shell, i.e., at $x=+ l / 2$, we have $N_x=0$, but $N_{x\phi}=-pl \sin \phi$. This means that part of the applied load is transferred to the end diaphragm by the shear force mechanism.

3.5 - Containment Vessels

3.5.1 - Fluid Tanks

Consider a vertical circular cylindrical tank of radius a and height H . Assume that it is filled with a fluid of density γ . The components of pressure loading are

$$P_x = 0, \quad P_\phi = 0, \quad P_r = \gamma(H - x) \quad (3-7)$$

Equations (3-1) to (3-3) give the membrane field of internal forces.

$$N_x = 0 \quad (3-8a)$$

$$N_{x\phi} = 0 \quad (3-8b)$$

$$N_\phi = \gamma a (H - x) \quad (3-8c)$$

3.5.2 - Pipes under Internal Pressure

As an example of thin-walled pipes, under internal pressure, we consider a circular cylindrical pipe, of radius a , located in a horizontal position and pressurized by a fluid of density γ . The pipe is assumed to be supported by two end ring supports, figure (3-5).

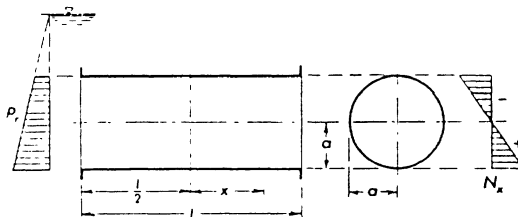


Figure (3-5) A horizontal thin-walled pipe under internal pressure

The pressure head, measured at the level of cylinder axis, is assumed to be p_0 . Thus the components of applied loading are

$$P_r = P_0 - \gamma a \cos\phi \quad (3-9a)$$

$$P_x = 0 \quad (3-9b)$$

$$P_\phi = 0 \quad (3-9c)$$

Using equations (3-1) to (3-3), or equivalently (3-4), we obtain the following membrane force field:

$$N_\phi = P_0 a - \gamma a^2 \cos\phi \quad (3-10a)$$

$$\begin{aligned} N_{\phi x} &= - \gamma a \sin \phi dx + f_1(\phi) \\ &= - \gamma a x \sin \phi + f_1(\phi) \end{aligned} \quad (3-10b)$$

$$\begin{aligned} N_x &= \int \gamma \cos \phi \cdot x dx - \frac{1}{a} \int \frac{df_1(\phi)}{d\phi} \cdot dx + f_2(\phi) \\ &= \gamma \frac{x^2}{2} \cos \phi - \frac{x}{a} \frac{df_1(\phi)}{d\phi} + f_2(\phi) \end{aligned} \quad (3-10c)$$

The unknown functions $f_1(\phi)$ and $f_2(\phi)$ are to be determined from the boundary conditions:

$$(N_x)_{x=0} = 0 \quad , \quad (N_x)_{x=l} = 0$$

Using these information in the expression (3-9c) we obtain

The constant C , representing the non-existing resultant end torsional couple may be set equal to zero. Therefore, the solution to this problem is

$$N_\phi = P_O \bar{a} - \gamma a^2 \cos \phi \quad (3-11a)$$

$$N_{x\phi} = \gamma a \left(\frac{l}{2} - x \right) \sin \phi \quad (3-11b)$$

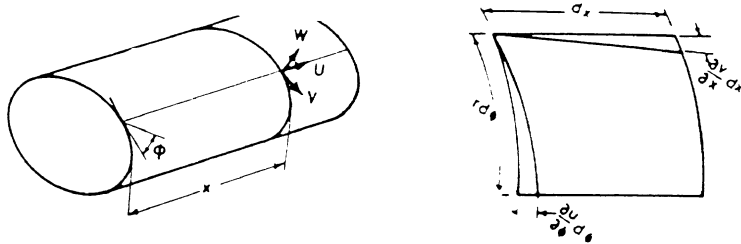
$$N_x = - \frac{\gamma}{2} x (l - x) \cos \phi \quad (3-11c)$$

If this cylinder were viewed as a *horizontal beam*, then the derived expressions for N_x and $N_{x\phi}$ could be interpreted as the longitudinal bending stress and shear stress, respectively. Figure (3-5) shows that N_x is linear in the sectional height.

3.6 - Membrane Deformation of Cylindrical Shells

The components of displacement field in a cylindrical shell are the longitudinal displacement, u , the transverse displacement, v , and the normal displacement, w , figure (3-6a). These quantities are functions of the coordinates x and ϕ .

In order to obtain the membrane displacement field in a cylindrical shell, with already known internal forces, we use the constitutive and the shell kinematic relations. We assume that the shell is made of a linearly elastic and isotropic material which obeys Hooke's law; the two elastic constants are Young's modulus E and Poisson's ratio v .



Figure(3-6) (a) Displacement components in a cylindrical shell,
(b) a deformed element of the shell

For a linearly elastic and isotropic cylindrical shell of thickness \$t\$ the constitutive relations are:

$$\begin{aligned}\epsilon_x &= \frac{1}{Et} (N_x - v N_\phi) \\ \epsilon_\phi &= \frac{1}{Et} (N_\phi - v N_x) \\ \gamma_{x\phi} &= \frac{2(1+v)}{Et} N_{x\phi}\end{aligned}\quad (3-12)$$

To derive the kinematic relations we consider a displaced configuration of the shell element, as shown in figure (3-6b). If we denote the axial strain by \$\epsilon_x\$, the transverse strain by \$\epsilon_\phi\$, and the shear strain by \$\gamma_{x\phi}\$, then we can write the linear strain-displacement relations as:

$$\begin{aligned}\epsilon_x &= \frac{\partial u}{\partial x} \\ \epsilon_\phi &= \frac{1}{r} \left(\frac{\partial v}{\partial \phi} + w \right) \\ \gamma_{x\phi} &= \frac{\partial v}{\partial x} + \frac{1}{r} \frac{\partial u}{\partial \phi}\end{aligned}\quad (3-13)$$

By combining two sets of relations (3-12) and (3-13) we obtain

$$\begin{aligned}\frac{\partial u}{\partial x} &= \frac{1}{Et} (N_x - v N_\phi) \\ \frac{\partial v}{\partial x} + \frac{1}{r} \frac{\partial u}{\partial \phi} &= \frac{2(1+v)}{Et} N_{x\phi} \\ \frac{w}{r} + \frac{1}{r} \frac{\partial v}{\partial \phi} &= \frac{1}{Et} (N_\phi - v N_x)\end{aligned}\quad (3-14)$$

Assuming that the membrane forces \$N_x, N_\phi, N_{x\phi}\$ are already determined, we can integrate the relations (3-14) in a sequential manner, to obtain

$$\begin{aligned} E\ddot{u} &= f(N_x - vN_\phi)dx + f_3(\phi) \\ E\ddot{v} &= 2(1+v)\int N_{x\phi} dx - Et \frac{1}{r} \int \frac{\partial u}{\partial \phi} dx + f_4(\phi) \\ E\ddot{w} &= r(N_\phi - vN_x) - Et \frac{\partial v}{\partial \phi} \end{aligned} \quad (3-15)$$

The functions $f_3(\phi)$ and $f_4(\phi)$ in the integration process can be determined for each shell from specific boundary conditions.

3.7 - Displacements of Cylindrical Vaults

Return to the circular cylindrical shell of figure (3-4). We would like to determine the displacement field in the shell under a dead weight loading of intensity p . As specific boundary conditions, we assume that at $x=+1/2$ we have $v=0$ and $w=0$.

If we substitute the membrane force expressions (3-5) into (3-15) we obtain the following:

$$\begin{aligned} E\ddot{u} &= \frac{Px}{a} \left(\frac{x^2}{3} - \frac{\ell^2}{4} + va^2 \right) \cos\phi \\ E\ddot{v} &= \frac{1}{8} P(\ell^2 - 4x^2) \left(\frac{5\ell^2 - 4x^2}{24a^2} + 4 + 3v \right) \sin\phi \\ E\ddot{w} &= -\frac{1}{8} P(\ell^2 - 4x^2) \left(\frac{5\ell^2 - 4x^2}{24a^2} + 4 + v \right) \cos\phi - Pa^2 \cos\phi \end{aligned} \quad (3-16)$$

Note that the constraint on the radial displacement, w , at $x=+1/2$ violates the requirements of the membrane action of the shell at that section. As a result, some bending will develop around that region, and can be predicted by the bending theory of cylindrical shells.

Numerical Example 3.1

As a numerical example of displacement calculation, assume the following numerical data for the cylindrical shell of figure (3-4):

$$a = 9.0 \text{ m}, t = 10.0 \text{ cm}, l = 20.0 \text{ m}$$

$$p = 400 \text{ kg/m}^2, v = 0.0, E = 2 \times 10^5 \text{ kg/cm}^2$$

The displacement of the shell at the point ($x=0, \phi=0$) is to be determined.

Solution

Evaluating the expressions (3-16), for the shell displacements, and substituting the assumed numerical values in the resulting expressions, we obtain

$$u_0 = \frac{1}{Eh} (0) = 0$$

$$v_0 = 0$$

$$\begin{aligned} w_0 &= \frac{1}{Et} \left[-\frac{p\ell^2}{8} \cdot \left(\frac{5\ell^2}{24a^2} + 4 \right) - pa^2 \right] \\ &= \frac{1}{2 \times 10^6} \left[-\frac{400 \times 400}{8} \times \left(\frac{5}{24} \times \frac{400}{81} + 4 \right) - 400 \times 81 \right] \\ &= 0.06 \text{ cm} = 0.6 \text{ mm} \end{aligned}$$

As we observe, the resulting displacement is very small. It would be interesting to compare this value with a relatively high lateral deflection of a beam having the same span and loading.

3.8 - Qualitative Description of Cylindrical Shells Behavior

The membrane behavior of cylindrical shells consists of an interaction of two behavioral components: (1) *the beam action*, and (2) *the arch action*. In the beam mode of action, the cylindrical shell behaves as a simply supported (or as a continuous beam) resting on longitudinal supports. In the arch mode of action, the applied forces are transferred in the transverse direction, i.e., along the arches of the shell.

Whether the cylindrical shell has mostly *the beam action* or *the arch action* depends on the shell geometry and the edge conditions. For example, longitudinal supports transfer the applied forces in the longitudinal direction.

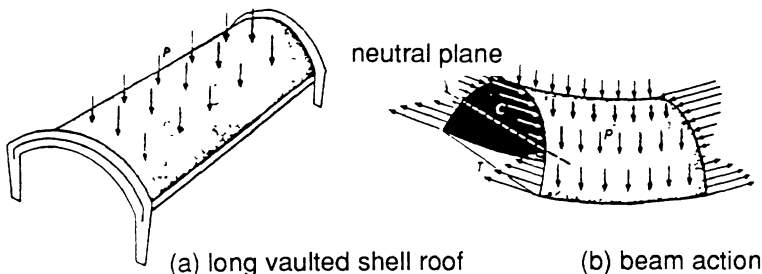


Figure (3-7) Beam action of long cylindrical vaults, (a) laterally loaded shell resting on longitudinal end arches, (b) longitudinal internal forces in the vault

Long cylindrical shells resting on end supports act like simply supported beams. A long shell acts like a beam, having as its section the shell profile, and as its span the span of the shell. The external bending moment at each section is supported by the resultant of compressive longitudinal membrane forces acting as the *compression flange*, and the tension in the edge beam acting as the *tension flange*, figure (3-7).

As we have seen in our membrane analysis of long vaults, the applied forces are transferred longitudinally to the end supports. The transfer of internal load to the end diaphragms or end arches takes place by the internal shear force mechanism, as shown in figure (3-8).

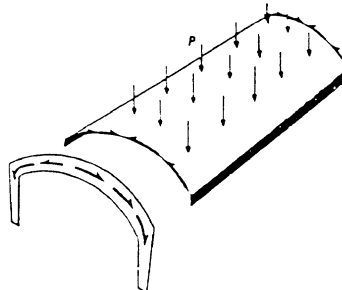


Figure (3-8) Shear force mechanism of applied forces to the end arches in a cylindrical vault

In an overall beam action of the long shell, part of the applied load could be transferred by internal shear forces to the longitudinal beams, as demonstrated in figure (3-9). However, if there are no edge beams, then because the free edge situation is incompatible with the requirements of the membrane theory, some bending field of forces will develop along the longitudinal edges

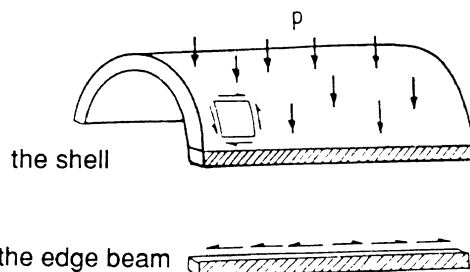


Figure (3-9) Shear force mechanism of load transfer to the longitudinal edge beam in a vault

The longer the shell is, the stronger is the beam action of the shell. On the other hand, in a short shell, the so-called *arch action* is more effective and the applied load is mostly transferred by the transverse arches.

Figure (3-10) shows the longitudinal internal stresses in two end supported cylinders, one long and the other short. As we see, the behavior of the longer shell is closer to the action of a simple beam, whereas that of the shorter shell is different.

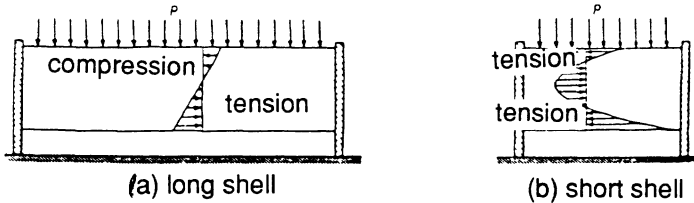


Figure (3-10) Comparative behaviors of long and short cylinders both resting on end supports

So far, in our qualitative presentation of cylindrical shells behavior, we have discussed the membrane action of the shell. As we pointed out earlier, in chapter 2, some bending fields can develop in shells. For example, end supports (diaphragms or arches) give rise to internal bending forces. In these cases the bending force field is needed to satisfy compatibility. The region of influence of the bending field depend on the end conditions, the loading, the thickness, and the length of the cylindrical shell.

Figure (3-11) shows how the behavior of long and short shells are influenced by the bending field. The effect of the bending field, caused by the end diaphragms, is local and confined to the ends of a long shell. In shorter shells, the influence of bending field is more pronounced. For very short shells, the bending field penetrates throughout the shell and affects the "whole system".

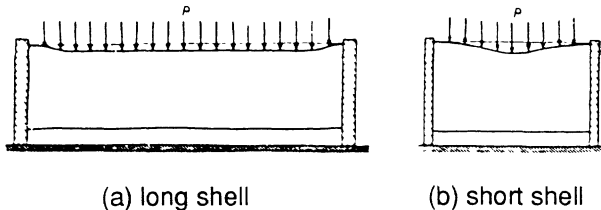


Figure (3-11) Comparative influence of the bending field on end-supported cylindrical shells, (a) a long shell, (b) a short shell

Figures (3-12) summarize the cylindrical shell behavioral patterns. These figures demonstrate clearly the beam action, figure(3-12a) and (3-12b); the arch action, figure (3-12c); the bending fields developed by the stiffening longitudinal beam, figure (3-12a), and end arches, figure (3-12c).

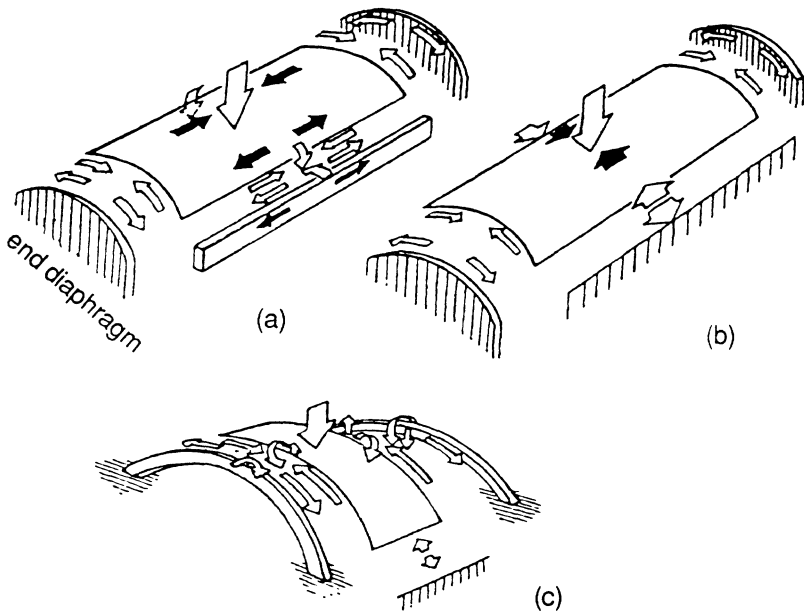


Figure (3-12) A graphical summary of cylindrical shell behavior, (a) long shell with rigid end diaphragms and torsion resisting edge beams, (b) long shell with rigid end diaphragms and simple longitudinal vertical supports, (c) short shell with torsion resisting end arches and simple longitudinal vertical supports

The qualitative understanding of the cylindrical shell behavior, arrived at in this section, is extremely useful in cylindrical shell design and analysis. The quantitative analysis of cylindrical shells for bending effects will be carried out in the next chapter.

Problems

P 3.1 - Consider a cylindrical vessel with elliptical profile as shown in figure (P 3.1). The vessel is in a horizontal position and is simply supported at its two ends by means of end rings or end diaphragms. Determine the internal forces in this shell for $p_x = 0$ and arbitrary distributions of p_f and p_r . Show that the resulting force field has the following form:

$$N_{x\phi} = -x(P_\phi + \frac{1}{a} \frac{\partial N_\phi}{\partial \phi})$$

$$N_x = -\frac{1}{8a} (\lambda^2 - 4x^2) \frac{d}{d\phi} (P_\phi + \frac{1}{a} \frac{\partial N_\phi}{\partial \phi})$$

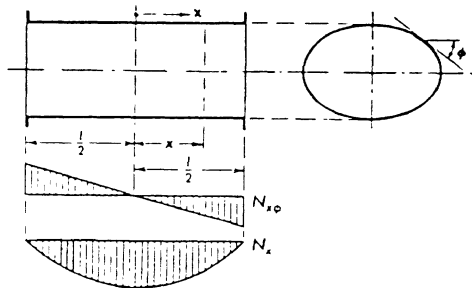


Figure (P 3-1)

P 3.2 - Consider a cylindrical vault having a parabolic profile as shown in figure (P 3-2). The equation of the profile curve is

$$\zeta^2 = 2r_0 \xi$$

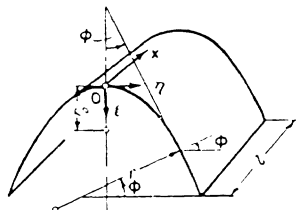


Figure (P 3-2)

wherein, r_0 is the radius of curvature of the parabola at the origin. At any other point, the radius of curvature can be expressed as

$$r = \frac{[1 + (d\xi/d\zeta)^2]^{3/2}}{(d^2\xi)/(d\zeta^2)}$$

and since

$$\frac{d^2\xi}{d\zeta^2} = \frac{1}{r_0}$$

so $\tan\phi = \frac{d\xi}{d\zeta}$, $r = \frac{r_0}{\sin^3\phi}$

Consider three types of applied loading

(1) Dead load of intensity p:

$$\begin{cases} P_x = 0 \\ P_\phi = -P \cos\phi \\ P_r = -P \sin\phi \end{cases}$$

(2) Snow load of intensity p:

$$\begin{cases} P_x = 0 \\ P_\phi = -P \sin\phi \cos\phi \\ P_r = -P \sin^2\phi \end{cases}$$

(3) Lateral wind load of intensity p:

$$\begin{cases} P_x = 0 \\ P_\phi = 0 \\ P_r = -P \cos\phi \end{cases}$$

Show that the internal force field for these loading systems are as follows:

(1) Membrane forces for dead loading:

$$N_\phi = -P \frac{r_0}{\sin^2\phi}$$

$$N_{\phi x} = \frac{P}{2} (\ell - 2x) \cos\phi$$

$$N_x = \frac{Px}{2r_0} (\ell - x) \sin^4\phi$$

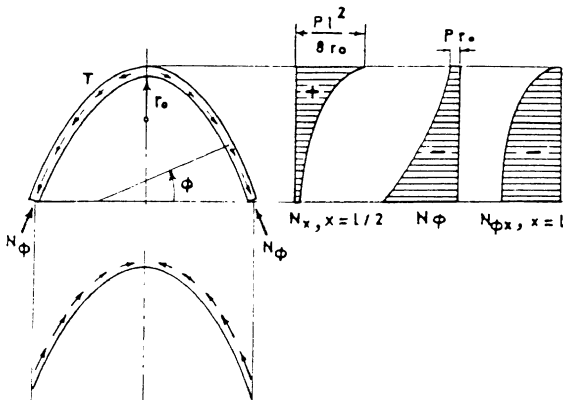
(2) Membrane forces for snow loading:

$$N_\phi = - P \frac{r_o}{\sin \phi}$$

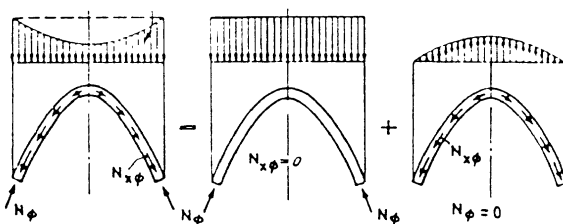
$$N_x = 0$$

$$N_{\phi x} = 0$$

Interpret these results and note that for snow loading, parabolic arches are funicular and hence the load is carried mainly in the transverse direction. By plotting the membrane force field for dead loading, reproduce the following figure:



Note that the effect of shell on the end diaphragm is in apparent contradiction to intuition. Verify this result and carry out a physical interpretation with the help of the following diagrams.



P 3.3 - A circular cylindrical barrel shell of length L_1 is supported by diaphragms at its ends A and B. The shell cantilevers out beyond B for a length L. Find the membrane forces in this shell under dead loading of intensity p.

3.4 - A vertical chimney of circular cross section and radius a is subjected to a wind load defined by $p_x = 0$, $p_\phi = 0$, $p_r = q \cos \theta$. Here θ is the horizontal angle and q is the intensity of wind load. Find the membrane stress resultants in this chimney shell. Compare the results with those obtained by classical cantilever beam theory.

3.5 - Consider a simply supported shell vault with a catenary cross section. The equation of the middle surface in the cross-sectional coordinate system y-z is given by,

$$z = -a(1 - 85h y / a)$$

Obtain the membrane stress resultants in the shell under uniformly distributed dead loading of intensity p.

References for Chapter Three

- 3.1 - W. Flügge, *Stresses in Shells*, Springer Verlag, Berlin, 1962
- 3.2 - A. M. Haas, *Design of Thin Concrete Shells*, John Wiley & Sons, New York, 1962
- 3.3 - S. Timoshenko, and S. Woinowsky-Krieger, *Theory of Plates and Shells*, 2nd Edition, McGraw-Hill Book Co., N.Y., 1959
- 3.4 - A. Pflüger, *Elementary Statics of Shells*, 2nd Edition, McGraw-Hill Book Co., N.Y., 1961
- 3.5 - M. Salvadori and R. Heller, *Structure in Architecture*, Prentice-Hall, INC., N.J., 1963

Chapter **4**

Bending Analysis of Circular Cylindrical Shells

4.1 - Introduction

A complete analysis of various cylindrical shell forms, for silos, pressure vessels, containment shells, containers, and shell roofs, would require an appropriate bending theory. A general bending theory would embody the membrane theory of shells. It would also predict the bending action of the shell. This chapter introduces a general bending theory of circular cylindrical shells. The theoretical basis of the present chapter forms the foundation of approximate bending theories for cylindrical shells. The special theories for cylinders, such as axisymmetric cylindrical shell theory and the bending theories of cylindrical vaulted roofs, developed in future chapters, can be considered as the offspring of the general theory presented in this chapter. The theoretical developments in this chapter will lead to a set of useful relations for treating a variety of practical shell analyses and design problems.

4.2 - General Governing Equations

The governing field equations of cylindrical shells include: **equilibrium equations**, **kinematic relations**, and **constitutive relations**.

4.2.1 - Equilibrium Equations

Consider the free-body diagram of a circular cylindrical shell element shown in figure (4-1). The superposition of the two force systems depicted in figures (4-1a) and (4-1b) would yield a complete system of internal forces acting on an element of the cylindrical shell. The internal forces are defined per unit width of the element. Figure (4-1) indicates the bending moments and twisting couples by double arrows. Figure (4-1) gives a complete picture of the internal forces, including the bending and the membrane forces.

In the developments which follow, we use the following abbreviations:

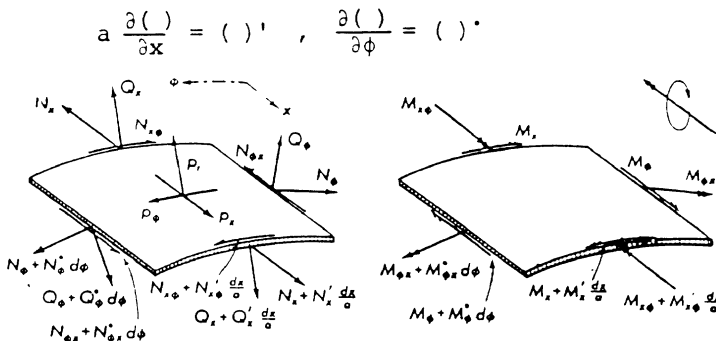


Figure (4-1) Free body of a cylindrical shell element with internal force variations and the external distributed forces

The equations of equilibrium of internal and external forces, along the x , ϕ , and r axes, are as follows:

$$N'_x + N'_{\phi x} + aP_x = 0 \quad (4-1a)$$

$$N'_\phi + N'_{x\phi} - Q_\phi + aP_\phi = 0 \quad (4-1b)$$

$$Q_\phi + Q'_x + N_\phi - aP_r = 0 \quad (4-1c)$$

Compared with the membrane equations for cylindrical shells, these equations contain extra terms emanating from the bending effects. When the bending field comes into play they are needed for providing the equilibrium and / or compatibility to the shell elements.

The moment equations of equilibrium, about the x , ϕ , and r axes, are:

$$\dot{M}_\phi + M'_{x\phi} - aQ_\phi = 0 \quad (4-2a)$$

$$\dot{M}'_x + M_{\phi x} - aQ_x = 0 \quad (4-2b)$$

$$aN_{x\phi} - aN_{\phi x} + M_{\phi x} = 0 \quad (4-2c)$$

Note that, due to the presence of the twisting couple $M_{\phi x}$, the membrane shear forces $N_{x\phi}$ and $N_{\phi x}$ need no longer be equal.

If we eliminate the two shear force functions Q_x and Q_ϕ from the two sets of equations (4-1) and (4-2), we obtain the following equilibrium equations:

$$N'_x + N'_{\phi x} + aP_x = 0 \quad (4-3a)$$

$$aN_\phi + aN'_{x\phi} - M_z - M'_{x\phi} + a^2P_\phi = 0 \quad (4-3b)$$

$$M'_\phi + M''_{x\phi} + M'_{\phi x} + M''_x + aN_\phi - a^2P_r = 0 \quad (4-3c)$$

$$aN_{x\phi} - aN_{\phi x} + M_{z x} = 0 \quad (4-3d)$$

There are ten unknown internal force components (N_x , N_ϕ , $N_{x\phi}$, $N_{\phi x}$, M_x , M_ϕ , $M_{\phi x}$, $M_{x\phi}$, Q_x , Q_ϕ), on the one hand, and six equilibrium equations, on the other. Therefore, the shell is statically indeterminate and hence requires extra relations for its analysis.

4.2.2 - Kinematic Relations

To derive the kinematical relations for circular cylinders, we use the basic kinematic assumptions outlined in section 2.5. If we denote the components of displacement field of the shell middle-plane by u, v, w , then we can express the displacement of an arbitrary point located at a distance z from the middle-surface in terms of these components. An outward radial displacement, w , is considered positive.

Figures (4-2a) and (4-2b) show the undeformed and the deformed longitudinal and transverse sections of the shell element. In these figures, points A_0 and A represent typical material points originally located on the shell middle-surface, and a distance z from the middle-surface, respectively. The components of displacement of the material point A are denoted by u_A, v_A, w_A .

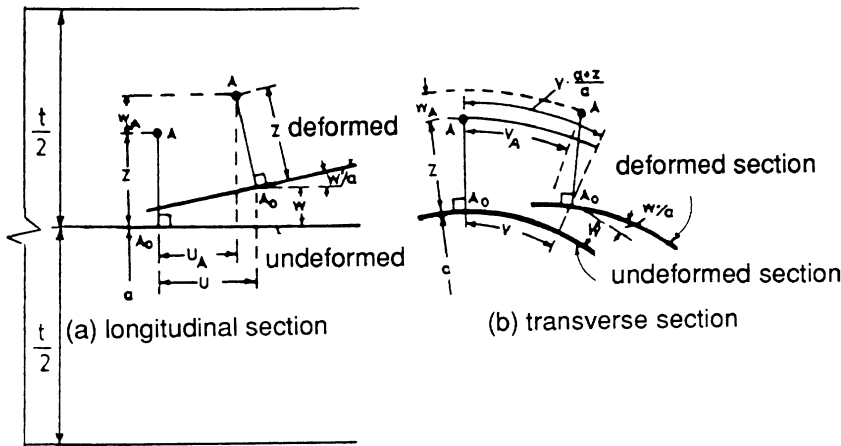


Figure (4-2) Undeformed and deformed sections of the shell,
(a) undeformed, (b) deformed

Using the basic kinematic assumptions of section 2.5, we can express the displacement components of an arbitrary material point located at a distance z in terms of the middle-surface displacement components as follows:

$$u_A^* = u - \frac{w}{a} z \quad (4-4)$$

$$v_A^* = \frac{a+z}{a} v - \frac{w}{a} z \quad (4-5)$$

$$w_A^* = w \quad (4-6)$$

Having found the displacement relationships, we can now formulate the strain-displacement relations. The components of strain in cylindrical coordinates can be expressed as

$$\epsilon_x = \frac{\partial u_A^*}{\partial x} = \frac{u_A^{*'}}{a} \quad (4-7a)$$

$$\epsilon_\phi = \frac{1}{a+z} \left(\frac{\partial v_A^*}{\partial \phi} + w_A^* \right) = \frac{v_A^{*'} + w_A^*}{a+z} \quad (4-7b)$$

$$\gamma_{x\phi} = \frac{\partial v_A^*}{\partial x} + \frac{1}{a+z} \frac{\partial u_A^*}{\partial \phi} = \frac{v_A^{*''}}{a+z} + \frac{u_A^{*'}}{a+z} \quad (4-7c)$$

Using relations (4-4), (4-5), and (4-6) we can write these as finally:

$$\epsilon_x = \frac{u'}{a} - z \frac{w''}{a^2} \quad (4-8a)$$

$$\epsilon_\phi = \frac{v}{a} - \frac{z}{a} \frac{\ddot{w}}{a+z} + \frac{w}{a+z} \quad (4-8b)$$

$$\gamma_{x\phi} = \frac{u}{a+z} + \frac{a+z}{a^2} v' - \frac{w'}{a} \left(\frac{z}{a} + \frac{z}{a+z} \right) \quad (4-8c)$$

These relations constitute the kinematic relations for circular cylindrical shells.

4.2.3 - Constitutive Relations

Throughout this book, we shall assume that the shells under consideration are composed of isotropic materials having linearly elastic behavior. Therefore, assuming a generalized plane state of stress, we may write the stress-strain relations, at any point of the shell as follows:

$$\sigma_x = \frac{E}{1-\nu^2} (\epsilon_x + \nu \epsilon_\phi) \quad (4-9a)$$

$$\sigma_\phi = \frac{E}{1-\nu^2} (\epsilon_\phi + \nu \epsilon_x) \quad (4-9b)$$

$$\tau_{x\phi} = \frac{E}{2(1+\nu)} \gamma_{x\phi} \quad (4-9c)$$

We can express these constitutive relations in terms of internal force resultants and the displacement components of the middle surface. In order to do so, we use the set of relations (2-1), (4-8), and (4-9). The combined constitutive and kinematic relations are:

$$N_\phi = \frac{D}{a} (v + w + \nu u') + \frac{K}{a^3} (w + \ddot{w}) \quad (4-10a)$$

$$N_x = \frac{D}{a} (u' + \dot{v} + \nu w) - \frac{K}{a^3} w'' \quad (4-10b)$$

$$M_\phi = \frac{K}{a^2} (w + \ddot{w} + \nu w'') \quad (4-10c)$$

$$M_x = \frac{K}{a^2} (w'' + \dot{\nu} w - u' - \nu \dot{v}) \quad (4-10d)$$

$$M_{\phi x} = \frac{K}{a^2} (-\nu \dot{v} (w' + \dot{u}) + \frac{1}{a} u' - \nu \dot{w}) \quad (4-10e)$$

48 Design and Analysis of Shell Structures

$$M_{x\phi} = \frac{K}{a^2} (1 - v) (w'' - v'') \quad (4-10f)$$

$$N_{\phi x} = \frac{D}{a} \frac{1 - v}{2} (\dot{u} + v') + \frac{K}{a^3} \frac{1 - v}{2} (\dot{u} - w'') \quad (4-10g)$$

$$N_{x\phi} = \frac{D}{a} \frac{1 - v}{2} (\dot{u} + v') + \frac{K}{a^3} \frac{1 - v}{2} (v' - w'') \quad (4-10h)$$

The two shell characteristic parameters, K and D, are:

$$D = \frac{Et}{1 - v^2}, \quad K = \frac{Et^3}{12(1 - v^2)} \quad (4-11)$$

From a physical point of view, the parameter K signifies the bending stiffness and D the membrane stiffness of the shell. Therefore, all terms containing K represent contributions of the bending field to the total field. So, if we assume no bending stiffness for the shell, i.e., if we disregard the terms containing K, in the above relations, we shall obtain the constitutive relations for a membrane elastic cylindrical shell.

The shell constitutive relations (4-10) can be cast in a more appealing and yet compact form. In looking back to relations (4-8) we recognize the middle-surface strain field, as defined by ϵ_x , ϵ_ϕ , and $\gamma_{x\phi}$ to be related to middle-surface displacement components as follows:

$$\bar{\epsilon}_x = \frac{u'}{a}, \quad \bar{\epsilon}_\phi = \frac{\dot{v} + w}{a}, \quad \bar{\gamma}_{x\phi} = \frac{\dot{u} + v'}{a} \quad (4-12)$$

Also, the terms containing thickness variable, z, are recognized to be contributions from the sectional curvature change and twist. Hence, using relations (4-8) we can write the change in the shell local curvature as well as the local twist in terms of parameters ψ_x , ψ_ϕ , and $\psi_{x\phi}$ as:

$$\psi_x = \frac{w''}{a^2}, \quad \psi_\phi = \frac{\ddot{w} + w}{a^2} \quad (4-13a)$$

$$\psi_{x\phi} = \frac{w'''}{a^2} + \frac{\dot{u} - v'}{2a^2} \quad (4-13b)$$

Now, if we insert the expressions (4-12) and (4-13) in relations (4-10), we obtain the following constitutive relations:

$$N_{\phi} = D(\bar{\varepsilon}_{\phi} + v\bar{\varepsilon}_x) + \frac{K}{a}\psi_{\phi} \quad (4-14a)$$

$$N_x = D(\bar{\varepsilon}_x + v\bar{\varepsilon}_{\phi}) - \frac{K}{a}\psi_x \quad (4-14b)$$

$$N_{\phi x} = \frac{D(1-v)}{2}\bar{\gamma}_{x\phi} + \frac{K(1-v)}{2a}(\psi_{x\phi} + \frac{\bar{\gamma}_{x\phi}}{2a}) \quad (4-14c)$$

$$N_{x\phi} = \frac{D(1-v)}{2}\bar{\gamma}_{x\phi} - \frac{K(1-v)}{2a}(\psi_{x\phi} - \frac{\bar{\gamma}_{x\phi}}{2a}) \quad (4-14d)$$

$$M_{\phi} = K(\psi_{\phi} + v\psi_x) \quad (4-14e)$$

$$M_x = K(\psi_x + v\psi_{\phi}) - \frac{\bar{\varepsilon}_x + v\bar{\varepsilon}_{\phi}}{a} \quad (4-14f)$$

$$M_{\phi x} = K(1-v)\psi_{x\phi} \quad (4-14g)$$

$$M_{x\phi} = K(1-v)(\psi_{x\phi} - \frac{\bar{\gamma}_{x\phi}}{2a}) \quad (4-14h)$$

These relations, are a set of fairly complete but useful forms of shell constitutive relations expressed in terms of internal force resultants. They also embody the kinematic relations. In these expressions, the terms containing K signify the contributions arising from the bending action of the shell.

4.3 - Displacement Equations of Circular Cylindrical Shells

The collection of equilibrium, kinematic, and constitutive equations, (relations (4-3) and (4-10)), constitute the field equations of bending theory of circular cylindrical shells. In passing, we note that by using the expressions for $N_{x\phi}$, $N_{\phi x}$, and $M_{\phi x}$ we can satisfy the last equation of (4-3) identically. Hence, the total of 11 equations correspond well with the total of 11 unknowns (internal forces and displacements).

By combining the relations (4-3) and (4-10), we can obtain the displacement equations governing the bending behavior of circular cylindrical shells. So, by substituting (4-10) into (4-3), and making some elementary manipulations, we obtain

$$u'' + \frac{1-v}{2} \ddot{u} + \frac{1+v}{2} v''' + vw' + k \left[\frac{1-v}{2} \ddot{u} - w''' \right] + \frac{1-v}{2} w'''' + \frac{P_x a^2}{D} = 0 \quad (4-15a)$$

$$\frac{1+v}{2} \dot{u}' + \ddot{v} + \frac{1-v}{2} v'' - \dot{w} + k \left[\frac{3}{2}(1-v)v'' \right] - \frac{3-v}{2} w'''' + \frac{P_x a^2}{D} = 0 \quad (4-15b)$$

$$vu' + \dot{v} + w + k \left[\frac{1-v}{2} u'''' - u''' - \frac{3-v}{2} v''' + w''' \right] + 2w'''' + \ddot{w} + 2\ddot{w} + w - \frac{P_x a^2}{D} = 0 \quad (4-15c)$$

The parameter k in these equations represents the ratio of bending to membrane stiffness. It has the following definition:

$$k = \frac{K}{Da^2} = \frac{t^2}{12a^2} \quad (4-16)$$

The displacement equations (4-15) governing the bending behavior of circular cylindrical shells are quite general. These equations can be solved by numerical schemes or, in some special cases, by analytical means. However, certain simplifications can be made to make them more useful for practical analysis and design. If we assume that the shell is relatively thin, then we may only retain those terms containing the parameter k which are of higher gradients, i.e., higher order of differentiation with respect to the x and ϕ variables. If we do so, we obtain the more simplified equations which read:

$$u'' + \frac{1-v}{2} \ddot{u} + \frac{1+v}{2} v''' + vw' + \frac{P_x a^2}{D} = 0 \quad (4-17a)$$

$$\frac{1+v}{2} u''' + \ddot{v} + \frac{1-v}{2} v'' + \dot{w} + \frac{P_\phi a^2}{D} = 0 \quad (4-17b)$$

$$vu' + \dot{v} + w + k(w'''' + 2w''' + w) - \frac{P_r a^2}{D} = 0 \quad (4-17c)$$

These equations can be simplified further. We shall discuss special theories based on these equations in the forthcoming sections and chapters.

4.4 - Circular Cylinders with Axisymmetric Loading

In a variety of practical situations, circular cylindrical shell structures are subjected to axisymmetric loadings. Circular silos, pressure vessels, and liquid as well as gas retaining cylindrical shells are some important cases in which cylindrical shells are subjected to axisymmetric loadings.

The behavior of a complete cylindrical shell under axisymmetric loading is also axisymmetric. This means that there are no variations with the hoop coordinate parameter, ϕ .

The governing equations of axisymmetric behavior of cylindrical shells can be conveniently derived from the general equations of the previous section by setting all derivatives with respect to ϕ equal to zero, and putting $p_\phi = 0$. We also note that, due to symmetry, $Q_\phi = 0$ and $M_{\phi x} = 0$, and hence $N_{x\phi} = N_{\phi x}$.

The equilibrium equations for the axisymmetric theory of cylinders are thus:

$$N'_x + aP_x = 0 \quad (4-18a)$$

$$N'_\phi + Q'_x - aP_r = 0 \quad (4-18b)$$

$$M'_x - aQ_x = 0 \quad (4-18c)$$

52 Design and Analysis of Shell Structures

The last two equations, representing the axisymmetric bending (now decoupled from the axial deformation) may be combined to yield the single equation:

$$aN_{\phi} + M''_x - a^2 P_r = 0 \\ \Rightarrow P_r = \frac{1}{a^2} M''_x + \frac{1}{a} N_{\phi} = \frac{d^2 M_x}{dx^2} + \frac{1}{a} N_{\phi} \quad (4-19)$$

The combined constitutive-kinematic relations of axisymmetric cylindrical shells can also be deduced from the general relations (4-10). By assuming axial symmetry and neglecting the terms containing K_z in the membrane force expressions, we obtain

$$N_{x\phi} = N_{\phi x} = 0 \quad (4-20a)$$

$$N_{\phi} = \frac{1}{a} D (w + vu') \quad (4-20b)$$

$$N_x = \frac{1}{a} D (u' + vw) \quad (4-20c)$$

$$M_{\phi} = \frac{1}{a^2} K (w + vw'') \quad (4-20d)$$

$$M_x = \frac{1}{a^2} K (w'' - u') \quad (4-20e)$$

$$M_{\phi x} = M_{x\phi} = 0 \quad (4-20f)$$

In order to derive a single differential equation on the radial displacement, we decouple the axial effects from radial bending by assuming that $p_x = 0$. By assuming a constant thickness shell, we obtain

$$Kw''' + Eta^2 w = P_r a^4 \quad (4-21)$$

and the following relations for the internal forces:

$$N_{\phi} = -\frac{1}{a} Dw(1 - v^2) \quad (4-22)$$

$$M_{\phi} = vM_x \quad M_x = \frac{1}{a^2} Kw''$$

If we define a parameter, β , from

$$\beta^4 = \frac{Et}{4a^2K} = \frac{3(1 - v^2)}{a^2 t^2} \quad (4-23)$$

Then, we obtain a single differential equation governing the axisymmetric behavior of circular cylindrical shells

$$\frac{d^4 w}{dx^4} + 4\beta^4 w = \frac{P_r}{K} \quad (4-24)$$

This fourth order differential equation resembles the equation of a beam resting on an elastic foundation and laterally loaded by the distributed force P_r . From a physical viewpoint, the equivalent elastic foundation effect comes from the inclined hoop force, N_ϕ , acting on a longitudinal "strip" of the shell in its radial beam-type behavior.

In this chapter, as in other chapters, we have treated *static* problems for shells. To deal with dynamic problems we must include the inertia effects in the equilibrium equations. The theory governing the axisymmetric vibrations of circular cylindrical shells is quite simple. In fact, all we have to do is to add a lateral inertia term to the right hand side of the equation (4-24).

4.5 - Some Axisymmetric Problems of Circular Cylinders

4.5.1 - General Solution to Axisymmetric Problems

The general solution to the fourth order differential equation (4-24) is obtained by superposition of two parts: a general solution to the corresponding homogeneous differential equation and a particular solution to the non-homogeneous equation. Thus

$$w = e^{\beta x} (C_1 \cos \beta x + C_2 \sin \beta x) + e^{-\beta x} (C_3 \cos \beta x + C_4 \sin \beta x) + f(x) \quad (4-25)$$

In this expression, the function $f(x)$ represents a *particular solution* to (4-24). To obtain the **general solution** to nonhomogeneous equation this particular solution is to be superimposed on the general solution to the corresponding homogeneous equation. Being a fourth order homogeneous differential equation, it would contain four integration constants C_1, C_2, C_3, C_4 .

The physical interpretation of the two parts of the solution is as follows:

The *particular solution* is the solution obtained by assuming a membrane action for the shell. This solution may not satisfy the prescribed boundary conditions of the shell which are sometimes the sources of bending effects.

The *general solution* to the *homogeneous* equation (i.e., the differential equation without the right hand side) gives the correction to the particular, i.e., membrane solution so that the prescribed boundary conditions can be satisfied. The integration constants C_1, C_2, C_3, C_4 are determined by the four boundary conditions (two at each edge) prescribed for each case.

4.5.2 - A Fundamental Problem

Consider the circular cylinder of figure (4-3) subjected to a distributed edge moment M_o and a distributed edge shear force Q_o .

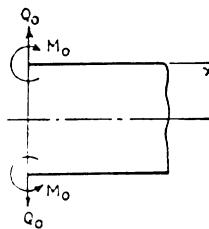


Figure (4-3) A circular cylindrical shell under edge effects

Since the shell of figure (4-3) is acted upon by the edge forces alone, the particular solution to this problem is identically zero, i.e., $f(x) = 0$. The edge effects should decay out as we move further away from the loaded edge. So that $C_1 = C_2 = 0$. The general solution to this problem is therefore

$$w = e^{-\beta x} (C_3 \cos \beta x + C_4 \sin \beta x) \quad (4-26)$$

Two remaining constants of integration can be determined from the prescribed force boundary conditions:

$$\begin{aligned} (M_x)_{x=0} &= +K \left(\frac{d^2 w}{dx^2} \right)_{x=0} = M_o \\ (Q_x)_{x=0} &= \left(\frac{dM_x}{dx} \right)_{x=0} = +K \left(\frac{d^3 w}{dx^3} \right)_{x=0} = Q_o \end{aligned} \quad (4-27)$$

By substituting the expression (4-26) into these end conditions and solving two resulting simultaneous equations for C_3 and C_4 , we obtain

$$C_3 = + \frac{1}{2\beta^3 K} (Q_o + \beta M_o) \quad , \quad C_4 = \frac{-M_o}{2\beta^2 K} \quad (4-28)$$

This gives the general solution, (4-26), for this problem as follows:

$$w = \frac{e^{-\beta x}}{2\beta^3 K} \left[\beta M_o (-\sin \beta x + \cos \beta x) + Q_o \cos \beta x \right] \quad (4-29)$$

This is the expression for the radial displacement of a circular cylinder under edge loading. The resulting hoop force and bending moment at any section can be determined from the relations (4-22). As we expect, all these field functions decay character with distance from the loaded edge.

4.5.3 - Thin Circular Cylinders under Internal Pressure

Now consider a circular cylinder subjected to a uniform internal pressure, p . Both ends of the shell are assumed to be fixed, figure (4-4).

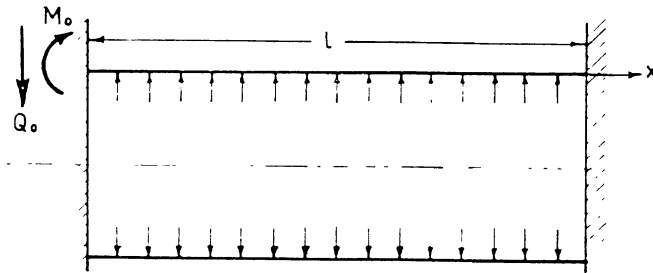


Figure (4-4) A closed-end thin circular cylinder under uniform internal pressure

Before entering into the analysis of this problem, we offer a physical observation on the expected behavior of this shell. If the ends of this cylinder were free from all restrictions, the shell under internal pressure would act as a membrane. The membrane hoop stress obtained from the membrane theory of cylindrical shells would be

$$\sigma_t = \frac{pa}{t} \quad (4-30)$$

and the resulting uniform radial expansion would be

$$D_0 = \frac{a\sigma_t}{E} = \frac{pa^2}{Et} \quad (4-31)$$

However, the imposed edge constraints inhibit the free membrane expansion of the shell. To compensate for the incompatibility of membrane action, a bending field develops at the edges and influences the shell behavior.

We assume that the cylinder is long enough so that the influence of the constraint at one end would not be felt at the other. Therefore, the edge effect solution, (4-26), can be applied to each end region. If we did not assume this, then for short cylinders we would have to obtain all four constants C_1, C_2, C_3, C_4 simultaneously.

The end conditions, being the same for both ends in this problem, are

$$(w)_{x=0} = 0 \quad , \quad \left(\frac{dw}{dx}\right)_{x=0} = 0 \quad (4-32)$$

Substituting the sum of the fundamental edge effect solution (4-29) and the membrane solution (4-31) into these relations, we obtain

$$-\frac{1}{2\beta^3 K}(\beta M_0 + Q_0) - D_0 = 0$$

$$\frac{1}{2\beta^2 K}(2\beta M_0 + Q_0) = 0$$

By solving these equations for Q_0 and M_0 , we find

$$Q_0 = -4\beta^3 K D_0 = -\frac{P}{\beta} \quad , \quad M_0 = 2\beta^2 K D_0 = \frac{P}{2\beta^2} \quad (4-33)$$

Having found the quantities M_0 and Q_0 , we can easily write down the expressions for the radial displacement, the bending moment, and the shear force at each section of the shell.

4.5.4 - Analysis of Liquid Retaining Cylindrical Shells

As one important application of these solutions, we analyze the structural behavior of a vertical cylindrical container filled with a liquid of density γ . We assume the container to be fixed at the bottom end and to be free at the top, figure (4-5).

The internal pressure at each point of the container is

$$P_r = \gamma(H - x) \quad (4-34)$$

So that the governing differential equation (4-24) becomes

$$\frac{d^4 w}{dx^4} + 4\beta^4 w = -\frac{\gamma(H - x)}{K} \quad (4-35)$$

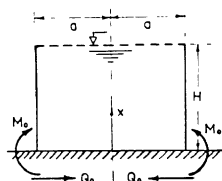


Figure (4-5) A liquid container fixed at the base

A particular solution to this equation is

$$f(x) = \frac{\gamma(H - x)}{4\beta^4 K} = \frac{\gamma(H - x)a^2}{Et} \quad (4-36)$$

From a physical point of view, this solution is the *membrane* displacement field of the same container having unconstrained edges. The general solution of the governing differential equation, with edge constraints, is

$$\begin{aligned} w = & e^{\beta x} (C_1 \cos \beta x + C_2 \sin \beta x) + e^{-\beta x} (C_3 \cos \beta x \\ & + C_4 \sin \beta x) + \frac{\gamma(H - x)a^2}{Et} \end{aligned} \quad (4-37)$$

If we assume the container to be high enough so that the effect of the constraint at the base would not be felt at the top, then we may set $C_1 = C_2 = 0$; then

$$w = e^{-\beta x} (C_3 \cos \beta x + C_4 \sin \beta x) + \frac{\gamma(H - x)a^2}{Et} \quad (4-38)$$

The remaining integration constants can be obtained through the use of the boundary conditions at $x = 0$, which are the same as (4-32); we obtain

$$C_3 = \frac{-\gamma a^2 H}{Et}, \quad C_4 = \frac{-\gamma a^2}{Et} \left(H - \frac{1}{\beta} \right)$$

The radial displacement is therefore:

$$w = \frac{\gamma a^2}{Et} \left\{ H - x - e^{-\beta x} \left[H \cos \beta x + \left(H - \frac{1}{\beta} \right) \sin \beta x \right] \right\} \quad (4-39)$$

Having determined the radial displacement function, $w(x)$, we can also write down the expressions for the hoop stress and the bending moment, at each section of the cylinder, as well as the value of constraining forces at the base. These expressions are

$$N_x = \gamma a \left[H - x - H e^{-\beta x} \cos \beta x + \left(\frac{1}{\beta} - H \right) e^{-\beta x} \sin \beta x \right] \quad (4-40a)$$

$$M_x = - \frac{\gamma a t}{\sqrt{12(1 - v^2)}} \left[\left(\frac{1}{\beta} - H \right) e^{-\beta x} \cos \beta x + H e^{-\beta x} \sin \beta x \right]$$

$$(M_x)_{x=0} = M_o = \left(1 - \frac{1}{\beta H} \right) \frac{\gamma a H t}{\sqrt{12(1 - v^2)}} \quad (4-40b)$$

Numerical Example 4.1

As a numerical example of analysis of cylindrical liquid containers, we consider a full vertical water tank having the dimensions as shown in the figure (4-6). The assumed numerical data are

$$\gamma = 1000 \text{ Kg/m}^3 \quad v = 0$$

$$a = 2.75 \text{ m} \quad , \quad t = 25 \text{ cm} = 0.25 \text{ m} \quad , \quad H = 3.65 \text{ m}$$

This liquid retaining tank is to be analyzed under the given conditions.

Solution:

First, we calculate the value of the parameter β :

$$\beta = \left[\frac{3(1 - v^2)}{a^2 t^2} \right]^{1/4} = 1.59^{-1/\text{m}}$$

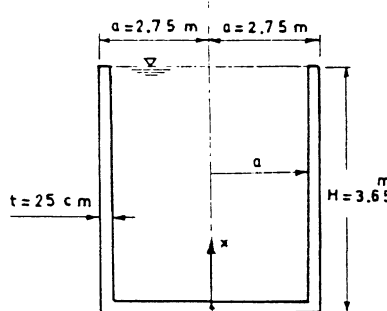


Figure (4-6) The cylindrical water tank of example 4.1

Referring to relations (4-40), we find the hoop force and the bending moment

$$N_{\phi} = 2750 \left[3.65 - x - 3.65e^{-1.59x} \cos 1.59x - 3.02e^{-1.59x} \sin 1.59x \right]$$

$$M_x = -198.1 \left[-3.02e^{-1.59x} \cos 1.59x + 3.65e^{-1.59x} \sin 1.59x \right]$$

$$M_x \Big|_{x=0} = +598.26 \text{ kg-m/m}$$

Because of our sign convention, the positive value for the bending moment at the base shows that the outer longitudinal fibers are in compression while the inner ones are in tension.

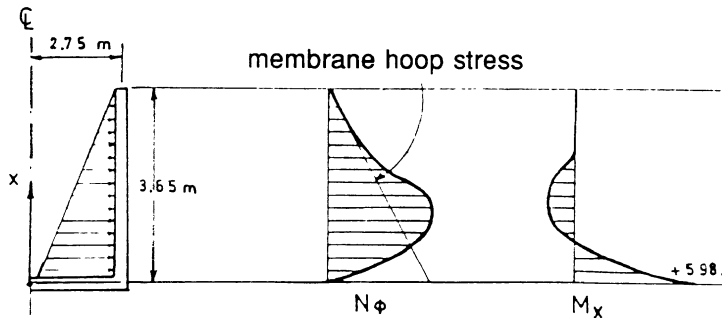


Figure (4-7) Variations of bending moment and hoop force along the height of the water container of example 4.1

Figure (4-7) shows the hoop stress and the bending moment variations with height. We observe that the maximum hoop stress occurs somewhere along the cylinder wall, and not at the base of the shell, as the membrane theory would have had predicted. In fact, the hoop force at the base, being proportional to w , is equal to zero.

Problems

P 4.1 - Consider a long pipe, of radius a , with a radial line load P (per unit width) applied around the circumference at the mid-length of the pipe, figure (P 4-1). Show that the longitudinal bending moment under the load is,

$$M_0 = \frac{P a}{4 \beta}$$

What would the expression for the bending moment under the load P be if the pipe had a relatively short length of $2L$ while being free at the both ends ?.

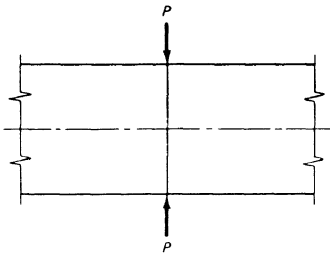


Figure (P 4-1)

P 4.2 - Consider a long pipe with stiffening rings spaced at $2L$ centers and subjected to a uniform external pressure p , figure (P4-2). Outline the general approach needed to analyze such a structure.(Hint: there are two redundant forces at the pipe ring junction which, due to symmetry, are the same on the two sides of the ring-pipe intersection. These redundant forces can be determined by writing the appropriate compatibility relations).

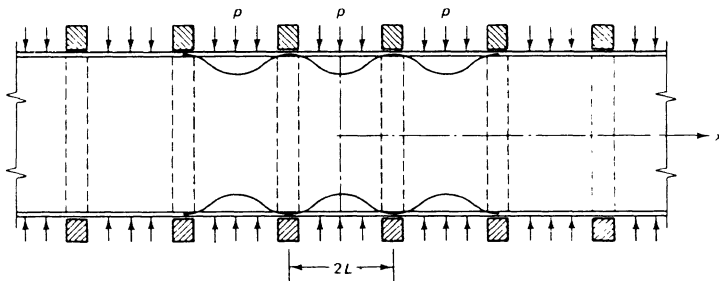


Figure (P 4-2) A ring stiffened pipe

References for Chapter Four

- 4.1 - W. Flügge, *Stresses in Shells*, Springer-Verlag, Berlin, 1962
- 4.2 - S. Timoshenko and S. Woinowsky-Krieger, *Theory of Plates and Shells*, 2nd edition, McGraw-Hill Book Co., N.Y., 1959
- 4.3 - G. P. Manning, *Reinforced Concrete Design*, Third edition, Longmans, Green and Co. Ltd., England, 1967
- 4.4 - Krishna and Jain, *Reinforced Concrete*, Vol.1,2, McGraw-Hill, New Delhi
- 4.5 - J. Faber and F. Mead, *Reinforced Concrete*, Third edition, E. and F.M. Spon Ltd., London, 1967

Chapter **5**

Design of Concrete Cylindrical Shell Roofs

5.1 - Introduction

Thin concrete cylindrical shells can cover the roofs of various buildings efficiently and aesthetically. Large roof spans of bus, railroad, and air terminals, sport stadia, and aircraft hangars have been effectively covered with reinforced concrete shells, many of which have been cylindrical. Cylindrical shell forms can be easily shored and easily reinforced. Cylindrical concrete shell roofs can also be constructed from the precast shell elements.

In previous chapters, we have discussed the membrane and the bending theories of cylindrical shells. Those theories, and their simplified versions, can be used in the design of concrete cylindrical shells. In the present chapter, we will present fundamentals of thin concrete shell roof design. We also present a number of design recommendations and practical analysis schemes. These design-analysis methodologies will be accompanied by a set of detailed design and analysis examples.

5.2 - Geometric Design of Cylindrical Shell Roofs

5.2.1 - Overall Dimensioning of the Shell

The first step in the structural design of a cylindrical shell roof is the design of the geometrical configuration of the shell and the structural elements associated with the shell body. Figures (5-1) show a number of choices which can be made for such a purpose. These simple shell modules include a single shell simply supported on end arches (or diaphragms), figure(5-1a); a group of simply supported shells, figure (5-1b); a continuous cylindrical shell with intermediate stiffening arches and supports, figure (5-1c).

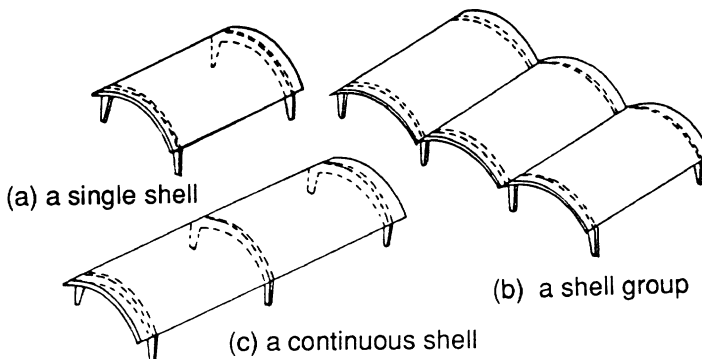


Figure (5-1) Examples of cylindrical roofs, (a) a simply supported single shell, (b) a group of simply supported shells, (c) a continuous shell

Cylindrical shell roofs are generally composed of the main shell together with some stiffening and / or supporting elements. These elements could form a collection consisting of **edge beams**, **stiffening arches**, and **end members**. Figure (5-2) shows a typical continuous cylindrical shell roof having these elements.

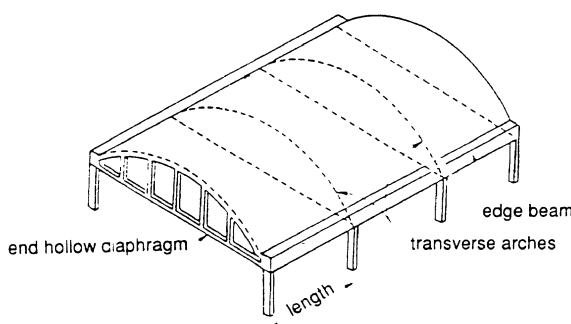


Figure (5-2) A continuous cylindrical shell roof with edge beams, transverse arches, and end members.

The end edge members themselves can have various forms. They can be in the form of a solid diaphragm, figure (5-3a); a tied arch (with or without verticals), figure (5-3b); a simple arch, figure (5-3c); an elevated grid, figure (5-3d); or an arched truss, figure (5-3e). Figures (5-3) show varieties of end-stiffening and supporting members associated with a shell roof structure.

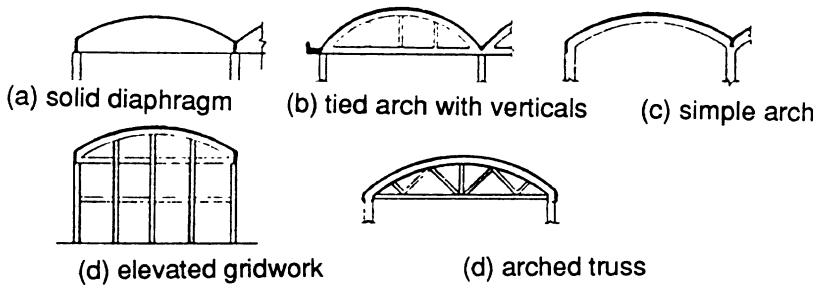


Figure (5-3) End members of a shell roof structure, (a) a diaphragm, (b) a tied arch , (c) a simple arch, (d) a grid-work, (e) an arched truss

A shell roof could be placed on vertical supports or on its foundation in a variety of ways. Figures (5-4) show some possible vertical support arrangements for cylindrical shell roof structures.

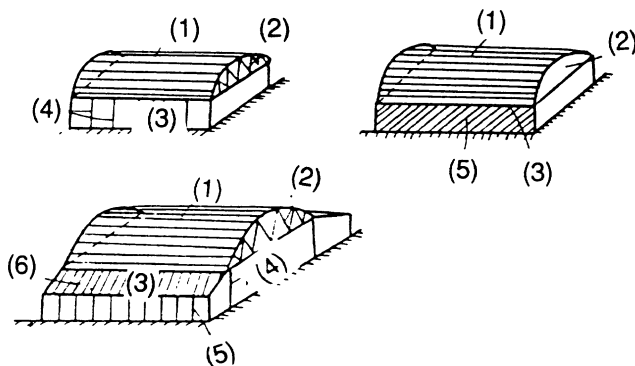


Figure (5-4) Some types of vertical supports for cylindrical shell roofs. Elements of these structures are: (1) the shell, (2) end diaphragm, (3) longitudinal edge member, (4) rows of columns, ((5) wall, (6) side sloped roof

We propose some suitable relative dimensions for cylindrical shell roofs in figure (5-5) and in its accompanying table. Figure (5-5a) relates to a group of cylindrical shells with an edge beam located at the longitudinal edge of the last shell located in the shell group.

The shell dimensions given in figure (5-5b) are for a particular type of cylindrical roof called *the Northlight shells*. This shell type is used to provide natural light through the roof. These shell types are particularly suitable for factory and manufacturing installations. The information presented in figure-table (5-5) serves as a useful guide in proportioning the cylindrical shell roofs.

Large shell spans, up to 120 meters can be constructed using plain or prestressed reinforced concrete material. These large spans are used in terminals, airplane hangars, sport stadia, and unobstructed storage places. In such cases, a number of transverse arches are normally constructed with the shell. These arches stiffen the shell and carry its load to the foundations. Shell lengths up to 30 meters can be made of non-prestressed reinforced concrete. For longer shell lengths, the shell should be prestressed. The longitudinal expansion joints are usually provided every 45 meters of the shell length.

l (m)	B (m)	r (m)	t (mm)	Approx. wt. per m ² (kg)
10	10	7	60	270
30	15	11	70	300
40	20	15	80	350
50	25	18	100	390

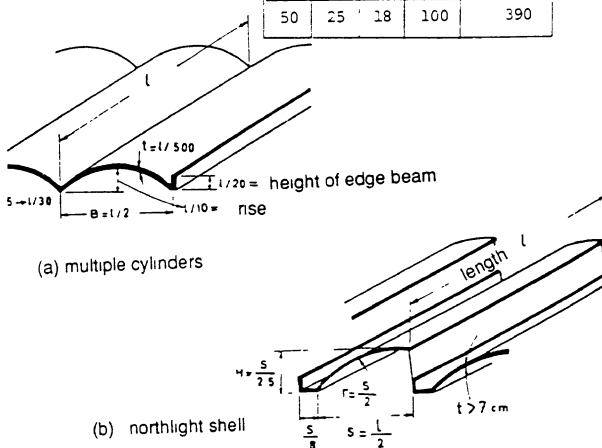


Figure-Table (5-5) Proposed relative dimensions for cylindrical shell roofs

5.2.2 - Dimensions of Edge Beams

The longitudinal edge beams of shells have two major function: (1) They carry the applied loads, which have been transferred to them by the mechanism of internal shear force, and transfer them in turn to the supports of the shell structure. (2) They provide additional stiffness for the thin shell body.

Edge beams may have a variety of shapes and dimensions. Depending on the structural needs and architectural constraints, they may have vertical or horizontal orientations. In figures (5-6) show some suitable relative dimensions for the edge beams. In addition to the dimensions cited in this set of figures, the shell designer may set the ratio of the height of edge beam to shell length somewhere between 1/25 to 1/20.

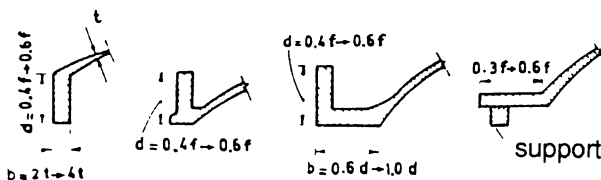


Figure (5-6) Proposed relative dimensions for the design of edge beams

5.2.3 - Profile, Central Angle, and Curvature of the Shell

In addition to the structural requirements, acoustic and architectural considerations affect the choice of shell profile, its radius of curvature, and the central angle of the profile. Shells with circular profile are easier and more economical to build. The central angle of such profiles is usually selected between 60 to 80 degrees. Higher central angles would result in shell geometries with steeper slopes. Placing of concrete on these slopes would then require double forming.

5.2.4 - Rise of the Shell

Appropriate values for the rise of the shell, relative to other shell dimensions, are proposed in figure-table (5-5). It is generally suggested that the rise of the shell be chosen larger than 1/10 of the chord width. For single shells, a total rise (the vertical distance from the crown to the bottom of edge beam) of 1/6 to 1/12, but not less than 1/15 of the chord width is considered appropriate.

5.2.5 - Shell Thickness

The choice of thickness of thin concrete shells is based on stability and construction requirements, not just on the strength design calculations. The stresses in reinforced shells under normal loadings are usually so small that the strength criteria are satisfied. However, the buckling instability of thin shells could lead to failure of the structure. Therefore, elastic stability of shells is an important criteria which must be fulfilled. Constructional limitations, such as the minimum thickness for concrete placement, would also influence the

choice of the shell thickness. As a general guideline, a thickness to chord width ratio of 1/300 to 1/200 could be considered a sound choice for concrete shell thickness.

The thickness of concrete shells is usually increased near the edge members, and gradually reduced to a constant design value. This simplifies the placing of reinforcement: It also prevents stress concentrations, and facilitates flow of forces to the edges and supporting members.

5.3 - Reinforcement of Concrete Cylindrical Roofs

Concrete materials have high compressive strength but low tensile resistance. Therefore, thin concrete shell roofs must be reinforced to acquire sufficient tensile strength. Reinforcing of the concrete shells is usually provided by means of steel reinforcing bars.

The existing codes of practice for shells normally require that the reinforcing bars be placed along the general directions of *principal tensile stresses*. However, deviations from these directions are also conditionally allowed by these codes. Figure (5-7) shows the stress trajectories (i.e., the principal stress directions) in a simply supported single cylindrical shell subjected to its own dead weight. These types of results will be obtained in the later sections of this chapter.

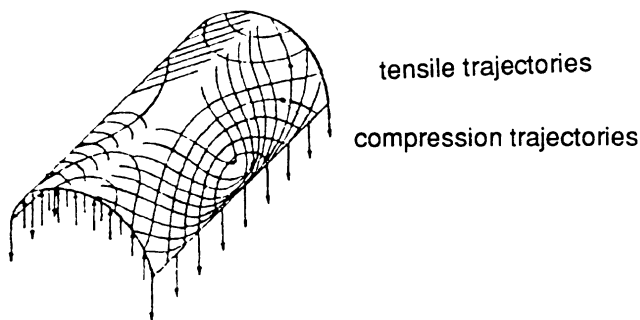


Figure (5-7) Stress trajectories in a simply supported cylindrical shell

As we know from the elementary courses on solid mechanics, the **stress trajectories** consist of two families of curves which are mutually orthogonal. In cylindrical shell roofs, one family of these curves represents the directions of principal *tensile* stresses while the other family of trajectories gives the directions of principal compressive stresses. In this sense, the behavior of the shell can be conceived to consist of a mesh of *cables* and *arches*.

As we noted earlier, thin shells are usually accompanied by stiffening and / or supporting members. These elements must be monolithic with the shell so that they can transfer the internal forces. On the other hand, these members produce a bending field. This bending field would require extra reinforcement which must be provided in addition to the membrane field reinforcements.

The knowledge of the bending field in the shell, is crucial in the design of the extra reinforcements. We presented a qualitative discussion of the cylindrical vaults behavior in chapter 3; that is useful in devising the general pattern of shell reinforcements, but a detailed design must be based on a quantitative analysis of the shell.

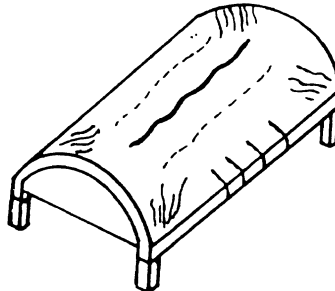
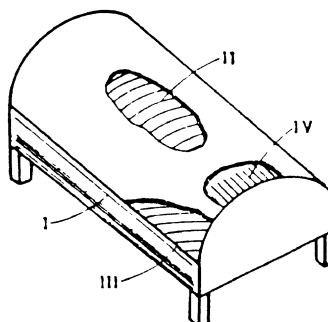


Figure (5-8) Pattern of possible cracks in a simply supported single shell

Tensile stresses in concrete shells tend to cause cracks in the concrete. Figure (5-8) shows the most probable cracking pattern in a single cylindrical shell. This figure shows the positions as well as the directions of the probable cracks.

The transverse cracks appearing in the longitudinal edges of figure (5-8) are due to longitudinal tensile force. The longitudinal cracks designated by solid and dotted lines can be caused by transverse bending moment. Finally, the inclined cracks at four corners of the shell are produced by the diagonal tension. these latter cracks are called *shear cracks* . In addition to these global crack field, local cracks may occur at the junctions of the shell with its stiffening members.

The pattern of shell reinforcement must naturally follow the probable cracking. The steel reinforcement should , in principle, be placed in the directions perpendicular to the possible cracks. Figure (5-9) shows a reinforcing pattern for the shell of figure (5-8). A review of figure (5-8) would easily lead to the reinforcement design strategy adopted in figure (5-9).



*Figure (5-9) Reinforcement pattern of the shell of figure (5-8),
(1) longitudinal reinforcement in the edge beam, (2) transverse
membrane and bending reinforcement, (3) shear reinforcement,
(4) negative moment bending reinforcement near the diaphragms.*

70 Design and Analysis of Shell Structures

Based on this knowledge and the current practice, we offer a practical construction tip for placing of reinforcements. The shear reinforcement which is to absorb the diagonal tension field is normally placed in the lower layer. The longitudinal reinforcement occupies the mid-layer; the transverse reinforcement is usually placed on the top. These structural reinforcements also serve as shrinkage, distribution, and temperature reinforcements.

The total amount of steel reinforcement in a cylindrical shell roof depends on the individual designs. However, as an initial crude estimate of steel consumption, the following formula could be used.

$$q = \frac{l(l + B)}{20f} + 6 \quad (5-1)$$

In this approximate formula, l is the shell length, B is the chord width, f is the rise of the shell, and q (in kilograms per square meters of shell surface) is the amount of the consumed reinforcement.

The values of principal stresses at each point of the shell can be obtained from the following relation:

$$N_p = \frac{N_x + N_\phi}{2} \pm \sqrt{\left(\frac{N_x - N_\phi}{2}\right)^2 + N_{x\phi}^2} \quad (5-2)$$

and the principal directions can also be determined from the following formula:

$$\tan 2\theta = \frac{2N_{x\phi}}{N_x - N_\phi} \quad (5-3)$$

Assuming that the internal forces N_x , N_ϕ , and $N_{x\phi}$ are determined through the analysis of the shell, we can determine the principal stresses and the principal directions at each point of the shell, and plot the stress trajectories for each case.

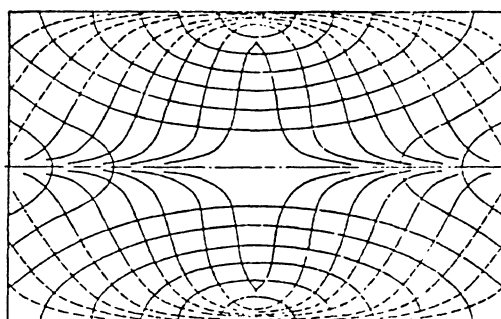


Figure (5-10) Plan of stress trajectories for a simply supported cylindrical vault under uniform dead load

Figure (5-10) shows the plan of stress trajectories for a uniformly loaded simply supported cylindrical vault. In this figure, the solid curves represent the directions of compressive principal stresses while the dashed lines represent the curves that are tangent to the directions of maximum tensile stresses.

According to the American Concrete Institute (ACI) code of reinforced concrete shell design, the reinforcement is to be placed in the general direction of *principal tensile stresses*. This code allows for slight deviations of reinforcement direction from principal direction. In this code, a directional error of 5 degrees or less is considered acceptable. However, due to constructional considerations, it is usually convenient to place the reinforcing bars in perpendicular directions. The codes have provisions for these cases. In these cases, the reinforcing network must be designed so that it can absorb the principal tensile stress at each point. This situation is shown in figure (5-11).

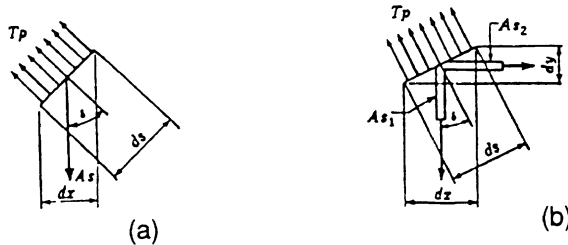


Figure (5-11) (a) Principal tensile force acting in some elemental direction, (b) contributions of perpendicular steel reinforcement to absorb the principal tensile stress

Referring to figure (5-11b), we can write the internal equilibrium equation can be written as

$$T_p ds = A_{s1} f_{s1} dx \cos \delta + A_{s2} f_{s2} dy \sin \delta \quad (5-4)$$

In this relation, A_{s1} and A_{s2} are the cross sectional areas (per unit shell width) of perpendicularly placed reinforcing bars, f_{s1} and f_{s2} are the stresses in reinforcing bars, T_p is the value of principal tensile force, and δ is its angle of inclination. Using the geometrical relations between ds , dx , and dy , we may rewrite the relation (5-4) as,

$$T_p = A_{s1} f_{s1} \cos^2 \delta + A_{s2} f_{s2} \sin^2 \delta \quad (5-5)$$

If we impose the requirement of strain compatibility, we arrive at the following relation between the stresses in reinforcing bars:

$$f_{s2} = f_{s1} \operatorname{tg} \delta \quad (5-6)$$

Therefore, for an orthogonal mesh of reinforcement we will have

$$T_p = f_{s1} (A_{s1} \cos^2 \delta + A_{s2} \sin^2 \delta \operatorname{tg} \delta) \quad (5-7)$$

This relation can be effectively used in designing reinforcement, i.e., in determining the area of reinforcing bars.

5.4 - Beam-Arch Method of Vaulted Roof Analysis

One of the simple methods for preliminary analysis and design of cylindrical shell roofs is called the **beam-arch method**. The "beam-arch" method makes use of combined beam and arch actions of cylindrical shells. In this method, **beam analysis** and **arch analysis** of the shell are carried out almost independently by the well-known simple theories of the structural analysis. The results of these analyses are, then, combined appropriately to yield the spatial behavior of the cylindrical shells.

In the following, we shall outline the principles of the "beam-arch" method for cylindrical vaults having an arbitrary profile. Later on, we shall also apply the method to the analysis of a vaulted roof problem.

The **beam-arch** method of vaulted roof analysis is composed of two steps: (1) **the beam analysis**, (2) **the arch analysis**.

(1) - Beam Analysis

In this stage, the shell is conceived as a *beam* resting on the end supports and behaving according to the classical beam theory. The beam has the profile of the cylindrical shell as its cross section and the length of the shell as its longitudinal span.

To perform the beam analysis of a circular cylindrical shell, we consider the profile of the shell to be as shown in figure (5-12). In this figure, ϕ_k is the half central angle, a is its radius, and t is the shell wall thickness. The origin of cross-sectional coordinate system $y-z$ coincides with the centroid of the section, designated by the letter G. This centroid is assumed to be located at a vertical distance of \bar{z} from the crown of the shell. For a circular sector shown in figure (5-12), the following formula for \bar{z} in terms of cross-sectional parameters (a and ϕ_k) can easily be derived:

$$\bar{z} = a \left(1 - \frac{\sin \phi_k}{\phi_k} \right) \quad (5-8)$$

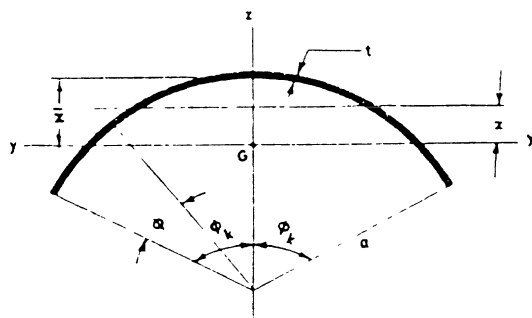


Figure (5-12) Cross section of a circular cylindrical vault used in the *beam-arch* analysis of cylindrical shells

The longitudinal membrane stress (expressed as force per unit width, N_x) can be calculated by the flexure theory of beams. The appropriate bending stress formula is

$$N_x = \left(\frac{M_{yy}}{I_{yy}} z \right) t \quad (5-9)$$

In this relation, M_{yy} is the bending moment of applied loads calculated about the y-y axis, I_{yy} is the second moment of cross sectional area with respect to y-y axis. A general formula for I_{yy} for a circular sector is

$$\begin{aligned} I_{yy} &= 2t \int_{\phi=0}^{\phi=\phi_k} ad\phi \left(a\cos\phi - \frac{a\sin\phi}{\phi_k} \right)^2 \\ &= a^3 t \left[\phi_k + \sin\phi_k (\cos\phi_k - \frac{2\sin\phi_k}{\phi_k}) \right] \end{aligned} \quad (5-10)$$

According to classical beam theory, the relations (5-8) to (5-10) are valid in a principal coordinate system for the cross section. For non-principal coordinates, we must use a more general beam formula.

The transverse shear stress (expressed by the membrane shear force, $N_{x\phi}$) can also be determined by a formula given in the classical beam theory. So, using the formula for the shear stresses in beams, we find

$$N_{x\phi} = \left(\frac{VQ}{I_{yy}(2t)} \right) t = \frac{VQ}{2I_{yy}} \quad (5-11)$$

In this relation, V is the total vertical shear force at any arbitrary section of the shell, the symbol Q represents the value of the first moment of the part of the areal section lying beyond the layer at which the magnitude of shear stress is to be calculated. A general formula for Q for a circular sector is

$$\begin{aligned} Q &= a \left(\frac{\sin\phi}{\phi} - \frac{\sin\phi_k}{\phi_k} \right) 2a\phi t \\ &= 2a^2 t \left(\sin\phi - \frac{\phi}{\phi_k} \sin\phi_k \right) \end{aligned} \quad (5-12)$$

The longitudinal and shear membrane forces N_x and $N_{x\phi}$, determined through beam analysis, are functions of x and ϕ . This completes the *beam analysis*.

(2) - Arch Analysis

The second stage of *beam-arch method*, consists of analysis of *transverse arches*. In this stage, a transverse arch having an arbitrarily small longitudinal width, dx , is taken out from the shell. Figure (5-13) shows the free-body diagram of such an arch *slice* cut out from some arbitrary location along the shell.

The free body diagram of figure (5-13) shows the applied loading as well as the effect of the rest of the system; this includes the longitudinally varying shear force which has already been determined. The longitudinal edge effects consist of horizontal shear forces and the bending moments, both distributed on the edges of the arch.

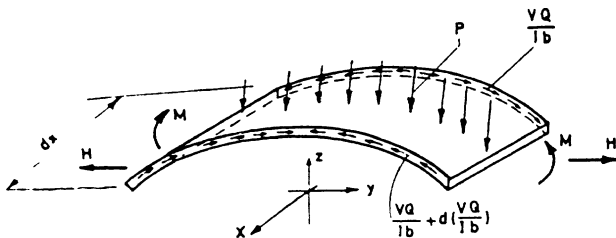
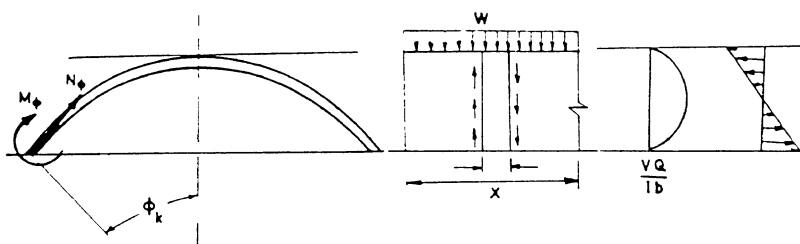


Figure (5-13) Free-body diagram of a transverse arch of a cylindrical shell

In the vertical equilibrium of transverse arches, the applied vertical forces are supported by the vertical component of the internal shear stresses. In this sense, one may conceive of this arch to have been *hanging* from the rest of the system, i.e., to have been vertically supported by the adjacent arches through which the applied load is ultimately transferred to the end supports. Figure (5-14) shows an arbitrary transverse arch in the shell and its role in supporting its share of the load.



(a) profile of the arch (b) lateral view of arch (c) internal stress in beam

Figure (5-14) The side and the end view of an arbitrary transverse arch in a cylindrical shell

For a uniformly distributed applied loading, the change of internal shear force, in the longitudinal direction, is

$$\frac{dN_{x\phi}}{dx} = \frac{d}{dx} \left(\frac{vQ}{2It} \cdot t \right) = \frac{Q}{2I_{yy}} \frac{dv}{dx} = \frac{Q}{2I_{yy}} w \quad (5-13)$$

and the vertical component of internal shear force is equal to

$$\frac{wQ}{2I} \sin(\phi_k - \phi) \quad (5-14)$$

Having defined the transverse arch and its loading, we can proceed with its analysis. Depending on the number of unknown boundary forces (M and / or H), the arch could be statically determinate or indeterminate; in any case, it can be analyzed by standard methods of structural analysis. The transverse arch analysis gives the transverse membrane force, N_ϕ , and the transverse bending moment, M_ϕ , are determined.

(3) Synthesis of Results of Beam and Arch Analyses

By combining the results of the beam and arch analyses we can find the internal force system in the shell, consisting of N_x , $N_{x\phi}$, N_ϕ , and M_ϕ . The strength of the shell roof can now be verified against the applied loads. The calculated internal forces can be used to design the proper shell reinforcement to support the prescribed loading.

The *beam-arch* method for cylindrical vaults can be displayed in a tabular form. Table (5-1) shows coefficients of internal force system for a circular cylindrical shell subjected to its dead weight and snow type loading. This table gives the internal forces for various values of the half central angle ϕ_k .

The *beam-arch* method of cylindrical shell analysis can be applied to a variety of design/analysis problems. The accuracy of predictions by this method is closely related to the premises of the classical beam theory. As a guideline, the following approximate rules could be used in assessing the domain of application of this method. Generally speaking, the *beam-arch* theory could be applied to the following cases:

- (a) Single shells with no edge beams provided that $l/a > 5$ (l is the length and a is the radius of the shell)
- (b) Long shells with edge beam of regular height, if $l/a > 3$
- (c) Shell units in a shell group with small edge beam, if $l/a > 1.67$
- (d) Shell units with edge beams in a shell group, if $l/a > 3$

Modified version of the beam-arch method may also be used for the analysis of *folded plates*; the topic which will be discussed in chapter 11.

Table (5-1) Internal forces in vaulted roofs according to Beam-Arch method

ϕ_k deg	ϕ	Case 1				Case 2			
		N_x (1)	N_ϕ (2)	S (3)	M_ϕ (4)	N_x (5)	N_ϕ (6)	S (7)	M_ϕ (8)
22.5	ϕ_k	-6.010	-1.411	0.000	-0.00292	-6.167	-1.433	0.000	-0.00309
	0.75 ϕ_k	-4.875	-1.189	2.211	0.00112	-5.003	-1.205	2.269	-0.00118
	0.50 ϕ_k	-1.482	-0.614	3.533	0.00232	-1.521	0.615	3.626	0.00245
	0.25 ϕ_k	4.137	0.049	0.084	-0.00235	4.245	0.065	3.165	0.00249
	0	11.927	0.361	0.000	-0.00662	12.239	0.384	0.000	-0.00702
25.0	ϕ_k	-4.855	-1.402	0.000	-0.00353	-5.012	-1.430	0.000	-0.00378
	0.75 ϕ_k	-3.937	-1.182	1.985	-0.00135	-4.064	-1.202	2.049	-0.00145
	0.50 ϕ_k	-1.193	-0.612	3.170	0.00280	-1.232	-0.613	3.273	0.00300
	0.25 ϕ_k	3.342	0.044	2.765	0.00282	3.451	0.064	2.855	0.00304
	0	9.617	0.347	0.000	-0.00797	9.929	0.374	0.000	-0.00857
27.5	ϕ_k	-4.000	-1.393	0.000	-0.00417	-4.158	-1.426	0.000	-0.00453
	0.75 ϕ_k	-3.242	-1.175	1.799	-0.00159	-3.370	-1.199	1.869	-0.00173
	0.50 ϕ_k	-0.980	-0.609	2.871	0.00331	-1.018	-0.610	2.985	0.00360
	0.25 ϕ_k	2.755	0.038	2.503	0.00332	2.863	0.063	2.602	0.00363
	0	7.908	0.331	0.000	-0.00938	8.220	0.363	0.000	-0.01025
30.0	ϕ_k	-3.350	-1.383	0.000	-0.00482	-3.508	-1.422	0.000	-0.00533
	0.75 ϕ_k	-2.714	-1.166	1.643	-0.00183	-2.842	-1.195	1.720	-0.00203
	0.50 ϕ_k	-0.817	-0.606	2.622	0.00384	-0.856	-0.607	2.746	0.00424
	0.25 ϕ_k	2.308	0.032	2.284	0.00383	2.417	0.061	2.392	0.00426
	0	6.608	0.314	0.000	-0.01082	6.920	0.352	0.000	-0.01204
32.5	ϕ_k	-2.844	-1.372	0.000	-0.00548	-3.002	-1.418	0.000	-0.00618
	0.75 ϕ_k	-2.303	-1.158	1.511	-0.00207	-2.431	-1.191	1.595	-0.00235
	0.50 ϕ_k	-0.691	-0.603	2.410	0.00438	-0.729	-0.603	2.544	0.00492
	0.25 ϕ_k	1.960	0.026	2.098	0.00434	2.069	0.060	2.215	0.00492
	0	5.596	0.297	0.000	-0.01227	5.908	0.339	0.000	-0.01393

Table (5-1) Continued, Internal forces in vaulted roofs according to Beam-Arch method

ϕ_k , deg	ϕ	N_x (1)	N_ϕ (2)	S (3)	M_ϕ (4)	N_x (5)	N_ϕ (6)	S (7)	M_ϕ (8)
35 0	ϕ_k	-2.442	-1.361	0.000	-0.00615	-2.601	-1.414	0.000	-0.00707
	0.75 ϕ_k	-1.977	-1.148	1.397	-0.00232	-2.105	-1.186	1.488	-0.00268
	0.50 ϕ_k	-0.591	-0.599	2.227	0.00491	-0.629	-0.600	2.372	0.00565
	0.25 ϕ_k	1.684	0.019	1.938	0.00484	1.793	0.058	2.064	0.00561
	0	4.794	0.278	0.000	-0.01370	5.105	0.326	0 000	-0.01591
37 5	ϕ_k	-2.118	-1.349	0.000	-0.00679	-2.278	-1.409	0.000	-0.00800
	0.75 ϕ_k	-1.174	-1.138	1.298	-0.00255	-1.842	-1.181	1.396	-0.00302
	0.50 ϕ_k	-0.510	-0.596	2 069	0.00544	-0.548	-0.596	2 224	0.00640
	0.25 ϕ_k	1.461	0.012	1.798	0.00532	1.571	0 057	1 933	0.00632
	0	4.146	0.260	0.000	-0.01509	4 458	0.312	0 000	-0 01796
40 0	ϕ_k	-1.853	-1.335	0.000	-0.00742	-2 013	-1.404	0 000	-0 00897
	0.75 ϕ_k	-1.498	-1.127	1.211	-0 00277	-1 627	-1.176	1.315	-0.00337
	0.50 ϕ_k	-0.443	-0.592	1 929	0 00595	-0 482	-0.592	2 095	0.00719
	0.25 ϕ_k	1.279	0.005	1 675	0 00578	1.389	0 055	1 819	0 00705
	0	3 616	0.241	0 000	-0 01641	3 928	0 297	0 000	-0 02006
45 0	ϕ_k	-1.449	-1.307	0 000	-0 00853	-1 610	-1.393	0 000	-0 01096
	0.75 ϕ_k	-1.170	-1.104	1 065	-0 00316	-1 299	-1.165	1 183	-0 00408
	0.50 ϕ_k	-0 343	-0 585	1 694	0 00688	-0 381	-0 583	1 882	0 00883
	0.25 ϕ_k	1 001	-0 011	1 468	0 00657	1 112	0 052	1 630	0 00854
	0	2.809	0 202	0 000	-0 01872	3 120	0 266	0 000	-0 02437
50 0	ϕ_k	-1.160	-1.276	0 000	-0 00939	-1 322	-1.380	0 000	-0 01301
	0.75 ϕ_k	-0.935	-1.1079	0.947	-0.00344	-1.065	-1.152	1.079	-0 00480
	0.50 ϕ_k	-0.271	-0.578	1.504	0.00762	-0.308	-0.574	1.713	0.01054
	0.25 ϕ_k	0.802	-0.029	1.300	0.00714	0.914	0.049	1 481	0.01002
	0	2.232	0.164	0 000	-0.02052	2 543	0.234	0 000	-0.02871
55 0	ϕ_k	-0.946	-1.242	0 000	-0.00989	-1.109	-1.367	0 000	-0.01506
	0.75 ϕ_k	-0.761	-1.053	0.849	-0.00358	-0.892	-1.139	0.995	-0.00549
	0.50 ϕ_k	-0.217	-0.572	1 347	0.00807	-0.255	-0.563	1 578	0.01227
	0.25 ϕ_k	0.655	-0.048	1 161	0.00712	0 767	0.045	1 360	0.01141
	0	1 805	0 128	0 000	-0 02130	2 115	0.201	0 000	-0.03293
60 0	ϕ_k	-0.783	-1.205	0 000	-0.00992	-0 947	-1.352	0 000	-0.01705
	0.75 ϕ_k	-0.629	-1.025	0 766	-0 00355	-0 761	-1 124	0 927	-0 00613
	0.50 ϕ_k	-0.177	-0.566	1 213	0 00815	-0 214	-0.552	1 467	0 01398
	0.25 ϕ_k	0.543	-0.068	1 043	0 00734	0 656	0 042	1 261	0 01275
	0	1.481	0.095	0 000	-0 02118	1 790	0 167	0 000	-0 03688

Numerical Example 5.1

A circular cylindrical internal shell belonging to a shell group is to be analyzed. This shell is shown in figure (5-15). The data of the problem are:

Length of the shell:

$$l = 20 \text{ m}$$

radius of shell profile:

$$r = 10 \text{ m}$$

shell thickness:

$$t = 10 \text{ cm}$$

half central angle:

$$\phi_k = 40^\circ$$

intensity of dead weight:

$$p_D = 250 \text{ kg/m}^2$$

intensity of live (snow) load:

$$p_L = 150 \text{ kg/m}^2$$

additional load due to local increase in thickness:

$$P = 60 \text{ kg/m}$$

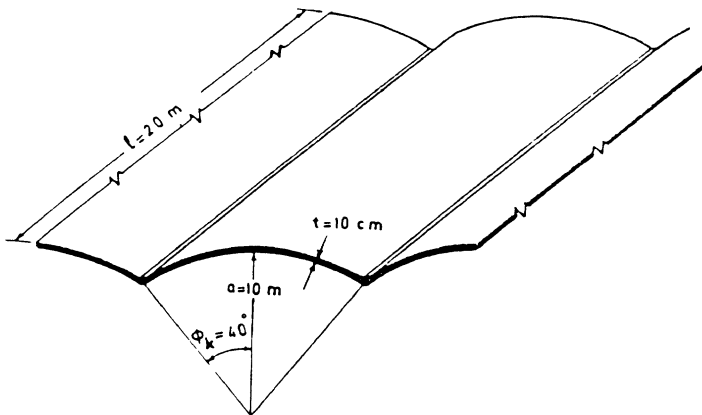


Figure (5-15) A view of the shell of example 5.1

Solution:

Location of cross sectional centroid:

$$\bar{z} = r(1 - \frac{\sin\phi_k}{\phi_k}) = 10(1 - \frac{0.643}{0.698}) = 0.793 \text{ m}$$

Value of the second moment of area:

$$\begin{aligned}
 I_{YY} &= r^3 t \left[\phi_k + \sin \phi_k (\cos \phi_k - \frac{2 \sin \phi_k}{\phi_k}) \right] + \\
 &= (10)^3 \left(\frac{10}{100} \right) \left[0.698 + 0.643 (0.766 - \frac{2 \times 0.643}{0.698}) \right] \\
 &= 0.587 + 0.10 = 0.687 \text{ m}^4
 \end{aligned}$$

To perform the numerical analysis of this symmetric problem, we consider one half of the cross section. Then, we divide it arbitrarily into 8 segments, figure (5-16), and from now calculate everything for these discrete segments.

Table (5-2)

point	angle from the crown (degrees)	Q (m^3)
0	40	0.
1	35	0.223
2	30	0.358
3	25	0.418
4	20	0.413
5	15	0.355
6	10	0.259
7	5	0.136
8	0	0.

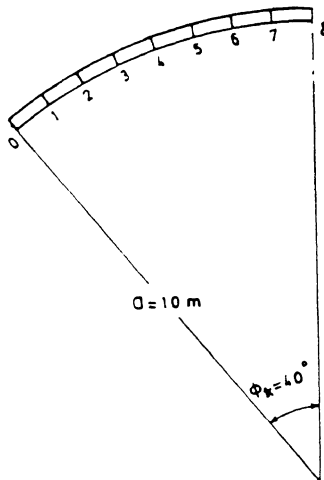


Figure (5-16) Divisions of half section

For future use, values of Q are calculated for each part of the cross section and are tabulated in table (5-2).

Beam Analysis:

The longitudinal bending moment, M_{yy} , and the longitudinal stress, N_{xx} , are calculated at the mid-length of the shell, where they are maximum, while the shear force, V , and related shear stress are calculated at the ends of the shell. The related calculations are shown below. The numerical results for discrete segments are given in table (5-3).

$$N_x = \left(\frac{M_{YY}}{I_{YY}} z \right) t \quad N_{x\phi} = \frac{VQ}{2I_{YY}}$$

$$\begin{aligned} M_{YY} &= \frac{w\ell^2}{8} = (2 \times 250 \times S + 120B + 60) \frac{(20)^2}{8} \\ &= (250 \times 10 \times 2 \times 0.698 + 150 \times 2 \times 10 \times 0.623 + 60) \frac{(20)^2}{8} \\ &= (3490 + 1869 + 60) \frac{(20)^2}{8} = \frac{5419 \times (20)^2}{8} = 270950 \text{ kg-m} \\ V &= \frac{wl}{2} = \frac{5419 \times 20}{2} = 54190 \text{ kg} \end{aligned}$$

$$Z = r(1 - \cos\phi) - \bar{z} = 9.207 - 10\cos\phi$$

$$N_x = \frac{M_{YY}}{I_{YY}} z t = \left(\frac{270950}{0.687} \times 0.1 \right) Z = 39418Z$$

$$N_{x\phi} = \frac{V}{2I_{YY}} Q = \frac{54190}{2 \times 0.687} Q = 39418Q$$

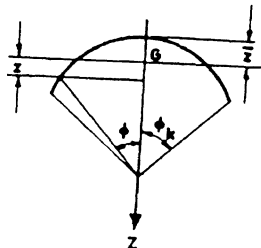


Table (5-3)

point	ϕ° from top	z m	Q m ³	N_x kg/m	$N_{x\phi}$ kg/m
0	40	1.547	0	60972	0
1	35	1.016	0.223	40038	8780
2	30	0.547	0.358	21562	14119
3	25	0.144	0.418	5683	16458
4	20	-0.190	0.413	-7476	16261
5	15	-0.452	0.355	-17817	14012
6	10	-0.641	0.259	-25260	10210
7	5	-0.755	0.136	-29748	5367
8	0	-0.793	0	-31248	0

Arch Analysis

Since the applied uniform loading is constant along the shell the shear force varies linearly in the longitudinal direction. Therefore, the longitudinal change of shear force, $N_{x\phi}$, i.e., its derivative with respect to x , is obtained by dividing the maximum values, calculated at the end supports, by $1/2$. These values as well as the vertical and horizontal components of shear force, for each discrete segment, are given in table (5-4).

Figure (5-17) shows the side view of half of the transverse arch together with its applied loading, as extracted from table (5-4). As we see, for this half arch, the vertical as well as the horizontal equilibrium equations are satisfied.

Table (5-4)

(1)	(2)	(3)	(4)	(5)	(6)	(7)	(8)	(9)	(10)
	ds	dy	dz	$\frac{\partial N_{x\phi}}{\partial x}$	$\frac{\partial N_{x\phi}}{\partial x} dy$	$\frac{\partial N_{x\phi}}{\partial x} dz$	$P_d \cdot ds$	$P_L \cdot dy$	$V = 7+8+9$
	m	m	m	$kg/m/m$	Kg/m	Kg/m	Kg/m	Kg/m	Kg/m
0	0.436	0.3403	0.2731	0.0	0	0	109.1	51.0	160.1
1	0.873	0.7148	0.5005	878.0	627.6	-439.5	218.2	107.2	-114.1
2	0.873	0.7557	0.4363	1411.9	1067.0	-616.1	218.2	113.4	-284.5
3	0.873	0.7909	0.3688	1645.8	1301.7	-607.0	218.2	118.6	-270.2
4	0.873	0.8200	0.2985	1626.1	1333.5	-485.3	218.2	123.0	-144.1
5	0.873	0.8429	0.2259	1401.2	1181.1	-316.5	218.2	126.4	28.1
6	0.873	0.8594	0.1515	1021.0	877.5	-154.7	218.2	128.9	192.4
7	0.873	0.8693	0.0761	536.7	466.6	-40.8	218.2	130.4	307.8
8	0.436	0.4362	0.0095	0.0	0	0	109.1	65.4	174.5

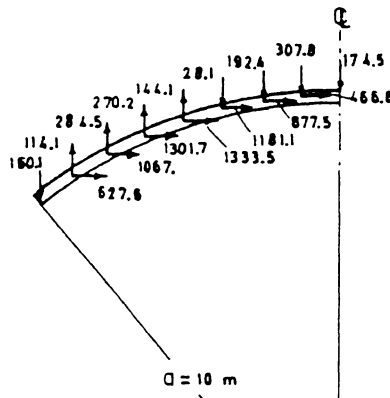


Figure (5-17) Free body diagram of half arch of example 5.1

82 Design and Analysis of Shell Structures

The longitudinal edges of the shell in figure (5-15) are fixed against rotation and horizontal translation. Therefore, the transverse arch can be considered a fixed arch. The redundant forces are taken to be the bending moment, M_o , and horizontal shear force, H , at the crown of the arch, as shown in the figure (5-18). To determine the redundant forces, we use the *energy theorems* of structural analysis, and in particular the method of *least work*.

The bending moments at the discretized arch segments of corresponding statically determinate arch, i.e., the arch from which the redundant forces M_o and H have been removed, are

$$m_8 = 0.0$$

$$m_7 = -174.5(0.4362 + \frac{0.8693}{2}) = -151.96 \text{ Kg-m}$$

$$m_6 = -151.96 - (307.8 + 174.5) \times \frac{(0.8693 + 0.8594)}{2}$$

$$-466.6 \times \frac{(0.0761 + 0.1515)}{2} = -621.94 \text{ Kg-m}$$

$$m_5 = -621.94 - (174.5 + 307.8 + 192.4) \times \frac{(0.8594 + 0.8429)}{2}$$

$$-(466.6 + 877.5) \times \frac{(0.1515 + 0.2259)}{2} = -1449.84 \text{ Kg-m}$$

$$m_4 = -1449.84 - (174.5 + 307.8 + 192.4 + 28.1)$$

$$\times \frac{(0.8429 + 0.8200)}{2} - (466.6 + 877.5 + 1181.1)$$

$$\times \frac{(0.2259 + 0.2985)}{2} = -2696.29 \text{ Kg-m}$$

$$m_3 = -2696.29 - (558.7) \times \frac{(0.82 + 0.7909)}{2} - (3858.7)$$

$$\times \frac{(0.2985 + 0.3688)}{2} = -4433.75 \text{ Kg-m}$$

$$m_2 = -4433.75 - 288.5 \times \frac{(0.7909 + 0.7557)}{2} - (5160.4)$$

$$\times \frac{(0.3688 + 0.4363)}{2} = -6734.17 \text{ Kg-m}$$

$$m_1 = -6734.17 - 4 \times \frac{(0.7557 + 0.7148)}{2} - 6227.4$$

$$\times \frac{(0.4363 + 0.5005)}{2} = -9654.02 \text{ Kg-m}$$

$$m_o = -9654.02 + 110.1(0.3403 + \frac{0.7148}{2}) - 6355$$

$$\times (0.2731 + \frac{0.5005}{2}) = -13164.77 \text{ Kg-m}$$

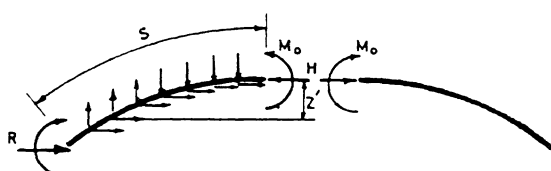


Figure (5-18) Redundant forces in the transverse arch of example 5.1

The expression for stored strain energy in the arch is

$$U = 2 \int_0^S \frac{M_i^2 ds}{2EI}$$

where

$$M_i = M_o + HZ' + m_i \quad Z' = a(1 - \cos\phi)$$

Now, we satisfy the compatibility requirements of no rotation and no lateral movement at the crown. Using the *principle of least action*, we express these requirements as follows:

$$\Delta H = \frac{\partial U}{\partial H} = 0 \quad , \quad \Delta \theta = \frac{\partial U}{\partial M_o} = 0$$

Therefore

$$\frac{\partial U}{\partial H} = 2 \int_0^S \frac{Z'}{EI} (M_o + HZ' + m_i) ds = 0$$

$$\frac{\partial U}{\partial M_o} = 2 \int_0^S \frac{1}{EI} (M_o + HZ' + m_i) ds = 0$$

Since the bending stiffness of the arch cross section, EI, has been assumed constant, these relations can be rewritten as

$$M_o \int_0^S z' ds + H \int_0^S z'^2 ds + \int_0^S z' m_i ds = 0$$

$$M_o \int_0^S ds + H \int_0^S z' ds + \int_0^S m_i ds = 0$$

Numerical calculations related to these integrals can be performed in a routine fashion; the final results are shown in table (5-5).

Table (5-5)

section	z'	ds	m_i	z'^2	$z' ds$	$z'^2 ds$	$m_i z' ds$	$m_i ds$
0	2.340	0.436	-13164.77	5.474	1.021	2.3883	-13438.91	-5744.21
1	1.808	0.873	-9654.02	3.271	1.578	2.854	-15235.94	-8424.72
2	1.340	0.873	-6734.17	1.795	1.169	1.566	-7873.25	-5876.67
3	0.937	0.873	-4433.75	0.878	0.818	0.766	-3625.12	-3869.18
4	0.603	0.873	-2696.29	0.364	0.526	0.317	-1419.01	-2352.96
5	0.341	0.893	-1449.84	0.116	0.297	0.101	-431.11	-1265.22
6	0.152	0.873	-621.94	0.023	0.133	0.020	-82.46	-542.75
7	0.038	0.873	-151.96	0.0014	0.033	0.0013	-5.05	-132.61
8	0	0.436	0	0	0	0	0	0

$$\Sigma = 6.981$$

$$\Sigma = 5.575 \quad \Sigma = 8.014 \quad \Sigma = -42110.85 \quad \Sigma = -28208$$

Using the calculated integrals, we write the compatibility relations:

$$\begin{cases} 5.575 M_o + 8.014 H = 42110.85 \\ 6.981 M_o + 5.575 H = 28208.32 \end{cases}$$

From which we obtain

$$M_o = -350.15 \text{ kg-m/m}$$

$$H = 5498.24 \text{ kg/m}$$

Once the quantities M_o and H have been determined, the internal forces can be easily obtained using only the equations of statics. These calculations and the resulting values of internal forces are presented in tables (5-6) and (5-7).

Table (5-6)

section	z'	m_1	M_o	HZ'	$M = M_\phi$ $\frac{Kg-m}{m}$
0	2.340	-13164.77	-350.15	12863.44	-651.48
1	1.808	-9654.02	-350.15	9943.46	-60.74
2	1.340	-6734.17	-350.15	7366.25	281.93
3	0.937	-4433.75	-350.15	5151.42	367.52
4	0.603	-2696.29	-350.15	3315.84	269.4
5	0.341	-1449.84	-350.15	1873.48	73.49
6	0.152	-621.94	-350.15	835.31	-136.78
7	0.038	-151.96	-350.15	209.23	-292.88
8	0	0	-350.15	0	-350.15

Table (5-7)

section	(1)	(2)	(3)	(4)	(5)	(6)	(7)
	ϕ	ΣV	ΣH	$\Sigma H \cos\phi$	$\Sigma V \sin\phi$	$N_\phi = 5 + 6$ Kg/m	
0	40	160.1	1356.8	1039.4	102.9	1142.3	
1	35	41	729.2	597.3	26.4	623.7	
2	30	-238.5	-337.8	-292.5	-119.3	-411.8	
3	25	-508.7	-1639.5	-1485.9	-215	-1700.9	
4	20	-652.8	-2973	-2793.7	-223.3	-3017	
5	15	-624.7	-4154.1	-4012.6	-161.7	-4174.3	
6	10	-432.3	-5031.6	-4955.2	-75.1	-5030.3	
7	5	-124.5	-5498.2	-5477.3	-10.9	-5488.2	
8	0	50	-5498.2	-5498.2	0	-5498.2	

The results of these calculations are summarized in the set of figures (5-19); these show the variations of internal forces across the shell profile.

Finally, we calculate the horizontal thrust, R, along the longitudinal edges of this inner shell; it is

$$R = H - \sum \frac{\partial N_x \phi}{\partial x} dy = 5498.2 - 6855.0 = -1356.8 \text{ Kg-m}$$

The lateral thrust, R, is negative; this means that the direction of R is *outwards* and not *inward*, as would have been the case for arches and frames. In other words, the inner shell has a tendency to *shrink inwards* along its longitudinal edges, so that the restraining effect of adjacent shells is to constrain this inward movement. This quality differs from our experience in the analysis of framed structures; and has its own structural implications in the design of such shells.

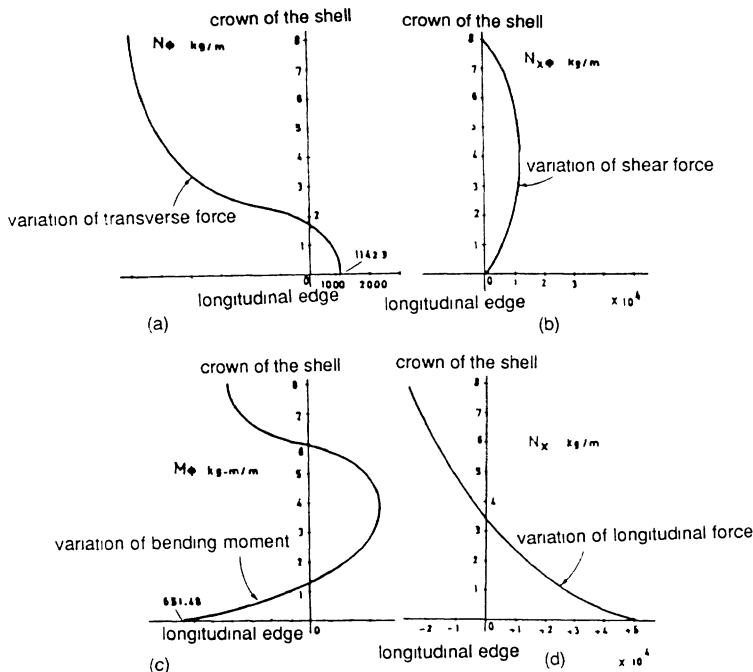


Figure (5-19) Plots of internal forces in the shell of example 5.1, (a) cross-sectional variations of N_ϕ at the mid-length, (b) sectional variation of $N_{x\phi}$ at the support, (c) sectional variation of M_ϕ in the mid-length, (d) sectional variation of N_x at the mid-length.

The analysis of this problem could have also been carried out with the help of table (5-1).

5.5 - Analysis of Cylindrical Vaults by ASCE Tables

Based on some simplified forms of bending theory of cylindrical shells, numerical calculations have been made for the shell vaults having various geometrical dimensions. These calculations have been tabulated and are available as a set of design-analysis tables. An **American Society of Civil Engineers (ASCE)** committee has been responsible for this task. Hence, these tables are normally referred to as **ASCE tables**.

Calculations in the ASCE manual are based on simplified versions of the exact cylindrical shell equations (Flügge equations). These calculations relate to the so-called "long shells" (for which $l/a > 1.67$) and short shells (for which $l/a < 1.67$).

The ASCE tables are based on the force method of structural analysis which has been outlined in previous chapters; the forces at the longitudinal edge of the shell are chosen as the redundant forces.

The ASCE tables use Fourier series expansions. All distributed applied loads, as well as distributed edge effects, are expanded into Fourier sine or cosine series in the longitudinal variable, x . Figures (5-20) show the first terms of the Fourier expansion of the redundant edge force distributions. Similar type of distributions are also assumed for the edge beams.

Note that the ASCE tables choose the origin of the transverse angular coordinate, ϕ , at the longitudinal edge of the shell. Therefore, the angle defining the normal to the surface at each point is measured from the normal to the shell at its longitudinal boundary.

In the analysis of cylindrical shells by the ASCE tables the following procedure should be followed:

(1) Membrane analysis

The membrane analysis of the shell is performed by using the tabulated coefficients.

(2) Edge effect bending analysis

The coefficients for the corrective bending edge effects are read from the appropriate table.

(3) Compatibility relations

Using the results of parts (1) and (2), we write a set of compatibility relations. By solving these relations for redundant edge force amplitudes, we obtain the unknown redundant edge forces.

(4) Superposition

Having obtained the redundant forces, we superpose the results of calculations performed in steps (1) and (2) and find the total force field in the shell.

The **ASCE tables** provide a set of coefficients for the internal forces in a variety of circular cylindrical vaults, including single shells with or without edge beams, and shell groups with or without edge members. The ASCE tables are included in the **appendix**.

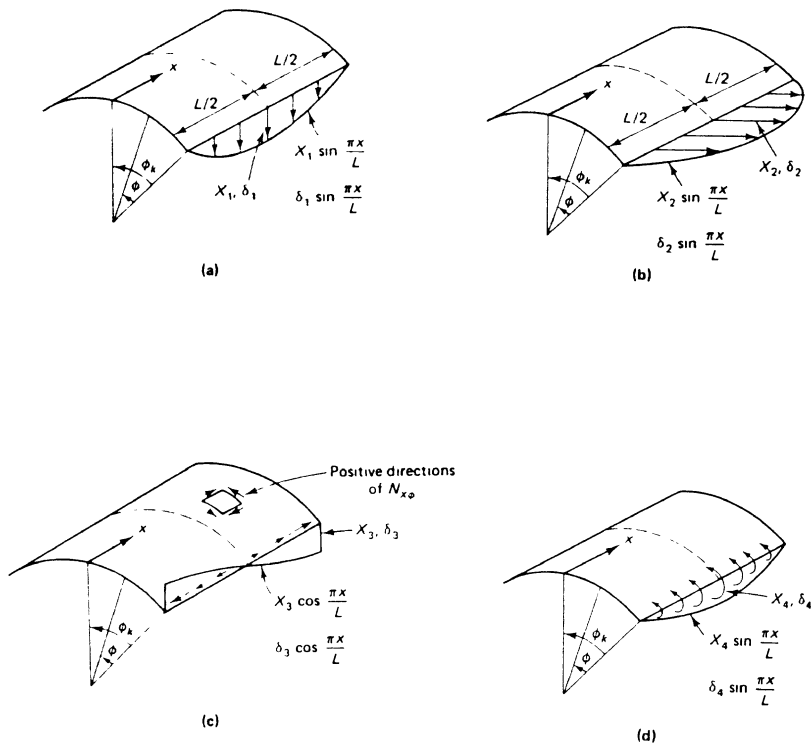


Figure (5-20) Redundant edge forces and corresponding edge displacements in the ASCE manual

5.6 - Design Examples of Reinforced Concrete Cylindrical Shell Roofs

In this section, we present some design examples of reinforced concrete shell roofs. We assume that the analysis of the shells under design has been carried out by the *beam-arch* method, the ASCE tables, or some computer program. In practical designs, differences in solutions obtained by different means of analysis are usually of secondary importance.

5.6.1 - Design of a Single Shell without Edge Beams

Consider a simply supported single thin reinforced concrete circular cylindrical vault as shown in figure (5-21). This shell is to be designed for the snow load of intensity 150 kg / m² which is imposed in addition to the shell weight. The allowable tensile stress is assumed to be equal to 1400 kg / cm².

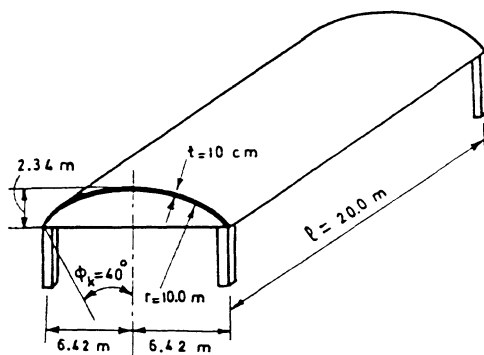


Figure (5-21) A single cylindrical vault with no edge beam

Design:

The overall dimensions of the shell are given in figure (5-21). The objective is to design the steel reinforcement for given shape.

Tables (5-8) and (5-9) summarize the results of analysis of this shell performed by using the ACI tables. We would have obtained similar results if we had analyzed the shell by other methods.

Table (5-8) Internal forces in the single simply supported shell of figure (5-21)

$$\frac{x}{l} = 0, \frac{1}{8}, \frac{1}{4}, \frac{3}{8}, \frac{1}{2}, \frac{x}{l}$$

ϕ^o	N_ϕ (Kg/m)				$N_{x\phi}$ (Kg/m)				N_x (Kg/m)				M_ϕ (Kg-m/m)							
	0	1/8	1/4	3/8	1/2	0	1/8	1/4	3/8	1/2	0	1/8	1/4	3/8	1/2	0	1/8	1/4	3/8	1/2
40	0	-2623	-4846	-6331	-6853	0	0	0	0	0	0	-1349	-2493	-3257	-3525	0	-505	-933	-1220	-1320
30	0	-2564	-4738	-6190	-6700	-2013	-1860	-1423	-770	0	0	-5513	-10186	-13308	-14405	0	-457	-844	-1102	-1193
20	0	-2115	-3907	-5105	-5526	-8447	-7804	-5973	-3233	0	0	-11591	-21418	-27984	-30290	0	-267	-494	-645	-698
10	0	-942	-1740	-2274	-2461	-14798	-13672	-10464	-5663	0	0	-1353	-2500	-3267	-3536	0	-34	-62	-81	-88
0	0	0	0	0	0	0	0	0	0	0	0	+52641	+97267	+127086	+137557	0	0	0	0	0

Table (5-9) Principal tensile stresses and directions in shell of figure (5-21)

ϕ^o	$x/l = 0$			$x/l = 1/8$			$x/l = 1/4$			$x/l = 3/8$			$x/l = 1/2$		
	N_{P_1}	N_{P_2}	θ	N_{P_1}	N_{P_2}	θ	N_{P_1}	N_{P_2}	θ	N_{P_1}	N_{P_2}	θ	N_{P_1}	N_{P_2}	θ
40	0	0	0	-2623	-1349	0	-4846	-2493	0	-6331	-3257	0	-6853	-3525	0
30	-2013	2013	45	-6412	-1665	26	-10535	-4389	14	-13390	-6108	6	-6700	-14405	0
20	-8477	8477	45	-15983	+2277	29	-23261	-2064	17	-28432	-4657	8	-5526	-30290	0
10	-14798	14798	45	-14821	+12590	45	-12526	+8351	44	-8455	+2914	42	-2461	-3536	0
0	0	0	0	0	+52641	0	0	+97267	0	0	+127086	0	0	+137557	0

Figure (5-22) shows variations of internal forces N_x , N_ϕ , and M_ϕ at the mid-length and the variation of $N_{x\phi}$ at the end support. For N_x , the numbers in this figure should be multiplied by a factor of 10000 (kg / m). For other force quantities, the multiplication coefficient of 1000 should be applied.

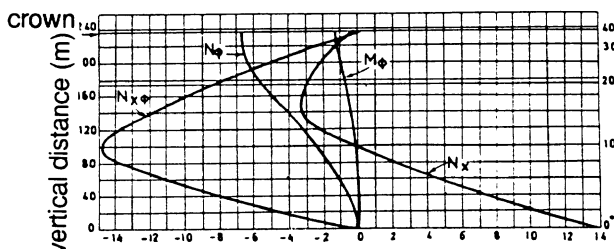


Figure (5-22) Variations of internal forces across the section of shell in figure (5-21)

Once the internal forces are known, the reinforcement design, for each subdivided region of the shell, can be carried out according to the standard **Working Stress Design (WSD)** method.

Figure (5-23) shows the plan of reinforcement pattern for the shell of figure (5-21). Due to the double axial symmetry, only a quarter of the shell is shown. Figure (5-24) shows a detailed section of the reinforcement at the corner region. The reinforcement of the shell in this region consists of longitudinal, transverse, and diagonal (shear) reinforcements.

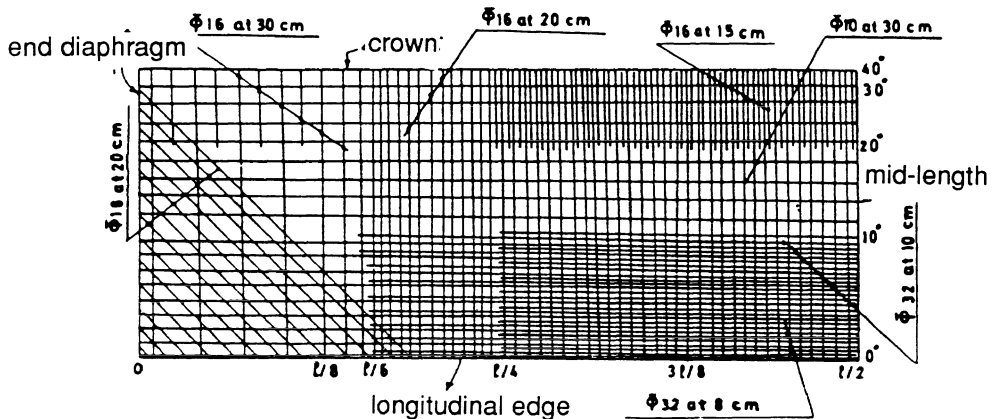


Figure (5-23) Quarter plan of reinforcement of shell in figure (5-21)

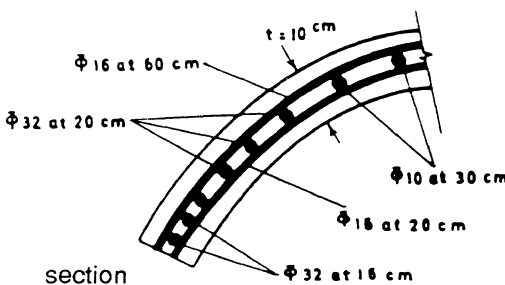


Figure (5-24) A detailed section of corner reinforcement of single shell in figure (5-21)

5.6.2 - Design of an Inner Shell in a Shell Group

As another design example, we consider a shell roof composed of a series of cylindrical shells as shown in figure (5-25). These shells are laterally connected to each other, with no edge beams. We will design an inner shell of this shell group. The given data are the same as for the single shell designed in the previous example.

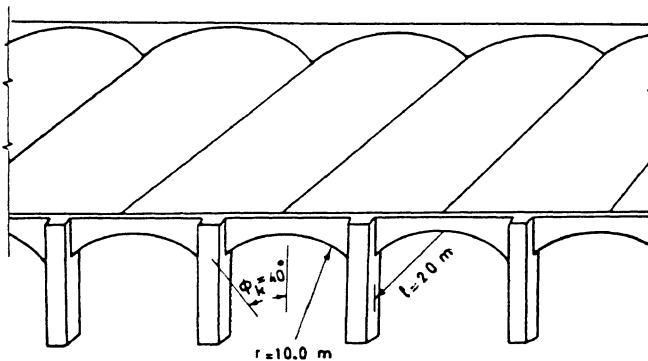


Figure (5-25) A system of multiple cylindrical vaults

To design an inner shell of the shell group, we take it out and analyze it using one of the methods discussed before. Figures (5-26) show the physically reasonable assumptions which can be made. These assumptions are also useful in the analysis of shells by computer programs.

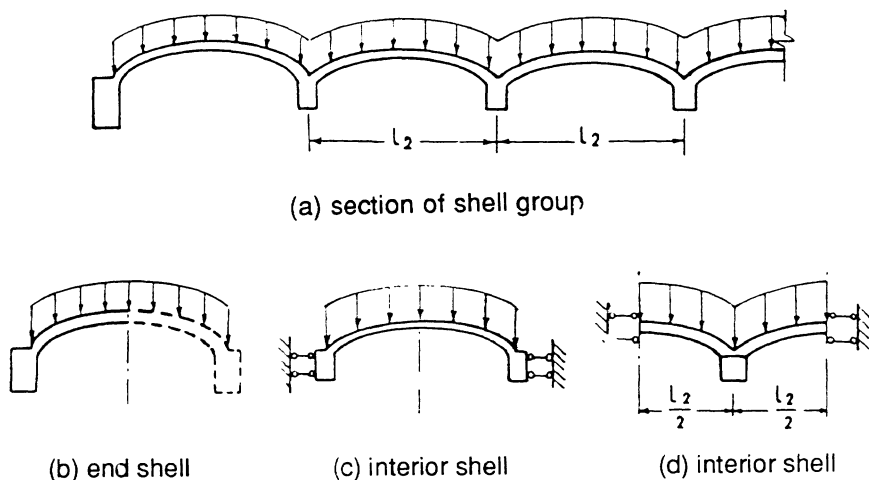


Figure (5-26) Assumptions on the behavior of inner and outer shells in a group of cylindrical shells

The results of analysis of an inner shell are summarized in tables (5-10) to (5-14).

Table (5-10)

$\frac{x}{l}$		N_c (Kg/m)				
c	$\frac{x}{l}$	0	1/8	1/4	3/8	1/2
40	0	-2601	-4807	-6281	-6798	
30	0	-2237	-4134	-5401	-5846	
20	0	-1241	-2293	-2996	-3243	
10	0	-24	-44	-57	-62	
0	0	507	937	1224	+1325	

Table (5-11)

$\frac{x}{l}$		N_x (Kg/m)				
c	$\frac{x}{l}$	0	1/8	1/4	3/8	1/2
40	0	-10422	-19257	-25160	-27233	
30	0	-9345	-17268	-22561	-24420	
20	0	-4492	-8300	-10844	-11738	
10	0	+7288	13466	17598	+19044	
0	0	+27635	51063	66717	72214	

Table (5-12)

$\frac{x}{l}$		N_{xc} (Kg/m)				
c	$\frac{x}{l}$	0	1/8	1/4	3/8	1/2
40	0	0	0	0	0	0
30	-7224	-6674	-5108	-2765	0	0
20	-12496	-11545	-8836	-4782	0	0
10	-11992	-11079	-8480	-4589	0	0
0	0	0	0	0	0	0

Table (5-13)

$\frac{x}{l}$		M_z (Kg-m/m)				
c	$\frac{x}{l}$	0	1/8	1/4	3/8	1/2
40	0	-121	-223	-292	-316	
30	0	-53	-98	-128	-139	
20	0	+110	204	266	+288	
10	0	117	216	282	+305	
0	0	-329	-608	-795	-860	

Table (5-14)

ϕ°	$x/l = 0$		$x/l = 1/8$		$x/l = 1/4$		$x/l = 3/8$		$x/l = 1/2$	
	N_{P_1}	N_{P_2}	N_{P_1}	N_{P_2}	N_{P_1}	N_{P_2}	N_{P_1}	N_{P_2}	N_{P_1}	N_{P_2}
40	0	0	-10422	-2601	-19257	-4807	-25160	-6281	-27233	-6798
30	-7224	+7224	-13352	1770	-19021	-2381	-22996	-4966	-24920	-5846
20	-12496	+12496	-14525	8792	-14629	4036	-13106	-734	-11738	-3243
10	-11992	+11992	-8035	15299	-4131	17553	-1179	18720	+19044	-62
0	0	0	507	27635	937	51063	1224	66717	+72214	+1325

Figure (5-27) shows variations of internal forces across the shell cross section. For the transverse moment, M_{ϕ} , the values of the table should be multiplied by 1000 (kg m / m). Also, for N_x a factor of 10000 (kg / m), and for N_{ϕ} and $N_{x\phi}$ a multiplication factor of 1000 (kg / m) should be applied.

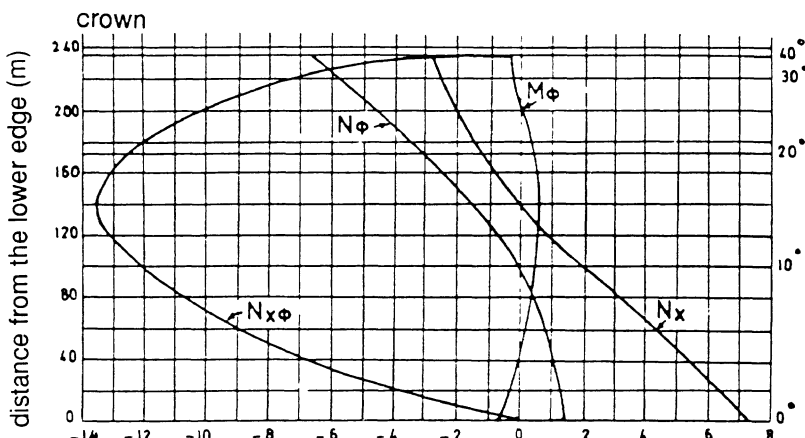


Figure (5-27) Variation of internal forces across the section of an inner shell in figure (5-26)

Figure (5-28) shows the quarter plan of reinforcing scheme of an inner shell from the shell group in figure (5-26).

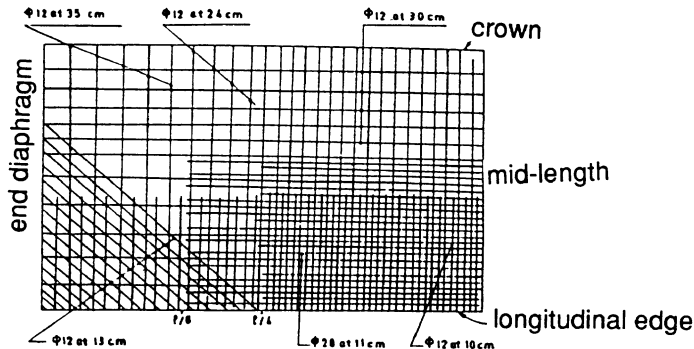


Figure (5-28) Quarter plan of reinforcement of an inner shell in the group of shell vaults shown in figure (5-26)

5.6.3 - Design of a Single Simply Supported Shell with Edge Beams

(1)Shell geometry, figure (5-29):

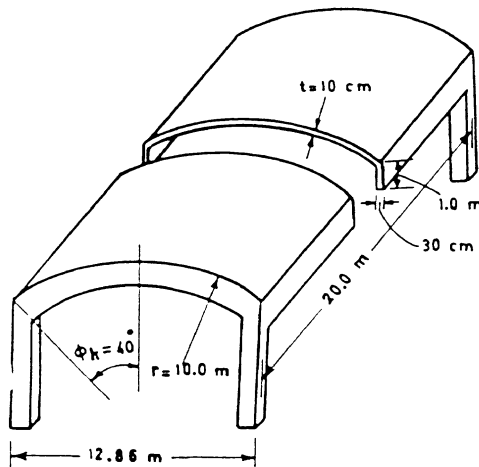


Figure (5-29) A single simply supported shell with edge beams
@Seismicisolation

96 Design and Analysis of Shell Structures

(2) Results of shell analysis:

Table (5-15)

$\frac{x/l}{\phi}$	0	1/8	1/4	3/8	1/2	N_x (kg/m)
40	0	-2581	-4769	-6232	-6745	
30	0	-3656	-6756	-8827	-9554	
20	0	-5718	-10566	-13806	-14943	
10	0	-5889	-10882	-14219	-15390	
0	0	-1055	-1949	-2546	-2756	

Table (5-16)

$\frac{x/l}{\phi}$	0	1/8	1/4	3/8	1/2	M_t (kg-m/m)
40	0	-130	-241	-315	-341	
30	0	-77	-142	-186	-201	
20	0	0	-1	-1	-1	
10	0	70	130	170	184	
0	0	0	0	0	0	

Table (5-17)

$\frac{x/l}{\phi}$	0	1/8	1/4	3/8	1/2	N_{xz} (kg/m)
40	0	0	0	0	0	
30	-2118	-1957	-1498	-811	0	
20	-5487	-5069	-3880	-2100	0	
10	-9862	-9111	-6973	-3774	0	
0	-12731	-11762	-9002	-4872	0	

Table (5-18)

ϕ	$x/l = 0$		$x/l = 1/8$		$x/l = 1/4$		$x/l = 3/8$		$x/l = 1/2$	
	N_{P_1}	N_{P_2}	N_{P_1}	N_{P_2}	N_{P_1}	N_{P_2}	N_{P_1}	N_{P_2}	N_{P_1}	N_{P_2}
10	0	0	-2581	-2188	-4769	-4043	-6232	-5283	-6745	-5718
30	-2118	+2118	-4987	-779	-7397	-3258	-8996	-4925	-9554	-5514
20	-5487	+5487	-9194	+1674	-12319	-1976	-14251	-3905	-14943	-4807
10	-9862	+9862	-12826	+5907	-14728	1759	-15348	-1598	-15390	-2952
0	-12731	+12731	-12858	+11184	-10127	+7959	-6417	3585	-2756	-310

3) Variations of internal forces in the cross section:

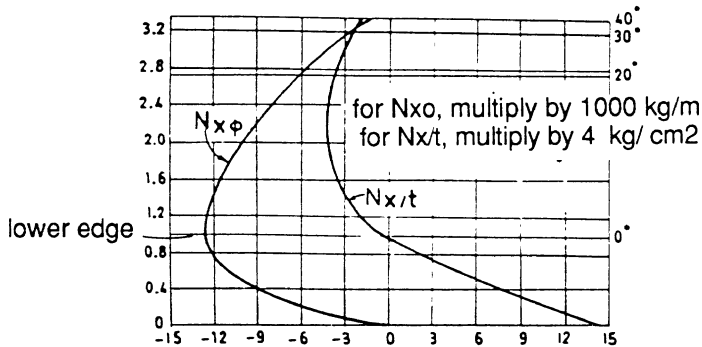


Figure (5-30) Variations of internal forces in the cross section of the shell in figure (5-29)

4) Plan of reinforcement:

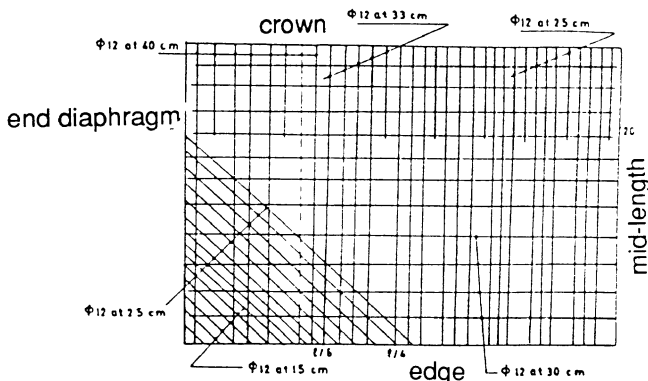


Figure (5-31) Quarter plan of reinforcement of the shell in figure (5-29)

5.6.4 - Design of an Inner Shell in a Shell Group with Edge Beams

1) Geometry of the system, figure (5-32):

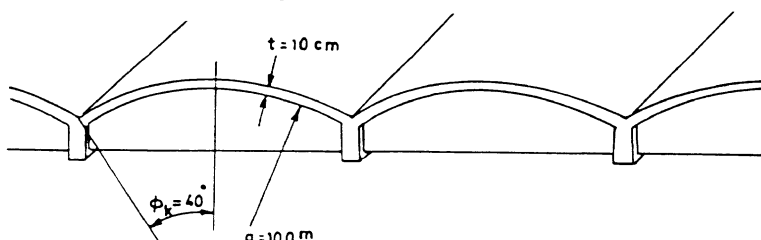


Figure (5-32) A shell group with edge beams

2) Results of shell analysis:

Table (5-19)

$\frac{x/l}{\phi}$	0	1/8	1/4	3/8	1/2	N_x (kg/m)
40	0	-2274	-4201	-5489	-5941	
30	0	-2091	-3864	-5048	-5464	
20	0	-1544	-2852	-3727	-4034	
10	0	-695	-1283	-1677	-1815	
0	0	232	428	559	605	

Table (5-20)

$\frac{x/l}{\phi}$	0	1/8	1/4	3/8	1/2	N_x (kg-m)
40	0	-5509	-10180	-13300	-14396	
30	0	-5585	-10320	-13484	-14595	
20	0	-5029	-9293	-12142	-13142	
10	0	-2367	-4373	-5713	-6184	
0	0	2906	5370	7017	7595	

Table (5-21)

$\frac{x/l}{\phi}$	0	1/8	1/4	3/8	1/2	M_y (kg-mv/m)
40	0	-92	-170	-223	-241	
30	0	-33	-60	-79	-85	
20	0	55	102	133	144	
10	0	67	124	162	175	
0	0	-191	-354	-462	-500	

Table (5-22)

$\frac{x/l}{\phi}$	0	1/8	1/4	3/8	1/2	$N_{x\phi}$ (kg-mv)
40	0	0	0	0	0	
30	-3678	-3583	-2742	-1484	0	
20	-7856	-7258	-5555	-3006	0	
10	-10603	-9857	-7544	-4083	0	
0	-10619	-9811	-7509	-4064	0	

Table (5-23)

ϕ^o	0	$x/l = 1/8$	$x/l = 1/4$	$x/l = 3/8$	$x/l = 1/2$
	\bar{p}_1	\bar{p}_2	\bar{p}_1	\bar{p}_2	\bar{p}_1
40	0	-5509	-2274	-10180	-4201
30	-3678	+3878	-7624	-11327	-2857
20	-7856	+7856	-10751	-4178	-12494
10	-10669	+10669	-11423	+8361	-10529
0	-10619	+10619	-6333	+11471	-5006
				+10804	+4047
					4144
					+7595
					-605

3) Reinforcement system:

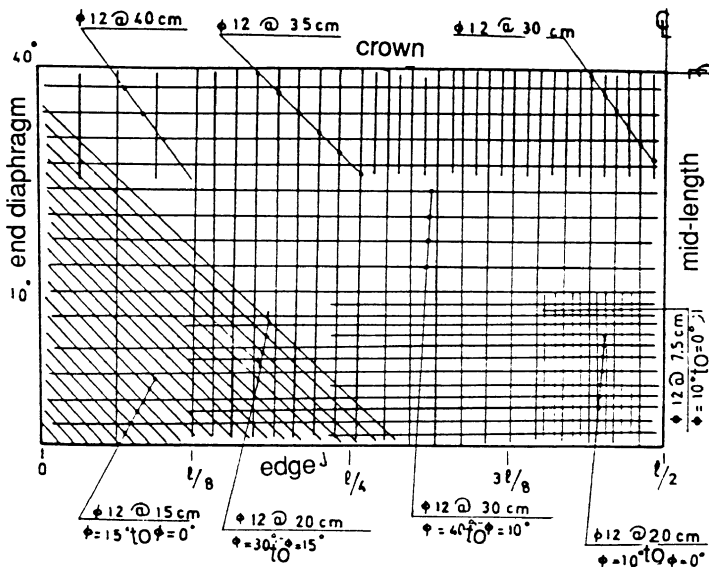


Figure (5-33) Quarter plan of reinforcement of the shell in figure (5-32)

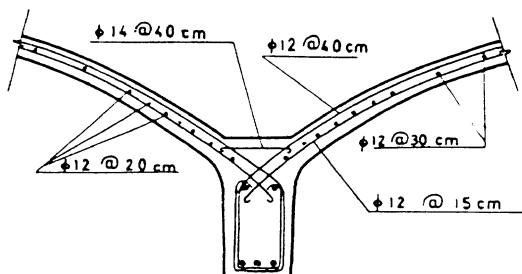


Figure (5-34) Detail of reinforcement at the intersection of the shells with edge beams in the shell group of figure (5-32)

Problems

P 5.1 - Analyze the inner shell of the multi-cylindrical shell roof shown in figure (P 5-1). The profiles of shells are semicircles. The shells are semicircular, of thickness t ; the width of the inner and the outer edge beams is $3t$, and the height of the edge beams is $5t$. The width of the shells is one half of the roof length. The system is subjected to its own dead load.

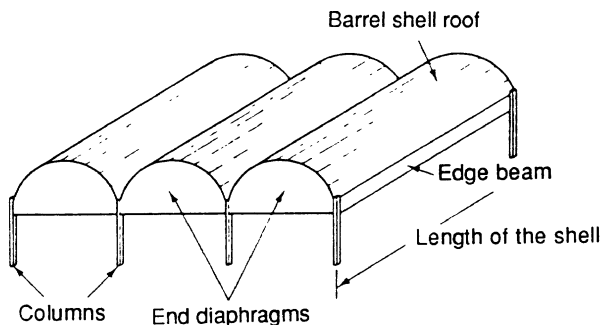


Figure (P 5-1) A multiple cylindrical shell roof

P 5.2 - Figure (P 5-2) shows a shell roof over a bus or train station. The length of the shell is 10.0 m, and it is supported by arched diaphragms which cantilever out from the columns. The radius of the circular shell section is 2.4 m. The intensity of applied load is 300 kg / m^2 distributed over the shell area. Analyze this shell by using the beam-arch method, and present a design of shell reinforcement.

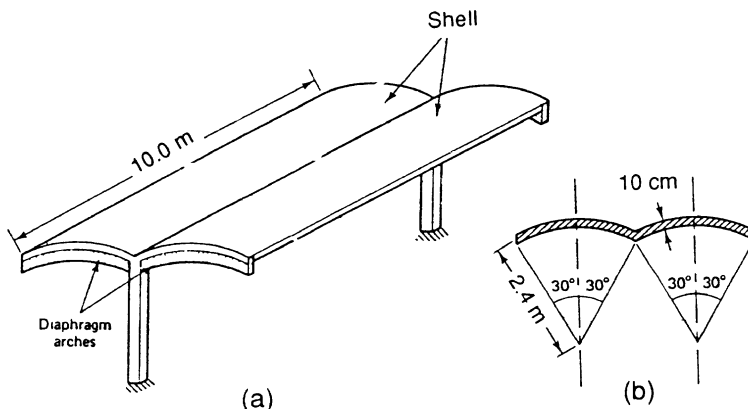


Figure (P 5-2) Barrel shell used as a platform cover (a) shell configuration, (b) shell cross section

References for Chapter Five

- 5.1 - M. Farshad, *Shell Structures*, Vol. I, 1986, Vol. II, 1987, Shiraz University Publications, Shiraz
- 5.2 - D. P. Billington, *Thin Shell Concrete Structures*, McGraw-Hill Book Co. N.Y., Revised edition, 1982
- 5.3 - G. S. Ramaswamy, *Design and Construction of Concrete Shell Roofs*, McGraw-Hill Book Co., N.Y., 1968
- 5.4 - J. E. Gibson, *The Design of Shell Roofs*, E. and F. N. Spon Ltd., London 1968
- 5.5 - *Design of Cylindrical Concrete Shell Roofs*, Manual of Engineering Practice, No. 31, American Society of Civil Engineers, New York, 1952
- 5.7 - C. B. Wilby, *Design Graphs for Concrete Shell Roofs*, Applied Science Publishers, Ltd., Barking, Essex, England, 1980
- 5.8 - *Coefficients for design of Cylindrical Concrete Shell Roofs*, Portland Cement Association, Skokie, Illinois, 1959
- 5.9 - J. Chinn, Cylindrical Shell Analysis Simplified by the Beam Method, ACI J., Vol. 55, May 1959
- 5.10 - V. N. Baikov, (ed.), *Reinforced Concrete Structures*, MIR Publishers, Moscow, English Translation 1978
- 5.11 - V. I. Murashev, E. Y. Sigalov, and V. N. Baikov, *Design of Reinforced Concrete Structures*, MIR Publishers, Moscow, 1968
- 5.12 - *Concrete Thin Shells*, ACI Publication, 1983
- 5.13 - V. S. Kelkar, and R. T. Sewell, *Fundamentals of the Analysis and Design of Shell Structures*, Prentice-Hall, INC., New Jersey, 1987
- 5.14 - ACI *Code of Reinforced Concrete Shell Design*, No. 334

Chapter 6

Membrane Analysis of Shells of Revolution

6.1 - Introduction

In this chapter we will study the membrane behavior of shells of revolution with double curvature. The shell types analyzed in the present chapter are a subclass of shells of revolution having non-zero positive Gaussian curvature. Shells with non-zero Gaussian curvature have non-developable surfaces. Hence they are stronger, stiffer, and more stable than shells with zero Gaussian curvature.

Domes have positive Gaussian curvature. These types of shells are used to cover the roofs of sport halls and large liquid storage tanks. The containment shield structure of nuclear power plants have also dome-like roofs. Various pressure vessels are either completely composed of a single rotational shell or have shells of rotation as their end caps.

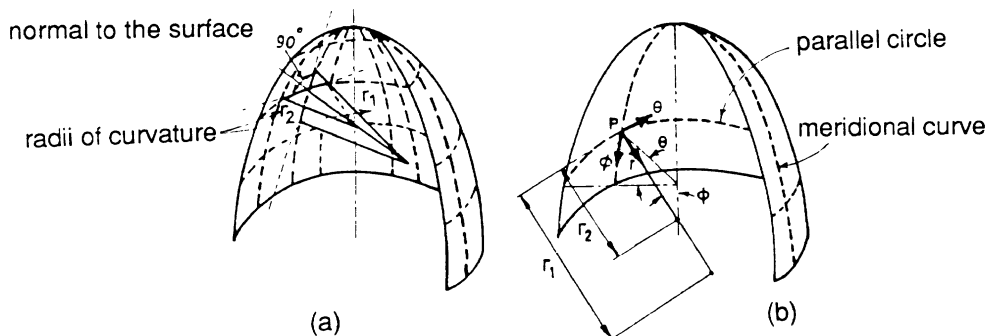
Conical shells, with zero Gaussian curvature, are a member of the class of shells of revolution. They are used to cover liquid storage tanks, and the nose cones of missiles and rockets.

In this chapter, we first derive the governing membrane equations of shells of revolution will be derived. Then, we apply them to the analysis of a number of shell problems including dome-like roofs cones. Later on, we determine the membrane displacement field of rotationally symmetric shells. These results will be used in later chapters in which more complete design and analysis of the shells of revolution are presented.

6.2 - Geometrical Description

At any point on the middle surface of a shell with non-zero Gaussian curvature we can define two principal radii of curvature. Figure (6-1a) shows two principal sections containing the normal to the shell at a point P. These sections create two plane curves with two local principal radii of curvature, r_1 and r_2 , as shown in figure (6-1a). One of these sections is called the *meridional curve* while the projection of another section on plane perpendicular to the axis of revolution creates the *parallel circles* on the shell surface.

The middle surface of a shell of revolution with non-zero positive Gaussian quadrature can be described rather like the earth. Thus through any point we may take two sections, one perpendicular to the axis of revolution, one containing the axis. The first cuts the shell in a *parallel curve* (circle of latitude) the other in a *meridian* (plane of longitude). At any point, the radius of curvature of the meridian is called r_1 , and the radius of parallel circle, r , is projected value of another principle radius of curvature which has been denoted by r_2 .



Figure(6-1) A partial perspective view of a surface of revolution showing the principal sections at a point P, the principal radii of curvature, the meridians and the parallel circles

Parallel circles form the perimeter of the base of a cone the apex of which is the center of curvature for r_2 . Due to rotational symmetry, the center of curvature of r_2 always lies on the axis of revolution. However, the center of curvature of r_1 does not have to lie on this axis.

Denote the angle between the normal to the surface at P with the axis of revolution by ϕ . We also denote the horizontal angular position of P, from some arbitrary origin, by the angle θ . The direction of the axis of revolution is assumed to coincide with the z axis.

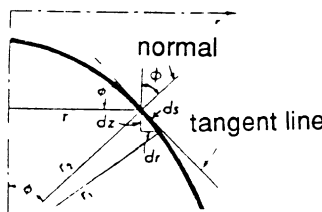


Figure (6-2) A meridional section of rotational shell showing the geometrical parameters of the shell surface

Referring to figure (6-2), the radius of parallel circle, r , at point P can be written as

$$r = r_2 \sin \phi$$

Also, referring again to figure (6-2), the following relations exist among the shell geometrical parameters.

$$\begin{aligned} r &= r_2 \sin \phi \\ ds &= r_1 d\phi \\ dr = ds \cos \phi, \quad dz = ds \sin \phi \end{aligned} \tag{6-1}$$

$$\frac{dr}{d\phi} = r_1 \cos \phi \tag{6-2}$$

$$\frac{dz}{d\phi} = r_1 \sin \phi \tag{6-3}$$

Combining the above relations, we obtain the following inter-relation between the surface parameters r_1 , r_2 , and ϕ .

$$\frac{1}{r} - \frac{dr}{d\phi} = \frac{r_1}{r_2} \cot \phi \tag{6-4}$$

6.3 - Governing Membrane Equations

To derive the membrane equilibrium equations for shells of revolution, we consider the free body diagram of an element of the shell, figure(6-3). The element shown in figure (6-3) is taken out from the shell by two pairs of infinitesimally adjacent sections. The first pair of sections are meridians while the second pair contain the normals at the corner points. Since these two intersections are principal sections, they are mutually orthogonal to each other.

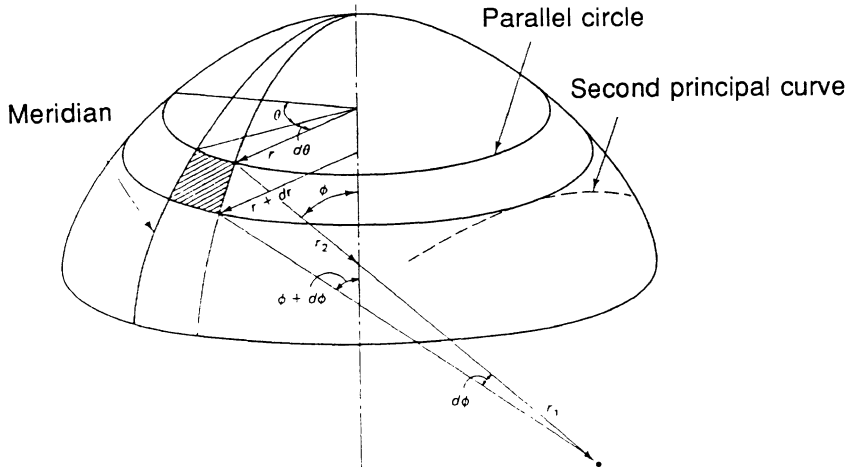


Figure (6-3) An infinitesimal element of a rotational surface

The free body diagram of figure (6-4) shows the internal membrane forces, N_ϕ , N_θ , $N_{\phi\theta}$, and their differential variations, N_ϕ designates the meridional force, N_θ the hoop force, and $N_{\phi\theta}$ the membrane shear force; the quantities p_r , p_ϕ , and p_θ represent the intensity of external distributed applied loading, in the r , ϕ , and θ directions, respectively.

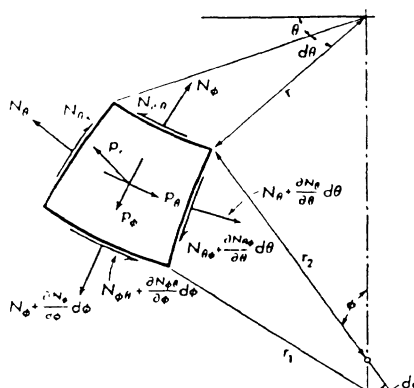
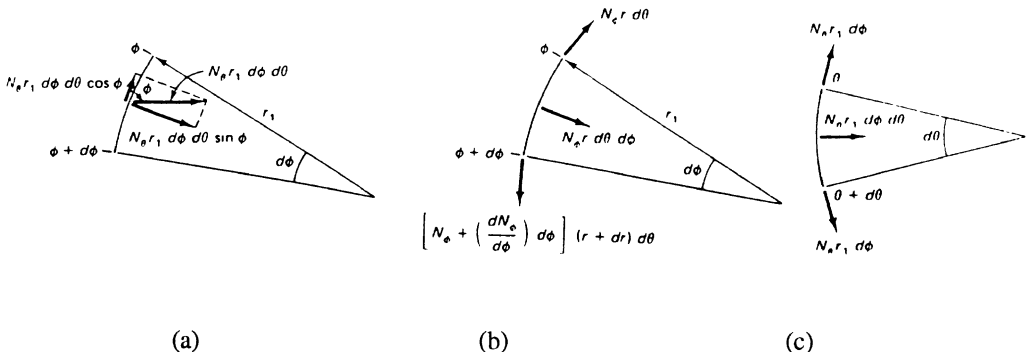


Figure (6-4) Free body diagram of a rotational shell element

We write the equations of equilibrium in the ϕ , θ , and r directions. Because of the double curvature, the membrane forces have projections in all three directions and thus contribute to all three equilibrium equations. Figures (6-5) show the contributions of N_ϕ and N_θ in various directions.



(a)

(b)

(c)

Figure (6-5) Meridional and hoop sections through the shell of revolution,(a) and (b) meridional sections, (c) hoop section

The equilibrium equation in the hoop direction is

$$\frac{\partial N_\theta \phi}{\partial \theta} r_1 d\theta d\phi + \frac{\partial}{\partial \phi} (r N_\phi) d\theta d\phi - N_\phi r_1 d\phi d\theta \cos \phi + P_\phi r r_1 d\theta d\phi = 0 \quad (6-5)$$

If we divide both side of this equation by $(d\phi d\theta)$ we obtain

$$\frac{\partial}{\partial \phi} (r N_\phi) + r_1 \frac{\partial N_\phi \phi}{\partial \theta} - r_1 N_\phi \cos \phi + P_\phi r r_1 = 0 \quad (6-6)$$

We derive the equilibrium equation in the ϕ direction in a similar fashion.

$$\frac{\partial}{\partial \phi} (r N_{\phi\phi}) + r_1 \frac{\partial N_\phi}{\partial \theta} + r_1 N_{\phi\phi} \cos \phi + P_\phi r r_1 = 0 \quad (6-7)$$

The third equilibrium equation is obtained by projecting all the forces in the direction normal to the shell, i.e., in the r direction. By doing so, we obtain

$$N_\theta r_1 \sin \phi + N_\phi r - P_r r r_1 = 0$$

which, upon division by ($r r_1$) yields

$$\frac{N_\phi}{r_1} + \frac{N_\theta}{r_2} = p_r \quad (6-8)$$

Equations (6-6), (6-7), and (6-8) constitute the governing equilibrium equations of the membrane theory for shells of revolution. These relations yield N_ϕ , N_θ , and $N_{\phi\theta}$, i.e., the membrane force field in the shell.

Note that the meridional and hoop forces N_ϕ , N_θ appear in all three equations. This indicates that a doubly curved shell is a complex and efficient structure; all three forces N_ϕ , N_θ and $N_{\phi\theta}$ contribute to carrying the load in any direction. The spatial interaction of internal forces, manifested in their presence in all equilibrium equations, is indicative of an efficient and profound behavior of doubly curved shells. This spatial collaboration is very rare in framed structures.

6.4 - Rotational Shells with Axisymmetric Loading

In a number of important loading cases, such as the dead weight and internal fluid pressure loading, geometrically complete shells of revolution have axisymmetric behavior. *Axisymmetric behavior* is independent of the variable θ . The loading, internal forces, and deformations can vary in the ϕ direction.

The membrane behavior of axially symmetric shell subjected to axisymmetric loading is axisymmetric, so that the membrane shear force, $N_{\phi\theta}$, is identically zero; and the directions of principal stresses coincide with the meridional and hoop directions.

The governing equations of axisymmetrically loaded shells of revolution can be easily obtained from the equations (6-6) to (6-8) by setting all derivatives with respect to θ equal to zero:

$$\frac{d}{d\phi} (r N_\phi) - r_1 N_\theta \cos\phi = - p_\phi r r_1 \quad (6-9a)$$

$$\frac{N_\phi}{r_1} + \frac{N_\theta}{r_2} = p_r \quad (6-9b)$$

The third equation is decoupled from the other two:

$$\frac{d}{d\phi} (r N_{\phi\theta}) + r_1 N_{\theta\phi} \cos\phi = - p_\theta r r_1 \quad (6-10)$$

Since $p_\theta = 0$, the last (and already decoupled) equation would be identically satisfied, and so we shall have $N_{\phi\theta} = 0$.

If we eliminate N_ϕ between the equations (6-9a) and (6-9b) we get:

$$\frac{d(rN_\phi)}{d\phi} \sin\phi + rN_\phi \cos\phi = r_1 r_2 P_r \cos\phi \sin\phi - r_1 r_2 P_\phi \sin^2\phi$$

Using the identity:

$$\frac{d(rN_\phi)}{d\phi} \sin\phi + rN_\phi \cos\phi = \frac{d}{d\phi} (rN_\phi \sin\phi) = \frac{d}{d\phi} (r_2 N_\phi \sin^2\phi)$$

and integrating the combined equilibrium relation we obtain:

$$N_\phi = \frac{1}{r_2 \sin^2\phi} [\int r_1 r_2 (P_r \cos\phi - P_\phi \sin\phi) \sin\phi d\phi] + C \quad (6-11)$$

This gives the meridional membrane force, N_ϕ ; the hoop force, N_θ , can be conveniently obtained from the relation (6-9b).

The relation (6-11) has a clear and useful physical interpretation. To provide this interpretation, we intersect the shell with a plane section normal to the axis of revolution at a point having an arbitrary normal angle ϕ . Figure (6-7) shows a sector of the shell lying above this plane section; it also shows the effect of the lower part on this piece, which consists of the internal meridional force uniformly distributed at the base of this sector. Figure (6-6) shows the resultant of applied axisymmetric loading is also shown, denoted by R .

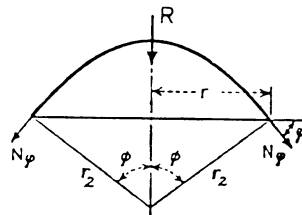


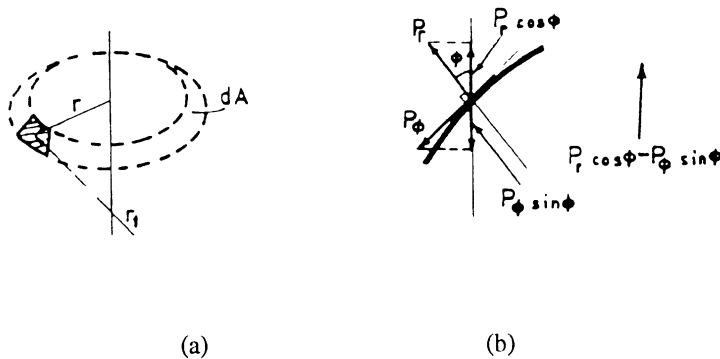
Figure (6-6) A sector of a shell of revolution showing the resultant of axisymmetric applied loads and the reactive membrane forces

Figure (6-7) shows a shell element and its meridional side view; an elemental area of the shell is

$$dA = 2\pi r r_1 d\phi = 2\pi r_1 r_2 \sin\phi d\phi$$

We can verify that the differential of applied forces projected in the direction of the shell axis of revolution has the value:

If we now go back to the integral (6-11) we note that the integral is the *resultant of applied loads* projected along the shell axis of revolution. We also note that the quantity $2\pi N_\phi (r_2 \sin^2\phi)$ is the sum of reactive forces projected along that axis. The constant C is the sum of applied concentrated forces, if any, along the shell axis of revolution. Therefore, the relation (6-11) is the equation of equilibrium for the global shell sector shown in figure (6-6).



Figure(6-7) (a) A ring section of the shell, (b) resultant of forces on an infinitesimal element

This procedure, called *the method of sections*, gives the membrane force field in the form:

$$N_\phi = - \frac{R}{2\pi r_2 \sin^2\phi} \quad (6-12)$$

$$N_\theta = + \frac{R}{2\pi r_1 \sin^2\phi} + P_r r_2 \quad (6-13)$$

In the following sections, the membrane theory developed in this section will be applied to a number of shells with axisymmetric loadings.

6.5 - Spherical Domes

6.5.1.- Membrane Forces

Consider a constant-thickness spherical dome of radius a acted upon by its own dead weight of intensity q . We analyze the shell by *the method of sections*.

The resultant, R , of applied dead load projected along the vertical axis of revolution is

$$R = 2\pi \int_0^\phi a^2 q \sin\phi d\phi = 2\pi a^2 q (1 - \cos\phi)$$

The relations (6-12) and (6-13) give the membrane internal forces

$$N_\phi = - \frac{a q (1 - \cos\phi)}{\sin^2\phi} = - \frac{aq}{1 + \cos\phi} \quad (6-14a)$$

$$N_\theta = aq \left(\frac{1}{1 + \cos\phi} - \cos\phi \right) \quad (6-14b)$$

Several interesting observations can be made concerning this solution. First, the expression (6-14a) always yields negative values for N_ϕ throughout the shell. Hence, the meridional force in a dome under its own weight is always compressive. Secondly, the hoop force, N_θ , is compressive at the top, but changes sign somewhere along the meridian and becomes tensile in the lower part of the shell. N_θ is zero when:

$$\frac{1}{1 + \cos\phi} - \cos\phi = 0 \quad (6-15)$$

The root of this transcendental equation is $\phi = 51^\circ 50'$.

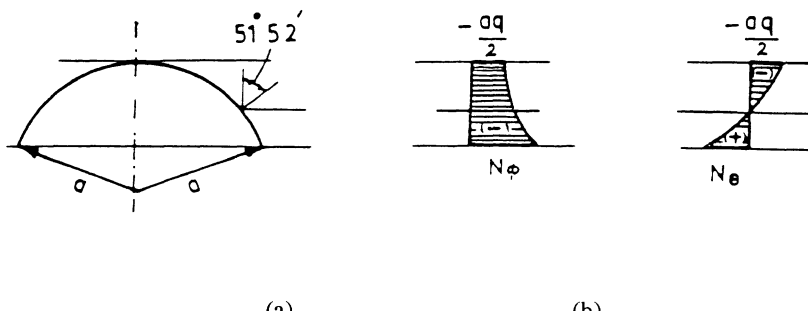


Figure 6-8: A spherical dome under its own weight, (a) the dome
© Seismic Isolation

Figure (6-8) shows plots of the solutions (6-14), i.e., variations of meridional and hoop stresses along the height of the dome. We observe that at $\phi = 0$, $N_\phi = N_\theta = -aq/2$. For a hemispherical dome, the absolute maximum of the both membrane forces is (aq).

It is interesting to know that the ancient engineers were well aware of this structural behavior of domes. When building domes with masonry materials, such as adobe brick, fired brick, and stone, which are relatively weak in tension, but strong in compression, they would confine their dome sector to the compression zone or, for high domes, would reinforce them in the tensile region. The hoop reinforcement would consist of wooden ties placed along the parallel circles; when tied together they would form a closed strengthening ring capable of absorbing tensile forces.

6.5.2. - Domes with skylight

In some occasions, the top sector of the domes is removed for some purpose. For example, domes can be provided with an open top for natural lighting; these roofs are called *domes with skylight*. In such cases, the shells are usually provided with a stiffening ring at the top, as well as one at the base, figure (6-9).

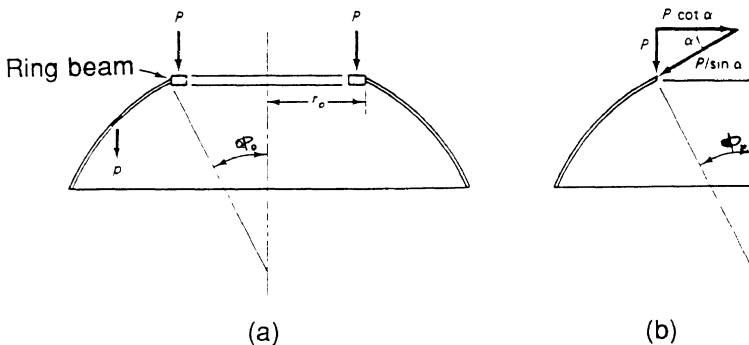


Figure (6-9) A spherical dome with a skylight and a ring at the top

The ring at the top region acts in compression and is meant to reduce the internal forces in the shell body. The weight of this ring is applied to the shell as a uniformly distributed line loading.

Assume that the weight per unit width of the top stiffening ring of the spherical dome of figure (6-9) is equal to P . Then, for a dome with skylight we have

$$R = 2\pi \int_{\phi_0}^{\phi} a^2 q \sin \phi d\phi + 2\pi P a \sin \phi_0$$

The expressions (6-12) and (6-13) yield:

$$N_{\phi} = -aq \frac{\cos \phi_o - \cos \phi}{\sin^2 \phi} - P \frac{\sin \phi_o}{\sin^2 \phi} \quad (6-16a)$$

$$N_{\theta} = aq \left(\frac{\cos \phi_o - \cos \phi}{\sin^2 \phi} - \cos \phi \right) + P \frac{\sin \phi_o}{\sin^2 \phi} \quad (6-16b)$$

Numerical Example 6.1

Consider a concrete shell of revolution having a parabola as its generating meridian, figure (6-10). The rise of this dome is $f = 15.0$ meters and the radius of its base parallel circle is $r_0 = 6.0$ meters. The dome has a constant thickness of $t = 10.0$ cm. The specific weight of concrete is assumed to be equal to 2400 kg/m^3 . In addition to its own weight, the dome is also subjected to snow load of 100.0 kg/m^2 uniformly distributed on a horizontal projection. Determine the maximum meridional and hoop stresses in the dome.

Solution:

If the dead load has intensity w , relations (6-12) and (6-13) give the membrane forces:

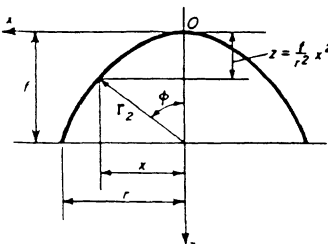
$$N_{\phi} = \frac{wC}{6K^2} \left[(1 + K^2)^2 - \sqrt{1 + K^2} \right], \quad K = \frac{2x}{c}$$

$$N_{\theta} = \frac{wC}{2} - \frac{N_{\phi}}{\sqrt{1+K^2}}$$

For a snow live load of intensity q , we have

$$N_{\phi} = \frac{qc}{4} \sqrt{1 + K^2}$$

$$N_{\theta} = \frac{qc}{4} \sqrt{1 + K^2}$$



$$z = f \frac{x^2}{r^2} = \frac{1}{c} x^2$$

$$c = \frac{r^2}{f}$$

Figure (6-10) Paraboloidal dome of example 6.1 and the equation of its meridional curve

In the present example,

$$C = (6.0)/15 = 2.4 \text{ kg/m}, \quad q = 100.0 \text{ kg/m}^2, \quad w = 2400 \times 0.10 = 240 \text{ kg/m}^2$$

The maximum compressive meridional force under combined loading occurs at the base of the dome. Hence, $K = (2 \times 6.0)/2.4 = 5.0$. Therefore,

$$\begin{aligned} N_\phi|_{\max} &= \frac{10.0 \times 2240 \times 2.40}{100 \times 6 \times 5^2} [(1+5^2)^2 - \sqrt{1+5^2}] \\ &+ \frac{100 \times 2.40}{4} \sqrt{1+5^2} = 2404.5 + 305.9 = 2710.4 \text{ kg/m} \end{aligned}$$

and the maximum meridional stress is

$$\sigma_\phi|_{\max} = \frac{2710.4 \times \frac{1}{100}}{10} = 2.71 \text{ kg/cm}^2$$

The maximum hoop force under combined loading is tensile and occurs at the base; its magnitude is:

$$\begin{aligned} N_0|_{\max} &= \frac{10 \times 2240 \times 2.40}{100 \times 2} - \frac{2404.5}{\sqrt{1+5^2}} + \frac{100 \times 2.40}{4} \sqrt{1+5^2} \\ &= 268.8 - 471.6 + 305.9 = 103.1 \text{ kg/m} \end{aligned}$$

The magnitude of corresponding maximum tensile hoop stress is:

$$\sigma_0|_{\max} = \frac{103.1 \times \frac{1}{100}}{10} = 0.10 \text{ kg/cm}^2$$

As we observe, the calculated values of maximal stresses are remarkably *low* for such a structure. In particular, the maximum tensile hoop stress is very small and can be carried by weak materials such as various masonry products. This is generally true for most shell structures. Many historical masonry shells which still remain after many centuries testify to this unique feature of shells.

6.6 - Fluid Storage Tanks

Thin shells have various applications as liquid storage tanks and fluid containers. In these applications, varieties of shell shapes may be envisaged, designed, and manufactured. In this section we present a membrane analysis of three types of these containment vessels.

6.6.1 - Spherical Liquid Storage Tank

The spherical tank, of radius a , such as the one shown in the figure (6-11a) is normally made of metal and is used to store liquids or gases. Complete spherical metallic tanks with radius a are usually placed on an elevated footing and supported by means of stiffening rings.

The applied internal pressure in the tank of figure (6-11) filled with a liquid of density γ is,

$$P_\phi = 0, \quad P_\theta = 0, \quad P_r = \gamma a (1 - \cos \phi) \quad (6-17)$$

Formula (6-11) gives:

$$\begin{aligned} N_\phi &= \frac{\gamma a^2}{\sin^2 \phi} \left[\int (1 - \cos \phi) \cos \phi \sin \phi d\phi + C \right] \\ &= \frac{\gamma a^2}{6 \sin^2 \phi} [(2 \cos \phi - 3) \cos^2 \phi + 6C] \end{aligned} \quad (6-18)$$

At the apex of the shell ($\phi = 0$), the denominator of the above expression vanishes resulting in N_ϕ infinite. Physically, this force must be actually zero at the apex. To have a finite value at the "regular" apex point, we evaluate the constant C so that this condition is satisfied. Hence, we evaluate the expression in the nominator at $\phi = 0$ and then set it to equal to zero. If we do so, we find $C = 1/6$. Substituting this value in (6-18), and making use of the formula (6-9b) we obtain

$$\begin{aligned} N_\phi &= \frac{\gamma a^2}{6} \frac{1 - \cos \phi}{1 + \cos \phi} (1 + 2 \cos \phi) \\ N_\theta &= \frac{\gamma a^2}{6} \frac{1 - \cos \phi}{1 + \cos \phi} (5 + 4 \cos \phi) \end{aligned} \quad (6-19)$$

The expressions (6-19) are valid for the part of the tank lying above ϕ_0 . For the lower part, we must find another proper value for the constant C which assures the finiteness of N_ϕ at $\phi = \phi_0$. By a manipulation similar to the previous one, this value comes out to be $C = 5/6$. Hence, for the lower part of the shell we find

$$\begin{aligned} N_\phi &= \frac{\gamma a^2}{6} \frac{5 - 5 \cos \phi + 2 \cos^2 \phi}{1 - \cos \phi} \\ N_\theta &= \frac{\gamma a^2}{6} \frac{1 - 7 \cos \phi + 4 \cos^2 \phi}{1 - \cos \phi} \end{aligned} \quad (6-20)$$

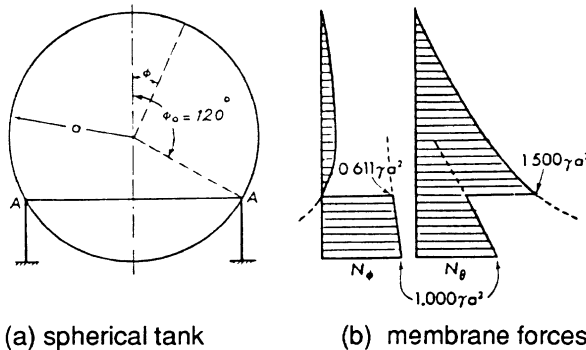


Figure (6-11) A spherical liquid storage tank

Variations of membrane forces in the liquid tank are plotted in figure (6-11b). Note that the internal force quantities are discontinuous at the ring section. This discontinuity is due to the presence of the supporting ring. In fact, due to presence of the ring element, a local bending field develops around the ring section. The membrane theory is of course incapable of determining the bending forces.

According to membrane theory, the difference in internal forces in the upper and lower parts of the shell, in figure (6-11a), must be absorbed by the stiffening supporting ring. The discontinuity in N_θ creates in the ring a compressive force of magnitude:

$$\frac{2\gamma a^2}{3} \frac{\cos\phi_0}{\sin\phi_0}$$

Also, the sum of the meridional forces at the ring section exerts a vertical component equal to:

$$\frac{2\gamma a^2}{3} \sin \phi_0$$

A preliminary design of the ring can be carried out on the basis of these quantities.

6.6.2 - Cylindrical Tanks with Spherical Ends

Figure (6-12) shows a liquid storage tank composed of cylindrical wall and spherical end shells. The tank is placed on an elevated ring support. The height of the cylinder is H and the radius of hemispherical end shells is a . The tank is filled with a liquid of density γ .

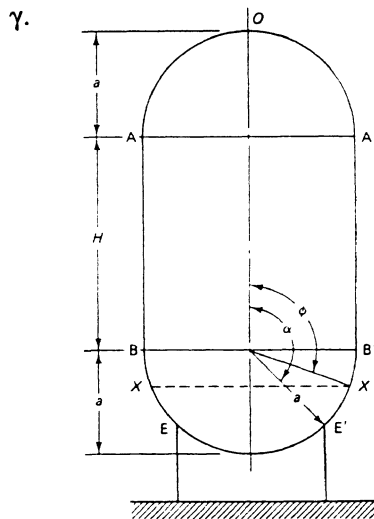


Figure (6-12) A cylindrical liquid storage tank having two spherical ends

The liquid pressure loading at the bottom spherical part of the tank is,

$$p_\phi = 0 \quad p_r = \gamma a \left(\frac{H}{a} + 1 - \cos \phi \right) \quad \phi \geq \frac{\pi}{2} \quad (6-21)$$

Substituting these values into the formula (6-11), and integrating from $\phi = \pi/2$ to $\phi = 0$, we obtain

$$N_\phi = \frac{\gamma a^2}{\sin^2 \phi} \left(\frac{\cos^3 \phi}{3} - \frac{\cos^2 \phi}{2} - \frac{H \cos^2 \phi}{a} \frac{1}{2} \right) + \frac{N_{\phi_0}}{\sin^2 \phi} \quad (6-22)$$

where N_{ϕ_0} is the value of N_ϕ evaluated at $\phi = \pi/2$. It is, on the other hand, equal to the value of N_ϕ at the level A. Their common value can be found by using the formula (6-11) again but with $H = 0$ and integrating it from $\phi = 0$ to $\phi = \pi/2$. It can also be found by the *method of sections* applied to an arbitrary section X-X. The resulted value of N_{ϕ_0} , found by either of these two schemes, is

$$N_{\phi_0} = \frac{\gamma a^2}{6} \quad (6-23)$$

Hence, from (6-22) we obtain

$$N_\phi = \frac{\gamma a^2}{\sin^2 \phi} \left(\frac{\cos^3 \phi}{3} - \frac{\cos^2 \phi}{2} + \frac{1}{6} - \frac{H \cos^2 \phi}{a} \frac{1}{2} \right) \quad (6-24)$$

which, after some simplification, yields

$$N_\phi = \frac{\gamma a^2}{6} \frac{(1 - \cos \phi)(1 + 2 \cos \phi)}{1 + \cos \phi} - \frac{\gamma a^2 H}{2} \frac{\cos^2 \phi}{a \sin^2 \phi} \quad \frac{\pi}{2} \leq \phi \leq \alpha \quad (6-25)$$

Also, from (6-9b) we have

$$N_\theta = \gamma a^2 \left(\frac{H}{a} + 1 - \cos \phi \right) - N_\phi \quad (6-26)$$

Substituting N_ϕ from (6-24) and simplifying, we obtain

$$N_\theta = \frac{\gamma a^2}{\sin^2 \phi} \left(\frac{5 - 6 \cos \phi - 3 \cos^2 \phi + 4 \cos^3 \phi}{6} \right) + \frac{\gamma a^2}{\sin^2 \phi} \left(\frac{2 - \cos^2 \phi}{2} \right) \frac{H}{a} \quad (6-27)$$

or

$$N_\theta = \frac{\gamma a^2}{6} \frac{(1 - \cos \phi)(5 + 4 \cos \phi)}{1 + \cos \phi} + \frac{\gamma a^2}{2} \frac{2 - \cos^2 \phi}{\sin^2 \phi} \frac{H}{a} \quad \frac{\pi}{2} \leq \phi \leq \alpha \quad (6-28)$$

The expressions (6-25) and (6-28) give values of N_ϕ and N_θ for $\pi/2 \leq \phi \leq \alpha$. For $\alpha \leq \phi$, the effect of the line load coming from the support reaction must also be incorporated.

The total support reaction, V , is equal to the weight of the liquid in the tank. Hence

$$V = \left(\frac{2}{3} \pi a^3 + \pi a^2 H + \frac{2}{3} \pi a^3 \right) \gamma = \left(\frac{4}{3} \pi a^3 + \pi a^2 H \right) \gamma \quad (6-29)$$

Using the relation (6-12), we add a term to the expression for N_ϕ from relation (6-24), to find (for $\alpha \leq \phi$), the following expression:

$$\begin{aligned} N_\phi &= \frac{\gamma a^2}{\sin^2 \phi} \left(\frac{\cos^3 \phi}{3} - \frac{\cos^2 \phi}{2} + \frac{1}{6} - \frac{H \cos^2 \phi}{a \cdot 2} \right) \\ &\quad + \frac{4}{3} \frac{\pi a^3 \gamma}{2 \pi a \sin^2 \phi} + \frac{\pi a^2 \gamma H}{2 \pi a \sin^2 \phi} \\ \text{or} \quad N_\phi &= \frac{\gamma a^2}{\sin^2 \phi} \left(\frac{\cos^3 \phi}{3} - \frac{\cos^2 \phi}{2} + \frac{5}{6} \right) + \frac{\gamma a^2 H}{2} \left(\frac{1 - \cos^2 \phi}{\sin^2 \phi} \right) \\ N_\phi &= \frac{\gamma a^2}{6} \left(\frac{2 \cos^2 \phi - 5 \cos \phi + 5}{1 - \cos \phi} \right) + \frac{\gamma a^2 H}{2} \quad \phi > \alpha \end{aligned} \quad (6-30)$$

The value of the hoop force, N_θ , for this region is

$$N_\theta = \frac{\gamma a^2}{6} \left(\frac{4 \cos^2 \phi - 7 \cos \phi + 1}{1 - \cos \phi} \right) + \frac{\gamma a^2 H}{2} \frac{H}{a} \quad \phi > \alpha \quad (6-31)$$

From expressions (6-30) and (6-31) we see that in the region $\alpha \leq \phi$ the membrane forces N_ϕ and N_θ are always positive. This is true since the shell below the ring support is actually "hanging" from the ring and thus carrying the load by tension. For $120^\circ \leq \phi$, N_ϕ and N_θ are given by the expressions (6-25) and (6-28).

Having obtained a general solution to cylinder-sphere pressure vessel, we now consider the following special cases :

(1) $H/a = 0$. In this case, we have the complete spherical tank which was treated before. In this case, N_θ is always positive (i.e., tensile) whereas N_ϕ is negative in the region $120^\circ \leq \phi$, as seen from (6-25).

For the metallic tanks buckling of the shell is a problem and so the compressive forces must be taken seriously. On the other hand, all metallic materials can sustain tensile stresses efficiently. Therefore, in the design of a metallic shell it would be desirable to place the support at such an angle that both N_ϕ and N_θ are tensile throughout the shell body.

(2) $H/a = 1$. In this case, in the region $112.5^\circ \leq \phi$, the meridional force N_ϕ is compressive. For H/a much larger than unity, N_ϕ would be compressive throughout the region $90^\circ \leq \phi$. Comparing this case with the previous one, we conclude that to insure the existence of a tensile N_ϕ field, the angle α , determining the location of the support, should vary from 90° (for very large H/a) to 120° (for $H/a = 0$). The expression (6-28) shows that the corresponding hoop forces N_θ will also be tensile.

In this liquid tank problem, as in the previous example, the internal forces at the ring support location are discontinuous. The role of the supporting and stiffening ring is to absorb the differences between the internal forces. Due to the incompatibility of deformation at two sides of the ring, some bending field develops in that region. This state of affairs is demonstrated in figure (6-13).

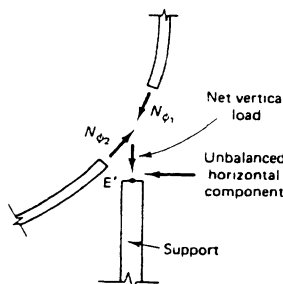


Figure (6-13) Interaction of forces at the ring support of a combined cylindrical and spherical pressure vessel

6.6.3 - Pressure Vessels

Pressure vessels are used to store pressurized liquids or gases; they must resist high internal fluid pressures. Pressure vessels are normally built of metals and / or composite materials. In such constructions, the stresses due to the weight of the vessel are negligible compared with the internal pressure-induced stresses.

Pressure vessels are normally shells of revolution. In this section, we will determine the internal membrane forces in axisymmetric pressure vessels with arbitrary meridional geometries.

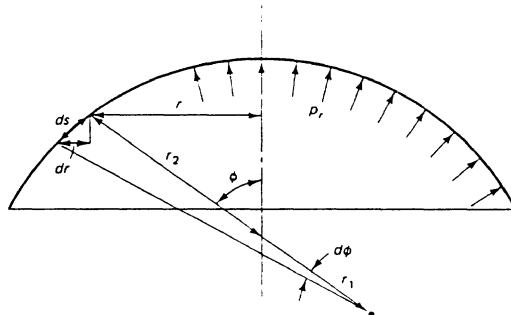


Figure (6-14) Part of a pressure vessel having an arbitrary meridional shape which intersects the axis of revolution

Consider a pressure vessel having an arbitrary meridional shape of radius r_1 , as shown in figure (6-14). If the internal pressure is assumed to be equal to p , then the applied force components will be

$$P_\theta = 0, \quad P_\phi = 0, \quad P_r = p \quad (6-32)$$

Substituting these values into the formula (6-11) we obtain

$$N_\phi = \frac{1}{r_2 \sin^2 \phi} \int_0^\phi r_1 r_2 p \cos \phi \sin \phi d\phi = \frac{p}{r_2 \sin^2 \phi} \int_0^r r dr \quad (6-33)$$

This integration can be performed without assuming a specific shell surface; using the expression (6-9b) we obtain:

$$N_\phi = \frac{1}{2} p r_2, \quad N_\theta = p r_2 \frac{2r_1 - r_2}{2r_1} \quad (6-34)$$

For the special case of a spherical pressure vessel of radius a , the expressions yield $N_\phi = N_\theta = pa/2$. For a cylindrical pressure vessel having $r_1 = \infty$, and $r_2 = a$, we find $N_\phi = pa/2$ and $N_\theta = pa$.

6.7 - Shells of Revolution with Nonaxisymmetric Loading

Shells structures can be subjected to loadings which are not axisymmetric. Examples of nonaxisymmetric loadings are: wind forces, earthquake effects, soil pressure on buried pipes, and temperature gradients in composite and / or metallic shells.

To perform a membrane analysis of rotationally symmetric shells under arbitrary loading, we must use all three coupled simultaneous partial differential equations (6-6), (6-7), and (6-8). If we eliminate N_θ from these equations, we obtain the following relations:

$$r_2 \frac{\partial N_\phi}{\partial \phi} \sin \phi + (r_1 + r_2) N_\phi \cos \phi + r_1 \frac{\partial N_\phi \theta}{\partial \theta} = - r_1 r_2 (P_\phi \sin \phi - \frac{P_r}{\partial N_\phi} \cos \phi) \quad (6-34a)$$

$$\begin{aligned} r_2 \frac{\partial N_\phi \theta}{\partial \phi} \sin \phi + 2r_1 N_\phi \theta \cos \phi - r_2 \frac{\partial N_\phi}{\partial \theta} \\ = - r_1 r_2 (P_\theta \sin \phi + \frac{\partial P_r}{\partial \theta}) \end{aligned} \quad (6-34b)$$

For a distributed loading we can expand the loading functions, p_ϕ , p_θ , and p_r , in terms of Fourier series. These expansions have the following forms:

$$\begin{aligned} P_\phi &= \sum_0^\infty p_{\phi n} \cos n\theta + \sum_1^\infty q_{\phi n} \sin n\theta \\ P_\theta &= \sum_1^\infty p_{\theta n} \sin n\theta + \sum_0^\infty q_{\theta n} \cos n\theta \\ P_r &= \sum_0^\infty p_{rn} \cos n\theta + \sum_1^\infty q_{rn} \sin n\theta \end{aligned} \quad (6-35)$$

For known loadings, the so-called "Fourier coefficients" $p_{\phi n}, p_{\theta n}, q_{\phi n}, \dots$, can be determined using Fourier series analysis.

Equations (6-34a,b) have solutions which are separable in θ and ϕ . For each value of n there are two different solutions: one in which p_ϕ , p_θ , N_ϕ , N_θ are functions of ϕ multiplied by $\cos n\theta$, while p_θ , $N_{\phi\theta}$ are functions of ϕ multiplied by $\sin n\theta$; another in which $\cos n\theta$ and $\sin n\theta$ are interchanged. Both solutions are found in the same way; for the first we write

$$P_\phi = p_{\phi n} \cos n\theta, \quad P_\theta = p_{\theta n} \sin n\theta, \quad P_r = p_{rn} \cos n\theta \quad (6-36)$$

$$N_\phi = N_{\phi n} \cos n\theta, \quad N_\theta = N_{\theta n} \cos n\theta, \quad N_{\phi\theta} = N_{\phi\theta n} \sin n\theta \quad (6-37)$$

where, $N_{\phi n}$, $N_{\theta n}$, and $N_{\phi\theta n}$ are, in general, functions of ϕ . Substituting these expressions into (6-37) and cancelling the common factor of $\cos n\theta$ in (6-34a), $\sin n\theta$ in (6-34b) we find

$$\frac{dN_{\phi n}}{d\phi} + \left(1 + \frac{r_1}{r_2}\right) N_{\phi n} \cot \phi + n \frac{N_{\phi\theta n}}{\sin \phi} \frac{r_1}{r_2} = r_1 (-P_{\phi n} + P_{rn} \cot \phi) \quad (6-38a)$$

$$\frac{dN_{\phi\theta n}}{d\phi} + 2 \frac{r_1}{r_2} N_{\phi\theta n} \cot \phi + n \frac{N_{\phi n}}{\sin \phi} = r_1 (-P_{\theta n} + \frac{n}{\sin \phi} P_{rn}) \quad (6-38b)$$

These ordinary differential equations can be solved analytically or numerically. Since equations (6-34) are linear we may superimpose any of these solutions to obtain other solutions; typical shell analyses and designs are based on just one or two terms.

6.8 - Wind-Induced Stresses in Domes

For a simple model of wind forces, acting on the shells of revolution, we assume the following distribution,

$$P_\phi = 0, \quad P_\theta = 0, \quad P_r = P_{r_1} \cos \theta = -P \sin \phi \cos \theta \quad (6-39)$$

For a hemispherical dome of radius a subjected to this wind effect. equations (6-38) become:

$$\begin{aligned} \frac{dN_{\phi n}}{d\phi} + 2 \cot \phi N_{\phi n} + \frac{n}{\sin \phi} N_{\phi\theta n} &= a (-P_{\phi n} + \cot \phi P_{rn}) \\ \frac{dN_{\phi\theta n}}{d\phi} + 2 \cot \phi N_{\phi\theta n} + \frac{n}{\sin \phi} N_{\phi n} &= a (-P_{\theta n} + \frac{n}{\sin \phi} P_{rn}) \end{aligned} \quad (6-40)$$

In terms of the new variables:

$$\begin{aligned} U &= N_{\phi n} + N_{\phi\theta n} \\ V &= N_{\phi n} - N_{\phi\theta n} \end{aligned} \quad (6-41)$$

the equations become:

$$\begin{aligned}\frac{dU}{d\phi} + (2\cot\phi + \frac{n}{\sin\phi})U &= a(-P_{\theta n} - P_{\phi n} + \frac{n+\cos\phi}{\sin\phi} P_{rn}) \\ \frac{dV}{d\phi} + (2\cot\phi - \frac{n}{\sin\phi})V &= a(P_{\theta n} - P_{\phi n} - \frac{n-\cos\phi}{\sin\phi} P_{rn})\end{aligned}\quad (6-42)$$

Each of these first order differential equations has the form:

$$\frac{dU}{d\phi} + P(\phi) \cdot U + q(\phi) = 0 \quad (6-43)$$

The general solution to this equation is

$$U = [C - \int q \exp(\int P d\phi) d\phi] \cdot \exp(-\int P d\phi) \quad (6-44)$$

With the help of relations (6-39) and (6-44) we find:

$$\begin{aligned}U &= \frac{1+\cos\phi}{\sin^3\phi} [A_1 + Pa(\cos\phi - \frac{1}{3}\cos^3\phi)] \\ V &= \frac{1-\cos\phi}{\sin^3\phi} [B_1 - Pa(\cos\phi - \frac{1}{3}\cos^3\phi)]\end{aligned}\quad (6-45)$$

Returning to the relations (6-41) and multiplying the resulting expressions, for the actual field variables $N_{\phi n}$ and $N_{\phi\theta n}$, by $\cos\theta$ and $\sin\theta$, respectively, we obtain

$$\begin{aligned}N_{\phi} &= \frac{\cos\theta}{\sin^3\phi} \left[\frac{A_1 + B_1}{2} + \frac{A_1 - B_1}{2} \cos\phi + Pa(\cos^2\phi - 1/3 \cos^4\phi) \right] \\ N_{\phi\theta} &= \frac{\sin\theta}{\sin^3\phi} \left[\frac{A_1 - B_1}{2} + \frac{A_1 + B_1}{2} \cos\phi + Pa(\cos\phi - 1/3 \cos^3\phi) \right]\end{aligned}$$

The integration constants A_1 and B_1 can be determined by imposing the physical condition that N_{ϕ} and $N_{\phi\theta}$ must be finite at $\phi = 0$. Hence, after some algebraic manipulations, we obtain the following final solution to the problem

$$\begin{aligned}N_{\phi} &= -\frac{Pa}{3} \frac{(2 + \cos\phi)(1 - \cos\phi)}{(1 + \cos\phi)\sin\phi} \cos\phi \\ N_{\phi\theta} &= -\frac{Pa}{3} \frac{(2 + \cos\phi)(1 - \cos\phi)}{(1 + \cos\phi)\sin\phi} \sin\theta \\ N_{\theta} &= -\frac{Pa}{3} \frac{(3 + 4\cos\phi + 2\cos^2\phi)(1 - \cos\phi)}{(1 + \cos\phi)\sin\phi} \cos\theta\end{aligned}\quad (6-46)$$

Plots of variations of internal forces in this shell are presented in figure (6-15). Note that because the loading and the behavior of the shell is not axisymmetric there is a nonzero membrane shear force field, as well as normal membrane forces. Therefore, the meridional curves and parallel circles no longer represent the principal directions of the internal stresses. For the present case, the plan form of the stress trajectories is shown in the figure (6-16).

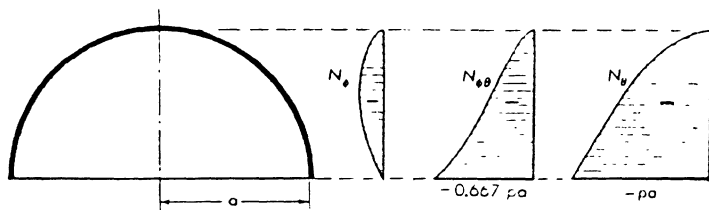


Figure (6-15) Variations of internal membrane forces in a hemispherical dome subjected to lateral wind loading

Having found the three components of membrane forces in the ϕ and θ directions we can use the well-known transformation formulas to find the membrane forces in an arbitrary direction. Specifically, we can determine the principal forces and the directions of principal stresses. Using such relations we can plot two orthogonal families of curves indicating the principal directions. These are called *the stress trajectories*. Figure (6-16) shows the plan of the stress trajectories for a hemispherical dome subjected to lateral wind forces.

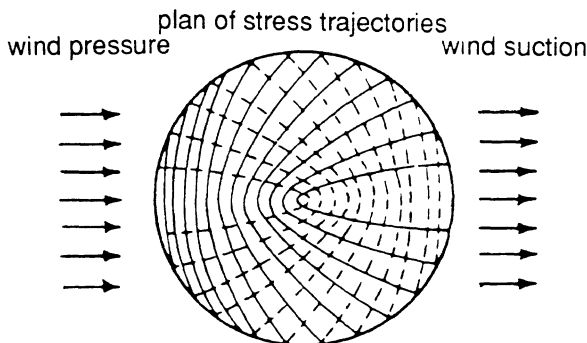


Figure (6-16) Stress trajectories in a spherical dome subjected to lateral wind loading

In figure (6-16), the solid and dashed lines indicate the compressive and tensile principal stresses, respectively. Thus, the behavior of the dome under wind forces can be conceived to consist of combined arch and cable actions.

6.9 - Displacements of Axisymmetric Shells

The displacement vector in a rotational shell of double curvature generally has meridional, hoop, and normal components. If the applied loading is symmetrical, then the hoop component of the displacement vector is zero. In these truly axisymmetric problems there are only the displacement components along the meridional and normal to the shell are to be determined.

Consider an infinitesimal element, AB, taken from the meridional section of the shell. This element is deformed into A'B', as shown in the figure (6-17). The positive meridional displacement, v , is taken in the direction of increasing ϕ , the positive normal displacement, w , is taken inwards.

The change of length of element AB is composed of two parts: one part arises from the meridional differential displacement, $(dv/d\phi) \times d\phi$; the other from the normal displacement, $(w) \times d\phi$. With the adopted the sign conventions, the total change of length of element AB is,

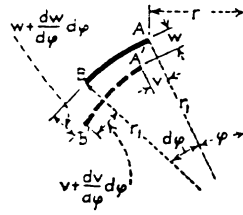


Figure (6-17) A meridional element of the shell and its symmetrically deformed configuration

The meridional strain is obtained by dividing the above change of length to the undeformed length of the element ($r_1 d\phi$). So, the expression for meridional strain is,

$$\epsilon_{\phi} = \frac{1}{r_1} \frac{dv}{d\phi} - \frac{w}{r_1} \quad (6-47)$$

As we see, the meridional component of strain is also affected by the normal displacement, w , as well as the meridional displacement, v . This result has a simple physical interpretation which is offered as follows:

Suppose that a spherical membrane "balloon" is inflated by an inner pressure. The balloon will expand symmetrically so that only there is a radial component of the displacement, w .

The meridional strain is equal to the change of diameter divided by the original diameter, i.e., (w/r) . In this example, $dv/d\phi = 0$.

To determine the hoop strain, we consider a hoop element of the shell. Figure (6-18) shows the change of radius, Δr , of the parallel circle passing through this element. Referring to this figure we find the following expression:

$$+\xrightarrow{-} \Delta r = v \cos \phi - w \sin \phi \quad (6-48)$$

The arrow above Δr indicates the assumed positive direction.

Since the circumferential length change is proportional to the the change in the radius, so the hoop strain is

$$\varepsilon_{\theta} = \frac{1}{r} (v \cos \phi - w \sin \phi)$$

and since $r = r_2 \sin \phi$ we may write

$$\varepsilon_{\theta} = \frac{v}{r_2} \cot \phi - \frac{w}{r_2} \quad (6-49)$$

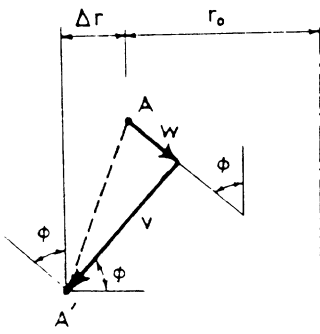


Figure (6-18) Shell displacement components leading to the change of radius of a typical parallel circle

Expressions (6-47) and (6-49) constitute the strain-displacement relations of a rotational shell undergoing axisymmetric deformation. If we eliminate the normal displacement function, w , between these relations, we obtain the following differential equation for the meridional displacement component v .

$$\frac{dv}{d\phi} - v \cot \phi = r_1 \varepsilon_{\phi} - r_2 \varepsilon_{\theta} \quad (6-50)$$

Having obtained the kinematic relations and equilibrium equations we now write down the third group of governing relations, i.e., the constitutive relations. If the shell is linearly elastic and isotropic, the two dimensional elastic constitutive relations, for a local state of plane stress, are

$$\begin{aligned}\varepsilon_z &= \frac{1}{Et} (N_\phi - v N_\theta) \\ \varepsilon_\phi &= \frac{1}{Et} (N_\theta - v N_\phi)\end{aligned}\quad (6-51)$$

Substituting these relations into (6-50) we obtain

$$\frac{dv}{dz} - v \cot \phi = \frac{1}{Et} [N_\phi(r_1 + vr_2) - N_\theta(r_2 + vr_1)] \quad (6-52)$$

Suppose that we have carried out a stress analysis the shell. Then we know the membrane forces, N_ϕ and N_θ . Furthermore, we can express the shell radii of curvature, r_1 and r_2 , as functions of ϕ . This means that the right-hand side of equation (6-52) is a known function of ϕ . Representing this function by $f(\phi)$, we may write the general form of equation (6-50) as

$$\frac{dv}{d\phi} - v \cot \phi = f(\phi) \quad (6-53)$$

To solve this equation, we make use of the following identity:

$$\frac{d}{d\phi} \left(\frac{v}{\sin \phi} \right) = \frac{\frac{dv}{d\phi} \sin \phi - v \cos \phi}{\sin^2 \phi} = \frac{1}{\sin \phi} \left(\frac{dv}{d\phi} - v \cot \phi \right)$$

Therefore

$$\frac{dv}{d\phi} - v \cot \phi = \sin \phi \frac{d}{d\phi} \left(\frac{v}{\sin \phi} \right) = f(\phi)$$

or

$$\frac{d}{d\phi} \left(\frac{v}{\sin \phi} \right) = \frac{1}{\sin \phi} f(\phi)$$

The general solution to the above equation, obtained by direct integration, is

$$v = \sin \phi \left[\int \frac{f(\phi)}{\sin \phi} d\phi + C \right] \quad (6-54)$$

Having obtained the meridional displacement function, v , we can now use either of the two relations (6-47) or (6-49) to find the normal component of displacement, w .

6.10 - Membrane Deformation of Spherical Domes

Consider the spherical dome of figure (6-8) subjected to its own weight. The membrane forces in this dome were obtained earlier and are given in relations (6-14). To determine the deformation field in this shell, we use the relations developed in section (6-9). Using the expressions (6-14), and noting that $r_1 = r_2 = a$, we rewrite the equation (6-52) in the following form:

$$\frac{dv}{d\phi} - v \cot \phi = \frac{a^2 q(1+v)}{Et} (\cos \phi - \frac{2}{1+\cos \phi}) \quad (6-55)$$

so that the function $f(\phi)$ is

$$f(\phi) = A (\cos \phi - \frac{2}{1+\cos \phi}) , \quad A = \frac{a^2 q(1+v)}{Et} \quad (6-56)$$

We substitute this expression into the general solution (6-54) and perform the integration on the variable ϕ to obtain:

$$\begin{aligned} \int \frac{f(\phi)}{\sin \phi} d\phi &= A \int \left[\frac{\cos \phi}{\sin \phi} - \frac{2}{(1+\cos \phi)\sin \phi} \right] d\phi \\ &= A \int \frac{\cos \phi + \cos^2 \phi - 2}{\sin \phi (1+\cos \phi)} d\phi = A \left[\int \frac{-\sin \phi}{1+\cos \phi} d\phi + \int \frac{\cos \phi - 1}{\sin \phi (1+\cos \phi)} d\phi \right] \\ \frac{1}{A} \int \frac{f(\phi)}{\sin \phi} d\phi &= \ln (1+\cos \phi) + \int \frac{\cos \phi - 1}{\sin \phi (1+\cos \phi)} d\phi \\ \int \frac{\cos \phi - 1}{\sin \phi (1+\cos \phi)} d\phi &= \int \frac{-2 \sin^2 \frac{\phi}{2}}{2 \sin^2 \frac{\phi}{2} \cos^2 \frac{\phi}{2} \cdot 2 \cos \frac{2\phi}{2}} = \int \frac{-\sin \phi / 2}{2 \cos^3 \phi / 2} d\phi \\ \cos \frac{\phi}{2} = x \implies -\frac{1}{2} \sin \frac{\phi}{2} d\phi &= dx \\ \int \frac{-\sin \phi / 2}{2 \cos^3 \phi / 2} d\phi &= \int \frac{dx}{x^3} = -\frac{1}{2x^2} = -\frac{1}{2 \cos^2 \phi / 2} = \frac{-1}{1+\cos \phi} \end{aligned}$$

Therefore

$$\begin{aligned} \frac{1}{A} \int \frac{f(\phi)}{\sin \phi} d\phi &= \ln (1+\cos \phi) - \frac{1}{1+\cos \phi} \\ v &= \frac{a^2 q(1+v)}{Et} \sin \phi \left[\ln (1+\cos \phi) - \frac{1}{1+\cos \phi} \right] + C \sin \phi \end{aligned} \quad (6-57)$$

At $\phi = \alpha$, we have $v = 0$, so that

$$C = \frac{a^2 q (1+v)}{Et} \left[\frac{1}{1+\cos\alpha} - \ln(1+\cos\alpha) \right]$$

With $v(\phi)$ determined, we can find $w(\phi)$ from either of the two relations (6-47) or (6-49); the latter gives:

$$w = -a\varepsilon_\theta + v \cot\phi = -\frac{a}{Et} N_\theta + v \cot\phi \quad (6-58)$$

In particular we may find the horizontal displacement at the base of the dome ΔH (at $\phi = \alpha$).

$$\Delta H = r \varepsilon_\theta = \frac{a^2 q}{Et} \left(\frac{1+v}{1-\cos\alpha} - \cos\alpha \right) \sin\alpha \quad (6-59)$$

Numerical Example 6.2

Determine the vertical displacement at the apex of a hemispherical dome under its own weight. The numerical data of the problem are:

$$\begin{aligned} a &= 6.0 \text{ m} , \quad t = 10 \text{ cm} , \quad \alpha = 60^\circ \\ q &= 150 \text{ kg/m}^2 \\ E &= 2 \times 10^5 \text{ kg/cm}^2 , \quad v = 0 \end{aligned}$$

Solution:

Using the expression (6-57) in (6-58), we have

$$w = -\frac{qa^2}{Et} \left(\frac{1}{1+\cos\phi} - \cos\phi \right) + \frac{a^2 q}{Et} \cos\phi \left[\ln(1+\cos\phi) - \frac{1}{1+\cos\phi} \right] + C \cos\phi$$

and since

$$C = \frac{a^2 q}{Et} \left[\frac{2}{3} + \ln(1.5) \right]$$

therefore

$$w = \frac{a^2 q}{Et} \left\{ -\left(\frac{1}{1+\cos\phi} - \cos\phi \right) + \cos\phi \left[\ln(1+\cos\phi) - \frac{1}{1+\cos\phi} \right] + \left(\frac{2}{3} - \ln 1.5 \right) \cos\phi \right\}$$

At the apex of the dome $\phi = 0$, we have

$$w = \frac{a^2 q}{Et} \left[+\frac{1}{2} + (\ln 2 - 1/2) - (\ln 1.5 - 2/3) \right] = \frac{(6.0)^2 \times 150 \times 0.954}{2 \times 10^5 \times 10} = 0.03 \text{ mm}$$

This dome has a relatively large span of $2a = 12.0$ meters. In spite of this, the central deflection is indeed very small. It would be instructive to compare this negligibly small value with relatively high central deflection of a beam element having the same span and loading conditions. We would conclude that a dome is several orders of magnitude stiffer than a corresponding beam structure. As was pointed out before, this high degree of structural stiffness is typical of all shell forms.

6.11 - Qualitative Description of Dome Behavior

The membrane field of internal forces in domes consists of a meridional force, a hoop force, and a membrane shear force, figure (6-19a). For axisymmetric loading of domes, the membrane shear is zero throughout and the internal force field consists of meridional and hoop forces only, figure (6-19b).

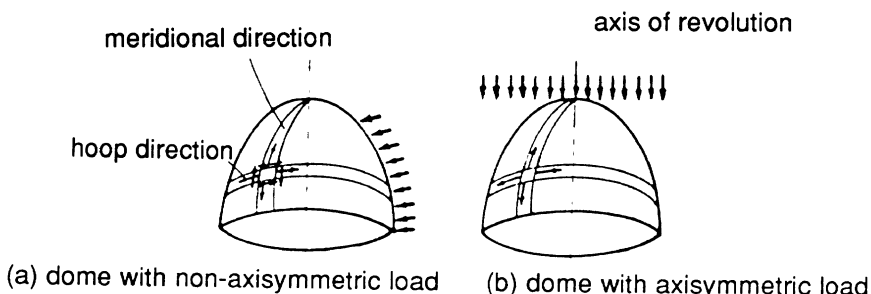


Figure (6-19) State of internal membrane force field in domes,(a) generally non-symmetrical loading, (b) symmetric loading

For axisymmetric loading of domes, the stress trajectories, i.e., the directions of principal normal stresses, will coincide with meridional and hoop curves; the shear stress is identically zero along these directions, figure (6-19b).

Figure (6-20a) show the stress trajectories for a symmetrically loaded continuously supported spherical dome. As we have seen before, from our membrane analysis of domes, the meridional force is compressive throughout the shell, while the hoop force has a change of sign from compression to tension. In this figure, the compression field of principal stresses are plotted by solid curves while the tension stress trajectories are sketched by dashed lines.

Figure (6-20b) shows the stress trajectories for a spherical dome with four concentrated supports under vertical symmetric loading. This figure reveals the flow of forces towards the supports and the resulting stress concentration near the point supports. A bending field will develop at these supports to compensate for the shortcomings of the membrane behavior.

The structural behavior of domes can be conceived as the interaction of two mechanisms: (1) *arch action* of the shell along the meridional direction; (2) *ring action* of the shell in the hoop direction. The interaction of these two mechanisms gives rise to an efficient spatial behavior of the doubly curved shell.

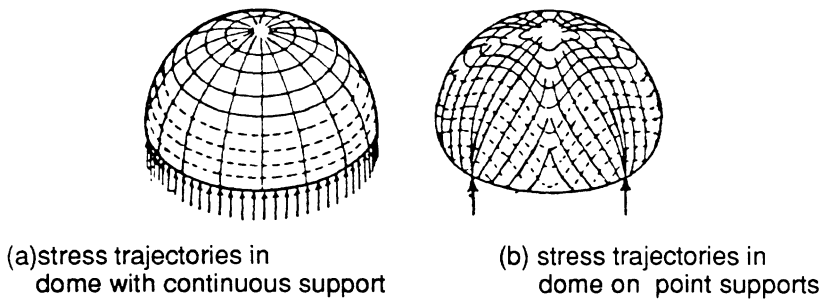


Figure (6-20) Compressive principal stresses (solid lines) and tensile principal stresses (dashed lines) in hemispherical domes under vertical loading; (a) distributed vertical support, (b) four point supports

Sometimes domes are provided with edge supporting and / or stiffening rings. For example, when there is only a vertical support (such as a supporting wall) the horizontal thrust must be absorbed by a ring, figure (6-21). To stiffen a dome the designer may place a stiffening ring at the intersection of the dome with other structural elements.

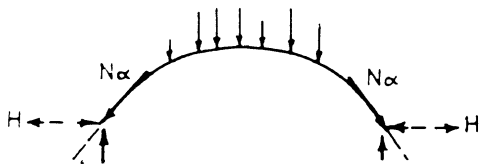


Figure (6-21) Vertical and horizontal edge forces in a dome

Figure (6-22a) shows a dome roof with an edge ring. Figure (6-22b) shows a liquid storage tank with a cylindrical wall, a dome roof, and a stiffening ring at the intersection of the two shell types.

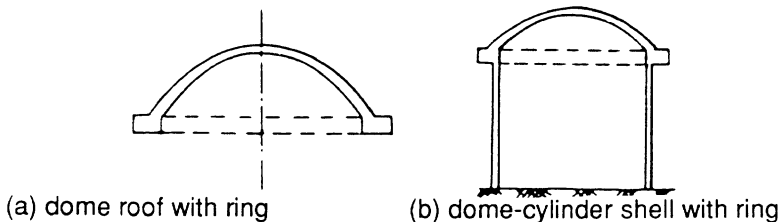


Figure (6-22) Domes with rings, (a) a dome with supporting ring, (b) a combined cylindrical liquid storage tank with a stiffening ring

The spatial load-bearing behavior of domes can be well contrasted to that of the arches. Figure (6-23) gives a graphical comparison between an *arch* and a *dome*. For example, the effect of boundary shear effect in the dome is local whereas the bending effect in an arch is global. Figure (6-23) show the variation of the bending moment caused by the edge shear in the shell and the bending moment diagram in an arch under edge force subjected to a distributed loading.

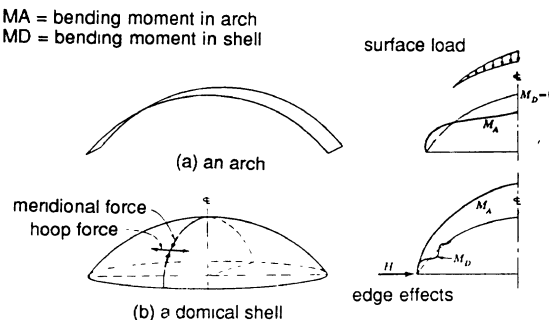


Figure (6-23) Comparison of a dome with an arch subjected to bending, (a) global propagation of bending effect in the arch, (b) local influence of edge shear in the shell

The overall membrane behavior of domes with or without rings is graphically represented in figures (6-24). All these domes have distributed supports and are subjected to axisymmetric vertical loading.

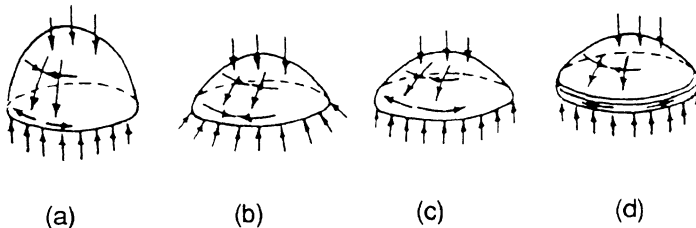


Figure (6-24) Membrane behavior of axisymmetrically loaded domes, (a) high rise dome with vertical support, (b) a low rise dome with vertical as well as horizontal support, (c) a low rise dome with vertical support, (d) a low rise dome with vertical support and and edge ring

The arrows in the figure (6-24a) show the sign of membrane field in a high rise dome with no ring and only a vertical support. The tangent to the meridional curve at the lower edge is assumed to be vertical. The meridional force remains compressive, but the hoop stress changes sign. In this shell, the hoop tension is taken by the shell itself and the edge meridional force is carried by the vertical support.

The membrane field (meridian and hoop stresses) in the low rise shell of figure (6-24b) is totally compressive. At the edges of this shell, the inclined meridional force is carried through the support, which is assumed to sustain vertical as well as lateral thrusting forces. The equilibrium requirements of membrane behavior are satisfied for this shell.

The support of low rise shell of figure (6-24c) can only carry vertical forces. Therefore, the horizontal thrust developed by meridional compression must be carried through the shell itself mainly by the mechanism of hoop action. Some tension will be induced in the lower parallel circles, as demonstrated in figure (6-24c). This is obviously contrary to the predictions of membrane theory; there must be a, some bending field in the lower part of this shell to satisfy the equilibrium requirements.

The low rise shell of figure (6-24d) has a supporting ring at the edge together with a vertical support; the horizontal thrust is totally carried by the ring.

6.12 - Conical Shells

Conical shells, as the name implies, have as their middle surface a complete cone, a truncated cone, or a sector of a conical surface. Conical shells are shells of revolution with zero Gaussian curvature. In spite of this feature, these shells are non-developable and thus offer a great resistance to buckling and collapse. Conical shells are used in roofing and flooring of liquid retaining tanks and reservoirs; as for the ends of pressure vessels; the nose cones of spacecrafts and missiles, the roofing of a station or a stand.

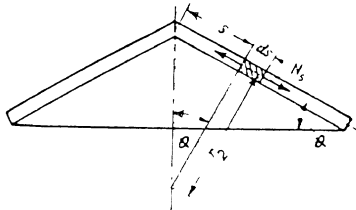


Figure (6-25) A conical shell

In order to perform the membrane analysis of a conical shell, we consider the conical shell of figure (6-25). One of the principal radii of curvature, i.e., r_1 , is infinite, and the meridional angle, ϕ , is constant. We define a new variable, s , as the meridional distance from the apex, and introduce the following change of variables

$$\begin{aligned} \phi &= & dS &= r_1 d\phi \\ r_1 &= \infty & N_\phi &= N_S \\ r_2 &= s \cot\phi & N_{\theta\phi} &= N_{\theta S} \end{aligned} \quad (6-60)$$

Using these new definitions in the membrane equilibrium equations, (6-6), (6-7), and (6-8), we obtain the following governing equations for conical shells

$$\begin{aligned} \frac{\partial}{\partial s} (rN_S) + \frac{\partial N_{\theta S}}{\partial \theta} - N_\theta \cos \phi + P_S r &= 0 \\ \frac{\partial}{\partial s} (rN_{\theta S}) + \frac{\partial N_\theta}{\partial \theta} + N_{\theta S} \cos \phi + P_\theta r &= 0 \\ \frac{N_S}{r_1} + \frac{N_\theta}{r_2} &= P_r \end{aligned} \quad (6-61)$$

For the special cases of symmetrical loadings, the above equations become

$$\frac{d}{ds} (N_S s) - N_\theta = - P_S s \quad (6-62a)$$

$$N_\theta = P_r s \cot \phi \quad (6-62b)$$

Adding up both sides of these relations, we obtain

$$\frac{d}{ds} (N_S S) = - (P_S - P_r \cot \phi) S$$

which, after integration, yields

$$N_S = - \frac{1}{S} \int (P_S - P_r \cot \phi) S ds + \frac{C}{S} \quad (6-63)$$

Expressions (6-63) and (6-62b) give the closed form solution to the membrane force field in axisymmetrically loaded conical shells.

As an example, we consider the **mushroom-type** conical shell shown in figure (6-25a). This shell rests on a single column support at its apex. The loading consists of the dead weight with intensity p . The load components are,

$$P_S = p \sin \alpha, \quad P_r = - p \cos \alpha \quad (6-64)$$

If we substitute these expressions into (6-62b) and (6-63) we find

$$\begin{aligned} N_\theta &= - p S \cos \alpha \cot \alpha \\ N_S &= - \frac{1}{S} \frac{p}{\sin \alpha} \frac{S^2}{2} + \frac{C}{S} \end{aligned} \quad (6-65)$$

To determine the integration constant, C , we use the condition that at the free edge of the shell ($s = l$) the value of meridional force, N_S , is zero; this boundary condition gives

$$C = \frac{p l^2}{2 \sin \alpha}$$

and therefore,

$$N_S = \frac{p}{2} \frac{l^2 - s^2}{S \sin \alpha} \quad (6-66)$$

Figure(6-26a) shows the membrane forces, N_θ and N_S . The meridional force, N_S , becomes infinite at the apex. This is what the membrane theory predicts. Actually, due to concentrated support at the apex, there is some bending field at the apex. Figure (6-26b) shows the sign of the internal forces in this shell.

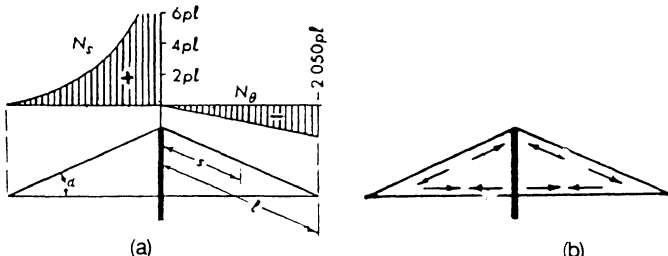


Figure (6-26) A mushroom-type conical shell under its own weight, (a) variation of membrane forces, (b) sign of membrane force field

If this conical shell had a continuous, rather than a point, support at its lower edge, figure (6-27), then the expression for N_θ would remain the same, but the meridional force would be

$$N_s = - \frac{PS}{2\sin \alpha} \quad (6-67)$$



Figure (6-27) Sign of membrane force field in a conical shell with distributed edge support

Figure (6-27) shows the sign of the internal forces for this case. The comparison of the two figures (6-27) and (6-26b) is instructive in the sense that it demonstrates the influence of supporting conditions on the conical shell behavior.

Problems

P 6.1 - Consider the pointed dome shown in figure (P 6-1). This dome has a continuous edge support and is acted upon by its own weight. The meridian is a circular arch of radius a . The angle of normal to meridional curve at the shell apex with the vertical is ϕ_0 . Hence, the principal radii of curvature are,

$$r_1 = a$$

and

$$r_2 = \frac{r}{\sin \phi} = a \left(1 - \frac{\sin \phi_0}{\sin \phi}\right)$$

Derive the following expressions for the membrane forces in this pointed dome.

$$\begin{aligned} N_\phi &= - \frac{Pa}{(\sin \phi - \sin \phi_0) \sin \phi} \int_{\phi_0}^{\phi} (\sin \phi - \sin \phi_0) d\phi \\ &= - \frac{Pa}{(\sin \phi - \sin \phi_0) \sin \phi_0} \\ N_\theta &= - \frac{Pa}{\sin^2 \phi} [(\phi - \phi_0) \sin \phi_0 - (\cos \phi_0 - \cos \phi) + (\sin \phi - \sin \phi_0) \cos \phi \sin \phi] \end{aligned}$$

Also, plot the membrane force field variation with the angle ϕ , and thus reproduce the diagrams shown in figure (P 6-1).

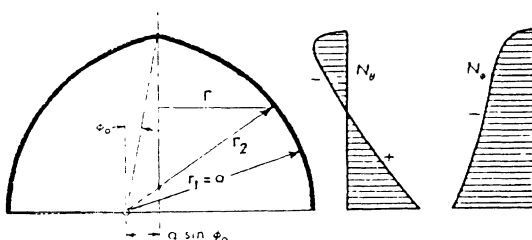


Figure (P 6-1): A pointed dome under its own weight

P 6.2 - A circular cylindrical grain silo is suspended from its top and has a conical bottom (hopper) as shown in figure (P 6-2). The thickness of the shell is t and the unit weight of shell material is g . The conical hopper is open at its bottom. Find the membrane forces in both shells. Explain why a ring may be needed at the junction of the two shells.

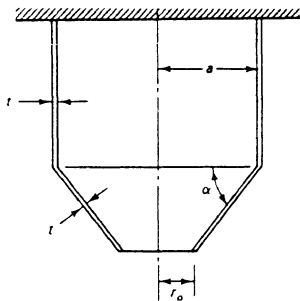


Figure (P 6-2) Grain silo consisting of cylindrical and conical portions

P 6.3 - A conical concrete liquid retaining tank having a dome roof is shown in figure (P 6-3). The tank is filled with water with specific weight of g , and the conical part is subjected to a line load, q (N/m), from the dome roof above as well as being subjected to its own weight. The unit weight of concrete is assumed to be g_c . Derive appropriate expressions for the membrane forces in this conical shell.

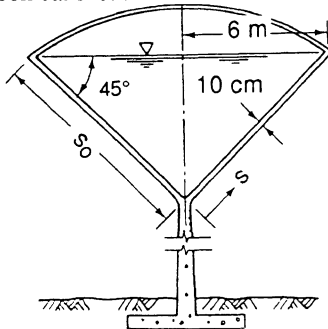


Figure (P 6-3) A conical water tank with dome-like roof

6.4 - Figure (P 6-4) shows a steel cylindrical pressure vessel with conical end caps. Using the membrane theory alone, design the thickness of steel required to resist the internal pressure of $p = 4.0$ bar. The yield stress of the steel is 4000 kg/cm^2 . Where may additional strengthening be required.

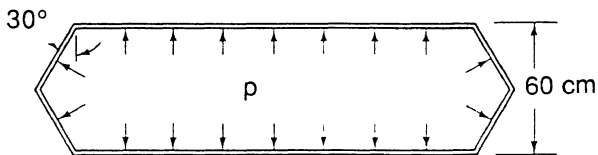


Figure (P 6-4) Cylindrical pressure vessel with conical caps

References for Chapter Six

- 6.1 - M. Farshad, *Shell Structures*, (in Farsi), Shiraz university Publications, Vol. I, 1986, Vol. II, 1987, Shiraz
- 6.2 - M. Salvadori and R. Heller, *Structure in Architecture*, Prentice-Hall, INC,N.J., 1963
- 6.3 - W. Flügge, *Stresses in Shells*, Springer Verlag, Berlin, 1962
- 6.4 - V. S. Kelkar and R. T. Sewell, *Fundamentals of the Analysis and Design of Shell Structures*, Prentice-Hall,INC.,N.J., 1987
- 6.5 - D.P. Billington, *Thin Shell Concrete Structures*, McGraw-Hill Book Co., revised edition, 1982

Chapter 7

Bending Analysis of Axisymmetric Shells

7.1 - Introduction

By the term "axisymmetric shells", in this chapter, we mean all *doubly curved* as well as conical shell forms which have an *axis of symmetry* and are loaded in an axisymmetric fashion. Shells of revolution such as domes, single sheet hyperbolic paraboloids (used in cooling towers), and conical shells fall in this category.

Domes, being doubly curved, are non-developable, synclastic shells; they are the strong, stiff and, stable. The membrane forces dominate the internal force field in a dome. Geometrical and force incompatibilities will cause some bending field to develop, but this bending field is local and is confined to the vicinity of geometrical variations, concentrated forces, and membrane-incompatible boundary conditions.

In chapter six, we discussed the membrane theory of shells of revolution with positive Gaussian curvature, including domes. In the present chapter, we develop a simplified bending theory for axisymmetric shells subject to axisymmetric loading. As a result, we will obtain the influence coefficients which are useful in the force method of axisymmetric shell analysis.

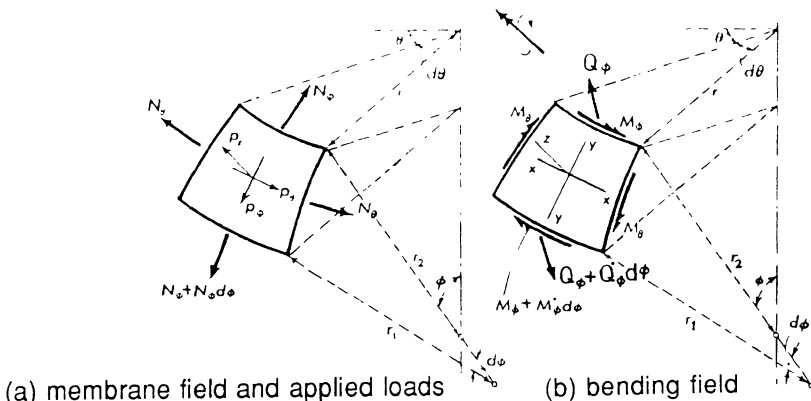
Sometimes axisymmetric shells, and in particular domes, are provided with edge rings. The analysis of domes with edge rings will also be carried out in this chapter. With such an analysis, one can analyze combined shell structures composed of cylindrical walls with dome- or cone-like roofs which are sometimes connected to each other by means of stiffening rings.

The analysis scheme developed in the present chapter can be applied to the design of dome roofs; cylindrical liquid retaining shells with dome roofs; pressure vessels; containment shells of nuclear power plants; as well as other types of axisymmetric shells.

7.2 - Governing Equations for Axisymmetric Shells

7.2.1 - Equilibrium Equations

Consider a shell of revolution subject to axisymmetric loading. Figure(7-1) shows the free-body diagram of an element of this shell. Figure (7-1a) shows the membrane forces and the applied distributed loading while the complementary figure (7-1b) demonstrates the bending force field developed in this shell element. Due to axial symmetry of geometrical and loading conditions, all variables involved are independent of the hoop parameter, q .



Figure(7-1) Free body diagram of a rotational shell with axisymmetric loading, (a) the membrane forces and applied distributed loads, (b) the bending field of internal forces in the shell

The equations of equilibrium consist of three force equations and three moment relations. Due to axisymmetric conditions, and assuming the applied load in θ direction, p_θ , to be zero, the force equation of equilibrium along the θ direction is satisfied identically as are the moment equations of equilibrium about the r and ϕ directions. We are left with three equations of equilibrium which we will now write down.

Because the shell has double curvature, the internal forces have projections in all directions. For example, when writing down the equilibrium of forces in the ϕ direction we should take into consideration the contribution of the shear force, Q_ϕ , as well as the membrane forces, N_ϕ and N_θ . Figure (7-2) shows the projections of membrane and the bending shear force in the ϕ and r directions.

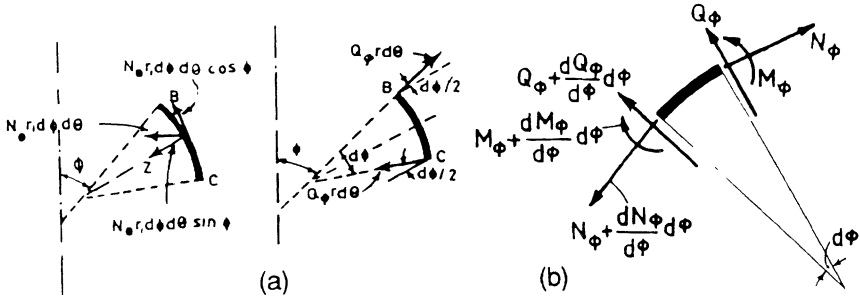


Figure (7-2) Meridional section through a shell element showing the internal forces and their projections, (a) membrane forces, (b) bending shear force

The force equations of equilibrium are, with the help of figure (7-2), written as follows:

$$\frac{d}{d\phi} (N_\phi r) - N_\theta r_1 \cos \phi - r Q_\phi + r r_1 P_\phi = 0 \quad (7-1)$$

$$N_\phi r + N_\theta r_1 \sin \phi + \frac{d(Q_\phi r)}{d\phi} - r r_1 P_r = 0 \quad (7-2)$$

These equations have a more general form than the membrane equations which were derived in chapter six. For instance, the load-bearing contribution of the bending shear force, Q_ϕ , appears in the equilibrium equations.

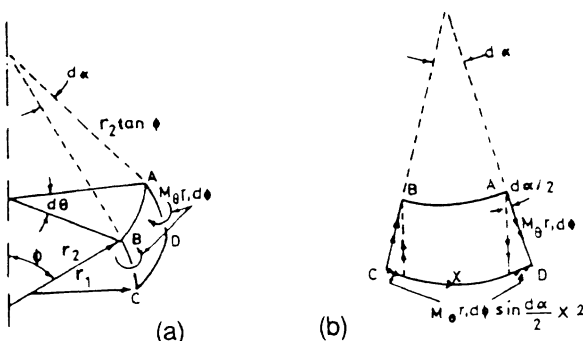


Figure (7-3) A rotationally symmetric shell element with geometrical parameters and hoop bending moments

To derive the moment equation of equilibrium about the θ axis, we make use of the figure (7-3). This figure shows the spatial configuration of shell element and the projections of bending as well as twisting couples. Some useful relations among the geometrical parameters represented in this figure are

$$r = r_2 \sin\phi$$

$$AB = rd\theta = r_2 \sin\phi d\theta$$

$$AB = r_2 \tan\phi \cdot d\alpha$$

$$d\alpha = \cos\phi d\theta$$

The moment equation of equilibrium for the shell element about the θ axis is

$$(M_\phi + \frac{dM_\phi}{d\phi} d\phi) (r + \frac{dr}{d\phi} d\phi) d\theta - M_\phi r d\theta - M_\theta r_1 \cos\phi d\phi d\theta - Q_\phi r_2 \sin\phi r_1 d\phi d\theta = 0$$

which can be simplified to:

$$\frac{d}{d\phi} (M_\phi r) - M_\theta r_1 \cos\phi - Q_\phi r_1 r = 0 \quad (7-3)$$

Equations (7-1), (7-2), and (7-3) constitute three relations among six unknown force quantities N_ϕ , N_θ , M_ϕ , M_θ , and Q_ϕ . This means that the shell is statically indeterminate and three more relations are needed to find the internal forces. These additional relations are provided by the kinematic and constitutive equations.

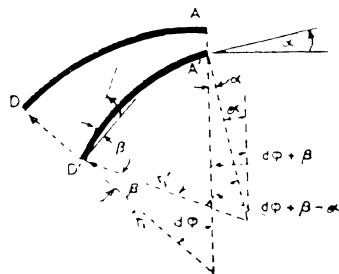
7.2.2 - Kinematic Relations

Kinematic relations relate the strains and the change of curvature with the components and gradients of the displacement vector. In this axisymmetric case, the displacement components are the displacement normal to the shell surface, w , and the displacement component along the meridian, v . These quantities are, in general, functions of meridional parameter, ϕ . Due to axial symmetry, the hoop displacement is identically zero. In chapter six, we have already obtained the following strain-displacement relations.

$$\epsilon_\phi = \frac{1}{r_1} \frac{dv}{d\phi} - \frac{w}{r_1}, \quad \epsilon_\beta = \frac{v}{r_2} \cot\phi - \frac{w}{r_2} \quad (7-4)$$

To derive the relations between curvature changes and displacement components, we consider a meridional section of the shell in the undeformed and deformed configurations,

as shown in the figure (7-4). In this figure, AD and A'D' represent the undeformed and deformed meridional sections, respectively.



Figure(7-4) The undeformed and deformed meridional sections of the axisymmetric shell

The angle which the tangent to the meridian at A makes with the initial direction of the tangent line is designated by α . This change in meridional tangents is brought about by both v and w displacement components. Figure (7-5a), shows the effect of meridional displacement on the infinitesimal rotation of the tangent. This part of rotation is designated by $\delta_1 = v / r_1$. Figure (7-5b) shows the effect of normal displacement on the angle of meridional rotation. This contribution is easily seen to be equal to $\delta_2 = (dw) / (r_1 d\phi)$. The total angle α is

$$\alpha = \delta_1 + \delta_2 = \frac{v}{r_1} + \frac{dw}{r_1 d\phi} \quad (7-5)$$

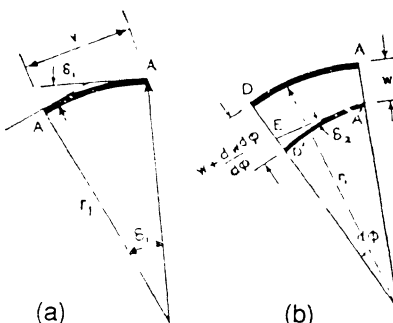


Figure (7-5) Meridional sections through axisymmetric shell element showing contributions of displacement components to the change of angle of tangent to the meridional curve at point A.

The angle between the meridional tangent and the tangent for a neighboring point D, figure (7-4), is simply equal to that of point A plus the differential change in α . Thus, if we designate this angle at point D by β , we have

$$r = \frac{v}{r_1} + \frac{dw}{r_1 d\phi} + \frac{d}{d\phi} \left(\frac{v}{r_1} + \frac{dw}{r_1 d\phi} \right) d\phi \quad (7-6)$$

Figure (7-4) shows that the central angle of the deformed element, A'D', is $(d\phi + \beta - \alpha)$ and so its length is equal to

$$A'D' = r'_1 (d\phi + \beta - \alpha)$$

in this relation, r'_1 is the meridional radius of curvature of the deformed element. If we neglect the second order effects of membrane stretching, we may assume $AD = A'D'$, so

$$r_1 d\phi = r'_1 (d\phi + \beta - \alpha)$$

hence,

$$\frac{1}{r'_1} = \frac{d\phi + \beta - \alpha}{r_1 d\phi}$$

so that the change of curvature of the meridian is as follows:

$$\frac{1}{r'_1} = \frac{1}{r'_1} - \frac{1}{r_1} = \frac{(\beta - \alpha)}{r_1 d\phi} \quad (7-7)$$

$$\frac{1}{r'_1} = \frac{d}{r_1 d\phi} \left(\frac{v}{r_1} + \frac{dw}{r_1 d\phi} \right)$$

To determine the change in the radii of parallel circles, i.e., the curvature change in the hoop direction, we consider the shell element shown in figure (7-6); the initial and deformed radii of curvature of the hoop element, AB, are designated by r_2 and r'_2 , respectively.

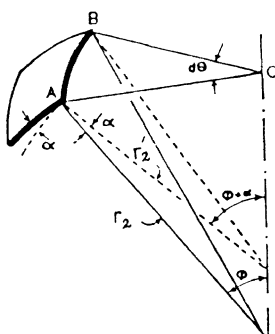


Figure (7-6) A hoop element of axisymmetric shell

Because of the axisymmetric behavior of the shell, the radius of curvature has the same rotation at A and B, namely the angle α . From figure (8-6), we can easily deduce the following relations:

$$AB = AOd\theta = r_2 \sin \phi d\theta$$

$$AB = r'_2 \sin (\phi + \alpha) d\theta$$

If we neglect the second order effect of the membrane change of length, we may write

$$\begin{aligned} r_2 \sin \phi d\theta &= r'_2 \sin (\phi + \alpha) d\theta \\ &= r'_2 (\sin \phi \cos \alpha + \sin \alpha \cos \phi) d\theta \end{aligned}$$

and since the angle α is infinitely small, we may write

$$\begin{aligned} \text{and so } r_2 \sin \phi &= r'_2 (\sin \phi + \alpha \cos \phi) \\ \frac{1}{r'_2} &= \frac{1 + \alpha \cot \phi}{r_2} \end{aligned}$$

Therefore, the curvature change in the hoop direction will be

$$x_\theta = \frac{1}{r'_2} - \frac{1}{r_2} = \frac{\cot \phi}{r_2}$$

Substituting for α from relation (7-5), we find the expression for the change of curvature in the hoop direction

$$x_\theta = \frac{\cot \phi}{r_2} \left(\frac{v}{r_1} + \frac{dw}{r_1 d\phi} \right) \quad (7-8)$$

Relations (7-4), (7-7), and (7-8) constitute the kinematic relations for axisymmetric behavior of shells of revolution. The strain components (in two perpendicular directions) in a shell layer located at a distance z , from the middle-surface, can generally be expressed as follows:

$$\begin{aligned} \epsilon_x^* &= \epsilon_1 - zx_1 \\ \epsilon_y^* &= \epsilon_2 - zx_2 \end{aligned} \quad (7-9)$$

For shells of revolution, the indices x and y , are usually interchanged with ϕ and θ . Moreover, very often the notations $X_1 = x_\theta$ and $X_2 = x_\phi$ are used interchangeably for the redundant forces in the shells of revolution.

7.2.3 - Constitutive Relations

We assume that the shell is made of a linearly elastic and isotropic material. In this case, for an arbitrary point of the shell located at a distance z from the middle surface, we may write the following generalized plane stress constitutive relations:

$$\begin{aligned}\sigma_{\phi}^* &= \frac{E}{1-\nu^2} (\epsilon_{\phi}^* + \nu \epsilon_{\theta}^*) \\ \sigma_{\theta}^* &= \frac{E}{1-\nu^2} (\epsilon_{\theta}^* + \nu \epsilon_{\phi}^*)\end{aligned}\quad (7-10)$$

Now, if we substitute these expressions into the relations (2-1), relating internal stresses to internal force resultants, and use the kinematic relations (7-4), (7-7), (7-8), we obtain

$$N_{\phi} = \frac{Et}{1-\nu^2} \left[\frac{1}{r_1} \left(\frac{dv}{d\phi} - w \right) + \frac{\nu}{r_2} (v \cot \phi - w) \right] \quad (7-11a)$$

$$N_{\theta} = \frac{Et}{1-\nu^2} \left[\frac{1}{r_2} (v \cot \phi - w) + \frac{\nu}{r_1} \left(\frac{dv}{d\phi} - w \right) \right] \quad (7-11b)$$

$$M_{\phi} = - \frac{Et^3}{12(1-\nu^2)} \left[\frac{1}{r_1} \frac{d}{d\phi} \left(\frac{v}{r_1} + \frac{dw}{r_1 d\phi} \right) + \frac{\nu}{r_2} \left(\frac{v}{r_1} + \frac{dw}{r_1 d\phi} \right) \cot \phi \right] \quad (7-11c)$$

$$M_{\theta} = - \frac{Et^3}{12(1-\nu^2)} \left[\left(\frac{v}{r_1} + \frac{dw}{r_1 d\phi} \right) \frac{\cot \phi}{r_2} + \frac{\nu}{r_1} \frac{d}{d\phi} \left(\frac{v}{r_1} + \frac{dw}{r_1 d\phi} \right) \right] \quad (7-11d)$$

These are the axisymmetric constitutive relations for linearly elastic shells of revolution. It is to be noted that in deriving these combined constitutive-kinematic relations, we have also used the kinematic relations for axisymmetric shell behavior.

We may write these relations symbolically as:

$$\begin{aligned}N_{\phi} &= D(\epsilon_{\phi} + \nu \epsilon_{\theta}) \\ N_{\theta} &= D(\epsilon_{\theta} + \nu \epsilon_{\phi}) \\ M_{\phi} &= -K(x_{\phi} + \nu x_{\theta}) \\ M_{\theta} &= -K(x_{\theta} + \nu x_{\phi})\end{aligned}\quad (7-12)$$

The parameters D and K have the following definitions:

$$D = \frac{Et}{1-v^2} \quad K = \frac{Et^3}{12(1-v^2)} \quad (7-13)$$

Where t is the shell thickness, and E, v are the elasticity parameters.

From the physical point of view, D signifies the **membrane stiffness** and K designates the bending stiffness of the shell.

The relations (7-12) show that the bending constitutive relations can be decoupled from the membrane constitutive relations. This conclusion follows the assumptions that we had made regarding the equality of undeformed and deformed lengths of the shell elements.

Relations (7-1), (7-2), (7-3), and (7-12) form the governing equations of linear elastic shells of revolutions with axisymmetric behavior.

7.3 - Reduction of Shell Equations

If we substitute the constitutive-kinematic relations (7-12) into the equilibrium equations (7-1) to (7-3), we obtain three simultaneous differential equations for three unknown functions v, w, and Q_ϕ . We could eliminate the variable Q_ϕ , signifying the lateral shear force, from these three equations. The result would be two simultaneous differential equations for the two displacement components, v and w. At this stage, it is more convenient to introduce the following new variables:

$$v^* = \frac{1}{r_1} (v + \frac{dw}{d\phi}) \quad (8-14)$$

$$u^* = r_2 Q_\phi \quad (8-15)$$

The variable v^* signifies the rotation of tangent to meridional curve i.e., the angle α . The variable u^* is directly proportional to the shear force, Q_ϕ .

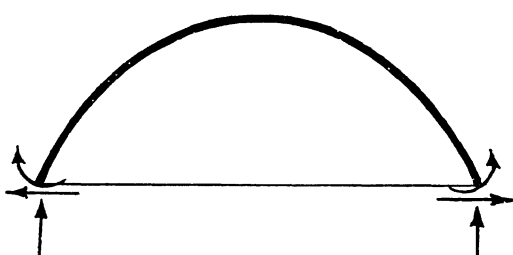


Figure (7-7) Base forces on a horizontal section of axisymmetric shell

To facilitate the change of variables, we rewrite the equilibrium equation (7-1) by considering the equilibrium of a global shell segment located above an angle ϕ , figure (7-7).

If we write the equation of equilibrium of the segment shown in figure (7-7), we obtain

$$2\pi r N_\phi \sin \phi + 2\pi r Q_\phi \cos \phi = 0$$

from which we deduce

$$N_\phi = - Q_\phi \cot \phi = - \frac{1}{r_2} U^* \cot \phi \quad (7-16)$$

Using the second equation of equilibrium (equation (7-2)) with $p_r = 0$ we find

$$r_1 N_\theta \sin \phi = - N_\phi r - \frac{d(Q_\phi r)}{d\phi}$$

Noting that $r = r_2 \sin \phi$, we may write this as:

$$N_\theta = - \frac{1}{r_1} \frac{d}{d\phi} (Q_\phi r) = - \frac{1}{r_1} \frac{dU^*}{d\phi} \quad (7-17)$$

We have thus succeeded in expressing the membrane forces in terms of new variables, U^* and V^* . In order to write the governing equations in terms of these new variables, we proceed as follows:

First, we cast the relations (7-11a) and (7-11b) into following forms:

$$\frac{dv}{d\phi} - w = \frac{r_1}{Et} (N_\phi - v N_\theta) \quad (7-18a)$$

$$v \cot \phi - w = \frac{r_2}{Et} (N_\theta - v N_\phi) \quad (7-18b)$$

To eliminate w between these equations, we subtract the second from the first to obtain

$$\frac{dv}{d\phi} - v \cot \phi = \frac{1}{Et} [(r_1 + v r_2) N_\phi - (r_2 + v r_1) N_\theta] \quad (7-19)$$

By differentiating both sides of relation (7-18b) we get

$$\frac{dv}{d\phi} \cot \phi - \frac{v}{\sin^2 \phi} - \frac{dw}{d\phi} = \frac{d}{d\phi} \left[\frac{r_2}{Et} (N_\theta - v N_\phi) \right] \quad (7-20)$$

We can easily eliminate the term $dv/d\phi$ between (7-19) and (7-20). The result is

$$v + \frac{dw}{d\phi} = r_1 V^* = \frac{\cot\phi}{Et} \left[(r_1 + vr_2) N_\phi - (r_2 + vr_1) N_\theta \right] - \frac{d}{d\phi} \left[\frac{r_2}{Et} (N_\theta - v N_\phi) \right] \quad (7-21)$$

If we substitute the expressions N_ϕ and N_θ , from relations (7-16) and (7-17), into these equations we obtain the following:

$$\frac{r_2}{r_1^2} \frac{d^2 U^*}{d\phi^2} + \frac{1}{r_1} \left[\frac{d}{d\phi} \left(\frac{r_2}{r_1} \right) + \frac{r_2}{r_1} \cot\phi - \frac{r_2}{r_1 t} \frac{dt}{d\phi} \right] \frac{dU^*}{d\phi} - \frac{1}{r_1} \left[\frac{r_1}{r_2} \cot^2\phi - v - \frac{v}{h} \frac{dt}{d\phi} \cot\phi \right] U^* = Et V^* \quad (7-22)$$

This equation is one of the two desired relations between U^* and V^* . To obtain another governing equation, we substitute for M_ϕ and M_θ from relations (7-11c) and (7-11d) into the equilibrium equation (7-3). By doing so, we obtain the second relation in the following form:

$$\frac{r_2}{r_1^2} \frac{d^2 V^*}{d\phi^2} + \frac{1}{r_1} \left[\frac{d}{d\phi} \left(\frac{r_2}{r_1} \right) + \frac{r_2}{r_1} \cot\phi + 3 \frac{r_2}{r_1 t} \frac{dt}{d\phi} \right] \frac{dV^*}{d\phi} - \frac{1}{r_1} \left(v - \frac{3v\cot\phi}{t} \frac{dt}{d\phi} + \frac{r_1}{r_2} \cot^2\phi \right) V^* = - \frac{U^*}{K} \quad (7-23)$$

We have expressed the governing equations of axisymmetric shells as two relations (7-22) and (7-23) in term of new variables U^* and V^* .

Equations (7-22) and (7-23) are valid for thin axisymmetric shells with varying thickness. For a shell with constant thickness, we have $dt/d\phi = 0$. In such a case, the *differential operators* in the left-hand side of those equations become identical,namely

$$L(\dots) = \frac{r_2}{r_1^2} \frac{d^2(\dots)}{d\phi^2} + \frac{1}{r_1} \left[\frac{d}{d\phi} \left(\frac{r_2}{r_1} \right) + \frac{r_2}{r_1} \cot\phi \right] \frac{d(\dots)}{d\phi} - \frac{r_1 \cot^2\phi}{r_1 r_2} (\dots) \quad (7-24)$$

With this notation, the two basic equations (7-22) and (7-23) can be written in more compact *operator forms* as follows

$$L(U^*) + \frac{v}{r_1} U^* = Et V^* \quad (7-25a)$$

$$L(V^*) - \frac{v}{r_1} V^* = - \frac{U^*}{K} \quad (7-25b)$$

This pair of second order differential equations can be combined to yield the following fourth order differential equation with ϕ as its independent variable. Operate on (7-25a) by L to obtain

$$LL(U^*) + vL\left(\frac{U}{r_1}\right) = EtL(V^*) \quad (7-26)$$

But (7-25b) shows that

$$L(V^*) = \frac{v}{r_1} V^* - \frac{U^*}{K} = \frac{v}{r_1 Et} \left[(L(U^*) + \frac{v}{r_1} U^*) - \frac{U^*}{K} \right]$$

so that equation (7-26) may be expressed as a fourth order equation in U^* :

$$LL(U^*) + vL\left(\frac{U}{r_1}\right) - \frac{v}{r_1} L(U^*) - \frac{v^2}{r_1^2} U^* = - \frac{Et}{K} U^* \quad (7-27)$$

The following fourth order equation on variable V^* can be obtained in a similar fashion.

$$LL(V^*) - vL\left(\frac{V}{r_1}\right) + \frac{v}{r_1} L(V^*) - \frac{v^2}{r_1^2} V^* = - \frac{Et}{K} V^* \quad (7-28)$$

These equations are valid for constant thickness axisymmetric shells having arbitrary meridional curves. For special shell types (for example spherical shells, cones, and toroidal shells), in which the meridional radius of curvature (r_1) is constant, we will have the following:

$$L\left(\frac{U}{r_1}\right) = \frac{1}{r_1} L(U)$$

Upon defining the parameter μ as

$$\mu^4 = \frac{Et}{K} - \frac{v^2}{r_1^2} \quad (7-29)$$

both of the equations (7-27) and (7-28) acquire the form

$$LL(\dots) + \mu^4 (\dots) = 0 \quad (7-30)$$

Operationally, this differential equation can be decomposed into the following components:

$$L [L(\dots) + i\mu^2(\dots)] - i\mu^2 [L(\dots) + i\mu^2(\dots)] = 0 \quad (7-31)$$

$$L [L(\dots) - i\mu^2(\dots)] + i\mu^2 [L(\dots) - i\mu^2(\dots)] = 0$$

By comparing the mathematical form of two above equations, we conclude that solutions to the following equation are also solutions to equations (7-31).

$$L(\dots) \pm i\mu^2(\dots) = 0 \quad (7-32)$$

Therefore, the problem of bending analysis of axisymmetric shells with constant thickness and constant r_1 reduces to solving the equation (7-32). As we shall see, the solution to this problem has a broad range of applications; it can be applied to edge-effect analysis of *other* axisymmetric shells with arbitrary meridional shapes.

7.4 - Edge Effects in Axisymmetric Shells

The edge effects in an axisymmetric shell of revolution consist of uniformly distributed bending moment, shear force, and vertical reaction, figure (7-8). Each of these edge forces produces a bending field in the shell. The stresses and deformations due to these bending fields must be superposed on the membrane field to obtain the total field of internal forces and deformations in the shell.

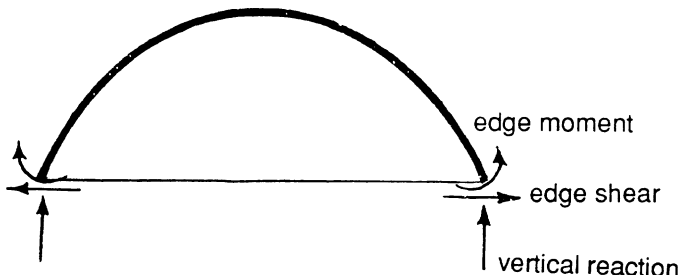


Figure (7-8) Edge forces in an axisymmetric shell

Calculations based on more exact theories and experimental results show that the influence of boundary conditions dies out rapidly away from the edges. In fact, at a distance located at approximately 20° away from the edges, the shell "does not feel" the bending effects brought about by the edge forces. The membrane force field predominates in the inner part of the shell.

The set of figures (7-9) show the spatial variations of internal forces and shell deformations due to distributed edge shear and bending moment. These results could be quantified by bending analyses and / or actual measurements of shell behavior. As we see, all internal forces and displacements due to edge forces "damp out" rapidly away from the boundary region.

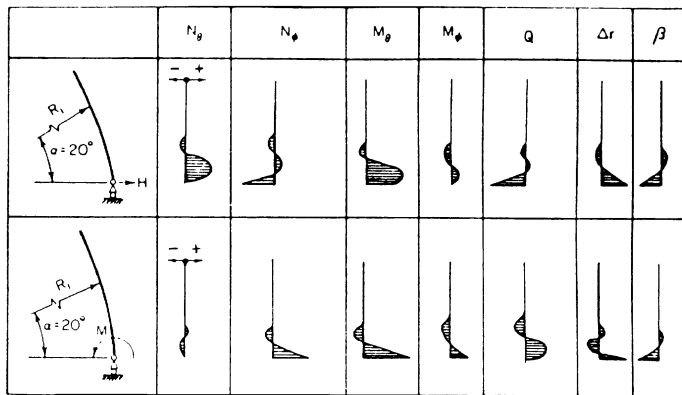


Figure (7-9) Internal forces and axisymmetric shell deformations due to edge effects

Even in the edge zone differences in shell configuration have little effect on the bending behavior. This means that we can determine this behavior approximately by using, say, a spherical shell, figure (7-11); we choose spherical shell because it is easily analyzed. Figure (7-9) shows the implication of this argument and its application in practical shell analyses.

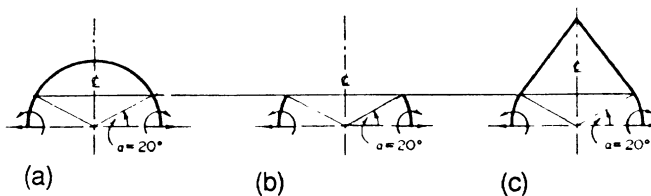


Figure (7-10) Localized action of edge shear and moment effects, (a) in a spherical shell, (b) in the boundary region of that shell, (c) in a shell with some other geometry

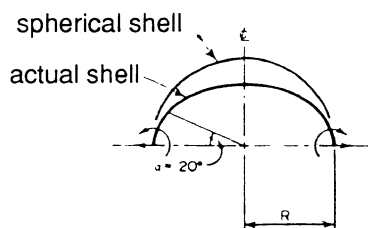


Figure (7-11) Replacement of an arbitrary shell with a spherical shell for edge effects analysis

7.5 - Analysis of Axisymmetric Shells for Edge Effects

In this section, we determine an approximate bending analysis of axisymmetric shells, known as *Geckeler's approximation*. This analysis is valid for a spherical shell of radius a but the results can also be used, as an approximation, for other shell axisymmetric shells.

For a spherical shell, the operator L , defined by relation (7-24) is

$$L(\dots) = \frac{1}{a} \left[\frac{d^2}{d\phi^2} (\dots) + \cot \phi \frac{d}{d\phi} (\dots) - \cot^2 \phi (\dots) \right] \quad (7-33)$$

so that equations (7-25), with the help of (7-15), may be written as

$$\begin{aligned} \frac{d^2 Q_\phi}{d\phi^2} + \cot \phi \frac{dQ_\phi}{d\phi} - (\cot^2 \phi - v) Q_\phi &= EtV^* \\ \frac{d^2 V^*}{d\phi^2} + \cot \phi \frac{dV^*}{d\phi} - (\cot^2 \phi + v) V^* &= -\frac{a^2 Q_\phi}{K} \end{aligned} \quad (7-34)$$

In Geckeler's approximation, of the above equations, only the functions themselves and their derivatives (gradients) of higher order are retained and the lower order derivatives are discarded. Recall that the functions V^* and Q_ϕ represent meridional rotation and lateral shear force, respectively. The Geckeler approximation is based on the physical argument that the boundary effects are localized and thus the higher order gradients are of greatest importance. Hence, in each equation, only the highest order derivative of the main function and the zero order derivative of another, coupling function, shall be retained.

On the basis of this argument, equations (7-24) are replaced by

$$\begin{aligned} \frac{d^2 Q_\phi}{d\phi^2} &= Et V^* \\ \frac{d^2 V^*}{d\phi^2} &= -\frac{a^2}{K} Q_\phi \end{aligned} \quad (7-35)$$

By eliminating the variable function V^* we obtain a fourth order differential equation on the function Q_ϕ .

$$\frac{d^4 Q_\phi}{d\phi^4} + 4\lambda^4 Q_\phi = 0 \quad (7-36)$$

in which

$$\lambda^4 = 3(1 - v^2) \left(\frac{a}{t}\right)^2 \quad (7-37)$$

The general solution to equation (7-36) is

$$Q_\phi = C_1 e^{\lambda\phi} \cos \lambda\phi + C_2 e^{\lambda\phi} \sin \lambda\phi + C_3 e^{-\lambda\phi} \cos \lambda\phi + C_4 e^{-\lambda\phi} \sin \lambda\phi \quad (7-38)$$

We recall that the coordinate parameter ϕ was originally taken as the angle between the normal to the shell surface and the vertical direction. Thus, the lower edge of the shell would be identified by the value $\phi = \alpha$. For shells with convex meridional curves ϕ would decrease towards the shell apex.

The last two terms in the general solution (7-38) increase as ϕ increases, i.e., as we move away from the edge. But we argued that edge effects must decrease as we move away from the edge. Therefore, we set $C_3 = 0 = C_4$, and obtain

$$Q_\phi = C_1 e^{\lambda\phi} \cos \lambda\phi + C_2 e^{\lambda\phi} \sin \lambda\phi \quad (7-39)$$

For convenience, we introduce a change of coordinate $\psi = \alpha - \phi$, figure (7-12), and replace the integration constants C_1 and C_2 by two new constants C and γ . With these alterations, the general solution (7-39) can be rewritten

$$Q_\phi = C e^{-\lambda\psi} \sin(\lambda\psi + \gamma) \quad (7-40)$$

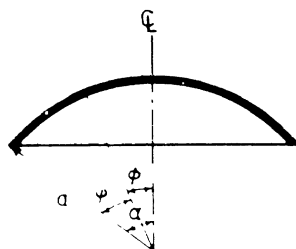


Figure (7-12) Different coordinate angles of an axisymmetric shell

Using the relations (7-15) to (7-17), we can now write down the expressions for V^* , N_ϕ , and N_θ

$$V^* = \frac{1}{Et} \frac{d^2 Q_\phi}{d\phi^2} = + \frac{2\lambda^2}{Et} C e^{-\lambda\psi} \cos(\lambda\psi + \gamma) \quad (7-41)$$

$$N_\theta = - \frac{dQ_\phi}{d\phi} = - \lambda \sqrt{2} C e^{-\lambda\psi} \sin(\lambda\psi + \gamma - \frac{\pi}{4}) \quad (7-42)$$

$$N_\phi = - Q_\phi \cot\phi = - \cot(\alpha - \psi) C e^{-\lambda\psi} \sin(\lambda\psi + \gamma) \quad (7-43)$$

To obtain the expressions for bending moments M_ϕ and M_θ , we use the relations (7-11c), (7-11d), and (7-14), set $r_1 = r_2 = a$ and neglect V^* compared with $dV^*/d\phi$. We obtain

$$M_\phi = - \frac{K}{a} \frac{dV^*}{d\phi} = \frac{a}{\lambda\sqrt{2}} C e^{-\lambda\psi} \sin(\lambda\psi + \gamma + \frac{\pi}{4}) \quad (7-44)$$

$$M_\theta = - \frac{K}{a} V^* \frac{dV}{d\phi} = \frac{av}{\lambda\sqrt{2}} C e^{-\lambda\psi} \sin(\lambda\psi + \gamma + \frac{\pi}{4}) \quad (7-45)$$

For our future use in the analysis of axisymmetric shells, we also need the expressions for shell rotation and displacement. The horizontal displacement, i.e., the change in radius of parallel circles is

$$\begin{aligned} \delta &= a \sin\phi \epsilon_\theta = \frac{a}{Et} \frac{\sin\phi}{\lambda\sqrt{2}} (N_\theta - v N_\phi) \\ &= - \frac{\sin\phi}{Et} \left(\frac{dU^*}{d\phi} - v U^* \cot\phi \right) \end{aligned} \quad (7-46)$$

If we neglect the term containing U^* , compared with $dU^*/d\phi$, we will have

$$\begin{aligned} \delta &= - \frac{\sin\phi}{Et} \frac{dU^*}{d\phi} = - \frac{a}{Et} \sin(\alpha - \psi) \times \\ &\quad \lambda\sqrt{2} C e^{-\lambda\psi} \sin(\lambda\psi + \gamma - \frac{\pi}{4}) \end{aligned} \quad (7-47)$$

Relations (7-41) to (7-47) approximate the bending field of forces and displacements in a spherical shell subjected to edge shear and bending moment. All of these fields have the *decaying* form that was demonstrated qualitatively in figures (7-9).

7.6 - Influence Coefficients for Axisymmetric Shells

As a useful by-product of this analysis, we now obtain the *flexibility influence coefficients* of axisymmetric shells, i.e., the displacements due to *unit edge forces*.

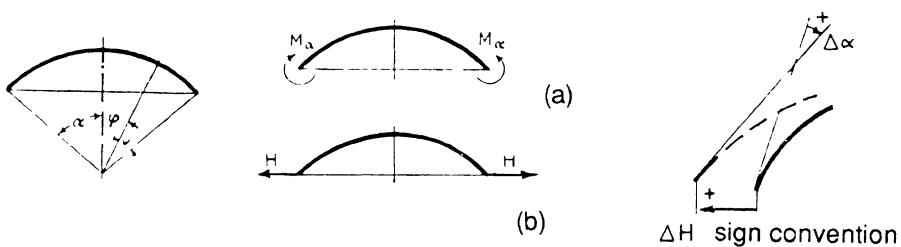


Figure (7-13) Axisymmetric shell under separate application of edge forces, (a) shear force, (b) bending moment

Consider figure (7-13b) in which the shell is acted upon by a uniformly distributed edge moment M_α . The boundary conditions are:

$$(M_\phi)_\phi = \alpha = M_\alpha \quad (7-48a)$$

$$(N_\phi)_\phi = \alpha = 0 \quad (7-48b)$$

If the condition (7-48b) is used in (7-43) it gives $\gamma = 0$. Substitution of (7-48a) into (7-44) gives

$$C = \frac{2M_\alpha \lambda}{a}$$

Having obtained the two integration constants C and γ , we can write down the expressions for internal edge forces and edge displacements due to the edge moment M_α . These values are tabulated in the third column of table (7-1). Specifically, for $M_\alpha = 1.0$ we shall get the bending moment flexibility influence coefficients.

As another basic solution, we consider the shell of figure (7-13c); the edge conditions for this shell are

$$\begin{aligned} (M_\phi)_\phi = \alpha &= 0 \\ (N_\phi)_\phi = \alpha &= -H \cos \alpha \end{aligned} \quad (7-49)$$

Proceeding along similar lines we find

$$\lambda = -\frac{\pi}{4}, \quad C = \frac{2H \sin \alpha}{\sqrt{2}}$$

Having found these constants, we can write the expressions for internal edge forces and edge displacements due to a distributed edge shear force, H. These results are tabulated in the second column of table (7-1). Again, for $H = 1.0$, these expressions give the flexibility influence coefficients of the shell due to a unit edge shear force.

Table (7-1) Flexibility influence coefficients for axisymmetric shells

		
N_ϕ	$-\sqrt{2} \cot(\alpha - \psi) \sin \alpha e^{-\lambda \psi} x$ $\sin(\lambda \psi - \frac{\pi}{4}) H$	$-\frac{2\lambda}{a} \cot(\alpha - \psi) e^{-\lambda \psi} x$ $\sin(\lambda \psi) M_\alpha$
N_θ	$-2\lambda \sin \alpha e^{-\lambda \psi} \sin(\lambda \psi - \frac{\pi}{2}) H$	$-\frac{2\sqrt{2}}{a} \lambda^2 e^{-\lambda \psi} \sin(\lambda \psi - \frac{\pi}{4}) M_\alpha$
M_ϕ	$\frac{a}{\lambda} \sin \alpha e^{-\lambda \psi} \sin(\lambda \psi) H$	$\sqrt{2} e^{-\lambda \psi} \sin(\lambda \psi + \frac{\pi}{4}) M_\alpha$
ΔH	$\frac{2a\lambda \sin^2 \alpha}{Et} H$	$\frac{2\lambda^2 \sin \alpha}{Et} M_\alpha$
$\Delta \alpha$	$\frac{2\lambda^2 \sin \alpha}{Et} H$	$\frac{4\lambda^3 M_\alpha}{Ea t}$

7.7 - Force Method of Axisymmetric Shells Analysis

The force method of axisymmetric shells analysis consists of: (1) the membrane analysis, (2) the bending analysis for the edge and / or boundary effects, and (3) superposition of membrane and bending analyses to satisfy the compatibility requirements.

In the force method, the redundant unknown quantities are the bending edge forces and / or the forces between two shell segments. Once these forces are determined, the other unknowns such as internal forces and shell displacements can be obtained by superposition of the membrane and the bending fields. The flexibility influence coefficients are useful for deriving the compatibility relations and for determining the unknown redundant edge forces.

In the following section, a sample example will be worked out to show the force method of axisymmetric shell analysis and also to demonstrate the relative quantitative contribution of the edge effects to the total field of forces and displacements.

7.8 - Sample Analysis of a Dome

As a numerical example of axisymmetric shells analysis, we consider a reinforced concrete spherical dome as shown in the figure (7-14). This dome is assumed to be constrained against rotation and translation at the lower edge. We would like to analyze this shell for a uniformly distributed dead load of intensity q . The given data of the problem are as follows:

$$\alpha = 28^\circ$$

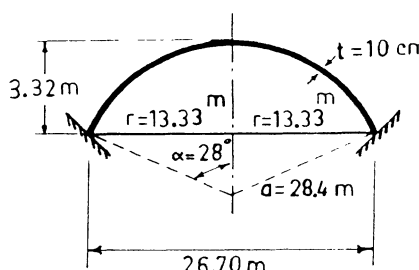
$$t = 0.1 \text{ m} = 10 \text{ cm.}$$

$$r_1 = r_2 = a = 28.4 \text{ m.}$$

$$v = 1/6 = 0.167$$

$$q = 440 \text{ Kg/m}^2$$

$$r = a \sin \alpha = 13.35 \text{ m.}$$



Solution:

Let us designate the redundant edge shear force and edge bending moment by the symbols X_1 and X_2 , respectively. In this problem, these are the bending constraints which are needed for deformation compatibility and are to be determined by the application of the force method.

(1) Membrane analysis

The membrane forces and the edge of displacements of spherical domes were determined in chapter six. Those expressions and their values for the present problem can be summarized as follows:

$$D_{10} = \frac{a^2 q}{E t} \left(\frac{1+v}{1+\cos\alpha} - \cos\alpha \right) \sin\alpha$$

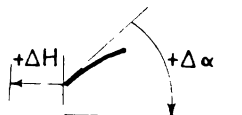
$$D_{10} = \frac{(28.4)^2 \times q}{E \times 0.1} \left(\frac{1+0.167}{1+\cos 28} - \cos 28 \right) \sin 28 = -997 \frac{q}{E}$$

$$D_{20} = \frac{aq}{Et} (2+v) \sin\alpha$$

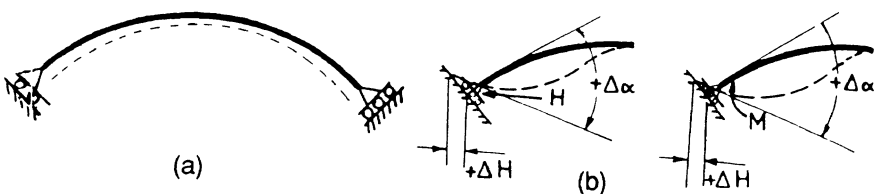
$$D_{20} = \frac{28.4 q}{E \times 0.1} (2+0.167) \sin 28 = 289 \frac{q}{E}$$

$$N_{\psi_O} = -aq \left(\frac{1}{1+\cos\psi} \right)$$

$$N_{v_O} = aq \left(\frac{1}{1+\cos\psi} - \cos\psi \right)$$



Here, D_{10} is the membrane horizontal displacement of the edge parallel circle and D_{20} is the membrane rotation of meridional curve at the edge of the shell. Figure (7-15) shows the schematics of membrane deformation and adopted sign conventions.



membrane deformation due to dead load

sign conventions

Figure (7-15) Deformation and assumed sign convention
for the shell of figure (7-14)

(2) Bending (corrective) analysis

To find the bending field of action, we first calculate the value of parameter λ which was defined by relation (7-37). Its numerical value for this problem is,

$$\lambda = \sqrt[4]{3(1-\nu^2) \left(\frac{a}{t}\right)^2} = 22$$

The influence coefficients necessary for bending analysis can be calculated by the help of table (7-1). If the i -th deformation component due to unit edge force $x_j = 1.0$ is denoted by D_{ij} , then the appropriate flexibility influence coefficients are,

$$x_1 = 1 : \begin{cases} D_{11} = \frac{2a\lambda \sin^2 \alpha}{Et} = + \frac{2754}{E} \\ D_{21} = \frac{2\lambda^2 \sin \alpha}{Et} = + \frac{4544}{E} \end{cases}$$

$$x_2 = 1 : \begin{cases} D_{12} = D_{21} = + \frac{4544}{E} \\ D_{22} = \frac{4\lambda^3}{Eat} = \frac{14997}{E} \end{cases}$$

The compatibility relations, requiring zero horizontal displacement and zero meridional rotation at the edge, are as follows:

$$\sum \Delta H = 0 \implies D_{11}x_1 + D_{12}x_2 + D_{10} = 0$$

$$\sum \Delta \alpha = 0 \implies D_{21}x_1 + D_{22}x_2 + D_{20} = 0$$

If we substitute the numerical values of influence coefficients and membrane deformations in these expressions, we obtain,

$$2754 x_1 + 4544 x_2 = 997 q$$

$$4544 x_1 + 14997 x_2 = - 289 q$$

and by solving these two simultaneous equations for X_1 and X_2 we find,

$$x_1 = 0.876 q = 347 \text{ Kg/m}$$

$$x_2 = - 0.258 q = - 113 \text{ Kg-m/m}$$

The negative sign in the value obtained for the edge moment indicates that the actual direction is contrary to what was assumed in the beginning of this problem. We also note that the edge shear force, X_1 , comes out to be positive. This means that the membrane shell has a tendency to move *inwards* and the effect of edge shear is to bring it back *outwards*,

so that the actual edge conditions can be satisfied. This result differs from what we would have expected from the analysis of a planar arch.

Once the redundant edge forces are found, we can use relations (7-42) to (7-47) to determine the internal forces and displacements due to edge effects. These calculations are summarized in tables (7-2) and (7-3).

Table (7-2)

Ψ degree	ψ radian	$\cot(\alpha-\psi)$	$\lambda\psi$ degree	$\lambda\psi$ radian	$e^{-\lambda\psi}$	$\sin \psi$	$\sin(\lambda\psi - \frac{\pi}{4})$	$\sin(\lambda\psi + \frac{\pi}{4})$	$\sin(\lambda\psi - \frac{\pi}{2})$	$\sin \alpha$
0	0	1.68	0	0	1.000	0	-0.707	0.707	-1.000	0.4695
1	0.0175	1.96	22	0.385	0.68	0.375	-0.391	0.921	-0.927	0.4695
2	0.0349	2.05	44	0.768	0.464	0.695	-0.017	1.000	-0.719	0.4695
5	0.0873	2.36	110	1.92	0.147	0.940	0.906	0.423	0.342	0.4695
10	0.1745	3.08	220	3.84	0.021	-0.643	0.087	-0.996	0.766	0.4695
20	0.3491	-12	440	7.68	0.0004	0.985	0.574	0.819	-0.174	0.4695
28	0.4987	-	616	10.75	0	-0.970	-0.515	-0.854	0.242	0.4695

Table (7-3)

Ψ	N_ϕ		N_θ		M_ϕ	
	x_1 coefficient	x_2 coefficient	x_1 coefficient	x_2 coefficient	x_1 coefficient	x_2 coefficient
0	-0.892	0	+20.6	+34.079	0	+1.00
1	-0.346	-0.774	+13.0	+12.816	+0.154	+0.89
2	-0.0107	-1.024	+6.89	+0.380	+0.195	+0.66
5	-0.209	-0.505	-1.04	-6.420	+0.084	+0.088
10	-0.0037	+0.064	-0.332	-0.0881	-0.008	-0.03
20	-0.00108	-0.0043	+0.0014	-0.0111	0	0
28	0	0	0	0	0	0

$$N_\phi : \text{coefficient } x_1 - \sqrt{2} \cot(\alpha-\psi) \sin \alpha e^{-\lambda\psi} \sin(\lambda\psi - \pi/4)$$

$$\text{coefficient } x_2 - \frac{2\lambda}{a} \cot(\alpha-\psi) e^{-\lambda\psi} \sin(\lambda\psi)$$

$$\text{coefficient } x_2 - 2\lambda \sin \alpha e^{-\lambda\psi} \sin(\lambda\psi - \pi/2)$$

$$\text{coefficient } x_2 - \frac{-2\sqrt{2}}{a} \lambda^2 e^{-\lambda\psi} \sin(\lambda\psi - \pi/4)$$

$$\text{coefficient } x_1 \frac{a}{\lambda} \sin \alpha e^{-\lambda\psi} \sin \lambda\psi$$

$$\text{coefficient } x_1 \frac{a}{\lambda} e^{-\lambda\psi} \sin(\lambda\psi +/- \pi/4)$$

(3) Superposition of membrane and bending analyses

Using the results of part (1) and part (2), we can present the bending and the membrane field of internal forces in the shell for a number of meridional angles, as shown in table (7-4)

Table (7-4)

ψ degree	0 edge	1	2	5	10	20	28
1. N_{ϕ_0} membrane T/m	-6.64	-6.44	-6.30	-6.26	-6.25	-6.25	-6.25
2. $N_{\phi_1} (H=x_1)$ T/m	+0.31	+0.12	+0.004	-0.073	-0.001	0	0
3. $N_{\phi_2} (M=x_2)$ T/m	0.0	+0.09	+0.12	+0.06	-0.007	0	0
4. $N_{\phi}^T / m^2 (q=440)$	-6.33	-6.23	-6.18	-6.28	-6.26	-6.25	-6.25
5. N_{θ_0} membrane T/m	-4.40	-5.3	-6.01	-6.19	-6.24	-6.25	-6.25
6. $N_{\theta_1} (H=x_1)$ T/m	+7.15	+4.51	+2.39	-0.36	-0.12	0	0
7. $N_{\theta_2} (M=x_2)$ T/m	-3.85	-1.45	-0.04	+0.73	+0.01	0	0
8. $N_{\theta}^T / m^2 (q=440)$	-1.12	-2.24	-3.66	-5.82	-6.35	-6.25	-6.25
9. M_{ϕ_0} membrane $T \cdot m / m$	0	0	0	0	0	0	0
10. M_{ϕ_1} $(H=x_1) T \cdot m / m$	0	+0.05	+0.07	+0.03	0	0	0
11. M_{ϕ_2} $(M=x_2) T \cdot m / m$	-0.11	-0.10	-0.07	-0.01	0	0	0
12. $M_{\phi} T \cdot m / m$	-0.11	-0.05	-0.00	+0.02	0	0	0

Using the numerical values of table (7-4), we can plot the variations of the internal forces in the shell on the meridional curve. The set of figures (7-16) show variations of meridional force, the hoop force, and the bending moment in the shell of figure (7-14). In these diagrams, the membrane field of forces is plotted and compared with the results of a more comprehensive bending analysis.

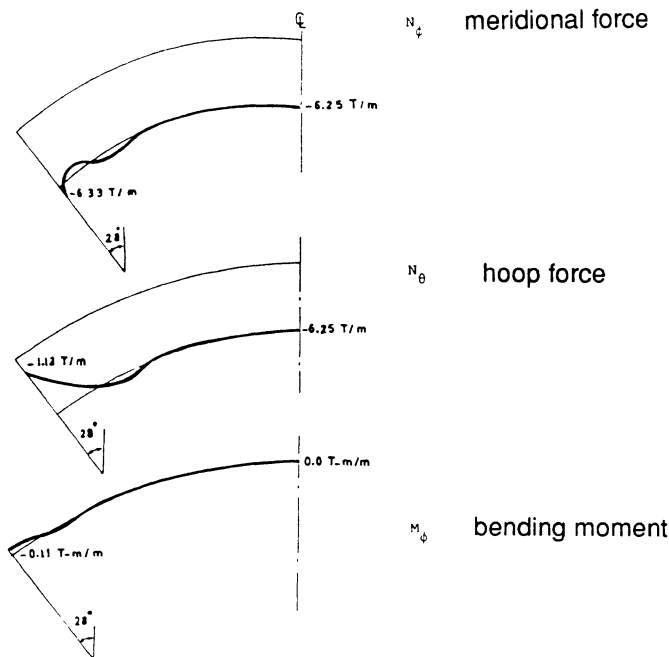


Figure (7-16) variation of internal forces in the dome of figure (7-14)

As we see, the influence of edge forces is quite local and damps out rapidly as we move away from the boundary zone. At an angle of about 5° the effect of edge constraint is quite insignificant.

The maximal values of internal forces could be determined from table (7-4). The maximum internal force quantities and their locations are as follows:

$$(N_\phi)_{\max} = -6.33 \text{ T/m.} \quad \text{at } \psi=0^\circ, \quad M_\phi = -0.11 \frac{\text{T-m}}{\text{m}}$$

$$(N_\theta)_{\max} = -6.25 \text{ T/m.} \quad \text{at } \psi=28^\circ, \quad M_\phi = 0$$

$$(M_\phi)_{\max} = -0.11 \text{ T-m/m.} \quad \text{at } \psi = 0^\circ$$

$$(\sigma_\phi)_{\max} = -6.33 \text{ Kg/Cm}^2, \quad (\sigma_\theta)_{\max} = -6.25 \text{ Kg/Cm}^2$$

As a final observation, we note that the internal stress system in the dome remains a pure compressive field at all points of the shell.

Problems

P 7.1 - Consider A conical elastic shell with a central angle α , the base radius a , and thickness t . The lower edge of this cone is fixed against rotation and translation. This shell is subjected to its own weight with intensity q . Perform a complete analysis of this shell.

P 7.2 - Consider the spherical tank of figure (6-11). Determine the bending field which would develop around the supporting ring of this shell.

P 7.3 - The presence of the upper ring in the spherical shell with the top opening of figure (6-9) is expected to produce some bending field in this region. Even in the absence of the ring a bending field may be produced around the free edge. Verify if there is a bending field there. If so, determine the bending field at the top of this shell.

P 7.4 - Find the bending field in the intersection of the cylindrical wall and its conical hopper of the silo structure shown in figure (P 6-2).

P 7.5 - Consider the conical water tank with a domed roof of figure (P 6-3). Perform a complete analysis of this shell structure.

P 7.6 - Determine the bending force field between the cylindrical wall and the conical end of the pressure vessel shown in figure (P 6-4).

References for Chapter Seven

- 7.1 - M. Farshad, *Shell Structures*, Vol. I, 1986, Vol. II, 1987, Shiraz University Publications, Shiraz
- 7.2 - D. P. Billington, *Thin Shell Concrete Structures*, McGraw-Hill Book Co. N.Y., Revised edition, 1982
- 7.3 - W. Flügge, *Stresses in Shells*, Springer-Verlag, Berlin, 1962
- 7.4 - S. Timoshenko and S. Woinowsky-Krieger, *Theory of Plates and Shells*, 2nd edition, McGraw-Hill Book Co., N.Y., 1959

Chapter 8

Design of Reinforced Concrete Domes

8.1 - Introduction

Domes have synclastic shell surfaces with positive Gaussian curvature. They are strong and structurally stable. Dome roofs can be constructed from steel, various fiber reinforced composites, and reinforced concrete materials. Precast shells made of these materials have also been constructed successfully.

Reinforced concrete domes are used to cover large spans of stadiums, memorial buildings, meeting halls, and other large assembly halls. They are also used to cover the **roofs of liquid retaining structures, silos**, as well as the roofs of **containment shells of nuclear power plants**. The end caps of concrete containment structures and **pressure vessels** are also made of these axisymmetric shells. Parts of shells of revolution and / or various combinations of these shell types can also be conceived and designed.

In chapter six, we discussed the membrane behavior of shells of revolution. In chapter seven, we presented the bending theory of axisymmetric shells. Using what we acquired in those two chapters, we can now venture into the design of domes, in particular, reinforced concrete domes.

In this chapter, we will discuss the design problems related to domes. Domes are usually accompanied by *edge rings*. These two must be designed so that the strength, stiffness, and stability of the whole shell structure is achieved. In the first part of the present chapter we will analyze domes with edge rings and will then apply this to the design of a reinforced concrete shell.

8.2 - Domes with Rings

A dome is often provided with an edge ring at its lower edge and / or with a ring somewhere along its parallel circles. Figures (8-1) show some cases in which edge rings are used with domes.

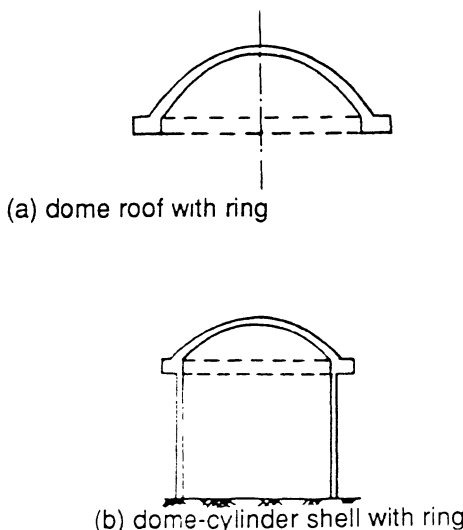


Figure (8-1) Domes connected to other structural members

Edge rings stiffen the shell and / or provide lateral support for the shell structure. The lateral support action of the rings is specially needed in cases where there are only vertical supports and thus the lateral thrusts are to be absorbed by the structure itself. For combined shells, figure (8-1b), the stiffening ring between two shells acts as a strengthening member which absorbs part of the bending field created by the curvature change from one shell to the other.

In metallic and composite shells, rings are needed to strengthen the shell against buckling. They are also required to distribute the line loadings and to transfer the shell loads to the supporting elements.

Edge beams in a shell structure create some bending field in the vicinity of the ring. This is due to the difference in stiffness between the shell and the ring and the ensuing violation of the membrane assumptions.

From the structural analysis point of view, a force field composed of shear force and bending moment as well as membrane forces would exist between the shell and its edge beam. The magnitudes of bending effects would be such that the deformation compatibility requirements are satisfied. These forces of dome-ring interaction are shown in figure (8-2).

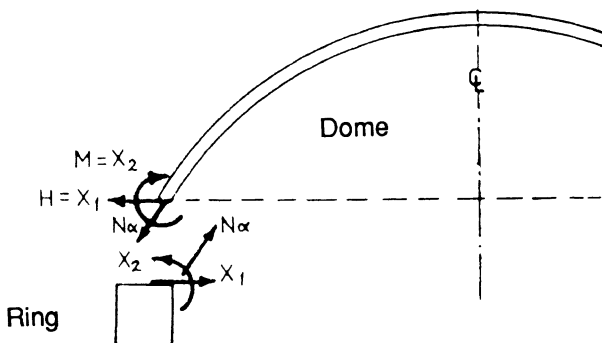


Figure (8-2) Interaction between an axisymmetric shell and its edge ring

8.3 - Force Method of "Dome-Ring" Analysis

8.3.1 - General Methodology

The general *force method* of structural analysis, outlined and used in previous chapters, can be used in the analysis of domes with rings and also domes with cylindrical walls. The ring in a dome acts as a *tie* capable of absorbing the horizontal forces; it is a deformable body integral with the shell and must be analyzed along with the shell.

A **dome-ring** structural system has its counterpart in linear framed structures. A dome with a ring resembles a framework having a tie at its lower base. The tie in the "dome-ring" structure can act in tension as well as in compression.

In order to understand the combined behavior of a "dome-ring" system, we use this analogy. In doing so, we utilize the knowledge and elementary analysis of framed structures. We shall therefore first discuss the force method as applied to a simple frame.

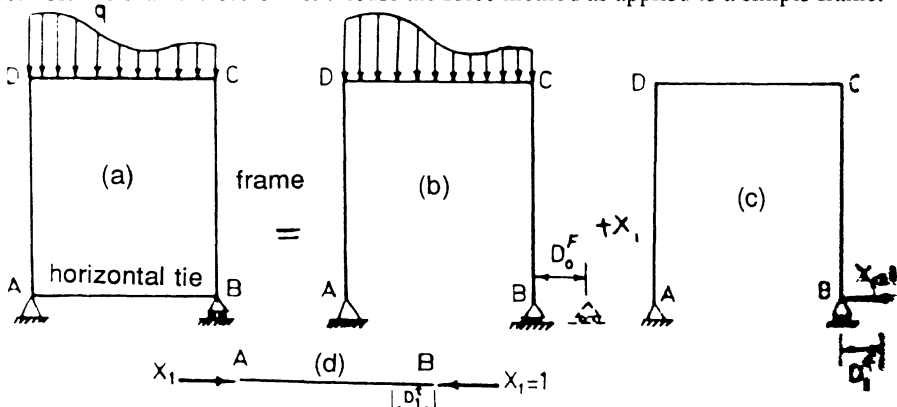


Figure (8-3) Force method of analysis applied to a portal frame with a tie

Figure (8-3a) shows a **portal frame** with a tie. A general approach to analysis of such a frame is depicted by figures (8-3b) and (8-3c). This frame is statically indeterminate having one degree of indeterminacy. The unknown force in the tie can be chosen as the redundant force. Figure (8-3b) is the associated statically determinate frame, i.e., the frame with the tie removed. The magnitude of redundant axial force in the tie is such that the compatibility requirement between the tie and the frame is fulfilled.

The statically determinate frame is structurally analogous to the membrane shell with the edge ring removed. Figure (8-3c) shows the influence of a unit horizontal thrust. Finally, figure (8-3d) shows the effect of tie deformation on the tied-frame behavior. These two latter figures correspond to the effect of edge forces, i.e., the edge ring on the shell structure.

The compatibility relation for the tied-frame of figure (8-3a) is

$$D_0^f + D_1^f x_1 = -D_1^t x_1$$

or

$$(D_1^f + D_1^t)x_1 + D_0^f = 0$$

giving

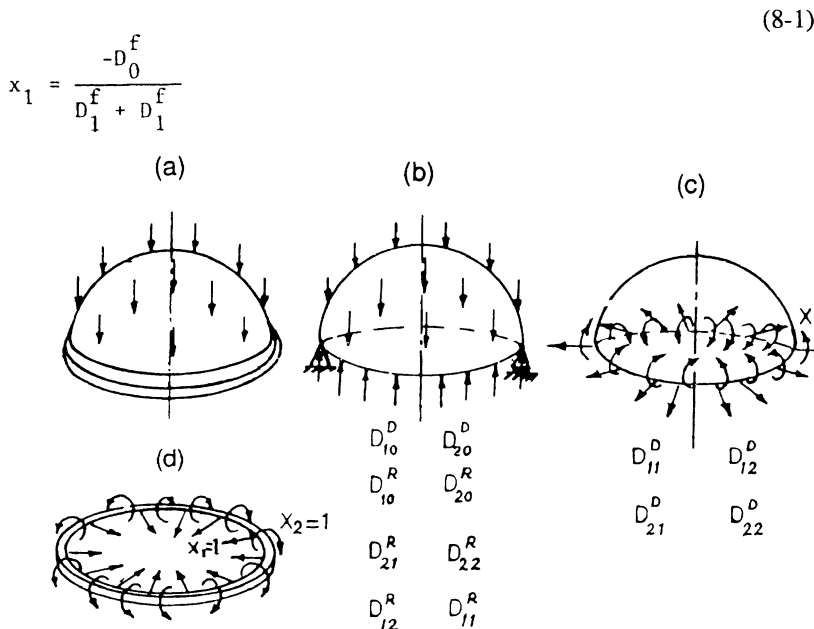


Figure (8-4) Ingredients of force method of "dome-ring" analysis

Figure (8-5) shows the details of the decomposition of the dome and its related deformation parameters. Figure (8-6) demonstrates the decomposition scheme of ring analysis as well as the deformation parameters to be calculated in the course of the ring analysis.

This analysis can be applied to a shell with a ring. Figure (8-4a) shows a dome with a ring. Figure (8-4b) depicts the same dome without the ring, acting as a (statically determinate) membrane shell. The membrane deformations in the dome and the deformations in the ring, due to membrane forces, are also defined alongside this figure. Figure (8-4c) demonstrates the edge forces and corresponding flexibility influence coefficients related to the dome. Finally, figure (8-4d) shows the ring together with related influence coefficients. In all these figures, D_{ij}^D and D_{ij}^R refer to influence coefficients related to dome and ring, respectively. The corresponding membrane deformations are denoted by D_{io}^D and D_{io}^R .

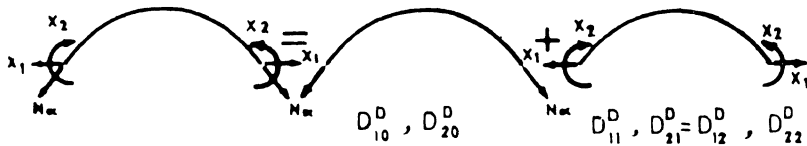


Figure (8-5) Decomposition of internal forces in the dome into membrane and bending fields

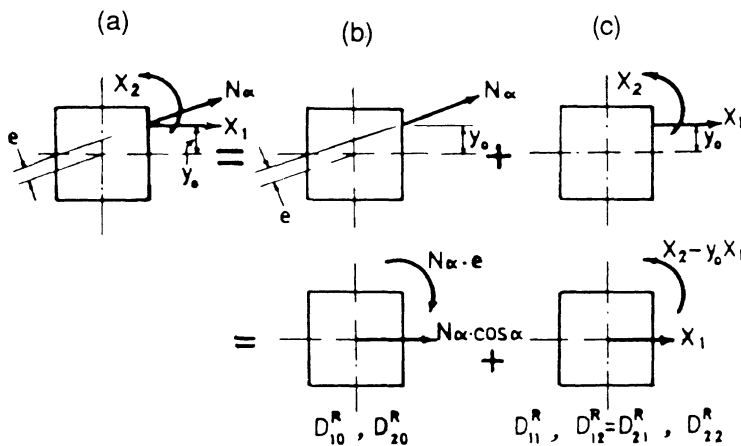


Figure (8-6) Decomposition of internal forces in the ring and their related deformations

Based on the foregoing discussion, we may now state the stages of any "dome-ring" analysis problem as follows:

- (1) **Analysis of the ring** under hoop force, unit radial force, and unit torsional couple.
- (2) **Membrane analysis of dome** for distributed forces as well as bending analysis of dome for unit value of edge effects.
- (3) **Matching of the dome and ring deformations** by imposition of compatibility relations. Determination of unknown "dome-ring" interaction forces from these relations.
- (4) **Superposition** of membrane and bending effects to find the total force and deformation in the **dome-ring** structure.

8.3.2 - Analysis of the Ring

Consider a linearly elastic circular ring of internal radius r and rectangular section $b \times h$. The ring is subjected to a uniformly distributed radial force, H , and a uniformly distributed twisting couple, M_a . Figure (8-7) shows the free-body diagrams of this ring segment.

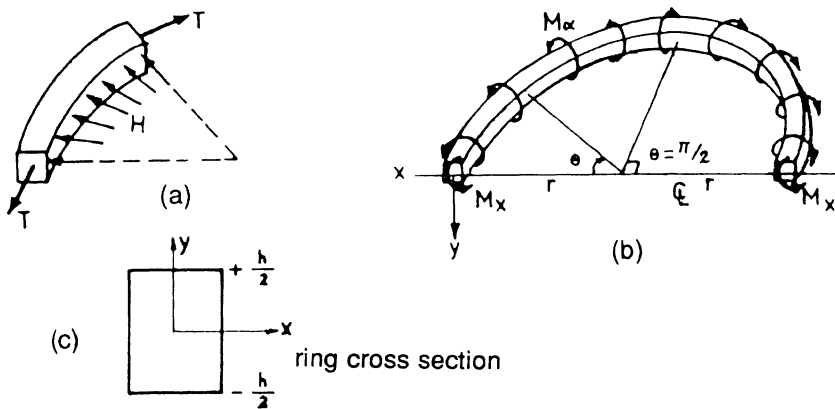


Figure (8-7) Free-body diagrams of a ring segment under radial force and twisting couple

Figure (8-7a) shows that the hoop force and the hoop stress are:

$$T = H \cdot r \quad , \quad \sigma_{\theta} = \frac{T}{A_R} \quad (8-2a)$$

and the corresponding hoop strain is

$$\epsilon_{\theta} = \frac{T}{E A_R} \quad (8-2b)$$

The change of length of this ring would be

$$\begin{aligned}\Delta_\theta &= 2\pi r \cdot \epsilon_\theta \\ \Delta_\theta &= \frac{2\pi r}{EA_R} \cdot T = \frac{2\pi r}{EA_R} Hr\end{aligned}\quad (8-3)$$

Therefore, the change of radius of this ring due to a radial force is expressed as follows:

$$\begin{aligned}\Delta H &= \epsilon_\theta \cdot r \\ \Delta H &= \frac{\Delta_\theta}{2\pi r} \times r \\ \Delta H &= \frac{-rT}{EA_R} = \frac{-r^2}{EA_R} \cdot H\end{aligned}\quad (8-4)$$

Now consider the free body diagram of half ring shown in figure (8-7b). The equation of moment equilibrium about the x-axis is

$$2M_x = 2 \int_0^{\pi/2} M_\alpha r \cdot \cos\theta d\theta$$

so

$$M_x = M_\alpha \cdot r \left[\sin \theta \right]_0^{\pi/2} = M_\alpha \cdot r \quad (8-5)$$

Figure (8-8a) shows the deformation of a section of this ring under the action of twisting couple M_α .

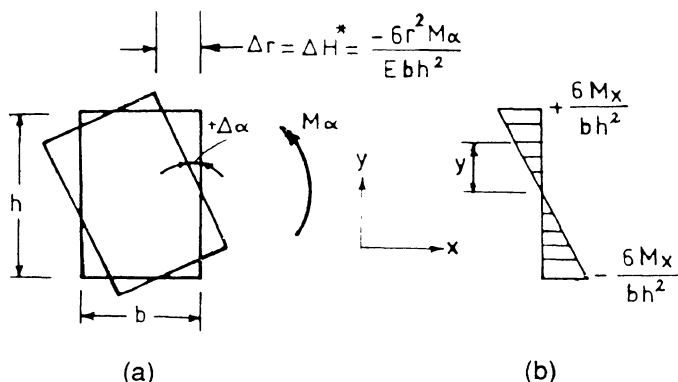


Figure (8-8) Torsional-bending deformation of the ring

Referring to figure (8-8a), and using the classical formula for bending of beams, we find the bending stress and corresponding hoop strain and change of ring radius as follows:

$$\sigma = \frac{M_x y}{I_R} \quad (8-6)$$

$$\epsilon_\theta^* = \frac{M_x y}{EI_R} \quad , \quad (\epsilon_\theta^*)_{\max} \Big|_{y=+h/2} = \frac{M_x \cdot -h/2}{Ebh^3/12} = \frac{6M_x}{Ebh^2}$$

$$\Delta r = -r(\epsilon_\theta^*)_{\max} = \frac{-6r^2 M_x}{Ebh^2} \alpha$$

$$(8-7)$$

Note that classical beam theory gives a bending stress which varies linearly with the height of a ring section. This is shown in figure (8-8b).

Assuming linear variation of torsion-induced hoop strain in the height of the ring section, and using simple bending stress formula, we find the torsion-induced change of ring perimeter to be

$$\Delta_\theta^* = 2\pi r \frac{M_x \cdot y}{EI_R} \quad (8-8)$$

and the corresponding change of ring radius:

$$\Delta H^* = \frac{-rM_x \cdot y}{EI_R} = -\frac{r^2 y}{EI_R} M_\alpha \quad (8-9)$$

Due to difference in the radius change, each section of the ring would undergo the following torsional rotation:

$$\Delta\alpha = \frac{|\Delta H|^*}{Y} = \frac{r^2}{EI_R} \cdot M_\alpha \quad (8-10)$$

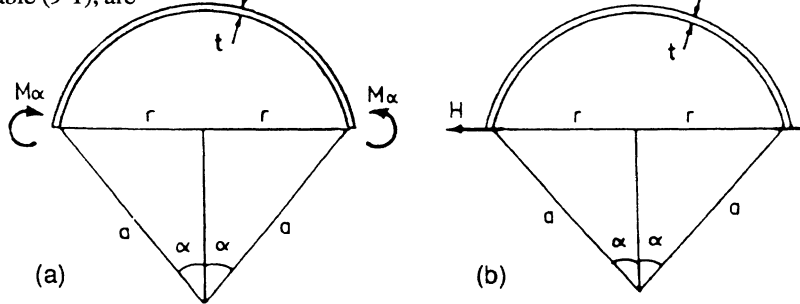
Relations (8-4) and (8-10) give the radius change and cross-sectional rotation of the ring under the uniformly distributed radial force H and twisting couple M_α . These relations are rewritten as follows:

$$\Delta H = \frac{-r^2}{Ebh} H \quad , \quad \Delta r = \frac{-12r^2 y}{Ebh^3} M_\alpha \quad , \quad \Delta\alpha = \frac{12r^2}{Ebh^3} M_\alpha \quad (8-11)$$

8.3.3 - Analysis of Domes Under Edge and Distributed Forces

The analysis of domes under distributed forces was carried out in chapter 6. In that chapter, we obtained the membrane force and deformation fields for domes. We now use those results for a more comprehensive "dome-ring" analysis.

In chapter 7 we derived the influence coefficients of a spherical dome subjected to uniformly distributed unit edge shear and edge moment. These coefficients were summarized in table (9-1), and we can use them here for the "dome-ring" analysis. Figure (8-9) shows the dome under edge forces. The related influence coefficients, as extracted from table (9-1), are



$$D_{11}^D = \frac{+2a\lambda \sin^2 \alpha}{Et}$$

$$D_{21}^D = \frac{+2\lambda^2 \sin \alpha}{Et}$$

$$D_{12}^D = \frac{+2 \lambda^2 \sin \alpha}{Et}$$

$$D_{22}^D = \frac{4\lambda^3}{Eat}$$

$$\lambda^4 = 3(1-\nu^2) \left(\frac{a}{t}\right)^2$$

Figure (8-9) dome subjected to uniformly distributed edge forces

8.3.4 - "Dome-Ring" Interaction

Figure (8-10a) shows part of a "dome-ring" structure resting on a vertical support. Figure (8-10b) shows the forces of interaction between the dome and the ring.

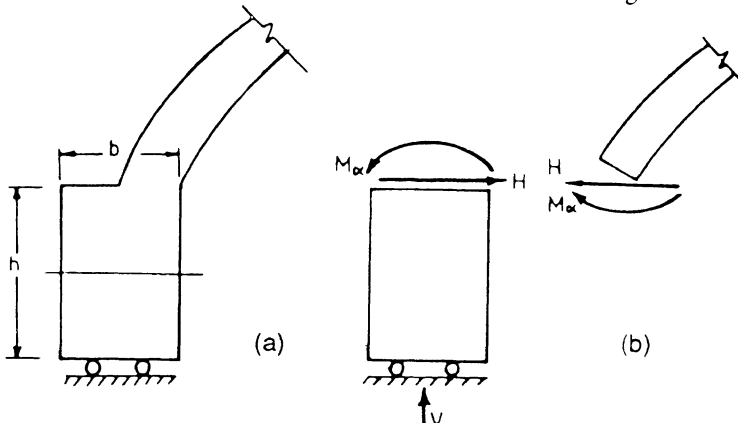


Figure (8-10) Bending forces of "dome-ring" interaction

Figure (8-11a) shows the membrane field of "dome-ring" interaction. The deformations caused by these sort of interaction and the adopted sign convention are shown in figures (8-11b) and (8-11c), respectively.

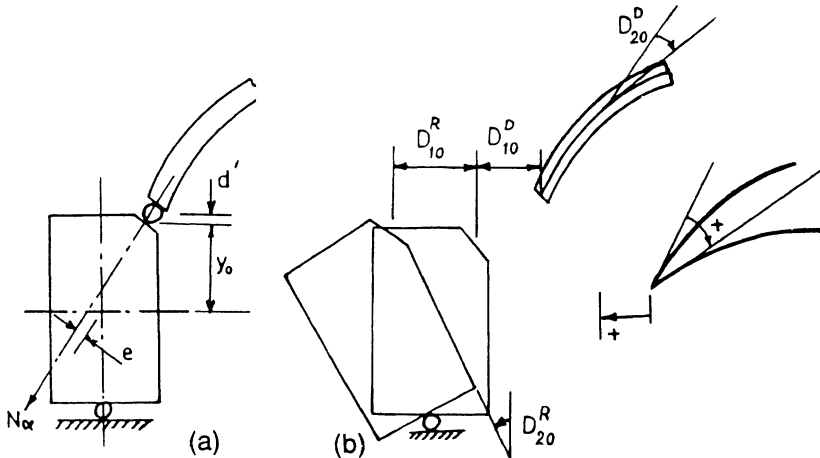


Figure (8-11) Membrane "dome-ring" interaction, (a) membrane meridional force, (b) membrane ring and dome deformations

In considering the "dome-ring" interaction, we use the spherical dome approximation. Based on our discussions of chapter 7, this approximation is justified. In what follows, we assume that the spherical dome has a radius a and a half central angle of α .

Figure (8-11a) shows that the components of meridional force at the base of the shell are

$$H_O = N_\alpha \cos \alpha \quad V_O = N_\alpha \sin \alpha \quad (8-13)$$

The vertical component is absorbed by the vertical support while the horizontal component is taken by the ring. The radial displacement of the ring due to this horizontal component is,

$$\Delta_{OH} = \frac{r^2}{EA_R} H_O = \frac{r^2}{EA_R} N_\alpha \cos \alpha \quad (8-14)$$

In the general case, the meridional force acts on the ring section with an eccentricity. Thus, assuming an eccentricity of e , we find that the torsional couple, induced by the membrane force, acting on the ring is $M_{O\alpha} = N_\alpha e$. The radial displacement of the ring due to this couple, derived in the previous section, is

$$\frac{r^2 y}{EI_R} M_{O\alpha} = \frac{r^2 y}{EI_R} N_\alpha e \quad (8-15)$$

We seek the radial displacement of the ring at the "dome-ring" junction. At this point, we have

$$Y_o = \frac{h}{2} - d'$$

in which

$$d' = \frac{t}{2} \cos \alpha$$

Since d' is usually very small, we may use the approximation $Y_o = h / 2$. Therefore, the total radial displacement of the ring is,

$$\Delta_H^R = D_{10}^R = \left(\frac{r^2}{EA_R} \cos \alpha + \frac{r^2 Y_o e}{EI_R} \right) N_\alpha \quad (8-16)$$

$$\Delta_\alpha^R = D_{20}^R = - \frac{r^2 e}{EI_R} N_\alpha \quad (8-17)$$

For a ring with rectangular cross section, the above relations become

$$D_{10}^R = (\cos \alpha + \frac{12 Y_o e}{h^2}) \frac{r^2 N_t}{Ebh} \quad (8-18)$$

$$D_{20}^R = - \frac{12 r^2 e N_t}{Ebh^3} \quad (8-19)$$

For example, if a spherical dome is acted upon by uniform dead weight of intensity q , then as we know, from chapter 7,

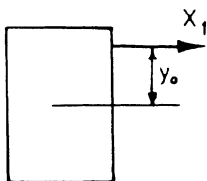
$$N_\alpha = \frac{-qa}{1+\cos \alpha}$$

Then we would have

$$D_{10}^D = + \frac{a^2 q}{Et} \left(\frac{1+v}{1+\cos \alpha} - \cos \alpha \right) \sin \alpha \quad (8-20)$$

$$D_{20}^D = + \frac{aq}{Et} (2+v) \sin \alpha \quad (8-20)$$

As another step in "dome-ring" interaction analysis, we subject the dome and the ring to the edge forces $H = X_1$ and $M_\alpha = X_2$, separately. Figure (8-12) shows that the ring deformation due to force X_1 , applied at Y_o , is



$$\Delta_{1H} = \frac{r^2}{EA_R} X_1$$

$$\Delta_{2H} = \frac{r^2 Y_0^2}{EI_R} X_1 \quad (e = Y_0)$$

$$\Delta_\alpha = - \frac{r^2}{EI_R} Y_0 X_1$$

Figure (8-12)

So, by combining these relations, and putting $X_1 = 1$, we have

$$D_{11}^R = \left(\frac{1}{A_R} + \frac{Y_0^2}{I_R} \right) \frac{r^2}{E} \quad (8-22)$$

$$D_{21}^R = - \frac{r^2 Y_0}{EI_R} \quad \text{+} \quad (8-23)$$

The ring deformation due to a torsional couple X_2 is

$$\Delta_H = - \frac{r^2 Y_0 X_2}{EI_R} \quad \Delta\alpha = \frac{r^2 X_2}{EI_R}$$

So, for $X_2 = 1$ we have

$$D_{12}^R = - \frac{r^2 Y_0}{EI_R} = D_{21}^R \quad (8-24)$$

$$D_{22}^R = \frac{r^2}{EI_R} \quad (8-25)$$

Therefore the *ring influence coefficients*, i.e, the ring deformation for unit radial force and unit twisting couple, observing the sign convention of figure (8-13), are

$$D_{11}^R = (1 + \frac{12 Y_0^2}{h^2}) \frac{r^2}{Ebh} \quad (8-26)$$

$$D_{12}^R = D_{21}^R = - \frac{12 r^2 Y_0}{Eb h^3} \quad (8-27)$$

$$D_{22}^R = \frac{12 r^2}{Eb h^3} \quad (8-28)$$

Figure (8-13)

At this stage, we are prepared to combine the influence coefficients of the dome and the ring to determine the influence coefficients for the "dome-ring" system. The *system influence coefficients* are,

$$\begin{aligned} D_{11} &= D_{11}^D + D_{11}^R \\ D_{12} &= D_{12}^D + D_{12}^R = D_{21} \\ D_{22} &= D_{22}^D + D_{22}^R \end{aligned} \quad (8-29)$$

This completes the "dome-ring" interaction analysis.

8.3.5 - Summary of "Dome-Ring" Analysis Relations

In the following relations, we adopt the sign conventions shown in figure (8-14).

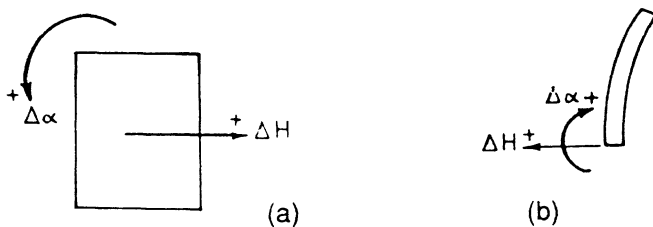


Figure (8-14) Sign conventions, (a) for the ring, (b) for the dome

(a) Membrane deformation field

(a-1) The dome

$$\Delta_{O_H}^D = D_{10}^D = \frac{r_2 \sin \phi}{E t} (N_z - v N_z) \quad (8-30)$$

$$\Delta_{O_1}^D = D_{20}^D = \frac{1}{E t} [N_\phi (r_1 + v r_2) - N_0 (r_2 + v r_1)] \quad (8-31)$$

For spherical rings with radius $r_1 = r_2 = a$,

$$\Delta_{O_H}^D = D_{10}^D = \frac{a^2 q}{E t} \left(\frac{1+v}{1+\cos \phi} - \cos \phi \right) \sin \phi \quad (8-32)$$

$$\Delta_{O_\alpha}^D = D_{20}^D = - \frac{a q}{E t} (2+v) \sin \phi \quad (8-33)$$

(a-2) The ring, figure (8-15):

$$D_{10}^R = (\cos \alpha + \frac{12Y_{0\alpha}}{h^2}) \frac{r^2 N_\alpha}{Ebh} \quad (8-34)$$

$$D_{20}^R = - \frac{12r^2 e}{Ebh^3} N_\alpha \quad (8-35)$$

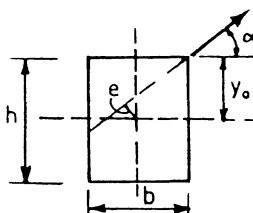


Figure (8-15) Eccentrically applied membrane force to the ring

For a spherical dome with vertical dead weight load q:

$$N_\alpha = - \frac{aq}{1 + \cos \alpha} \quad (8-36)$$

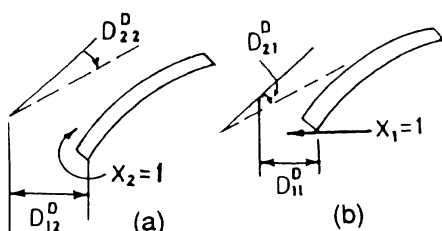
(b) Bending field - The influence coefficients

(b-1) The dome, figure (8-16):

$$D_{11}^D = \frac{2\alpha \lambda \sin^2 \alpha}{Et} \quad (8-37)$$

$$D_{12}^D = D_{21}^D = \frac{2\lambda^2 \sin \alpha}{Et} \quad (8-38)$$

$$D_{22}^D = \frac{4\lambda^3}{Ea t} \quad (8-39)$$



Figure(8-16) Positive sign convention for the influence coefficients of the dome

(b-2) The ring, figure (8-17):

$$D_{11}^R = \left(1 + \frac{12Y_o^2}{h^2}\right) \frac{r^2}{Ebh} \quad (8-40)$$

$$D_{12}^R = D_{21}^R = -\frac{12r^2 Y_o}{Ebh^3} \quad (8-41)$$

$$D_{22}^R = \frac{12r^2}{Ebh^3} \quad (8-42)$$

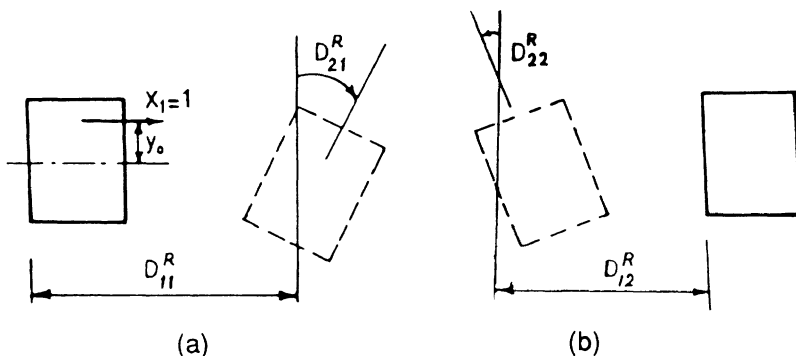


Figure (8-17) Positive sign convention for the ring influence coefficients

8.3.6 - Application of the Force Method

Having obtained all necessary influence coefficients and membrane deformations, we are now prepared to apply the final relations of the force method to the "dome-ring" system. We must satisfy the compatibility relations which express the continuity of radial displacement and rotation at the "dome-ring" junction. These are

$$(D_{10}^D + D_{11}^D x_1 + D_{12}^D x_2) = - (D_{10}^R + D_{11}^R x_1 + D_{12}^R x_2) \quad (8-43a)$$

$$(D_{20}^D + D_{21}^D x_1 + D_{22}^D x_2) = - (D_{20}^R + D_{21}^R x_1 + D_{22}^R x_2) \quad (8-43b)$$

Using the parameters defined in relations (8-29) we write the compatibility relations as

$$D_{11} x_1 + D_{12} x_2 + D_{10} = 0 \quad D_{10} = D_{10}^D + D_{10}^R \quad (8-44a)$$

$$D_{12} x_1 + D_{21} x_2 + D_{20} = 0 \quad D_{20} = D_{20}^D + D_{20}^R \quad (8-44b)$$

By solving these linear simultaneous algebraic equations, we determine the two unknown redundant forces X_1 and X_2 ; they are

$$x_1 = H = - \frac{D_{22}D_{10} - D_{12}D_{20}}{D_{22}D_{11} - D_{12}^2} \quad (8-45a)$$

$$x_2 = M_\alpha = - \frac{D_{11}D_{20} - D_{12}D_{10}}{D_{22}D_{11} - D_{12}^2} \quad (8-45b)$$

The final step in the "dome-ring" problem is to combine the bending field induced by these forces with the membrane field.

Sometimes, the shell structure consists of a "dome-ring-wall" system, as in a large cylindrical container. In these cases, two sets of compatibility relations are required: that between the dome and the ring and that between the ring and the cylindrical wall. Presently, we do have all the ingredients to write these compatibility relations. Therefore, the problems of cylindrical walls with domed roofs having a ring can also be treated in a similar fashion. This type of problem will be treated in chapter 11.

8.4 - Buckling Considerations in the Design of Domes

Domes have doubly curved, synclastic, nondevelopable surfaces, and are generally very stable. Nevertheless, the buckling must be considered in the choice of dome thickness. Construction requirements also play a major role in the choice of shell thickness for thin reinforced concrete domes.

In chapter 13 we discuss the buckling of shells, and give formulas for the buckling loads of domes. We can use those data in the actual design of reinforced concrete domes.

8.5 - Design Guides for Dome Geometry

The relative dimensions of concrete domes vary with the particular situation, service conditions, and the means of construction. We present some general guidelines for the initial design and quantity estimates related to concrete domes.

Figure (8-18) presents a design chart representing the appropriate rise to span ratios of concrete domes. Table (8-1) gives the ratios of the span, thickness, central angle, rise, and radius of spherical domes.

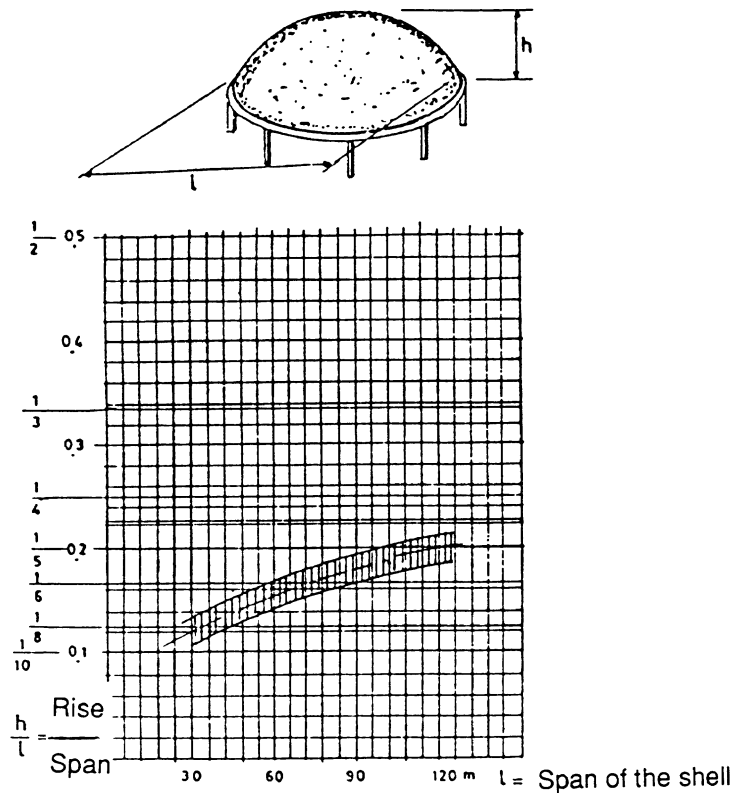
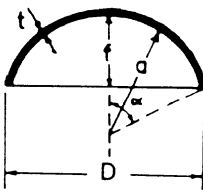


Figure (8-18) Appropriate Proportions of rise to span ratio for concrete domes

Table (8-1) Appropriate dimensions for spherical concrete domes

section	D meter	t cm	α deg	f meter	a meter
	30 . 0	7 . 5	30	4 . 02	30 . 0
	40 . 0	7 . 5	45	6 . 22	21 . 22
	45 . 0	9 . 0 (7.5)	30	5 . 36	40 . 0
	55 . 0	10. 0 (9.0)	45	8 . 29	28 . 29
	60 . 0	11. 5 (10.0)	30	6 . 03	45 . 0
			45	9 . 32	31 . 82
			30	7 . 37	55 . 0
			45	11. 40	38 . 90
			30	8 . 04	60 . 0
			45	12. 43	42 . 43

8.6 - Design of a Reinforced Concrete "Dome-Ring" Roof

In this section, we present the design of a reinforced concrete shell roof composed of a dome with a ring all resting on a vertical support. The dome is assumed to be part of a sphere with half central angle $\alpha = 28^\circ$. The geometrical details of dome shell connection are depicted in figure (8-19). The purpose of this problem is to design the reinforcing steel in the dome and the ring. The reinforcement steel has an assumed allowable tensile stress of 1200 kg / cm², and

$$a = 29.0 \text{ m}$$

$$t = 10 \text{ cm} = 0.1 \text{ m}$$

$$\alpha = 28^\circ$$

$$h = 45 \text{ cm} = 0.45 \text{ m}$$

$$b = 20 \text{ cm} = 0.20 \text{ m}$$

$$q = 300 \text{ kg/m}^2$$

$$E = 2 \times 10^5 \text{ Kg/cm}^2$$

$$\nu = 0.0$$

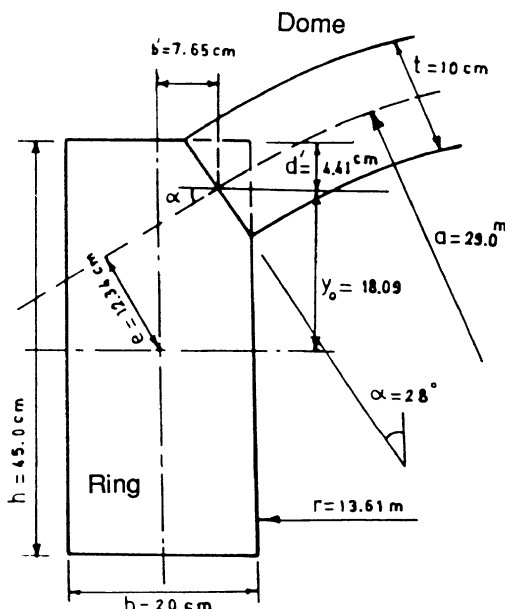


Figure (8-19) A design problem of a reinforced concrete dome with a ring

Design:

To design this shell structure, we must first determine the internal force field in the "dome-ring" system. For this purpose, we employ the method developed in the earlier sections of this chapter. The numerical calculations based on the force method of shell analysis are carried out in the following.

The numerical values of parameters Y_0 , e , d' , and λ are

$$\begin{aligned} d' &= \frac{t}{2} \times \cos \alpha = 5 \times 0.88 = 4.41 \text{ cm} & \sin \alpha &= 0.47 \\ Y_0 &= \frac{h}{2} - d' = 22.50 - 4.41 = 18.09 \text{ cm} & \cos \alpha &= 0.88 \\ b' &= \frac{b}{2} - \frac{t}{2} \sin \alpha = 10.00 - 2.35 = 7.65 \text{ cm} \\ e &= (\frac{h}{2} - d' - b' \tan \alpha) \cos \alpha = (22.50 - 4.41 - 4.07) 0.88 = 12.34 \text{ cm} \\ r &= a \sin \alpha - \frac{t}{2} \sin \alpha = 13.61 \text{ m} \\ \lambda^4 &= 3(1-v^2) \left(\frac{a}{t}\right)^2 = 3\left(\frac{29.0}{0.1}\right)^2 = 25.23 \times 10^4 \longrightarrow \lambda = 22.41 \end{aligned}$$

Now we calculate the numerical values for the flexibility influence coefficients and the membrane deformations. By direct substitution of assumed data in the appropriate formulas we obtain:

$$\begin{aligned} D_{11}^D &= \frac{1}{E} \frac{2a\lambda \sin^2 \alpha}{t} = \frac{1}{E} \cdot \frac{2 \times 29.0 \times 22.41 \times (0.47)^2}{0.1} = \frac{1}{E} 2871.21 \\ D_{12}^D &= \frac{1}{E} \frac{2\lambda^2 \sin \alpha}{t} = \frac{1}{E} \cdot \frac{2 \times (22.41)^2 (0.47)}{0.1} = \frac{1}{E} 4720.76 = D_{21}^D \\ D_{22}^D &= \frac{1}{E} \frac{4\lambda^3}{at} = \frac{1}{E} \cdot \frac{4(22.41)^3}{29.0 \times 0.1} = \frac{1}{E} 15523.43 \end{aligned}$$

$$\begin{aligned} D_{11}^R &= \frac{1}{E} \left(1 + \frac{12Y_0}{h^2}\right) \frac{r^2}{bh} = \frac{1}{E} \left(1 + \frac{12 \times (18.09)^2}{(45)^2}\right) \frac{(13.61)^2}{0.45 \times 20} = \frac{1}{E} 6049. \\ D_{12}^R &= -\frac{1}{E} \frac{12r^2 Y_0}{bh^3} = -\frac{1}{E} \frac{12 \times (13.61)^2 \times 0.1809}{0.20 \times (0.45)^3} = -\frac{1}{E} 22063.2 \\ D_{22}^R &= \frac{1}{E} \frac{12r^2}{bh^3} = \frac{1}{E} \frac{12(13.61)^2}{0.20 \times (0.45)^3} = \frac{1}{E} 121963.5 \end{aligned}$$

Deformation of the dome and the ring due to distributed loading:

$$\begin{aligned}
 D_{10}^D &= \frac{a^2 q}{E t} \left(\frac{1+v}{1+\cos \alpha} - \cos \alpha \right) \sin \alpha \\
 &= \frac{(29)^2 \times q}{E \times 0.1} \left(\frac{1}{1+0.88} - 0.88 \right) 0.47 = - \frac{1}{E} 1375.88 q \\
 D_{20}^D &= \frac{aq}{Et} (2+v) \sin \alpha = \frac{29q}{E \times 0.1} (2) 0.47 = \frac{1}{E} 27260 q \\
 D_{10}^R &= (\cos \alpha + \frac{12Y_{oe}}{h^2}) \frac{r^2}{Ebh} \left(\frac{-aq}{1+\cos \alpha} \right) = - 69935.62 \frac{q}{E} \\
 D_{20}^R &= - \frac{12r^2 e}{Ebh^3} \left(- \frac{qa}{1+\cos \alpha} \right) = + 232158.86 \frac{q}{E}
 \end{aligned}$$

Influence coefficients of the "dome-ring" system:

$$\begin{aligned}
 ED_{11} &= 2871.21 + 6049.37 = 8920.58 \\
 ED_{12} &= 4720.76 - 22063.2 = - 17342.47 \\
 ED_{22} &= 15523.43 + 121963.5 = + 137486.93 \\
 ED_{10} &= - 1375.88q - 69935.62q = - 71311.50 q \\
 ED_{20} &= 272.60 q + 232158.86 q = + 232431.46 q
 \end{aligned}$$

If we substitute these values in the parametric solution of the compatibility relations, i.e., expressions (8-45), we find

$$H = - \frac{(137486.93)(-71311.50) - (-17342.44)(232431.46)}{(137486.93)(8920.58) - (-17342.44)} q = + 6.24q$$

$$M_\alpha = - \frac{(8920.58)(232431.46) - (-17342.44)(-71311.50)}{(137486.93)(8920.58) - (-17342.44)} = - 0.904q$$

So, for $q = 300 \text{ kg/m}^2$ we have

$$H = + 6.24 \times 300 = 1872 \text{ kg/m}$$

$$M_\alpha = - 0.904 \times 300 = - 271.2 \frac{\text{kg-m}}{\text{m}}$$

Having obtained the edge forces, we can now use the expressions in table (9-1) to determine the bending field in the dome. The appropriate expressions are

$$\begin{aligned} M_\phi &= \frac{a}{\lambda} \sin \alpha e^{-\lambda \psi} \sin \lambda \psi H + \sqrt{2} e^{-\lambda \psi} \sin(\lambda \psi + \frac{\pi}{4}) M_\alpha \\ N_\theta &= -2 \lambda \sin \alpha e^{-\lambda \psi} \sin(\lambda \psi - \frac{\pi}{2}) H - \frac{2\sqrt{2}}{a} \lambda^2 e^{-\lambda \psi} \sin(\lambda \psi - \frac{\pi}{4}) M_\alpha \\ N_\phi &= -\sqrt{2} \cot(\alpha - \psi) \sin \alpha e^{-\lambda \psi} \sin(\lambda \psi - \frac{\pi}{4}) H - \frac{2\lambda}{a} \cot(\alpha - \psi) e^{-\lambda \psi} \sin(\lambda \psi) M_\alpha \end{aligned}$$

Here $\psi = \alpha - \phi$. If we substitute the numerical values in the above relations, we obtain the following expressions for our problem.

$$\begin{aligned} M_\phi &= 1138.57 e^{-\lambda \psi} \sin \lambda \psi - 383.53 e^{-\lambda \psi} \sin(\lambda \psi + \pi/4) \\ N_\theta &= -39434.43 e^{-\lambda \psi} \sin(\lambda \psi - \pi/2) + 13283.74 e^{-\lambda \psi} \sin(\lambda \psi - \frac{\pi}{4}) \\ N_\phi &= -2647.41 \cot(\alpha - \psi) \underbrace{e^{-\lambda \psi}}_{\sin \alpha} \sin(\lambda \psi - \frac{\pi}{4}) + 419.14 \cot(\alpha - \psi) e^{-\lambda \psi} \sin \lambda \psi \end{aligned}$$

To determine the complete internal force field, we must add to these bending forces the internal membrane forces. The calculations related to determination of bending and membrane fields are summarized in tables (8-2) and (8-3).

Table (8-2)

ψ		$\sin \lambda \psi$	$\sin(\lambda \psi + \frac{\pi}{4})$	$\sin(\lambda \psi - \frac{\pi}{2})$	$\sin(\lambda \psi - \frac{\pi}{4})$	$\cot \gamma (\alpha - \psi)$	$e^{-\lambda \psi}$
DEG.	Rad.						
0.0	0.0	0.0	+0.71	-1.00	+0.71	+1.88	+1.00
3.0	0.05	+0.92	+0.93	-0.39	+0.38	+2.14	+0.33
6.0	0.10	+0.71	+0.069	+0.70	+1.0	+2.48	+0.11
9.0	0.15	-0.37	-0.92	+0.93	+0.40	+2.90	+0.03
12.0	0.21	-1.0	-0.72	+0.02	-0.69	+3.49	+0.01
15.0	0.26	-0.40	+0.36	-0.91	-0.93	+4.03	+0.003
28.0	0.49	-1.0	-0.74	+0.04	-0.68	—	0

Table (8-3)

		bending field			membrane field			total field		
ϕ^o	ψ^o	M_ϕ	N_θ	N_ψ	M_ψ	N_θ^*	N_ψ^{**}	M_ϕ	N_θ	N_ψ
28	0.0	-271.2	29998.84	1652.8	0.0	-3061.2	-4620.4	-271.2	26936.8	-2967.6
25	3.0	214.52	6269.4	-55.58	0.0	-3321.1	-4563.8	214.52	2948.3	-4619.4
22	6.0	77.29	-1369.05	-223.43	0.0	-3552.1	-4514.4	77.29	-4921.15	-4737.8
19	9.0	-2.02	-927.4	-53.55	0.0	-3754.2	-4471.8	-2.02	-4681	-4527.3
16	12.0	-7.9	-91.01	14.15	0.0	-3927.1	-4435.9	-7.9	-4526.9	-4421.8
13	15.0	-1.7	66.93	12.13	0.0	-4070.6	-4406.5	-1.7	-4003	-4394.4
0	28.0	0	0	0	0.0	-4350.0	-4350.0	0	-4350	-4350

$$* N_\theta = aq \left(\frac{1}{1 + \cos\phi} - \cos\phi \right) \quad ** N_\psi = -aq(1 + \cos\phi)$$

Using the numerical values of table (8-3) we plot the variations of internal forces in this dome in figures (8-20a) to (8-20c). For comparison, we present the plots of the membrane field. As we see, the influence of the bending field, arising from the edge ring, is local and *dies out* as we move away from the boundary region.

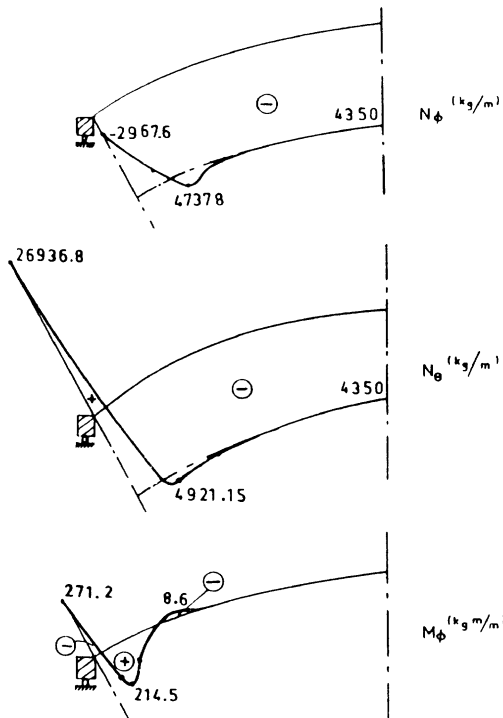


Figure (8-20) Variation of internal membrane (dashed) and bending forces in the "dome-ring" shell of figure (8-18)

The reinforcement design of the dome is based on finding the hoop and meridional reinforcements. The hoop reinforcement (per unit width of the shell) which would be needed in the lower part of the dome is determined with help of diagram (8-19b). The required reinforcement is:

$$A_{\theta} = \frac{26941.7}{1200} = 22.45 \text{ cm}^2/\text{m}$$

We note from diagram (8-19b) that beyond the meridional angle $\psi = 5^\circ$ the hoop stresses are compressive. Hence, at the upper part of the dome there would be no need for any calculated reinforcement. However, a minimum reinforcement is placed there to control the shrinkage of concrete as well as to absorb the stresses caused from temperature changes.

We see from diagram (8-19a) that the meridional force is compressive throughout the shell. Hence, from the structural viewpoint, there would be no need for a designed reinforcement along the meridional direction. However, we provide the shell with a minimum amount of shrinkage and temperature steel which, in this case, is chosen to be 14 mm diameter bars placed 40 cm apart.

In addition to the mesh-type reinforcement, the dome must be provided with bending reinforcement at the lower region. This bending reinforcement is determined with the help of diagram (8-19c):

$$A_{\phi} = \frac{272.3 \times 100}{0.875 \times 7 \times 1200} = 3.70 \text{ cm}^2/\text{m}$$

Having designed the reinforcement for the dome, we now determine the reinforcing steel for the *ring*. The bending moment at a typical section of the ring is

$$M_x = M_{\phi} \cdot r = -271.2 \times 13.61 \text{ } \text{kg-m} = -3691.0 \text{ } \text{kg-m}$$

so, the required bottom reinforcement would be

$$A_s = \frac{3691.0 \times 100}{0.875 \times 40 \times 1200} = 8.79 \text{ cm}^2$$

In addition to this, we should strengthen the ring for torsional effects; for this purpose, we provide the ring with top reinforcement as well as transverse *closed* stirrups.

Figure (8-21) shows the plan of dome reinforcement designed according to this procedure. Note that, for the presently assumed axisymmetric loading, the reinforcement pattern is axisymmetric, but for a compact presentation, all three types of reinforcements are shown in a single figure.

Figure (8-22) shows the detail of ring reinforcement as well as detail of "dome-ring" connection.

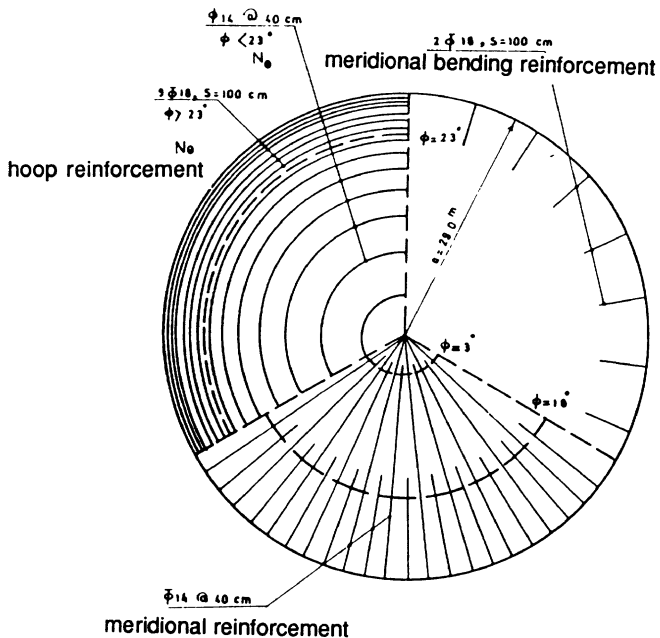


Figure (8-21) plan of reinforcement of the dome of figure (8-19)

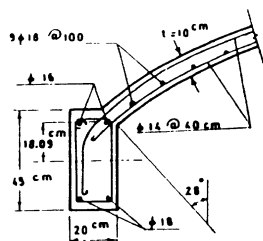


Figure (8-22) Detail of ring reinforcement and the "dome-ring" connection of the shell in figure (8-19)

The dome under design consideration must also be checked for buckling strength. In chapter 13, we will present a number of formulas for the buckling loads of the shells of revolution shall be presented. Those guidelines will show that the thickness of 10 cm of the dome is quite adequate to withstand buckling.

Problems

P 8.1- The concrete dome roof of a hall is supported on a cylindrical wall (or beams over columns) around its circumference as shown in figure (P8-1). A 2.4 m-wide annular slab surround the dome, acting as an overhead canopy. The loading on the dome is 3000 N/m^2 over the surface area, and the loading on the slab is 500 N/m^2 . Dimensions for the dome and the slab are shown. Poisson's ratio is assumed to be zero, and modulus of elasticity for concrete is assumed equal to 2000 N/mm^2 .

- (1) Analyze this dome for the applied loading.
- (2) Determine the steel reinforcement needed for this dome. The allowable stress of steel is assumed equal to 150 N/mm^2 .

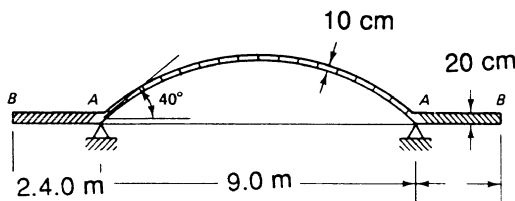


Figure (P 8-1)

P 8.2- Determine the steel reinforcement for the concrete dome of example 7.8. Use the steel bars with an allowable stress of 1500 kg/cm^2 .

References for Chapter Eight

- 8.1 - M. Farshad, *Shell Structures*, (In Farsi) Two volumes, Vol.: I 1986, Vol. II: 1987, University of Shiraz Publications, Shiraz
- 8.2 - W. Flügge, *Stresses in Shells*, Springer Verlag, New York, 1973
- 8.3 - D.P. Billington, *Thin Shell Concrete Structures*, 2nd ed., McGraw-Hill Book Company, New York, 1982
- 8.4 - V. S. Kelkar, and R. T. Sewell, *Fundamentals of the Analysis and Design of Shell Structures*, Prentice-Hall, INC., New Jersey, 1987

Chapter 9

Analysis of Shells with Arbitrary Geometry

9.1 - Introduction

Varieties of surfaces from which various shells may be designed and constructed are practically infinite. With the advent of such materials as reinforced concrete, prestressed concrete, ferro-cement, fiber-reinforced concrete, composites, and reinforced plastics, the varieties of shell geometries have been further increased. The choice of a particular surface geometry for the shell depends on the functional, structural, and architectural requirements.

Simple shell geometries, such as cylindrical forms and the shells of revolutions, can also be combined to give more elaborate shell forms suited for specific purposes. The set of figures (9-1) show some examples of combined shells and / or shells having new geometrical shapes. The structural design and analysis of combined or arbitrarily shaped shells, however, requires a methodology of its own to which the present chapter is devoted.

In the first part of this chapter, we will determine the membrane equilibrium equations for shells with general geometrical forms. Then, to solve these equations and to determine the membrane forces, we present an analytical technique, called *the method of stress functions*. In a later section of this chapter, we develop a simplified theory of shallow shells. This theory can be used in the bending analysis of many shells. In particular, this theory will be applied to the analysis and design of **Hyperbolic Paraboloid** shells which will be treated in the following chapter.

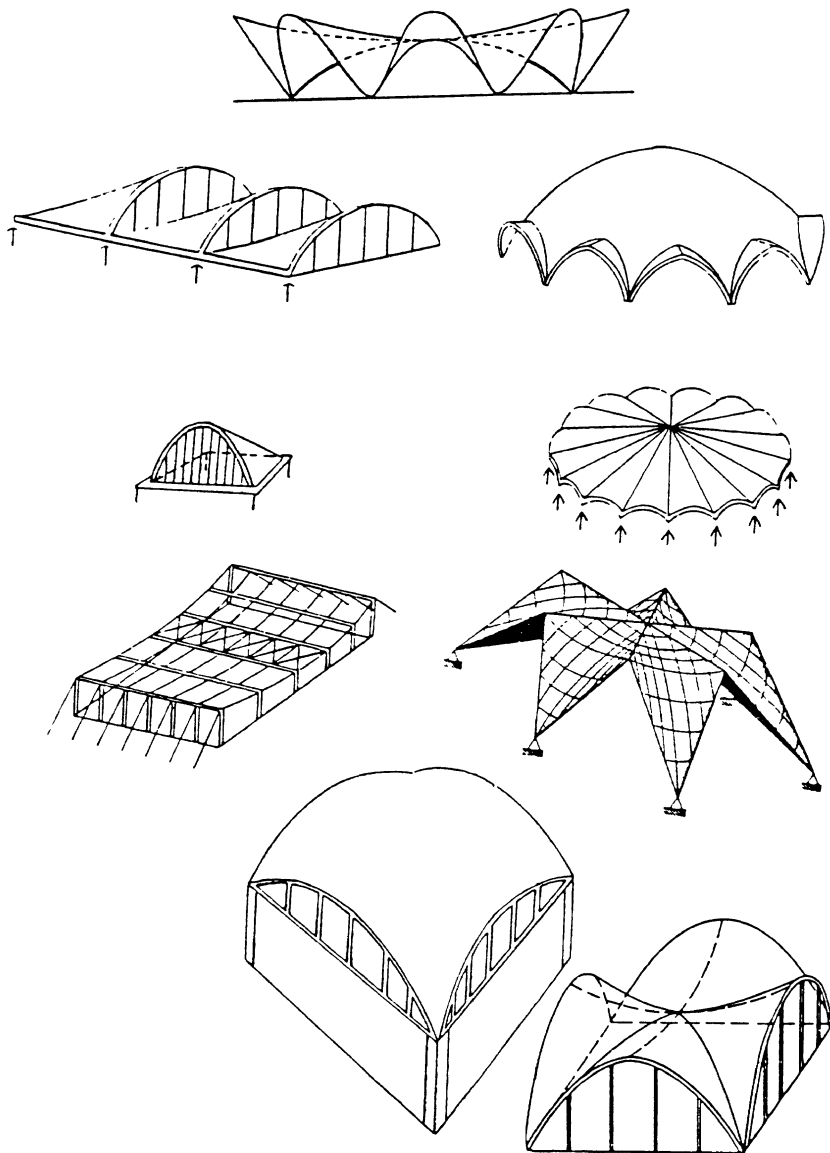


Figure (9-1) Examples of shells with various geometrical shapes

9.2 - Membrane Theory of General Shells

9.2.1 - Geometrical Description of Arbitrary Surfaces

To derive the governing equilibrium equations of general shells, we consider an element of shell mid-surface as shown in figure (9-2). In this figure, ABCD is an infinitesimal surface element, separated from the shell by two pairs of planes. This element is assumed to have an infinitesimal rectangular horizontal projection, A'B'CD'. The horizontal plane is identified by the orthogonal x-y coordinate system. The z axis is then oriented along the vertical direction. The symbols ϕ and ψ , denote the angles between the tangents, at point A, to the sides of this surface element and the x and the y directions, respectively. The sides of the infinitesimal element in horizontal projection, A'B'CD', are assumed to be equal to dx and dy .

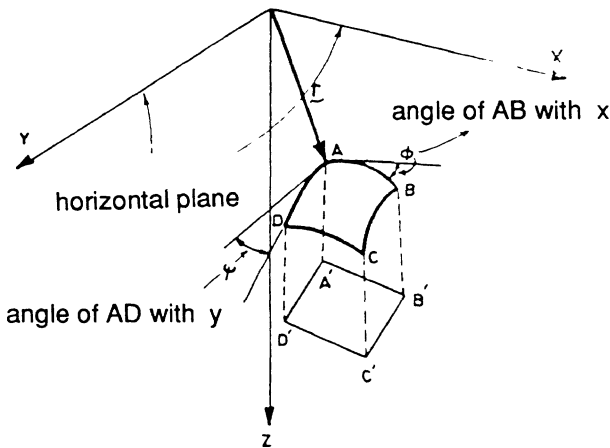


Figure (9-2) An infinitesimal element of a general surface and its horizontal projection

We denote the unit vectors along the x, y, and z axes, of the global Cartesian coordinate system xyz, by \mathbf{i} , \mathbf{j} , and \mathbf{k} , respectively. The position vector, \mathbf{r}_A , of the corner point A can be written as

(9-1)

Since the unit vectors (\hat{i} , \hat{j} , \hat{k}) are constant the partial derivatives of \hat{r} in this system can be expressed as

$$\frac{\partial \hat{r}}{\partial x} = \hat{i} + \frac{\partial z}{\partial x} \hat{k} \quad (9-2)$$

$$\frac{\partial \hat{r}}{\partial y} = \hat{j} + \frac{\partial z}{\partial y} \hat{k}$$

Therefore, the lengths of line segments AB and AD are, respectively

$$|\frac{\partial \hat{r}}{\partial x}| dx = \sqrt{1 + (\frac{\partial z}{\partial x})^2} dx = \sqrt{1 + p^2} dx \quad (9-3)$$

and

$$|\frac{\partial \hat{r}}{\partial y}| dy = \sqrt{1 + (\frac{\partial z}{\partial y})^2} dy = \sqrt{1 + q^2} dy \quad (9-4)$$

In these relations

$$p = \frac{\partial z}{\partial x} \quad q = \frac{\partial z}{\partial y}$$

In figure (9-2), the quantities p and q have the following geometrical interpretation:

$$\begin{aligned} p &= \tan \phi \\ q &= \tan \psi \end{aligned} \quad (9-5)$$

so that

$$\cos \phi = \frac{A'B'}{AB} = \frac{1}{\sqrt{1 + p^2}} \quad (9-6)$$

$$\cos \psi = \frac{A'D'}{AD} = \frac{1}{\sqrt{1 + q^2}}$$

The spatial angle, ω , between the generally non-orthogonal sides AB and AD, of the spatial shell element, can be determined by calculating the inner (scalar) product of their respective vectors. So

$$\left(\frac{\partial \tilde{r}}{\partial x}\right) \cdot \left(\frac{\partial \tilde{r}}{\partial y}\right) = \frac{\partial Z}{\partial x} \cdot \frac{\partial Z}{\partial y} = pq \quad (9-7)$$

Equating this to the equivalent expression

$$\begin{aligned} \left(\frac{\partial \tilde{r}}{\partial x}\right) \cdot \left(\frac{\partial \tilde{r}}{\partial y}\right) &= \left|\frac{\partial \tilde{r}}{\partial x}\right| \cdot \left|\frac{\partial \tilde{r}}{\partial y}\right| \cos\omega \\ &= \sqrt{1 + p^2} \sqrt{1 + q^2} \cos\omega = pq \end{aligned} \quad (9-8)$$

we obtain

$$\cos\omega = \frac{pq}{\sqrt{1+p^2} \sqrt{1+q^2}} \quad (9-9)$$

Furthermore, the infinitesimal surface area of ABCD is:

$$dA = (AB) (AD \sin\omega) \quad (9-10)$$

The value of elemental area, dA , can also be calculated by forming the vector product of two vectors representing the sides AB and AD. The resulting expression is,

$$dA = \sqrt{1 + p^2 + q^2} dx dy \quad (9-11)$$

We now have all the geometrical ingredients and can proceed with the membrane analysis of shells with arbitrary geometry.

9.2.2 - Methodology of Membrane Analysis of General Shells

In order to carry out membrane analysis of shells with arbitrary geometry we use a well-established methodology in which the *stress function* solution scheme is employed.

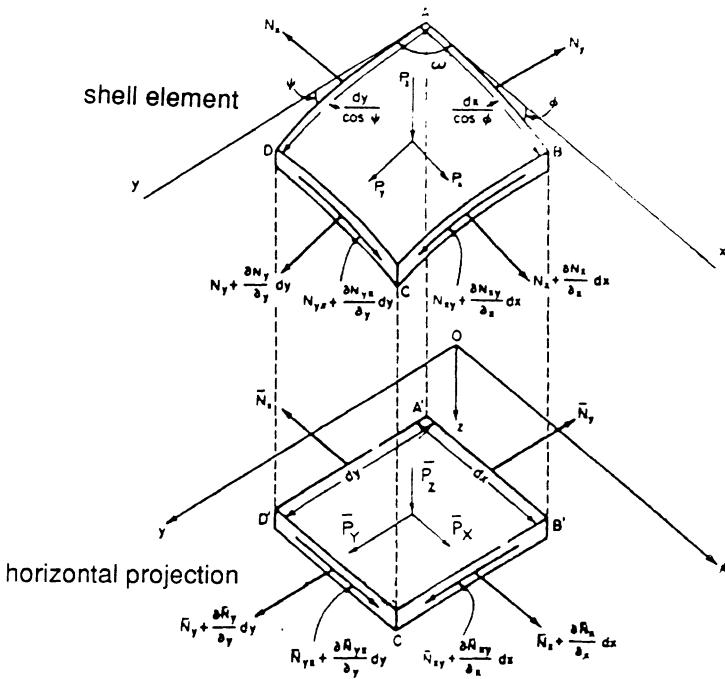


Figure (9-3) Free body diagram of an arbitrary shell element and its horizontal projection.

Consider an infinitesimal element of the shell having a rectangular horizontal projection, as shown in the figure (9-3). Figure (9-3) shows the free-body diagram of the actual shell element as well as the so-called "free-body diagram" of its horizontal projection. In this figure, the quantities N_x , N_y , and N_{xy} are the actual internal membrane forces, while the quantities \bar{N}_x , \bar{N}_y , and \bar{N}_{xy} designate the corresponding fictitious *in-plane* forces acting on the horizontally projected element.

The two sets of forces, i.e., the actual membrane forces (N_x, N_y, N_{xy}) and their plane-stress projections ($\bar{N}_x, \bar{N}_y, \bar{N}_{xy}$), can be related using the shell geometry. Referring to figure (9-3), and using the relations obtained before, we can write the relation between N_x and its horizontal projection (\bar{N}_x) as

$$\bar{N}_x dy = N_x dy \frac{\cos\phi}{\cos\psi}$$

or

$$N_x = \bar{N}_x \sqrt{\frac{1 + p^2}{1 + q^2}} \quad (9-12)$$

In a similar fashion, we obtain

$$N_y = \bar{N}_y \sqrt{\frac{1 + q^2}{1 + p^2}} \quad (9-13)$$

and

$$N_{xy} = \bar{N}_{xy} \quad (9-14)$$

Moreover, the actual distributed applied loads (p_x, p_y, p_z) can be related to their corresponding horizontal projections ($\bar{p}_x, \bar{p}_y, \bar{p}_z$). If the projected area is designated by dA' , then the relation between the actually applied forces and their horizontal projections would be,

$$\bar{p}_{x,y,z} dA' = p_{x,y,z} dA$$

or

$$\bar{p}_{x,y,z} dx dy = p_{x,y,z} \sqrt{1 + p^2 + q^2} dx dy$$

Which, in expanded form, gives

$$\bar{p}_x = p_x \sqrt{1 + p^2 + q^2}$$

$$\bar{p}_y = p_y \sqrt{1 + p^2 + q^2} \quad (9-15)$$

$$\bar{p}_z = p_z \sqrt{1 + p^2 + q^2}$$

We now have the relations between the actual membrane forces and their horizontal projections. Hence, if we could determine the force field of horizontal projection of the shell, then we could, in principle, use these relations to find the actual membrane force field for the given shell.

Thus we have converted the problem of spatial shell analysis to that of a *plane stress analysis* together with another problem which, as we shall see, is much easier to handle analytically than the original shell problem.

9.2.3 - Equilibrium Equations of General Shells

We first refer to the free body diagram of the projected shell element of figure (9-3) the horizontal view of which is shown in figure (9-4). The equilibrium equations for the projected field are the usual ones for a plane element, namely

$$\sum F_x = 0 \implies \frac{\partial \bar{N}_x}{\partial x} + \frac{\partial \bar{N}_{xy}}{\partial y} + \bar{P}_x = 0 \quad (9-16)$$

$$\sum F_y = 0 \implies \frac{\partial \bar{N}_y}{\partial y} + \frac{\partial \bar{N}_{xy}}{\partial x} + \bar{P}_y = 0 \quad (9-17)$$

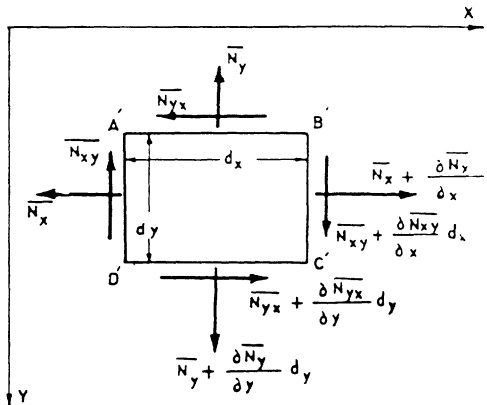


Figure (9-4) Top view of free body diagram of the projected rectangular element

To write down the third equilibrium equation, i.e., the equilibrium of actual forces in the vertical (z) direction, we go back to the actual shell element ABCD of figure (9-4). We now write the vertical equilibrium relation for the *actual forces* (N_x, N_y , and N_{xy}) but we try to express this equation of equilibrium in terms of the projected *fictitious forces* \bar{N}_x, \bar{N}_y , and \bar{N}_{xy} .

The vertical projection of the actual membrane force acting normal to the side AD, in terms of its fictitious counterpart, is

$$N_x \cdot AD \cdot \tan\phi = N_x (\sqrt{1 + q^2} \cdot dx) \frac{p}{\sqrt{1 + p^2}}$$

$$= N_x \sqrt{\frac{1 + q^2}{1 + p^2}} pdy = \bar{N}_x \frac{\partial z}{\partial x} dy$$

Similarly, the vertical projection of the membrane force normal to the side BC is

$$\bar{N}_x \frac{\partial z}{\partial x} dy + \frac{\partial}{\partial x} (\bar{N}_x \frac{\partial z}{\partial x}) dx dy$$

Therefore the resultant of these two forces is

$$\frac{\partial}{\partial x} \left[\bar{N}_x \left(\frac{\partial z}{\partial x} \right) \right] dx dy$$

In a similar fashion, the resultant of vertical projections of forces normal to the sides AB and CD are found to be

$$\frac{\partial}{\partial y} (\bar{N}_y \frac{\partial z}{\partial y}) dx dy$$

The vertical projection of the membrane shear force acting on the side AD is

$$\bar{N}_{xy} \cdot AD \cdot \tan\phi = \bar{N}_{xy} \frac{\partial z}{\partial y} dy$$

and the vertical component of corresponding force acting on BC is

$$\bar{N}_{xy} \frac{\partial z}{\partial y} dy + \frac{\partial}{\partial x} (\bar{N}_{xy} \frac{\partial z}{\partial y}) dx dy$$

The resultant of these two forces is

$$\frac{\partial}{\partial x} \left[\bar{N}_{xy} \left(\frac{\partial z}{\partial x} \right) \right] dx dy$$

The resultant of vertical projections of shear forces acting on the sides AB and CD is similarly

$$\frac{\partial}{\partial y} \left[\bar{N}_{xy} \left(\frac{\partial z}{\partial y} \right) \right] dx dy$$

The contribution of externally applied forces to the equilibrium equation in the vertical direction is ($\bar{P}_z \, dx \, dy$).

Summing up the projections of internal force resultants and the external forces in the vertical direction, and keeping track of proper signs, we obtain the following vertical equilibrium equation for the actual shell element

$$\frac{\partial}{\partial x} (\bar{N}_x \frac{\partial z}{\partial x}) + \frac{\partial}{\partial y} (\bar{N}_y \frac{\partial z}{\partial y}) + \frac{\partial}{\partial x} (\bar{N}_{xy} \frac{\partial z}{\partial y}) + \frac{\partial}{\partial y} (\bar{N}_{xy} \frac{\partial z}{\partial x}) + \bar{p}_z = 0 \quad (9-18)$$

This equation can be written in the expanded form:

$$\begin{aligned} \bar{N}_x \frac{\partial^2 z}{\partial x^2} + 2\bar{N}_{xy} \frac{\partial^2 z}{\partial x \partial y} + \bar{N}_y \frac{\partial^2 z}{\partial y^2} + (\frac{\partial \bar{N}_x}{\partial x} + \frac{\partial \bar{N}_{xy}}{\partial y}) \frac{\partial z}{\partial x} \\ + (\frac{\partial \bar{N}_y}{\partial y} + \frac{\partial \bar{N}_{xy}}{\partial x}) \frac{\partial z}{\partial y} + \bar{p}_z = 0 \end{aligned} \quad (9-19)$$

If we use the relations (9-16) and (9-17) in this equation, we obtain

$$\bar{N}_x \frac{\partial^2 z}{\partial x^2} + 2\bar{N}_{xy} \frac{\partial^2 z}{\partial x \partial y} + \bar{N}_y \frac{\partial^2 z}{\partial y^2} = -\bar{p}_z + \bar{p}_x \frac{\partial z}{\partial x} + \bar{p}_y \frac{\partial z}{\partial y} \quad (9-20)$$

To write this relation in an abbreviated form, we introduce the symbols

$$r = \frac{\partial^2 z}{\partial x^2}, \quad s = \frac{\partial^2 z}{\partial x \partial y}, \quad t = \frac{\partial^2 z}{\partial y^2} \quad (9-21)$$

With these notations, equation (9-20) is

$$r \bar{N}_x + 2s \bar{N}_{xy} + t \bar{N}_y = -\bar{p}_z + p \bar{p}_x + q \bar{p}_y \quad (9-22)$$

The set of equations (9-16), (9-17), and (9-20) constitute the governing equilibrium equations for membrane shells of arbitrary geometry. The relations (9-12), (9-13), and (9-14) give the actual membrane forces in terms of calculated projected forces.

9.2.4 - Solution of Membrane Equations by Stress Function

We solve the system of partial differential equations (9-16), (9-17), and (9-18) by *the method of stress function*. We introduce a generating function, $\Phi(x,y)$, called the **stress function** and we define it as follows:

$$\begin{aligned}\bar{N}_x &= \frac{\partial^2 \Phi}{\partial y^2} - \int \bar{p}_x dx \\ \bar{N}_y &= \frac{\partial^2 \Phi}{\partial x^2} - \int \bar{p}_y dy \\ \bar{N}_{xy} &= - \frac{\partial^2 \Phi}{\partial x \partial y}\end{aligned}\tag{9-23}$$

These expressions satisfy equation (9-16) and (9-17) identically. The third equation, i.e., equation (9-20) yields,

$$\begin{aligned}\frac{\partial^2 z}{\partial x^2} \frac{\partial^2 \Phi}{\partial y^2} - 2 \frac{\partial^2 z}{\partial x \partial y} \frac{\partial^2 \Phi}{\partial x \partial y} + \frac{\partial^2 z}{\partial y^2} \frac{\partial^2 \Phi}{\partial x^2} &= \bar{p}_x \frac{\partial z}{\partial x} + \bar{p}_y \frac{\partial z}{\partial y} - \bar{p}_z \\ &+ \frac{\partial^2 z}{\partial x^2} \int \bar{p}_x dx + \frac{\partial^2 z}{\partial y^2} \int \bar{p}_y dy\end{aligned}\tag{9-24}$$

This relation is a second order linear partial differential equation on the unknown stress function, $\Phi(x,y)$; it has variable coefficients which are dependent on the shell geometry. For a shell with specified shape, they are known functions of x and y . The right hand side of this equation is a known forcing function which depends on the applied loading as well as the shell geometrical configuration. The formulation of the problem is completed by the specification of the appropriate boundary conditions.

From a mathematical point of view, any second order partial differential equation can be classified as being of *hyperbolic*, *parabolic*, or *elliptic* type, depending on the sign and magnitudes of the coefficients of the second order terms; these depend on the shell geometry. This classification has physical importance. Hyperbolic equations have the property that the disturbances *propagate*, in the shell proper, whereas elliptic equations describe non-propagating features. For a detailed discussion of this subject, the reader is referred to standard books on partial differential equations.

The governing equations derived in this section will be solved analytically and / or by numerical schemes. In the following chapter, we will apply this method to analyze one of the most widely used types of shells, Hyperbolic Paraboloid shells. This method can also be used to find analytical solutions to shells having Elliptic Paraboloids and Conoids as their middle surfaces.

9.3 - Bending Theory of Shallow Shells

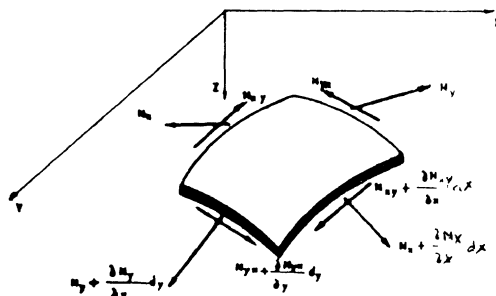
To perform a comprehensive analysis of shells with arbitrary geometry, and in particular those discussed in this chapter we require a bending theory. By application of a proper bending theory, we can determine, for example, the bending field developed around the edge beams of a hyperbolic paraboloid shell.

The analytical treatment of general shell equations is difficult. Numerical solutions to shell equations can be obtained by the Finite Element and / or Finite Difference methods. Analytic solutions though crude be, demonstrate the useful interplay between various parameters.

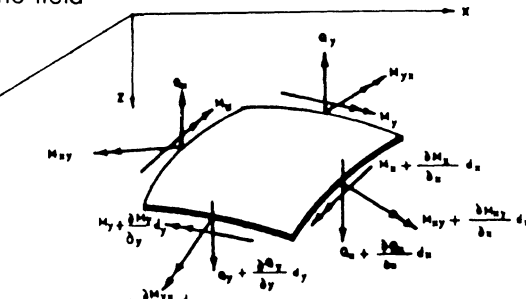
The bending theory of general shells can be simplified to yield equations which can be solved analytically and numerically. One of such simplifications is the so-called "shallow shell theory", based on the **assumptions**:

- (1) The slope of the shell (roof) is small.
- (2) The curvature of the shell, as well as the changes in curvature of the shell, are small. As a guideline, the range of rise to span ratio of less than 1/5 is suggested for shallow shells.
- (3) The loading as well as shell boundaries are such that the applied loads are carried primarily by the in-plane forces.
- (4) The deformations normal to the shell surface are greater than the in-plane deformations.

For practical purposes, many Hyperbolic Paraboloid shells and also Conoidal shells may be considered to be *shallow shells*. This approximate theory is also referred to as **Vlasov Theory** of shallow shells.



(a) membrane field



(b) bending field

Figure (9-5) An element of an arbitrary shallow shell

Consider a shell with a general middle surface defined by the equation $z = z(x,y)$ in an orthogonal Cartesian coordinate system. According to our previous definitions, we have,

$$\frac{\partial^2 z}{\partial x^2} = r \quad \text{Curvature of the surface in the } x \text{ direction} \quad (9-25a)$$

$$\frac{\partial^2 z}{\partial x \partial y} = s \quad \text{Torsion of the shell surface} \quad (9-25b)$$

$$\frac{\partial^2 z}{\partial y^2} = t \quad \text{Curvature of the surface in the } y \text{ direction} \quad (9-25c)$$

With these definitions and related interpretations, we now proceed to derive the governing equations of linearly elastic shallow shells.

(a) Equations of Equilibrium

Consider an infinitesimal element of a shallow shell. Figures (9-5) show the membrane and the bending fields of internal forces acting on this element. We assume that the shell is acted upon by a general distributed force having the components p_x , p_y , and p_z along x , y , and z axes, respectively. In this treatment, z axis is assumed to lie along the vertical direction. Thus, $x-y$ plane defines the horizontal surface.

The equilibrium equations have the following forms:

Equilibrium of forces along x axis

$$\frac{\partial N_x}{\partial x} + \frac{\partial N_{yx}}{\partial y} + p_x = 0 \quad (9-26a)$$

Equilibrium of forces along y axis

$$\frac{\partial N_y}{\partial y} + \frac{\partial N_{xy}}{\partial x} + p_y = 0 \quad (9-26b)$$

Equilibrium of forces along z axis

$$\frac{\partial Q_x}{\partial x} + \frac{\partial Q_y}{\partial y} + N_x \frac{\partial^2 z}{\partial x^2} + 2N_{xy} \frac{\partial^2 z}{\partial x \partial y} + N_y \frac{\partial^2 z}{\partial y^2} + p_z = 0 \quad (9-26c)$$

Equilibrium of moments about z axis

$$M_{yx} = -M_{xy} \quad (9-26d)$$

Equilibrium of moments about x axis

$$\frac{\partial M_y}{\partial y} + \frac{\partial M_{xy}}{\partial y} - Q_y = 0 \quad (9-26e)$$

Equilibrium of moments about y axis

$$\frac{\partial M_x}{\partial x} + \frac{\partial M_{xy}}{\partial x} - Q_x = 0 \quad (9-26f)$$

Equations (9-26e) and (9-26f) can be rewritten as

$$Q_y = \frac{\partial M_y}{\partial y} + \frac{\partial M_{xy}}{\partial x}$$

$$Q_x = \frac{\partial M_x}{\partial x} + \frac{\partial M_{xy}}{\partial y} \quad (9-27)$$

If we substitute the expressions for Q_x and Q_y from these relations into (9-26c) we obtain

$$\frac{\partial^2 M_x}{\partial x^2} + 2 \frac{\partial^2 M_{xy}}{\partial x \partial y} + \frac{\partial^2 M_y}{\partial y^2} + N_x \frac{\partial^2 z}{\partial x^2} + 2N_{xy} \frac{\partial^2 z}{\partial x \partial y} + N_y \frac{\partial^2 z}{\partial y^2} + p_z = 0 \quad (9-28)$$

(b) Kinematic Relations

The displacement field of the mid-surface of the shell is assumed to have three components defined by the functions u , v , and w . Inspired by the corresponding relations for cylindrical shells, we assume the following strain-displacement relations for shallow shells.

$$\epsilon_x = \frac{\partial u}{\partial x} - rw \quad (9-29a)$$

$$\epsilon_y = \frac{\partial v}{\partial y} - tw \quad (9-29b)$$

$$\gamma_{xy} = \frac{\partial u}{\partial y} + \frac{\partial v}{\partial x} \quad (9-29c)$$

In these relations, ϵ_x , ϵ_y , γ_{xy} are the strain components of an arbitrary point in the shell thickness. As we note, in the present approximation, the influence of normal displacement component, w , (which in this approximate theory is assumed to be the same as vertical displacement) is highlighted. In other words, the gradients of other components are neglected in comparison with those of the function w .

The relations between the change in curvature and also the twist of the shell, on one hand, and the displacement gradients, on the other hand, are,

$$\begin{aligned} \chi_x &= \frac{\partial^2 w}{\partial x^2} \\ \chi_y &= \frac{\partial^2 w}{\partial y^2} \\ \chi_{xy} &= \frac{\partial^2 w}{\partial x \partial y} \end{aligned} \quad (9-30)$$

These are the desired kinematic relations for shallow shells.

(c) Constitutive Relations

The constitutive relations for a linearly elastic and isotropic shallow shell, assuming the decoupling of membrane and bending relations, can be expressed as follows:

$$N_x = \frac{Et}{1 - \nu^2} (\epsilon_x + \nu \epsilon_y) \quad (9-31a)$$

$$N_y = \frac{Et}{1 - \nu^2} (\chi_y + \nu \chi_x) \quad (9-31b)$$

$$N_{xy} = N_{yx} = \frac{Et}{2(1+\nu)} \chi_{xy} \quad (9-31c)$$

$$M_x = -k(\chi_x + \nu \chi_y) \quad (9-31d)$$

$$M_y = -k(\chi_y + \nu \chi_x) \quad (9-31e)$$

$$M_{xy} = -k(1-\nu) \chi_{xy} \quad (9-31f)$$

In these relations, the parameters D and K are the *membrane* and *bending stiffnesses* of the shell, respectively.

$$D = \frac{Et}{1 - \nu^2} \quad K = \frac{Et}{12(1 - \nu^2)}$$

@ Seismicisolation

By combining the three types of basic relations, i.e., equilibrium, kinematic and constitutive relations we obtain the governing equations of Vlasov theory of shallow shells. The synthesis procedure is as follows:

By differentiating both sides of relations (9-29a) and (9-29b) twice, with respect to y and x respectively, and after adding up both sides of resulting relations, we obtain

$$\frac{\partial^2 \epsilon_x}{\partial y^2} + \frac{\partial^2 \epsilon_y}{\partial x^2} = \frac{\partial^2 u}{\partial x \partial y} + \frac{\partial^3 u}{\partial y \partial x^2} - r \frac{\partial^2 w}{\partial y^2} - t \frac{\partial^2 w}{\partial x^2} \quad (9-32)$$

and from the relation (9-29c)

$$\frac{\partial^2 \gamma_{xy}}{\partial x \partial y} = \frac{\partial^3 u}{\partial x \partial y^2} + \frac{\partial^3 u}{\partial y \partial x} - 2s \frac{\partial^2 w}{\partial x \partial y} \quad (9-33)$$

Now, by combining relations (9-32) and (9-33) we obtain

$$\frac{\partial^2 \epsilon_x}{\partial y^2} + \frac{\partial^2 \epsilon_y}{\partial x^2} = \frac{\partial^2 \gamma_{xy}}{\partial x \partial y} - r \frac{\partial^2 w}{\partial y^2} + 2s \frac{\partial^2 w}{\partial x \partial y} - t \frac{\partial^2 w}{\partial x^2} \quad (9-34)$$

At this stage, we consider special loading types in which only the applied loading has a vertical component P_z and the other loading components are identically zero. This is common for practical roof shell design problems.

To reduce the number of governing equations, we now introduce a stress function, $\Phi(x,y)$, and we define it in the following fashion:

$$N_x = \frac{\partial^2 \phi}{\partial y^2}, \quad N_y = \frac{\partial^2 \phi}{\partial x^2}, \quad N_{xy} = -\frac{\partial^2 \phi}{\partial x \partial y} \quad (9-35)$$

Also, we rewrite the equation (9-34) in the following form:

$$\left(\frac{\partial^2 \epsilon_x}{\partial y^2} - \frac{\partial^2 \gamma_{xy}}{\partial x \partial y} + \frac{\partial^2 \epsilon_y}{\partial x^2} \right) + (r \frac{\partial^2 w}{\partial y^2} - 2s \frac{\partial^2 w}{\partial x \partial y} + t \frac{\partial^2 w}{\partial x^2}) = 0 \quad (9-36)$$

If we make use of constitutive relations (9-31), the strain displacement relations (9-29) and stress function relations (9-35) in the above relation, we obtain

$$\nabla^4 \phi + Et \nabla_k^2 w = 0 \quad (9-37)$$

$$\nabla_k^2 \equiv (r \frac{\partial^2}{\partial y^2} - 2s \frac{\partial^2}{\partial x \partial y} + t \frac{\partial^2}{\partial x^2})$$

In which

$$\nabla^4 = \left(\frac{\partial^2}{\partial x^2} + \frac{\partial^2}{\partial y^2} \right) \left(\frac{\partial^2}{\partial x^2} + \frac{\partial^2}{\partial y^2} \right) = \frac{\partial^4}{\partial x^4} + 2 \frac{\partial^4}{\partial x^2 \partial y^2} + \frac{\partial^4}{\partial y^4} \quad (9-38)$$

Now, substituting relations (9-31d), (9-31e), and (9-31f), and also relations (9-30) and (9-35), into the equation (9-38), we obtain

$$-K\nabla^4 w + \nabla_k^2 \phi + p_z = 0$$

or

$$K\nabla^4 w - \nabla_k^2 \phi = p_z \quad (9-39)$$

Equations (9-37) and (9-39) constitute the governing equations of Vlasov theory of shallow shells. Equation (9-37) expresses the compatibility of deformations, while equation (9-39) relates to the equilibrium of externally applied and internal forces.

These equations for shallow shells contain more special theories as their offsprings:

(1) **Theory of flat plates** - For a flat plate, the initial curvature is zero. In this case, the governing equations of shallow shells become decoupled and take the following forms:

$$K\nabla^4 w = p_z \quad , \quad \nabla^2 \phi = 0 \quad (9-40)$$

These equations govern a laterally loaded thin plate as well as the same plate loaded by in-plane forces and acting in plane stress.

(2) **Membrane shallow shells** - In this case, the bending stiffness of the shell, K , is assumed to be zero. The governing equation of this membrane shell is derived from shallow shell equations to be,

$$\nabla^2 \phi = p_z \quad (9-41)$$

The governing field equations of shallow shells must be supplemented by appropriate boundary conditions. These equations can then be solved analytically by means of series expansions or otherwise. Numerical solution of shallow shell problems can be obtained by Finite-Element or Finite-Difference methods.

In the following chapter, the theory of shallow shells will be applied to analyze and design Hyperbolic Paraboloid shells.

Problems

P 9.1 - Figure (P 9-1a) shows a conoidal shell roof with windows which is used for roofing of factories, assembly halls and other places. A conoidal surface is an anticlastic surface having negative Gaussian curvature. A conoid is a ruled surface that can be generated by sliding a straight line on two different curves called the directrices. As a special case, one of these directrices may be a straight line, Figure (P 9-1b). The general equation of a conoidal surface is,

$$z = f_1(y) - \frac{x}{L}[f_1(y) - f_2(y)]$$

where $f_1(y)$ and $f_2(y)$ are the equations of plane directrices, y is the vertical coordinate x is the longitudinal, and L is the length of the conoid. In a special case that $f_1(y) = 0$ and $f_2(y)$ is a parabola, then

$$z = -\frac{f}{L}\left[1 - \frac{y^2}{b^2}\right]$$

Where f is the rise of the parabola and b is the half-width of the shell

- (1) Derive the appropriate governing equation for the membrane field in parabolic conoidal shell subjected to uniform loading of intensity q_0 .
- (2) Determine the membrane force field in the parabolic conoid. Show that the membrane shear force has the following expression:

$$N_{xy} = -\frac{\partial^2 \phi}{\partial x \partial y} = -\frac{q_0}{a} \left(\frac{\sqrt{1 + a^2 x^2 y^2}}{y} \right) + \frac{n}{2y}$$

here:

$$n = -\frac{2q_0}{a} \quad a = \frac{2f}{lb^2}$$

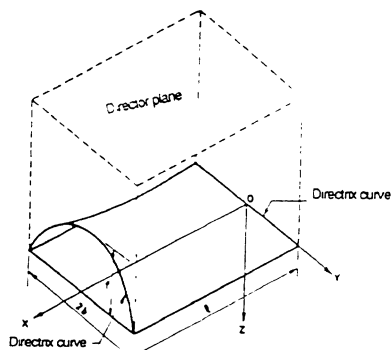
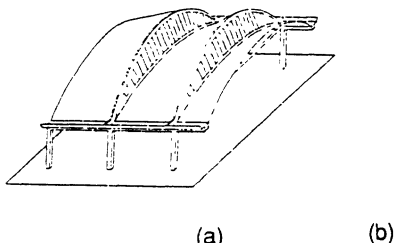


Figure (P 9-1) Conoidal shells, (a) Application, (b) Definition

P 9.2 - Consider a **cooling tower shell** which has a **hyperbolic paraboloid of one sheet** as its middle surface. This surface is generated by rotating a parabola about a non-intersecting vertical axis. If the axis of revolution is identified by the vertically oriented Z-axis, and if x-y axes characterize the horizontal plane, then the equation of this surface can be written as

$$(x^2 + y^2) / a^2 - z^2 / b^2 = 1$$

where a and b are two constant parameters of the surface. The x-y plane is chosen at the section B-B; the so-called the **throat** of the cooling tower.

This surface has negative Gaussian curvature: $1/R = 1/r_1 1/r_2$.

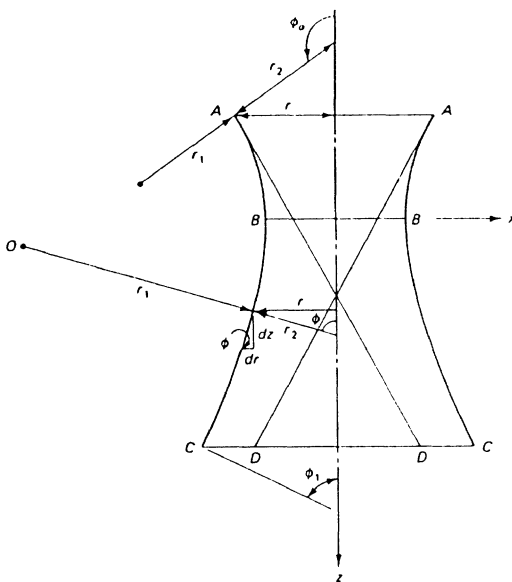


Figure (P 9-2) A cooling tower shell having hyperbolic paraboloid of one sheet as its middle surface

- (1) Write down the expressions for two principal radii of curvature, r_1, r_2 , in terms of the constants a and b and the angle ϕ of the shell normal with the vertical (see figure (P 9-2)).
- (2) Derive the expressions for the membrane forces, N_ϕ and N_θ , in this cooling tower subjected to its own weight. The shell is assumed to have a uniform thickness.

References for Chapter Nine

9.1 - M. Farshad, *Shell Structures*, (in Farsi), Shiraz University Press, Vol. I, 1986, Vol. II, 1987

9.2 - G. S. Ramaswamy, *Design and Construction of Concrete Shell Roofs*, McGraw-Hill Book Co., N. Y., 1968

9.3 - W. Flügge, *Stresses in Shells*, Springer Verlag, Berlin, 1962

9.4 - A. M. Haas, *Design of Thin Concrete Shells*, John Wiley & Sons, New York, 1962

9.5 - V.Z. Vlasov, *General Theory of Shells and its Applications in Engineering*, NASA Technical Translations, NASA TTF-99, 1964

Chapter 10

Design of Hyperbolic Paraboloid Shells

10.1 - Introduction

Hyperbolic paraboloid shells are doubly curved shells with negative Gaussian curvature; they are called **HP** or **Hypar** shells, and a subclass of them are called **Saddle-type** shells.

Hyperbolic paraboloid shells are structurally efficient and many constructional and aesthetic advantages: they are used to cover large spans, vast roofed areas, and a variety of other roofed spaces, figure (10-1); they are used as foundations for special structures; they can be prefabricated simply.

The theoretical tools for the membrane and bending analysis of HP shells were prepared in chapter nine. In the present chapter, the solution methodologies of that chapter will be applied to the analysis and design of hyperbolic-paraboloid shell structures. In addition to quantitative analyses, we will also present qualitative discussion of the overall structural behavior of these shells.

In a later section of this chapter, results of simplified theory of shallow shells, developed in chapter seven, will be applied to predict the bending field developed around the edge members of hyperbolic paraboloid shells. Based on this theory, practical formulas are presented which give the analytical expressions for bending forces in the HP shells. Some design guides for HP shells are given in this chapter, and a sample design example of a reinforced concrete HP shell is carried out in detail.

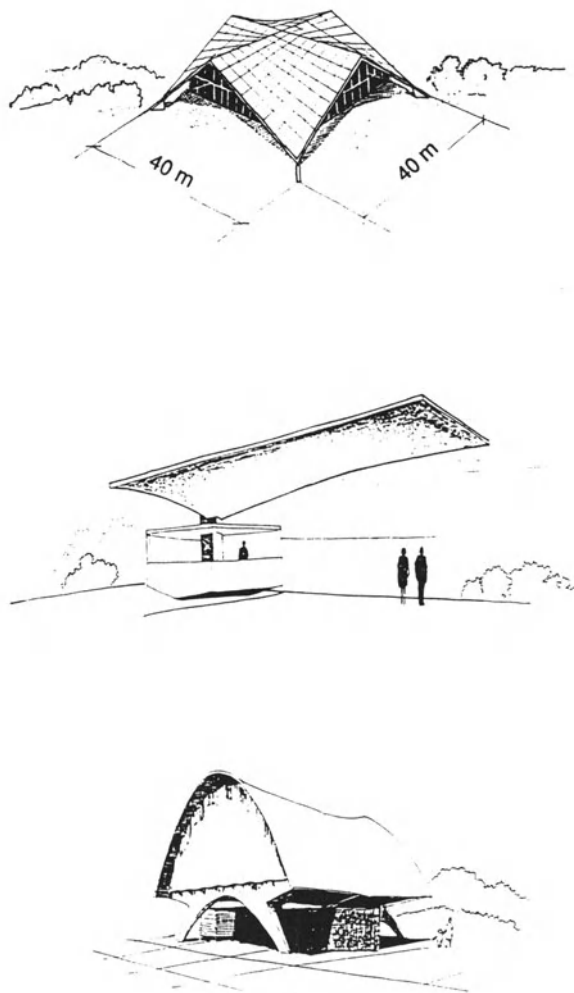
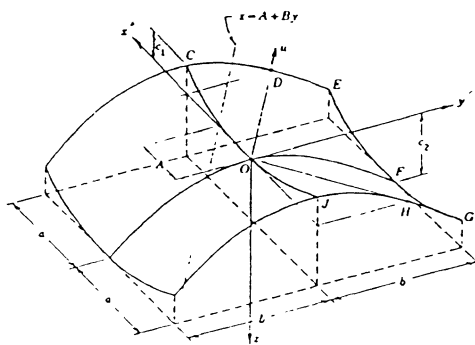


Figure (10-1) Examples of hyperbolic paraboloid shells

10.2 - Geometrical description

A *hyperbolic paraboloid* surface is generated by sliding a concave parabola on another plane, but convex, parabolic curve. The surface thus generated has a negative double curvature, and is therefore a non-developable surface; it can also be categorized as an *anticlastic* surface.



Figure(10-2) A hyperbolic paraboloid surface

Figure (10-2) shows a particular type of hyperbolic paraboloid surface generated by an upward parabola sliding perpendicularly on a downward parabola. If we assume a common stationary point, o, for both curves and take that point as the origin of a Cartesian coordinate system x'y'z', then we can express the equation of this surface as follows:

$$z = \frac{y'^2}{f_2} - \frac{x'^2}{f_1} \quad (10-1)$$

in which

$$f_1 = \frac{a^2}{c_1}, \quad f_2 = \frac{b^2}{c_2}$$

We can easily verify that the intersection of vertical planes, parallel to the x'z and y'z planes, with this surface would create plane *parabolic* curves. On the other hand, the intersection of this surface with horizontal planes, z = constant, generates *hyperbolas* having equations

$$\frac{y'^2}{f_2} - \frac{x'^2}{f_1} = \pm c$$

The name *hyperbolic-paraboloid* thus originates from this feature of the surface that has families of *hyperbolas* and *parabolas* as its intersections with horizontal and vertical planes, respectively, figure (10-3).

If we intersect the surface with the particular horizontal intersecting plane $z = 0$, we obtain

$$\frac{y'^2}{f_2} - \frac{x'^2}{f_1} = 0 \quad (10-2)$$

or

$$\left(\frac{y'}{\sqrt{f_2}} - \frac{x'}{\sqrt{f_1}} \right) \left(\frac{y'}{\sqrt{f_2}} + \frac{x'}{\sqrt{f_1}} \right) = 0 \quad (10-3)$$

The above equation represents two intersecting straight lines which pass through the origin, o , while remaining on the hyperbolic parabolic surface at all their points. Hence, these two lines could be considered to be the *straight-line generators* of the HP surface. These lines are, in fact, the *asymptotes* of horizontal hyperbolas. The tangent of the inclination of these lines with the x' -axis is

$$\tan \omega = \sqrt{\frac{f_2}{f_1}} \quad (10-4)$$

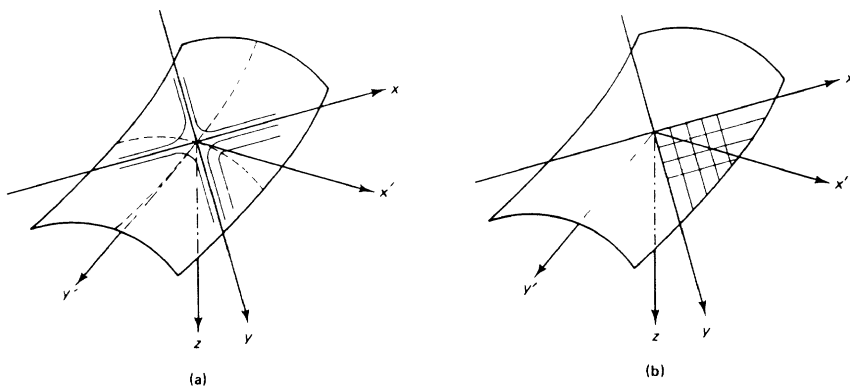


Figure (10-3) A hyperbolic paraboloid surface with two set of coordinate systems, (a) parabolas and hyperbolas, (b) straight line generators

Now, we choose the directions of these asymptotic lines as a new horizontal coordinate system, and we designate their directions by x and y . In figure (10-3), two sets of coordinate systems, one being tangent to generating parabolas and the other being oriented along the straight line generators, are shown. If the angle between two coordinate systems is designated by ω , we can write the relation for coordinate transformation as follows:

$$\begin{aligned} x' &= (y - x) \cos \omega \\ y' &= (y + x) \sin \omega \end{aligned} \quad (10-5)$$

If we substitute these expressions, for the new coordinate variable, into (10-1) we obtain the equation of hyperbolic parabolic surface in the coordinate system xyz. This equation is expressed as

$$z = \frac{4\sin^2\omega}{f_2} xy \quad (10-6)$$

In a particular case that $f_1 = f_2$, we have, $\tan \omega = 1$. In that case, the equation for the surface assumes the following simple form

$$z = \frac{2}{f_2} xy = \frac{1}{c} xy \quad (10-7)$$

By inspecting this equation we observe that the result of intersecting this surface with horizontal planes are hyperbolas having the coordinate axes x and y as their asymptotes.

A very interesting feature of the hyperbolic paraboloid surfaces, as seen in equation (10-5), is that by intersecting the surface with vertical planes, parallel to x or the y axes (i.e., $y = \text{constant}$ or $x = \text{constant}$), we obtain the equations of *straight lines*. This means that we can generate a hyperbolic parabolic surface by sliding a straight line on two other non intersecting lines.

Figure (10-4) shows part of a HP surface generated in this fashion. Obviously, the generated surface is doubly curved. It is also non-developable and has non-zero negative curvature. Surely, by intersecting the surface of figure (10-4) with a pair of orthogonal planes, we shall obtain two intersecting parabolas.

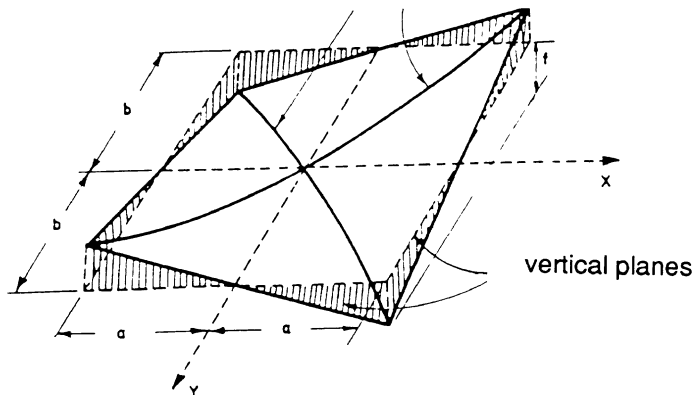


Figure (10-4) A hyperbolic parabolic surface generated by straight lines and also by parabolas

From what we have said here we conclude that a HP surface can have straight lines as its *generators*. This feature is shown in figure (10-5). If the x-y plane (Indicated by x-y axes and two orthogonal dashed lines) is horizontal, then the corner point of the shell with horizontal coordinates $x = a$ and $y = b$, is seen to have a rise of $z = f$. Inserting these coordinates in the equation (10-7), we obtain $c = a b / f$. So, the equation of this surface would read as

$$z = (f/a b) xy.$$

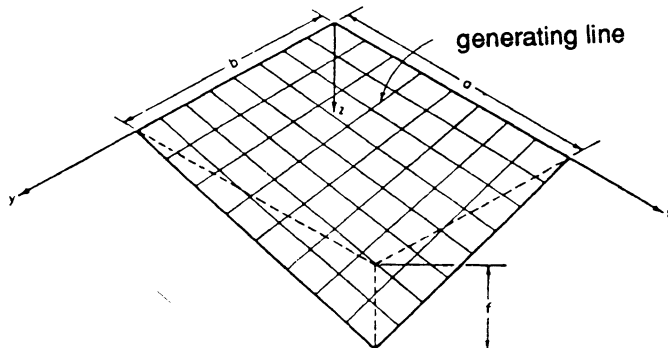


Figure (10-5) A hyperbolic parabolic surface with straight lines generators

Figures (10-6) show some examples of HP surfaces composed of fundamental modules with straight line generators. In these figures, the coordinate axes ox and oy are located in the horizontal plane and thus represent the horizontal datum.

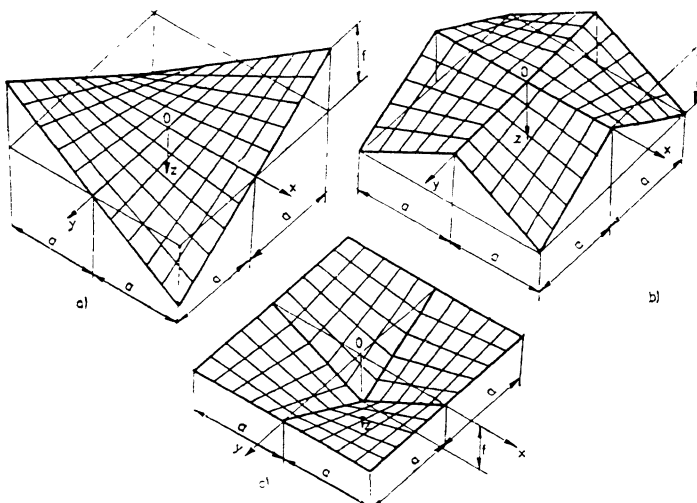


Figure (10-6) Geometrical shapes of some HP shells with straight line generators

Figure (10-6a) is a single module shell which, in practice, could be situated on two supports located diagonally at the lower corners. Figure (10-6b) is a four module shell which is usually supported at four corners; this type of shell is sometimes referred to as *hipped hypar* shell. Figure (10-6c) shows an inverted umbrella shape or mushroom-type shell, since it is supported at its middle point by a single column.

Generation of a HP shell surface, by straight lines, has practical significance: it means that the forming of concrete HP shells can be carried out by using separate pieces of rectilinear shoring.

In some schemes of prefabrication, use can be made of the foregoing geometrical feature of straight-line generated HP shells. For example, a low cost construction scheme can be developed in which the molding of concrete precast shells could be achieved by a heap of soil. In this method, a heap of shapeless soil could be very conveniently shaped by means of a long straight plank sliding over two straight directrices. in this fashion, an "earthen mold" on which the concrete shell can be easily cast would be economically generated. Figure (10-7) shows a picture of a case in which this method was applied successfully to construct a number of *precast* concrete HP shells.

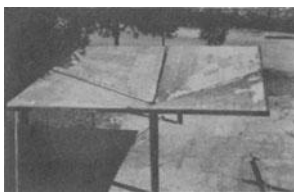
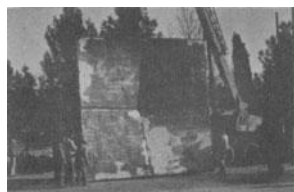


Figure (10-7) A precast HP shell from a series of shells being lifted from an earthen mold (a project executed by the author)

10.3 - Membrane Analysis of HP Shells

In this section we will analyze the behavior of HP shells having straight generators as their straight edges by using the membrane theory developed in previous chapter.

Consider a straight-edge hyperbolic paraboloid shell with the mid-surface equation of the form,

$$z = \frac{xy}{c} = \frac{f}{ab} xy \quad (10-8)$$

We use the governing membrane differential equation (7-24). If we evaluate the second-order derivatives of $z(x,y)$ and substitute them into the equation (7-24), we obtain the following equation:

$$-\frac{2}{c} \frac{\partial^2 \Phi}{\partial x \partial y} = -\bar{p}_z + \frac{y}{c} \bar{p}_x + \frac{x}{c} \bar{p}_y \quad (10-9)$$

To carry out the analysis further, we must now specify the applied loading. Suppose that the shell is subjected to a load uniformly distributed with intensity p on the horizontal projection. Snow loading is one of this type. In this case, the equation (10-9) becomes

$$\frac{\partial^2 \Phi}{\partial x \partial y} = \frac{1}{2} cp \quad (10-10)$$

This can easily be integrated twice with respect to x and y , to give

$$\Phi(x,y) = \frac{1}{2} cp xy + F_1(x) + F_2(y) \quad (10-11)$$

Here, $F_1(x)$ and $F_2(y)$ are two integration functions to be determined from the boundary conditions. Now, the internal forces are given by the equation (9-23):

$$\bar{N}_{xy} = -\frac{1}{2} cp = -\frac{ab}{2f} p$$

$$\bar{N}_x = \sqrt{\frac{c^2 + y^2}{c^2 + x^2}} \frac{d^2 F_2}{dy^2} \quad (10-12)$$

$$\bar{N}_y = \sqrt{\frac{c^2 + x^2}{c^2 + y^2}} \frac{d^2 F_1}{dx^2}$$

Using relations (9-12) to (9-14), we find

$$N_{xy} = -\frac{1}{2} cp, \quad N_x = \frac{d^2 F_2}{dy^2}, \quad N_y = \frac{d^2 F_1}{dx^2} \quad (10-13)$$

which shows that N_x is a function of y only, and N_y a function of x only.

A HP shell may have a variety of edge conditions. Sometimes HP shells may be provided with the so-called **edge members**. In a majority of practical cases, edge members are comparatively stiff in their own plane, but can not sustain loadings applied in the lateral direction, figure (10-8). In such cases, either or both of the normal forces, N_x and N_y , would vanish at the boundaries normal to their direction so that $F_1(x)$ and $F_2(y)$ would be assumed to be identically zero. Consequently, the normal membrane forces are identically zero throughout the shell and we are left with a *pure shear* membrane force field existing throughout the HP shell.

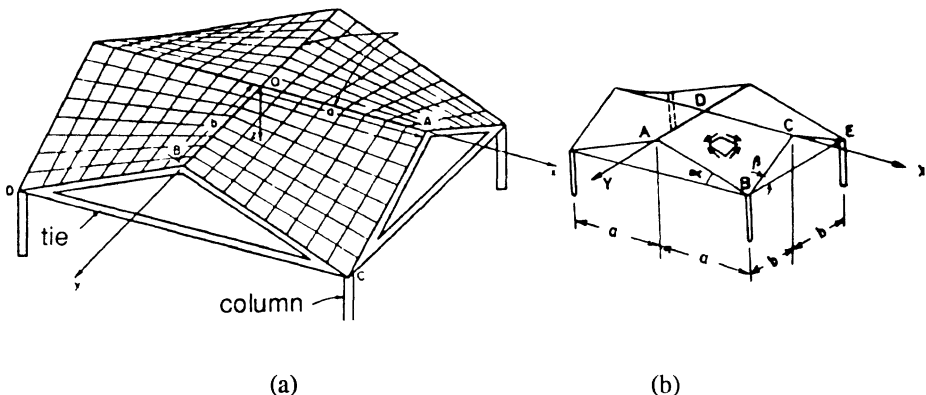


Figure (10-8) A combined HP shell composed of four hypar units resting on vertical corner supports

Consider the HP shell roof shown in figure (10-8a), composed of four HP shell segments. The whole shell structure rests at its four corners on vertical column supports. The applied loading is assumed to be uniformly distributed with intensity p on the horizontal projection of the shell.

The state of stress at a typical element of the shell is determined using relations (10-13) and the prescribed boundary conditions. The internal membrane force field along each generator line consists of a pure shear force of constant magnitude,

$$\tau = N_{xy} = -c p / 2 = -a b p / 2 f$$

Figure (10-8b) shows the state of stress in an element of the shell. A more detailed picture of stress and force distribution in the shell is presented in figure (10-9).

The principal stresses at any point corresponding to this pure shear are a tensile stress τ in the direction parallel to DB and a compressive stress τ in the direction parallel to AC.

Note that the membrane field is inversely proportional to the shell rise, f . Thus, according to membrane theory, shells with higher rise value have more reserved strength and thus are stronger than shells with lower rise. To arrive at a more definite conclusion about the actual

strength of the shell, however, the stability requirements must also be taken into consideration.

According to membrane theory, there exists a distributed internal shear force system at the edges of the shell of figure (10-9). To satisfy the equilibrium requirements of membrane theory, these edge shears must be transferred to vertical supports by means of some intermediate members. Two types of such members are needed: *edge beams* and *ridge beams*; members such as AB and BC are *edge beams*, and AD and CD are *ridge beams*.

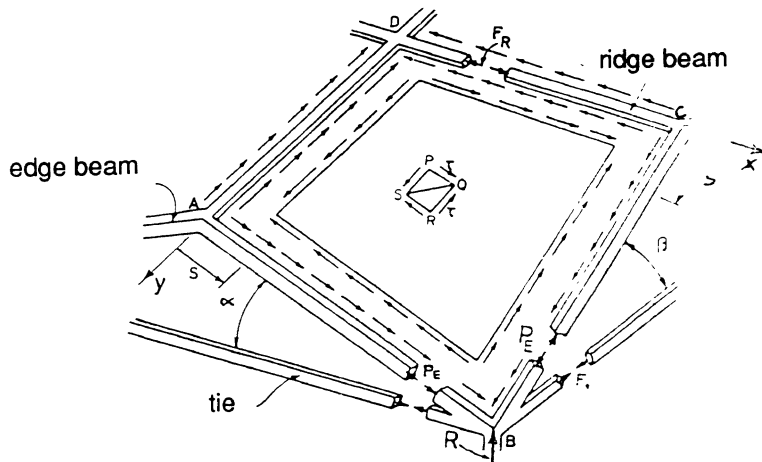


Figure (10-9) Internal force distribution in a segment of the HP shell of figure (10-8)

The internal membrane shear force, τ , in being transferred to the *edge* and *ridge* beams causes axial forces in those members. In the present case, figure (10-9) shows that the axial forces in both the edge beams and the ridge beams happen to be compressive. In other cases, either of these axial forces may be tensile.

The magnitudes of axial compressive forces in the boundary members of the shell of figure (10-8) are

$$(F_E)_{AB} = N_{xy} \cdot s = N_{xy} \frac{x}{\cos\alpha} = - \frac{ab}{2f} \frac{px}{\cos\alpha} \quad (10-14)$$

$$(F_E)_{BC} = N_{xy} \cdot s = N_{xy} \frac{y}{\cos\beta} = - \frac{ab}{2f} \frac{py}{\cos\beta}$$

At the corners of the structure, the edge beams produce axial thrusts as well as vertical forces. The vertical forces are carried by the vertical column supports, but the horizontal thrusts must be absorbed by tie members. Figure (10-8) shows horizontal ties carrying the axial thrust in tension.

The resultant of vertical forces at each corner, to be supported by the column, is

$$R = \frac{ab}{2f} \frac{pa}{\cos\alpha} \cdot \sin\alpha + \frac{ab}{2f} \frac{pb}{\cos\beta} \cdot \sin\beta = pab \quad (10-15)$$

and the axial compressive force in, for example, the ridge beam CD is equal to:

$$F_R = 2(a - x)N_{xy} = -c(a - x)p \quad (10-16)$$

As we see, the axial force the ridge beam is zero at the outer boundary (the edge) and is maximum at the center.

Numerical Example 10.1

Consider the hyperbolic paraboloid shell roof shown in figure (10-10). The assumed shell dimensions are,

$$a = b = 3.0 \text{ m}, \quad f = 1.0 \text{ m}, \quad t = 10.0 \text{ cm} \text{ (shell thickness)}$$

This shell is to be analyzed for an applied distributed loading of intensity $p = 400 \text{ kg/m}^2$, which is assumed uniformly distributed on the horizontal projection of the shell.

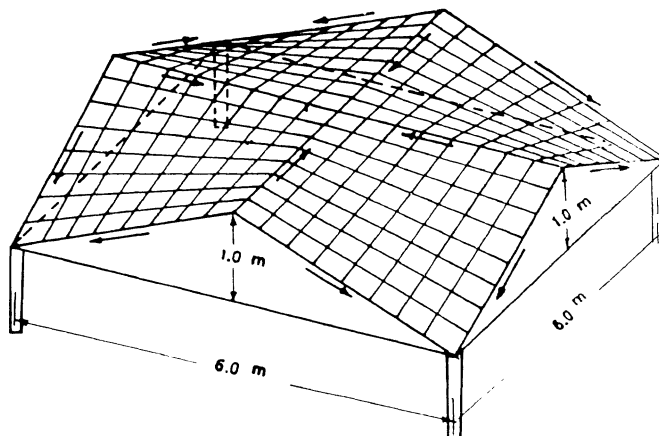


Figure (10-10) HP Shell roof of example 10.1

Solution:

The constant value of membrane shear force field is

$$N_{xy} = -\frac{1}{2} \frac{ab}{f} p = -\frac{1}{2} \times \frac{3 \times 3}{1.0} \times 400 = -1800 \text{ kg/m}$$

The principal stresses associated with this internal force can be obtained from the following well-known formula:

$$\tau\sigma = t \left[\frac{\sigma_x + \sigma_y}{2} \pm \sqrt{\left(\frac{\sigma_x - \sigma_y}{2}\right)^2 + \sigma_{xy}^2} \right]$$

which gives

$$N = \tau\sigma = \pm \bar{N}_{xy} = \mp 1800 \text{ kg/m}$$

from which we find

$$\sigma = \mp \frac{1800}{0.1} = \mp 18000 \text{ kg/m}^2 = \mp 18 \text{ kg/cm}^2$$

The maximum value of compressive force in the edge beam is

$$F_E|_{\max} = -\frac{ab}{2f} \cdot \frac{pa}{\cos\alpha}, \quad \cos\alpha = \frac{a}{\sqrt{f^2 + a^2}} = \frac{3}{\sqrt{10}}$$

$$= -\frac{3 \times 3}{2 \times 1.0} \cdot \frac{400 \times 3}{3 / \sqrt{10}} = -5692 \text{ kg} = -5.692 \text{ Ton}$$

the maximum value of compressive force in the ridge beam is

$$F_R = -\frac{ab}{f} \cdot a \cdot p$$

$$= -\frac{3 \times 3 \times 3}{1.0} \cdot 400 = -10800 \text{ kg} = -10.8 \text{ Ton}$$

the tensile force in the horizontal tie is

$$F_t = (F_E)_{\max} \cdot \cos\alpha = 5692 \times \frac{3}{\sqrt{10}} = +5400 \text{ kg} = +5.4 \text{ Ton}$$

Finally, the vertical force transferred to the column is

$$R = pab = (3 \times 3 \times 400) = 3600 \text{ kg} = 3.6 \text{ Ton}$$

This completes the membrane analysis of the present example. As we see, the level of internal tensile and compressive stresses is quite *low*. We have observed the same structural feature in other shell types.

10.4 - Description of Membrane Behavior of HP Shells

According to the membrane theory, the state of stress in a HP shell element, oriented along the straight-edge generators, is a *pure shear* which remains constant throughout the shell.

The principal stresses make 45° with the straight-line generators; one principal stress is tensile, the other compressive; both are constant throughout the shell.

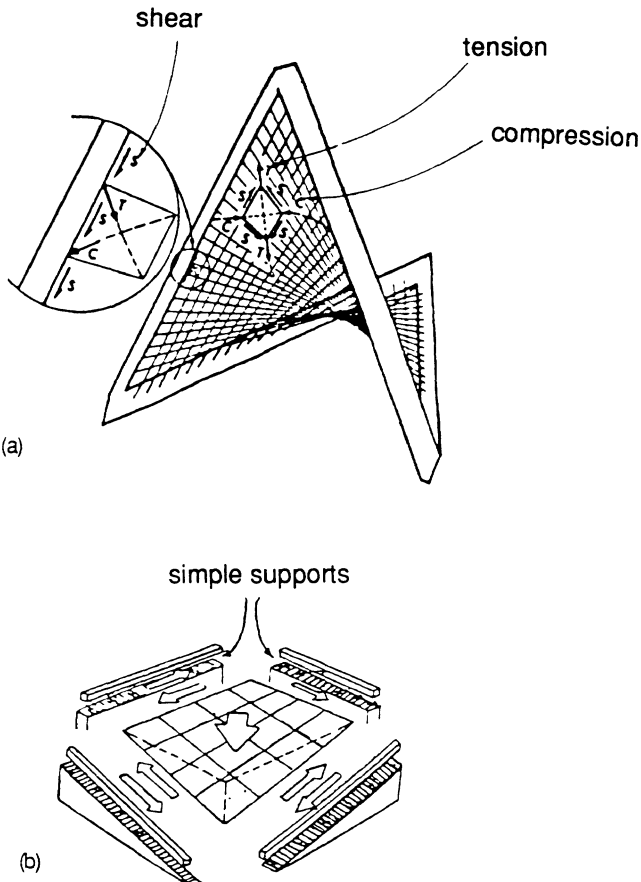


Figure (10-11) An overall view of membrane behavior of HP shells with straight edge generators, (a) shear force field and corresponding principal stresses and transfer of edge shear to edge beams, (b) transfer of shell forces to simple vertical supports

In HP shells having edge members, the applied load is normally transferred to the edge and the ridge beams which, in turn, carry the induced axial forces to the shell supports.

Figure (10-11) shows the membrane behavior of HP shells with straight edge boundaries and edge beams. Figure (10-11a) shows the internal stress field and the shear stress transfer to the edge beam.

Figure (10-11b) demonstrates the mechanism of load transfer from the shell to the edge beams. This shell is assumed to have simple continuous supports, suitable for the realization of membrane conditions.

Figures (10-12) show the flow of internal forces from the shell body to the edge members of the shells depicted in figures (10-6).

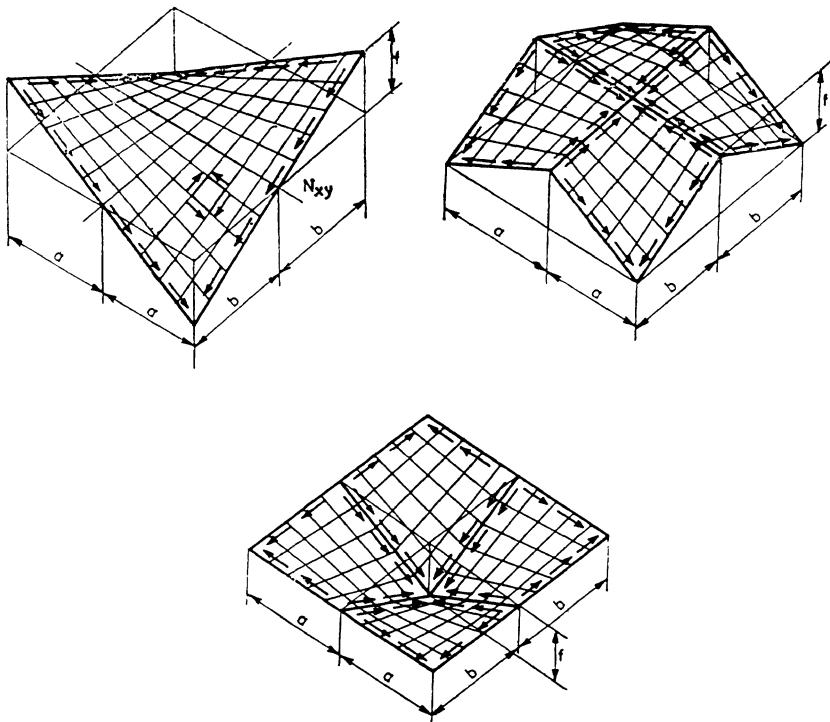


Figure (10-12) Transfer of internal forces to the edge members in some HP shell types

We conclude that the structural action of the HP shell arises from the interaction of two mechanisms: (1) a *cable action* of the shell along the directions of principal tensile stresses, and (2) an *arch action* along the lines of maximum compressive stresses.

A HP shell is an anticlastic surface, i.e., it has negative Gaussian curvature. The *cable* and *arch* mechanisms interact in two "opposite" fashions: the applied load induces *compression* in the "inner-built" arches while it also causes *tension* in the "internal" cables, figure (10-13). The applied force is thus distributed between these two "in-built" structural elements; the over-compression of the arches is hindered by the cables that tend to "pull up" the arches at each point; this increases the elastic stability of HP shells.

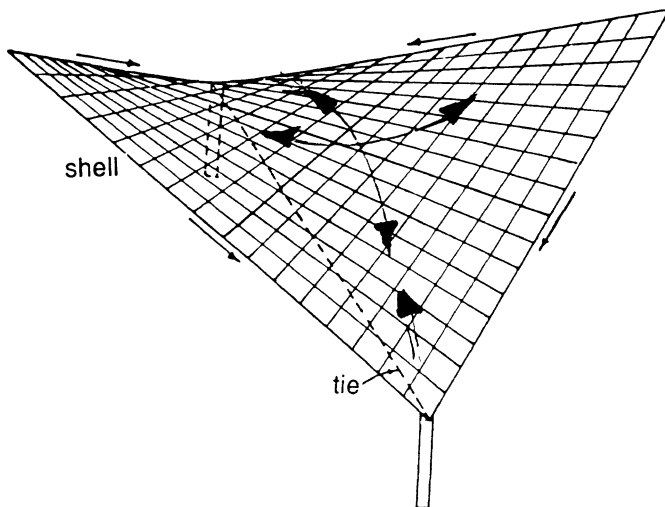


Figure (10-13) Cable action and arch action in an HP shell with two supports

The sign of the axial force developed in the edge and ridge beams of HP shells depends on the shell configuration and the supporting conditions. Figures (10-14) show the state of axial forces in the edge and ridge beams of two HP shells.

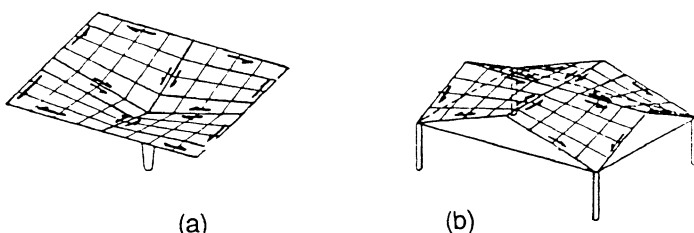


Figure (10-14) State of axial forces in edge and ridge beams of two types of HP shells

The HP shells considered so far had square horizontal plans; other shapes are possible. Figures (10-15) show some examples of HP shells with straight line boundaries having various horizontal projections; they are all composed of basic HP shell units having arbitrary quadrilateral shapes.

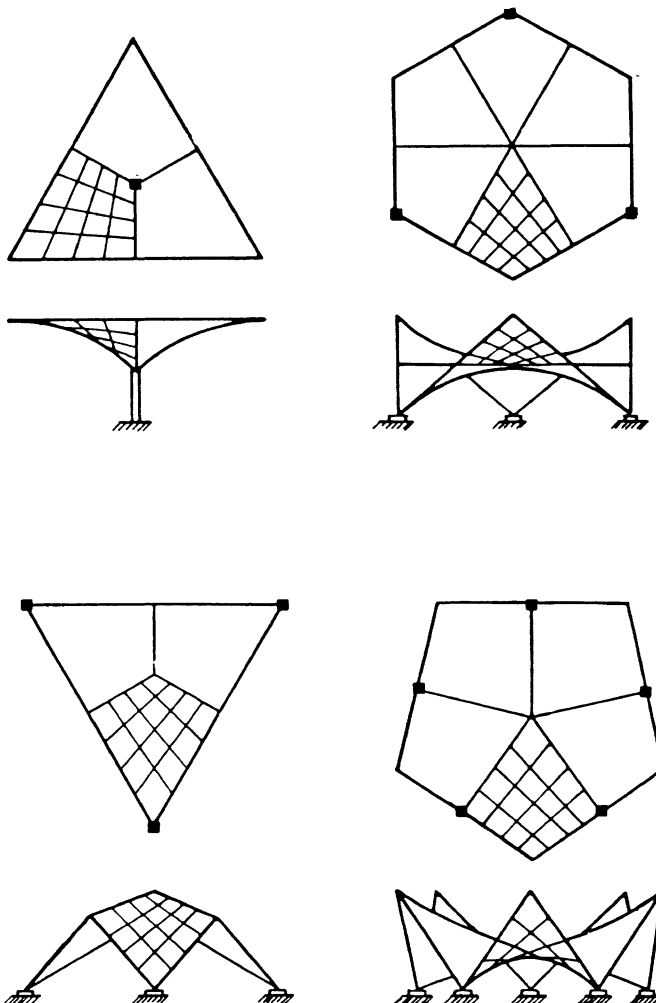


Figure (10-15) HP shells with various horizontal plans.

So far we have analyzed the behavior of the hyperbolic paraboloid shells with straight edge generators. There are HP shells which have other configurations and boundary formations. There are many shapes of HP shells that have curved, parabolic edges. One may combine simpler HP shells to construct a number of useful shell configurations. Figure (10-16) shows a HP shell with curved edges.

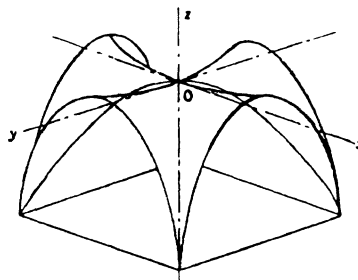


Figure (10-16) A hyperbolic parabolic shell with curved edges. In this figure, boundary curve is the generating parabola

Figure (10-17) demonstrates the membrane behavior of the HP shell shown in figure (10-16). Again, the *arch* and the *cable* actions interact efficiently. The curved edges act as compression arches which carry the shear forces, transferred to them by the shell, to the shell supports. There is some boundary field at the support which is compensated by the bending mechanisms of load transfer.

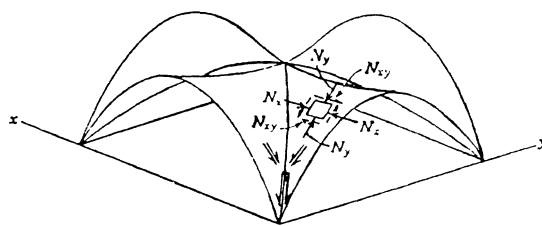


Figure (10-17) The membrane load transfer mechanisms in a hyperbolic paraboloid shell with curved boundaries

Note that all these conclusions are based on the predictions of membrane theory. In actual situations, there will be some bending field. The magnitudes of the bending forces and the range of penetration of the bending field into the shell will depend on the source of the bending field as well as the geometrical properties of the specific shell.

The stability of HP shells must also be considered in their design. However, as we have pointed out before, the membrane theory gives a very useful overall picture of the shell behavior. Some designers have designed large HP shells using only membrane theory together with their intuitive knowledge of HP shell behavior.

10.5 - Bending Field in Hyperbolic Paraboloid Shells

In this section, we present an approximate bending analysis of HP shells based on the theory of shallow shells developed in the previous chapter.

The results of this section were obtained by Loof who has used Vlasov theory of shallow shells to find the bending field of moment and shear in the square HP shells with straight line generators.

Loof's results for two different boundary conditions in a square HP shell shown in figure (10-18) are as follows:

(I) Shell with fixed edges

$$M_y = -0.511 \text{ ga}^2 \left(\frac{f}{t}\right)^{-4/3} \quad (7-85)$$

$$Q_y = +1.732 \text{ ga} \left(\frac{f}{t}\right)^{-1} \quad (7-86)$$

In these formulas, M_y and Q_y are the bending moment and the shear force in the mid-length of the shell edge. The parameter g represents the intensity of uniformly distributed vertical load; f and t denote the rise and the thickness of the shell, respectively.

(II) Shell with hinged edge

Consider part of a HP shell structure with simply supported edges as shown in figure (10-15). At the hinged edge, the bending moment is zero but the non-zero transverse shear force is,

$$Q_y = +0.577 \text{ ga} \left(\frac{f}{t}\right)^{-1}$$

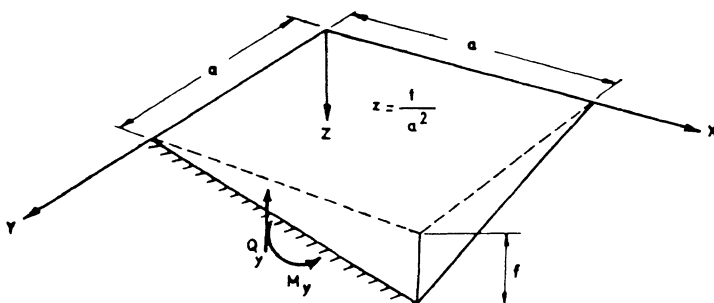


Figure (10-18) A square hyperbolic paraboloid shell with simply supported edges

The maximum bending moment occurs at a section located at a distance y_1 from the edge, where

$$y_1 = 0.55 \left(\frac{f}{t} \right)^{-1/3} a$$

and the corresponding bending moment is,

$$M_y = +0.149 g a^2 \left(\frac{f}{t} \right)^{-4/3}$$

These formulas show that the bending moment is reduced by increasing the shell rise, and increased by increasing the shell thickness.

Figure (10-19) shows a log-log plot of the variation of dimensionless bending moment in a HP shell with dimensionless parameter (f/t) . The limiting value for very small quantities of (f/t) corresponds to the bending moment in a flat plate.

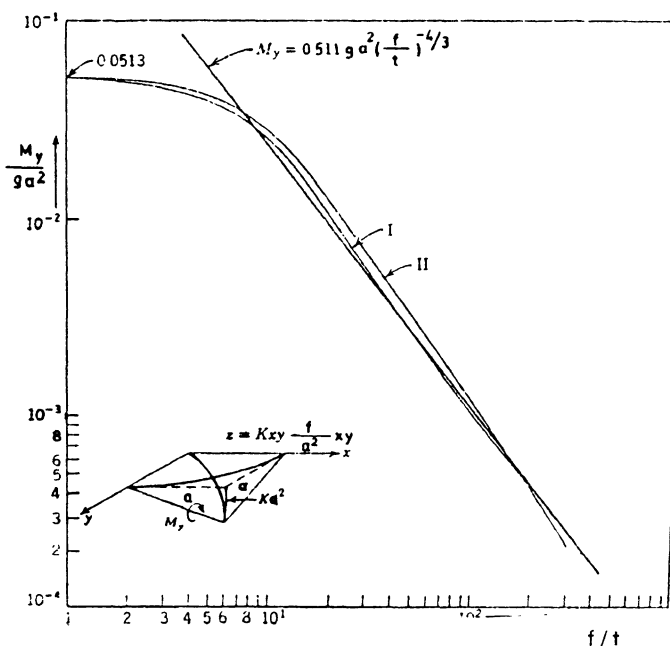


Figure (10-19) Variation of bending moment in a square HP shell with dimensionless parameter f / t

Figure (10-20) shows the variation of bending moment versus the dimensionless length parameter. Figures (10-19) and (10-20) show that the differences in boundary condition have little effect within the shell body.

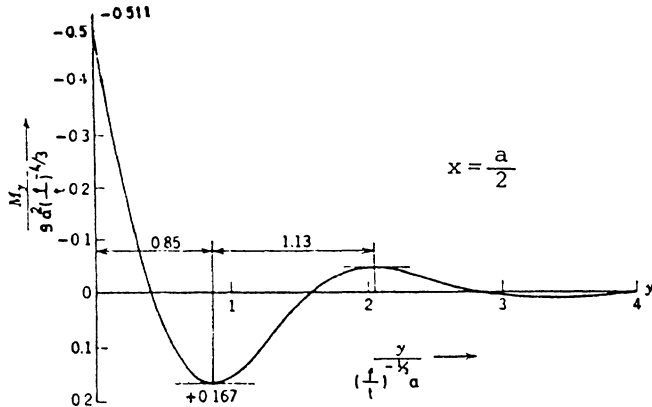
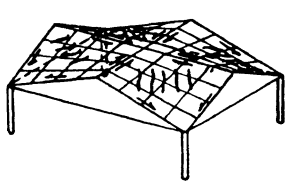


Figure (10-20) Change of bending moment in a square HP shell with distance from the edge

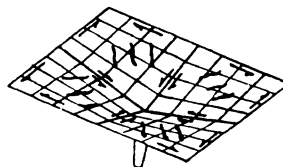
10.6 - General Design Considerations of HP Shells

Hyperbolic paraboloid shells are among the most favoured shell types. Since they can be generated by straight lines, they can be formed by using rectilinear planks or prefabricated forms.

A simple state of stresses in a membrane HP shell is another feature which can be used to great advantage. As we have learned, the internal force system in a membrane HP shell consist mostly of a pure shear which gives rise to two principal stresses, one being tensile and the other compressive.



(a) A HP shell on four columns



(b) an inverted umbrella HP shell

Figure (10-21) Possible membrane cracking pattern in two types of HP shells under vertical loading

Concrete HP shells need tensile reinforcement; ideally this should be placed along the directions of principal tensile stresses, figure (10-22,I), but for ease of construction is often placed along the straight line generators, figure (10-22 II). Figures (10-21) show the probable cracking patterns in HP shells; against which the shell must be reinforced.

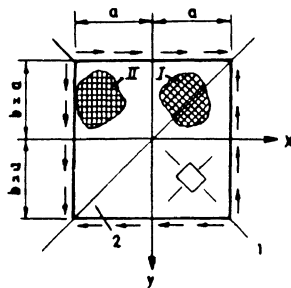


Figure (10-22) Two possible plans of reinforcement for a HP shell supported along the outer straight boundary and subjected to uniform vertical loading

The edge beams and point supports induce some bending field in the HP shells. The extent of bending field is dependent on the geometrical parameters of the shell as well as the edge conditions. Reinforcements are needed to strengthen the shell against the bending field arising from these sources. To achieve an efficient transfer of loads, from the shell to the edge members, one must design the system in such a fashion that the monolithicity of the whole shell structure is assured.

We now present some guidelines for the choice of appropriate dimensions for the preliminary design of two HP shell types; a hyped shell and an inverted umbrella type reinforced concrete shell.

Figure (10-23b) presents appropriate proportions for the preliminary design of the reinforced concrete HP shell, of figure (10-23b); this having a generally rectangular plan and resting on four corner supports. This graph gives appropriate proportions of rise to long span ratio with long span, for a number of short span values.

Figure (10-24) and its related table (10-1) give some guidance in the design of an inverted umbrella type shell. This table gives appropriate dimensions for the edge members.

In designing of hyperbolic paraboloid shells we must consider the buckling behavior of the structure. The arch strips oriented along the compressive diagonal are compressed, and therefore may buckle. Moreover, the axial force in the edge members of the shell are, in most cases, compressive forces. So, the edge members of a HP shell could also be prone to buckling. Hence, the shell thickness as well as the dimensions of edge members should be controlled to satisfy the stability considerations.

In chapter 13, of this book, the stability of shells is discussed. In the same chapter, some formulas for the critical buckling loads and buckling modes of hyperbolic paraboloid shells are presented. Use may be made of those results in the actual design of HP shell Structures.

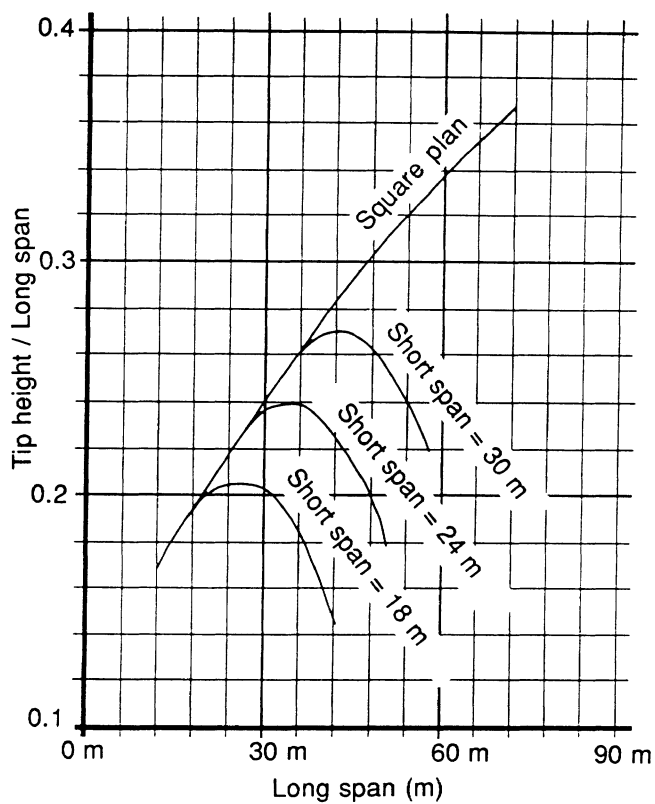
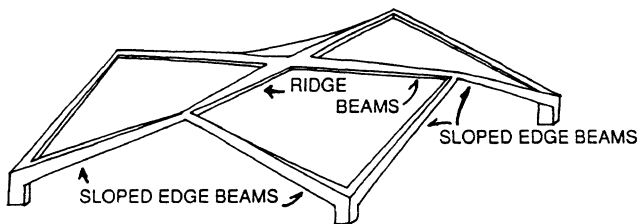
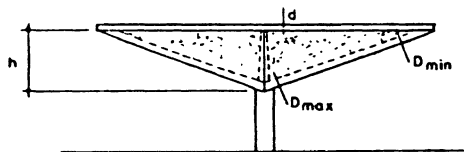
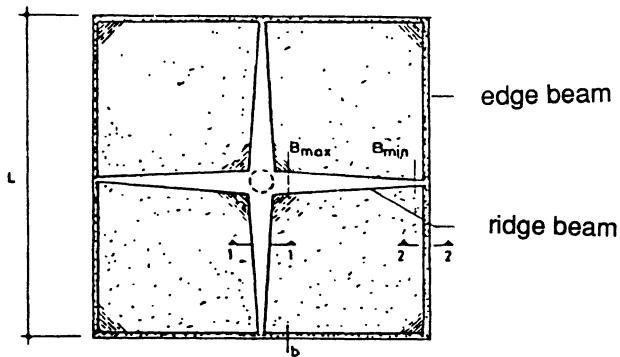
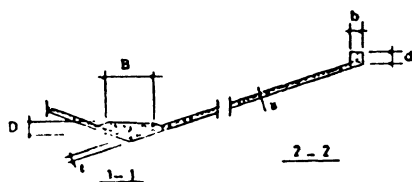


Figure (10-23) Appropriate proportions for the preliminary design of a reinforced concrete HP shell with four corner supports



View of the inverted mushroom-type HP shell



section of the HP shell

Figure (10-24) Dimensions involved in the design of reinforced concrete HP shells of inverted umbrella type

@Seismicisolation

Table (10-1) Appropriate dimensions for reinforced concrete mushroom-type HP shells

L m	h m	t cm	B _{max} cm	D _{max} cm	B _{min} cm	D _{min} cm	b cm	d cm
12	1.5	9	50	8	15.5	8	25	25
12	3.0	9	25	8	15.5	8	25	25
12	4.5	9	18	8	15.5	8	25	25
12	6.0	9	13	8	15.5	8	25	25
12	7.5	9	10	8	15.5	8	25	25
18	3.0	10.5	68	13	15.5	8	30	30
18	4.5	9	45	13	15.5	8	25	25
18	6.0	9	35	13	15.5	8	25	25
18	7.5	9	28	13	15.5	8	25	25
18	9.0	9	23	13	15.5	8	25	25
18	10.5	9	20	13	15.5	8	25	25
24	4.5	15.5	88	18	15.5	8	40	40
24	6.0	9	65	18	15.5	8	35	35
24	7.5	9	53	18	15.5	8	30	30
24	9.0	9	45	18	15.5	8	30	30
24	10.5	9	38	18	15.5	8	25	25
24	12.0	9	33	18	15.5	8	25	25
30	6.0	23	105	20	15.5	8	60	60
30	7.5	13	85	20	15.5	8	50	50
30	9.0	10.5	70	20	15.5	8	40	40
30	10.5	9	60	20	15.5	8	35	35
30	12.0	9	53	20	15.5	8	35	35
30	13.5	9	48	20	15.5	8	35	35
30	15.0	9	43	20	15.5	8	35	35

10.7 - Design of a Reinforced Concrete HP Shell Roof

As a design example, we treat the reinforced concrete HP shell shown in the figure (10-24). The thickness of the shell is 10.0 cm.; the assumed uniformly distributed vertical loading is $p = 400 \text{ kg/m}^2$; this includes the dead weight of the concrete (which is assumed to weigh 2.5 t/m^3). The steel reinforcement as well as the edge members of this shell are to be designed. The allowable tensile strength of the reinforcing steel is 1400 kg/cm^2 .

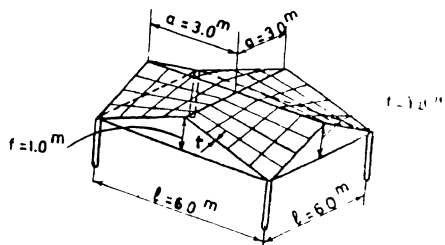


Figure (10-25) The HP shell roof of sample design example

(1) Membrane analysis

Using membrane theory of HP shells, we find

$$\tau = \bar{N}_{xy} = -\frac{1}{2} \frac{ab}{f} \cdot p = -\frac{3 \times 3}{2 \times 1} \cdot 400 = -1800 \text{ kg/m}$$

$$F_E|_{\max} = \tau \cdot \frac{a}{\cos\alpha} = -1800 \times \frac{3\sqrt{10}}{3} = -5692.1 \text{ kg}$$

$$F_R|_{\max} = 2\tau a = -2 \times 1800 \times 3 = -10800 \text{ kg}$$

$$P_t = \text{Force in the tie} = F_E|_{\max} \cdot \cos\alpha = +5692.1 \times \frac{3}{\sqrt{10}} = 5400 \text{ kg}$$

$$P_c: \text{Force in the column} = p \cdot a^2 = 400 \times (3)^2 = 3600 \text{ kg}$$

(2) Bending analysis

Considering that the edge beams cannot resist torsion, we may assume that the edges can rotate freely, and use Loof formula for hinged edges. Accordingly, the edge shear force and maximum bending moment are

$$M_y|_{\max} = +0.149 \text{ pa}^2 \left(\frac{f}{t}\right)^{-4/3}$$

$$y_1 = 0.55 \left(\frac{f}{t}\right)^{-1/3} a$$

$$Q_y = +0.577 \text{ pa} \left(\frac{f}{t}\right)^{-1}$$

Therefore

$$M_y|_{\max} = +0.149 \times 400 \times (3)^2 \times \left(\frac{1}{0.1}\right)^{-4/3} = 24.9 \text{ kg-m/m}$$

$$y_1 = 0.55 \left(\frac{1}{0.1}\right)^{-1/3} \times 3 = 0.77 \text{ m}$$

$$Q_y = +0.577 \times 400 \times 3 \times \left(\frac{1}{0.1}\right)^{-1} = +69.24 \text{ kg/m}$$

(3) Shell Reinforcement

To design the reinforcing steel mesh, to be placed along the straight line generators, we use the following relations:

$$T_p = f_{s_1} (A_{s_1} \cos^2 \delta + A_{s_2} \sin^2 \delta \tan \delta)$$

$$\delta = 45^\circ, \quad A_{s_1} = A_{s_2}, \quad f_{s_1} = 1400 \text{ kg/cm}^2$$

$$T_p = 2f_s \cos^2 \delta \times A_s$$

Thus, the required area of tensile mesh reinforcement would be

$$A_s = \frac{T_p}{2f_s \cos^2 \delta} = \frac{1800}{2 \times (1400) \times \left(\frac{\sqrt{2}}{2}\right)^2} = 1.29 \text{ cm}^2$$

To design the reinforcement for bending moment, we use the *working stress method*, as follows. Let n represent the modular ratio, and let f_s and f_c designate the allowable stresses in the steel reinforcement and concrete. Also, let k and J indicate the characteristic parameters identifying the location of neutral axis and the moment arm of the internal forces. Then, using the bending strain diagram we find the following expressions:

$$k = \frac{1}{1 + f_s/nf_c} = \frac{1}{1 + 1400/9 \times 0.45 \times 250} = 0.42$$

$$J = 1 - k/3 = 0.86$$

Now, if the parameter d , called the effective depth, is the distance from the point of action of the resultant of the concrete compression to the centroid of steel reinforcement, then by applying simple statics we find the area of steel reinforcement as

$$A_s = \frac{M}{f_s J d} = \frac{24.9 \times 100}{1400 \times 0.86 \times 7} = 0.295 \text{ cm}^2/\text{m}$$

Hence, the steel ratio would be

$$\rho = \frac{A_s}{b \cdot d} = \frac{0.295}{100 \times 7} = 0.0004 < \rho_{\min} = 0.0035$$

Since the calculated steel ratio is smaller than that prescribed by ACI codes on concrete shells, the prescribed minimum reinforcement is provided for this shell. The *provided* steel cross sectional area is,

$$\rho_{\min} = 0.0035$$

$$A_s = \rho b d = 0.0035 \times 100 \times 7 = 2.45 \text{ cm}^2$$

$$A_{s\phi 12} = 1.13 \text{ cm}^2 \implies \phi 12 @ 30 \text{ cm}$$

Another minimum reinforcement value to be observed in designing flexural members is given by **ACI code** in terms of the yield stress f_y . Its expression is,

$$\rho_{\min} = \frac{14.06}{f_y} = \frac{14.06}{2800} = 0.00502$$

Since the provided reinforcement is higher in value than this magnitude, hence the design is also satisfactory from the bending point of view.

To design the edge elements, we assume an overall dimensioning of (15 cm x 20 cm) for each of the edge and ridge beams. The intensity of dead weight of the edge elements is,

$$w = 0.15 \times 0.20 \times 2.5 = 0.075 \text{ T/m}$$

Calculations related to design of edge members follow.

Maximum bending moment:

$$M_{\max} = \frac{\omega l^2}{8} = \frac{75 \times (\sqrt{10})^2}{8} = 93.75 \text{ kg-m}$$

Effective depth of edge beams:

$$d = 17 \text{ cm}$$

Bending steel reinforcement for the edge beams:

$$A_s = \frac{M}{f J d} = \frac{93.75 \times 100}{1400 \times 0.86 \times 17} = 0.433 \text{ cm}^2$$

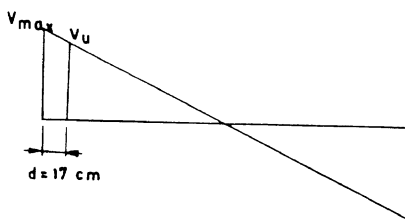
We compare this calculated steel ratio with the minimum required reinforcement:

$$\rho = \frac{0.433}{15 \times 17} = 0.0017 < \rho_{\min} = 0.00502$$

Based on these calculations, the longitudinal reinforcement in edge beam would be

$$A_s = 0.00502 \times 15 \times 17 = 1.28 \text{ cm}^2$$

We design the shear reinforcement for the edge beams as follows. First, we plot the shear force diagram in the edge beams as shown in figure (10-25). According to ACI code of practice of reinforced concrete, the design shear is to be taken at a distance equal to the effective depth of the member from the support. This design shear force is shown in the following figure.



Shear force diagram of the edge beam

The routine calculations for design of shear reinforcement are carried out as follows:

Maximum shear force:

$$V_{\max} = \frac{wl}{2} = \frac{75 \times \sqrt{10}}{2} = 118.9 \text{ kg}$$

Design shear force:

$$V_u = 75 \times (\frac{\sqrt{10}}{2} - 0.17) = 105.84 \text{ kg}$$

Design shear stress:

$$\tau_u = \frac{V_u}{0.85bd} = \frac{105.84}{0.85 \times 15 \times 17} = 0.488 \text{ kg/cm}^2$$

Shear stress carried by concrete (ACI code)

$$v_c = 0.53\sqrt{f'_c} = 0.53 \times \sqrt{250} = 8.38 \text{ kg/cm}^2$$

Limit of no required stirrups:

$$\frac{1}{2}v_c = 4.19 \text{ kg/cm}^2$$

$$v_u < v_c$$

Minimum shear reinforcement:

$$A_{v_{\min}} = \frac{3.52b \cdot s}{f_y}$$

Spacing of shear stirrups is determined through the following considerations:

$$s \leq d/2$$

$$s \leq d/4 \quad \text{when} \quad v_u - v_c > 1.06\sqrt{f'_c} = 1.06\sqrt{250} = 16.76 \text{ kg/cm}^2$$

$$s < \frac{17}{2} = 8.5 \quad \rightarrow \quad s = 8 \text{ cm}$$

$$s_{\max} = \frac{A_{v_{\min}} \times f_y}{3.52 \times b} = \frac{\frac{2A_s}{\phi 10} \times 2800}{3.52 \times 15} = \frac{2 \times 0.79 \times 2800}{3.52 \times 15} = 84 \text{ cm}$$

Figure (10-26) shows the reinforcement detail of the edge members.

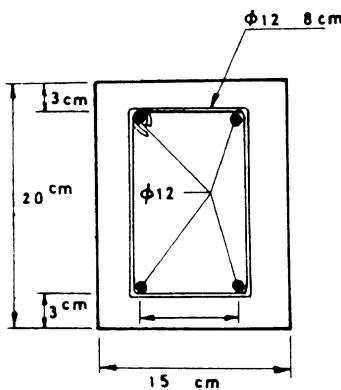


Figure (10-26) Reinforcement detail of edge beams of the designed shell

The design of ridge beams can be carried out in a completely similar fashion. Figure (10-27) shows the reinforcement detail of one of the four ridge beams

Having designed various part of this shell structure, we can now put the designs together and present an overall design sketch for the whole system. The design sketches for this example are presented in figures (10-27) to (10-29).

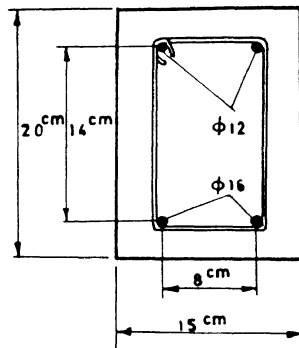


Figure (10-27) Reinforcement detail of the ridge beams

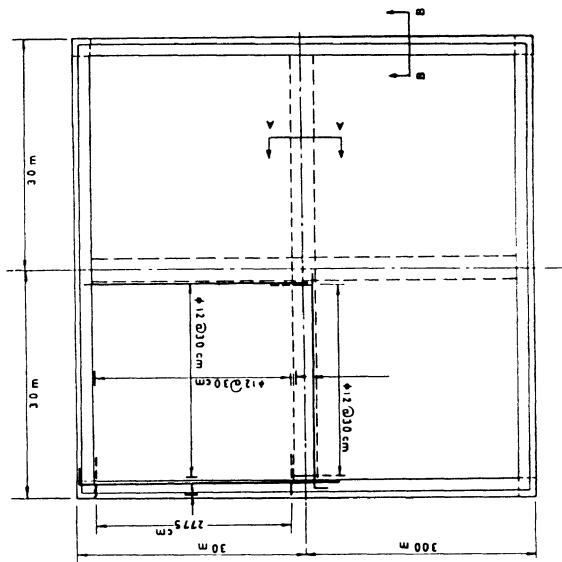
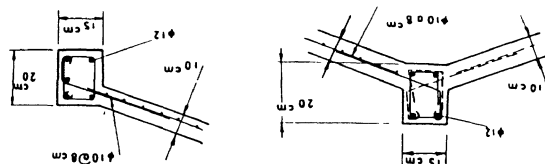


Figure (10-28) Plan of reinforcement for shell of figure (10-24)



(a) detail of edge beam

(b) detail of the ridge beam

Figure (10-29) Details of reinforcements at the intersection of the shell with the edge and ridge beams

Problems

P 10.1 - Consider the relatively shallow reinforced HP shell of figure (P 10-1) resting on four corner supports. This shell has a uniform thickness. The weight per unit surface area is p_z . Show that the expressions for the projected membrane forces in this shell are,

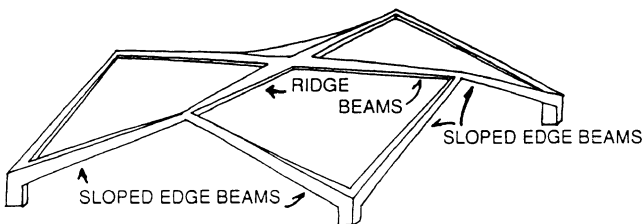


Figure (P 10-1)

Here $k = c / a b$ and $f_1(y)$ and $f_2(x)$ are functions resulting from the integrations. Using these expressions, find the expressions for the true membrane stress resultants in the shell.

P 10.2 - A reinforced concrete HP shell with a rectangular plan is to be designed as the roofing of a sport center. The general geometrical shape of a hipped shell shown in figure (P 10-1) has been chosen for this purpose. The characteristic dimensions are as follows:

$$L_1 = 40 \text{ m}, L_2 = 80 \text{ m}, h = 15 \text{ m}$$

The density of combined reinforced concrete material is assumed to be equal to 2500 kg/cm^2 . The steel reinforcement to be used in this structure has a yield limit of 400 N/mm^2 . The compressive strength of concrete is 30 N/mm^2 . Design the main shell as well as its edge members for its dead load.

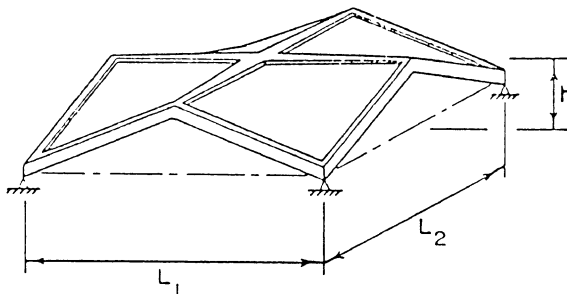


Figure (P 10-2)

P 10.3 - Figure (P 10-3) shows a reinforced concrete HP shell which is to be used as a footing to carry a heavy load P . This footing has a square plan of dimension $2a$ and a rise of f . Perform an analysis of this shell footing under each of the following assumptions:

- (a) the soil reaction, p , is uniform.
- (b) the soil reaction is proportional to the vertical displacement of the shell (This case corresponds to a shell resting on a Winkler foundation).

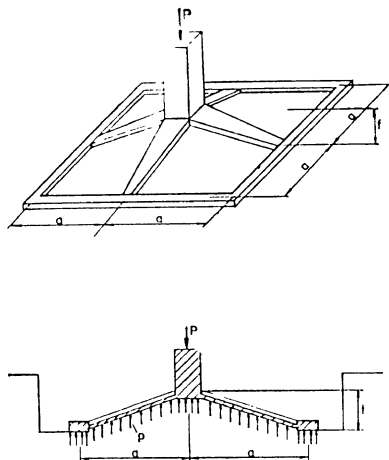


Figure (P 10-3) Hyperbolic paraboloid shaped footing

References for Chapter Ten

- 10.1 - M. Farshad, *Shell Structures*, (in Farsi), Shiraz University Press, Vol. I, 1986, Vol. II, 1987
- 10.2 - M. Salvadori, and R. Heller, *Structure in Architecture*, Prentice-Hall, INC., 1963
- 10.3- A. M. Haas, *Design of Thin Concrete Shells*, John Wiley & Sons, New York, 1962
- 10.4 - C. Faber, *Candela: The Shell Builder*, Reinhold Publishing Corporation, New York, 1963
- 10.5 - F. Candela, "General Formulas for Membrane Stresses in Hyperbolic Paraboloid Shells", ACI Journal, Proceeding, Vol. 57, No. 4, PP 353-371, 1960
- 10.6 - W.C.Schonbrich, " Analysis of Hyperbolic Paraboloid Shells", *Concrete Thin Shells*, ACI Special Publication,SP-28,1971
- 10.7 - V.N. Baikov, (ed), *Reinforced Concrete Structures*, MIR Publishers, Moscow, 1968
- 10.8 - J. Christiansen, (editor), *Hyperbolic Paraboloid Shells-State of the Art*, American Concrete Institute, SP-110, Detroit, 1988
- 10.9 - V. Gioncu, *Thin Reinforced Concrete Shells*, John Wiley & Sons Ltd., Chichester, 1979
- 10.10 - M. Melaragno, *An Introduction to Shell Structures - The art and Science of Vaulting*, Von Nostrand Reinhold, New York, 1991

Chapter 11

Analysis and Design of Folded Plates

11.1 - Introduction

Folded plate structures are composed of a number of flat plates connected to each other. They have many uses: in roofing of large spans in an architecturally appealing appearance; as box girders in bridges and overpasses; as bunkers in silo structures; as sheet piles.

In this chapter, we present the analysis and design of prismatic folded plates. Although folded plates can be analyzed by numerical schemes such as the Finite Element method, but the analytical calculations of this chapter aid the understanding of the structural behavior of folded plates.

11.2 - General Features of Folded Plates

There exist a large variety of folded plate structures used in different engineering and architectural applications. Figures (11-1) show some examples of the used of folded plates.

A **prismatic folded plate** is formed by connecting a number of rectangular plates so that their lines of junction remains parallel to a fixed line. figures (11-1a) and (11-1b).

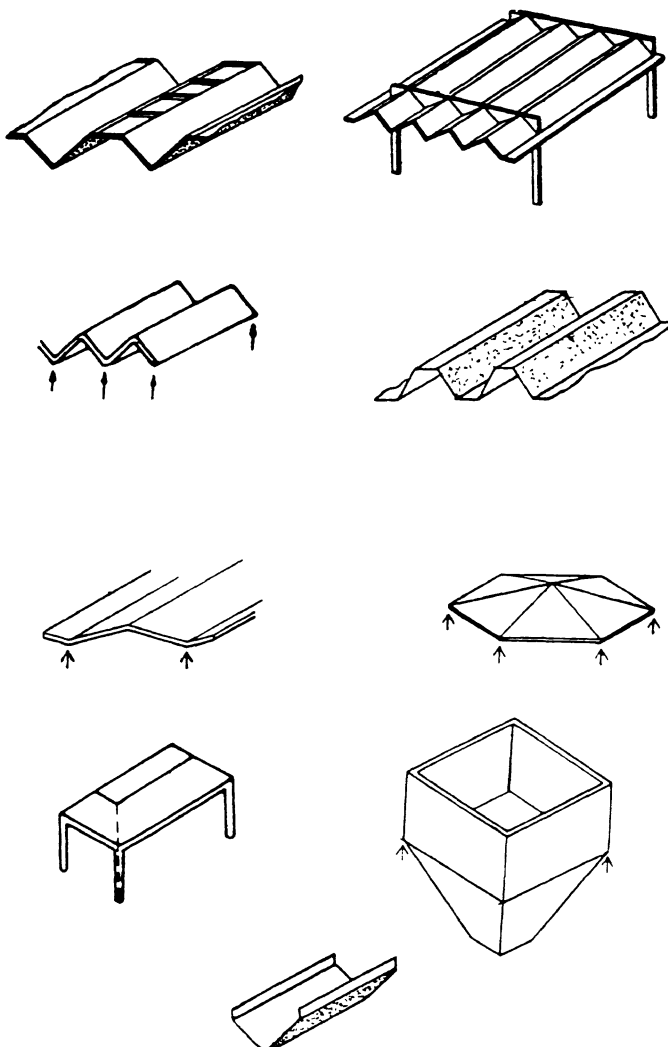


Figure (11-1) Examples of folded plate structures

Folded plates are degenerate shells: in the flat plate parts the curvature is zero, while at the corners, i.e., at the plates junctions, the curvature is infinite. The simple geometrical configuration of folded plates makes the manufacturing of metallic, composite, and polymeric folded plates quite simple. Forming of reinforced concrete folded plates is much easier than for other shell forms. Thus there are great economic advantages in the constructional aspects of folded plates as compared with more complicated curved shell configurations.

A simple paper experiment, shown in figure (11-2), demonstrates the structural efficiency gained by forming an otherwise structurally inefficient flat piece of paper into a folded plate: placing the material further away from the axis of flexure, makes the system much stiffer than a flat plate. The folded plate shape of the figure (11-2b) is a truly load bearing stiff structure. This structure is a prismatic folded plate. Other nonprismatic efficient shapes could also be generated with the same piece of material.

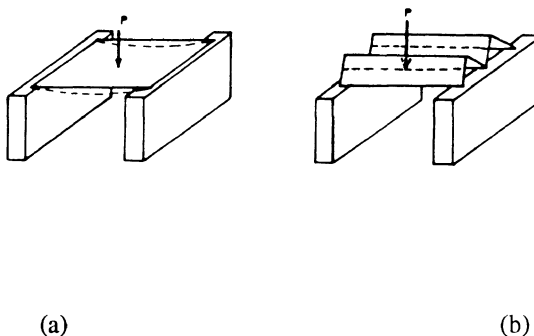


Figure (11-2) A simple paper experiment showing the structural efficiency of folded plates, (a) a paper sheet with bending load carrying inefficiency, (b) a folded plate made of paper sheet of figure (11-2a) demonstrating the strength and stiffness of folded plate forms

By folding a flat plate into a folded plate, we completely change the internal force system as well as the load carrying mechanisms. In a folded plate structure, in-plane (membrane) forces are generated in both directions; The internal force field is truly spatial and the applied force is mainly carried by the generated in-plane forces, not by bending in a flat plate structure. In this sense, a folded plate is a **form-resistant** structure. Its strength and stiffness to weight ratio are much higher than those of flat plate and planar framed structures.

Consider the folded plate roof structure shown in figure (11-3); it can be characterized by the plate dimensions, slopes, lateral span, and the length on the structure. So far as the span (b) length (l) relation is concerned, the prismatic folded plates can be classified as being long ($l/b > 2$), short ($l/b < 2$), and intermediate. This classification is similar to the one presented for cylindrical shell roofs.

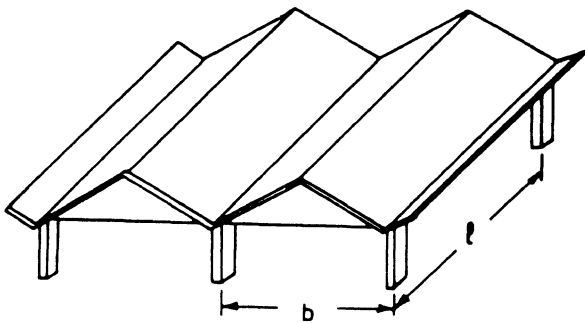


Figure (11-3) A prismatic folded plate roof

Long folded plates resting on end supports behave like beams, figure (11-4). In short folded plates, the lateral action, i.e., the action of the folded strips becomes important.

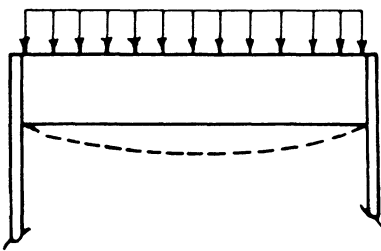


Figure (11-4) Beam action of a long folded plate

The behavior of an intermediate prismatic folded plate is truly spatial; it behaves like a beam, but it is modified by the action of the transverse folded strips. The longitudinal load transfer emanates from the action of inclined plates. This is referred to as the **plate action**. The lateral load transfer takes place by folded strips acting as a continuous beam and undergoing bending deformation; this is called the **slab action** of the folded plate, figure (11-5).

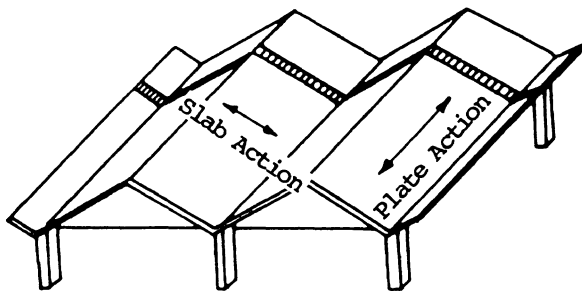


Figure (11-5) Plate action and slab action of a prismatic folded plate

The structural behavior of a prismatic folded plate, resting on end supports, can thus be described as follows:

- (1) First, the applied loads act on transverse folded slab strips causing these strips to undergo bending as a continuous beam resting on flexible supports located at the intersection of the inclined plates. The supporting reaction, R, comes from the longitudinal plates, figure (11-6).

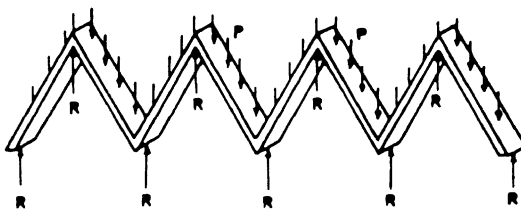


Figure (11-6) transverse slab action of a prismatic folded plate

- (2) The transverse folded slab strips transfer their loads to the end supports by means of the longitudinal plates action of the folded plate. The vertical reactive force, R, will act as a longitudinally distributed applied force on the inclined longitudinal plates. Each plate will receive a share of this distributed force. To determine the share of each plate, the vertical reactive force must be resolved into two components lying in the plane of two adjacent plates, figure (11-7).

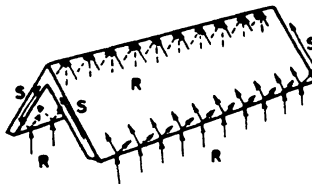


Figure (11-7) Resolution of transverse slabs reactive forces

The longitudinal plates will carry their share of transferred reactive forces to the end supports; in doing so, each inclined plate acts as an inclined deep beam loaded in its own plane.

(3) The totality of implicit transverse slabs and longitudinal plates act in such a fashion that the integral behavior of the *whole* structure is preserved. This means that the action of each individual element takes place in conformity with the equilibrium and compatibility requirements of the *whole* folded plate structure.

This qualitative discussion on the behavior of prismatic folded forms the basis for analytical determination of internal forces and deformations in folded plates presented in the forthcoming sections.

11.3 - General Design Considerations of Prismatic Folded Plates

Prismatic folded plate roofs are normally supported by the end diaphragms resting on end columns; the end diaphragms can be solid, or may be in the form of end frames and / or trusses.

There are many prismatic folded plate sections from which a design choice can be made; folded plate sections having triangular and trapezoidal shapes are very common since the forming of such sections is repeatable and their construction is relatively easy; folded plate sections made of a number of slanted plates forming a prism are favoured. They approximate cylindrical roofs by a number of flat surfaces; their forming is simple compared with a curved cylindrical surface.

Figures (11-8) suggests initial choices for geometrical parameters of reinforced concrete folded plates. Folded plates may also have stiffening and / or supporting edge beams, and the general design considerations described for cylindrical shell roofs are applicable. In the Figures (11-8) present appropriate relative dimensions for lateral span and slopes of inclined plates in a folded plate roof.

In prismatic reinforced concrete folded plate roofs, the length of the folded plate (L) is usually greater than the lateral span (b) depending on the architectural planning. The rise of a folded plate is normally chosen in the range of $1/10$ to $1/7$. The choice of a particular folded plate geometry depends on architectural and functional requirements.

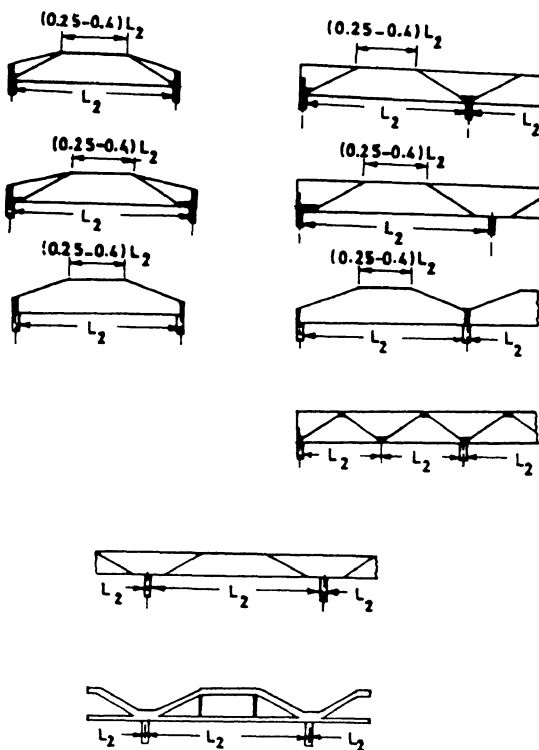
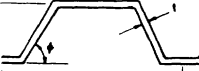


Figure (11.8) Appropriate relative dimensions of some RC folded plates

Table (11-1) Appropriate proportions for two types of reinforced concrete folded plates

Reinforcement per kg/ horz.projection	Thickness, t Centimeter	Rise (Meter)		Width (Meter)	Length (Meter)
		Max	Min		
	0.11-0.08	10.0	1.2	0.8	4.5
	0.19-0.13	10.0-15.0	1.8	1.8	12.0
	0.26-0.18	10.0-15.0	2.25	1.5	22.5
	0.36-0.28	12.5-15.0	3.0	2.0	30.0
	0.14-0.11	7.5	1.5	0.75	12.0
	0.21-0.14	7.5-9.0	1.8	1.2	18.0
	0.28-0.18	7.5-10.0	2.3	1.5	22.5
	0.42-0.28	10.0-12.5	3.0	1.95	30.0

The thickness of concrete folded plates is determined by stability and construction requirements, not strength only. In reinforced concrete folded plates, the steel reinforcement, in some sections, consists of three layers of reinforcement. The structural and concrete cover requirements place a limit on the minimum thickness of folded plates. Some regions of a folded plate may be in compression, so that there may be local or global buckling; this can be a determining factor for minimum.

Table (11-1) presents some appropriate proportioning of two types of reinforced concrete folded plates, including the average thickness, and the approximate magnitude of steel reinforcement (per unit horizontal projection). This table may be used in dimensioning reinforced concrete folded plate roofs and in the initial estimation of required material.

11.4 - Methodology of Analysis of Folded Plates

There are several methods by which the folded plates and, in particular, prismatic folded plates could be analyzed. In addition to numerical schemes, such as *Finite Element method*, the folded plates could be analyzed by a number of analytical methods. One of these, is the arch-beam method which, in principle, is similar to the beam-arch method of cylindrical shell analysis. Another method, is the limit analysis technique employed for ductile yielding structures. A third method, of elastic analysis of folded plates, is based on combined lateral-longitudinal behavior of folded plates described in section 11.2. We shall employ this analytic methodology to analyze the folded plates of the forthcoming sections.

A general comprehensive analysis of elastic prismatic folded plate consists of three parts: **the preliminary analysis, the corrective analysis, and superposition**. For the initial design of folded plates, the preliminary analysis proves to be sufficient. The corrective

analysis is only needed as a refinement in the later stages of design, specially for relatively flexible folded plate structures.

11.4.1 - Preliminary Analysis

Here the combined transverse slab and longitudinal plate actions are analyzed under the assumption that the plate intersections are immovable; the displacement of longitudinal lines of plates intersections is constrained. The preliminary analysis consists of two following stages:

(a) Transverse slab analysis

It is assumed that transverse plates act as *one-way slabs* and thus could be modeled by strips of unit width. Such a strip acts as a continuous folded beam resting on immovable supports. The supports are located at the junctions of inclined plates. In this slab action, the transverse strips undergo lateral deflections having components along the folded strips as well as components normal to each strip element.

In performing transverse slab analysis, we may use the classical *moment distribution* method of continuous beam analysis. The loading on a typical transverse strip consists of actual applied forces per unit width of the strips.

The transverse slab analysis determines the support reactions. These reactive forces are oriented along the vertical directions.

(b) Longitudinal plates analysis

To perform such analysis, it is assumed that each of the longitudinal plates, constituting the folded plate structure, act as beams resting on end supports and undergoing deformations in their own plane.

The transverse slab analysis yielded longitudinally distributive reactive forces. These reactions were actually provided by the longitudinal plates. Thus, the action of transverse strips would be forces equal in magnitude to these reactions but opposite in direction of these reactions. Therefore, loading on longitudinal plates consists of components of reactive forces determined in the previous step (with their signs changed) resolved in the plane of the adjacent plates.

The analysis of individual longitudinal plates can be carried out by means of classical beam theory; this determines the linearly varying bending stresses in each plate, and the deflection of each plate in its plane. This deflection must satisfy the boundary conditions at the ends of the folded plate structure.

(c) Matching of plates

The analysis of each longitudinal inclined plates yields a bending stress and deflection field independent from the stress and deflection fields in the other plates. In the folded plate structure the plates are connected along the plates junctions; it is this connectivity that creates an efficient folded plate structure; this interaction imposes certain constraints on the stresses and deformations in the individual plates.

The plates are *matched* for equilibrium and compatibility; the bending stresses at the points of intersection of two adjacent plates must be equal; the deflections of two adjacent plates must be compatible.

11.4.2 - Corrective Analysis

The *preliminary analysis* of folded plates gives an equilibrated force field and a compatible deformation field for the whole folded plate structure assuming immovable lines of plate junctions. In reality, the plates junctions are not totally constrained in space; and there will be some lateral movement of the lines of plate intersections which in turn will affect the stress and deformation fields.

This phenomenon resembles the "*sidesway*" appearing in framed structures. The lateral movement of plate junctions would alter the stress and deformation field in the folded plate. The magnitude and influence of such movement would depend on the features of the folded plate structure.

The corrective analysis, taking into account the movement of plate junctions, can be carried out in similar fashion as to the *sidesway analysis* of frames. The procedure is to apply unit lateral displacement to each junction and to determine the influence of these unit deflections on the structure.

Having obtained these *influence coefficients* we write the compatibility relations for each junction. In writing such compatibility relations we use appropriate geometrical relations at the junctions.

The **corrective analysis**, like the preliminary analysis, has three stages:

- (a) Analysis of transverse slabs
- (b) Analysis of longitudinal plates
- (c) Matching of plates

11.4.3 - Compatibility Analysis and Superposition of Results

The results of preliminary and corrective analyses must be superimposed to yield the complete force and deformation fields in the monolithic folded plate structure. The superposition must be carried out so that the compatibility requirements at the plates junctions are fulfilled. By writing down the appropriate compatibility relations, the actual lateral displacements at the junctions of adjacent plates are determined.

The results of corrective analysis, assuming unit displacements, are then used to fined the corrective internal forces produced by these displacements (settlements). Superposition of corrective analysis and preliminary analysis would then yield the complete solution to the folded plate problem.

11.5 - Basic Steps in the Folded Plates Analysis

11.5.1 - Schematics of analysis

The set of figures (11-9) to (11-11) summarize the three steps in the preliminary analysis. Figure (11-9) shows the variation of transverse bending moment in transverse slab action, and the vertical reactions, R_1, R_2, R_3, \dots , assuming constrained junctions.

Figure (11-10) shows the action of longitudinal plates; forces equal and opposite to the reactions, R_i , are applied and are resolved into two components along the adjacent plates. Figure (11-10b) shows the adopted positive sign conventions are also indicated; the parameters ϕ_i indicate the orientation of inclined plates with respect to the horizontal direction.

Figure (11-11) shows the bending stresses obtained from the analysis of the longitudinal plates. The bending stresses at the line of junction of two adjacent plates are, in general, unequal. Since adjacent plates are monolithically attached to each other, the bending stresses at the junction must be equal. To achieve this equalization there must be an equilibrating shear force, τ_{12} , at the junction. This shear force is to be determined by a process of redistribution of bending stresses, as outlined in the following section.

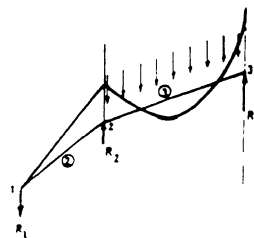


Figure (11-9) Part of a folded plate section showing the transverse slab action, distribution of the transverse bending moment, and reactive forces at the plates junctions

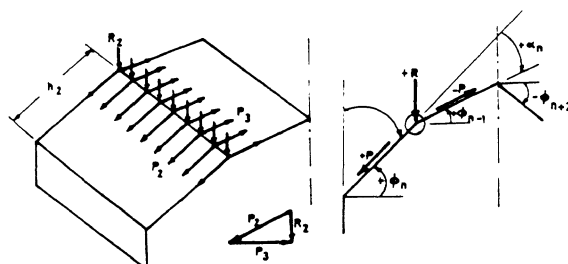


Figure (11-10) Longitudinal plates action, (a) resolution of junction forces into components in the plane of plates, (b) the positive sign convention

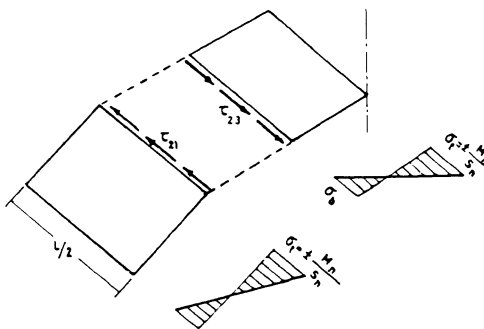


Figure (11-11) Bending stresses in the individual plates and the junction shear resulting from plates matching

11.5.2 - Shear Stresses at Plates Junctions

Consider two adjacent plates in a prismatic folded structure, numbered (n) and (n+1) in figure (11-12). The components of applied in-plane forces, figure (11-10), produce bending moments in these plates. The bending moments produce linearly varying bending stresses. According to classical beam theory, the maximum stresses occur at the extreme fibers of each beam, which are located at the plates junctions. In the figure (11-12), these maximum values are indicated by σ_n and σ_{n+1} .

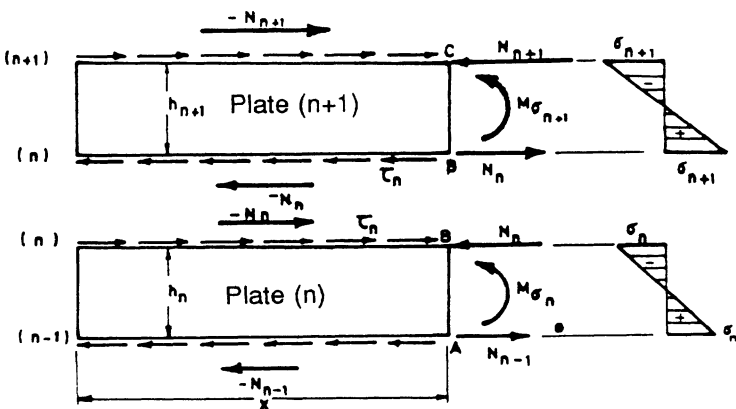


Figure (11-12) Bending stresses in two individual adjacent plates in a folded plate structure and the required shear stresses at junctions for stress matching

In a monolithic folded plate, the stress in the common fiber located at a plate junction must have the same value when considered as a fiber in either of the adjacent plates; the difference between two stresses σ_n and σ_{n+1} vanishes by virtue of a compensating shear stress, τ_n , at the junction.

Figure (11-12) shows this shear stress and its resultant, N_n , over the length of the plate. If we consider each longitudinal plate as a relatively deep beam then, figure (11-12) shows that the bending stresses are produced by the shear forces as well as the junction reactions. Thus, every one of these longitudinal plates is acted upon by a resultant axial force, produced by edge shears, a bending moment, again due to edge shears, and the bending moment produced by the junction reactions.

To achieve a stress matching between two adjacent plates, we should calculate the total stress in the longitudinal junction fiber caused by the bending and shear actions, for each plate, and so determine the required equalizing stresses.

Figure (11-12) shows that the resultant junction shear force is

$$N_{n-1} = - \int_0^x \tau_{n-1} dx, \quad N_n = \int_0^x \tau_n dx, \quad N_{n+1} = \int_0^x \tau_{n+1} dx \quad (11-1)$$

The expressions for complete longitudinal stress at the common fiber, calculated for plates (n+1) and (n) are, respectively

$$\frac{M_{o,n+1}}{S_{n+1}} + \frac{N_n h_{n+1}}{2S_n} + \frac{N_n}{A_{n+1}} - \frac{N_{n+1}}{A_{n+1}} + \frac{N_{n+1} h_{n+1}}{2S_{n+1}} \quad (11-2)$$

$$- \frac{M_{o,n}}{S_n} - \frac{N_{n-1} h_n}{2S_n} + \frac{N_{n-1}}{A_n} - \frac{N_n}{A_n} - \frac{N_n h_n}{2S_n} \quad (11-3)$$

In these relations, (h_n, A_n) and (h_{n+1}, A_{n+1}) are the (thickness, cross-sectional area) of plates (n) and (n+1), respectively, The quantities S_n and S_{n+1} are the section moduli of plates (n) and (n+1), namely

$$S_n = \frac{t_n h_n^2}{6}, \quad S_{n+1} = \frac{t_{n+1} h_{n+1}^2}{6} \quad (11-4)$$

Now, we match the two plates. The equilibrium constraint is that the bending stress at the common junctional fiber must be the same; by equating (11-2) and (11-3) we obtain

$$\frac{N_{n-1}}{A_n} + 2\left(\frac{N_n}{A_n} + \frac{N_n}{A_{n+1}}\right) + \frac{N_{n+1}}{A_{n+1}} = -\frac{1}{2}\left(\frac{M_{o,n}}{S_n} + \frac{M_{o,n+1}}{S_{n+1}}\right) \quad (11-5)$$

This equation relates the shear forces at three subsequent junctions (n-1), (n) and (n+1), and resembles the well-known three moment equation for continuous beams.

11.5.3 - Distribution of Junctional Shear Forces

The junction shear forces are required to satisfy the stress equilibrium at the plate junctions; they must compensate for the unbalanced bending stresses. Therefore, the unbalanced bending stresses must be converted to compensating shear forces. Since equation (11-5) shows that there is coupling between shear forces at several junctions, the unbalanced stresses should be distributed among several junctions.

The concept of liquidating the unbalanced bending stresses, by means of distribution, is quite similar to the concept of moment distribution in statically indeterminate structures. In this case, the unbalanced stresses, expressed in terms of shear forces, are to be distributed among several junctions.

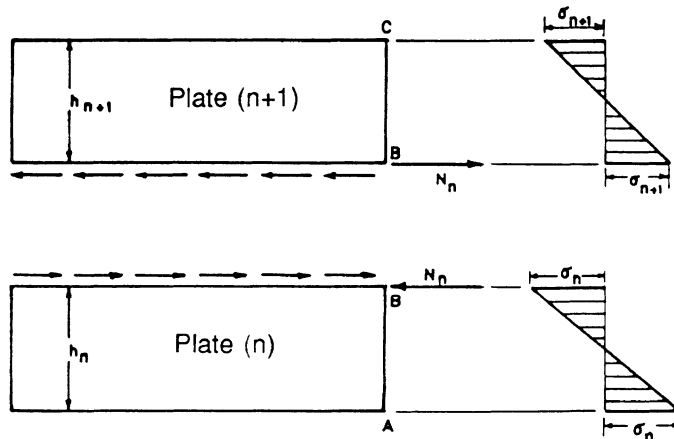


Figure (11-13) Shear stress at the junction of two adjacent plates

To determine the share of each adjacent plate in the balancing stress, i.e., to find the **distribution factor**, we proceed as follows: Consider adjacent plates (n) and (n+1), again as shown in figure (11-13). By imposing the condition of stress equality at the junction B we obtain

$$\frac{N_n}{A_{n+1}} + \frac{N_n h_{n+1}}{2S_{n+1}} + \sigma_{n+1} = - \frac{N_n}{A_n} - \frac{N_n h_n}{2S_n} + \sigma_n \quad (11-6)$$

Which upon substitution of S_n and S_{n+1} from (11-4) is rewritten as

$$\frac{4N_n}{A_{n+1}} + \sigma_{n+1} = \frac{-4N_n}{A_n} + \sigma_n \quad (11-7)$$

Let us rewrite relation (11-7) as

$$4N_n \left(\frac{1}{A_n} + \frac{1}{A_{n+1}} \right) = (\sigma_n - \sigma_{n+1}) \quad (11-8)$$

This relation shows that the unbalanced stresses σ_n and σ_{n+1} can be equalized by addition of certain shear forces as indicated in the above relation.

We find the share of each plate in the balancing force as follows:

For plate (n):

$$D_n = -\frac{4N_n}{A_n} = -(\sigma_n - \sigma_{n+1}) \frac{A_{n+1}}{A_n + A_{n+1}} \quad (11-9)$$

For plate (n+1):

$$D_{n+1} = \frac{4N_n}{A_{n+1}} = (\sigma_n - \sigma_{n+1}) \frac{A_n}{A_n + A_{n+1}} \quad (11-10)$$

Figure (11-14) shows the share of each of two adjacent plates from the unbalanced equivalent shear force.

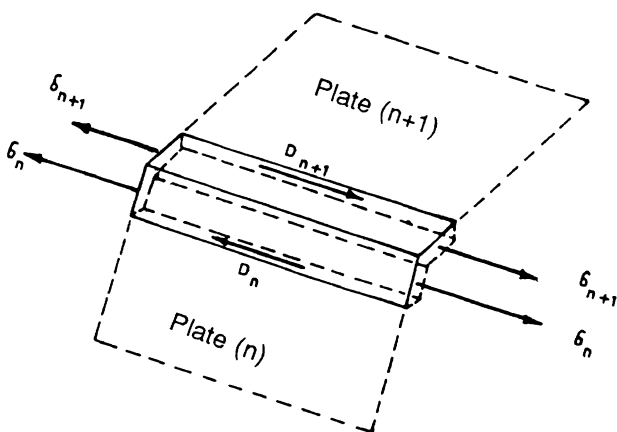


Figure (11-14) The share of each of two adjacent plates in the balancing shear force

Using relations (11-9) and (11-10), we obtain the corresponding distribution factors, D_n and D_{n+1}

$$D_{n+1} = \Delta\sigma \frac{\frac{1}{A_{n+1}}}{\frac{1}{A_n} + \frac{1}{A_{n+1}}} \quad (11-11)$$

$$D_n = -\Delta\sigma \frac{\frac{1}{A_n}}{\frac{1}{A_n} + \frac{1}{A_{n+1}}} \quad (11-12)$$

Here $\Delta\sigma = \sigma_n - \sigma_{n+1}$ is the equivalent unbalanced shear stress. The coefficients D_n and D_{n+1} are called **shear distribution factors** at the junction n of the folded plate structure. We note that the share of each plate is proportional to its shear compliance, i.e., the inverse of shear stiffness of each plate acting as a beam. This becomes evident if we would multiply the cross-sectional areas, appearing in the nominators and denominators of (11-11) and (11-12), by a common factor of the shear modulus, G . As we know (by ignoring a common shape factor), the quantity GA is the shear stiffness of a beam section.

The condition of equilibrium requires that the plates in which the unbalanced forces are distributed must be in equilibrium. To satisfy the equilibrium requirements, part of the share allocated to each plate should be *transferred* to the other edge of the plate. This event is similar to bending moment transfer in continuous beams.

Figure (11-13), and the equilibrium requirements in each plate, show that the shear stresses carried over to edges a and b are

$$\frac{N_n}{A_{n+1}} - \frac{N_n h_{n+1}}{2S_{n+1}} = - \frac{2N_n}{A_{n+1}} = - \frac{1}{2} (\sigma_n - \sigma_{n+1}) \frac{A_n}{A_n + A_{n+1}} \quad (11-13)$$

$$-\frac{N_n}{A_n} + \frac{N_n h_n}{2S_n} = \frac{2N_n}{A_n} = + \frac{1}{2} (\sigma_n - \sigma_{n+1}) \frac{A_{n+1}}{A_n + A_{n+1}} \quad (11-14)$$

The transferred quantity in each plate is, in magnitude, one half of the share of that plate from the unbalanced stresses. Therefore, taking the algebraic sign into consideration, we conclude that the **carry over factor** for each plate is equal to $-1/2$; this is the same carry over factor for uniform continuous beams.

11.5.4 - Summary of Analysis Procedure

We are now able to analyze prismatic folded plates with various configurations. We recapitulate the results of the forgoing discussions:

(1) perform the **preliminary analysis**, including transverse slab and longitudinal analyses, and redistribution of unbalanced shear forces to arrive at a stress compatible force system in the constrained folded plate. The method is similar to moment distribution, but is called **shear distribution**.

(2) Perform the **corrective analysis**. Introduce unit deflection at each junction, carry out the related force analysis along the lines indicated for the preliminary analysis. We must assume an appropriate longitudinal distribution for lateral displacement at each junction. For example, for a simply supported folded plate, a sinusoidal distribution of deflections and forces is an appropriate assumption.

(3) Fulfill the deformation compatibility at the junctions by writing the kinematic relations **matching the adjacent plates**, and so find the actual lateral displacements of the junctions. Multiply these quantities by the results of unit lateral displacements to find the actual corrections.

(4) **Superpose** the results of preliminary analysis (part (1)) and corrective analysis (part (3)) to find the complete force and displacement field in the folded plate structure.

In the following section, we apply this methodology to the analysis of a reinforced concrete folded plate roof.

11.6 - Analysis of a RC Folded Plate Roof

Consider the simply supported reinforced concrete single prismatic folded plate roof structure shown in figure (11-15). Figure (11-16) shows the cross section of this folded plate. This symmetric folded plate is composed of five plates, two of which act as the edge beams for the structure; it rests on two solid end diaphragms.

The present folded plate can be considered as a spatial flat plate approximation to the cylindrical roof designed in chapter 5; we would expect that the force systems in the two structures to be similar.

The applied loading to the folded plate of figure (11-15) is assumed to be as follows:

Dead weight of reinforced concrete (assuming a 10cm thick folded plate) 240 kg/m^2

Weight of additional load	50 kg/m^2
---------------------------	---------------------

Live load	100 kg/m^2
-----------	----------------------

Total vertical load	390 kg/m^2
---------------------	----------------------

Additional weight of the edge beam (15 cm x 80 cm)	330 kg/m
--	--------------------

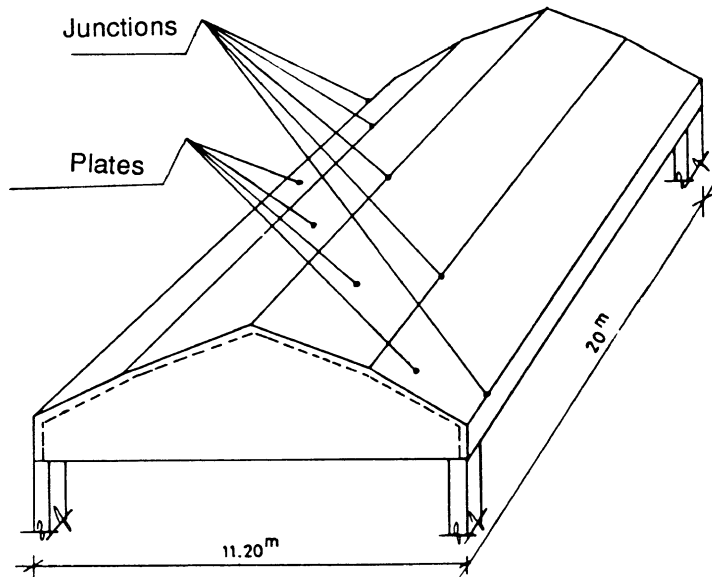


Figure (11-15) A simply supported symmetrical single folded plate

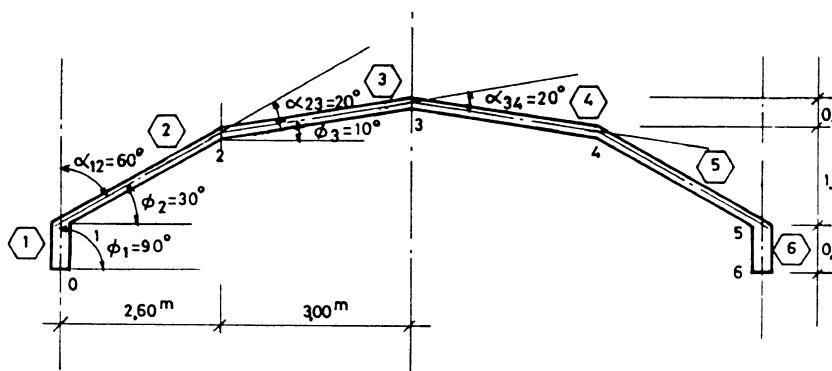


Figure (11-16) Cross section of the folded plate of figure (11-15)

@Seismicisolation

The geometrical features of the folded plate structure are given in tables (11-2) and (11-3).

Table (11-2) Geometrical properties of the folded plate of figure (11-15)

Plate	h (cm)	t (cm)	$A = th$ (cm^2)	$S = \frac{th^2}{6}$ (cm^3)	ϕ	$\sin\phi$	$\cos\phi$
1	90	15	1350	20250	90	1.00	0.0
2	300	10	3000	150000	30	0.50	0.866
3	305	10	3050	155040	10	0.179	0.985

Table (11-3) Orientation of constituent plates of figure (11-15)

Junction	α	$\sin\alpha$	$\cot\alpha$
0	0	0.00	—
1	60	0.866	0.577
2	20	0.342	2.75
3	20	0.342	2.75

Analysis:

To perform the analysis of continuous transverse slabs by means of moment distribution method, we need the moment distribution factors; these factors relate to continuous transverse strips acting in bending; they are not the shear distribution factors that we have discussed before in relation to the unbalance shear distribution between the longitudinal plates.

The moment distribution factors are proportional to the flexural stiffness ($4 E I / h$) of the transverse strips. For a strip element with one end hinged, the distribution factor is multiplied by $3/4$. By doing so, we need not to carry the moment to the hinged end. In the present case, the lower ends of two edge beam are free while their upper ends are free to rotate, i.e., to be hinged.

The moment distribution factors are calculated in table (11-4). In this table, the junction and plate numbers refer to the numbering chosen and shown in figure (11-16).

Table (11-4) Moment distribution factors of transverse slabs

Junction	Plate	Relative stiffness	Coeff. of moment distribution
0	1	—	—
1	1	$K_{10} = 0$	0
	2	$K_{12} = 4$	1.000
2	2	$K_{21} = (\frac{3}{4})(4) = 3$	0.433
	3	$K_{23} = 4 \times \frac{3}{3.05}$	0.567
3	3	$K_{32} = 4 \times \frac{3}{3.05}$	0.500
	4	$K_{34} = 4 \times \frac{3}{3.05}$	0.500

(1) Preliminary analysis

(a) Transverse slab analysis

We consider a continuous transverse strip of unit width located at the mid-length of the folded plate. At this stage, we assume that this strip behaves as a continuous beam on fixed supports. The well-known *moment distribution method* can be used to find the bending moments in this statically indeterminate beam. The distribution and carry-over factors are given in table (11-3). With the help of these factors, the unbalanced moment distribution in this continuous strip can be carried out.

Table (11-4) summarizes the moment distribution process. Having obtained the moments, each segment of this continuous strip can be considered and the shear forces at its ends can be determined by statics. Finally, the end shear forces can be combined to find the reactive forces at the junctions of strip segments, i.e., at the plate junctions. These values are also calculated in table (11-4). Figure (11-17) shows a half profile of the folded plate and the reactive forces at the plate junctions, as determined in table (11-4).

Table (11-4) Moment distribution in a continuous transverse strip of folded plate, the bending moments, shear forces and reactions at the strips junctions

		1	2	3	Junction	
0	10	12	21	2 3	32	Member
		1.000	0.433	0.567	0.500	Coeff. of moment Distribution
		+380	+380	-298	+298	kg-m/m Fix-end moment
		-35.5	-46.5			Distribution
				-23.3		Carry over
0		+344.5	-344.5	+274.7	kg-m/m	Final moment
0		-133	+133	+23	-23	M/h Cosφ Kg/m Moment reac
+330		+585	+585	+59.5	+595	$\frac{Mh}{2}$ Kg/m Vertical shear
+330		+452	+718	+618	+572	kN/m Total shear force
	+782		+1336		+1144	kg/m Reactions at junctions

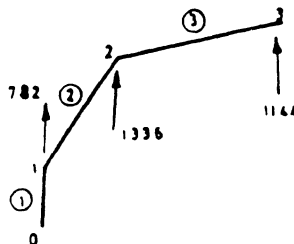


Figure (11-17) Reactive forces at the junctions of a transverse strip

(b) Longitudinal plates analysis

At this stage, we resolve the reactions to the forces obtained in the previous stage, along the inclined longitudinal plates. If we designate the received force share of plate i at its edge j by the symbol P_{ij} , we have

$$P_{10} = 0$$

$$P_{11} = 782 \text{ Kg/m}$$

$$P_{21} = 0$$

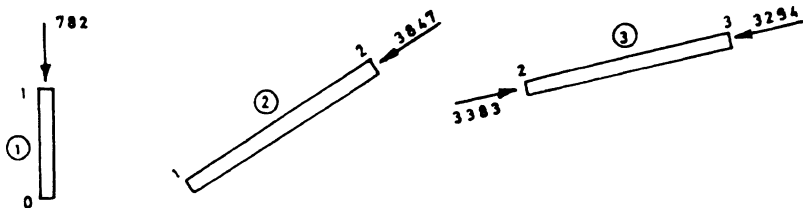
$$P_{22} = 1336 \frac{\cos\phi_3}{\sin\alpha_2} = 1336 \frac{0.985}{0.342} = 3847 \text{ Kg/m}$$

$$\alpha_2 = \alpha_{23}$$

$$P_{32} = -1336 \frac{\cos\phi_2}{\sin\alpha_2} = -1336 \frac{0.866}{0.342} = -3383 \text{ Kg/m}$$

$$P_{33} = 1144 \frac{\cos\phi_2}{\sin\alpha_2} = 1144 \frac{0.985}{0.342} = 2294 \text{ Kg/m}$$

These component forces can be combined to yield the forces transferred to each longitudinal plate. The result is shown in figures (11-18).



Figures (11-18) Forces transferred to longitudinal plates

The longitudinal plates can, now, be analyzed as simply supported beams under uniform loading. The maximum bending moments and bending stresses in these plates can be obtained by the classical beam formulas. These calculations are performed in the following.

$$P_3 = P_{32} + P_{33} = 3294 - 3383 = -89 \text{ Kg/m}$$

$$M = \frac{P_3 l^2}{8} = \frac{-89 \times 20^2}{8} = -4450 \text{ Kg-m}$$

$$\sigma_t = -\sigma_b = \frac{M}{S} = \frac{4450 \times 100}{155040} = 2.87 \text{ Kg/cm}^2$$

$$P_2 = P_{21} + P_{22} = 0 + 3847 = 3847 \text{ Kg/m}$$

$$M = \frac{P_2 l^2}{8} = \frac{3847 \times 20^2}{8} = 192350 \text{ Kg-m}$$

$$\sigma_t = -\sigma_b = - \frac{192350 \times 100}{150000} = -128.2 \text{ Kg/cm}^2$$

$$P_1 = P_{10} + P_{11} = 0 + 782 = 782 \text{ Kg/m}$$

$$M = \frac{P_1 l^2}{8} = \frac{782 \times 20^2}{8} = 39100 \text{ Kg-m}$$

$$\sigma_t = -\sigma_b = - \frac{39100 \times 100}{20250} = -193.1 \text{ Kg/cm}^2$$

Figure (11-19) plots the results of the stress calculations in each longitudinal plate, treated independently from the other plates. As we see, the stresses at the common longitudinal junction fibers are not equal. Therefore, there is an unbalanced shear force which is to be distributed between two adjacent plates. If the shear distribution factor for the junction i of the plate j is designated by the D_{ij} , then relations (11-11) and (11-12) give

$$D_{01} = 0$$

$$D_{11} = \frac{\frac{1}{A_1}}{\frac{1}{A_1} + \frac{1}{A_2}} = \frac{A_2}{A_1 + A_2} = \frac{3000}{1350 + 3000} = 0.69$$

$$D_{12} = \frac{\frac{1}{A_2}}{\frac{1}{A_1} + \frac{1}{A_2}} = \frac{A_1}{A_1 + A_2} = \frac{1350}{1350 + 3000} = 0.31$$

$$D_{22} = \frac{\frac{1}{A_2}}{\frac{1}{A_2} + \frac{1}{A_3}} = \frac{A_3}{A_2 + A_3} = \frac{3050}{3000 + 3050} = 0.50$$

$$D_{\dots} = 0.50$$

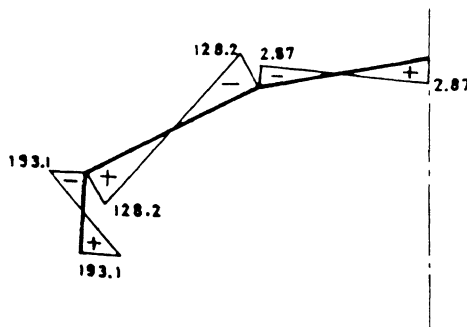


Figure (11-19) Unbalanced bending stresses in the longitudinal plates

Moreover, the carry over factors are

$$C_{10} = C_{12} = C_{21} = C_{23} = -0.5$$

$$C_{01} = C_{32} = 0$$

We should note that, due to symmetry, the shear stress at the junction 3 is zero. So, no shear carry over is to take place to that junction.

The unbalanced shear distribution process is summarized in table (11-5). Figure (11-20) shows the final result of balanced stresses in the longitudinal plates.

Table (II-5) unbalanced shear force distribution among the longitudinal plates

0	2	3		Junction
1	2	3		Member
0	0.69	0.31	0.50	Coeff. of moment Dist
-0.5		-0.5	-0.5	Carry-over factor
+193.1	-193.1	+128.2	-128.2	Stresses at fixed edges
+221.7	-99.6	+62.7	-62.7	Distribution
-110.8	-31.3	+49.8	+31.3	Distribution
+82.3	+28.6	-2.7	-15.7	Sum
	-21.6	+9.7	-25.0	Distribution
+10.8		+12.5	-4.85	Carry over
+93.1	+7	+19.5	-45.6	Sum
	+8.6	-3.9	+2.5	Distribution
-4.3		-1.25	-1.9	Carry over
+888	15.6	+14.4	-45.0	Sum
	-0.83	+0.37	+0.95	Distribution
+0.4		-0.48	-0.2	Carry-over
+89.2	+14.8	+14.4	-44.1	Final stresses
			+23.5	

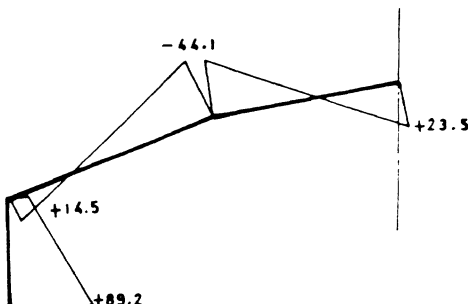


Figure (II-20) Balanced bending stress distribution in the longitudinal plates

At this stage, the longitudinal plate are in equilibrium. The deformations of these plates should also be compatible; this leads to some relations which we shall now derive.

Figure (11-21) shows the displacements of the longitudinal plates, δ_i in their own planes. These quantities are the displacements of longitudinal plates at the mid-length of the folded plate. Figure (11-21) also shows the lateral displacements, Δ_i of the plates junctions, and the conventional positive directions of these displacements are also depicted.

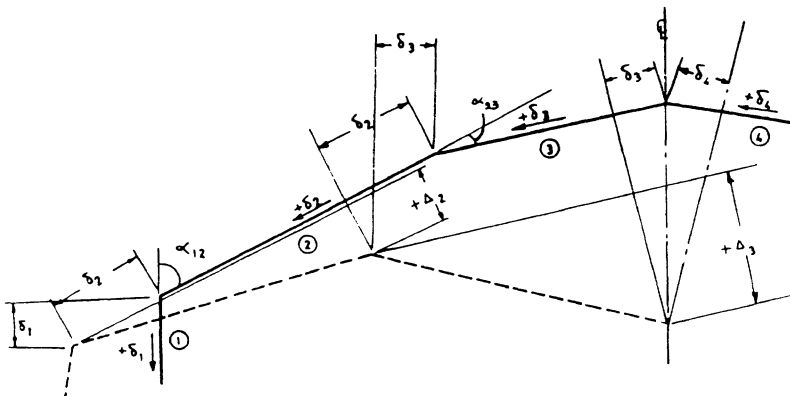


Figure (11-21) Displacements of longitudinal plates and their positive directions

It can be shown that the in-plane displacements of the plates and the lateral displacement of the plates junctions are related by the following kinematical relation.

$$\Delta_n = -\frac{\delta_{n-1}}{\sin \alpha_{n-1}} + \delta_n (\cot \alpha_{n-1} + \cot \alpha_n) - \frac{\delta_{n+1}}{\sin \alpha_n} \quad (11-15)$$

In this relation, the subscript n designates the longitudinal plate number.

The master relation (11-15), for the present problem yields

$$\Delta_2 = -1.15\delta_1 + 3.32\delta_2 - 2.92\delta_3$$

$$\Delta_3 = -2.92\delta_2 + 5.5\delta_3 - 2.92\delta_4 \quad (11-16)$$

Now, as we know, for a uniformly loaded simply supported beam having a rectangular cross section, the relations between the bending stresses, maximum bending moment and maximum deflection are as follows:

$$\delta = \frac{5Ml^2}{48EI} , \quad M = \frac{\sigma_b - \sigma_t}{2} s$$

$$\delta = \frac{5(\sigma_b - \sigma_t)sl^2}{2 \times 48EI}$$

$$\frac{s}{I} = \frac{2}{h}$$

$$\delta = \frac{\sigma_b - \sigma_t}{h} \left(\frac{5}{48} \frac{s^2}{E} \right)$$

In these relations, σ_b and σ_t are the bending stresses at the bottom and top fibers of the beam, respectively. Using these relations together with the results of table (11-5), we can find the displacement of plate i in the preliminary analysis, δ_{io} . Thus, we obtain

$$\delta_{30} = \frac{(-441 - 23.5)}{3.05} \cdot \frac{5}{48} \cdot \frac{20^2 \times 100}{1.4 \times 10^5} = -0.66 \text{ cm}$$

$$\delta_{20} = \frac{(+14.5 + 44.1)}{3.00} \cdot \frac{5}{48} \cdot \frac{20^2 \times 100}{1.4 \times 10^5} = +0.58 \text{ cm}$$

$$\delta_{10} = \frac{(+89.2 - 14.5)}{0.90} \cdot \frac{5}{48} \cdot \frac{20^2 \times 100}{1.4 \times 10^5} = +2.47 \text{ cm}$$

Figure (11-22) shows the deformed state of the folded plate at its mid-length as predicted by the preliminary analysis.

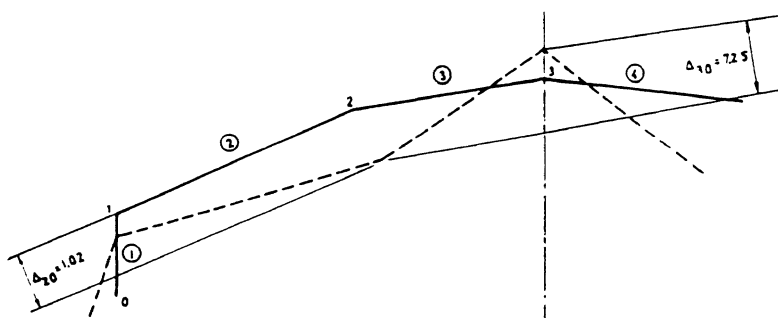


Figure (11-22) Deformation of the folded plate at its mid-length according to preliminary analysis

(2) Corrective analysis

The preliminary analysis was based on the assumption that the junction points were immovable, whereas some lateral displacement, as shown in figure (11-22) was obtained in that stage of analysis. In reality, junctions displace laterally. This displacement is not the same as that obtained in the preliminary analysis. Some correction is required to achieve a deformation compatibility of the adjacent plates. This is done in the "corrective analysis".

The corrective analysis consists of introducing unit lateral displacements at each junction, in a sequential manner, and finding the force and deformation fields due to these individual lateral "sideways". Then, a set of displacement compatibility equations are written which would yield the true lateral displacements. Note that, for each one of these unit lateral displacements, an analysis similar to that of the preliminary analysis (consisting of slab and plate analyses) should be performed.

In figures (11-23) and (11-24) the unit lateral displacements of plates number 2 and 3 are depicted.

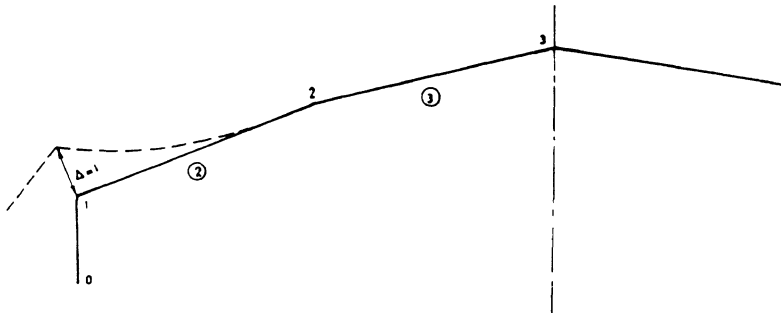


Figure (11-23) Unit lateral displacement of Plate 2

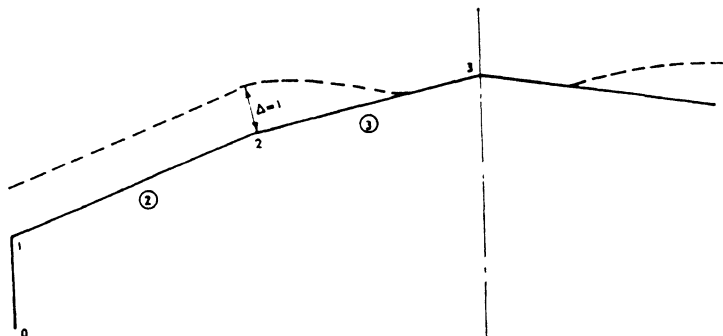


Figure (11-24) Unit Lateral displacement of plate 3

For a transverse slab, the end moments due to the unit displacements shown in figures (11-23) and (11-24) are

For the pattern of figure (11-23)

$$M_2^F = \frac{3EI_2\Delta}{h_2^2} = \frac{3 \times 1.4 \times 10^5 \times (1 \times \frac{10^3}{12}) \times 1}{(300)^2} = 389 \text{ kg-m/m}$$

For the pattern of figure (11-24)

$$M_2^F = M_3^F = \frac{6 \times 1.4 \times 10^5 \times (1 \times \frac{10^3}{12}) \times 1}{(305)^2} = 753 \text{ kg-m/m}$$

Now, we repeat the moment distribution procedure for each of these two patterns. These calculations are performed in tables (11-6) and (11-7). The corresponding end reactions are also obtained.

Table (11-6)

<u>$\Delta_2 = 1 \text{ cm}$</u>					
0	1	2	3	Distribution	
10	12	21	23	Member	
0.000	1.000	0.433	0.561	Distribution factor	
		-389	0	Fixed end moment	
		+168	+221	Distribution	
				+110.5	
0	0	-221	+221	110.5	Final moment
+85.1	-85.1	-110.4	+110.4		M/h Cost
+85.1	-195.5		2 x 110.4 = 220.8		Final reaction

Table (11-7)

<u>$\Delta_3 = 1 \text{ cm}$</u>					
0	1	2	3	Junction	
10	12	21	23	Member	
0.000	1.000	0.433	0.567	Distribution factor	
			-753	-753	
0	0	+32.6	+427	Fixed-end moment	
				213.5	Carry-over
0	0	+32.6	-32.6	-539.5	Final moment
-125.5	+125.5	+288	-288		M/h Cost
-125.5	413.5	2 x (-288) = -576			Reactions

The results of calculations performed in tables (11-6) and (11-7) are depicted in the figures (11-25).

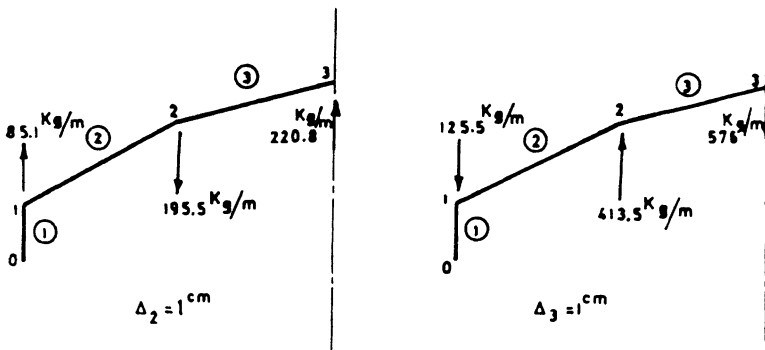


Figure (11-25) End reactions due to unit lateral displacements

To analyze the simply supported longitudinal plates, we assume a sinusoidal distribution for the loadings shown in figures (11-25). The related differential equation is,

$$EIv'' = q_0 = P \sin \frac{\pi x}{\lambda} \quad (11-17)$$

From which, we obtain

$$M(x) = EIv''' = \frac{\lambda^2}{\pi^2} P \sin \frac{\pi x}{\lambda} \quad (11-18)$$

So, the maximum moment at the mid-span would be,

$$M = \frac{P\lambda^2}{\pi^2} \quad (11-19)$$

and the related maximum bending stresses,

$$\sigma_b = -\sigma_c = \frac{M}{S} = \frac{P\lambda^2}{\pi^2 S} \quad (11-20)$$

Therefore, the maximum in-plane displacement of each longitudinal plate is,

$$\delta = \left(\frac{\sigma_b - \sigma_t}{hE} \right) \frac{l^2}{\pi^2} \quad (11-21)$$

Now, having carried out the analysis of transverse slabs for unit lateral displacements, and having obtained the above relations, we can perform the corrective analysis of longitudinal plates. The procedure resembles the preliminary analysis. The details of the calculations are as follows:

Loadings on longitudinal plates:

For $\Delta_2 = 1$ cm

$$P_{10} = 0$$

$$P_{11} = 85.1 \text{ Kg/m}$$

$$P_{21} = 0$$

$$P_{22} = -195.5 \frac{\cos \phi_3}{\sin \alpha_2} = -195.5 \frac{0.985}{0.342} = -563 \text{ Kg/m}$$

$$P_{32} = 195.5 \frac{\cos \phi_3}{\sin \alpha_2} = 195.5 \frac{0.866}{0.342} = +495 \text{ Kg/m} \quad \begin{matrix} \alpha_2 = \alpha_{23} \\ \alpha_3 = \alpha_{34} \end{matrix}$$

$$P_{33} = (2 \times 110.4) \frac{\cos \phi_4}{\sin \alpha_3} = 220.8 \frac{0.985}{0.342} = +636 \text{ Kg/m}$$

For $\Delta_3 = 1$ cm

$$P_{10} = 0$$

$$P_{11} = -125.5 \text{ Kg/m}$$

$$P_{21} = 0$$

$$P_{22} = +413.5 \frac{0.985}{0.342} = 1191 \text{ Kg/m}$$

$$P_{32} = -413.5 \frac{0.866}{0.342} = -1047 \text{ Kg/m}$$

$$P_{33} = (-288 \times 2) \frac{0.985}{0.342} = -1659 \text{ Kg/m}$$

Figures (11-26) and (11-27) show these loadings applied to each plate.

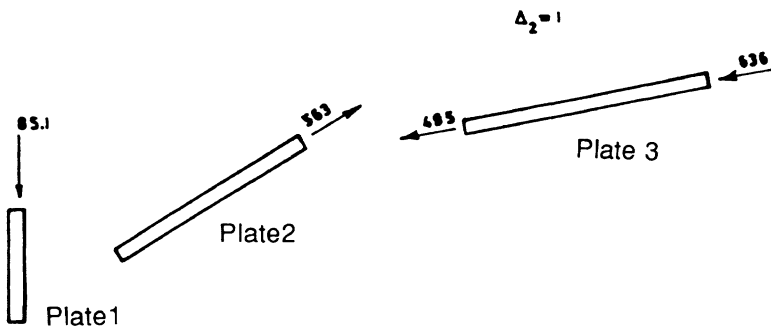


Figure (11-26)

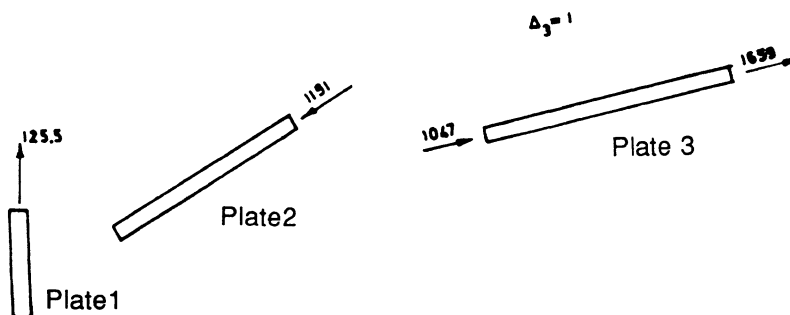


Figure (11-27)

Stresses at the junctions:

For $\Delta_2 = 1$ cm

$$\sigma_b = -\sigma_t = \frac{P\ell^2}{S} = \frac{(636 + 495) \times 20^2 \times 100}{\pi^2 \times 155040} = +29.6 \text{ kg/cm}^2 \quad \text{Plate 3}$$

$$\sigma_b = -\sigma_t = \frac{-563 \times 20^2 \times 100}{\pi^2 \times 150000} = -15.2 \text{ kg/cm}^2 \quad \text{Plate 2}$$

$$\sigma_b = -\sigma_t = \frac{85.1 \times 20^2 \times 100}{\pi^2 \times 20250} = +17.0 \text{ kg/cm}^2 \quad \text{Plate 1}$$

For $\Delta_3 = 1 \text{ cm}$

$$\sigma_b = -\sigma_t = \frac{-(1659 + 1047) \times 20^2 \times 100}{\pi^2 \times 155040} = -70.7 \text{ kg/cm}^2 \quad \text{Plate 3}$$

$$\sigma_b = -\sigma_t = \frac{1191 \times 20^2 \times 100}{\pi^2 \times 150000} = +32.2 \text{ kg/cm}^2 \quad \text{Plate 2}$$

$$\sigma_b = -\sigma_t = \frac{-125.5 \times 20^2 \times 100}{\pi^2 \times 20250} = -25.1 \text{ kg/cm}^2 \quad \text{Plate 1}$$

Figures (11-28) and (11-29) show the results of longitudinal plates analysis. At this stage, the bending stresses at the junctions are not equal and should be equalized by a shear stress distribution.

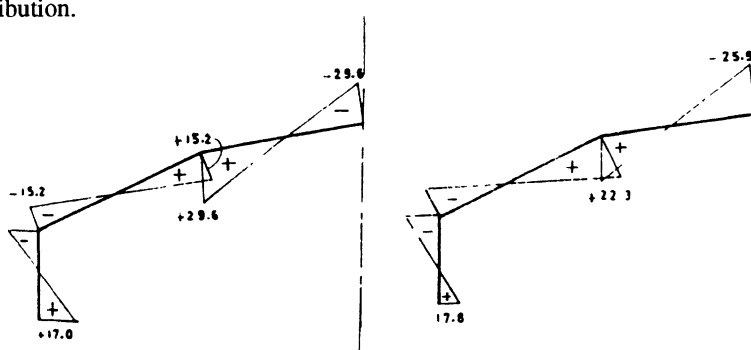


Figure (11-28) Bending stresses for $\Delta_2 = 1 \text{ cm}$

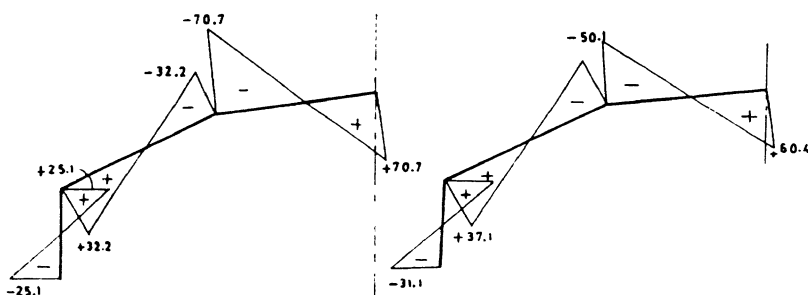


Figure (11-29) Bending stresses for $\Delta_3 = 1 \text{ cm}$

The results of unbalanced shear force distribution (in the corrective analysis) are presented in tables (11-8) and (11-9).

Table (11-8) Corrective shear force distribution, $\Delta_2 = 1 \text{ cm}$

1		2		3		Plate
0	0.69	0.31	0.500	0.500		Distribution factor
$-\frac{1}{2}$		$-\frac{1}{2}$		$-\frac{1}{2}$		Carry-over factor
+17.0	-17.0	-15.2	+15.2	+29.6	-29.6	Stresses at fixed edges
0	+1.24	-0.56	+7.2	-7.2	0	Distribution
-0.6	0	-3.6	+0.28	0	+3.6	Carry over
+16.4	-15.8	-19.4	+22.7	+22.4	-26.0	Sum
0	-2.5	+1.1	-0.15	+0.15	0	Distribution
+1.3	0	+0.1	-0.6	0	-0.1	Carry over
+17.7	+18.3	-18.2	+22.0	+22.6	-26.1	Sum
0	+0.1	0	+0.3	-0.3	0	Distribution
0	0	-0.2	0	0	+0.2	Carry over
+17.7	-18.2	-18.4	22.3	22.3	-25.9	Sum
0	-0.1	+0.1	0	0	0	Distribution
+0.1	0	0	0	0	0	Carry over
+17.8	-18.3	-18.3	+22.3	+22.3	-25.9	Sum

Table (11-9) Corrective shear force distribution, $\Delta_3 = 1 \text{ cm}$

1		2		3		Plate
0	0.69	0.31	0.500	0.500		Distribution factor
$-\frac{1}{2}$		$-\frac{1}{2}$		$-\frac{1}{2}$		Carry-over factor
-25.1	+25.1	+32.2	-32.2	-70.7	+70.7	Stresses at fixed edges
0	+4.9	-2.2	-19.3	+19.3	0	Distribution
-2.5	0	+9.6	11	0	-96	Carry over
-27.6	+30	+39.6	-50.4	-51.4	+61.1	Sum
0	+6.6	-3.0	-0.5	+0.5	0	Distribution
-3.3	0	+0.3	+1.5	0	-0.3	Carry over
-30.9	+36.6	+36.9	-49.4	-50.9	+60.8	Sum
0	+0.2	-0.1	-0.7	+0.7	0	Distribution
-0.1	0	+0.4	0	0	-0.4	Carry over
-31	+36.8	+37.2	-50.1	-50.2	+60.4	Sum
0	+0.3	-0.1	-0.1	+0.1	0	Distribution
-0.1	0	0	+0.1	0	0	Carry over
-31	+37.1	+37.1	-50.1	-50	+60.4	Sum

In-plane displacements of longitudinal plates:**The formula:**

$$\delta = \frac{\sigma_b - \sigma_t}{hE} \frac{l^2}{\pi^2}$$

For $\Delta_2 = 1$ cm

$$\delta_3 = \frac{(22.3 + 25.9)400 \times 100}{3.05 \times 1.4 \times 10^5 \times \pi^2} = 0.46 \text{ cm}$$

$$\delta_2 = \frac{(-18.3 - 22.3)400 \times 100}{3.00 \times 1.4 \times 10^5 \times \pi^2} = -0.39 \text{ cm}$$

$$\delta_1 = \frac{(+17.8 + 18.3)400 \times 100}{0.90 \times 1.4 \times 10^5 \times \pi^2} = 1.16 \text{ cm}$$

For $\Delta_3 = 1$ cm

$$\delta_3 = \frac{(-50.1 - 60.4)400 \times 100}{3.05 \times 1.4 \times 10^5 \times \pi^2} = -1.05 \text{ cm}$$

$$\delta_2 = \frac{(37.1 + 50.1)400 \times 100}{3.00 \times 1.4 \times 10^5 \times \pi^2} = 0.84 \text{ cm}$$

$$\delta_1 = \frac{(-31.1 - 37.1)400 \times 100}{0.90 \times 1.4 \times 10^5 \times \pi^2} = -2.19 \text{ cm}$$

The total in-plane displacement of each longitudinal plate is obtained by superposition of the results of preliminary and corrective analyses. So, if the actual lateral displacements of junctions 2 and 3 are denoted by the symbols Δ_2 and Δ_3 , respectively, then the total displacements of the plates at their mid-span would be,

$$\delta_1 = 2.47 + 1.16\Delta_2 - 2.19\Delta_3$$

$$\delta_2 = 0.58 - 0.39\Delta_2 + 0.84\Delta_3 \quad (11-22)$$

$$\delta_3 = -0.66 + 0.46\Delta_2 - 1.05\Delta_3$$

Now, if we substitute the relations (11-16) into (11-22) we obtain the following compatibility relations for the actual lateral displacements of plates junctions.

$$\begin{aligned} \Delta_2 &= -1.15(2.47 + 1.16\Delta_2 - 2.19\Delta_3) + 3.32(0.58 - 0.39\Delta_2 + 0.84\Delta_3) \\ &\quad - 2.92(-0.66 + 0.46\Delta_2 - 1.05\Delta_3) \end{aligned}$$

$$\Delta_2 = +1.0123 - 3.972\Delta_2 + 8.3733\Delta_3 \quad (11-23)$$

$$\begin{aligned} \Delta_3 &= -2.92(0.58 - 0.39\Delta_2 + 0.84\Delta_3) + 5.5(-0.66 + 0.46\Delta_2 - 1.05\Delta_3) \\ &\quad - 2.92(0.66 - 0.46\Delta_2 + 1.05\Delta_3) \end{aligned}$$

$$\Delta_3 = -7.2508 + 5.012\Delta_2 - 11.2938\Delta_3 \quad (11-24)$$

If we solve two simultaneous equations for Δ_2 and Δ_3 we find

$$\Delta_2 = -2.52 \text{ cm}$$

$$\Delta_3 = -1.62 \text{ cm}$$

Having determined the actual lateral displacements of the plates junctions, we can obtain the correction by multiplying the unit load corrections by the magnitude of actual displacements.

(3) Superposition of preliminary and corrective solutions

To obtain a complete solution to the folded plate problem of figure (11-15) the preliminary and corrective solutions must be superposed. This superposition is carried out in tables (11-10) and (11-11) and (11-12).

Table (11-10) Longitudinal stress in the folded plate (kg/m²)

Junctions	0	1		2		3
Preliminary anal	+89.2	+14.5	+14.5	-44.1	-44.1	+23.5
Corrective anal						
$\Delta_2 = 1\text{ cm}$	+17.8	-18.3	-18.3	+22.3	+22.3	-25.9
$\Delta_2 = -2.52\text{ cm}$	-44.86	+46.12	+46.12	-56.20	-56.20	+65.27
$\Delta_3 = 1\text{ cm}$	-31.1	+37.1	+37.1	-50.1	-50.1	+60.4
$\Delta_3 = -1.62\text{ cm}$	+50.38	-60.10	-60.10	+81.16	+81.16	-97.83
Total correction	+5.52	-18.98	-13.98	+24.96	+24.96	-32.58
Final results	+94.7	+0.52	+0.52	-19.14	-19.14	-9.08

Table (11-11) Transverse bending moments in the mid-length of the folded plate (kg-m/m)

		Plate 2		Plate 3	
Preliminary analysis 0		+208	-344.5	+137	-274.7
Corrective analysis					
$\Delta_2 = 1\text{ cm}$	0		+221		-110.5
$\Delta_2 = -2.52\text{ cm}$	0		-556.9		+278.3
$\Delta_3 = 1\text{ cm}$	0		-326.0		+539.5
$\Delta_3 = -1.63\text{ cm}$	0		+528.1		-874.0
Total correction	0		-28.8		-595.7
Final results	0	+193.5	-373.3	-175	-870.4

Table (11-12) Shear force in the mid-length of the folded plate (kg/m x 10³)

Junctions	0	01 **	1	12	2	23	3
Preliminary	0		-70.0		-35.6		0
Corrective analysis							
$\Delta_2 = 1\text{ cm}$	0		+0.34		-5.7		0
$\Delta_2 = 2.52\text{ cm}$	0		-0.86		+14.4		0
$\Delta_3 = 1\text{ cm}$	0		-4.1		+15.4		0
$\Delta_3 = -1.62\text{ cm}$	0		+6.6		-25.0		0
Total correction	0		+5.74		-10.6		0
Final results	0	-48.0	-64.3	-57.6	-46.2	-14.3	0

To find the shear stress at each point of the folded plate, we need to know the longitudinal variation of the shear force. We assume that the shear force has the same variation as the moment M_n and loading P_n . So, to find the shear stress, τ , we do as follows:

From the **preliminary analysis**, we have

$$M_n = M_{\max} \left(\frac{4x}{l} - \frac{4x^2}{l^2} \right) \quad (11-27)$$

$$N_o = N_{C\max} \left(\frac{4x}{l} - \frac{4x^2}{l^2} \right) \quad (11-28)$$

in which N_o is the shear force obtained in the preliminary analysis. The shear stress, according to preliminary analysis, is,

$$\tau = \frac{4N_o \max}{t l} \left(1 - \frac{2x}{l} \right) \quad (11-29)$$

The **corrective analysis** gives

$$M = M_{\max} \sin \frac{\pi x}{l} \quad (11-30)$$

Table (11-13) principal stresses in the folded plate of figure (11-15)

Plate		A(x = 0)	B(x = $\frac{L}{8}$)	C(x = $\frac{L}{4}$)	D(x = $\frac{3L}{8}$)	E(x = $\frac{L}{2}$)
3	Junction 3	0	0	0	0	0
	Plate	0	-3.97	-6.81	-8.51	-9.08
		+2.86	+0.67	+0.19	+0.04	0
		-2.86	-6.84	-10.77	-13.27	-14.11
	Junction 2	+7.24	+2.67	+0.86	+0.18	0
2		-7.24	-11.04	-15.22	-18.12	-19.14
	Plate	+11.52	+6.84	+3.24	+0.86	0
		-11.52	-10.91	-10.22	-9.59	-9.31
	Junction 1	+12.86	+9.77	+6.63	+3.46	+0.52
		-12.86	-9.54	-6.23	-2.97	0
1	Junction 1	+8.57	+6.55	+4.49	+2.40	+0.52
	Plate	-8.57	-6.32	-4.10	-1.91	0
		+6.4	+22.32	+36.12	+44.71	+47.61
		-6.4	-1.49	-0.41	-0.08	0
	Junction 0	0	+41.43	+71.03	+88.78	+94.70
		0	0	0	0	0

So, the corrective shear force would be

$$\bar{N} = \bar{N}_{\max} \sin \frac{\pi x}{\lambda} \Rightarrow \tau = \frac{\pi \bar{N}_{\max}}{t \ell} \cos \frac{\pi x}{\lambda} \quad (11-31)$$

Therefore, the expression for the total shear stress is

$$\tau = \left(\frac{N_{o \max}}{t} \right) \left(1 - \frac{2x}{\lambda} \right) + \frac{\pi \bar{N}_{\max}}{t \ell} \cos \frac{\pi x}{\lambda} \quad (11-32)$$

In practice, we assume a linear longitudinal variation for the shear stress. On this basis, we may write

$$\tau = \frac{4(N_{o\ max} + \bar{N}_{max})}{t_s} \left(1 - \frac{2x}{l}\right) \quad (11-33)$$

At this stage, we can determine the principal stresses at each point of the folded plate. The appropriate known relation is

$$\sigma_p = \frac{\sigma_x}{2} \pm \sqrt{\tau^2 + \left(\frac{\sigma_x}{2}\right)^2} \quad (11-34)$$

Table (11-13) shows calculations related to determination of principal stresses at several points of the folded plate are performed; the (+) and (-) signs designate compressive and tensile forces, respectively. Points A, B, C, and D, in table (11-13), identify the design points at which the principal stress calculations are carried out.

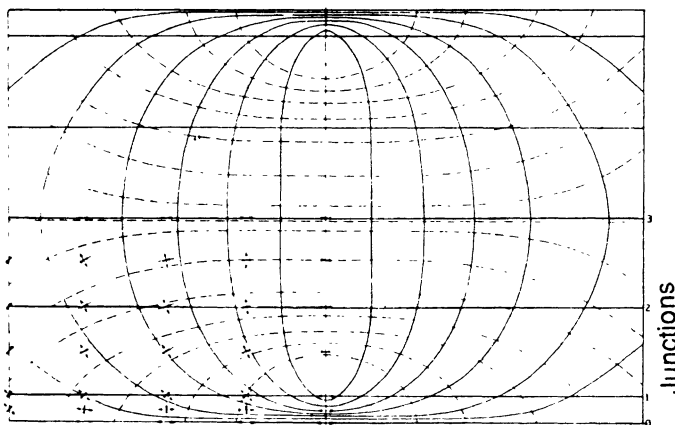


Figure (11-30) Plan of stress trajectories for figure (11-16)

Figure (11-31) shows the plan of stress trajectories in the folded plate of figure (11-16). In this figure, the compressive and tensile directions are depicted by the dotted and solid lines, respectively.

The results of this folded plate roof problem are similar to those obtained in chapter 5 for the single simply supported cylindrical roof with edge beams.

The values obtained in table (11-13) could be used to design reinforcement for the concrete in the folded plate roof. The steel reinforcement would consist basically of longitudinal bars, transverse bars, and inclined bars placed at the corner region. The pattern of reinforcement is similar to that of single simply supported cylindrical shell with edge beams.

Problems

P 11.1 - A prismatic folded plate roof may be considered as a geometrical approximation to a continuously curved cylindrical vault. Thus it is to be expected that the stress and deformation fields in a folded plate would be approximately the same as the corresponding fields in a cylindrical roof having the same overall dimensions and loadings. To investigate the validity of this statement, consider the series of design examples of cylindrical shell roofs presented in chapter 5. Assume some appropriate folded plate substitutes for those shells. Design each folded plate and compare the results with the ones presented for cylindrical shells.

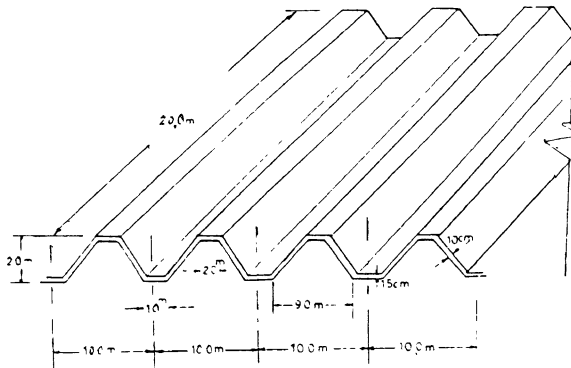
P 11.2 - A large space is to be covered by a reinforced concrete folded plate roof. Figure (P 11-2a) shows the overall geometrical dimensions of this roof. Figure (P 11-2b) shows the transverse section of one of the repeating units. Analyze this structure and design the required steel reinforcement. For your analysis and design, the following data may be assumed.

Intensity of dead load: 300 kg/m²

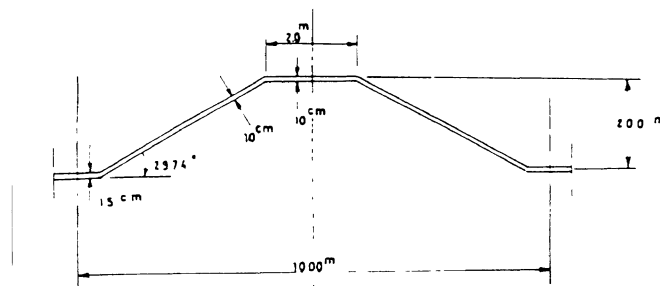
Intensity of live load: 100 kg/m² (on the projected horizontal surface)

$f_c = 200 \text{ kg/cm}^2$, $f_y = 3000 \text{ kg/cm}^2$

$E_s = 2000000 \text{ kg/cm}^2$, $E_c = 200000 \text{ kg/cm}^2$



(a) A perspective view



(b) Transverse section of one of the units

Figure (P 11-2) A prismatic folded plate roof

References for Chapter Eleven

- 11.1 - M. Farshad, *Shell Structures*, Vol. I, 1986, Vol. II, 1987, Shiraz University Publications, Shiraz
- 11.2 - D. P. Billington, *Thin Shell Concrete Structures*, McGraw-Hill Book Co. N.Y., Revised edition, 1982
- 11.3 - G. S. Ramaswamy, *Design and Construction of Concrete Shell Roofs*, McGraw-Hill Book Co., N.Y., 1968
- 11.4 - M. Salvadori and R. Heller, *Structure in Architecture*, Prentice-Hall, INC., N.J., 1963
- 11.5 - "Phase I Report on Folded Plate Construction", Report of the Task Committee on Folded Plate Construction, Journal of the Structural Division, Proc. of ASCE, Dec. 1963, pp 365-406

Chapter 12

Design of Liquid Retaining Shells

12.1 - Introduction

Liquid retaining shell structures are made of steel, concrete, reinforced plastics, and other reinforced materials; they may have circular shape or other geometrical forms; they could be located underground, over of the ground, and / or on elevated towers. Circular containers could be roofed by cones or domes; they could also have cones or flat plates as their base. In the present chapter, emphasis will be mainly placed on the design aspects of *reinforced concrete* circular containers.

In the first part of this chapter, we discuss general design considerations related to cylindrical liquid storage shells. We will use the membrane theory of cylindrical shells developed in chapter three and the bending theory presented in chapter four. We will also develop a theory of axisymmetric behavior of circular cylindrical shells for quick reference. In the later parts of present chapter, we treat circular containers with various top and bottom conditions.

12.2 - Classifications of Liquid Containers

Liquid retaining tanks may be classified according to shape, size, location, application, and materials of construction.

(1) Configuration

Liquid storage structures may be cylindrical, rectangular, conical, combined, or some other shape.

(2) Size

They may be small, medium or large. Volumes less than 50 m^3 are *small*, from 150 to 500 m^3 are *medium*, from 1000 m^3 to 2500 m^3 are *large*, over 5000 m^3 are *very large*.

(3) Location

Liquid storage containers could be buried (underground), half-buried, situated on the ground, figure(12-1), or be placed on elevated foundations, figure (12-2) and / or towers. Accordingly, they would be called *buried*, *half-buried*, *ground*, and *elevated* tanks.

(4) Application

Liquid retaining tanks could be water tanks, gas tanks, and / or pressure vessels.

(5) Materials of Construction

Liquid retaining structures could be reinforced concrete containers, steel tanks, etc.

12.3 - General Design Considerations

12.3.1 - Shape Design

Figures (12-1) show examples of ground-based liquid retaining shells. Figures (12-2) show some examples of customarily shapes for elevated water tanks. The ground based containers could be located underground.

Elevated water tanks can have a variety of top and bottom systems. The set of figures (12-3) show some of these arrangements. In overall shape design of elevated tanks, the diameter to height ratio is customarily chosen between one and two. For initial design, an average ratio of 1.5 is recommended.

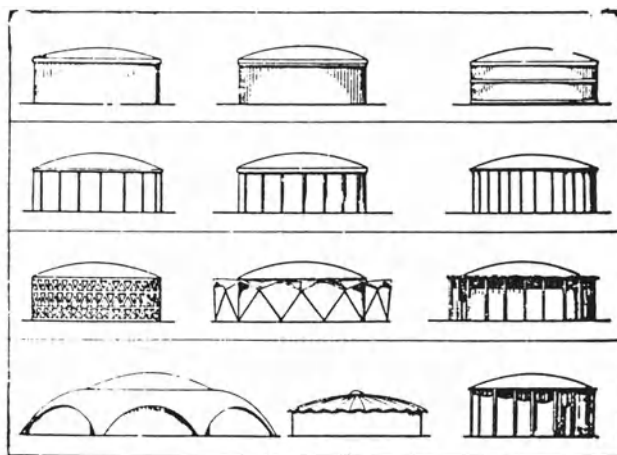


Figure (12-1) Examples of ground-based liquid retaining shells

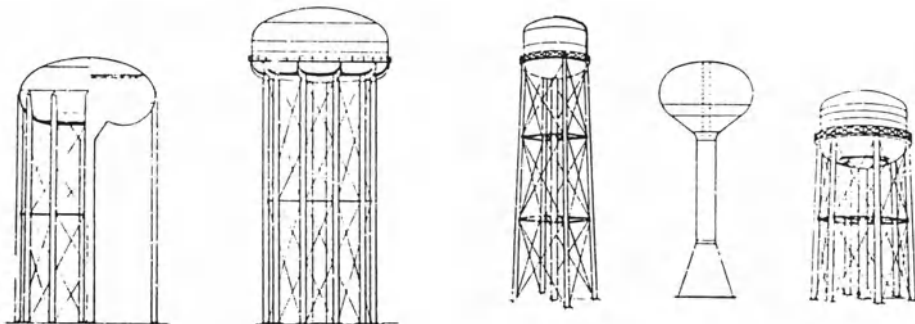


Figure (12-2) Examples of elevated water containers

@Seismicisolation

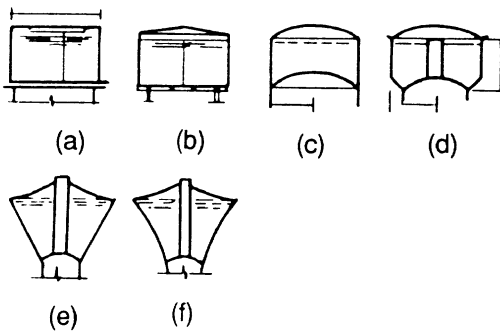


Figure (12-3) Examples of elevated water tanks, (a) circular tank with flat bottom, (b) circular tank with flat bottom and conical roof, (c) circular tank with domed roof and bottom, (d) circular tank with domed roof and bottom together with a conical transition to its bottom, (e) conical tank with doubly curved top and bottom

Elevated tanks, and specially reinforced concrete water tanks, can have various floor systems; often the tank bottom must be stiffened. Moreover, the elevated tanks require some sort of stiffening rib-ring which transfers the vertical forces to the elevated support and / or strengthens the tank against the local effects of point supports. Figures (12-4) show some arrangement of these flat and domed floor rib systems.

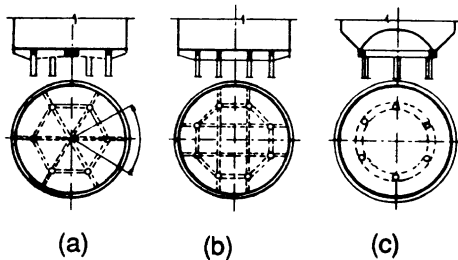


Figure (12-4) Stiffening ribs in the bottom of elevated tanks

For larger elevated tanks, the bottom rib system must be more elaborate. Figure (12-5) shows a network of beams which, together with a ring, form the stiffening system of a large tank.

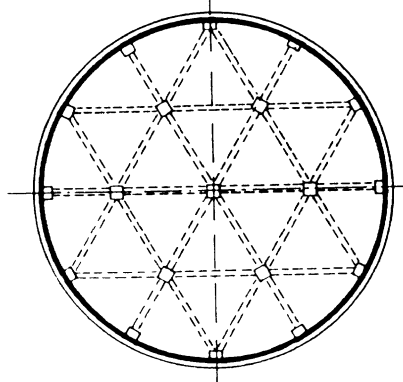


Figure (12-5) Stiffening beam network for floor of an elevated water tank

There are many kinds of towers for elevated water tanks. The towers could be shells or any other continuous structural systems (figures (12-6)). In some cases, the tank and tower can be a single monolithic structure; then the water tank is a natural continuation of its elevated support. Figures (12-6c) and (12-6d) show two models of this arrangement. The elevated supports could also be in the form of an spatial framework and / or a spatial grid system. Figures (12-7) show three examples of such systems.

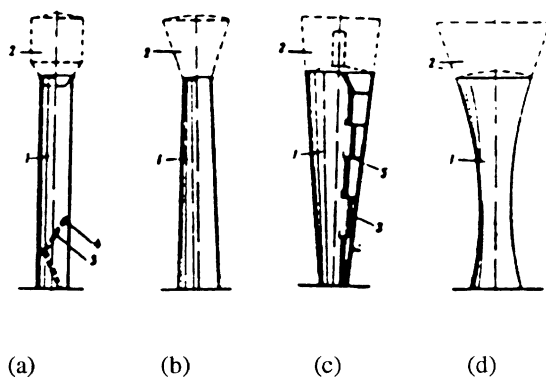


Figure (12-6) Constituting elements of elevated tanks with continuous shell-type supports: (1) the tower, (2) the tank, (3) the stairway, (4) metallic stairway stands, (5) concrete stairway

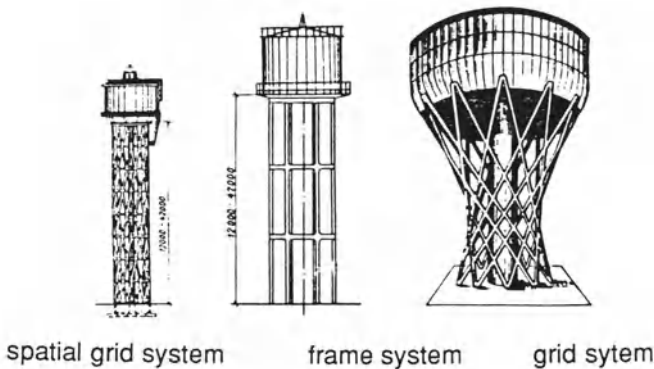


Figure (12-7) Examples of water tanks on elevated spatial grid-work

12.3.2 - Serviceability Design

In addition to requiring structural strength and stability, liquid retaining structures should be designed and constructed so that they do not leak. Therefore, the requirement of "serviceability" would include the structural as well as functional criteria, which in this case, is the efficient containment of the contained fluid.

Water-tightness must be part of the serviceability requirement; construction joints and water-stops must be provided with special connections so that no liquid could leak out from these joints. Figures (12-8) to (12-13) show some of the details which could be used in the construction joints of reinforced concrete water conduits and containers.

For reinforced concrete containers, there must be no cracking in the concrete. Thus, cracking conditions put a limit on serviceability of concrete liquid retaining structures. In order to satisfy this requirement, the stress in the concrete and the strain level in the reinforcing steel must lie below certain limits. These limits are specified by some codes of practice.

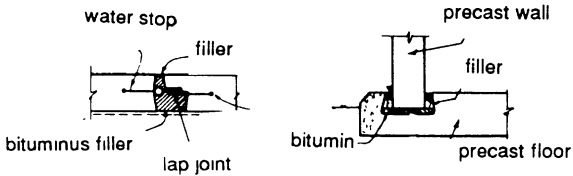


Figure (12-8)

Figure (12-9)

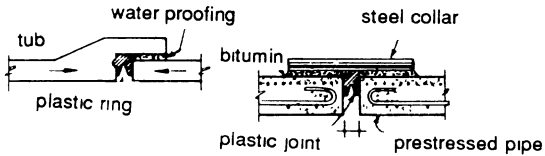


Figure (12-10)

Figure (12-11)

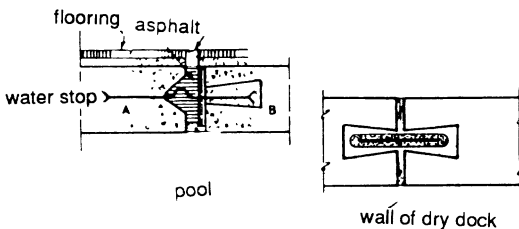


Figure (12-12)

Figure(12-13)

12.4 - Loading Conditions

Liquid retaining structures are subjected to hydrostatic fluid pressure, soil pressure, temperature gradients, dead weight loads, and dynamic loadings arising from wind and earthquake effects. In larger reservoirs, additional hydrodynamic loading due to the motion of contained fluid could be produced; this motion called *slushing*.

The **hydrostatic forces** vary linearly along the height of the tank. The wind and earthquake forces are, however, more complicated to be described by simple analytical formulas. As a

fairly good approximation for wind forces, we may assume the following expression for the intensity of radial load:

$$q(x, \theta) = q(x) \cos \theta \quad (12-1)$$

If we assume that the applied **wind loading** does not vary with height, then the expression (12-1) reduces to

$$q = p_0 \cos \theta \quad (12-2)$$

Here p_0 is the maximum intensity of the wind pressure.

The applied force diagram corresponding to this approximation is shown in figure (12-14).

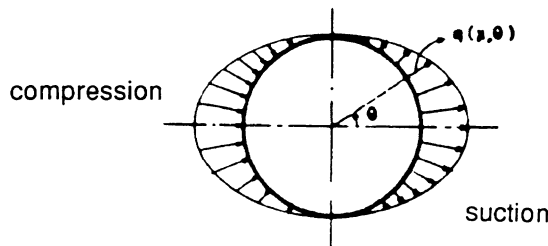


Figure (12-14) Circumferential variation of wind pressure loading on the wall of cylindrical vessel

The earthquake forces are body forces arising from the motion of the wall and the contained fluid. The static fluid pressure on the wall is,

$$p(x) = \gamma x \quad (12-3)$$

If we assume that the earthquake loading is proportional to fluid pressure on the wall at each point, Then

$$q(x, \theta) = c \gamma x \cos \theta \quad (12-4)$$

In addition to these loadings , the buried containers could be subjected to forces applied by the surrounding soil and also the surcharge loads of vehicles and / or superstructures.

12.5 - Axisymmetric Behavior of Circular Containers

In chapter 4, we developed the general bending theory of circular cylindrical shells and a special theory of axisymmetric behavior of thin circular cylinders.

In the present chapter, that special theory will be used for the design and analysis of cylindrical containers subjected to axisymmetric pressure and dead weight loading. We recapitulate the basic features of the axisymmetric theory.

Consider a thin circular cylindrical wall of radius a , as shown in the figure (12-15). This shell wall is assumed to be subjected to internal radial pressure as well as axisymmetric vertical forces. The free body diagram of an element of this shell is shown in figure (12-16).

In order to derive the governing equations of axisymmetric behavior of circular cylindrical shells, we could use the general theory developed in chapter 4. The theory of axisymmetric behavior of cylindrical shell can be derived from general equations by setting all derivatives with respect to q equal to zero. Moreover, in the axisymmetric behavior, the hoop shear force and twisting moments are identically zero everywhere. By taking these features into account, we now derive the particular theory of axisymmetric behavior of circular cylindrical shells.

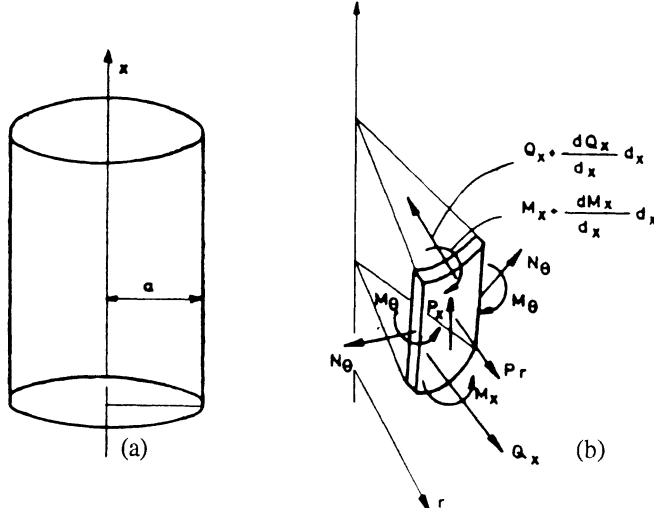


Figure (12-15) (a) A circular cylindrical shell wall,
(b) Free body diagram of an element of the shell

The equilibrium equations for the axisymmetric shell element of figure (12-16) are,

$$\frac{dN_x}{dx} + p_x = 0 \quad (12-5)$$

$$\frac{dQ_x}{dx} + \frac{1}{a} N_\theta - p_r = 0 \quad (12-6)$$

$$\frac{dM_x}{dx} - Q_x = 0 \quad (12-7)$$

The membrane strain displacement relations, as derived in chapter 4 are

$$\epsilon_x = \frac{du}{dx} , \quad \epsilon_\theta = \frac{w}{a} \quad (12-8)$$

For a linear elastic behavior, the membrane constitutive relations are

$$N_x = \frac{Et}{1-v^2} (\epsilon_x + v\epsilon_\theta) \quad (12-9)$$

$$N_\theta = \frac{Et}{1-v^2} (\epsilon_\theta + v\epsilon_x) \quad (12-10)$$

As an approximation, we decouple the axial deformation from the hoop and the bending fields. The constitutive relation for hoop force can be rewritten as

$$N_\theta = \frac{Et}{1-v^2} \left(\frac{w}{a} + v \frac{du}{dx} \right) = \frac{Et}{a} w \quad (12-11)$$

Finally, the axisymmetric moment-curvature relations, as deduced from the general equations of chapter 4 are

$$M_x = K \frac{d^2 w}{dx^2} \quad K = \frac{Et^3}{12(1-v^2)} \quad (12-12)$$

$$M_\theta = v M_x \quad Q_x = K \frac{d^3 w}{dx^3} \quad (12-13)$$

If we combine two equilibrium equations (12-6) and (12-7), we obtain

$$\frac{d^2 M_x}{dx^2} + \frac{1}{a} N_\theta = p_r \quad (12-14)$$

and if we substitute the expressions (12-11) and (12-12) into (12-14), we get

$$\frac{d^2}{dx^2} \left(K \frac{d^2 w}{dx^2} \right) + \frac{Et}{a^2} w = p_r \quad (12-15)$$

For a homogeneous shell with uniform thickness, K is constant. So, we will have

$$K \frac{d^4 w}{dx^4} + \frac{Et}{a^2} w = p_r \quad (12-16)$$

We now define the same parameter, β , as defined in chapter 4 as

$$\beta^4 = \frac{Et}{4a^2 K} = \frac{3(1-\nu^2)}{a^2 t^2} \quad (12-17)$$

The key governing equation of a uniform cylindrical shell in its axisymmetric behavior becomes

$$\frac{d^4 w}{dx^4} + 4\beta^4 w = \frac{p_r}{K} \quad (12-18)$$

This equation has exactly the same form as derived in chapter 4. As we have seen, the general solution to this equation is

$$w = e^{\beta x} (A \cos \beta x + B \sin \beta x) + e^{-\beta x} (C \cos \beta x + D \sin \beta x) + f(x) \quad (12-19)$$

In which, $f(x)$ is a particular solution. From a physical viewpoint, this particular solution is always the solution to the corresponding membrane problem, i.e., the membrane shell subjected to the prescribed distributed loading.

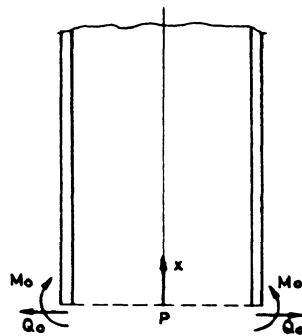


Figure (12-17) Edge forces at one end of a cylindrical liquid container

For a circular cylindrical liquid retaining shell of height H , filled with liquid with density γ , the particular solution (as found in chapter 4) is

$$f(x) = \frac{P_r}{4\beta^4 K} = \frac{P_r a^2}{Et} = \frac{\gamma(H-x)}{4K\beta^4} \quad (12-20)$$

The four integration constants A,B,C,D may be found from four boundary conditions (two at each edge). However, as we have argued before, for actual water tanks the edge conditions at two ends do not influence each other. Therefore, two of these constants (involving positive exponential terms) are set to zero and the two remaining are found from two boundary conditions. With this assumption, the solution to homogeneous equation would reduce to

$$w = e^{-\beta x} (C \cos \beta x + K \sin \beta x) \quad (12-21)$$

Having this solution, we can study the influence of edge forces on the shell. This was done in detail in chapter 4; we can repeat it.

For the shell of figure (12-17), subjected to edge forces, M_o and Q_o , the expressions for constants C and D are,

$$\begin{aligned} C &= + \frac{1}{2\beta^3 K} (Q_o + \beta M_o) \\ D &= - \frac{M_o}{2\beta^2 K} \end{aligned} \quad (12-22)$$

For this case, the general solution (12-19) becomes

$$w = \frac{1}{2\beta^3 K} [\beta M_o \psi(\beta x) + Q_o \theta(\beta x)] + f(x) \quad (12-23)$$

Useful expressions for shell deformation and forces are:

$$\frac{dw}{dx} = \frac{-1}{2\beta^2 K} [2\beta M_o \theta(\beta x) + Q_o \phi(\beta x)] + \frac{d}{dx} f(x) \quad (12-24)$$

$$M = \frac{1}{2\beta} [2\beta M_o \phi(\beta x) + Q_o \xi(\beta x)] + \frac{d}{du} f(x) \quad (12-25)$$

$$Q = -[2\beta M_o \xi(\beta x) - Q_o \psi(\beta x)] + \frac{d^3}{du^2} f(x) \quad (12-26)$$

In writing down these expressions, the functional quantities ξ, ϕ, θ, ψ have been defined for the sake of compactness. These quantities are all functions of the dimensionless variable βx :

$$\phi(\beta x) = e^{-\beta x} (\cos \beta x + \sin \beta x)$$

$$\psi(\beta x) = e^{-\beta x} (\cos \beta x - \sin \beta x) \quad (12-27)$$

$$\theta(\beta x) = e^{-\beta x} \cos \beta x$$

$$\xi(\beta x) = e^{-\beta x} \sin \beta x$$

These functions are evaluated for different values of (βx) and the results are tabulated and given in table (12-1). This table can be useful in variety of analysis and design problems.

Table (12-1) Numerical values of the functions appearing in the displacement and force fields of circular cylindrical shells

βx	ϕ	ψ	θ	ξ	βx	ϕ	ψ	θ	ξ
0	1.0000	1.0000	1.0000	0	3.0	-0.0423	-0.0563	-0.0493	0.0071
0.1	0.9907	0.8100	0.9003	0.0903	3.1	-0.0431	-0.0469	-0.0450	0.0019
0.2	0.9651	0.6398	0.8024	0.1627	3.2	-0.0431	-0.0383	-0.0407	-0.0024
0.3	0.9267	0.4888	0.7077	0.2189	3.3	-0.0422	-0.0306	-0.0364	-0.0058
0.4	0.8784	0.3564	0.6174	0.2610	3.4	-0.0408	-0.0237	-0.0323	-0.0085
0.5	0.8231	0.2415	0.5323	0.2908	3.5	-0.0389	-0.0177	-0.0283	-0.0106
0.6	0.7628	0.1431	0.4530	0.3099	3.6	-0.0366	-0.0124	-0.0245	-0.0121
0.7	0.6997	0.0599	0.3798	0.3199	3.7	-0.0341	-0.0079	-0.0210	-0.0131
0.8	0.6354	-0.0093	0.3131	0.3223	3.8	-0.0314	-0.0040	-0.0177	-0.0137
0.9	0.5712	-0.0657	0.2527	0.3185	3.9	-0.0286	-0.0008	-0.0147	-0.0140
1.0	0.5083	-0.1108	0.1988	0.3096	4.0	-0.0258	0.0019	-0.0120	-0.0139
1.1	0.4476	-0.1457	0.1510	0.2967	4.1	-0.0231	0.0040	-0.0095	-0.0136
1.2	0.3899	-0.1716	0.1091	0.2807	4.2	-0.0204	0.0057	-0.0074	-0.0131
1.3	0.3355	-0.1897	0.0729	0.2626	4.3	-0.0179	0.0070	-0.0054	-0.0125
1.4	0.2849	-0.2011	0.0419	0.2430	4.4	-0.0155	0.0079	-0.0038	-0.0117
1.5	0.2384	-0.2068	0.0158	0.2226	4.5	-0.0132	0.0085	-0.0023	-0.0108
1.6	0.1959	-0.2077	-0.0059	0.2018	4.6	-0.0111	0.0089	-0.0011	-0.0100
1.7	0.1576	-0.2047	-0.0235	0.1812	4.7	-0.0092	0.0090	0.0001	-0.0091
1.8	0.1234	-0.1985	-0.0376	0.1610	4.8	-0.0075	0.0089	0.0007	-0.0052
1.9	0.0932	-0.1899	-0.0484	0.1415	4.9	-0.0059	0.0087	0.0014	-0.0073
2.0	0.0667	-0.1794	-0.0563	0.1230	5.0	-0.0046	0.0084	0.0019	-0.0065
2.1	0.0439	-0.1675	-0.0618	0.1057	5.1	-0.0033	0.0080	0.0023	-0.0057
2.2	0.0244	-0.1548	-0.0652	0.0895	5.2	-0.0023	0.0075	0.0026	-0.0049
2.3	0.0080	-0.1416	-0.0668	0.0748	5.3	-0.0014	0.0069	0.0028	-0.0042
2.4	-0.0056	-0.1282	-0.0669	0.0613	5.4	-0.0006	0.0064	0.0029	-0.0035
2.5	-0.0166	-0.1149	-0.0656	0.0492	5.5	0.0000	0.0058	0.0029	-0.0029
2.6	-0.0254	-0.1019	-0.0636	0.0383	5.6	0.0005	0.0052	0.0029	-0.0023
2.7	-0.0320	-0.0895	-0.0608	0.0287	5.7	0.0010	0.0046	0.0028	-0.0018
2.8	-0.0369	-0.0777	-0.0573	0.0204	5.8	0.0013	0.0041	0.0027	-0.0014
2.9	-0.0403	-0.0666	-0.0534	0.0132	5.9	0.0015	0.0036	0.0026	-0.0010
					6.0	0.0017	0.0031	0.0022	-0.0007

12.6 - Force Method of Container Shells Analysis

The fundamentals of the force method for shells analysis were outlined in earlier chapters; the force method of analysis was presented in detail in chapter 4. In this section, the same method will be used for the analysis of liquid retaining shell structures.

The basic steps in the formulation of shell equations according to force method are: solve the membrane problem; obtain the flexibility influence coefficients; write the compatibility relations; solve these equations.

12.6.1 - Influence Coefficients

Equations (12-24) to (12-26) show that the expressions for edge displacement and edge rotation, due to edge loads Q_0 and M_0 are

$$w(x=0) = \frac{1}{2\beta^3 K} (\beta M_0 + Q_0) \quad (12-28)$$

$$\frac{d}{dx} w(x=0) = -\frac{1}{2\beta^2 K} (2\beta M_0 + Q_0)$$

To find the flexibility influence coefficients, we should consider unit edge forces and to evaluate the edge displacement and edge rotation due to these unit effects. Figure (12-18) shows the meaning and symbols of influence coefficients as well as the edge deformations due to applied distributed forces, i.e., the membrane deformations.

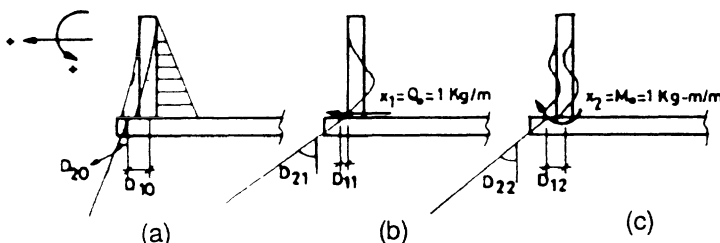


Figure (12-18) Edge deformation of a cylindrical shell, (a) membrane deformation, (b) edge deformations due to unit edge shear, (c) edge deformations due to unit edge moment

The expressions for influence coefficients, as derived from relations (12-28), are

$$D_{11} = \frac{1}{2\beta^3 K}$$

$$D_{12} = -D_{21} = \frac{1}{2\beta^2 K}$$

$$D_{22} = \frac{-1}{\beta K}$$

For a liquid filled container, with radius a and height H , the edge deformations due to liquid pressure are easily derived from the expression (12-20); they are

$$D_{10} = w(x=0) = +\frac{\gamma a^2 H}{Et} , \quad D_{20} = \frac{d}{dx} w(x=0) = \frac{-\gamma a^2}{Et} \quad (12-30)$$

12.6.2 - Analysis of "Wall - Base" Interaction

(1) Hinged Wall to Base Connection

In this case, $Q_0 \neq 0$, $M_0 = 0$. Then, the only required compatibility relation is

$$D_{11}x_1 + D_{10} = 0$$

from which, we obtain

$$x_1 = -\frac{D_{10}}{D_{11}} = -\frac{\frac{\gamma a^2 H}{Et}}{\frac{1}{2\beta^3 K}} = -\frac{\gamma a^2 H}{\frac{Et}{2\beta^3 K}}$$

or

$$x_1 = Q_0 = -\frac{(3)^{3/4}}{6(1-v^2)^{1/4}} \gamma a^2 \left(\frac{t}{a}\right)^{1/2} \left(\frac{H}{a}\right) \quad (12-31)$$

The bending field is

$$w = \frac{1}{2\beta^3 K} Q_0 \theta(\beta x)$$

$$N_\theta = \frac{Et}{a} \cdot \frac{1}{2\beta^3 K} Q_0 \theta(\beta x) \quad (12-32)$$

$$M_x = \frac{1}{\beta} Q_0 \theta'(\beta x)$$

@Seismicisolation

The assumed hinged condition can be realized in concrete liquid retaining shells. Figure(12-19) shows a design-construction detail of wall-floor connection in which this assumption is fulfilled.

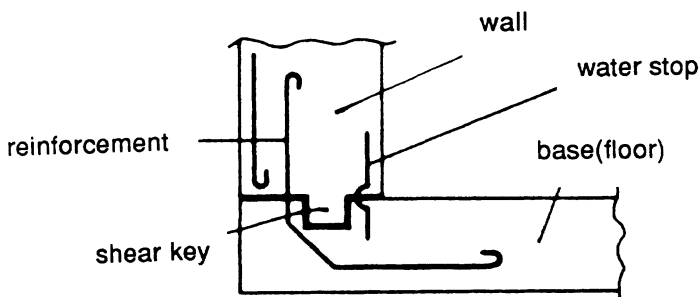


Figure (12-19) A hinged wall-floor connection in a reinforced concrete circular container

To determine the complete force field, the membrane forces must be superposed on the solution given in (12-32). The schematic diagram of complete field is shown in figure (12-20).

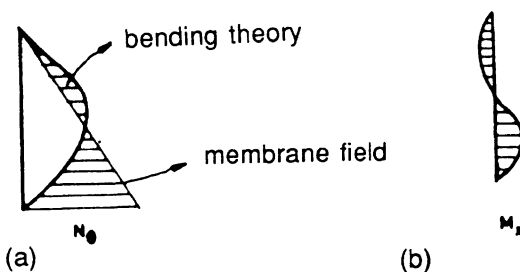


Figure (12-20) Schematic diagram of internal forces in a cylindrical wall with hinge base, (a) hoop force, (b) bending moment

(2)- Wall Fixed to Its Base

This case is realized when the stiffness of a monolithic container base is very high compared to the wall stiffness. In such a case, the radial displacement and wall rotation at the lower end would be equal to zero. Thus the required compatibility relations are

$$D_{11}X_1 + D_{12}X_2 + D_{10} = 0$$

(12-33)

$$D_{21}X_1 + D_{22}X_2 + D_{20} = 0$$

By solving these two simultaneous equations for unknown edge forces X_1 and X_2 , we obtain the following general formula:

$$\frac{X_1}{\gamma a^2} = \frac{-\left(\frac{t}{a}\right)^{1/2}}{\left[3(1-v^2)\right]^{1/4}} \quad \frac{H}{a} - \frac{1}{2\left[3(1-v^2)\right]^{1/4}} \left(\frac{t}{a}\right)^{1/2}$$
(12-34)

$$\frac{X_2}{\gamma a^3} = \frac{\left(\frac{t}{a}\right)}{2\left[3(1-v^2)\right]^{1/2}} \quad \left(\frac{H}{a}\right) - \frac{1}{\left[3(1-v^2)\right]^{1/4}} \left(\frac{t}{a}\right)^{1/2}$$

The bending field resulting from these edge effects can now be determined by substituting X_1 and X_2 into the expressions (12-23) to (12-26). The hoop force N_θ can be obtained from relation (12-11). To find the complete force field resulting from these edge forces we must add the membrane field to this bending field solution. Graphs of variation of internal forces in the shell are shown in figure (9-21).

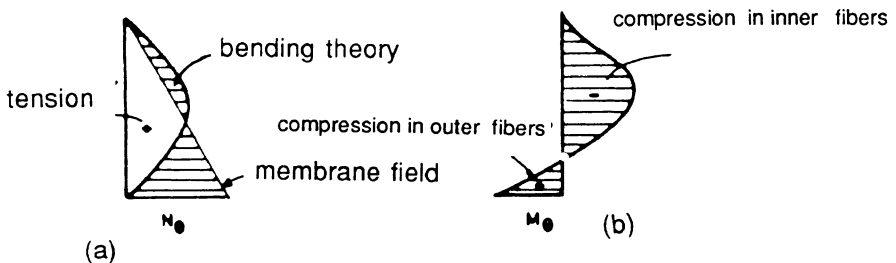


Figure (12-21) Variation of internal forces in cylindrical wall fixed to its base

In order to cast these expressions into more useful forms, we define a dimensionless parameter, Z, as follows:

$$z = \frac{H}{\sqrt{ta}} \quad (12-35)$$

with such definition, the expressions (12-34) can be rewritten as

$$\frac{x_1}{a} = - \frac{\left(\frac{t}{a}\right)^{1/2}}{[3(1-v^2)]^{1/4}} \left\{ \frac{z\sqrt{ta}}{a} - \frac{1}{2[3(1-v^2)]^{1/4}} \left(\frac{t}{a}\right)^{1/2} \right\}$$

$$\frac{x_2}{a} = \frac{\left(\frac{t}{a}\right)}{2[3(1-v^2)]^{1/2}} \left\{ \frac{z\sqrt{ta}}{a} - \frac{1}{[3(1-v^2)]^{1/4}} \left(\frac{t}{a}\right)^{1/2} \right\}$$

or

$$\begin{aligned} \frac{x_1}{ya^2} &= - \frac{\left(\frac{t}{a}\right)}{[3(1-v^2)]^{1/2}} \left\{ z - \frac{1}{2[3(1-v^2)]^{1/4}} \right\} \\ \frac{x_2}{ya^3} &= \frac{\left(\frac{t}{a}\right)^{3/2}}{2[3(1-v^2)]^{1/2}} \left\{ z - \frac{1}{[3(1-v^2)]^{1/4}} \right\} \end{aligned} \quad (12-36)$$

Now, we define the dimensionless base shear force and base shear bending moment as

$$v = \frac{x_1}{yH\sqrt{ta}} \quad , \quad M = \frac{x_2}{yHta} \quad (12-37)$$

with this definition, the expressions (12-36) assume the following forms:

$$v = \frac{-1}{[3(1-v^2)]^{1/4}} \left\{ 1 - \frac{1}{2[3(1-v^2)]^{1/4}} \cdot \frac{1}{z} \right\} \quad (12-38)$$

$$M = \frac{1}{2[3(1-v^2)]^{1/2}} \left\{ 1 - \frac{1}{[3(1-v^2)]^{1/4}} \cdot \frac{1}{z} \right\}$$

Figures (12-22) show variations of base shear and base bending moment in terms of the parameter Z.

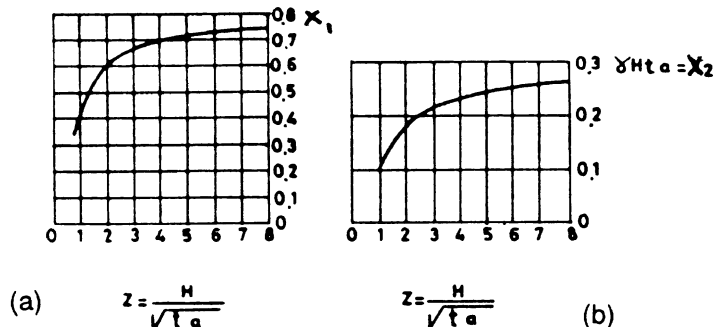


Figure (12-22) Variation of: (a) base shear and, (b) base moments with dimensionless height parameter, z , in a cylindrical tank with fixed base

(3) Semi-Rigid Wall to Base Connection

This case is realized whenever the *wall-base* connection is monolithic and the wall stiffness is comparable to that of the base. In this case, the rotation of the wall must be equal to that of its base. The wall is subjected to linearly varying hydrostatic pressure while the base is resting on its *tensionless foundation* and is acted upon by the uniform pressure equal to $q = \gamma H$. Figure (12-23) shows a situation in which part of the base has a tendency to be lifted from its foundation in order to fulfill the compatibility requirement with the wall.

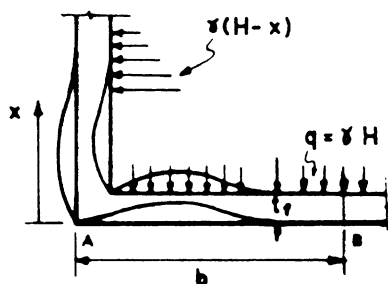


Figure (12-23) Behavior of a semi-rigid wall-base system

To analyze this case, we use an approximate method employing the *moment-area theorem* well-known in structural analysis. Viewing figure (12-23), we note the width, b , of lifted "ring" region is unknown and is to be determined together with unknown redundant base forces.

Using moment-area theorem for a radial strip of the circular base, we may write expressions for edge rotation and lateral displacement of the base plate as follows:

$$\phi_{AB} = \frac{1}{3K_f} M_O b - \frac{qb^3}{24K_f} \quad (12-39a)$$

$$w_{AB} = \frac{1}{6K_f} M_O b^2 - \frac{qb^4}{24K_f} \quad (12-39b)$$

Due to high axial stiffness of the wall, the lateral displacement of the base plate at the edge can be assumed to be zero. Hence, by setting the second expression equal to zero, we find

$$b = 2\sqrt{\frac{M_O}{q}}$$

Substituting this value into (12-39b), we find

$$\phi_{AB} = \frac{1}{3K_f} \sqrt{\frac{M_O^3}{q}} = D_{22} x_2 \quad (12-40)$$

Having determined this expression, we can now use the classical plate theory to write down the expressions for the influence coefficients of circular plate at its edge. These coefficients are

$$D_{11}^f = \frac{-a(1-\nu)}{Et}$$

$$D_{12}^f = 0 \quad (12-41)$$

$$D_{22}^f x_2 = \frac{-1}{3K_f} \sqrt{\frac{x_2^3}{q}} \quad D_{22}^b = \frac{-1}{3K_f} \sqrt{\frac{x_2}{q}}$$

On the other hand, we had previously determined the influence coefficients for the cylindrical wall (expressions (12-29)). Therefore, we can, now, combine two sets of influence coefficients to determine the **flexibility influence coefficients** for the **wall-base system**. These expressions are

$$D_{11} = D_{11}^W + D_{11}^f = - \left[\frac{1}{2B^3 K} + \frac{a(1-\nu)}{Et} \right]$$

$$D_{12} = -D_{21} = D_{12}^W + D_{12}^f = + \frac{1}{2B^2 K} \quad (12-42)$$

$$D_{22} = D_{22}^W + D_{22}^f = \frac{-1}{4K} - \frac{1}{3K_f} \sqrt{\frac{x_2}{q}}$$

We can write down the compatibility relations for the case of wall-base system:

$$D_{11}x_1 + D_{12}x_2 + D_{10} = 0$$

$$D_{12}x_1 + D_{22}x_2 + D_{20} = 0$$

From these we obtain

$$\left[\frac{1}{2\beta^2 K} - \frac{a(1-v)}{Et} \right] x_1 + \frac{1}{2\beta^2 K} x_2 = \frac{-\gamma a^2 H}{Et} \quad (12-43)$$

$$\frac{1}{2\beta^2 K} x_1 - \left(\frac{1}{K} + \frac{1}{3K_f} \sqrt{\frac{x_2}{q}} \right) x_2 = \frac{\gamma a^2}{Et}$$

12.6.3 - Analysis of Wall to Roof Connection

In this analysis, the parameters related to roof slab and cylindrical wall are identified by subscripts s and w, respectively. The x-coordinate is assumed to have the top of the wall as its origin, figure (12-24). We also note that the in-plane stiffness of flat plate roof slab is so high that the in-plane radial deformation of the roof slab may be neglected. So, at x = 0, we may assume w = 0.

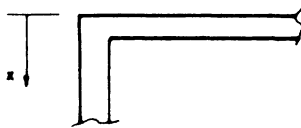


Figure (12-24)

For the cylindrical wall, the expressions (12-28) yield:

$$\text{Due to } M_O: \quad w_1 = \frac{M_O}{2\beta^2 K} \quad \frac{dw_1}{dx} = -\frac{M_O}{\beta K} \quad (12-44a)$$

$$\text{Due to } Q_O: \quad w_2 = \frac{Q_O}{2\beta^2 K} \quad \frac{dw_2}{dx} = -\frac{Q_O}{2\beta^2 K} \quad (12-44b)$$

The radial displacement must be zero at the top, i.e.,

$$w_1|_{x=0} + w_2|_{x=0} = w|_{x=H} = 0$$

Using relations (12-44a) and (12-44b), relation $Q_O = -\beta M_O$, adding up the resulting expressions, we arrive at relations applicable to the case of the wall monolithic with roof slab. In this fashion, the condition $w = 0$ at $x = 0$ will be satisfied. Then, the wall-slab rotation at the top would be

$$\frac{dw}{dx} = -\frac{M_O}{\beta K} + \frac{M_O}{2\beta K} = -\frac{M_O}{2\beta K} \quad (12-45)$$

In this case, the expressions for internal force field in the wall will be

$$\begin{aligned} M_x &= M_O e^{-\beta x} \cos \beta x \\ Q_x &= -M_O \beta e^{-\beta x} (\sin \beta x + \cos \beta x) \\ N_\theta &= 2M_O \beta^2 a e^{-\beta x} \sin \beta x \end{aligned} \quad (12-46)$$

and the rotation of the wall at the top is

$$\left. \frac{dw}{dx} \right|_{x=0} = \frac{-\gamma a^2}{D(1-\nu^2)} - \frac{1}{2\beta K} x_2 \quad (12-47)$$

Now, we consider various case of loading conditions of wall-roof-slab structural system. A general case of loaded roof slab is shown in figure (12-25).

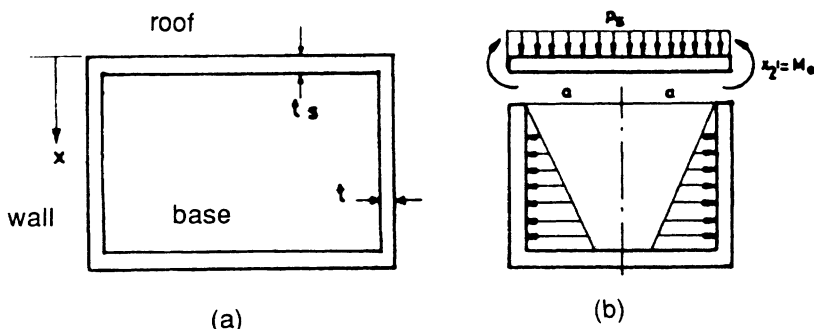


Figure (12-25) A cylindrical container with monolithic wall to base and wall-to-roof connection

To perform an analysis of the **wall-roof-slab system**, we need the expression for lateral deformation of a circular elastic plate. The deformation of plates can be determined through the use of plate theory. Treatment of this theory is not given in the present text but is dealt with in books on the analysis of plates. Only the result of such analyses will be used in this section. To make this presentation more useful, the results of circular plates analyses are compiled in table (12-2).

Table (12-2) Internal force and deformation field in elastic circular plates

$w(r)$: lateral deflection

M_r : radial bending moment

M_t : hoop bending moment

M_a : bending moment in the center

w	$\frac{qr^4}{64K} + C_1 \frac{r^2}{4} + C_2 \log \frac{r}{a} + C_3$	$\frac{M_a}{2K(1+v)}(a^2 - r^2)$	$\frac{q}{64K}(a^2 - r^2)^2$	$\frac{q}{64K}(a^2 - r^2)(\frac{5+v}{1+v}a^2 - r^2)$
$\frac{\partial w}{\partial r}$	$\frac{qr^3}{16K} + C_1 \frac{r}{2} + C_2 \frac{1}{r}$	$-\frac{M_a r}{K(1+v)}$	$-\frac{qr}{16K}(a^2 - r^2)$	$-\frac{q}{16K}(\frac{3+v}{1+v}a^2 - r^2)$
$\frac{d w}{dr}$	$\frac{3ar^2}{16K} + \frac{C_1}{2} - C_2 \frac{1}{r^2}$	$-\frac{M_a}{K(1+v)}$	$-\frac{q}{16K}(a^2 - 3r^2)$	$-\frac{q}{16K}(\frac{3+v}{1+v}a^2 - 3r^2)$
C_1		$-\frac{2M_a}{K(1+v)}$	$-\frac{qa^2}{8K}$	$-\frac{qa^2}{8K}\frac{3+v}{1+v}$
C_2		0	0	0
C_3		$\frac{M_a a^2}{2K(1+v)}$	$\frac{qa^4}{64K}$	$\frac{qa^2}{64K}\frac{5+v}{1+v}$
M_r	$-K(\frac{d^2w}{dr^2} + \frac{v\partial w}{\partial r})$	$+M_a$	$\frac{q}{16}[a^2(1+v) - r^2(3+v)]$	$\frac{q}{16}(3+v)(a^2 - r^2)$
M_t	$-K(\frac{1}{r}\frac{\partial w}{\partial r} + v\frac{d^2w}{dr^2})$	$+M_a$	$\frac{q}{16}[a^2(1+v) - r^2(1+3v)]$	$\frac{q}{16}[a^2(3+v) - r^2(1+3v)]$
M_a		$+M_a$	$-\frac{a^2}{8}$	0
M_a		$+M_a$	$\frac{qa}{16}(1+v)$	$\frac{qa}{16}(3+v)$

Using this table, and referring to figure (12-25), we can write

$$\frac{dw}{dr} \Big|_{r=a} = \frac{-p_s a^3}{8k_s(1+\nu)} - \frac{a}{k_s(1+\nu)} x_2$$

in which $k_s = \frac{Et^3}{12(1-\nu^2)}$ is the bending stiffness of circular plate.

Now, since the wall-roof connection is assumed monolithic, the compatibility of rotations must be fulfilled. Therefore we have,

$$\frac{-\gamma a^2}{D(1-\nu^2)} - \frac{1}{2\beta K} \cdot x_2 = \frac{p_s a^3}{8k_s(1+\nu)} + \frac{a}{k_s(1+\nu)} x_2$$

from which we obtain

$$x_2 = -\frac{\frac{\gamma a^2}{D(1-\nu^2)} + \frac{p_s a^3}{8k_s(1+\nu)}}{\frac{1}{2\beta K} + \frac{a}{k_s(1+\nu)}} \quad (12-48)$$

Having obtained the expression for edge moment, x_2 , we can write the expressions for displacement and force field in the wall and the roof slab; we consider two special cases:

(1) Full container with no load on the roof

In this case, $p_s = 0$, so we have

$$w = \frac{\gamma a^3}{D(1-\nu^2)} \frac{x}{a} - \frac{k_s(1+\nu)}{2K\beta a + k_s(1+\nu)} \frac{1}{\beta a} e^{-\beta x} \sin x \quad (12-49)$$

$$M_x = \frac{2\gamma K k_s \beta a^2}{D(1-\nu) 2K\beta a + k_s(1+\nu)} e^{-\beta x} \cos \beta x$$

(2) Empty container with loaded roof

In this case, $q = 0$, so we have

$$w = \frac{p_s a^3}{8\beta [2K\beta a + k_s(1+\nu)]} e^{-\beta x} \sin \beta x \quad (12-50)$$

$$M_x = -\frac{p_s a^3}{4} \frac{K\beta}{2K\beta a + k_s(1+\nu)} e^{-\beta x} \cos \beta x$$

(3) General case- Full container with loaded roof

The force and deformation fields can be determined by superposition of the expressions in cases (1) and (2).

The foregoing analytical results can be tabulated or plotted as design guides to the proportioning of cylindrical containers. In addition to these analytical results, numerical calculations can also be performed by means of, for example, the Finite Element method. To provide some examples of design tables, tables (12-3) and (12-4) are presented. In these tables, the coefficients for the moments and the hoop forces in cylindrical walls, with various loading and boundary conditions, are given.

Table (12-3a) Moments and hoop forces in cylindrical shell walls with various loading and boundary conditions

Moments in cylindrical wall, M_x											
Triangular load											
Fixed base, free top											
$M_x = - \text{coef} \times uH^2 \text{ ft lb per ft}$											
Negative sign indicates tension in the outside											
Coefficients at point											
H^2	Dt	0.1H	0.2H	0.3H	0.4H	0.5H	0.6H	0.7H	0.8H	0.9H	1.0H
0.4	-0.005	+0.014	+0.021	+0.007	-0.042	-0.150	-0.302	-0.529	-0.816	-1.1205	
0.8	+0.011	+0.037	+0.063	+0.080	+0.070	+0.023	-0.068	-0.224	-0.465	-0.795	
1.2	+0.012	+0.042	+0.077	+0.103	+0.112	+0.090	+0.022	-0.108	-0.311	-0.602	
1.6	+0.011	+0.041	+0.075	+0.107	+0.121	+0.111	+0.058	-0.051	-0.232	-0.505	
2.0	+0.010	+0.035	+0.068	+0.099	+0.120	+0.115	+0.075	-0.021	-0.185	-0.436	
3.0	+0.006	+0.024	+0.047	+0.071	+0.090	+0.097	+0.077	+0.012	-0.119	-0.333	
4.0	+0.003	+0.015	+0.028	+0.047	+0.066	+0.077	+0.069	+0.023	-0.080	-0.268	
5.0	+0.002	+0.008	+0.016	+0.029	+0.046	+0.059	+0.059	+0.028	-0.058	-0.222	
6.0	+0.001	+0.003	+0.008	+0.019	+0.032	+0.046	+0.051	+0.029	-0.041	-0.187	
8.0	0.0000	+0.001	+0.002	+0.008	+0.016	+0.028	+0.038	+0.029	-0.022	-0.146	
10.0	0.0000	0.0000	+0.001	+0.004	+0.007	+0.019	+0.029	+0.028	-0.012	-0.122	
12.0	0.0000	-0.0001	+0.001	+0.002	+0.003	+0.013	+0.023	+0.026	-0.005	-0.104	
14.0	0.0000	-0.0000	0.0000	-0.0000	+0.001	+0.008	+0.019	+0.023	-0.001	-0.090	
16.0	0.0000	-0.0000	-0.001	-0.002	-0.001	+0.004	+0.013	+0.019	-0.001	-0.079	

Tension in circular rings, N_r											
Triangular load											
Fixed base, free top											
$N_r = - \text{coef} \times uH^2 \text{ lb per ft}$											
Positive sign indicates tension											
Coefficients at point											
H^2	Dt	0.0H	0.1H	0.2H	0.3H	0.4H	0.5H	0.6H	0.7H	0.8H	0.9H
0.4	-0.149	-0.134	-0.120	-0.101	+0.082	+0.066	+0.049	+0.029	+0.014	+0.004	
0.8	-0.263	-0.239	-0.215	-0.190	+0.160	+0.130	+0.096	+0.063	+0.034	+0.010	
1.2	-0.283	-0.271	-0.254	-0.234	+0.209	+0.180	+0.142	+0.099	+0.054	+0.016	
1.6	-0.265	-0.268	-0.268	-0.266	+0.250	+0.226	+0.185	+0.134	+0.075	+0.023	
2.0	-0.234	-0.251	-0.273	-0.285	+0.285	+0.274	+0.232	+0.172	+0.104	+0.031	
3.0	-0.134	-0.203	-0.267	-0.322	+0.357	+0.362	+0.330	+0.262	-0.157	+0.052	
4.0	-0.067	-0.164	-0.256	-0.339	+0.403	+0.429	+0.409	+0.334	-0.210	-0.073	
5.0	-0.025	-0.137	-0.245	-0.346	+0.428	+0.477	+0.469	+0.398	-0.259	+0.092	
6.0	-0.018	-0.119	-0.234	-0.344	+0.441	+0.504	+0.514	+0.447	+0.301	-0.112	
8.0	-0.011	-0.104	-0.218	-0.335	+0.443	+0.534	+0.575	+0.530	+0.381	-0.151	
10.0	-0.011	-0.098	-0.208	-0.323	+0.437	+0.542	+0.608	+0.589	-0.440	-0.179	
12.0	-0.005	-0.097	-0.202	-0.312	+0.429	+0.543	+0.628	+0.633	-0.494	-0.211	
14.0	-0.001	-0.098	-0.200	-0.306	+0.420	+0.539	+0.639	+0.666	-0.541	-0.241	
16.0	0.000	-0.099	-0.199	-0.300	+0.414	+0.531	+0.641	+0.677	-0.552	-0.265	

Table (12-3b) Moments and hoop forces in cylindrical shell walls with various loading and boundary conditions

Moments in cylindrical wall, M_x											
Trapezoidal load											
Hinged base, free top											
$M_x = - \text{coef} \times (wH^3 + pH^2) \text{ ft-lb per ft}$											
Negative sign indicates tension in the outside											
DI		Coefficients at point									
II^1		Bottom									
DI		0.1H	0.2H	0.3H	0.4H	0.5H	0.6H	0.7H	0.8H	0.9H	1.0H
0.4		+0.0020	+0.0072	+0.0151	+0.0230	+0.0301	+0.0348	+0.0357	+0.0312	+0.0197	0
0.8		+0.0019	+0.0064	+0.0133	+0.0207	+0.0271	+0.0319	+0.0329	+0.0292	+0.0187	0
1.2		+0.0016	+0.0058	+0.0111	+0.0177	+0.0237	+0.0280	+0.0296	+0.0263	+0.0171	0
1.6		+0.0012	+0.0044	+0.0091	+0.0145	+0.0195	+0.0236	+0.0255	+0.0232	+0.0155	0
2.0		+0.0009	+0.0033	+0.0073	+0.0114	+0.0158	+0.0199	+0.0219	+0.0205	+0.0145	0
3.0		+0.0004	+0.0018	+0.0040	+0.0063	+0.0092	+0.0127	+0.0152	+0.0153	+0.0111	0
4.0		+0.0001	+0.0007	+0.0016	+0.0033	+0.0057	+0.0083	+0.0109	+0.0118	+0.0092	0
5.0		0.0000	+0.0001	+0.0006	+0.0016	+0.0034	+0.0057	+0.0080	+0.0094	+0.0078	0
6.0		0.0000	0.0000	+0.0002	+0.0008	+0.0019	+0.0039	+0.0062	+0.0078	+0.0068	0
8.0		0.0000	0.0000	-0.0002	-0.0000	+0.0007	+0.0020	+0.0038	+0.0057	+0.0054	0
10.0		0.0000	0.0000	-0.0002	-0.0001	+0.0002	+0.0011	+0.0025	+0.0043	+0.0045	0
12.0		0.0000	0.0000	-0.0001	-0.0002	-0.0000	+0.0005	+0.0017	+0.0032	+0.0039	0
14.0		0.0000	0.0000	-0.0001	-0.0001	-0.0001	0.0000	+0.0012	+0.0026	+0.0033	0
16.0		0.0000	0.0000	-0.0000	-0.0001	-0.0002	-0.0004	+0.0008	+0.0022	+0.0029	0

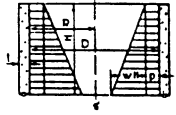
Tension in circular rings, N_t											
Triangular load											
Hinged base, free top											
$\Delta_t = \text{coef} \times wH^2 \text{ lb per ft}$											
Positive sign indicates tension											
DI		Top									
II^2		Coefficients at point									
DI		0.0H	0.1H	0.2H	0.3H	0.4H	0.5H	0.6H	0.7H	0.8H	0.9H
0.4		+0.474	-0.440	-0.395	-0.352	+0.308	+0.264	+0.215	+0.165	+0.111	+0.057
0.8		+0.423	-0.402	-0.381	-0.358	+0.330	+0.297	+0.249	+0.202	+0.145	+0.076
1.2		+0.350	-0.355	-0.361	-0.362	+0.358	+0.343	+0.309	+0.256	+0.186	+0.098
1.6		+0.271	-0.303	-0.341	-0.369	+0.385	+0.385	+0.362	+0.314	+0.233	+0.124
2.0		+0.205	-0.260	-0.321	-0.373	+0.411	+0.434	+0.419	+0.369	+0.280	+0.151
3.0		+0.074	-0.179	-0.281	-0.375	+0.449	+0.506	+0.519	+0.479	+0.375	+0.210
4.0		+0.017	-0.137	-0.253	-0.367	+0.469	+0.545	+0.579	+0.553	+0.447	+0.256
5.0		-0.008	-0.114	-0.235	-0.356	+0.469	+0.562	+0.617	+0.666	+0.563	+0.294
6.0		-0.011	-0.103	-0.223	-0.343	+0.463	+0.566	+0.639	+0.643	+0.547	+0.327
8.0		-0.015	-0.096	-0.208	-0.324	+0.443	+0.564	+0.661	+0.697	+0.621	+0.386
10.0		-0.008	-0.095	-0.200	-0.311	+0.428	+0.552	+0.666	+0.730	+0.678	+0.433
12.0		-0.002	-0.097	-0.197	-0.302	+0.417	+0.541	+0.664	+0.720	+0.677	+0.477
14.0		0.000	-0.098	-0.197	-0.299	+0.408	+0.531	+0.659	+0.761	+0.752	+0.513
16.0		+0.002	-0.100	-0.198	-0.299	+0.403	+0.521	+0.650	+0.764	+0.776	+0.546

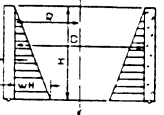
Table (12-4a) Moments and hoop forces in cylindrical shell walls with various loading and boundary conditions

Moments in cylindrical wall, M_x									
Triangular load									
Fixed base, free top									
$M_x = - \text{coeff} \times wH^2 / 12 \text{ ft lb per ft}$									
Negative sign indicates tension in the outside									
Coefficients at point									
Bottom									
H^2 / D^2	$0.1H$	$0.2H$	$0.3H$	$0.4H$	$0.5H$	$0.6H$	$0.7H$	$0.8H$	$0.9H$
0.4	+ .0005	+ .0014	- .0021	+ .0007	- .0042	- .0150	- .0302	.0529	- .0816
0.8	+ .0011	+ .0037	- .0063	+ .0080	+ .0070	+ .0023	- .0058	.0224	- .0465
1.2	+ .0012	+ .0042	- .0077	+ .0103	+ .0112	+ .0090	- .0022	.0108	- .0311
1.6	+ .0011	+ .0041	- .0075	+ .0107	+ .0121	+ .0111	- .0058	.0051	- .0232
2.0	+ .0010	+ .0035	- .0068	+ .0099	+ .0120	+ .0115	+ .0075	- .021	- .0185
3.0	+ .0006	+ .0024	- .0047	+ .0071	+ .0090	+ .0097	+ .0077	.0012	- .0119
4.0	+ .0003	+ .0015	- .0028	+ .0047	+ .0066	+ .0077	+ .0069	.0023	- .0080
5.0	+ .0002	+ .0008	- .0016	+ .0029	+ .0046	+ .0059	+ .0059	.0028	- .0058
6.0	+ .0001	+ .0003	- .0008	+ .0019	+ .0032	+ .0046	+ .0051	.0029	- .0041
8.0	0.0000	+ .0001	- .0002	+ .0008	+ .0016	+ .0028	+ .0038	.0029	- .0022
10.0	0.0000	- .0000	- .0001	+ .0004	+ .0007	+ .0019	+ .0029	.0028	- .0012
12.0	0.0000	- .0001	- .0001	+ .0002	+ .0003	+ .0013	+ .0023	.0026	- .0005
14.0	0.0000	- .0000	- .0000	- .0000	+ .0001	+ .0008	+ .0019	.0023	- .0001
16.0	0.0000	- .0000	- .0001	- .0002	- .0001	+ .0004	+ .0013	.0019	+ .0001

Tension in circular rings, N_x									
Triangular load									
Fixed base, free top									
$N_x = \text{coeff} \times wH^2 / 12 \text{ lb per ft}$									
Positive sign indicates tension									
Coefficients at point									
Top									
H^2 / D^2	$0.1H$	$0.2H$	$0.3H$	$0.4H$	$0.5H$	$0.6H$	$0.7H$	$0.8H$	$0.9H$
0.4	- .0149	- .0134	- .0120	- .0101	- .0082	- .0066	- .0049	- .0029	- .0014
0.8	- .0263	- .0239	- .0215	- .0190	- .0160	- .0130	- .0096	- .0063	- .0034
1.2	- .0283	- .0271	- .0254	- .0234	- .0209	- .0180	- .0142	- .0099	- .0054
1.6	- .0265	- .0268	- .0268	- .0266	- .0250	- .0226	- .0185	- .0134	- .0075
2.0	- .0234	- .0251	- .0273	- .0285	- .0285	- .0274	- .0232	- .0172	- .0104
3.0	- .0134	- .0203	- .0267	- .0322	- .0357	- .0362	- .0330	- .0262	- .0157
4.0	- .0067	- .0164	- .0256	- .0339	- .0403	- .0429	- .0409	- .0334	- .0210
5.0	- .0025	- .0137	- .0245	- .0346	- .0428	- .0477	- .0469	- .0398	- .0259
6.0	- .0018	- .0119	- .0234	- .0344	- .0441	- .0504	- .0514	- .0447	- .0301
8.0	- .0011	- .0104	- .0218	- .0335	- .0443	- .0534	- .0575	- .0530	- .0381
10.0	- .0011	- .0098	- .0208	- .0323	- .0437	- .0542	- .0608	- .0589	- .0440
12.0	- .0005	- .0097	- .0202	- .0312	- .0429	- .0543	- .0628	- .0633	- .0494
14.0	- .0002	- .0098	- .0200	- .0306	- .0420	- .0539	- .0639	- .0666	- .0541
16.0	0.0000	- .0099	- .0199	- .0304	- .0412	- .0531	- .0641	- .0687	- .0582

Table (12-4b) Moments and hoop forces in cylindrical shell walls with various loading and boundary conditions

Moments in cylindrical wall, M_z										
Trapezoidal load										
Hinged base, free top										
$M_z = - \text{coef} \times (uH^4 + pH^4) \text{ ft lb. per ft.}$										
Negative sign indicates tension in the outside										
										
H^4		Coefficients at point								
Dt		0.1H	0.2H	0.3H	0.4H	0.5H	0.6H	0.7H	0.8H	0.9H
0.4	+0.0020	+0.0072	+0.151	+0.230	+0.301	+0.348	+0.357	+0.312	+0.197	0
0.8	+0.0019	+0.0064	+0.133	+0.207	+0.271	+0.319	+0.329	+0.292	+0.187	0
1.2	+0.0016	+0.0058	+0.111	+0.177	+0.237	+0.280	+0.296	+0.263	+0.171	0
1.6	+0.0012	+0.0044	+0.091	+0.145	+0.195	+0.236	+0.255	+0.232	+0.155	0
2.0	+0.0009	+0.0033	+0.073	+0.114	+0.158	+0.199	+0.219	+0.205	+0.145	0
3.0	+0.0004	+0.018	+0.040	+0.063	+0.092	+0.127	+0.152	+0.153	+0.111	0
4.0	+0.0001	+0.007	+0.016	+0.033	+0.057	+0.083	+0.109	+0.118	+0.092	0
5.0	.0000	+0.001	+0.006	+0.016	+0.034	+0.057	+0.080	+0.094	+0.078	0
6.0	.0000	.0000	+0.002	+0.008	+0.019	+0.039	+0.062	+0.078	+0.068	0
8.0	.0000	.0000	-0.002	.0000	+0.007	+0.020	+0.038	+0.057	+0.054	0
10.0	.0000	.0000	-0.002	-0.001	+0.002	+0.011	+0.025	+0.043	+0.045	0
12.0	.0000	.0000	-0.001	-0.002	.0000	+0.005	+0.017	+0.032	+0.039	0
14.0	.0000	.0000	-0.001	-0.001	-0.001	.0000	+0.012	+0.026	+0.033	0
16.0	.0000	.0000	0.000	-0.001	-0.002	-0.004	+0.008	+0.022	+0.029	0

Tension in circular rings, N_t										
Triangular load										
Hinged base, free top										
$N_t = \text{coef} \times uH^4 \text{ lb. per ft.}$										
Positive sign indicates tension										
										
H^4		Coefficients at point								
Dt		0.0H	0.1H	0.2H	0.3H	0.4H	0.5H	0.6H	0.7H	0.8H
0.4	+0.474	+0.440	+0.395	+0.352	+0.308	+0.264	+0.215	+0.165	+0.111	+0.057
0.8	+0.423	+0.402	+0.381	+0.358	+0.330	+0.297	+0.249	+0.202	+0.145	+0.076
1.2	+0.350	+0.355	+0.361	+0.362	+0.358	+0.343	+0.309	+0.256	+0.186	+0.098
1.6	+0.271	+0.303	+0.341	+0.369	+0.385	+0.385	+0.365	+0.362	+0.314	+0.233
2.0	+0.205	+0.260	+0.32	+0.373	+0.411	+0.434	+0.419	+0.369	+0.280	+0.151
3.0	+0.074	+0.179	+0.281	+0.375	+0.449	+0.506	+0.519	+0.479	+0.375	+0.210
4.0	+0.017	+0.137	+0.253	+0.367	+0.469	+0.545	+0.579	+0.553	+0.447	+0.256
5.0	-0.000	+0.114	+0.235	+0.356	+0.469	+0.562	+0.617	+0.606	+0.503	+0.259
6.0	-0.011	+0.103	+0.223	+0.343	+0.463	+0.566	+0.639	+0.643	+0.547	+0.327
8.0	-0.015	+0.096	+0.208	+0.324	+0.443	+0.564	+0.661	+0.697	+0.621	+0.386
10.0	-0.008	+0.095	+0.200	+0.311	+0.428	+0.552	+0.666	+0.730	+0.678	+0.433
12.0	-0.002	+0.097	+0.197	+0.302	+0.417	+0.541	+0.664	+0.734	+0.720	+0.477
14.0	0.000	+0.098	+0.197	+0.299	+0.408	+0.531	+0.659	+0.761	+0.752	+0.513
16.0	+0.002	+0.100	+0.198	+0.299	+0.403	+0.521	+0.650	+0.764	+0.776	+0.536

12.7 - An Example of Cylindrical Container Analysis

In this section, we present a comprehensive numerical example consisting of analysis of a liquid retaining reinforced concrete tank with various base and roof conditions. The circular cylindrical container to be analyzed is shown in figure (12-26). The analysis should be performed for following cases:

- (1) Hinged wall to base connection
- (2) Fixed rigid base
- (3) Flexible base of thickness $t_f = 30 \text{ cm}$.
- (4) Full tank with no load on its flat roof
- (5) Empty tank with roof under uniformly distributed load of $p_s = 500 \text{ kg/m}^2$.

In all cases, we assume that the Poisson's ratio, n , of concrete is equal to zero.

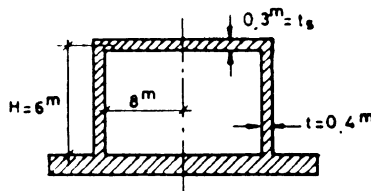


Figure (12-26) A reinforced concrete cylindrical container

Analysis:

In the analysis that follows, we assume that the conditions at one end of the cylinder wall do not affect the field at the other end: the wall-base and wall-roof interactions have been decoupled from one another; combined fields can easily be determined by superposition of these simple cases.

(1) Hinged wall-base problem

From relations (12-31), with $v = 0$, we have

$$x_1 = Q_o = -\frac{3^{3/4}}{6} \gamma a^2 \left(\frac{t}{a}\right)^{1/2} \left(\frac{H}{a}\right)$$

$$\frac{H}{a} = \frac{6}{8} = 0.75 \quad , \quad \frac{t}{a} = \frac{0.4}{8} = 0.05$$

$$x_1 = Q_o = -\frac{3^{3/4}}{6} (1000)(8)^2 (0.05)^{1/2} (0.75) = 4077.7 \text{ kg/m}$$

Scimic isolation

also

$$\beta = \left[\frac{3(1-v^2)}{a^2 t^2} \right]^{1/4} = \left[\frac{3}{8^2 (0.4)^2} \right]^{1/4} = 0.7357 \text{ m}^{-1}$$

$$K = \frac{Et^3}{12(1-v^2)} = \frac{2 \times 10^5 \times 10^4 (0.4)^3}{12} = 106.7 \times 10^{+5} \text{ kg-m}^2/\text{m}$$

The internal force field in the shell will be:

$$\begin{aligned} N_\theta &= \frac{Et}{a} w = 10^6 \frac{Q_O}{2\beta^3 K} \theta(\beta x) + \frac{\gamma(H-x)a^2}{Et} \\ &= 10^6 \left[\frac{-4077.7}{2(0.7357)^3 (106.7 \times 10^5)} \theta(\beta x) + \frac{(1000)(8)^2(6-x)}{2 \times 10^9 \times 0.4} \right] \end{aligned}$$

$$N_\theta = [-4.79 \times 10^4 \theta(\beta x) + 8000(6-x)] \text{ kg/m}$$

$$M_x = \frac{1}{\beta} Q_O \xi(\beta x) = \frac{-4077.7}{0.7357} \xi(\beta x) = -5542.6 \xi(\beta x)$$

Variations of internal forces in the wall along the height of the shell are shown in figures (12-27)

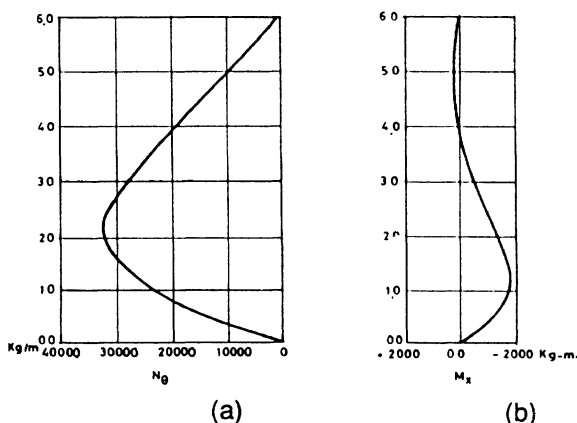


Figure (12-27) Variation of internal forces of the container shown in figure (12-26) having a hinged wall to base connection, (a) hoop force, (b) bending moment

(2) Wall with rigid base

In this case, first we rewrite relations (12-33) as

$$x_1 = -\gamma a^2 \frac{\left(\frac{t}{a}\right)^{1/2}}{[3(1-v^2)]^{1/4}} \left[\left(\frac{H}{a}\right) - \frac{1}{2[3(1-v^2)]^{1/4}} \left(\frac{t}{a}\right)^{1/2} \right]$$

$$x_2 = \gamma a^3 \frac{\left(\frac{t}{a}\right)}{2[3(1-v^2)]^{1/2}} \left[\left(\frac{H}{a}\right) - \frac{1}{[3(1-v^2)]^{1/4}} \left(\frac{t}{a}\right)^{1/2} \right]$$

Utilizing these expressions, we obtain

$$x_1 = Q_o = -1000(8)^2 \frac{(0.05)^{1/2}}{3^{1/4}} \left[0.75 - \frac{1}{2(3)^{1/4}} (0.05)^{1/2} \right] = -7231 \text{ kg/m}$$

$$x_2 = M_o = 1000(8)^3 \frac{0.05}{2(3)^{1/2}} \left[0.75 - \frac{1}{3^{1/4}} (0.05)^{1/2} \right] = 4286 \text{ kg-m/m}$$

The internal force field in the cylindrical wall is

$$N_\theta = \frac{Et}{a} w = \frac{Et}{a} \left\{ \frac{1}{2\beta^3 K} [\beta M_o \psi(\beta x) + Q_o \theta(\beta x)] + \frac{\gamma(H-x)}{Et} a^2 \right\}$$

$$= \frac{2 \times 10^9 \times 0.4}{8} \left\{ \frac{1}{2(0.736)^2 (106.7 \times 10^5)} [4286 \psi(\beta x) \right.$$

$$\left. - \frac{7231}{0.736} \theta(\beta x)] + 8000(6-x) \right\}$$

$$M_x = \frac{1}{2\beta} [2\beta M_o \phi(\beta x) + 2Q_o \xi(\beta x)] = 4286 \phi(\beta x) - \frac{2 \times 7231}{0.736} \xi(\beta x)$$

or

$$N_\theta = 8.5 \times 10^4 [0.436 \psi(\beta x) - \theta(\beta x)] + 8000(6-x)$$

$$M_x = 4286 [\phi(\beta x) - 2.226 \xi(\beta x)]$$

@Seismicisolation

Variations of these forces along the cylindrical wall are shown in figure (12-28).

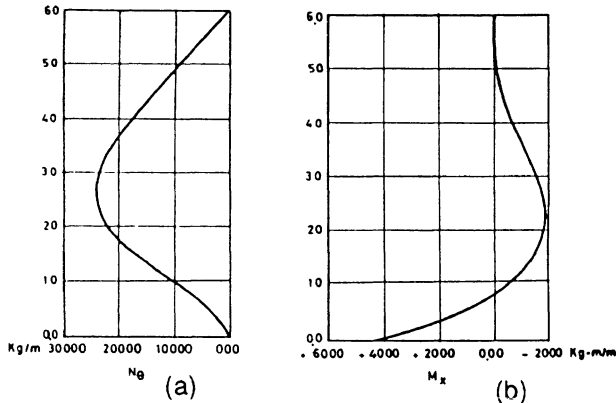


Figure (12-28) Variation of internal forces in cylindrical wall of problem (12-26), with a rigid base, (a) hoop force, (b) bending moment

(3) Wall with flexible base slab

The bending stiffness of the wall, k , and the base slab, k_f , are

$$k = \frac{Et^3}{12(1-\nu^2)} = \frac{2 \times 10^9 (0.4)^3}{12} = 1.067 \times 10^7 \text{ kg-m}^2/\text{m}$$

$$k_f = \frac{Et_f^3}{12(1-\nu^2)} = \frac{2 \times 10^9 (0.3)^3}{12} = 0.45 \times 10^7 \text{ kg-m}^2/\text{m}$$

The numerical value of parameter β is

$$\beta = \left(\frac{3}{a^2 t^2}\right)^{1/4} = \left(\frac{3}{8^2 (0.4)^2}\right)^{1/4} = 0.736^{-1/\text{m}}$$

and the magnitude of maximum pressure applied to base slab is

$$q = \gamma H = 1000 \times 6 = 6000 \text{ kg/m}^2$$

The influence coefficients, relations (12-42), are

$$\lambda_{11} = -\left[-\frac{1}{2B^2K} + \frac{a(1-\nu)}{Et_f}\right] = -\left[-\frac{1}{2(0.736)^2(1.067) \times 10^7} + \frac{8}{2 \times 10^9 (0.3)}\right] = 1.039 \times 10^{-7}$$

$$\lambda_{12} = \frac{1}{2B^2K} = \frac{1}{2(0.736)^2(1.067) \times 10^7} = 0.865 \times 10^{-7}$$

$$\lambda_{22} = -\left[\frac{1}{BK} + \frac{1}{\sqrt{q}} \cdot \frac{1}{3k_f} \sqrt{x_2}\right] = -\left[\frac{1}{0.736(1.069 \times 10^7)} + \frac{1}{\sqrt{6000}} \times \frac{1}{3(0.45 \times 10^7)} \sqrt{x_2}\right]$$

$$= -1.273 \times 10^{-7} - 0.956 \times 10^{-3} \sqrt{x_2}$$

We can write the compatibility relations (12-43) as

$$1.039x_1 + 0.865x_2 = -4800$$

$$-0.865x_1 - 1.273x_2 - 0.956 \times 10^{-3} \sqrt{x_2} = 800$$

The solution to this non-linear simultaneous equations is

$$x_2 = 2974.67 \text{ Kg-m/m}, \quad x_1 = -7096.33 \text{ Kg/m}$$

$$b = 2\sqrt{\frac{x_2}{q}} = 2 \sqrt{\frac{2974.67}{6000}} = 1.408 \text{ m}$$

Having obtained the values of edge forces x_1 and x_2 , we can write the expressions for internal force variations as in the previous cases.

(4) Full container with unloaded roof slab

In this case, the numerical values for essential parameters are

$$\beta = 0.736 \quad K = 1.067 \times 10^7 \text{ kg-m/m}$$

$$k_a = \frac{Et_3}{12(1-\nu^2)} = \frac{2 \times 10^3 \times (0.3)^3}{12} = 0.45 \times 10^7 \text{ kg-m}^2/\text{m}$$

$$D = \frac{Et_3}{(1-\nu)} = \frac{2 \times 10^3 \times 0.4}{1} = 80 \times 10^7 \text{ kg/m}$$

Therefore, the internal displacement and force field in the cylinder wall is

$$w = \frac{1000(8)^3}{(80)10^7} \left[\frac{x}{8} - \frac{0.45 \times 10^7}{2 \cdot (1.067)(10^7)(0.736)(8) + (0.45) \times 10^7} \cdot \frac{1}{(0.736)(8)} e^{-\beta x} \sin x \right]$$

or

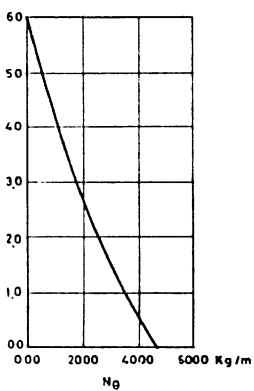
$$w = 6.4 \times 10^{-4} \left[\frac{x}{8} - 5.874 \times 10^{-3} \xi(x) \right]$$

and

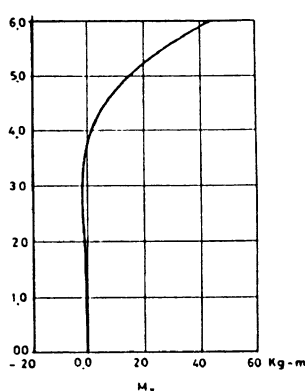
$$N_\theta = \frac{Et}{a} w = 6.4 \times 10^{-4} \left[\frac{x}{8} - 5.874 \times 10^{-3} \xi(\beta x) \right]$$

$$M_x = \frac{2 \times 1000(1.067 \times 10^7)(0.45 \times 10^7)(0.736)(8)^2}{80 \times 10^7 \cdot 2 \times 1.067 \times 10^7 \times 0.736 \times 8 + 0.45 \times 10^7} e^{-\beta x} \cos \beta x = 43.460(\beta x)$$

Figures (12-29) show variations of internal forces in the wall of this problem.



(a)



(b)

Figure (12-29) Variations of internal forces in the wall of the container shown in figure (12-26) for the case of full container with unloaded roof slab. (a) hoop force, (b) bending moment

(5) Empty container with loaded roof slab

We have assumed that the roof slab is subjected to uniformly distributed vertical load of $p_s = 500 \text{ kg/m}^2$. In this case, we use relations (12-49) and (12-50). The resulting expressions for displacement and force field in the cylinder wall are

$$\begin{aligned} w &= \frac{500 \times (8)^3}{8 \times 0.736 \cdot 2 \times 1.067 \times 10^7 \times 0.736 \times 8 + 0.45 \times 10^7} e^{-\beta x} \cos \beta x \\ &= 3.342 \times 10^{-4} \xi(\beta x) \\ N &= \frac{Et}{a} w = \frac{2 \times 10^9 \times 0.4}{8} w = 10^8 w \\ M_x &= \frac{-500(8)^3}{4} \cdot \frac{(1.067 \times 10^7)(0.736)}{2 \times 1.067 \times 10^7 \times 0.736 \times 8 + 0.45 \times 10^7} e^{-\beta x} \cos \beta x \\ &= -3.863 \times 10^3 \theta(\beta x) \end{aligned}$$

Figures (12-30) show variations of internal forces in this cylinder wall.

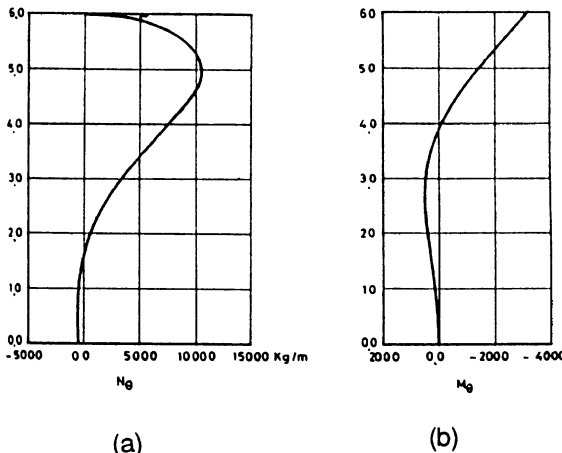


Figure (12-30) Variation of internal forces in the liquid container of figure(12-26) assuming empty tank and uniformly loaded roof slab, (a) hoop force, (b) bending moment

As we have mentioned before, the combined field of forces and deformations can be easily determined by simple linear superposition of these individual solutions.

12.8 - Design of a Reinforced Concrete Container

A reinforced concrete circular cylindrical liquid retaining tank, figure (12-31) will be designed in this section. Overall dimensions of the tank are,

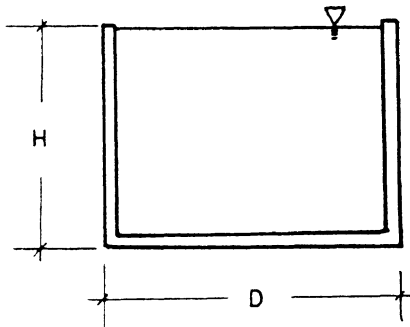


Figure (12-31) A reinforced concrete circular cylindrical liquid retaining tank

This container is assumed to be free at the top and to be monolithic with its base, which is of a relatively thick slab. The properties of concrete and reinforcing materials are as follows:

Modular ratio (ratio of Young modulus of steel to Young modulus of concrete):
 $n = 14$

Compressive strength of the concrete (28 days cylinder sample):

$$f_c = 200 \text{ kg/m}^2$$

Allowable tensile stress in concrete for direct hoop tension:

$$\sigma_t = 12 \text{ kg/cm}^2$$

Allowable tensile stress of concrete in bending:

$$\sigma_{tb} = 17 \text{ kg/cm}^2$$

Allowable tensile stress in reinforcing steel bars:

$$f_s = 1000 \text{ kg/cm}^2$$

Design:

We assume a trial thickness value of 12.5 cm for the cylinder wall. Numerical values of parameters needed for necessary calculations are

$$I = \frac{bt^3}{12} = \frac{t^3}{12}$$

$$\beta^4 = \frac{t}{4a^2 I} = \frac{3}{a^2 t^2}$$

$$\beta^4 = \frac{3}{(450)^2 (12.5)^2} = 9.47 \times 10^{-8}, \quad \beta = 1.75 \times 10^{-2} \text{ cm}^{-1}$$

$$e^{\beta H} = e^{1.75 \times 10^{-2}} \times 400 = 1097$$

$$\sin \beta H = 0.657 \quad \cos \beta H = 0.754$$

$$\beta^4 I = \frac{t}{4a^2} = 0.155 \times 10^{-4}$$

Since the base slab is thick and its connection to the wall is monolithic, the relations for a fixed base can be used. Calculations to determine the internal force field have been performed before and will not be repeated here. Without entering into the detailed, but straightforward calculations, we only present the final results in the form of force diagrams as shown in figure (12-32). These results have been obtained assuming the coupled interaction of both ends of the cylinder. Had we assumed that the ends effects were decoupled, the results would have not been affected too much.

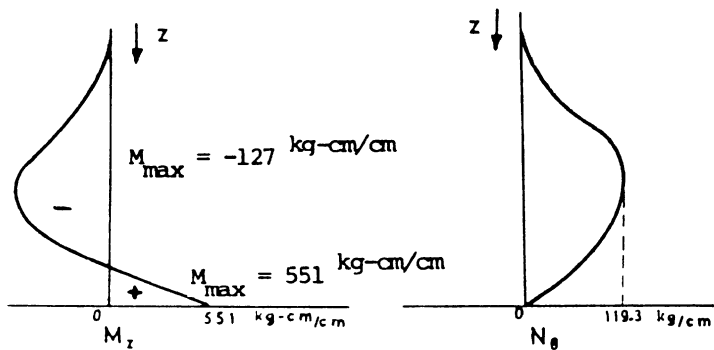


Figure 12-32. Internal force diagrams in the container of figure (12-31)

Having determined the internal force field, we are now ready to design the required tensile reinforcements

The **hoop reinforcement** to carry the maximum hoop force is

$$A_s = \frac{119.3}{1000} = 0.119 \text{ cm}^2/\text{cm} = 11.9 \text{ cm}^2/\text{m}$$

On the other hand, according to, for example, IS (Indian Standards), the minimum steel ratio is

$$\rho_{\min} = \frac{A_{\min}}{bh} = 0.3 - \frac{2.5}{35} \times 0.1 = 0.2938$$

So, the corresponding minimum hoop reinforcement would be

$$A_{s,\min} = \rho_{\min} \cdot bh = \frac{0.293}{100} \times 100 \times 12.5 = 3.66 \text{ cm}^2/\text{m}$$

We also need to check the maximum tensile stress in the concrete, so that we are assured that there is no cracking in the concrete, and therefore no leakage. The tensile hoop stress in the concrete is

$$\sigma_c = \frac{119.3}{12.5 + (14-1) \times 0.119} = 8.5 \text{ kg/cm}^2 < 12 \text{ kg/cm}^2$$

So we are assured that there will be no vertical cracking of the cylinder wall.

The maximum **vertical steel reinforcement** in the *inner side* of the wall is

$$A_s = \frac{M}{f_s \cdot jd} = \frac{551}{1000 \times 0.835 \times 10.9} = 0.0605 \text{ cm}^2/\text{cm} = 6.05 \text{ cm}^2/\text{m}$$

Vertical steel required at the *outer part* is

$$A_s = \frac{M}{f_s \cdot jd} = \frac{127}{1000 \times 0.835 \times 9.4} = 0.0162 \text{ cm}^2/\text{cm} = 1.62 \text{ cm}^2/\text{m}$$

The **minimum** area of steel reinforcement, placed in the inner and outer faces of the wall thickness is

In the inner face:

$$A_{s,\min} = \frac{0.293}{100} \times 1 \times 12.5 = 0.0366 > 0.0162$$

in the outer face:

$$A_{s,\min} = \rho_{\min} \cdot bt = \frac{0.293}{100} \times 1 \times 14 = 0.0460 \text{ cm}^2/\text{cm} < 0.0605$$

The reinforcing steel bars should be reduced proportionately at the sections with smaller hoop force and bending moment.

Figure (12-33) shows the reinforcing detail in a vertical section through the container.

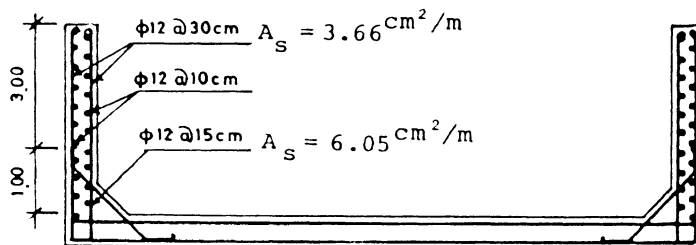


Figure (12-33) A vertical section through the container of design problem, figure (12-31), showing details of reinforcements

12.9 - Some Considerations on Reinforcements Detail

In designing of reinforced concrete liquid retaining tanks, due consideration must be given to the detailing of the reinforcing system; improper detailing could lead to local and sometimes global failures; a poor detailing could make an otherwise properly designed container unserviceable; proper detailing is particularly important at the location of water stops, construction joints, and the corner points. Figures (12-34) show two types of proper corner reinforcement details and a third one which is considered inappropriate.

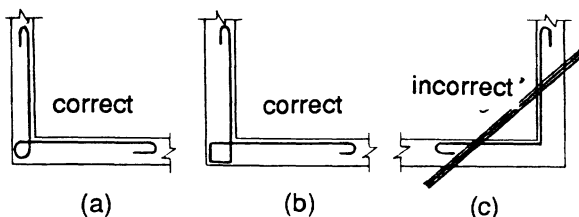


Figure (12-34) Correct and incorrect reinforcement detailing at an intersection. (a) and (b) correct, (c) incorrect

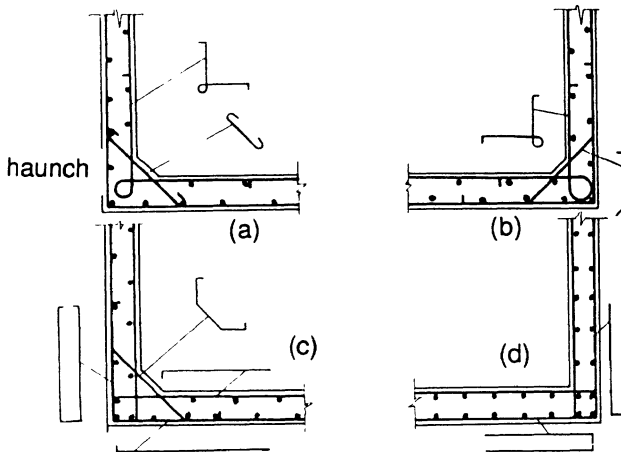


Figure (12-35) Some possible arrangements of reinforcement detailing at the corners of reinforced concrete liquid retaining structures

To facilitate placing of reinforcement at the intersections, and also to facilitate placing of fresh concrete, the corners of wall to base junction can be provided with horizontal and vertical **haunches**. The set of figures (12-35) show proper reinforcement detailing in reinforced concrete containers with or without haunches.

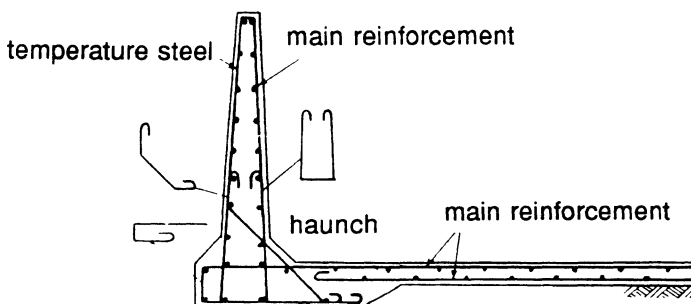


Figure (12-36) Detailing of reinforcement in a large container with wall heel

Particularly in large containers, wall footings are provided by a "heel", figure (12-36). This "heel" acts as a stiffening horizontal ring for the wall-base system; it also helps to distribute the load of the wall to the foundation bed in a more uniform fashion. Moreover, if the structure has a heel, it is easier to place reinforcement and concrete in a crowded area; this would lead to better joint quality.

12.10 - Cylindrical Walls with Domed Roofs

In some cases, and specially when the diameter of cylindrical wall is large and no inner columns are permitted, the roof would be a dome. Other cylindrical shell structures may have domed roofs: nuclear power plant containment shells and large circular halls are examples. The cylindrical wall can be connected to its domed roof with or without a stiffening ring.

We analyze and design wall-dome shell systems by means of the "force method" of shell analysis. Fundamentals of this method have been discussed in various places of this text. In the previous sections of the present chapter, this method was applied to the analysis of cylindrical wall with flat roof. Now we apply the same method to the analysis of **wall-dome system**.

Consider the cylindrical wall-dome system shown in figure (12-37a). The **force method** of analysis, consisting of membrane analysis, corrective (bending) analysis, and superposition of fields, will be applied in the following fashion.

(1) Membrane analysis

The horizontal, H , and vertical, V , components of membrane reactions at the base of the dome are

$$H = N_\alpha \cos \alpha$$

$$V = N_\alpha \sin \alpha$$

The vertical component is carried by the wall in a membrane state and thus would not induce radial displacement in the wall. The horizontal component produces radial displacement as well as rotation in the wall. The values of these deformations are

$$D_{10}^S = \frac{1}{2\beta^2 K} N_\alpha \cos \alpha \quad (12-51)$$

$$D_{20}^S = \frac{1}{2\beta^2 K} N_\alpha \cos \alpha$$

These membrane deformations are shown in figure (12-37b). If the cylinder is a container filled with liquid, then the membrane deformation produced by internal pressure must also be added to the above expressions. For a container filled up to the point of intersection, these additive terms would be

$$D_{20}^S = \frac{-\gamma a^2}{E t_s}, \quad D_{10}^S = 0 \quad (12-52)$$

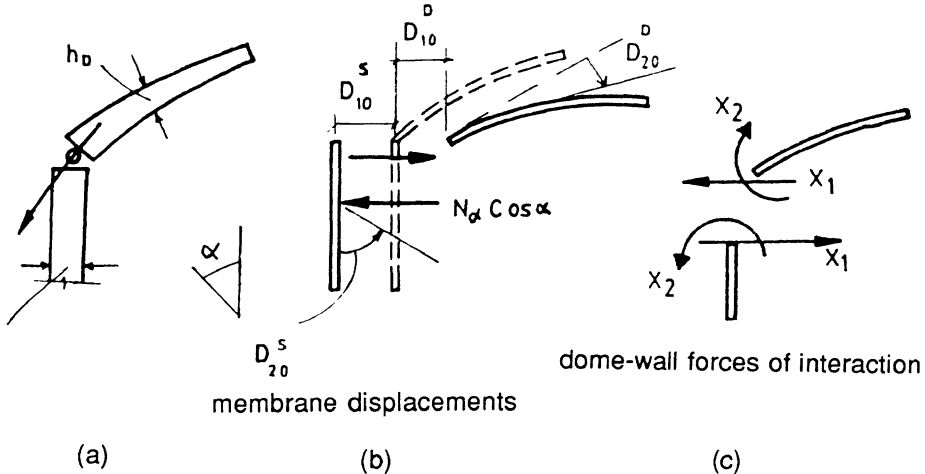


*Figure (12-37) Force method of cylindrical wall-dome analysis,
(a) the membrane wall-dome system, (b) membrane deformations,
(c) unknown bending forces in the wall-dome intersection*

(2) Bending analysis

In the chapters 4 and 9, on the bending analysis of domes and cylindrical shells, we have developed the expressions for the influence coefficients of domes and cylinders. Using those results, and referring to wall-dome system of figure (12-37c), we can write the influence coefficients at the wall-dome intersection as follows:

$$D_{10} = D_{10}^D + D_{10}^S = D_{10}^D + \frac{1}{2\beta^3 K} N_\alpha \cos \alpha$$

$$D_{20} = D_{20}^D + D_{20}^S = D_{20}^D - \frac{1}{2\beta^2 K} N_\alpha \cos \alpha$$

$$D_{11} = D_{11}^D + D_{11}^S = \frac{2a\lambda \sin^2 \alpha}{E \bar{t}_D} - \frac{1}{2\beta^3 K} \quad (12-53)$$

$$D_{12} = D_{12}^D + D_{12}^S = \frac{2\lambda^2 \sin \alpha}{E \bar{t}_D} + \frac{1}{2\beta^2 K}$$

$$D_{22} = D_{22}^D + D_{22}^S = \frac{4\lambda^3}{E a \bar{t}_D} - \frac{1}{\beta K}$$

Having determined the influence coefficients of the system, we can now write the compatibility relations for the structure. These equations are

$$D_{11}X_1 + D_{12}X_2 + D_{10} = 0 \quad (12-54)$$

$$D_{21}X_1 + D_{22}X_2 + D_{20} = 0$$

Substituting the relevant values from relations (12-51) to (12-53) into these equations, and solving these equations for the unknown forces, X_1 and X_2 , we complete the corrective (bending) analysis.

(3) Superposition

The results of membrane and bending analyses performed in (1) and (2) should be superposed to yield the total field in the cylindrical wall-dome system.

In the following section, we present a sample design example using the results of this analysis.

12.11 - Design of a Cylindrical "Wall-Dome" Container

Consider a monolithic reinforced concrete container consisting of a cylindrical wall, a spherical shell roof, and a rigid base, as shown in figure (12-38). Geometrical and material features of this system are

$$\begin{aligned} a &= 30^{\text{m}}, \alpha = 26^{\circ}, v = 0, t = 10^{\text{cm}} & n &= 14 & \lambda &= 3\left(\frac{30}{0.1}\right)^2 = 22.8 \\ t_s &= 35^{\text{cm}}, R = 13^{\text{m}}, H = 6.5^{\text{m}}, & q &= 240 \text{ Kg/m}^2 & K &= E \frac{35^3 \times 10^{-6}}{12} = 3.57 \times 10^{-3} E \\ & & & & \beta &= \frac{3}{13^2 \times (0.35)^2} = 0.62^{\text{l/m}} \end{aligned}$$

The goal is the design of this structure including the reinforcement design of the wall as well as its domed roof. Allowable concrete and steel stresses are assumed to be the same as in the previous example. The wall is assumed to be high enough so that the boundary effects at one end can be decoupled from those at the other. The container is assumed to be filled with water.

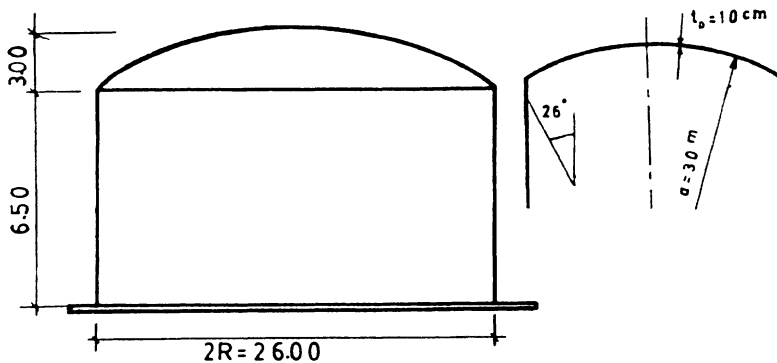


Figure (12-38) A reinforced concrete cylindrical wall-dome container

1). Analysis of the system:

(a) "Wall-dome" interaction

Membrane deformations:

$$ED_{10} = 1.473 \times 10^3 q + \frac{1}{2 \times 0.62^3 \times 3.57 \times 10^{-3}} \times \frac{30 \times 0.9}{1 + 0.9} q \\ = 2357760$$

$$ED_{20} = 0.263 \times 10^3 q - \frac{1}{2 \times 0.62^3 \times 3.57 \times 10^{-3}} \times \frac{30 + 0.9}{1 + 0.9} q \\ = -1179504$$

Influence coefficients:

$$ED_{11} = \frac{2 \times 30 \times 22.8 \times 0.438^2}{0.1} - \frac{1}{2 \times 0.62^3 \times 3.57 \times 10^{-3}} = 2036$$

$$ED_{12} = \frac{2 \times 22.8^2 \times 0.438}{0.1} + \frac{1}{2 \times 0.62^2 \times 3.57 \times 10^{-3}} = 4918$$

$$ED_{22} = \frac{4 \times 22.8^3}{30 \times 0.1} - \frac{1}{0.62 \times 3.57 \times 10^{-3}} = 15351$$

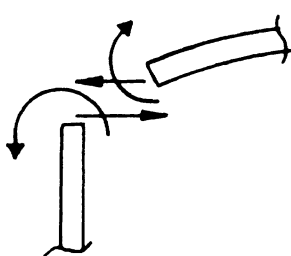
Compatibility relations:

$$D_{10} + D_{11}X_1 + D_{12}X_2 = 0$$

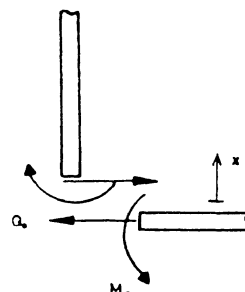
$$D_{20} + D_{21}X_1 + D_{22}X_2 = 0$$

$$X_1 = H = -5940 \text{ Kg/m} , \quad X_2 = M_\alpha = 1980 \text{ Kg-m/m}$$

Noting the negative sign of H , and referring to figure (12-39a), we conclude that the direction of horizontal force must be reversed.



(a)



(b)

Figure (12-39) Forces of interaction in the structure shown in figure (12-38), (a) bending effects at the wall-dome junction, (b) bending effects at the wall-base junction

(b) Wall-base interaction

This type of analysis was performed before. Using those relations, and referring to figure (12-39b), we see that the shear force and bending moment at the junction of wall and its base are

$$\frac{Q_O}{\gamma a^2} = \frac{\left(\frac{t}{a}\right)^{1/4}}{\left[3(1-v^2)\right]^{1/4}} \times \left\{ \frac{H}{a} - \frac{1}{2[3(1-v^2)]^{1/4}} \cdot \left(\frac{t}{a}\right)^{1/2} \right\}$$

$$\frac{Q_O}{1000 \times 13^2} = \frac{\left(\frac{35}{1300}\right)^{0.5}}{3^{1/4}} \times \left\{ \frac{6.5}{13} - \frac{1}{2 \times 3^{1/4}} \cdot \left(\frac{35}{1300}\right)^{0.5} \right\}$$

$$\Rightarrow Q_O = -9222 \text{ Kg/m}$$

$$\frac{M_O}{\gamma a^3} = \frac{M_O}{1000 \times 13^3} = \frac{\frac{35}{1300}}{2[3]^{0.5}} \times \left\{ \frac{6.5}{13} - \frac{1}{3^{1/4}} \cdot \left(\frac{35}{1300}\right)^{0.5} \right\}$$

$$\Rightarrow M_O = 6408 \text{ Kg-m/m}$$

Now we can use the results of corrective analyses performed in part (a) and (b) to find the total internal force field in the system.

The membrane force field in the cylindrical container is

$$N_\theta = \frac{Et}{a} w = \frac{Et}{a} \frac{\gamma a^2 (H-x)}{Et} = 13000 (6.5 - x)$$

The force field in the cylinder produced by wall-dome interaction is

$$M_x = 1980 [\phi(\beta x) + 4.84 \xi(\beta x)]$$

$$N_\theta = 19691 [\psi(\beta x) + 4.84 \theta(\beta x)]$$

and the force field due to wall-base interaction is determined to be

$$N_0 = \frac{Et}{a} w = \frac{Et}{a} \cdot \frac{1}{2\beta^3 K} [\beta M_O \psi(\beta x) + Q_O \theta(\beta x)] = 63733 [\psi(\beta x) - 2.321 \theta(\beta x)]$$

$$M_x = K \frac{d^2 w}{dx^2} = K \cdot \frac{1}{2\beta K} [2\beta M_O (\beta x) + 2Q_O \xi(\beta x)] = 6408 [\psi(\beta x) - 2.321 \xi(\beta x)]$$

These fields are combined as shown in table (12-5).

Table (12-5) Calculations of wall-dome container problem, figure (12-39)

x (m)	β_x	functional coefficients				N_θ Kg/m	N_θ Kg/m	M_x (Kg-m/m)	N_ξ Kg/m	M_x (Kg-m/m)	N_θ (Kg/m)	M_x (Kg-m/m)
		$\zeta(\beta_x)$	(β_x)	$\xi(\beta_x)$	$\xi(\beta_x)$							
0.0	0	1.000	1.000	1.000	0	84500	-1106	-184	-84191	6408	-797	6224
0.50	0.31	0.9218	0.4755	0.6987	0.2231	78000	-2074	-193	-73050	2589	2876	2396
1.50	0.93	0.552	-0.0792	0.2365	0.3158	65000	-5212	-67	-40031	-1160	19756	-1227
2.50	1.55	0.2171	-0.2070	-0.00495	0.2122	52000	-8606	466	-12460	-1765	30934	-1299
3.0	1.86	0.1053	-0.1933	-0.04408	0.1493	45500	-9241	964	-5799	-1546	30460	-582
3.5	2.17	0.03025	-0.1586	-0.0642	0.0944	39000	-8007	1639	-611	-1210	30382	429
4	2.48	-0.0144	-0.1176	-0.066	0.0516	32500	-4548	2463	2268	-860	30220	1603
5	3.1	-0.0431	-0.0469	-0.0450	0.0019	19500	20980	4119	3667	-304	44147	3815
6	3.72	-0.0336	-0.0071	-0.0203	-0.0132	6500	75952	3963	2550	-19	85002	3944
6.5	4.0	-0.0258	0.0019	-0.0120	-0.0139	0	114995	1980	1654	41	115160	2021

2) Reinforcement design

Hoop reinforcement:

If the allowable tensile stress is 1000 kg/cm² for reinforcing steel, the hoop reinforcement required at the top of the wall would be

$$A_s = \frac{115160}{1000} = 115.16 \text{ cm}^2/\text{m}$$

To control the cracking of concrete due to hoop tension, we first calculate the tensile stress in the concrete, that is

$$\sigma_t = \frac{115160}{35 \times 100 + (14 - 1) \times 119.32} = 22.80 \text{ Kg/cm}^2$$

This value is higher than the prescribed allowable stress, so, the concrete may crack. To reduce this possibility, we can increase the thickness of the shell at this region, or provide the wall with an stiffening ring at the top. The magnitude of hoop reinforcement could be reduced at lower parts of the cylinder. In all regions, the stress in the concrete must also be calculated so that the cracking of the concrete can be controlled.

In all parts of the shell, a minimum hoop reinforcement of the following magnitude should be placed in the wall:

$$\rho_{\min} = 0.3 - \frac{250}{350} \times 0.1 = 0.228\%$$

$$A_{s,\min} = 0.228 \times 100 \times \frac{35}{100} = 98 \text{ cm}^2/\text{m} < A_s$$

We must choose an appropriate wall thickness to prevent cracking. The wall thickness calculation, based on allowable bending stress, is as follows:

$$\sigma_{bc} = \frac{M}{S} = \frac{6}{t^2} M \leq \sigma_{tb} \quad t = \sqrt{\frac{6M}{\sigma_{tb}}}$$

$$t = \sqrt{\frac{6224 \times 6}{17}} = 46.9 \text{ cm} > 35 \text{ cm}$$

We conclude that the assumed wall thickness of 35 cm is not sufficient for the lower region of the container; there the bending moment requires a thicker wall. A possible solution would be to provide the container with a "haunch" at the lower part, i.e., at the wall base junction.

Vertical reinforcement:

The next step is to determine the value of required bending reinforcement which is placed vertically along the shell wall. The allowable bending moment, corresponding to minimum reinforcement ($A_{s\min} = 7.98 \text{ cm}^2$), is

$$7.98 = \frac{M}{26.55 \times 1000} \rightarrow M = 2118.69 \text{ Kg-m/m}$$

In most parts of the wall this bending capacity is higher than the existing bending moment. hence, a minimum vertical reinforcement would suffice in the middle region of the wall. We place a minimum reinforcement throughout the wall and then provide the lower and upper parts with additional reinforcements.

In the top and bottom regions, the following values for additional vertical bending reinforcements could be calculated.

In the lower region:

$$A_s = \frac{(6224 - 2453) \times 100}{26.55 \times 1000} = 14.2 \text{ cm}^2/\text{m}$$

In the upper region:

$$A_s = \frac{(3944 - 2453) \times 100}{26.55 \times 1000} = 5.62 \text{ cm}^2/\text{m}$$

The minimum vertical reinforcement is placed at both faces of the wall thickness. However, the additional reinforcements are placed at each side of the wall required for the corresponding sign of the bending moment.

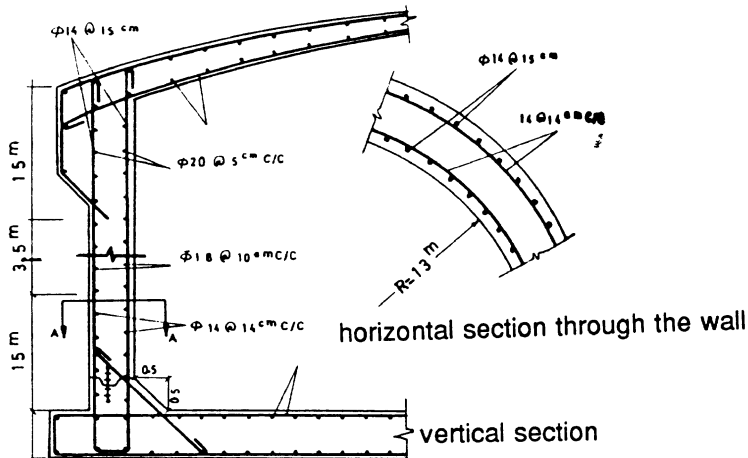


Figure (12-40) Design detail of the reinforced concrete container, shown in figure (12-39)

Figure (12-40) shows the reinforced detail of the container. In this figure, the dome and the base are also provided with appropriate steel reinforcements. The calculations pertaining to design of these latter reinforcements were not presented in this section. The design of the dome of this container can proceed along the lines detailed in chapter 8.

Problems

P 12.1 - The elevated tank shown in figure (P 12-1) is called an Intze tank. The main feature of an Intze tank is that the cylindrical wall is connected to a domed bottom by means of a conical shell; the lateral thrust at the wall bottom intersection is reduced and only a remaining vertical reaction must be carried to the vertical supports. Therefore, an Intze tank does not require a thrust ring.

The reinforced concrete Intze tank of figure (P 12-1) is to contain 100 m³ of water. The sum of dead and live load on the domed roof of this tank is 4000 N/mm². It is assumed that the maximum water level in the tank (freeboard) is 30 cm below the top of the wall.

(1) Find the membrane and bending forces in the wall and the roof. In your calculations, assume that the Young's modulus of the wall and the roof are the same, and the Poisson's ratios are zero. Plot the internal force diagrams.

(2) Design the reinforcement for the wall and the roof assuming allowable stresses for the reinforcing steel and concrete equal to $f_s = 100 \text{ N/mm}^2$ and $f_{ct} = 2 \text{ N/mm}^2$ (concrete tension), $f_{cc} = 15 \text{ N/mm}^2$ (concrete compression), respectively.

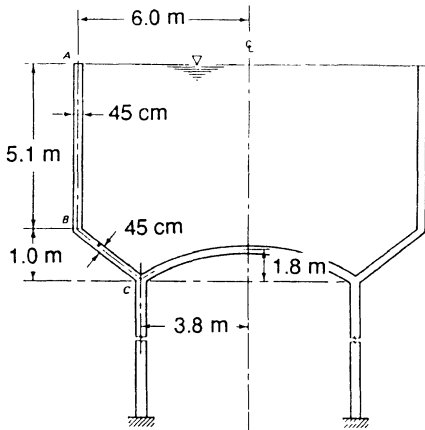


Figure (P 12-1) An Intze tank

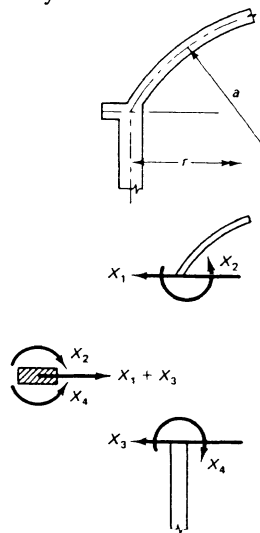


Figure (P 12-2)

P 12.2 - On some occasions, the cylindrical wall of a container is connected to its domed roof by means of a stiffening ring. Consider the container of section 12.11 again. In the present problem, assume that there is a stiffening ring between the wall and its roof. Perform the design of the wall with such ring. Choose some appropriate dimensions for the ring, design reinforcement for it.

(Hint: figure (P.12-2) shows the wall-roof junction with the ring. As you see, there are four redundant forces. Write four compatibility equations relating these redundant forces. Find the redundant forces and then determine the force fields in the wall and the roof).

References for Chapter Twelve

12.1 - M. Farshad, *Shell Structures*, Vol. I, 1986, Vol. II, 1987, Shiraz University Publications, Shiraz

12.2 - D. P. Billington, *Thin Shell Concrete Structures*, McGraw-Hill Book Co. N.Y., Revised edition, 1982

12.3 - S. Timoshenko and S. Woinowsky-Krieger, *Theory of Plates and Shells*, 2nd edition, McGraw-Hill Book Co., N.Y., 1959

12.4 - Krishna, and Jain, *Reinforced Concrete*, Vol. I and II, McGraw-Hill Book Company, New Delhi

12.5 - G. P. Manning, *Reinforced Concrete Design*, Third edition, Longmans, Green and Co. Ltd., England, 1967

Chapter 13

Buckling of Shells

13.1 - Introduction

Deformable bodies may become unstable under certain loading conditions and thus have a premature failure. The phenomenon of instability is particularly important for *thin* shells subjected to compressive forces. In such cases, the loadings which produce instability modes of failure are several orders of magnitudes smaller than the forces causing material collapse of the structure. A special mode of shell instability is the *buckling* of shells which occurs under certain static or dynamic loading conditions.

The design of thin shells is normally dominated by the stability considerations and not merely the material strength requirements. Hence, the stability analysis of thin shells acquires prime importance in various problems related to the design of shells.

In the present chapter, we derive a systematic, but simplified, analysis of shell buckling and obtain some useful relations between the so-called critical loads and shell parameters. In addition, we will present a set of useful relations for the linear buckling analysis of shells, and some buckling design recommendations.

13.2 - Concepts of Stability and Instability

Instability is a universal phenomenon which may occur in various material bodies. The fundamental concepts of stability and instability are clarified through the following definitions:

The state of a system is the collection of values of the system parameters at any instant of time. For example, the positions of material points in a structure and the temperature field at various points constitute the state of that system. The state of a system depends on **system parameters** and **environmental conditions**. For example, in a shell structure, the system parameters are geometrical and material properties, and the environmental conditions are the applied forces and thermal conditions.

Stability - *The state of a system, at any instant of time, is called **stable** if the relatively small changes in system parameter and / or environmental conditions would bring about relatively small changes in the existing state of the system.*

Instability - *The state of a system at any instant of time is called **unstable** if relatively small changes in system parameter and / or environmental conditions would cause major changes in the existing state.*

Stability and Instability of Equilibrium - The equilibrium state of a system is called *stable* if small perturbations in that state, caused by load changes or other effects, would be confined to a vicinity of the existing equilibrium state. The equilibrium state of a system is called *unstable* if slight changes in conditions related to that state would force the system away from that equilibrium state; an unstable system would find other equilibrium state(s); the new equilibrium state(s) may be in the vicinity of the initial state or may be far away from the initial equilibrium configuration.

The concepts of stable and unstable equilibrium are illustrated in figure (13-1). This figure shows a small ball lying on a smooth surface. According to the foregoing definitions, the equilibrium state 1 is stable while state 2 is unstable. The relativity of the foregoing definitions is clearly demonstrated in this figure; the state 1 may be stable in a certain limited region, but be unstable in a larger domain.

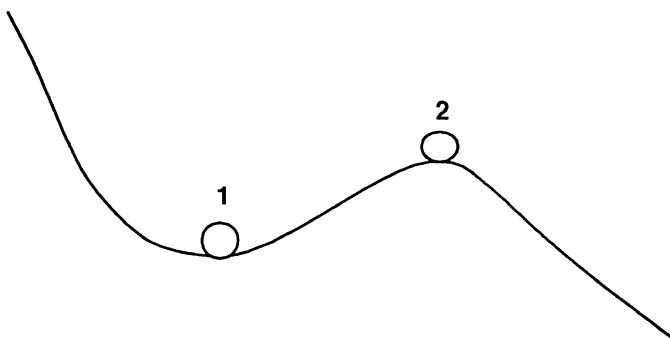


Figure (13-1) Concept of stability and instability of equilibrium

Buckling is a special mode of instability of equilibrium which may occur in deformable bodies subjected mostly to compressive loadings. So far as the structural problems are concerned, an existing state of equilibrium or trend of behavior of the structure subjected to applied loadings and / or temperature variations could be altered and the structure could acquire a new equilibrium state or a new trend of behavior. This phenomenon is termed the *buckling* of that particular structure. A well known example of elastic buckling instability is the flexural buckling of an axially compressed slender elastic column subjected to a concentric compressive force.

The type of applied loading affects the modes of elastic instability. Loading systems are classified as *conservative* or *nonconservative*. Dead loadings, such as the weight of structures, are conservative forces; time dependent loadings, and the forces which depend on the state of the system are generally nonconservative. Conservative loadings are derivable from a potential function whereas nonconservative forces have no generating potential. From this viewpoint, frictional forces are nonconservative.

Elastic bodies subjected to conservative forces may loose their current equilibrium state and find other equilibrated configurations; this mode of elastic instability is normally of the *buckling* type. The equilibrium of the same elastic bodies subjected to nonconservative forces may become *dynamically* unstable; the system could undergo oscillations with increasing amplitude. This mode of elastic instability is called *flutter*. Thin panels or shells in contact with flowing fluids could develop a flutter mode of elastic instability.

13.3 - Types of Loss of Static Stability

Ideal structures could loose their stability in one of the following types:

- (1) Bifurcation of Equilibrium
- (2) Limitation of Equilibrium

13.3.1 - Bifurcation of Equilibrium

One of the salient feature of static elastic instability, i.e., buckling, is the *bifurcation* of equilibrium state. At a certain stage of loading, the state of equilibrium of a structure may reach a point of bifurcation in which there are *two* possible paths (states) of equilibrium. The intersection of these two paths corresponds to the so called "bifurcation" of equilibrium because at such point two states of equilibrium can exist for the same load. Beyond the bifurcation point, the system can have one of the two choices of behavior. It can stay in its initial equilibrium regime or it could *diverge* from the *primary path* and follow a new path, the *secondary path*, of deformation. From the physical point of view, the structure chooses the path corresponding to a minimum of total energy of the system.

The bifurcation point of an equilibrium state marks the *critical state* of behavior of an elastic system. The primary path, i.e., the initial state of equilibrium, beyond the bifurcation point is an unstable path while the secondary equilibrium path is stable. The loading condition corresponding to a bifurcation point is normally called the *critical load*.

As a **simple example** of bifurcation type of instability, we consider the problem of a straight slender elastic straight column subjected to axial compressive force. If the force retains its original direction, then it is conservative. Under the applied compressive force,

this column would first undergo axial shortening; the amount of axial shortening is linearly proportional to the applied force. This trend of behavior, i.e., axial shortening of an otherwise straight column is called the *primary path* of equilibrium of this column. With increase of applied force the column is further compressed but still retains its straight configuration until the so-called bifurcation point is reached. A certain value of axially applied force would mark the bifurcation point.

With further increase in the applied force, beyond the bifurcation point, the column can follow one of the two following paths: (1) it can remain straight and to undergo further pure axial contraction, or (2) acquire a *bent* form and undergo lateral as well as axial deformation. This bent equilibrium state is certainly a new trend of behavior that is different from its straight configuration. This bent form of the compressed column is called *buckling*. The straight form of equilibrium, beyond the bifurcation point, is unstable in the sense that a small *perturbation* could alter that straight configuration and bring the column to a *bent* position; the bent configuration of the column is stable figure (13-2).

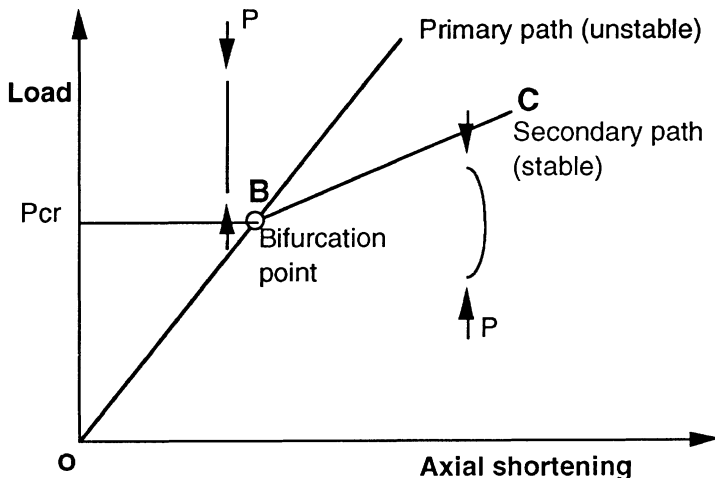


Figure (13-2) Behavior of axially compressed elastic column

The buckling of such elements as concentrically loaded straight bars and rings under uniform external pressure, as normally demonstrated by figure(13-2), is marked by bifurcation of equilibrium. In these elements, with the passage of applied load through critical state(s), the structure passes from an unbuckled shape to adjacent buckled configuration(s).

The existence of two equilibrium paths, emanating from a *bifurcation point*, and the fact that the system chooses the buckled shape beyond that point, is characteristic of a buckling type which is usually referred to as *classical buckling*. In figure (13-2), a classical buckling load (P_{cr}) can be determined by linear theories of stability analysis. For example, the classical linear theory of slender compressive members yields the well-known Euler buckling load. The Euler buckling load is directly proportional to bending rigidity of the member and is inversely proportional to the square of its length (third power of radius for rings and arches).

According to the shape of the post critical curve, two types of bifurcation of equilibrium can be distinguished:

(1) Stable symmetrical bifurcation

Figure (13-3a) shows a model of this type of bifurcation. If the applied load is below the critical value, P_{cr} , the strut remains straight. Beyond the critical value, the strut deviates lateral from the straight configuration. By the application of equilibrium equation, we find the load deformation relation in the postbuckling stage to be:

$$P = \frac{c}{1} \frac{\theta}{\sin \theta} \approx \frac{c}{1} \left[1 + \frac{1}{3} \left(\frac{\Delta}{l} \right)_2^2 \right] \quad (13-1)$$

Figure (13-3b) shows the load-deformation curve, p as a function of Δ , plotted on the basis of the above equation. Figure (13-3c) shows the load-deformation plot of the same relation, this time as function of δ . It can be observed that both of these postcritical plots are ascending curves showing that the post critical state of this system is stable, since the increase of deformation requires an increase in the applied loading.

(2) Labile symmetrical bifurcation

Another type of divergence of equilibrium path is called the "labile bifurcation". Labile bifurcation may be symmetric or nonsymmetric depending on the type of loading and the structure.

Figure (13-3d) shows a simple model in which symmetric labile bifurcation could be realized. The nonlinear load-deformation relation of this system is

$$P = \frac{k_1}{2} \cos \theta \approx \frac{k_1}{2} \left[1 - \frac{1}{2} \left(\frac{\Delta}{l} \right)_2^2 \right] \quad (13-2)$$

Figures (13-3e) and (13-3f) show that, beyond the bifurcation point, both curves have a *descending* trend. This means that for an equilibrium state to be preserved, the applied loading must be *decreased*. This is the case for some types of shell structures.

(3) Labile unsymmetrical bifurcation

A model of labile unsymmetrical bifurcation is shown in figure (13-3g). The nonlinear load-deformation relation for this case is,

$$P = \frac{k_1}{8} \left(1 - \frac{3}{4} \theta + \frac{\theta^2}{3} \right) \left[1 - \frac{3}{4} \left(\frac{\Delta}{l} \right)_1 + \frac{1}{3} \left(\frac{\Delta}{l} \right)_2^2 \right] \quad (13-3)$$

Figures (13-3h) and (13-3i) show plots of this load-deformation relation. This trend is characteristic of the structures in which the *postbuckling deformation* can only occur in a preferred direction; this phenomenon can occur in some imperfect structures.

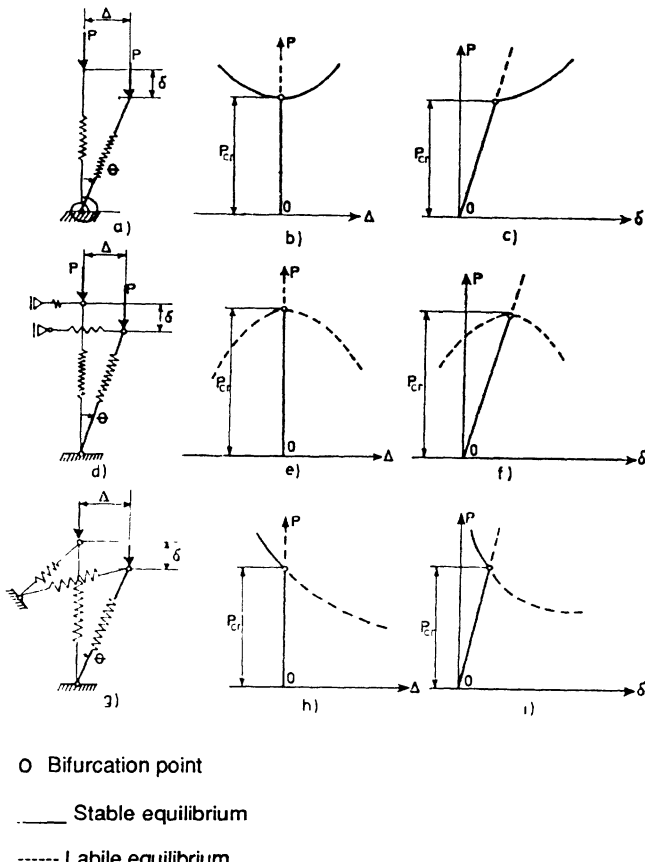


Figure (13-3) Types of bifurcation of equilibrium, (a) Model of stable symmetrical bifurcation, (b) and (c) postcritical behavior of system(a), (d)Model of labile symmetrical bifurcation, (e) and (f) postcritical behavior of the system (d), (g) model of labile unsymmetrical bifurcation, (h) and (i) post critical behavior of system (g)

13.3.2 - Limitation of equilibrium

The loss of stability through the so-called "limitation of equilibrium" is characteristic of structures which carry the transverse loading mainly by compressive axial forces. Shallow arches and shallow shells are examples of such structures. In structures undergoing this type of instability there is no bifurcation point. The load-deformation curve of such systems is continuous and consists of a single curve with no branches; this curve has some stationary maximum and minimum points; the critical load corresponds to one of these maxima.

A well-known type of *limitation of equilibrium instability* is referred to as the **snap-through buckling**. Snap-through buckling is a mode of instability in which an elastic system, under certain loading, may pass from an equilibrium state to a non-adjacent equilibrium configuration. Figure (13-4) shows the force deformation relation of a shallow arch with restrained ends. The branch OB of the load deformation curve describes the predominantly linear behavior of the arch. At the stationary point B, corresponding to a maximum applied force, the system "jumps" from a deformed state, marked by point B, to another deformation state much further away from its neighboring deformed configurations. In figure (13-4), this state is marked by another stationary point on the deformation path which is denoted by C. Compressed shallow arches and shells can "snap-through" their bases and deform into reversed shapes undergoing *tensile* (instead of compressive) deformations.

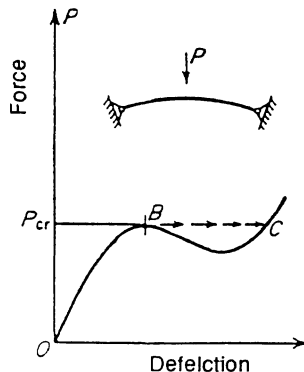


Figure (13-4) Snap-through buckling of a shallow arch with constrained ends

13.4 - An Overview of Shell Buckling

The equilibrium of thin elastic shells subjected to certain force fields may become unstable and the shell may undergo **prebuckling**, **buckling**, and **postbuckling** deformation. The occurrence of buckling in thin shells is quite probable due to the fact that the thickness to span ratio of shells is usually much lower than other structural elements.

The response of thin shells to compressive forces is essentially very different from the behavior of other structural elements such as struts, columns, and plates; some types of thin shells are extremely sensitive to geometrical and loading imperfections.

Geometrical imperfections include all deviations in the shape of the structural member from an ideally assumed geometrical configuration. Thus, a slightly crooked column, in comparison with a perfectly straight bar is considered imperfect. In the case of shells, the geometrical imperfection is marked by deviation of middle surface geometry from a conceived ideal shape.

Loading imperfections, are probable deviations of magnitudes and / or directions of applied forces from assumed values and / or directions. As an example, an eccentrically applied axial force to a straight column can be considered an imperfect loading. Loading imperfections, may be quantified by the so-called "imperfection parameters"; in the column problem, the axial force eccentricity could be chosen as an imperfection parameter.

Experiments performed on column and plates, under in-plane compressive conservative forces, have shown that such elements are relatively *insensitive* to slight geometric and loading imperfections. This is not the case in shell problems.

Buckling experiments carried out on shells have shown that some shells are very *sensitive* to geometrical and loading imperfections. Thus the buckling load of laboratory shell samples are normally smaller than the critical loads that a perfect system could sustain. This is, on one hand due the fact that the actual shells are, by production, never geometrically perfect and also that an ideally perfect conceived loading can never be produced and, on the other hand, due to **imperfection sensitivity** of real shells.

The imperfection sensitivity of shells has important analysis and design implications; to obtain a realistic estimate of buckling strength of shells, geometrical and loading imperfections must be taken into account. *Prebuckling deformation* is important and must be considered in the analysis scheme.

The comparative behavior of bars, plates, and shell forms is schematically depicted in figure (13-5). In these curves, graphs of variations in buckling load with some index of imperfection parameter are plotted.

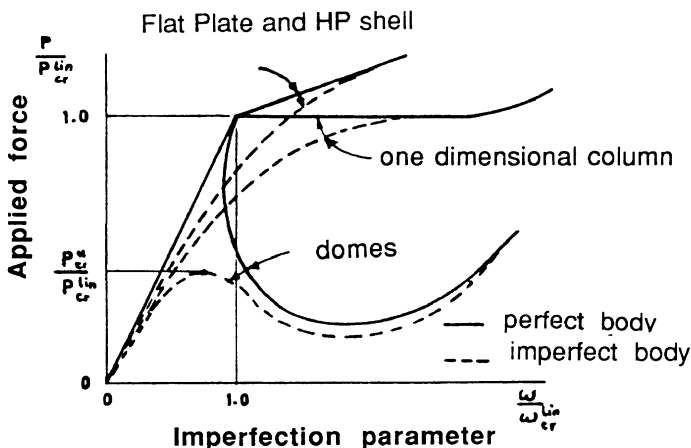


Figure (13-5) Schematic representation of buckling behavior of various structural elements

In figure (13-5), the solid lines represent the perfect system while the dotted curves demonstrate the behavior of related system in an imperfect condition. As we see, bar and plate-like elements are virtually insensitive to imperfections while domes are highly sensitive to imperfections.

It is also noted from figure (13-5) that for bar and plate problems there is no buckled form of equilibrium at loading smaller than the critical load, i.e., post buckling branch never drops below the primary prebuckling path. This means that the loss of stiffness after buckling is not great enough to cause the buckled shape to be maintained at lower load levels. This is not so for shell structures. As we see in figure (13-5), the *loss of stiffness* after buckling is so great that the buckled shapes can be maintained in static equilibrium only by the return of the system to an earlier state of loading, which may be by several orders of magnitude smaller than the buckling load.

Theories of shell buckling which are linear and based on perfect system, predict behavior which is not materialized. Linear stability theories are capable of predicting the buckling "threshold" and in particular the bifurcation point. On the other hand, it so happens that in some systems and, for example, in the imperfect systems, the bifurcation point does not essentially exist. Now, in the cases of for example, struts and columns the buckling load of imperfect system could be predicted by linear theories through the proper interpretation of the load deformation relation. For example, in some cases a drop in the value of applied force required to sustain a state of equilibrium can be interpreted as the threshold of elastic instability. However, in shell structures, with sufficiently large imperfection, the structure can pass from an unbuckled equilibrium state to a *nonadjacent* buckled equilibrium state even *before* the classical buckling load predicted by the linear theories is reached.

Figure (13-6) shows an axially compressed cylindrical shell. In this figure, OB represents the prebuckling branch and the curve BC signifies the classical postbuckling behavior of the shell. The arrows in figure (13-4) indicate possible occurrences of buckling far below the classical buckling stage. In real situations, depending on the degree of imperfections, the true buckling load could still be even smaller. It is in such situations that a behavioral trend having no distinct bifurcation point is manifested by the shell. This trend is sketched as dashed curve in figure (13-5).

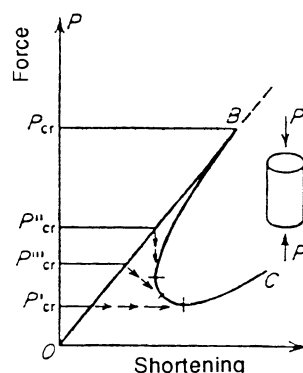


Figure (13-6) Buckling behavior of axially compressed cylindrical shell

To sum up, the prebuckling and post buckling behavior of shells form two inseparable parts of a single process that is the stability behavior of the shells. Linear theory of shells is not sufficient to predict the complete behavior and we must use **nonlinear theories** which are mathematically elaborate and analytically difficult. Nevertheless, the stability analysis of shells by means of linear theories yields some useful information about the buckling behavior of shells. Particularly, closed-form analytical expressions demonstrating the interplay of various parameters affecting the stability with appropriate correction and statistical coefficients could be implemented in those relations so that reliable design relations would be obtained. With such justification, we will now perform **linear stability analyses** of some shell forms in the following sections.

13.5 - Methodology of Linear Stability Analysis of Shells

The goal of linear stability analysis of shells is the determination of critical buckling loads and the corresponding buckled configurations. In linear stability analysis we assume the existence of a bifurcation point, and an adjacent equilibrium state. Moreover, in the analyses that follow, we assume that the shells have a perfect geometry and a perfect loading system.

The general methodology of linear buckling instability analysis of shells can be summarized as follows:

- (1) Consider a **deformed equilibrated state** infinitesimally close to the initial unbuckled configuration. The unbuckled equilibrium state is assumed to coincide with the initial geometry of the shell. These are the assumptions that are also normally made for the stability analysis of other types of structures.
- (2) Derive the **kinematic, constitutive, and equilibrium equations** for a shell element in the buckled equilibrium state. The adjacent buckled state is an equilibrium state, so the equations of equilibrium can be written for such equilibrium configuration. We assume a linear elastic and isotropic behavior.
- (3) On constructing these equations we derive a set of simultaneous **homogeneous partial differential equations** in which the **critical buckling load** appears as an unknown parameter.

The stability problem described by these equations is mathematically an **eigenvalue problem**. An eigenvalue problem is a problem which has only trivial solution unless the existing free parameter acquires certain values. With those values, the homogeneous problem has a nontrivial solution.

The special parameter values are called the **eigenvalues** or synonymously the **characteristic values**; the corresponding nonzero solutions are called the **eigenfunctions** or **characteristic functions** (eigenvectors).

From a physical point of view, the trivial solution corresponds to the prebuckled (undeformed) configuration. The eigenvalues are the values of critical buckling loads and the buckling modes are the eigenfunctions of the problem.

13.6 - Buckling of Circular Cylindrical Shells

Consider a circular cylindrical shell subjected to distributed loading. Figure (13-7) shows a complete circular cylinder and figure (13-7b) shows a sector of cylindrical shell. In both figures components (u, v, w) of the buckling displacement field are shown and their assumed positive directions are indicated.

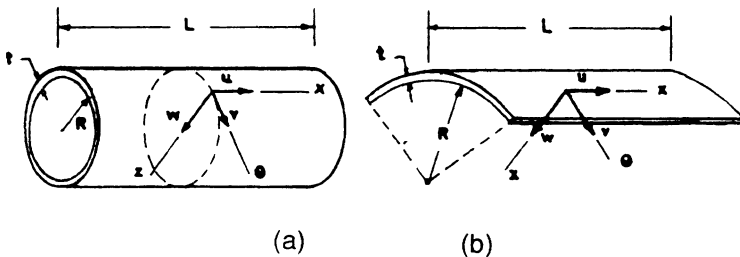


Figure (13-7) Circular cylindrical shells showing components of buckling deformations and the coordinate system

Consider an element OABC in its deformed (buckled) configuration. Figure (13-8a) shows the forces, (13-8b) the moments, with their respective derivatives. The buckled shape being infinitesimally close to prebuckled configuration, the displacement components, representing the buckled state, are infinitesimally small.

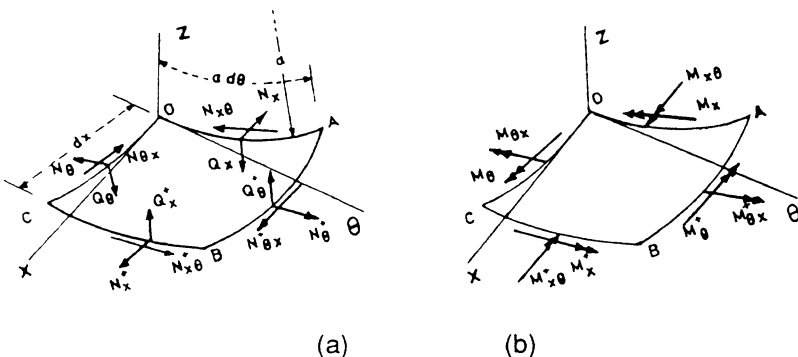


Figure (13-8) Forces on a deformed element of cylindrical shell in its buckled state

(1) Equations of equilibrium

To derive the equilibrium equation for the deformed shell element of figure (13-8), we obtain the displacement gradients necessary for projecting the forces in the various directions; these are shown in table (13-1).

Table (13-1)

Rotation of AB relative to OC	Rotation of BC relative to OA Axis of rotation	
$d\theta + \left(\frac{\partial v}{a \partial \theta} + \frac{\partial^2 w}{a \partial \theta^2} \right) dx$	$\frac{1}{a} \left(\frac{\partial v}{\partial x} + \frac{\partial^2 w}{\partial x \partial \theta} \right) dx$	About x axis
$- \left(\frac{\partial^2 w}{\partial \theta \partial x} + \frac{\partial v}{\partial x} \right) dx$	$- \frac{\partial^2 w}{\partial x^2} dx$	About y axis
$\left(\frac{\partial^2 v}{\partial \theta \partial x} - \frac{\partial w}{\partial x} \right) dx$	$\frac{\partial^2 v}{\partial x^2} dx$	About z axis

The equilibrium equation for forces along x-axis, is

$$\begin{aligned} \frac{\partial N_x}{\partial x} dx d\theta + \frac{\partial N_{\theta x}}{\partial \theta} d\theta dx - N_\theta \left(\frac{\partial^2 v}{\partial \theta \partial x} - \frac{\partial w}{\partial x} \right) d\theta dx \\ - N_{x\theta} \frac{\partial^2 v}{\partial x^2} dx d\theta - Q_x \frac{\partial^2 w}{\partial x^2} dx d\theta - Q_\theta \left(\frac{\partial^2 w}{\partial \theta \partial x} + \frac{\partial v}{\partial x} \right) d\theta dx = 0 \end{aligned}$$

Other two force equations of equilibrium can also be similarly derived. The three equilibrium equations for the forces along x, θ , z axes are

$$\begin{aligned} a \frac{\partial N_x}{\partial x} + \frac{\partial N_{\theta x}}{\partial \theta} - a Q_x \frac{\partial^2 w}{\partial x^2} - a N_{xy} \frac{\partial^2 v}{\partial x^2} - Q_\theta \left(\frac{\partial v}{\partial x} + \frac{\partial^2 w}{\partial \theta \partial x} \right) \\ - N_\theta \left(\frac{\partial^2 v}{\partial \theta \partial x} - \frac{\partial w}{\partial x} \right) = 0 \end{aligned} \quad (13-4a)$$

$$\begin{aligned} \frac{\partial N_\theta}{\partial \theta} + a \frac{\partial N_{x\theta}}{\partial x} + a N_x \frac{\partial^2 v}{\partial x^2} - Q_x \left(\frac{\partial^2 v}{\partial \theta \partial x} - \frac{\partial w}{\partial x} \right) \\ - Q_\theta \left(1 + \frac{\partial v}{a \partial \theta} + \frac{\partial^2 w}{a \partial \theta^2} \right) = 0 \end{aligned}$$

$$\begin{aligned} a \frac{\partial Q_x}{\partial x} + \frac{\partial Q_\theta}{\partial \theta} + N_{x\theta} \left(\frac{\partial v}{\partial x} + \frac{\partial^2 w}{\partial \theta \partial x} \right) + a N_x \frac{\partial^2 w}{\partial x^2} \\ + N_\theta \left(1 + \frac{\partial v}{a \partial \theta} + \frac{\partial^2 w}{a \partial \theta^2} \right) + N_{\theta x} \left(\frac{\partial v}{\partial x} + \frac{\partial^2 w}{\partial x \partial \theta} \right) + qa = 0 \end{aligned} \quad (13-4b)$$

In these equations, q is the applied radial force. The equations (13-4) include the nonlinear effects arising from projections of internal forces having smaller (higher order) magnitudes. If we neglect these nonlinear terms we obtain the equations:

$$a \frac{\partial N_x}{\partial x} + \frac{\partial N_{\theta x}}{\partial \theta} = 0 \quad (13-5a)$$

$$\frac{\partial N_\theta}{\partial \theta} + a \frac{\partial N_{x\theta}}{\partial x} - Q_\theta = 0 \quad (13-5b)$$

$$\begin{aligned} a \frac{\partial Q_x}{\partial x} + \frac{\partial Q_\theta}{\partial \theta} + N_\theta + a N_x \frac{\partial^2 w}{\partial x^2} + N_{x\theta} \left(\frac{\partial v}{\partial x} + \frac{\partial^2 w}{\partial \theta \partial x} \right) \\ + N_\theta \left(\frac{1}{a} \frac{\partial v}{\partial \theta} + \frac{1}{a} \frac{\partial^2 w}{\partial \theta^2} \right) + N_{\theta x} \left(\frac{\partial v}{\partial x} + \frac{\partial^2 w}{\partial x \partial \theta} \right) = -qa \end{aligned} \quad (13-5c)$$

In addition to the force equations of equilibrium, there are three moment equations; they are

$$a \frac{\partial M_{x\theta}}{\partial x} - \frac{\partial M_\theta}{\partial \theta} - a M_x \frac{\partial^2 v}{\partial x^2} - M_{\theta x} \left(\frac{\partial^2 v}{\partial \theta \partial x} - \frac{\partial w}{\partial x} \right) + a Q_\theta = 0 \quad (13-6a)$$

$$\frac{\partial M_{\theta x}}{\partial \theta} + a \frac{\partial M_x}{\partial x} + a M_{x\theta} \frac{\partial^2 v}{\partial x^2} - M_y \left(\frac{\partial^2 v}{\partial \theta \partial x} - \frac{\partial w}{\partial x} \right) - Q_x a = 0 \quad (13-6b)$$

$$M_x \left(\frac{\partial v}{\partial x} + \frac{\partial^2 w}{\partial x \partial \theta} \right) + a M_{x\theta} \frac{\partial^2 w}{\partial x^2} + M_{\theta x} \left(1 + \frac{\partial v}{a \partial \theta} + \frac{\partial^2 w}{a \partial \theta^2} \right) - M_\theta \left(\frac{\partial v}{\partial x} + \frac{\partial^2 w}{\partial x \partial \theta} \right) + a (N_{x\theta} - N_{\theta x}) = 0 \quad (13-6c)$$

If we discard nonlinear terms, we obtain the linearized moment equations of equilibrium:

$$\begin{aligned} aQ_\theta &= \frac{\partial M_\theta}{\partial \theta} - a \frac{\partial M_{x\theta}}{\partial x} \\ aQ_x &= \frac{\partial M_{\theta x}}{\partial \theta} + a \frac{\partial M_x}{\partial x} \\ N_{x\theta} &= N_{\theta x} \end{aligned} \quad (13-7)$$

Now we combine the two set of equilibrium equations (13-5) and (13-7); we eliminate Q_θ and Q_x and we neglect the effect of shear force Q_θ in equation (13-5b). We obtain the following condensed equations of equilibrium.

$$\begin{aligned} a \frac{\partial N_x}{\partial x} + \frac{\partial N_{\theta x}}{\partial \theta} &= 0 \\ \frac{\partial N_\theta}{\partial \theta} + a \frac{\partial N_{x\theta}}{\partial x} &= 0 \\ a^2 \frac{\partial^2 M_x}{\partial x^2} + a \frac{\partial^2 M_{\theta x}}{\partial x \partial \theta} - a \frac{\partial^2 M_{x\theta}}{\partial x \partial \theta} + \frac{\partial^2 M_\theta}{\partial \theta^2} \\ - a N_\theta + a^2 N_x \frac{\partial^2 w}{\partial x^2} + a N_{x\theta} \left(\frac{\partial v}{\partial x} + \frac{\partial^2 w}{\partial \theta \partial x} \right) \\ + N_\theta \left(\frac{\partial v}{\partial \theta} + \frac{\partial^2 w}{\partial \theta^2} \right) + a N_{\theta x} \left(\frac{\partial v}{\partial x} + \frac{\partial^2 w}{\partial x \partial \theta} \right) &= -qa^2 \end{aligned} \quad (13-8)$$

We derived the constitutive and kinematic relations in chapter 4; we repeat them here. The relations (4-14), (4-15), and (4-16) (with coupling terms dropped) are rewritten as follows:

(2) Constitutive relations:

$$\begin{aligned}
 N_x &= D(\epsilon_x + v\epsilon_\theta) \\
 N_\theta &= D(\epsilon_\theta + v\epsilon_x) & D = \frac{Et}{12(1-v^2)} \\
 N_{x\theta} &= D \frac{1-v}{2} \gamma_{x\theta} \\
 M_x &= K(\psi_x + v\psi_\theta) \\
 M_\theta &= K(\psi_\theta + \theta\psi_x) & K = \frac{Et^3}{12(1-v^2)} \\
 M_{x\theta} &= K(1-v)\psi_{x\theta}
 \end{aligned} \tag{13-9}$$

(3) Kinematic relations:

$$\begin{aligned}
 \epsilon_x &= \frac{\partial u}{\partial x}, \quad \epsilon_\theta = \frac{1}{a} \left(\frac{\partial v}{\partial \theta} + w \right), \quad \gamma_{x\theta} = \frac{1}{a} \frac{\partial u}{\partial \theta} \\
 \psi_x &= \frac{\partial \beta_x}{\partial x} = - \frac{\partial^2 w}{\partial x^2} \\
 \psi_\theta &= \frac{1}{a} \frac{\partial \beta_\theta}{\partial \theta} = - \frac{1}{a^2} \frac{\partial w}{\partial \theta} \\
 \psi_{x\theta} &= \frac{1}{2} \left(\frac{1}{a} \frac{\partial \beta_x}{\partial \theta} + \frac{\partial \beta_\theta}{\partial x} \right)
 \end{aligned} \tag{13-10}$$

If we combine the governing equations (13-8), (13-9), and (13-10), we arrive at a set of equations in terms of displacement components. However, we only substitute part of the constitutive and kinematic relations into the equilibrium equations to get the following relations:

$$a \frac{\partial N_x}{\partial x} + \frac{\partial N_{x\theta}}{\partial \theta} = 0 \quad (13-11a)$$

$$a \frac{\partial N_{x\theta}}{\partial x} + \frac{\partial N_\theta}{\partial \theta} = 0 \quad (13-11b)$$

$$K \nabla^4 w + \frac{1}{a} N_\theta - (N_x \frac{\partial^2 w}{\partial x^2} + \frac{2}{a} N_{x\theta} \frac{\partial^2 w}{\partial x \partial \theta} + \frac{1}{a^2} N_\theta \frac{\partial^4 w}{\partial \theta^2}) = q \quad (13-11c)$$

in which

$$\nabla^4 w = \frac{\partial^4 w}{\partial x^4} + \frac{2}{a^2} \frac{\partial^4 w}{\partial x^2 \partial y^2} + \frac{1}{a^4} \frac{\partial^4 w}{\partial \theta^4} \quad (13-12)$$

Equations (13-11) are a set of nonlinear governing relations suitable for stability analysis of quasi-shallow cylindrical shells.

To obtain the linear stability equations, we drop the nonlinear terms shown in parenthesis in equation (13-11c) we obtain

$$a \frac{\partial N_x}{\partial x} + \frac{\partial N_{x\theta}}{\partial \theta} = 0 \quad (13-13a)$$

$$a \frac{\partial N_{x\theta}}{\partial x} + \frac{\partial N_\theta}{\partial \theta} = 0 \quad (13-13b)$$

$$K \nabla^4 w + \frac{1}{a} N_\theta = q \quad (13-13c)$$

Now, we use the remaining constitutive and kinematic relations to express the forces N_x , N_θ , $N_{x\theta}$ in terms of the displacement components. If we carry out this substitution, we find the following set of simultaneous differential equations in terms of the displacement components.

$$a^2 \frac{\partial^2 u}{\partial x^2} + \frac{1-v}{2} \frac{\partial^2 u}{\partial \theta^2} + \frac{1+v}{2} a \frac{\partial^2 v}{\partial x \partial \theta} + va \frac{\partial w}{\partial x} = 0 \quad (13-14)$$

$$\frac{1+v}{2} a \frac{\partial^2 u}{\partial \theta \partial \theta} + \frac{1-v}{2} a \frac{\partial^2 v}{\partial x^2} + \frac{\partial^2 v}{\partial \theta^2} + \frac{\partial w}{\partial \theta} = 0$$

$$K \nabla^4 w + \frac{1}{a^2} D \left(\frac{\partial v}{\partial \theta} + w + va \frac{\partial u}{\partial x} \right) = q$$

By performing certain algebraic manipulations, we can achieve a partial decoupling of these equations. If we eliminate function variables u and v from the those equations, and rearrange the first two relations, we obtain

$$\nabla^4 u = - \frac{v}{a} \frac{\partial^3 w}{\partial x^3} + \frac{1}{a^2} \frac{\partial^3 w}{\partial x \partial \theta^2} \quad (13-15a)$$

$$\nabla^4 v = - \frac{2+v}{a^2} \frac{\partial^3 w}{\partial x^2 \partial \theta} - \frac{1}{a^4} \frac{\partial^3 w}{\partial \theta^3} \quad (13-15b)$$

$$K \nabla^8 w + \frac{1-v^2}{a^2} D \frac{\partial^4 w}{\partial x^4} = \nabla^4 q \quad (13-15c)$$

in which

$$\nabla^8 w = \nabla^4 (\nabla^4 w)$$

Relations (13-10) to (13-13) constitute another form of the governing stability equations of quasi-shallow cylindrical shells. The membrane shell equations can be easily derived from these relations by setting the bending stiffness, K , equal to zero. If we do so, we obtain the equations

$$a \frac{\partial N_x}{\partial x} + \frac{\partial N_{x\theta}}{\partial \theta} = 0$$

$$a \frac{\partial N_{x\theta}}{\partial x} + \frac{\partial N_\theta}{\partial \theta} = 0 \quad (13-16)$$

$$N_\theta = qa$$

These equations express the governing relations of the cylindrical shell in its unbuckled state. As we recall, we assumed that there is no bending deformation in the prebuckled state. This assumption is compatible with the premises of linear stability theory of shells.

By solving the equations (13-15) we can determine the membrane force field in the prebuckled state.

Having obtained the force field in the prebuckled state of the shell, we can perform linear stability analysis. At this stage, the prebuckled force field N_x , N_θ , $N_{x\theta}$ are known, so the terms in parenthesis of equation (13-11) are no longer nonlinear. We must distinguish between the unknown hoop force N_θ (in the buckled state) appearing outside the parenthesis and the known parenthesized prebuckled hoop force, denoted by the same symbol.

From the linearized version of the stability equations (13-11) we can obtain the stability equations for flat plates subjected to in-plane as well as out of plane loading, by letting $a \rightarrow \infty$. As the result the second term in equation (13-11c) would be eliminated.

13.7 - Buckling of Circular Cylinders under Axial Force

13.7.1 - General Modes of Cylinders Buckling under Axial force

In a complete circular cylindrical shell of intermediate length, subjected to axial force (uniformly distributed on the end section) there are three possible modes of buckling:

(1) Ring buckling

Ring buckling consists of an axisymmetric deformation with longitudinal waves along the length of the cylinder, figure (13-9a); there are no axially oriented nodes.

(2) Chessboard mode

The so-called "chess-board" mode of buckling has longitudinal and circumferential waves of deformation; the deformed shape of the cylinder will consist of a regular pattern of "inward" and "outward" deformations resembling a chess-board, figure (13-9b).

(3) Diamond-shape buckling

The so-called "diamond shape" buckling of cylinders occurs in the post buckling stage of loading. Under certain conditions, the critically loaded shell "snaps" from one equilibrium shape to another which requires less energy to be maintained. The second deformed shape has a pattern of "diamond type" inward and outward deformations, figure (13-9c).

The length of the cylinder is one of the main parameters influencing the general buckling mode; **ring modes** occur in very short cylinders, figure (13-10a); **diamond modes** occur in moderately long cylinders, figure (13-10b).

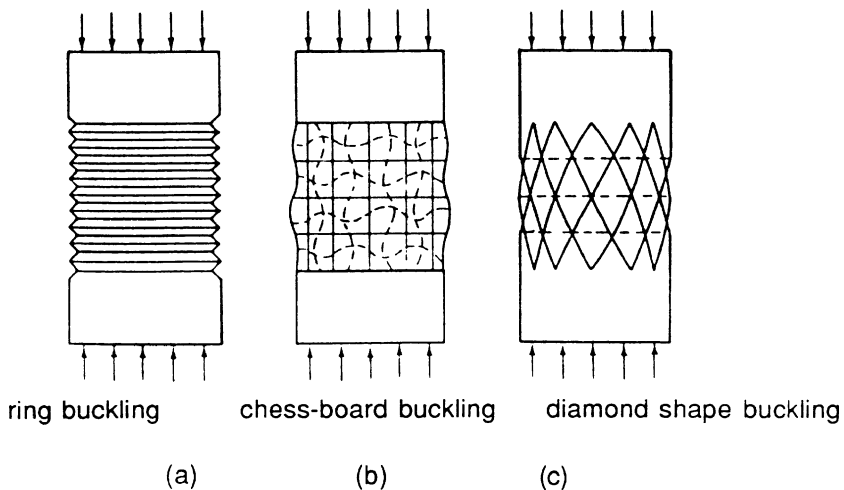


Figure (13-9) Theoretical buckling modes of circular cylindrical shells with intermediate length, (a) ring buckling, (b) chessboard buckling, (c) diamond pattern of buckled shape

If the cylinder is very long, another nonsymmetric "overall" buckling may occur, figure(13-10c). This mode of buckling occurs mostly in tubular members and the piping systems under axial loading.

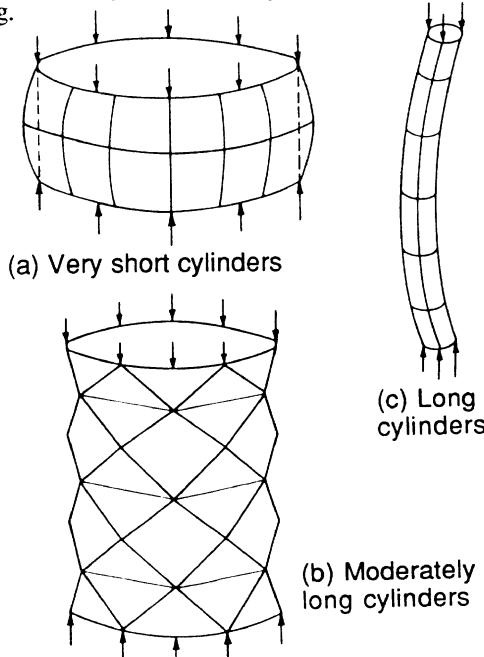


Figure 13-10 Effect of cylinder length the buckling modes, (a) very short cylinder, (b) moderately long cylinder, (c) very long cylinder

13.7.2 - Buckling of Axially Loaded Cylindrical Shells

We assume that the membrane forces N_θ and $N_{\theta x}$ are small compared with the axial force N_x and thus can be neglected. Implementing this assumption, and neglecting the nonlinear terms in equations (13-4) and (13-6), we obtain the equilibrium equations

$$a \frac{\partial N_x}{\partial x} + \frac{\partial N_{\theta x}}{\partial \theta} = 0 \quad (13-17a)$$

$$\frac{\partial N_\theta}{\partial \theta} + a \frac{\partial N_{x\theta}}{\partial x} + a N_x \frac{\partial^2 v}{\partial x^2} + \frac{\partial M_{x\theta}}{\partial x} - \frac{\partial M_\theta}{a \partial \theta} = 0 \quad (13-17b)$$

$$aN_x \frac{\partial^2 w}{\partial x^2} + N_\theta + a \frac{\partial^2 M_x}{\partial x^2} + \frac{\partial^2 M_{\theta x}}{\partial x \partial \theta} + \frac{\partial^2 M_\theta}{a \partial \theta^2} - \frac{\partial^2 M_{x\theta}}{\partial x \partial \theta} = 0 \quad (13-17c)$$

Using the constitutive and kinematic relations we can express these equations in terms of displacement components. We define the following parameters:

$$\alpha = \frac{t^2}{12a^2}, \quad N = \frac{N_x(1-v^2)}{Et} \quad (13-18)$$

After substituting expressions (13-9) and (13-10) into equations (13-17), we obtain

$$\frac{\partial^2 u}{\partial x^2} + \frac{1+v}{2a} \frac{\partial^2 v}{\partial x \partial \theta} - \frac{v}{a} \frac{\partial w}{\partial x} + \frac{1-v}{2} \frac{\partial^2 u}{a^2 \partial \theta^2} = 0 \quad (13-19a)$$

$$\frac{1+v}{2} \frac{\partial^2 u}{x} + \frac{a(1-v)}{2} \frac{\partial^2 v}{\partial x^2} + \frac{\partial^2 v}{a \partial \theta^2} - \frac{\partial w}{a \partial \theta} \quad (13-19b)$$

$$+ \alpha \left[\frac{\partial^2 w}{a \partial \theta^2} + \frac{\partial^3 w}{a \partial \theta^3} + a \frac{\partial^3 w}{\partial x^2 \partial \theta} + a(1-v) \frac{\partial^2 v}{\partial x^2} \right] - aN \frac{\partial^2 v}{\partial x^2} = 0$$

$$-aN \frac{\partial^2 w}{\partial x^2} + v \frac{\partial u}{\partial x} + \frac{\partial v}{a \partial \theta} - \frac{w}{a} \quad (13-19c)$$

$$- \alpha \left[\frac{\partial^3 u}{a \partial \theta^3} + (2-v)a \frac{\partial^3 v}{\partial x^2 \partial \theta} + a \frac{\partial^4 w}{\partial x^4} + \frac{\partial^4 w}{a \partial \theta^4} + 2a \frac{\partial^4 w}{\partial x^2 \partial \theta^2} \right] = 0$$

These stability equations must be complemented by the appropriate boundary conditions. The boundary conditions would consist of prescription of proper combinations of the displacement components, their derivatives, and the end forces.

As a particular problem, we assume the cylinder to have simple end conditions:

$$w = 0 \quad , \quad \frac{\partial^2 w}{\partial x^2} = 0$$

To solve the homogeneous simultaneous partial differential equations (13-19) for the shell with simple end conditions, we proceed as follows. Consider a series solution of the form:

$$\begin{aligned} u &= \sum_{nm} A \sin n\theta \cos \frac{m\pi x}{l} \\ v &= \sum_{nm} B \cos n\theta \sin \frac{m\pi x}{l} \\ w &= \sum_{nm} C \sin n\theta \sin \frac{m\pi x}{l} \end{aligned} \quad (13-20)$$

This assumed solution satisfies the prescribed end conditions. If we substitute the expressions (13-20) into equations (13-19), and perform the necessary algebraic manipulations assuming $\lambda = (\pi m a / l)$, for one term of series expansion, we obtain

$$\begin{aligned} A(\lambda^2 + \frac{1-v}{2}n^2) + B\frac{n(1+v)}{2}\lambda + Cv\lambda &= 0 \\ A\frac{n(1+v)}{2}\lambda + B\left[\frac{(1-v)}{2}\lambda^2 + a^2 + \alpha(1-v)\lambda^2 + \alpha n^2 - \lambda^2 N\right] \\ + C[n + \alpha n(n^2 + \lambda^2)] &= 0 \\ Av\lambda + Bn[1 + \alpha[n^2 + (2-v)\lambda^2]] \\ + C[1 - \lambda^2 N + \alpha(\lambda^2 + n^2)^2] &= 0 \end{aligned}$$

These homogeneous algebraic equations can be rewritten in matrix form:

$$\begin{bmatrix} (\lambda^2 + \frac{1-v}{2}n^2) & \frac{n(1+v)}{2}\lambda & v\lambda \\ \frac{n(1+v)}{2}\lambda & \frac{1-v}{2}\lambda^2 + n^2 + \alpha(1-v)\lambda^2 + \alpha n^2 - \lambda^2 N & n + \alpha n(n^2 + \lambda^2) \\ v\lambda & n(1 + \alpha[n^2 + (2-v)\lambda^2]) & 1 - \lambda^2 N + \alpha(\lambda^2 + n^2)^2 \end{bmatrix} \begin{bmatrix} A \\ B \\ C \end{bmatrix} = 0 \quad (13-21)$$

This system of equations constitutes an *eigenvalue* problem. The undetermined loading parameter N plays the role of *eigenvalue*. One solution to this equation is: A = B = C = 0; this corresponds to the unbuckled state. To obtain a nontrivial solution, we must set the determinant of this equation to zero; if we neglect small terms, and solve the resulting algebraic equation for N, we obtain

$$N_{cr} = \frac{N_x(1 - v^2)}{Et} = \frac{R}{S} \quad (13-22)$$

Where

$$R = (1 - v^2) \lambda^4 + \alpha [(n^2 + \lambda^2)^4 - (2 + v)(3 - v) \lambda^4 n^2] \quad (13-23)$$

$$+ 2 \lambda^4 (1 - v^2) - \lambda^2 n^4 (7 + \lambda) + \lambda^2 n^2 (3 + v) + n^4 - 2 n^6]$$

$$S = \lambda^2 \{ (n^2 + \lambda^2)^2 + \frac{2}{1-v} (\lambda^2 + \frac{1-v}{2} n^2) [1 + \alpha (n^2 + \lambda^2)^2] \quad (13-24)$$

$$- \frac{2v^2 \lambda^2}{1-v} + \frac{2\alpha}{1-v} (\lambda^2 + \frac{1-v}{2} n^2) [n^2 + (1 - v) \lambda^2]\}$$

This analysis includes the *ring* and *chessboard* buckling modes as special cases. For *chessboard* buckling modes, we take the length parameter, l, very large in (13-22); we find

$$N_{cr} = \frac{N_x(1 - v^2)}{Et} = \alpha \frac{(n^2 + \lambda^2)^2}{\lambda^2} + \frac{(1 - v^2) \lambda^2}{(n^2 + \lambda^2)^2} \quad (13-25)$$

N_{cr} is a function of λ ; the value of λ which would yield the minimum value of critical load, N_{cr} , is given by

$$\frac{(n^2 + \lambda^2)^2}{\lambda^2} = \sqrt{\frac{1 - v^2}{\alpha}} = \frac{2a}{t} \sqrt{3(1 - v^2)} \quad (13-26)$$

The minimum buckling load is

$$N_{cr} = \frac{N_x(1 - v^2)}{Et} = 2a \sqrt{\alpha(1 - v^2)} \quad (13-27)$$

and the minimum axial stress for *chessboard* buckling in the cylinder is

$$\sigma_{cr} = \frac{(N_x)_{cr}}{t} = \frac{E}{\sqrt{3(1-\nu^2)}} \frac{t}{a} \quad (13-28)$$

The corresponding chessboard buckling mode, i.e., the eigenfunction, is determined by substituting (13-27) into equation (13-21). The resulting radial displacement component is

$$w = CS \sin \frac{m\pi x}{l} \sin n\theta \quad (13-29)$$

The first mode of radial deformation is obtained by setting $m = 1$; it consists of a half-sine wave in the longitudinal direction accompanied by $2n$ half-sine waves in the circumferential direction. The result is a *chessboard* pattern of buckling.

Note that in this linear stability analysis, as in any other, the amplitude of buckled shape remains undetermined; this can be found by using a nonlinear postbuckling theory.

The *ring* mode of buckling can be studied in a similar fashion. It so happens that, for long cylindrical shells, the critical stress values for the *chessboard* and *ring* bucklings are equal.

To render the buckling formula (13-28) more useful for practical shell design problems, we must apply some correction factors. For example, for reinforced concrete cylindrical shells the following corrective coefficient has been proposed:

$$c = 1 - 0.9(1 - e^{-\frac{l}{16}\sqrt{\frac{a}{t}}}) \quad (13-30)$$

This correction is said to be valid in the following range:

$$0.5 < \frac{l}{a} < 5$$

$$100 < \frac{a}{t} < 3000$$

The buckling formula (13-28) can be used for estimation of cylindrical shells subjected to bending. In that case, the following correction factor has been proposed:

$$c = 1 - 0.73(1 - e^{-\frac{l}{16}\sqrt{\frac{a}{t}}}) \quad (13-31)$$

Design buckling strength can be estimated by multiplying the theoretical values by these correction factors.

13.7.3 - Buckling of Cylindrical Shells under External Pressure

The buckling analysis of circular cylindrical shells subjected to uniform external pressure is similar to the previous section. In this case, however, the effect of hoop forces are more important, so hoop effects must be retained in the governing equations. In this section the details of stability analysis will be omitted and only the results will be presented.

(1) Very long cylinders with free ends:

Critical buckling external pressure:

$$p_{cr} = \frac{1}{4(1-\nu^2)} E \left(\frac{t}{a}\right)^3 \quad (13-32)$$

Critical buckling hoop stress:

$$\sigma_{cr} = \frac{1}{4(1-\nu^2)} E \left(\frac{t}{a}\right)^2 \quad (13-33)$$

(2) Short cylinder with ends held circular, but otherwise unconstrained:

Critical buckling pressure:

$$p_{cr} = 0.807 \sqrt[4]{\frac{1}{(1-\nu^2)^3} \left(\frac{L}{a}\right)^2} E \frac{t^2}{L a} \quad (13-34)$$

(3) Closed-end cylinders subjected to both axial and lateral pressure (axisymmetric buckling):

Critical buckling pressure:

$$p_{cr} = \frac{2 E}{\sqrt{3(1-\nu^2)}} \left(\frac{t}{a}\right)^2 \quad (13-35)$$

Critical buckling hoop stress:

$$\sigma_{cr} = \frac{E}{\sqrt{3(1-\nu^2)}} \left(\frac{t}{a}\right) \quad (13-36)$$

13.8 - Buckling of Concrete Cylindrical Roofs

The mode of buckling of concrete cylindrical roofs depends on the applied loading as well as the span to length ratio of the cylinder:

- (1) For **long cylinders** ($l_1 / l_2 > 4$) the beam action of the shell is strong and hence the longitudinal bending stresses are predominant. In these types of shells, the instability mode consists of buckling of longitudinal strips in the mid-length of the shell at its crown region, figure (13-11a). The first mode of buckling consists of a single localized wave in the longitudinal and transverse direction.
- (2) For **short cylinders** ($l_1 / l_2 < 1$), the arch action becomes important: the applied loads are carried predominantly in the transverse direction. The mode of instability consists of buckling waves appearing in the transverse direction, figure (13-11b). The action of such shells resembles that of cylinders under lateral pressure.
- (3) For cylinders with **intermediate lengths** ($1 < l_1 / l_2 < 4$), the applied loads are transferred both in the longitudinal and transverse directions; the buckling modes of these types of shells are influenced by both the beam and the arch actions, figure (13-11c).

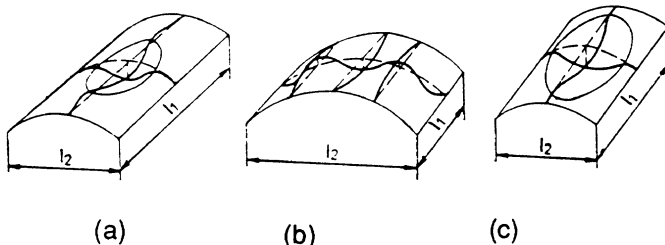


Figure (13-11) Buckling modes of roof cylinders, (a) long shell, (b) short shell, (c) Intermediate shell

One of the phenomena that can occur in postbuckling of open cylinders, as well as closed tubes, is the *flattening* of such shells. In open cylinders, due to longitudinal bending, the longitudinal edges are pushed outwards, causing an increase of the shell radius. For closed tubes this phenomenon is called the *Brazier effect*. The longitudinal stresses are responsible for this particular phenomenon.

13.9 - Buckling Formulas for Shells of Revolution

Shells of revolution subjected to applied loading may buckle if the applied load is increased beyond a certain limit. To perform a stability analysis of the shells of revolution, the governing equations of a shell element in its deformed (buckled) state must be derived. In this section, detailed stability analysis of such shells will not be carried out, but merely the results of linear stability analysis of shells of revolution will be presented.

(1) Complete spherical shell under uniform external pressure

Critical buckling pressure:

$$p_{cr} = \frac{2E}{\sqrt{3(1-\nu^2)}} \left(\frac{t}{a}\right)^2 \quad (13-37)$$

Critical buckling stress:

$$\sigma_{cr} = \frac{E}{\sqrt{3(1-\nu^2)}} \left(\frac{t}{a}\right) \quad (13-38)$$

(2) Long conical shell with semi-vortex angle α under axial vortex load P (axisymmetric buckling):

Critical buckling pressure:

$$P_{cr} = \frac{2\pi E \cos^2 \alpha}{\sqrt{3(1-\nu^2)}} \quad (13-39)$$

13.10 - Buckling of Domes

13.10.1 - Buckling Modes of Domes

The spherical dome is part of a complete spherical shell. Thus we can use the formulas presented for complete spherical shells to find the buckling loads of domes. However, there are some differences in the buckling behaviors of domes and complete spheres:

- (1) In complete spherical shells, the instability of the shell could inflict the whole shell, figure (13-12a), or may be of snap-through type confined a limited region, figure (13-12b). The occurrence of one of these two instability modes depends mainly on the thickness, shell radius, and the central angle (or equivalently the base radius, r_0) of the dome. As an approximate formula, we may say that if $r_0 > 3.8 \sqrt{t}$ then the buckling would be local, otherwise it would extend to the whole shell.

(2) For spherical domes, the loss of stability can appear by symmetrical, figure (13-12a), or unsymmetrical deformations, figure (13-12b). Both of these instability modes can extend to the whole shell surface.

(3) The postcritical behavior of spherical domes differs from that of complete spheres. A dome can pass to a postbuckling equilibrium position produced by deformations much larger than those of the corresponding complete sphere.

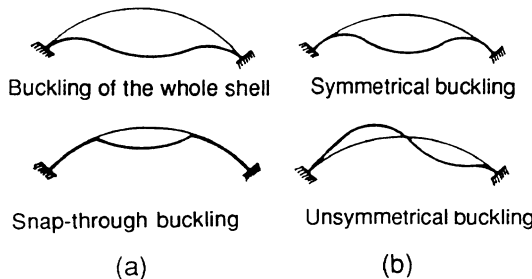


Figure (13-12) Symmetrical and non symmetrical buckling modes of the domes.

13.10.2 - Buckling of Concrete Domes

Domes are doubly curved, synclastic, and nondevelopable surfaces. Therefore, they are generally very strong and highly stable. The critical stability loads of concrete domes are usually much higher than those of concrete shells with single curvature. Nevertheless, thin concrete domes with large spans are susceptible to buckling; indeed the buckling considerations are one of the main design criteria of such shells.

In the previous section, we presented some theoretical buckling loads for spherical shells. In this section, we complement those relations by additional approximate formulas suitable for designing concrete domes.

The theoretical buckling load for a doubly curved elastic shell having the values of principal curvature $1/R_1$ and $1/R_2$, under the dead load, is

$$q_{cr} = \frac{2Et^2}{\sqrt{3(1-\nu^2)}} \frac{1}{R_1} \frac{1}{R_2} \quad (13-40)$$

In this relation, q_{cr} is the intensity of buckling dead load, E and ν are the Young's modulus and Poisson's ratio, respectively.

For a spherical shell, in which $R_1 = R_2 = a$, relation (13-40) yields:

$$q_{cr} = \frac{2E}{\sqrt{3(1-\nu^2)}} \left(\frac{t}{a}\right)^2 = \alpha E \left(\frac{t}{a}\right)^2, \quad \alpha = \frac{2}{\sqrt{3(1-\nu^2)}} \quad (13.41)$$

Experimental investigations yield buckling loads much less than the theoretical ones given here. This is due to imperfection sensitivity of shells which dramatically affects the stability behavior of shells. On this basis, some building codes recommend values of a *reduction parameter* for design purposes which lies in the region 0.05 and 0.1.

Based on these considerations, a more practical formula for the buckling strength of shells with double curvature would be

$$q_{cr} = 0.05 E \frac{t^2}{R_1 R_2} \quad (13-42)$$

If the ratio of elastic parameter E to the 28 day compressive strength of concrete cylindrical sample (denoted by f'_c) is assumed to be 1000, then formula (13-42) gives

$$\frac{q_{cr}}{f'_c} = 50 \frac{t^2}{R_1 R_2}$$

which, for a spherical shell of radius a, yields

$$\frac{q_{cr}}{f'_c} = 50 \left(\frac{t}{a} \right)^2 \quad (13-43)$$

As an example, for a shell having $t/a = 1/200$, we would have

$$\frac{q_{cr}}{f'_c} = 50 \times \frac{1}{4} \times 10^{-4}$$

and if $f'_c = 200 \text{ kg/cm}^2$, then

$$q_{cr} = 2.5 \text{ Ton/m}^2$$

The buckling load of the shell is quite high, several times higher than its service load.

13.11 - Buckling of Hyperbolic Paraboloid Shells

13.11.1 - General Buckling Behavior of HP Shells

As we have seen, in a HP shell under lateral loading, the membrane force field along the straight line generators consists of a state of relatively pure shear. This shear gives rise to a compressive and a tensile principal stresses in the diagonal directions. Thus, the loss of stability of a hyperbolic paraboloid shell is expected to occur in the compressed direction. This is in fact the case and the resulting buckling mode consists of half waves as well as complete waves along one of the diagonals, Figure (13-13a).

A compressed strip of the shell, cut along the compressed direction, could be conceived to act as an arch on an elastic foundation, figure (13-13b). This foundation effect comes from the restoring action of the stretched strips in the opposite direction, figure (13-13c).

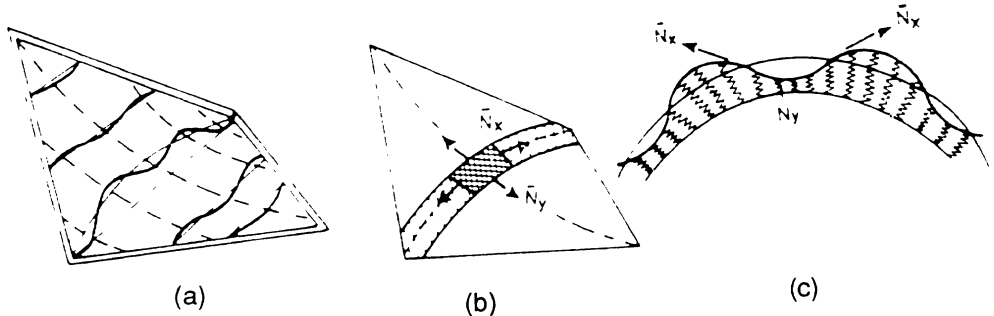


Figure (13-13) Buckling behavior of hyperbolic paraboloid shells, (a) the buckling mode, (b) elastic foundation model of interacting arches, (c) internal compressive and tensile forces

13.11. 2 - Buckling Formulas for Hyperbolic Paraboloid Shells

Based on linear stability analysis of HP shell roofs, the details of which are not given here, some approximate buckling formulas for the HP shell can be derived. These formulas will be presented in the following.

Consider a HP shell roof shown in figure (13-14), subjected to a uniformly distributed vertical load of intensity p . If t indicates the shell thickness and the parameters a , b , and f represent the overall dimensions, then the intensity of critical buckling load of this shell can be expressed as

$$p_{cr} = \frac{2 E}{\sqrt{3(1-v^2)}} \left(\frac{t}{c}\right)^2 \quad (13-44)$$

wherein, $c = a b / f$ could be interpreted as being the *torsion curvature* of the HP shell. With such interpretation, this formula, resembles that given for a complete spherical shell.

The length of half-wave of buckling produced in the compressed direction can be expressed by the following approximate formula:

$$\Lambda = \frac{2 E}{2 \sqrt{3(1-v^2)}} \sqrt{a b} \sqrt{\frac{t}{f}} \quad (13-45)$$

Experiments performed on hyperbolic paraboloid shells confirm the relations presented in this section. Some of the conclusions of experimental works are,

- (1) The loss of stability is produced by formation of waves in the compressive direction.
- (2) Initial imperfections reduce the critical loading.
- (3) In the postbuckling stage, redistribution of internal forces takes place.
- (4) Due to shear transfer to the edge beams, compressive forces are produced in the edge members. On some occasions, the limit of critical loading is governed by the buckling of the edge members.

Problems

P 13.1 - A circular ring of radius R and cross-sectional bending rigidity EI, as shown in figure (P13-1), is subjected to constant external dead pressure loading , p. The dotted curve show a possible mode of buckling of this ring. Show that the lowest critical pressure of this ring can be obtained by the following formula:

$$p_{cr} = \frac{3EI}{R^3}$$

Find the expression for the corresponding buckling modes of this ring.

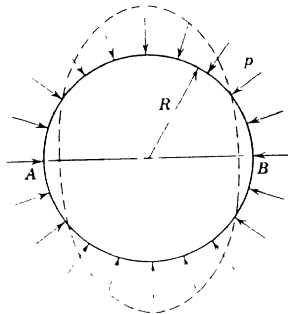
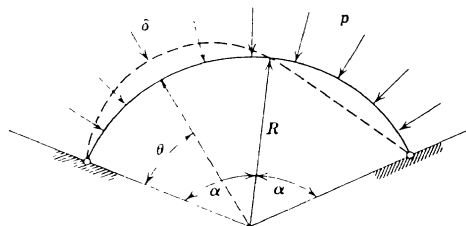


Figure (P 13-1)

P 13.2 - A segment of a circular ring, of radius R and central angle 2α and bending stiffness EI, forms an arch with hinged ends as shown in figure (P13-2). This arch is subjected to a uniform dead pressure loading with intensity p. A possible mode of buckling of this are is shown by the dotted line in this figure.Show that the intensity of lowest critical pressure is obtainable from the following formula:

$$p_{cr} = \frac{3EI}{R^3} \left(\frac{\pi^2}{\alpha^2} - 1 \right)$$



P 13.3 - A thin-walled circular cylindrical tube, of thickness t and internal radius r , is subjected to internal pressure, p , via a compressed piston on which the force F is acting, figure (p13-3). Assume that the cylinder is long and there is no friction between the piston and the cylinder wall. Could this cylinder buckle under internal pressure?. If so, what is the critical internal pressure which causes the overall buckling of this cylinder?.

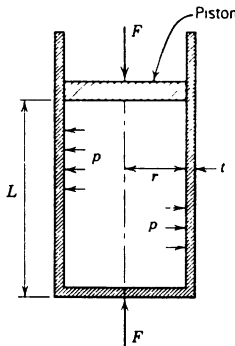


Figure (P 13-3)

References for Chapter Thirteen

- 13.1 - M. Farshad, *Shell Structures*, Vol. I, 1986, Vol. II, 1987, Shiraz University Publications, Shiraz
- 13.2 - S. P. Timoshenko and J. H. Gere, *Theory of Elastic Stability*, McGraw-Hill Book Co., New York, 1961
- 13.3 - J. G. A. Croll and A.C. Walker, *Elements of Structural Stability*, The Macmillan Press Ltd, London, 1972
- 13.4 - I. Kollar and E. Dulacska, *Buckling of Shells for Engineers*, John Wiley & Sons, Toronto, 1984
- 13.5 - R. Narayanan (ed), *Shell Structures-Stability and Strength*, Elsevier Applied Science Publishers, London, 1985
- 13.6 - W. Flügge (ed), *Handbook of Engineering Mechanics*, McGraw-Hill ,New York, 1962
- 13.7 - E. Ramm, (editor), *Buckling of Shells*, Proceedings of a State of Art Colloquium, Springer Verlag, Berlin, 1982
- 13.8 - D.O. Brush, and Bo. O. Almroth, *Buckling of Bars, Plates, and Shells*, McGraw-Hill, Book Company, New York, 1975
- 13.8 - V. Gioncu, *Thin Reinforced Concrete Shells*, John Wiley & Sons, Chichester, 1979
- 13.9 - L. H. Donnel, *Beams, Plates and Shells*, McGraw-Hill Book Company, New York, +976
- W. T. Koiter, (editor), *The Theory of The Elastic Shells*, Proc. IUTAM Symp., North-Holland, Amsterdam, 1960
- J. M. Hutchinson, and W. T. Koiter, Post-Buckling Theory, Applied Mechanics Review, Vol. 12, PP 1353-1366, 1970

Appendix A

Notation:

p_E	Intensity of dead loading (per unit area of shell middle surface)
p_s	Intensity of snow load (per unit area of horizontal projection)
$p = \gamma H$	Hydrostatic pressure (normal to the shell middle surface); H is the fluid height and γ is the specific weight of the fluid
p_w	Intensity of wind loading, per unit area of the projection normal to the wind direction
P_L	Weight of the opening for natural light and/or northlight
E	Young modulus
G	Shear modulus
ν	Poisson's ratio
N_ϕ	Meridional force
N_θ	Hoop force
S	Membrane shear force

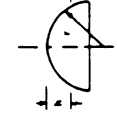
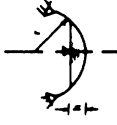
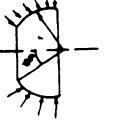
Unless otherwise specified, it is assumed that the shells are supported continuously at their lower edges.



Spherical Shells

System	Loading	N_ϕ	N_θ	T
	$P_x = P_E \sin\phi$ $P_z = P_E \cos\phi$	$-P_E r \frac{\cos\phi_o - \cos\phi}{\sin^2\phi}$ $P_E r \frac{1}{1 + \cos\phi}$	$\frac{\cos\phi_o - \cos\phi}{\sin^2\phi} \cdot r$ $P_E r \left(\frac{1}{1 + \cos\phi} - \cos\phi \right)$	0 Without opening
H1	$P_x = P_S \sin\phi \cos\phi$ $P_z = P_S \cos^2\phi$	$-P_S \frac{r}{2} (1 - \frac{\sin^2\phi_o}{\sin^2\phi})$ $-P_S \frac{r}{2}$	$P_S \frac{r}{2} (1 - \frac{\sin^2\phi_o}{\sin^2\phi} - 2\cos^2\phi)$ $-P_S \frac{r}{2} \cos 2\phi$	0 Without opening
H2	$P_x = P_S \sin\phi$ $P_z = P_S \cos^2\phi$	$-P_S \frac{r}{2} (1 - \frac{\sin^2\phi_o}{\sin^2\phi})$ $-P_S \frac{r}{2}$	$-P_S \frac{r}{2} (1 - \frac{\sin^2\phi_o}{\sin^2\phi} - \frac{\cos^2\phi_o}{\sin^2\phi} - 3\cos\phi)$ $-P_S \frac{r}{2} \cos 2\phi$	0 Without opening

Spherical Shells

System	Loading	N_ϕ	N_θ	T
	$c_2 \quad p_z = \gamma(r - r\cos\phi - h)$	$-\frac{\gamma r^2}{6} \left(\frac{h}{r} \right) \frac{1}{\sin\phi} \left(\frac{h}{r} \left(3 - \frac{h}{r} \right) - 3 \right) +$ $1 - \frac{2\cos^2\phi}{1+\cos\phi}$	$0 \quad \text{for points above water level}$ $-\gamma r^2 n_l - \cos\phi \cdot \frac{h}{r} \cdot N_\phi \quad \text{for points below water level}$	0
	$c_3 \quad p_z = -\gamma(r - r\cos\phi - h)$	$\frac{1}{\sin\phi} \frac{r^2}{6} \left(\frac{h}{r} \left(3 - \frac{h}{r} \right) \right)$ $\gamma \frac{r^2}{6} \left[\left(3 - \frac{h}{r} \right) - 1 + \frac{2\cos^2\phi}{1+\cos\phi} \right]$	$0 \quad \text{for points above water level}$ $-\gamma \frac{h^2}{6} \left(3 - \frac{h}{r} \right) \frac{1}{\sin\phi} \quad \text{for points below water level}$	0
	$d \quad p_z = p$	$-p \frac{r}{2} \left(1 - \frac{\sin^2\phi_o}{\sin^2\phi} \right)$	$-p \frac{r}{2} \left(1 + \frac{\sin^2\phi_o}{\sin^2\phi} \right) \quad \phi_o \approx 0 \text{ without opening}$ $-p \frac{r}{2} \quad \phi_o \approx 0$	0

Spherical Shells

System	Loading	N_ϕ	N_θ	T
f P_L	edge load	$-P_L \frac{\sin\phi_0}{\sin\phi}$	$P_L \frac{\sin\phi_0}{\sin^2\phi}$	0
g P_L	line load	$-P_L \frac{1}{2\pi r \sin\phi}$	$P_L \frac{1}{2\pi r \sin^2\phi}$	0

Spherical Shells

System	Loading	N_ϕ	N_θ	T
	$-P_w \frac{r \cos\theta \cos\phi}{3 \sin^3\phi} \times [13(\cos\phi_0 - \cos\phi) - 3\sin^2\phi - 2\cos^4\phi]$	$P_w \frac{r \cos\theta}{3 \sin^3\phi} \times [13(\cos\phi_0 - \cos\phi)]$	$-P_w \frac{r \sin\theta}{3 \sin^3\phi} \times [13(\cos\phi_0 - \cos\phi)]$	$-P_w \frac{r \sin\theta}{3 \sin^3\phi} \times [13(\cos\phi_0 - \cos\phi)]$
e	$P_z = P_w \frac{r \cos\theta \sin\phi}{3 \sin^3\phi} \times [2(3\cos\phi - \cos^3\phi)]$	$P_w \frac{r \cos\theta \sin\phi}{3 \sin^3\phi} \times [2(3\cos\phi - \cos^3\phi)]$	$P_w \frac{r \cos\theta \sin^2\phi}{3 \sin^3\phi} \times [2(3\cos\phi - \cos^3\phi)]$	$P_w \frac{r \cos\theta \sin^2\phi}{3 \sin^3\phi} \times [2(3\cos\phi - \cos^3\phi)]$

Spherical Shells

System	Loading	N_ϕ	N_0	T
		$\frac{Yr}{(R + r \sin\phi)} \sin\phi [-Rh(\sin\phi_0 - \sin\phi) + \frac{rh}{2}(\cos^2\phi_0 - \cos^2\phi) + \frac{Rr}{2}(\sin\phi_0 - \sin\phi) \times \cos\phi_0 - \sin\phi \cos\phi + \phi \cdot h_0] + \frac{r^2}{3} (\cos^3\phi_0 - \cos^3\phi)$	$-\frac{Y}{\sin^2\phi} [(h - r \cos\phi)(R + r \sin\phi) \times \sin\phi + Rh(\sin\phi_0 - \sin\phi) \cdot \frac{rh}{2}(\cos^2\phi_0 - \cos^2\phi) + Rr(\sin\phi_0 - \sin\phi) \cdot \frac{Rr}{2} \times (\sin\phi_0 \cos\phi_0 - \sin\phi \times \cos\phi - \phi \cdot \phi_0) + \frac{2}{3}(\cos^3\phi_0 - \cos^3\phi)]$	0
c	$p_z = r(h - r \cos\phi)$	$(R + r \sin\phi) \sin\phi [Rh \sin\phi + \frac{rh}{2} \sin^2\phi - \frac{Rr}{2} \sin^2\phi (\sin\phi \cos\phi - \phi)] + \frac{r^2}{2} (\sin\phi \cos\phi \cdot \phi) - \frac{1}{3}(\cos^3\phi_0 - \cos^3\phi)$	$-\frac{Y}{\sin^2\phi} [\frac{rh}{2} \sin^2\phi \cdot \frac{Rr}{2} (\sin\phi \cos\phi - \phi) - r^2 (\cos\phi \sin^2\phi - \frac{1}{3} \cos^3\phi)]$	0
d	$p_z = p$	$-\frac{p}{2(R + r \sin\phi)} \sin\phi [(R + r \sin\phi)^2 - (R + r \sin\phi_0)^2]$	$-\frac{p}{2R} [2R \sin\phi_0 \cdot r(\sin^2\phi_0 + \sin^2\phi)]$	0
f	p_L	$-\frac{p_L}{2} \frac{R + r \sin\phi_0}{R + r \sin\phi}$	$\frac{p_L}{2} \frac{R + r \sin\phi_0}{\sin\phi}$	0



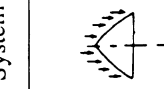
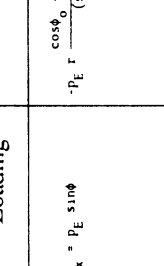
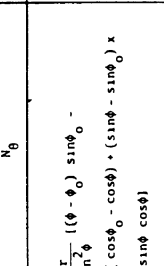
Other types of shells of revolution

 r_0 Radius of base circle

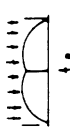
System	Loading	N_ϕ	N_θ	T
a Parabola	$P_x = P_E \sin\phi$ $P_z = P_E \cos\phi$	$\frac{r_o}{r_E} \frac{1 - \cos^3\phi}{\sin^2\phi \cos\phi}$	$-P_E \frac{r_o}{3} \frac{2 + 3 \cos^2\phi + \cos^3\phi}{\sin^2\phi}$	0
b Parabola	$P_x = P_S \sin\phi \cos\phi$ $P_z = P_S \cos^2\phi$	$-P_S \frac{r_o}{2} \frac{1}{\cos\phi}$	$-P_S \frac{r_o}{2} \cos\phi$	0
c Parabola	$P_z = \gamma(h + \frac{r_o}{2} t g\phi)$	$\frac{r_o}{r_E^2} (h(2t g^2\phi + 1) + \frac{1}{4} t g^2\phi)$	$+ r_o t g\phi (t g^2\phi + \frac{1}{4}) \cos\phi$	0
d Parabola	$P_z = p$	$-P \frac{r_o}{2} \frac{1}{\cos\phi}$	$-P \frac{r_o}{2} \frac{1 + \sin^2\phi}{\cos\phi}$	0

Shells of revolution

(1) Axis of revolution intersects the meridional curve

System	Loading	N_ϕ	N_θ	T
	$P_x = P_E \sin\phi$ $P_z = P_E \cos\phi$	$-P_E r \frac{\cos\phi - \cos\phi - (\phi - \phi_0) \sin\phi}{(\sin\phi - \sin\phi_0)^2 \sin\phi}$ $\times (\cos\phi - \cos\phi) + (\sin\phi - \sin\phi_0) \times$ $\times \sin\phi \cos\phi)$	$-P_E \frac{r}{\sin^2\phi} ((\phi - \phi_0) \sin\phi -$ $\times (\cos\phi - \cos\phi) + (\sin\phi - \sin\phi_0) \times$ $\times \sin\phi \cos\phi)$	0
	$P_x = P_S \sin\phi \cos\phi$ $P_z = P_S \cos^2\phi$	$-P_S \frac{r}{2} (1 - \frac{\sin\phi_0}{\sin\phi})$	$-P_S \frac{r}{2} (\cos 2\phi + 2 \sin\phi \sin\phi_0 -$ $\frac{\sin^2\phi_0}{\sin^2\phi})$	0
	$P_x = P_E \sin\phi$ $P_z = P_E \cos\phi$ $R = 2P_E^2(r\phi_0 \times \sin\phi_0 \cdot 2\sin^2\frac{\phi}{2})$	$1 - \frac{\cos\phi + \phi \sin\phi}{\sin\phi(\sin\phi + \sin\phi)}$	$-P_E r(\cos\phi - \frac{1 - \cos\phi}{\sin^2\phi} \cdot$ $+ \sin\phi_0(\cot\phi - \frac{\phi}{\sin^2\phi}))$	0

Shells of revolution

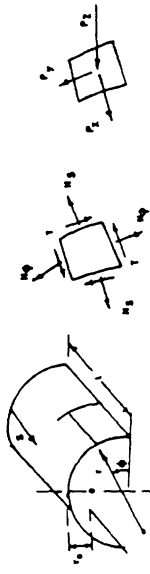
System	Loading	N_ϕ	N_θ	T
	$P_x = P_S \sin\phi \cos\phi$ $P_z = P_S \cos^2\phi$ $R = P_S \pi r^2 \sin^2\phi_0$	b $\frac{r \sin\phi + 2\sin\phi}{r \sin\phi + \sin\phi_0}$ $-P_S \frac{r}{2} (\cos 2\phi - 2\sin\phi \sin\phi_0)$ 0		



System	Loading	N_ϕ	N_θ	T
	$P_x = P_I \sin\phi$ $P_z = P_I \cos\phi$	$P_I \frac{R(\phi - \phi_0) + \frac{r}{2}(\cos\phi_0 - \cos\phi)}{(K + \frac{1}{r}) \sin\phi}$ $\frac{-P_I}{\sin\phi} [(R + rs\sin\phi) \cos\phi - R(\phi - \phi_0)]$ $\cdot r (\cos\phi_0 - \cos\phi)$	$\Phi_0 = -\phi_1$	0

Other types of shells of revolution

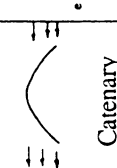
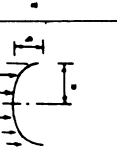
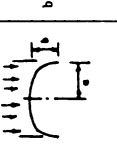
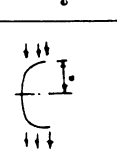
System	Loading	N_ϕ	N_0	τ
	$P_x = P_z \sin\phi$	$-P_z \cdot 2r_0 \frac{\Phi \sin\phi + \cos\phi - 1/3 \cos^3\phi - 2/3}{(\Phi\phi + \sin 2\phi) \sin\phi}$	$-P_z r_0 \left[\frac{1 - \cos^3\phi}{\sin\phi} - \frac{\Phi}{2} \right] \cos\phi -$ $-1/2 \sin^2\phi]$	0
	$P_t = P_z \cos\phi$	$-P_z \frac{r_0 \cdot 2\Phi + \sin 2\phi}{\sin\phi}$	$-P_z \frac{2\Phi + \sin 2\phi}{\sin\phi} x$ $\times (4 \cos^2\phi - \frac{2\Phi}{\sin\phi} - 1)$	0
	$P_x = P_s \sin\phi\cos\phi$	$-P_s \frac{r_0 \cdot 2\Phi + \sin 2\phi}{\sin\phi}$	$P_E \frac{[(b^2 + a^2)t_g^2\phi)^{1/2}}{2t_g\phi} \times (\frac{1}{2} x$ $\times \ln \frac{(1+t)}{\sqrt{b^2 + a^2 t_g^2\phi}} + \frac{1}{b} -$ $\frac{\sqrt{1 + t_g^2\phi}}{1 + t_g^2\phi}) - a^2/b^2 \cdot \frac{2}{t_g^2\phi} \cdot$ $\frac{2}{b^2 + a^2 t_g^2\phi}$	0
	$P_z = P_s \cos\phi$	$\frac{P_E}{2} \frac{\sqrt{a^2 t_g^2\phi + b^2} (a^2 - \frac{2b^2}{b^2 + a^2 t_g^2\phi})}{\sin\phi\cos\phi} +$ $\frac{b^2 \ln \frac{(1+t)}{\sqrt{b^2 + a^2 t_g^2\phi}}}{b(c + \sqrt{1 + t_g^2\phi})}$ $\epsilon = \frac{\sqrt{a^2 - b^2}}{b}$	$\frac{P_E}{2t_g\phi} \frac{[(b^2 + a^2 t_g^2\phi)^{1/2}] \times (\frac{1}{2} x$ $\times \ln \frac{(1+t)}{\sqrt{b^2 + a^2 t_g^2\phi}} + \frac{1}{b} -$ $\frac{\sqrt{1 + t_g^2\phi}}{1 + t_g^2\phi}) - a^2/b^2 \cdot \frac{2}{t_g^2\phi} \cdot \frac{2}{b^2 + a^2 t_g^2\phi}$	0
	$P_x = P_z \sin\phi$	$\frac{P_E}{2} \frac{a^2 \sqrt{1 + t_g^2\phi}}{b^2 + a^2 t_g^2\phi}$	$\frac{-P_z a^2}{2} \frac{b^2 - a^2 t_g^2\phi}{b^2 + a^2 t_g^2\phi} \cdot$ $\frac{1}{\sqrt{b^2 + (a^2 - b^2) \sin^2\phi}}$	0
	$P_t = P_z \cos\phi$	$P_z = P$	$\frac{P^2}{2b^2} \frac{b^2 - (a^2 - b^2) \sin^2\phi}{\sqrt{b^2 + (a^2 - b^2) \sin^2\phi}}$	0
	$P_x = P_s \sin\phi\cos\phi$	$\frac{P^2}{2} \frac{1}{\sqrt{b^2 + (a^2 - b^2) \sin^2\phi}}$	$\frac{P^2}{2b^2} \frac{b^2 - (a^2 - b^2) \sin^2\phi}{\sqrt{b^2 + (a^2 - b^2) \sin^2\phi}}$	0
	$P_z = P_s \cos\phi$	$P_z = P$	$\frac{P^2}{2b^2} \frac{b^2 - (a^2 - b^2) \sin^2\phi}{\sqrt{b^2 + (a^2 - b^2) \sin^2\phi}}$	0



Cylindrical Vaults

System	Loading	N_S	N_u	T
Circle	$P_y = -P_E \cos\phi$ $P_z = P_E \sin\phi$	$-P_E \frac{s}{r} (t - s) \sin\phi$	$-P_E r \sin\phi$	$-P_E (t - 2s) \cos\phi$
Circle	$P_y = -P_S \sin\phi \cos\psi$ $P_z = P_S \sin^2\phi$	$P_S \frac{3s}{2r} (t - s) (1 - 2s \sin^2\phi)$	$-P_S r \sin^2\phi$	$-P_S (\frac{t}{2} - s) 3 \sin\phi \cos\phi$
Circle	$P_z = P_u \cos\phi$	$-P_u \frac{t}{2r} (t - s) \cos\phi$	$-P_u r \cos\phi$	$P_u (\frac{t}{2} - s) \sin\phi$
Parabola	$P_y = -P_F \cos\phi$ $P_z = P_F \sin\phi$	$P_F \frac{s}{2r_O} (t - s) \sin^4\phi$	$-P_F \frac{r_o}{\sin^2\phi}$	$P_F (\frac{t}{2} - s) \cos\phi$

Cylindrical Vaults

System	Loading	N_S	N_ϕ	T
Catenary		$P_w \frac{3}{2T_0} \frac{(1-s)}{2(Y+s \sin \phi)} x$ $x(2+s \sin^2 \phi) \cos \phi$	$-P_w T_0 \frac{\cos \phi}{\sin \phi}$	$P_w (\frac{1}{2} - s) \frac{1 + \cos^2 \phi}{\sin \phi}$
	$P_y = -P_E \cos \phi$ $P_z = P_E \sin \phi$	$P_E \frac{s(t-s)(Y+\pi/4)}{2a(Y+s \sin \phi)^3} x$ $x(Y(1-6 \sin^2 \phi) - (2Y^2 + 3 \sin^2 \phi) \sin \phi)$	$-P_E \frac{a}{Y+\pi/4} x$ $x(Y + \sin \phi) \sin \phi$	$P_S (s - \frac{1}{2}) x$ $x \frac{(2Y + \sin \phi) \cos \phi}{Y + \sin \phi}$
	$P_y = -P_S \sin \phi \cos \phi$ $P_z = P_S \sin 2 \phi$	$P_S \frac{s(t-s)(Y+\pi/4)}{2a(Y+s \sin \phi)^3} x$ $x(Y(8 - 15 \sin^2 \phi) \sin \phi + (3Y^2 + 4 \sin^2 \phi) x)$ $x(1 - 2 \sin^2 \phi)$	$P_S \frac{a}{Y+\pi/4} x$ $x(Y + \sin \phi) \sin^2 \phi$	$P_S (s - \frac{1}{2}) x$ $x \frac{(3Y + 4 \sin \phi) \sin \phi \cos \phi}{Y + \sin \phi}$
	$P_y = P_w \cos \phi$ $P_z = P_w \cos 2 \phi$	$P_w \frac{s(t-s)(Y+\pi/4)}{2a(Y+s \sin \phi)^3} x$ $x \cos \phi (1 + Y^2 + 2 \sin^2 \phi + 4Y \sin \phi)$	$-P_w \frac{a}{Y+\pi/4} x$ $x(Y + \sin \phi) \cos \phi$	$P_w (s - \frac{1}{2}) \frac{1 - 2 \sin^2 \phi - Y \sin \phi}{Y + \sin \phi}$

Cylindrical Vaults

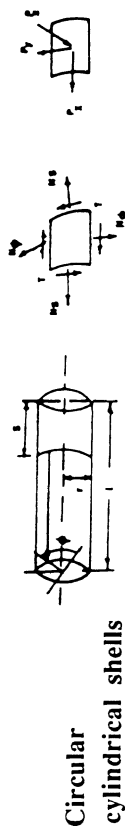
System	Loading	N_S	N_θ	T
Parabola 	$P_y = -P_S \sin\phi \cos\phi$ $P_z = P_S \sin^2\phi$	0	$-P_S \frac{r_o}{\sin\phi}$	0
Parabola 	$P_y = -P_S \sin\phi \cos\phi$ $P_z = P_S \sin^2\phi$	$P_w \frac{S}{2r_o} (t - s) \sin\theta \cos\theta \times$ $x(3 + 2 \sin^2\phi)$	$-P_w r_o \frac{\cos\phi}{\sin\phi}$	$P_w (\frac{t}{2} - s) \frac{1 + 2 \cos^2\phi}{\sin\phi}$
Cycloid 	$P_y = -P_E \cos\phi$ $P_z = P_E \sin\phi$	$-P_E \frac{3S}{2r_o} (t - s)$	$-P_E r_o \sin^2\phi$	$-P_E (\frac{t}{2} - s) 3 \cos\phi$
Cycloid 	$P_y = -P_S \sin\phi \cos\phi$ $P_z = P_S \sin^2\phi$	$P_S \frac{2S}{r_o} (t - s) \frac{1 - 2 \sin^2\phi}{\sin\phi}$	$-P_S r_o \sin^3\phi$	$-P_S (\frac{t}{2} - s) 4 \sin\phi \cos\phi$
Cycloid 	$P_y = -P_w \cos\phi$ $P_z = P_w \sin^2\phi$	$-P_w \frac{S}{r_o} (t - s) \times$ $x (1 - \cos\phi)$	$-P_w r_o \sin\phi \cos\phi$	$-P_w (\frac{t}{2} - s) \frac{1 - 2 \sin^2\phi}{\sin\phi}$

Cylindrical Vaults

System	Loading	N_S	N_E	T
Ellipse a b	$P_y = -P_E \cos\phi$ $P_z = P_E \sin\phi$	$-P_L \frac{\zeta}{2} (\ell - s) \times$ $\times \frac{3a^2 b^2}{a^2 b^2 n^2} \sin\phi$ $= a^2 (n \cos^2\phi + b^2 \sin^2\phi)$	$-P_E a^2 b^2 \frac{\sin\phi}{n^2}$	$-P_L \left(\frac{\ell}{2} - s \right) \times$ $\times \frac{2}{2a^2 + (a^2 - b^2)} \sin\phi \cos\phi$
Ellipse b a	$P_y = -P_S \sin\phi \cos\phi$ $P_z = P_S \sin^2\phi$	$-P_S \frac{35(\ell - s)}{2a^2 b^2 n^2} \times$ $\times [b^2 (a \cos^2\phi - b^2 \sin^2\phi) +$ $+ 2n^2 (\sin^2\phi - \cos^2\phi)]$	$-P_S a^2 b^2 \frac{\sin^2\phi}{n^2}$	$P_S \left(\frac{\ell}{2} - s \right) \times$ $\times \frac{35 \sin\phi \cos\phi}{n^2} (b^2 - m)$
Ellipse c a	$P_y = -P_E \cos\phi$ $P_z = P_E \sin\phi$	$-P_E \frac{5(\ell - s) \cos\phi}{2a^2 b^2 n^2} [n^2 +$ $+ 3(b^2 - a^2)(1 - 3 \sin^2\phi) -$ $- 6(b^2 - a^2) \sin^2\phi \cos^2\phi]$	$-P_E a^2 b^2 \frac{\cos\phi}{n^2}$	$P_E \frac{5}{2} \left(\frac{\ell}{2} - s \right) \frac{b^2 - a^2}{n^2} \times$ $\times (1 + \cos\phi) \sin\phi$
Catenary a	$P_y = -P_E \cos\phi$ $P_z = P_E \sin\phi$	0	$-P_E \frac{r_o}{\sin\phi}$	0
Catenary b	$P_y = -P_S \sin\phi \cos\phi$ $P_z = P_S \sin^2\phi$	$P_S \frac{5}{2r_o} (\ell - s) \sin^2\phi \times$ $\times (1 - 2 \sin^2\phi)$	$-P_S r_o$	$-P_S \left(\frac{\ell}{2} - s \right) \sin\phi \cos\phi$

Circular cylindrical shells

System	Loading	N_s	N_ϕ	T
a	$P_y = -P_E \cos\phi$	$-P_E \frac{3}{r} (t - s) \sin\phi$	$-P_E r \sin\phi$	$-P_E (t - 2s) \cos\phi$
b	$P_z = P_E \sin\phi$	$P_E \frac{t^2}{6r} - vr - \frac{s}{r} (t - s) \sin\phi$	$-P_E r \sin\phi$	$-P_E (t - 2s) \cos\phi$
c	$P_z = -Y/h \cdot r \sin\phi$	$-r \frac{s}{2} (t - s) \sin\phi$	$rr \left(\frac{h}{2} - s \right) \cos\phi$	
		$-Y \left(\frac{t^2}{12} - vr^2 - \frac{s}{2} (t - s) \right) x$ $x \sin\phi - vr^2$	$rr \left(\frac{h}{2} - s \right) \cos\phi$	



System	Loading	N_s	N_0	T
	a $p_x = p_E$	$-p_l s$	$-pr$	0
	b $p_x = p$	0	γrs	0
	c $p_x = -\gamma s$	0	0	$-p_w s \sin \phi$
	d $p_x = p_w \cos \phi$	$p_w \frac{s^2}{2r} \cos \phi$	$p_w r \cos \phi$	$-p_w s \sin \phi$
	e $p_x = p_w \cos \phi$	$p_w \frac{s^2}{2r} \cos \phi$	$p_w r \cos \phi$	$-p_w s \sin \phi$



Conical shells

System	Loading	N_s	N_θ	T
a	$P_x = P_E \sin\phi$ $P_z = P_E \cos\phi$	$-P_F \frac{s^2}{2s} \frac{1}{\sin\phi}$	$-P_E s \frac{\cos^2\phi}{\sin\phi}$	0
b	$P_x = P_S \sin\phi \cos\phi$ $P_z = P_S \cos^2\phi$	$-P_S \frac{s^2 - s_0^2}{2s} \cot\phi$	$-P_S s \frac{\cos^3\phi}{\sin\phi}$	0
c ₁	$P_z = r(h + s \sin\phi)$	$\frac{r}{s} \left(h \frac{s^2 - s_0^2}{2} \cot\phi + \frac{s^2 - s_0^2}{3} \cos\phi \right)$	$-rs(h \cot\phi + s \cos\phi)$	0
c ₂		$-rs \frac{h}{2} \cot\phi + \frac{s}{3} \cos\phi$	$rs(h \cot\phi + s \cos\phi)$	0

Conical shells

System	Loading	N_s	η_b	ψ
	$c_2 \quad p_z = \gamma(ssin\phi - h)$	0 Points above water level $-\frac{\gamma(1 - \cos\phi)}{6s^2} h^3 + s^2 (2s\cot\phi - 3h\cot^2\phi)$	0 Points below water level $-\gamma s(\cos\phi - h\cot\phi)$	0
	$c_3 \quad p_z = \gamma(h - ssin\phi)$	$\frac{\gamma h^3}{6s^2} \frac{\cos\phi}{\sin\phi}$ $\frac{s^2}{2} (3h\cot\phi - 2s\cos\phi)$	0 Points above water level $\gamma s(h\cot\phi - s\cos\phi)$	0
	$d \quad p_z = p$	$-p \frac{s^2 - s^2}{2s} \cot\phi$ $-p \frac{1}{2} \cot\phi$	$s_o = 0$ Complete cone $-p s \cot\phi$	0
	$f \quad p_L \quad$ Edge load $g \quad p_L \quad$ axisymmetric	$-p_L \frac{k_0}{s} \frac{1}{\sin\phi}$ $-p_L \frac{1}{2s} \frac{1}{\sin\phi \cos\phi}$	$s_o = 0$ for line load alone -	0 0
	$e \quad p_z = p_w \sin\phi \times \cos\theta$	$-p_w \frac{2}{3} \frac{\cos\phi}{\sin\phi} - \frac{1}{s^2} \times (\cos\phi - \frac{1}{\cos\phi})$ $-\frac{2}{s^2} \frac{1}{3\cos\phi} \cos\theta$ $-p_w \frac{s}{2} (\cos\phi - \frac{1}{3\cos\phi}) \cos\theta$	$-p_w \cos\phi \cos\theta$ Complete cone $-p_w s \cos\phi \cos\theta$	$\frac{s^3 - s^3}{p_w} \frac{x}{x \sin\theta}$ -



Conical shells with free edges
(supported at the apex)

System	Loading	N_S	N_θ	T
a	$P_x = P_L \sin\phi$ $P_x = P_E \cos\phi$	$P_L \frac{t^2 - s^2}{2s} \frac{1}{\sin\phi}$	$-P_E s \frac{\cos^2\phi}{\sin\phi}$	0
b	$P_x = P_S \sin\phi \cos\phi$ $P_z = P_S \cos^2\phi$	$P_S \frac{t^2 - s^2}{2s} \cot\phi$	$-P_S s \frac{\cos^3\phi}{\sin\phi}$	0
c	$P_z = P$	$P \frac{t^2 - s^2}{2s} \cot\phi$	$P_S \cot\phi$	0
e	$P_z = P_w \sin\theta \cos\phi$	$P_w \left(\frac{t^3 - s^3}{3s} - \frac{t^2 - s^2}{7s} \sin^2\phi \right) \frac{\cos\theta}{\cos\phi}$	$-P_w s \cos\theta \cos\phi$	$\frac{t^3 - s^3}{3s} \frac{P_w}{\sin\theta}$

Equation of surface		Boundary conditions	
$z = \frac{xy}{n} + n = \frac{a^2}{c}$		$N_x = 0$ $N_y = 0$ $N_z = n$	
System	Loading	N_x	N_y
	p_z	$-p_f \frac{1}{2} t_n \frac{x + \sqrt{x^2 + y^2 + n^2}}{\sqrt{y^2 + n^2}}$ $x \frac{\cos\psi}{\cos\phi}$	$-p_f \frac{1}{2} t_n \frac{y + \sqrt{x^2 + y^2 + n^2}}{\sqrt{x^2 + n^2}}$ $x \frac{\cos\phi}{\cos\psi}$
	$p_z = -p_s \cos\gamma$	0	0
			$p_s \frac{a^2}{2c}$

Hyperbolic Paraboloid shells

System	Loading	N_x	N_y	T
	$p_n = r(h - \frac{xy}{n})$	$\frac{y}{2n^2} (\frac{x}{4} + \frac{y^2}{2} (5x^2 + n^2)) - 4nhxy \frac{\cos\psi}{\cos\phi}$	$\frac{y}{2n^2} (\frac{1}{4} + \frac{y^2}{2} (5x^2 + n^2)) - 4nhxy \frac{\cos\phi}{\cos\psi}$	$\frac{y}{2n} (h - \frac{xy}{n}) x$ $x (x^2 + y^2 + n^2)$
	$p_n = p$	$- p \frac{2xy}{n} \frac{\cos\psi}{\cos\phi}$	$- p \frac{2xy}{n} \frac{\cos\phi}{\cos\psi}$	$p \frac{x^2 + y^2 + n^2}{2n}$
	$p_n = p_n \sin t \psi$	$-p_n \frac{y}{n} (\frac{x}{\sqrt{x^2 + y^2 + n^2}})^2$ $x \sin t \psi \frac{-\frac{x}{\sqrt{x^2 + y^2 + n^2}}}{\cos\phi}$	$-p_n \frac{x}{y} (\frac{y}{\sqrt{x^2 + y^2 + n^2}})^2$ $x \sin t \psi \frac{\frac{y}{\sqrt{x^2 + y^2 + n^2}}}{\cos\phi}$	$p_n \frac{y^2}{2n}$ $x \sin t \psi \frac{y}{\sqrt{x^2 + y^2 + n^2}} \cos\phi$

Appendix B

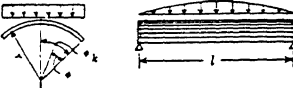
Notation:

Definition	unit	Table	Text
Longitudinal force	Force/unit length	T_x	N_x
Membrane shear force	Force/unit length	S	$N_{x\phi} = N_{\phi x}$
Transverse force	Force/unit length	T_ϕ	N_ϕ
Transverse moment	Force-length/length	M_ϕ	M_ϕ
Shell thickness	Length	t	t
Radius of shell profile	Length	$r = a$	r
Transverse angular coordinate (measured from normal to the shell at its lower edge)	Radian	ϕ	ϕ
Half central angle of the shell	Radian	ϕ_k	ϕ_k
Length of the shell	Length	$l = L$	l
Subscript for edge forces		$()_L$	
Horizontal displacement of the edges	Length	ΔH	
Vertical displacement of the edges	Length	ΔV	

Source of tables:

"Design of Cylindrical Shell Roofs", Manual 31, American Society of Civil Engineers, New York, 1952

(ASCE Table 1B) Membrane Forces and Displacements in Simply Supported Cylindrical Shells; Loads Varying Longitudinally from Zero at the Ends to Maximum Positive at the Middle

(a) UNIFORM TRANSVERSE LOAD						(b) DEAD WEIGHT LOAD					
											
Longitudinal Force T_x — $p_0 r \left[\left(\frac{l}{r} \right)^2 \times \text{Col. (1)} \right] \sin \frac{\pi z}{l}$						Longitudinal Force T_x — $p_d r \left[\left(\frac{l}{r} \right)^2 \times \text{Col. (7)} \right] \sin \frac{\pi z}{l}$					
Shearing Force S — $p_0 r \left[\left(\frac{l}{r} \right) \times \text{Col. (2)} \right] \cos \frac{\pi z}{l}$						Shearing Force S — $p_d r \left[\left(\frac{l}{r} \right) \times \text{Col. (8)} \right] \cos \frac{\pi z}{l}$					
Transverse Force T_ϕ — $p_0 r \times \text{Col. (3)} \times \sin \frac{\pi z}{l}$						Transverse Force T_ϕ — $p_d r \times \text{Col. (9)} \times \sin \frac{\pi z}{l}$					
Vertical Displacement ΔV — $p_0 r \frac{l^4}{\pi^2 t E} \left[\left(1 + \frac{1}{2} (\pi r/l)^2 + \frac{1}{12} (\pi r/l)^4 \right) \times \text{Col. (4)} \right] \sin \frac{\pi z}{l}$						Vertical Displacement ΔV — $p_d r \frac{l^4}{\pi^2 t E} \left[\left(\frac{2\pi}{\pi l} \right)^2 + \frac{2}{\pi^2} + \left(\frac{r}{l} \right)^4 \times \text{Col. (10)} \right] \sin \frac{\pi z}{l}$					
Horizontal Displacement ΔH — $\pm p_0 r \frac{l^4}{\pi^2 t E} \left\{ \left(\frac{r}{l} \right)^4 \times \text{Col. (5)} + \left[1 + \frac{1}{2} \left(\frac{\pi r}{l} \right)^2 + \frac{1}{12} \left(\frac{\pi r}{l} \right)^4 \right] \times \text{Col. (6)} \right\} \times \sin \frac{\pi z}{l}$						Horizontal Displacement ΔH — $\pm p_d r \frac{l^4}{\pi^2 t E} \left[\left(\frac{r}{l} \right)^4 \times \text{Col. (11)} \right] \times \sin \frac{\pi z}{l}$					
$\phi = \phi$	T_x	S	T_ϕ	ΔV	ΔH	T_x	S	T_ϕ	ΔV	ΔH	
	(1)	(2)	(3)	(4)	(5)	(6)	(7)	(8)	(9)	(10)	(11)
0	-0.3040	0	-1.0000	0.12319	0	0	-0.2026	0	-1.0000	1.0000	0
5	-0.2993	-0.0829	-0.9924	0.12180	0.0872	-0.00009	-0.2019	-0.0555	-0.9982	0.9924	0.0888
10	-0.2558	-0.1633	-0.9698	0.11766	0.1736	-0.00064	-0.1998	-0.1105	-0.9848	0.9688	0.1710
15	-0.2623	-0.2387	-0.9330	0.11102	0.2588	-0.00213	-0.1937	-0.1648	-0.9659	0.9330	0.2500
20	-0.2329	-0.3069	-0.8830	0.10225	0.3420	-0.00490	-0.1904	-0.2178	-0.9397	0.8830	0.3214
25	-0.1954	-0.3658	-0.8214	0.09170	0.4016	-0.00930	-0.1837	-0.2690	-0.9063	0.8214	0.3834
30	-0.1520	-0.4140	-0.7300	0.08080	0.4500	-0.01539	-0.1754	-0.3183	-0.8660	0.7500	0.4330
35	-0.1040	-0.4487	-0.6710	0.06771	0.5736	-0.02325	-0.1660	-0.3652	-0.8191	0.6710	0.4698
40	-0.0528	-0.4702	-0.3868	0.05337	0.6428	-0.03272	-0.1552	-0.4092	-0.7660	0.5868	0.4924
45	0	-0.4775	-0.5000	0.04354	0.7071	-0.04355	-0.1433	-0.4502	-0.7071	0.5000	0.5000
50	0.0528	-0.4702	-0.4132	0.03272	0.7660	-0.05537	-0.1302	-0.4877	-0.6428	0.4132	0.4924
55	0.1040	-0.4487	-0.3290	0.02325	0.8191	-0.06771	-0.1162	-0.5215	-0.5720	0.3290	0.4698
60	0.1520	-0.4140	-0.2500	0.01539	0.8860	-0.08001	-0.1013	-0.5513	-0.5900	0.2500	0.4330
65	0.1954	-0.3658	-0.1786	0.00930	0.9063	-0.09170	-0.0856	-0.5769	-0.4226	0.1736	0.3830
70	0.2129	-0.3069	-0.1170	0.00490	0.9397	-0.10222	-0.0693	-0.5982	-0.3420	0.1170	0.3214
75	0.2623	-0.2387	-0.0669	0.00213	0.9269	-0.11102	-0.0524	-0.6139	-0.2258	0.0669	0.2500
80	0.2856	-0.1633	-0.0301	0.00063	0.9848	-0.11768	-0.0351	-0.6269	-0.1736	0.0301	0.1710
85	0.2793	-0.0829	-0.0076	0.00009	0.9962	-0.12190	-0.0177	-0.6342	-0.0872	0.0076	0.0868
90	0.3040	0	0	0	1.0000	-0.12319	0	-0.6366	0	0	0

(ASCE Table 2A) Symmetrical Edge Loads on Simply Supported Cylindrical Shells; Stress Resultants at Various Values of ϕ

	Vertical Edge Load			Horizontal Edge Load			Shear Edge Load			Edge Moment Load						
*	(1)	(2)	(3)	(4)	(5)	(6)	(7)	(8)	(9)	(10)	(11)	(12)	(13)	(14)	(15)	(16)
(a) Basic Formulas and Loading Diagrams																
Longitudinal Force $T_{\phi=0}$																
$V_L \left[\left(\frac{1}{r} \right)^3 \times \text{Col. (1)} \right] \sin \frac{\pi z}{l}$																
Longitudinal Force $T_{\phi=90^\circ}$																
$H_L \left[\left(\frac{1}{r} \right)^3 \times \text{Col. (5)} \right] \sin \frac{\pi z}{l}$																
Shearing Force $S_{\phi=0}$																
$V_L \left[\frac{1}{r} \times \text{Col. (2)} \right] \cos \frac{\pi z}{l}$																
Shearing Force $S_{\phi=90^\circ}$																
$H_L \left[\frac{1}{r} \times \text{Col. (6)} \right] \cos \frac{\pi z}{l}$																
Transverse Force $T_{\phi=0}$																
$H_L \left[\frac{1}{r} \times \text{Col. (7)} \right] \times \sin \frac{\pi z}{l}$																
Transverse Force $T_{\phi=90^\circ}$																
$H_L \left[\frac{1}{r} \times \text{Col. (10)} \right] \cos \frac{\pi z}{l}$																
Transverse Moment $M_{\phi=0}$																
$V_L \left[r \times \text{Col. (8)} \right] \sin \frac{\pi z}{l}$																
$M_L \left[r \times \text{Col. (12)} \right] \sin \frac{\pi z}{l}$																
Transverse Moment $M_{\phi=90^\circ}$																
$H_L \left[r \times \text{Col. (16)} \right] \sin \frac{\pi z}{l}$																
(b) $r/l = 100$ and $r/l = 0.1$																
Longitudinal Force $T_{\phi=0}$																
$S_L \left[\left(\frac{1}{r} \right)^3 \times \text{Col. (9)} \right] \sin \frac{\pi z}{l}$																
Shearing Force $S_{\phi=0}$																
$S_L \left[\frac{1}{r} \times \text{Col. (10)} \right] \cos \frac{\pi z}{l}$																
Shearing Force $S_{\phi=90^\circ}$																
$S_L \left[\frac{1}{r} \times \text{Col. (11)} \right] \sin \frac{\pi z}{l}$																
Transverse Force $T_{\phi=0}$																
$T_s \left[\frac{1}{r} \times \text{Col. (12)} \right] \cos \frac{\pi z}{l}$																
Transverse Force $T_{\phi=90^\circ}$																
$T_s \left[\frac{1}{r} \times \text{Col. (13)} \right] \sin \frac{\pi z}{l}$																
Transverse Moment $M_{\phi=0}$																
$M_L \left[\frac{1}{r} \times \text{Col. (14)} \right] \sin \frac{\pi z}{l}$																
Transverse Moment $M_{\phi=90^\circ}$																
$M_L \left[\frac{1}{r} \times \text{Col. (15)} \right] \cos \frac{\pi z}{l}$																

(ASCE Table 2A) (continued)

Φ	Vertical, Wind Load				Horizontal, Erock Load				Span End Load				End Moment Load			
	T _x (1)	S (2)	T _y (3)	M _φ (4)	T _x (5)	S (6)	T _y (7)	M _φ (8)	T _x (9)	S (10)	T _y (11)	M _φ (12)	T _x (13)	S (14)	T _y (15)	M _φ (16)
(b) (Continued)																
Φ = .35	-3.430	0	-0.305	-0.37083	-0.0061	0	+0.0096	+0.1754	-0.00774	0	-0.0243	-0.0015	-0.0310	0	-0.0051	+0.0642
20	-1.320	-0.1921	-0.320	-0.320	-0.0013	-0.0013	-0.0013	-0.0013	-0.0295	-0.0213	-0.0014	-0.0014	-0.0076	-0.0037	+0.0636	-0.0030
20	-1.320	-0.1921	-0.320	-0.320	-0.0013	-0.0013	-0.0013	-0.0013	-0.0634	-0.0213	-0.0015	-0.0015	-0.0076	-0.0037	+0.0636	-0.0030
10	+1.422	-2.301	-0.2781	-0.1121	-0.0016	-0.0016	-0.0016	-0.0016	-0.0155	-0.0155	-0.0015	-0.0015	-0.0076	-0.0037	+0.0636	-0.0030
0	+6.615	0	+0.477	-0.1441	+0.0080	+0.0041	+0.0041	+0.0041	+0.0848	+0.0012	+0.0012	+0.0012	+0.0081	+0.0081	+0.0081	+0.0081
Φ = .40	+0	0	+0.016	+0.016	+0.0016	+0.0016	+0.0016	+0.0016	+0.0312	+0.0016	+0.0016	+0.0016	+0.0081	+0.0081	+0.0081	+0.0081
20	-2.210	0	-2.631	-0.4018	-0.0165	0	+0.0954	+0.075	-0.02347	-0.0279	-0.00422	-0.0179	-0.0156	-0.0156	-0.0156	-0.0156
30	-1.860	-1.138	-2.084	-0.3683	-0.0019	-0.00068	-0.00068	-0.00068	+0.0836	+0.0201	-0.0161	-0.0161	-0.0156	-0.0156	-0.0156	-0.0156
20	-0.578	-1.830	-1.305	-0.2691	+0.0176	-0.00312	-0.00312	-0.00312	+0.0420	+0.0162	-0.0162	-0.0162	-0.0156	-0.0156	-0.0156	-0.0156
10	+1.516	-1.611	-0.165	-0.1352	+0.0156	+0.0081	+0.0081	+0.0081	+0.0835	+0.0167	-0.0167	-0.0167	-0.0156	-0.0156	-0.0156	-0.0156
0	+4.534	0	+0.413	0	-0.0431	0	+0.0631	0	+0.7600	0	+0.2682	+0.0100	0	+0.0098	0	+0.0098
Φ = .45	-1.662	0	-2.231	-0.4355	-0.0359	0	+0.0973	+0.2779	-0.0536	0	-0.0315	-0.00311	-0.1280	0	-0.0437	0.9382
40	-0.516	0	-0.334	-0.4274	-0.0409	-0.0034	+0.0819	+0.2743	-0.0539	-0.0292	-0.0160	-0.0160	-0.0160	-0.0325	+0.0402	-0.0402
30	-1.098	-1.180	-1.116	-0.3053	+0.0633	-0.0016	-0.0016	-0.0016	+0.0612	+0.0401	-0.0258	-0.0258	-0.0258	-0.0447	-0.0447	-0.0447
20	-0.369	-1.553	-0.763	-0.2562	+0.0162	-0.0059	-0.0059	-0.0059	+0.0158	+0.0809	-0.0358	-0.0358	-0.0358	-0.0535	-0.0535	-0.0535
10	+1.110	-2.663	-0.1077	-0.2553	+0.0160	+0.0175	+0.0175	+0.0175	+0.072	+0.0722	+0.0722	+0.0722	+0.0722	+0.0722	+0.0722	+0.0722
0	+3.407	0	+0.107	0	-0.185	0	+0.0630	+0.0175	+0.0771	0	+0.2378	+0.0100	-0.0002	+0.0680	+0.0680	+0.0680
Φ = .50	-1.051	0	-1.931	-0.4541	-0.0693	0	+0.0966	+0.3326	-0.0331	0.0271	-0.0150	-0.0042	-0.0037	-0.0042	-0.0085	-0.0218
40	-0.918	-0.558	-1.741	-0.4265	-0.0213	-0.0213	+0.0650	+0.3320	-0.0320	-0.0198	-0.0123	-0.0123	-0.0123	-0.0123	-0.0123	-0.0123
30	-0.619	-0.969	-0.181	-0.2379	-0.02379	-0.0030	+0.0281	+0.3028	-0.0320	-0.0276	-0.0196	-0.0124	-0.0124	-0.0124	-0.0124	-0.0124
20	-0.001	-1.141	-0.1141	-0.1141	+0.0374	+0.0357	+0.0357	+0.0357	+0.0738	+0.1187	-0.0188	-0.0188	-0.0188	-0.0188	-0.0188	-0.0188
10	+0.998	-0.330	-0.417	-0.2706	+0.2488	0	+0.2947	0	+0.6428	0	+0.2138	+0.0030	-0.0002	+0.0287	+0.0287	+0.0287
0	+2.388	0	+0.206	0	-0.206	0	+0.0000	+0.0000	+0.0000	0	+0.0000	-0.0002	-0.0002	+0.0000	+0.0000	+0.0000
(c) r/t = 100 and r/l = 0.2																
Φ = .30	-5.160	0	-3.120	-0.3028	-0.0742	0	-0.0885	-0.1219	-0.0276	-0.0196	-0.0042	-0.0005	-0.549	-0.0013	-0.0009	-0.0009
20	-3.410	-5.331	-2.632	-0.2965	-0.0723	-0.0292	-0.0737	-0.1041	-0.0276	-0.0196	-0.0042	-0.0005	-0.549	-0.0013	-0.0009	-0.0009
10	-1.763	-3.228	-0.787	-0.1935	+0.0700	-0.0087	+0.03427	-0.0678	-0.0275	-0.0196	-0.0042	-0.0005	-0.549	-0.0013	-0.0009	-0.0009
0	+10.02	0	+0.300	0	-0.300	0	+0.1140	0	+0.3690	0	+0.0000	-0.0002	-0.0002	+0.0000	+0.0000	+0.0000

(ASCE Table 2A) (continued)

ϕ	Vertical Edge Load				Horizontal Edge Load				Shear Edge Load				Edge Moment Load			
	T_s (1)	S (2)	T_ϕ (3)	M_ϕ (4)	T_s (5)	S (6)	T_ϕ (7)	M_ϕ (8)	T_s (9)	S (10)	T_ϕ (11)	$M_\phi \cdot$ (12)	T_s (13)	S (14)	T_ϕ (15)	M_ϕ (16)
(c) (Continued)																
$\phi = 35^\circ$	-3.087	0.833	-2.871	-0.3347	-0.1532	0	+0.0603	+0.1501	-0.1487	0	-0.0458	-0.0024	-0.0112	0	-0.1014	+0.8637
30	-2.939	-2.156	-2.744	-0.3248	-0.1290	-0.0398	+0.0622	+0.1559	-0.1334	-0.0394	-0.0106	-0.0012	-0.0112	-0.142	-0.2331	-0.8669
20	-1.639	-2.396	-1.807	-0.2514	+0.0561	-0.0634	+0.0624	+0.1301	-0.1062	-0.0845	-0.0106	-0.0018	-0.0112	-0.142	-0.2331	+0.8669
10	+1.501	-2.394	-1.802	-0.1302	+0.1526	+0.0074	+0.0244	+0.0781	+0.0278	+0.0280	+0.0308	+0.0001	-0.0001	-0.0128	+0.0486	+0.8114
0	+7.434	0	+0.574	0	+0.524	0	+0.8192	0	+0.6159	+0.2000	0	0	0	0	+0.0001	+0.8662
$\phi = 10^\circ$																
$\phi = 40^\circ$	-1.764	-2.319	-2.388	-0.3556	-0.1366	-0.189	+0.0306	+0.162	-0.1273	0	-0.0525	-0.0035	-0.0035	-0.121	-0.2982	-0.8156
30	-1.640	-0.447	-2.105	-0.3219	-0.1351	-0.185	+0.0408	+0.1662	-0.1680	-0.0526	-0.0187	-0.0035	-0.0039	-0.121	-0.2982	-0.8156
20	-0.063	-1.897	-1.251	-0.2747	-0.1353	-0.188	+0.0180	+0.167	-0.1683	-0.0526	-0.0187	-0.0035	-0.0039	-0.121	-0.2982	-0.8156
10	+1.111	-1.753	-0.169	-0.168	-0.163	0	+0.7657	+0.1657	-0.0870	+0.0468	+0.0111	-0.0034	-0.0037	-0.121	-0.2982	+0.8156
0	+5.836	0	+0.634	0	+0.634	0	+0.8110	+0.1610	-0.0870	+0.0468	+0.0111	-0.0034	-0.0037	-0.121	-0.2982	+0.8156
$\phi = 45^\circ$																
$\phi = 45^\circ$	-0.775	0.917	-1.634	-0.3619	-0.1659	0	+0.0670	+0.1741	-0.1067	0	-0.0577	-0.0050	-0.0050	-0.2074	-0.7345	+0.7549
30	-0.820	-0.317	-1.867	-0.3556	-0.1667	-0.1493	+0.0567	+0.1748	-0.1068	-0.0588	-0.0287	-0.0055	-0.0055	-0.2074	-0.7345	+0.7549
20	-1.062	-0.313	-1.584	-0.3219	-0.1668	-0.1493	+0.0568	+0.1749	-0.1068	-0.0588	-0.0287	-0.0055	-0.0055	-0.2074	-0.7345	+0.7549
10	+0.532	-1.317	-0.910	-0.2747	-0.1675	-0.1558	+0.0381	+0.1750	-0.1070	-0.0598	-0.0297	-0.0066	-0.0066	-0.2074	-0.7345	+0.7549
0	+5.344	0	+0.534	0	+0.534	0	+0.8103	+0.1753	-0.1073	-0.0598	-0.0297	-0.0066	-0.0066	-0.2074	-0.7345	+0.7549
$\phi = 50^\circ$																
$\phi = 50^\circ$	+0.052	0.228	-1.487	-0.3493	-0.1469	0	+0.5813	+0.2514	-0.0848	0	-0.0601	-0.0065	-0.0065	-2.814	-0.6113	+0.6113
40	-0.291	-0.291	-1.413	-0.3313	-0.1469	-0.0848	+0.7040	+0.2525	-0.0714	-0.0419	-0.0168	-0.0056	-0.0056	-1.781	-0.8119	+0.8119
30	-1.016	-0.383	-1.246	-0.2786	-0.1073	-0.0848	+0.3827	+0.2525	-0.0714	-0.0419	-0.0168	-0.0056	-0.0056	-1.781	-0.8119	+0.8119
20	-1.214	-0.383	-1.053	-0.2786	-0.1073	-0.0848	+0.3828	+0.2526	-0.0714	-0.0419	-0.0168	-0.0056	-0.0056	-1.781	-0.8119	+0.8119
10	+0.381	-1.127	-0.110	-0.0943	-0.0943	-0.0848	+0.5624	+0.3610	+0.9171	+0.1015	+0.2557	-0.0125	+0.0513	-0.0125	-0.0125	-0.8119
0	+3.670	0	+0.7656	0	+0.7656	0	+2.318	0	+0.6128	0	+0.4748	+0.2000	0	0	0	+0.8119
$\phi = 30^\circ$																
$\phi = 30^\circ$	-4.709	0.881	-3.362	-0.2769	-0.2662	-0.0014	+0.6571	+0.1009	-0.2618	-0.1174	-0.0596	-0.0024	-0.0024	-2.101	-0.7879	+0.7879
30	-4.656	-2.381	-2.632	-0.2347	-0.2347	-0.1275	+0.6572	+0.0661	-0.2618	-0.1182	-0.0596	-0.0023	-0.0023	-2.101	-0.7879	+0.7879
20	-1.053	-3.000	-0.837	-0.2347	-0.2347	-0.1275	+0.6572	+0.0661	-0.2618	-0.1182	-0.0596	-0.0023	-0.0023	-2.101	-0.7879	+0.7879
10	+12.43	0	+0.560	0	+0.560	0	+0.8600	+0.0635	-0.3000	+0.3000	+0.3000	-0.0750	+0.0750	-0.0750	-0.0750	-0.0750
0	0	0	0	0	0	0	0	0	0	0	0	0	0	0	0	0

 (d) $r/l = 100$ and $r/l = 0.3$

ϕ	Horizontal Edge Load				Shear Edge Load				Edge Moment Load			
	T_s (1)	S (2)	T_ϕ (3)	M_ϕ (4)	T_s (5)	S (6)	T_ϕ (7)	M_ϕ (8)	T_s (9)	S (10)	T_ϕ (11)	M_ϕ (12)
(e) (Continued)												
$\phi = 0^\circ$	-0.0001	-0.0001	-0.0001	-0.0001	-0.0001	-0.0001	-0.0001	-0.0001	-0.0001	-0.0001	-0.0001	-0.0001
0	-0.0001	-0.0001	-0.0001	-0.0001	-0.0001	-0.0001	-0.0001	-0.0001	-0.0001	-0.0001	-0.0001	-0.0001

(ASCE Table 2A) (continued)

Φ	Vertical Edge Load			Horizontal Edge Load			Stream Edge Load			Elongation Edge Load			Elongation Moment Load			
	T_s (1)	S (2)	T_ϕ (3)	M_ϕ (4)	T_s (5)	S (6)	T_ϕ (7)	M_ϕ (8)	T_s (9)	S (10)	T_ϕ (11)	M_ϕ (12)	T_s (13)	S (14)	T_ϕ (15)	M_ϕ (16)
(d) (Continued)																
$\Phi = 15^\circ$	-2.156 30	0 -2.106 -2.106	-0.565 -1.817 -1.817	-2.682 -2.941 -2.941	-0.2903 -0.3823 -0.3823	0 -0.1511 -0.1511	0.6079 -0.1937 -0.1937	-0.1362 -0.1338 -0.1338	-0.2140 -0.0568 -0.0568	0 -0.0635 -0.0635	-0.0635 -0.0635	-3.493 -0.0945 -0.0945	-0.7613 -0.7613	10.7084 10.7254		
	10	+0.513 0	-2.156 0	-0.182 +0.674	-1.118 0	+0.2301 0	+0.2698 0	-0.2500 +0.0800	+0.1137 +0.0456	-0.0211 -0.0218	-0.0137 -0.0137	-3.761 -3.761	+0.1018 +0.1018	10.7161 10.7252		
	0	+10.04	0	-1.118	0	-0.1118	0	+0.0753	+0.0098	+0.0456	+0.0456	-9.163	0	+0.372 +0.372	+0.9680	
$\Phi = 10^\circ$	-0.216 30	0 -1.030	0 -1.030	-0.275 -1.862	-0.1977 -0.1865	-0.2853 -0.1865	-0.1767 -0.1767	-0.1763 -0.1553	-0.1658 -0.1658	0 -0.0877	-0.0736 -0.0736	-5.193 -0.0068 -0.0068	-2.988 -2.988	-1.609 -1.609	+0.6074 +0.6074	
	20	-2.106 -2.106	-2.106 -2.106	-2.106 -2.106	-1.203 -1.1862	-1.406 -1.406	-1.406 -1.406	-1.406 -1.406	-1.406 -1.406	-1.406 -1.406	-0.1238 -0.1238	-0.1238 -0.1238	-5.193 -0.0068 -0.0068	-2.988 -2.988	-1.609 -1.609	+0.6074 +0.6074
	10	-2.106 0	-2.106 0	-2.106 0	-2.106 0	-2.106 0	-2.106 0	-2.106 0	-2.106 0	-2.106 0	-0.1238 -0.1238	-0.1238 -0.1238	-5.193 -0.0068 -0.0068	-2.988 -2.988	-1.609 -1.609	+0.6074 +0.6074
	0	+10.04	0	-0.1033	0	+0.1033	0	-0.1033	+0.0098	+0.0098	+0.0098	-14.38	0	0	+1.000	
$\Phi = 15^\circ$	+1.000 15	0 -1.030	0 -1.030	-0.358 -0.358	-0.1033 -0.1033	-0.1033 -0.1033	-0.1033 -0.1033	-0.1033 -0.1033	-0.1033 -0.1033	-0.1033 -0.1033	-0.0930 -0.0930	0	-14.38	0	-1.000	
	40	-1.030 0	-0.358 0	-0.1033 0	-0.1033 0	-0.1033 0	-0.1033 0	-0.1033 0	-0.1033 0	-0.1033 0	-0.0930 -0.0930	0	-14.38	0	-1.000	
	30	-1.030 0	-0.358 0	-0.1033 0	-0.1033 0	-0.1033 0	-0.1033 0	-0.1033 0	-0.1033 0	-0.1033 0	-0.0930 -0.0930	0	-14.38	0	-1.000	
	20	-1.030 0	-0.358 0	-0.1033 0	-0.1033 0	-0.1033 0	-0.1033 0	-0.1033 0	-0.1033 0	-0.1033 0	-0.0930 -0.0930	0	-14.38	0	-1.000	
	10	-1.030 0	-0.358 0	-0.1033 0	-0.1033 0	-0.1033 0	-0.1033 0	-0.1033 0	-0.1033 0	-0.1033 0	-0.0930 -0.0930	0	-14.38	0	-1.000	
	0	+10.04	0	-0.1033	0	+0.1033	0	-0.1033	+0.0098	+0.0098	+0.0098	-14.38	0	-14.38	-1.000	
(e) $r/\ell = 100$ and $r/\ell = 0.4$																
$\Phi = 70^\circ$	-3.568 30	0 -3.560	-3.512 -3.512	-3.175 -2.592	-0.2104 -0.2018	-0.736 -0.638	-0.2032 -0.1936	-0.1362 -0.1338	-0.0210 -0.0218	-0.0947 -0.0856	-0.3118 -0.1568	0 -0.1563	-0.0772 -0.0631	-0.0028 -0.0010	-0.870 -0.870	
	20	-1.030 0	-1.030 0	-1.030 0	-1.030 0	-1.030 0	-1.030 0	-1.030 0	-1.030 0	-1.030 0	-1.030 0	-1.030 0	-0.0545 -0.0545	-0.0545 -0.0545	-0.870 -0.870	
	10	-1.030 0	-1.030 0	-1.030 0	-1.030 0	-1.030 0	-1.030 0	-1.030 0	-1.030 0	-1.030 0	-1.030 0	-1.030 0	-0.0545 -0.0545	-0.0545 -0.0545	-0.870 -0.870	
	0	+12.46 0	-0.1033 0	+0.1033 0	-0.1033 0	-0.1033 0	-0.1033 0	-0.1033 0	-0.1033 0	-0.1033 0	-0.0930 -0.0930	-0.0930 -0.0930	-21.76 -21.76	0	-1.000	

(ASCE Table 2A) (continued)

♦	Vertical Floor Load				Horizontal Earth Load				Shear Earth Load				Wind Moment Load			
	T _s (1)	S (2)	T _♦ (3)	M _♦ (4)	T _s (5)	S (6)	T _♦ (7)	M _♦ (8)	T _s (9)	S (10)	T _♦ (11)	M _♦ (12)	T _s (13)	S (14)	T _♦ (15)	M _♦ (16)
(e) (Continued)																
Φ = 35°	-0.217	0	-2.261	-0	-1.518	0.3878	0.670	-0.1001	-0.2518	0	-0.0842	-0.0040	-8.18	0	-1.860	0.5064
30	-0.166	-0.062	-0.220	-0	-1.214	-0.0723	-0.723	-0.1078	-0.2316	-0.0672	-0.0716	-0.0047	6.82	2.173	-1.574	0.5463
15	-0.152	-0.052	-0.205	-0	-1.183	-0.0677	-0.690	-0.0852	-0.2040	-0.0672	-0.0673	-0.0040	6.69	2.169	-1.564	0.5463
0	+0.151	-0.052	-0.195	-0.0182	+0.396	-0.0577	-0.690	-0.0852	-0.2040	+0.0673	+0.0673	+0.0040	0	0	+1.064	+1.064
40° = 40	+2.485	0	-1.221	-0.204	-2.664	-1.171	1.026	-0.1088	-0.1512	0.851	-0.0818	-0.0040	-11.15	0.928	-3.211	0.3806
30	+0.117	+0.013	-1.512	-0.194	-1.123	-1.171	0.656	+0.1088	-0.1515	-0.0851	-0.0567	-0.0039	4.83	-4.928	-0.164	+0.451
20	-4.206	-0.278	-1.700	-0.1580	+2.058	-0.6130	-0.1013	+0.1023	-0.1515	-0.0850	-0.0566	-0.0017	+8.71	-3.904	+1.250	+0.6068
10	-2.814	-0.249	-0.749	-0.0662	+2.405	-0.6316	-0.1216	+0.1223	-0.1515	-0.0850	-0.0566	-0.0017	+11.30	-2.733	+1.764	+0.7018
0	+17.20	0	+0.613	0	-7.122	+0.665	-0.746	+0.4000	-0.0728	0	+0.0728	0	-33.39	0	+1.000	+1.000
Φ = 45°	+4.326	0	-0.119	-0.1513	-3.817	-0.005	-0.372	+0.0890	-0.0053	-0.0652	-0.0054	-0.0054	-12.50	0	-4.617	+0.2210
40	+3.663	+1.126	-0.277	-0.1526	-3.361	-1.005	-0.230	+0.0823	-0.0053	-0.0652	-0.0054	-0.0054	-12.50	0	-4.168	+0.2112
30	+0.018	+2.020	-1.246	-0.1561	-0.150	-2.079	-0.703	-0.1060	-0.2030	-0.0673	-0.0673	-0.0040	0	0	-6.250	-0.3816
20	-6.034	-0.008	-1.886	-0.1477	-1.376	-0.1015	+1.638	+0.1083	-0.0344	-0.1112	-0.0158	-0.0015	+12.55	0.971	+2.411	+0.5011
10	-3.355	-3.104	-0.784	-0.0784	+3.104	+1.260	+1.497	+0.0731	+0.3651	+0.0110	+0.0216	+0.0000	+11.51	+4.702	+2.303	+0.7116
0	+0.707	0	-0.707	0	-10.78	0	+0.707	0	+1.388	+0.4000	0	0	0	-30.59	0	+0.000
Φ = 50°	+4.073	0	+0.784	-0.0881	-4.377	-0.5	-1.043	+0.0545	-0.0216	0	-0.0305	-0.0045	-11.45	0	-5.473	+0.1510
40	+2.870	+2.328	-0.150	-0.1576	-2.858	-2.155	-0.384	-0.0716	-0.0276	-0.0025	-0.0016	-0.0016	-7.65	-4.182	+3.775	+0.1504
30	-2.133	+2.116	-0.150	-0.1576	-2.858	-2.155	-0.384	-0.0716	-0.0276	-0.0025	-0.0016	-0.0016	-7.65	-4.182	+3.775	+0.1504
20	-6.881	-0.213	-2.118	-0.1244	+5.125	-1.065	-0.1657	-0.1165	-0.0882	-0.0113	-0.0025	+0.0100	+13.82	-1.157	+3.201	+0.5081
10	-3.019	-0.310	-0.001	-0.0724	-3.212	+0.800	+2.539	+0.1881	-0.0770	-0.0125	-0.0010	+0.0003	+10.19	+5.359	+2.668	+0.7098
0	+20.35	0	+0.766	0	-13.50	0	-0.613	+0.4000	+1.450	0	-0.0667	+0.0003	-41.80	0	0	+1.000
(f) - r/t = 100 and r/t = 0.5																
Φ = 30°	-1.757	0	-2.870	-0.2010	-1.420	0	-0.767	+0.0780	-0.1010	0	-0.0912	-0.0030	-10.64	0	-1.770	0.5085
20	-3.508	-1.321	-2.524	-0.1738	-0.108	-0.037	-0.5108	+0.0932	-0.0727	-0.1063	-0.1773	-0.0368	-12.54	-0.48	-3.877	+0.1585
10	+2.262	-3.378	-0.006	-0.0060	+1.616	+0.0381	+1.076	+0.0489	+0.0489	+0.4554	-0.1263	+0.0654	-12.54	+0.246	+0.008	+0.740
0	+20.22	0	+0.500	0	-3.767	0	-0.866	+0.4000	+1.450	0	-0.0667	+0.0003	-41.80	0	0	+1.000

(ASCE Table 2A) (*continued*)

$$(6) \quad r/t = 100 \text{ and } r/\lambda = 0.6$$

(ASCE Table 2A) (continued)

ϕ	Vertical Edge Load				Horizontal Edge Load				Shear Edge Load				Edge Moment Load				
	T_s (1)	S (2)	T_b (3)	M_b (4)	T_s (5)	S (6)	T_b (7)	M_b (8)	T_s (9)	S (10)	T_b (11)	M_b (12)	T_s (13)	S (14)	T_b (15)	M_b (16)	
(a) (Continued)																	
$\phi = 35^\circ$	5.530	0	+0.999	-0.1294	-1.187	0	+0.085	+0.0231	-0.0245	0	-0.0617	-0.0036	-21.54	0	-4.900	+0.2286	
30	+3.984	+1.371	-1.194	-0.1294	-1.072	-1.072	+0.085	+0.0381	-0.0238	-0.0617	-0.0049	-0.0034	-17.56	-5.639	-4.667	+0.2334	
20	+5.521	+1.142	-2.096	-0.1294	-1.625	+1.008	+0.085	+0.0381	-0.0238	-0.1738	-0.0016	+0.0014	+8.73	+8.73	+0.457	+0.457	
10	-7.862	-3.492	-1.432	-0.0731	4.617	+0.5579	+0.0477	+0.4825	+0.1215	+0.0821	+0.0021	+0.0021	+2.778	+2.844	+0.6789	+0.6789	
0	+31.29	0	+0.574	0	-11.74	0	+0.891	+2.453	+0.6000	0	+0.0000	0	-6.87	0	+1.000	+1.000	
(b) $r/l = 200$ and $\gamma l = 0.1$																	
$\phi = 40^\circ$	0	0	0	0	0	0	0	0	0	0	0	0	-20.91	0.058	-6.113	+0.1748	
40	+8.026	+3.389	+0.412	-0.0987	-2.518	0	+0.0778	-0.0578	-0.0565	-0.0653	-0.0034	-0.0034	-10.34	8.625	-3.216	+0.1447	
30	+2.640	+3.389	-0.650	-0.0987	-2.498	+0.632	+0.0500	-0.1750	-0.0885	-0.0601	-0.0020	-0.0020	-16.62	+0.0012	+3.566	+0.6842	
20	-8.598	-4.118	-2.347	-0.1016	-1.016	+1.341	+0.1016	+0.1503	-0.1750	-0.1554	-0.0018	-0.0018	+2.63	+0.0012	+0.0012	+1.000	
10	-8.783	-4.118	-1.651	-0.0671	+5.659	+1.341	+0.0673	+0.1503	-0.1750	-0.1554	-0.0018	-0.0018	+75.81	+0.0004	+0.0004	+1.000	
0	+34.71	0	+0.643	0	-17.02	0	-0.706	-0.038	+0.038	+0.0000	+0.0000	+0.0000	-75.81	0	0	+1.000	
(c) $r/l = 200$ and $\gamma l = 0.1$																	
$\phi = 45^\circ$	0	0	0	0	0	0	0	0	0	0	0	0	-15.56	0	-4.156	-0.0364	
45	+7.904	+2.058	+1.346	-0.0283	-5.885	-1.550	-1.258	-0.0115	+0.0166	+0.0166	-0.0267	-0.0026	-14.36	-4.156	-0.0122	+0.1633	
30	+6.985	+2.058	+1.415	-0.0283	-5.885	-1.550	-1.258	-0.0115	+0.0166	+0.0166	-0.0267	-0.0026	-14.36	-4.156	-0.0122	+0.1633	
20	-8.846	-4.055	-1.082	-0.0283	-5.885	-1.550	-1.258	-0.0115	+0.0166	+0.0166	-0.0267	-0.0026	-14.36	-4.156	-0.0122	+0.1633	
10	-7.803	-4.055	+1.452	-0.0283	-5.885	-1.550	-1.258	-0.0115	+0.0166	+0.0166	-0.0267	-0.0026	-14.36	-4.156	-0.0122	+0.1633	
0	+34.56	-0	+0.707	0	-20.64	0	+0.707	0	+0.0023	+0.0023	+0.0023	+0.0023	-0.0004	+0.0004	+0.0004	+0.1633	
(d) $r/l = 200$ and $\gamma l = 0.1$																	
$\phi = 50^\circ$	0	0	0	0	0	0	0	0	0	0	0	0	-8.26	0	-5.666	-0.0650	
40	+6.029	+2.055	+1.647	-0.0038	-4.847	0	-0.0114	+0.1678	+0.1678	-0.0073	-0.0015	-0.0015	-8.26	-4.83	-4.344	-0.0164	
30	+4.086	+2.055	+1.283	-0.0192	-3.656	-2.446	-0.851	-0.0100	+0.0523	+0.0523	-0.0689	-0.0151	-0.0017	-8.00	-4.83	-4.344	-0.0164
20	-1.803	+3.754	-1.294	-0.0627	-0.458	-3.469	+0.919	-0.0574	-0.2030	-0.2030	-0.0305	-0.0191	-0.0018	-1.03	-0.635	-0.635	-0.1835
10	-9.145	+0.659	-2.736	-0.0932	+6.530	-1.539	+2.469	-0.0897	-0.2862	-0.2862	-0.1225	-0.0245	-0.0010	-1.86	-5.014	-5.014	-0.4225
0	+6.445	-4.528	-1.501	-0.0624	+6.010	+2.570	+2.141	-0.0596	+0.3899	+0.3899	-0.1463	-0.0675	+0.0003	+20.05	+3.658	+3.658	+0.6366
	+31.83	0	+0.766	0	-22.64	0	+0.643	0	+0.6000	+0.6000	0	+0.6000	0	-70.37	0	0	+0.000

(ASCE Table 2A) (continued)

$\phi = 35^\circ$	Vertical Floor Load				Horizontal Floor Load				Shear Edge Load				End Moment Load			
	T_x (1)	S (2)	T_y (3)	M_ϕ (4)	T_x (5)	S (6)	T_y (7)	M_ϕ (8)	T_x (9)	S (10)	T_y (11)	M_ϕ (12)	T_x (13)	S (14)	T_y (15)	M_ϕ (16)
-3.373	0	-2.917	-0.3062	-0.0319	0	-0.0733	-0.0243	-0.0015	-0.2011	-0.0536	-0.0133	+0.0623	-0.0536	-0.0133	+0.0623	
-3.173	-0.937	-8.01	-0.3581	-0.0727	-0.0039	-0.0175	-0.0035	-0.0035	-0.0115	-0.0014	-0.0014	-0.0120	-0.0120	-0.0120	-0.0120	
-3.046	-2.382	-6.61	-0.2774	-0.0152	-0.0031	-0.0161	-0.0031	-0.0031	-0.0115	-0.0014	-0.0014	-0.0114	-0.0114	-0.0114	-0.0114	
-2.90	-1.673	-3.10	-0.337	-0.1111	-0.0032	-0.0151	-0.0032	-0.0032	-0.0115	-0.0014	-0.0014	-0.0114	-0.0114	-0.0114	-0.0114	
-1.9	-0.574	0	-0.358	-0.00675	-0.0032	-0.0167	-0.0032	-0.0032	-0.0115	-0.0014	-0.0014	-0.0114	-0.0114	-0.0114	-0.0114	
(b) (Continued)																
$\phi = 40^\circ$	-2.193	0	-2.826	-0.4041	-0.0791	-0.0341	-0.09782	-0.0237	-0.0670	0	-0.0125	-0.0022	-0.0022	-0.0022	-0.0022	-0.0022
-3.0	-1.813	-1.137	-2.015	-0.3677	-0.0303	-0.0341	-0.09712	-0.0205	-0.0658	-0.0158	-0.0028	-0.0028	-0.0028	-0.0028	-0.0028	-0.0028
-3.0	-0.678	-1.806	-0.220	-0.2090	-0.00577	-0.0219	-0.0969	-0.0177	-0.0619	-0.0158	-0.0029	-0.0029	-0.0029	-0.0029	-0.0029	-0.0029
-10	-1.181	-1.699	-0.0483	-0.1354	-0.0178	-0.0246	-0.09695	-0.0121	-0.0625	-0.0154	-0.0035	-0.0035	-0.0035	-0.0035	-0.0035	-0.0035
0	-0.460	0	-0.4613	0	-0.2213	0	-0.7660	0	-0.0002	-0.0020	-0.0002	-0.0002	-0.0002	-0.0002	-0.0002	-0.0002
$\phi = 45^\circ$	-1.415	0	-2.167	-0.4305	-0.1591	-0.0416	-0.2747	-0.0585	-0.0311	-0.0031	-0.0031	-0.0031	-0.0031	-0.0031	-0.0031	-0.0031
-45	-1.381	-0.385	-2.106	-0.3226	-0.1386	-0.0418	-0.2439	-0.0585	-0.0127	-0.0028	-0.0028	-0.0028	-0.0028	-0.0028	-0.0028	-0.0028
-30	-1.097	-1.081	-0.635	-0.3029	-0.0816	-0.0838	-0.1561	-0.0441	-0.0239	-0.0032	-0.0032	-0.0032	-0.0032	-0.0032	-0.0032	-0.0032
-20	-0.550	-1.505	-0.798	-0.2550	-0.1623	-0.1635	-0.1371	-0.0812	-0.0126	-0.0037	-0.0018	-0.0018	-0.0018	-0.0018	-0.0018	-0.0018
-10	-1.175	-1.323	-0.148	-0.1251	-0.1167	-0.0570	-0.1510	-0.071	-0.1213	-0.0121	-0.0028	-0.0028	-0.0028	-0.0028	-0.0028	-0.0028
0	-0.207	0	-0.4387	0	-0.207	0	-0.4371	0	-0.1071	-0.1071	-0.1000	-0.1000	-0.1000	-0.1000	-0.1000	-0.1000
$\phi = 50^\circ$	-0.838	0	-1.75	-0.4457	-0.1831	-0.2911	-0.3273	-0.0250	-0.0346	0	-0.0346	-0.0014	-0.0014	-0.0014	-0.0014	-0.0014
-45	-0.818	0	-1.61	-0.4195	-0.1746	-0.3378	-0.3492	-0.0251	-0.0125	-0.0068	-0.0026	-0.0026	-0.0026	-0.0026	-0.0026	-0.0026
-30	-0.562	-1.61	-0.908	-0.3229	-0.3456	-0.1012	-0.1615	-0.0255	-0.0125	-0.0068	-0.0024	-0.0024	-0.0024	-0.0024	-0.0024	-0.0024
-20	-0.311	-1.227	-0.517	-0.2308	-0.3210	-0.0318	-0.1439	-0.0202	-0.0167	-0.0067	-0.0016	-0.0016	-0.0016	-0.0016	-0.0016	-0.0016
-10	-0.907	-1.111	-0.284	-0.1142	-0.1615	-0.1245	-0.1201	-0.1167	-0.1175	-0.0987	-0.0271	-0.0271	-0.0271	-0.0271	-0.0271	-0.0271
0	-3.402	0	-0.766	0	-0.7384	0	-0.6128	0	-0.1000	-0.1000	-0.1000	-0.1000	-0.1000	-0.1000	-0.1000	-0.1000

(i) $r/h = 200$ and $r/l = 2$

(ASCE Table 2A) (continued)

♦	Vertical Edge Load				Horizontal Edge Load				Shallow Edge Load				Deep Moment Load				
	T _v	S	T _h	M _h	T _v	S	T _h	M _h	T _v	S	T _h	M _h	T _v	S	T _h	M _h	
(1)	(2)	(3)	(4)	(5)	(6)	(7)	(8)	(9)	(10)	(11)	(12)	(13)	(14)	(15)	(16)		
(i) (Continued)																	
$\phi = 35^\circ$	-2.669	0	-2.120	-0.3204	-0.5655	0	0.5655	+0.8832	+0.1560	-0.1455	0	-0.0466	-0.0027	-3.344	0	-0.7035	+0.8373
30	-2.990	-0.624	-2.124	-0.3204	-0.5253	-0.1446	-0.5253	+0.9000	+0.1531	-0.1313	-0.0366	-0.0410	-0.0025	-2.686	-0.8382	-0.8425	
20	-2.635	-0.834	-1.655	-0.2507	+0.2416	-0.2183	-0.2183	+0.9868	+0.1291	-0.0100	-0.0363	-0.0114	-0.0023	-1.373	-0.319	+0.1200	+0.8487
10	+0.948	-4.23	-0.570	-0.1313	-0.5710	+0.0604	-0.9767	+0.0783	+0.8191	+0.6331	-0.0368	+0.0358	+0.0002	-1.3518	+0.4350	+0.4355	+0.0000
0	0	0	0	0	0	0	0	0	0	0	0	0	0	0	0	0	0
$\phi = 0^\circ$	-0.324	0.318	-2.221	-0.3221	-0.3365	1.1323	-0.4724	-0.4955	+0.6621	+0.1847	-0.1144	-0.0503	-0.0037	5.117	0.117	-0.7422	-0.7549
90	-0.324	0.318	-2.221	-0.3221	-0.3365	-0.4724	-0.4724	-0.3660	+0.5224	+0.1760	-0.0838	-0.0572	-0.0331	-2.270	-0.2270	-0.2270	-0.8388
20	-0.257	-0.228	-1.125	-0.3010	-0.3231	-0.8653	-0.8653	-0.1027	+0.1027	+0.1027	+0.1458	+0.0292	-0.0755	-0.0213	-0.8390	-0.8390	-0.8390
10	-0.178	-0.090	-0.125	-0.2331	-0.2331	-0.3231	-0.3231	-0.1027	+0.1027	+0.1027	+0.1324	+0.0292	+0.0292	+0.0292	+1.095	+0.0292	+0.0292
0	0	0	0	0	0	0	0	0	0	0	0	0	0	0	0	0	0
$\phi = 45^\circ$	+0.337	0	+0.090	+0.090	+0.1343	0	-2.851	+0.1324	+0.1324	+0.1324	+0.1324	+0.7650	+0.5858	+0.0200	-13.55	+0.0200	+0.0200
45	+1.358	0	+0.344	-1.210	-0.3140	-1.967	-0.5171	-0.5171	+0.3169	+0.1973	-0.0743	0	-0.0414	-0.0047	7.076	-0.8462	-0.8462
30	+1.046	0	+0.344	-1.210	-0.3140	-1.725	-0.5171	-0.5171	+0.3877	+0.1967	-0.0769	-0.0215	-0.0442	-0.0045	-6.231	-0.5827	-0.5827
20	-3.033	-0.788	-0.770	-1.409	-0.2789	-0.6113	-0.6113	-0.5050	+0.1204	+0.1204	+0.1281	-0.0516	-0.0242	-0.0223	-0.0316	-0.5216	-0.5216
10	-3.035	-0.788	-0.770	-1.409	-0.2789	-0.6113	-0.6113	-0.5110	+0.1204	+0.1204	+0.1281	-0.0516	-0.0242	-0.0223	-0.0316	-0.5216	-0.5216
0	0	0	0	0	0	0	0	0	0	0	0	0	0	0	0	0	0
$\phi = 90^\circ$	+0.985	0	-2.169	-0.027	-0.1087	-1.486	+0.0994	+0.159	+0.0935	+0.2164	-0.0071	+0.0436	+0.0031	-5.706	+1.273	+1.273	+0.0200
90	0	0	0	0	0	0	0	0	0	0	0	0	0	0	0	0	0
$\phi = -90^\circ$	+2.886	0	-0.312	-0.2988	-2.918	0	-0.2665	+0.1807	-0.0385	-0.0445	-0.0226	-0.0049	-0.0032	-6.502	-0.4461	-0.4461	
30	+1.860	+1.105	-1.055	-0.2885	-0.2662	-1.798	-1.381	+0.1445	+0.1836	-0.0445	-0.0226	-0.0049	-0.0032	-6.350	-0.4461	-0.4461	
20	-1.45	-0.689	-1.055	-0.1867	+0.1904	-1.675	-1.016	+0.1889	+0.1889	-0.0420	-0.0146	-0.0140	-0.0041	-5.433	-0.5106	-0.5106	
10	-1.45	-0.689	-1.055	-0.1867	+0.1904	-1.675	-1.016	+0.1655	+0.1655	-0.0420	-0.0146	-0.0140	-0.0041	-4.459	-0.5106	-0.5106	
0	0	0	0	0	0	0	0	0	0	0	0	0	0	0	0	0	0
$\phi = 0^\circ$	+12.38	0	-0.079	-0.0895	-0.0895	-0.079	-0.079	-0.079	-0.079	-0.079	-0.079	-0.079	-0.079	-0.079	-0.079	-0.079	-0.079
$\phi = 30^\circ$	-2.875	1	-3.087	-0.2688	-1.018	0	-0.8833	+0.1065	-0.2481	-0.1187	-0.0759	-0.0535	-0.0023	-8.01	-0.2906	-0.2906	
30	-3.544	-1.727	-2.395	-0.2300	-0.1270	-1.142	-0.0251	-0.3975	+0.0558	+0.0561	-0.1187	-0.0236	-0.0023	-8.01	-0.2906	-0.2906	
10	-1.005	-0.351	-0.350	-0.1921	-0.1921	-0.2118	-0.0251	-0.1038	+0.0360	+0.0360	-0.1126	+0.0402	-0.0023	-9.20	+0.158	+0.158	+0.0000
0	0	0	0	0	0	0	0	0	0	0	0	0	0	0	0	0	0

 (j) $r/l = 200$ and $r/l = 0.3$

ϕ	Vertical Edge Load				Horizontal Edge Load				Shallow Edge Load				Deep Moment Load				
	T _v	S	T _h	M _h	T _v	S	T _h	M _h	T _v	S	T _h	M _h	T _v	S	T _h	M _h	
(1)	(2)	(3)	(4)	(5)	(6)	(7)	(8)	(9)	(10)	(11)	(12)	(13)	(14)	(15)	(16)		
(k) (Continued)																	
$\phi = 30^\circ$	-2.875	0	-3.087	-0.2688	-1.018	0	-0.8833	+0.1065	-0.2481	-0.1187	-0.0759	-0.0535	-0.0023	-8.01	-0.2906	-0.2906	
30	-3.544	-1.727	-2.395	-0.2300	-0.1270	-1.142	-0.0251	-0.3975	+0.0558	+0.0561	-0.1187	-0.0236	-0.0023	-8.01	-0.2906	-0.2906	
10	-1.005	-0.351	-0.350	-0.1921	-0.1921	-0.2118	-0.0251	-0.1038	+0.0360	+0.0360	-0.1126	+0.0402	-0.0023	-9.20	+0.158	+0.158	+0.0000
0	0	0	0	0	0	0	0	0	0	0	0	0	0	0	0	0	0

(ASCE Table 2A) (continued)

ϕ	Vertical End Load				Horizontal End Load				Shear End Load				Floor Moment Load			
	T_x (1)	S (2)	T_y (3)	M_ϕ (4)	T_x (5)	S (6)	T_y (7)	M_ϕ (8)	T_x (9)	S (10)	T_y (11)	M_ϕ (12)	T_x (13)	S (14)	T_y (15)	M_ϕ (16)
(j) (Continued)																
$\phi = 35^\circ$	+ 1.157 35	0 + 0.434 20	- 2.003 - 0.250 - 2.937 - 0.907	- 0.2659 - 0.134 - 0.2908 - 0.903	- 3.540 - 1.763 - 1.001 - 0.1119	0 + 0.5163 + 0.3879 + 0.2927 + 0.1119	+ 0.5377 + 0.6157 + 0.5051 + 1.184	+ 0.1233 + 0.1230 - 0.087 - 0.098	- 0.1777 - 0.1650 - 0.1115 - 0.1118	- 0.0475 - 0.0475 - 0.0475 - 0.0475	- 0.0616 - 0.0548 - 0.0548 - 0.0548	- 0.0033 - 0.0033 - 0.0033 - 0.0033	- 12.73 - 10.23 - 5.57 - 3.52	- 2.708 - 3.260 - 4.414 - 4.427	+ 0.6320 + 0.6414 + 0.6414 + 0.6414	
$\phi = 40^\circ$	0 + 18.06	0 + 0.574	- 2.003 - 0.250 - 2.937 - 0.907	- 0.2659 - 0.134 - 0.2908 - 0.903	- 3.540 - 1.763 - 1.001 - 0.1119	0 + 0.5163 + 0.3879 + 0.2927 + 0.1119	+ 0.8192 0 + 0.8192 0	+ 0.1233 + 0.1230 - 0.087 - 0.098	- 0.1777 - 0.1650 - 0.1115 - 0.1118	- 0.0475 - 0.0475 - 0.0475 - 0.0475	- 0.0616 - 0.0548 - 0.0548 - 0.0548	- 0.0033 - 0.0033 - 0.0033 - 0.0033	- 12.73 - 10.23 - 5.57 - 3.52	- 2.708 - 3.260 - 4.414 - 4.427	+ 0.6320 + 0.6414 + 0.6414 + 0.6414	
$\phi = 45^\circ$	+ 1.401 45	0 + 0.613	- 2.003 - 0.250 - 2.937 - 0.907	- 0.2659 - 0.134 - 0.2908 - 0.903	- 3.540 - 1.763 - 1.001 - 0.1119	0 + 0.5163 + 0.3879 + 0.2927 + 0.1119	+ 0.8192 0 + 0.8192 0	+ 0.1233 + 0.1230 - 0.087 - 0.098	- 0.1777 - 0.1650 - 0.1115 - 0.1118	- 0.0475 - 0.0475 - 0.0475 - 0.0475	- 0.0616 - 0.0548 - 0.0548 - 0.0548	- 0.0033 - 0.0033 - 0.0033 - 0.0033	- 12.73 - 10.23 - 5.57 - 3.52	- 2.708 - 3.260 - 4.414 - 4.427	+ 0.6320 + 0.6414 + 0.6414 + 0.6414	
$\phi = 50^\circ$	+ 1.551 50	0 + 0.626	- 2.003 - 0.250 - 2.937 - 0.907	- 0.2659 - 0.134 - 0.2908 - 0.903	- 3.540 - 1.763 - 1.001 - 0.1119	0 + 0.5163 + 0.3879 + 0.2927 + 0.1119	+ 0.8192 0 + 0.8192 0	+ 0.1233 + 0.1230 - 0.087 - 0.098	- 0.1777 - 0.1650 - 0.1115 - 0.1118	- 0.0475 - 0.0475 - 0.0475 - 0.0475	- 0.0616 - 0.0548 - 0.0548 - 0.0548	- 0.0033 - 0.0033 - 0.0033 - 0.0033	- 12.73 - 10.23 - 5.57 - 3.52	- 2.708 - 3.260 - 4.414 - 4.427	+ 0.6320 + 0.6414 + 0.6414 + 0.6414	
(k) $r/l = 200$ and $r/l = 0.4$																
$\phi = 30^\circ$	+ 1.124 30	0 - 3.463	- 2.479 - 0.295	- 0.2211 - 0.1947	- 2.025 - 0.9430	- 0.2211 - 0.9430	+ 0.5943 + 0.9092	+ 0.0868 + 0.0868	- 0.2817 - 0.1583	0 - 0.1339	- 0.0710 - 0.1302	- 0.0026 - 0.0018	- 20.19 - 20.19	- 0.433 - 0.433	- 3.173 - 3.173	- 0.5013 - 0.5013
$\phi = 20^\circ$	- 8.853 20	- 4.094 - 3.408	+ 2.518 - 1.407	+ 0.437 - 0.1117	+ 0.274 - 0.0700	+ 0.1947 + 0.1947	+ 1.111 + 1.191	+ 0.0868 0	- 0.1118 - 0.1098	0 - 0.1029	+ 0.0493 + 0.4000	+ 0.0026 + 0.0018	+ 21.57 + 21.57	+ 0.435 + 0.435	+ 3.618 + 3.618	+ 0.610 + 0.610
$\phi = 10^\circ$	- 4.273 10	- 4.273 - 2.528	- 2.518 - 1.407	- 0.437 - 0.1117	- 0.274 - 0.0700	+ 2.491 + 1.987	+ 4.214 + 0.6128	+ 2.483 0	- 0.1118 - 0.1098	0 - 0.1029	+ 0.0493 + 0.4000	+ 0.0026 + 0.0018	+ 21.57 + 21.57	+ 0.435 + 0.435	+ 3.618 + 3.618	+ 0.610 + 0.610
$\phi = 0^\circ$	+ 4.273 0	- 4.273 - 2.528	- 2.518 - 1.407	- 0.437 - 0.1117	- 0.274 - 0.0700	- 17.75 0	- 17.75 + 0.6128	- 17.75 0	- 0.1118 - 0.1098	0 - 0.1029	+ 0.0493 + 0.4000	+ 0.0026 + 0.0018	+ 21.57 + 21.57	+ 0.435 + 0.435	+ 3.618 + 3.618	+ 0.610 + 0.610

(ASCE Table 2A) (continued)

♦	Vertical Edge Load			Horizontal Edge Load			Shear Edge Load			Front Moment Load		
	T _s	S	T _e	M _φ	(1)	(2)	T _s	S	T _e	M _φ	T _s	S
(k) (Continued)												
♦ = .35	+ 6.673	+ 7.12	- 0.705	- 0.1850	- 4.632	- 0.1617	+ 0.0837	- 0.1462	- 0.0635	- 0.0032	- 22.50	0
30	+ 6.603	+ 6.14	- 1.039	- 0.1820	- 3.951	- 1.261	+ 0.0848	- 0.1482	- 0.0630	- 0.0030	- 7.05	- 5.635
20	- 6.203	- 2.206	- 2.061	- 0.1617	+ 2.308	- 1.889	+ 0.153	- 0.1152	- 0.0617	- 0.0017	- 11.73	+ 0.4179
10	- 3.087	- 3.382	- 1.613	- 0.1631	+ 1.356	+ 0.6587	+ 0.0862	- 0.0866	- 0.0621	+ 0.0539	+ 3.583	+ 0.5937
0	+ 34.19	0	+ 0.674	0	- 13.36	0	+ 0.8192	+ 0.3204	+ 0.0822	+ 0.0539	0	+ 1.000
♦ = .40	-	-	-	-	-	-	-	-	-	-	-	-
40	+ 11.34	0	+ 0.768	- 0.1216	- 7.637	0	- 0.0122	+ 0.0723	+ 0.0319	0	- 0.0148	- 32.34
30	+ 3.302	+ 4.447	- 0.465	- 0.1253	- 2.692	- 0.0367	- 0.0122	- 0.0781	- 0.0171	- 0.0032	- 1.323	- 1.289
20	- 10.30	+ 2.161	- 2.620	- 0.1409	+ 5.333	- 2.418	+ 0.0815	- 0.1367	- 0.0818	- 0.0036	- 10.73	- 4.242
10	- 10.34	- 4.580	- 1.955	- 0.0831	+ 6.811	+ 1.620	+ 0.1857	+ 0.0704	+ 0.2120	- 0.0845	+ 31.74	+ 0.5868
0	+ 39.09	0	+ 0.643	0	- 19.78	0	+ 0.7060	+ 0.0704	+ 0.14	+ 0.4000	0	+ 1.000
♦ = .45	-	-	-	-	-	-	-	-	-	-	-	-
40	+ 8.587	0	+ 0.772	+ 1.394	- 7.228	0	- 1.602	+ 0.0190	+ 0.0037	0	- 0.0006	- 22.45
30	+ 8.557	+ 2.427	- 0.835	- 0.033	- 6.936	- 1.011	- 1.410	+ 0.0375	+ 0.0198	- 0.0013	- 20.2	- 5.970
20	- 1.527	+ 3.169	- 3.68	- 0.1505	- 6.109	- 1.010	- 1.410	+ 0.0375	+ 0.0198	- 0.0012	- 13.43	- 2.116
10	- 0.650	+ 4.513	- 2.909	- 0.0857	- 7.382	- 2.215	+ 2.250	+ 0.0800	+ 0.2390	- 0.0012	- 23.35	- 8.250
0	+ 38.68	0	+ 0.707	0	- 23.68	0	+ 0.7071	+ 0.0800	+ 1.826	+ 0.4000	0	+ 1.000
♦ = .50	-	-	-	-	-	-	-	-	-	-	-	-
40	+ 7.414	+ 3.616	+ 2.207	+ 0.0042	- 6.122	0	- 0.0134	+ 0.1395	0	+ 0.0147	- 0.0013	- 13.14
30	+ 4.947	+ 4.440	+ 1.124	- 0.0267	- 4.489	- 3.008	- 1.161	+ 0.0151	+ 0.0405	+ 0.0042	- 0.0015	- 11.30
20	- 2.266	+ 4.440	- 1.556	- 0.0810	+ 0.935	- 4.116	+ 0.9827	+ 0.0776	- 0.1446	+ 0.0332	- 0.0017	- 10.95
10	- 10.69	+ 3.819	- 3.975	+ 0.2945	+ 7.557	- 1.711	+ 2.811	+ 0.1179	- 0.2195	- 0.0793	- 0.0011	- 19.84
0	- 7.142	- 3.081	- 1.774	- 0.0835	+ 6.437	+ 3.015	+ 2.378	+ 0.0892	+ 0.2113	- 0.1076	+ 0.0402	+ 23.36
	+ 35.00	0	+ 0.766	0	- 25.44	0	+ 0.6428	+ 0.6428	+ 1.810	+ 1.000	0	+ 1.000
											- 8.42	0
(l) r/l = 200 and r/l = 0.5												
♦ = .30:	+ 6.008	+ 7.701	- 1.578	- 0.1695	- 4.032	- 1.230	+ 0.2225	+ 0.0656	- 0.2115	- 0.0075	- 36.86	- 5.818
30	+ 6.001	+ 6.626	- 1.263	- 0.1657	- 1.657	+ 1.353	+ 0.8452	+ 0.0654	- 0.1971	- 0.0018	- 2.00	- 1.174
20	- 1.218	+ 1.972	- 1.972	- 0.0557	- 1.353	+ 0.1528	+ 0.8452	+ 0.0652	+ 0.2253	+ 0.0306	+ 43.35	+ 0.5258
10	+ 4.335	0	+ 1.500	0	- 13.29	0	+ 0.8650	+ 0.0652	+ 0.5000	- 0.0017	- 107.5	+ 1.30
0	-	-	-	-	-	-	-	-	-	-	0	+ 1.000

(ASCE Table 2A) (continued)

ϕ	Vertical Edge Load				Horizontal Edge Load				Shear Edge Load				Edge Moment Load			
	T_s (1)	S (2)	T_b (3)	M_b (4)	T_s (5)	S (6)	T_b (7)	M_b (8)	T_s (9)	S (10)	T_b (11)	M_b (12)	T_s (13)	S (14)	T_b (15)	M_b (16)
(I) Continued																
$\phi = 35^\circ$	-4.12	0.92	0	+0.520	-0.106	-7.760	-0.627	-0.6687	+0.0480	+0.0560	-0.1784	-0.0228	-0.0027	-41.17	-9.181	+0.1851
30	+0.14	3.193	0	-0.151	-0.151	-0.371	-1.925	-0.308	+1.253	+0.0670	-0.1818	-0.00866	-0.00015	+16.53	-10.62	-0.2222
20	-8.763	+1.022	-2.425	-0.1266	+1.266	+1.367	+1.926	+1.030	+0.0564	+0.1280	+0.0516	-0.0001	+1.439	-16.90	+0.4668	
10	-16.09	-4.481	-2.417	-0.0897	+0.574	-22.16	0	+0.8102	+0.2774	+0.5080	0	+1.205	+5.26	+5.747	+0.7504	
0	+32.21	0	+0.574	0	0	0	0	0	0	0	0	-142.8	0	0	+1.000	
$\phi = 40$	+4.3	0.93	0	+1.903	-0.0443	-8.698	0	-1.529	+0.0185	+0.1093	-0.075	-0.0298	-0.0020	-32.96	-10.30	-0.072
30	+5.401	4.888	+0.146	-0.12	-0.12	+0.912	+0.912	+3.933	+0.0357	+0.0398	-0.075	-0.0052	-0.0034	-15.29	-5.586	+0.1889
20	-12.79	+3.838	-3.838	-0.9860	-0.9860	-3.817	-0.9860	-0.9860	+0.945	+0.945	+0.945	+0.0333	+0.0333	+3.942	+9.4588	
10	-4.53	-3.471	-3.471	-0.633	-0.633	-3.21	-0.633	-0.633	-0.7660	-0.7660	-0.7660	+0.5800	+0.5800	-133.3	0	+1.000
0	+23.33	0	0	0	0	0	0	0	0	0	0	0	0	0	0	0
$\phi = 45^\circ$	+1.0	0.22	0	+2.135	+0.0045	-7.196	-0.907	-1.959	-0.0031	+0.1446	+0.0466	+0.0132	-0.0011	-18.31	0	-0.981
30	+0.9	1.885	+2.771	+2.135	-0.0045	-0.757	-1.907	-1.675	+0.0031	+0.1446	+0.0466	+0.0132	-0.0011	-17.78	-4.98	-0.0771
20	+0.957	+2.868	-0.565	-0.016	-0.016	-1.610	-4.438	-0.286	+0.0131	-0.1100	-0.0637	-0.0034	-0.0014	-8.90	-13.02	+0.1523
10	-12.61	+2.686	-3.208	-0.102	-0.102	+7.723	-2.850	+2.505	+0.0881	-0.3155	-0.0870	-0.0070	-0.0011	+20.73	-10.69	+0.4876
0	-12.62	-5.653	-2.457	-0.0832	-0.0832	+9.498	+2.791	+2.554	+0.0750	+0.2211	-0.1467	+0.0389	-0.0001	+38.31	+8.33	+0.0688
$\phi = 50$	+4.8	0.96	0	+0.707	0	-0.91	0	+0.7071	0	+2.539	+0.5900	0	0	-123.1	0	+1.000
30	+5.720	0	+2.151	+0.0279	-4.333	0	-1.931	-0.0295	+0.1739	+0.0001	+0.0205	+0.0002	-4.66	0	-6.575	-0.104
20	+5.105	+3.070	+1.205	-0.0015	-0.0015	-4.411	-2.438	-1.238	-0.0037	+0.0777	+0.0001	-0.777	-3.00	-3.00	-0.0518	
10	-0.025	+1.652	-1.014	-0.0656	-0.0656	-1.252	-4.161	-0.6816	+0.0569	-0.1578	+0.0593	-0.0387	-0.0013	-10.31	-0.96	+0.1915
0	-10.40	+1.897	-3.112	-0.0833	-0.0833	+7.432	-2.639	+2.813	-0.1013	-0.2919	-0.0794	-0.0364	-0.0011	+16.18	-9.65	+0.5157
-12.65	-5.639	-2.613	-0.0832	+1.150	+3.115	-3.155	-0.0913	-0.2411	-0.1221	+0.0366	-0.0000	+41.78	+0.30	7.575	+0.8127	
0	+12.10	0	0	0	0	0	0	0	0	0	0	-116.1	0	0	+1.000	
(m) $r/t = 200$ and $t/t = 0.6$																
$\phi = 30$	+1.3	4.1	0	-0.550	-0.1215	-7.494	-0.177	+0.0159	+0.2086	+0.0512	-0.1233	-0.0732	-0.0021	-5.95	-8.721	+0.2689
20	-2.95	1.174	-2.106	-0.1221	-0.1221	-0.317	-2.725	+0.756	+0.0513	+0.3019	-0.1613	-0.0010	+4.01	-20.04	-0.4012	
10	-19.88	-3.751	-2.621	-0.0867	-0.0867	-8.746	10.171	-0.281	0	+3.003	+0.6000	-0.0332	-0.0001	-166.4	0	+0.6938
0	+61.86	0	10.500	0	0	0	0	0	0	0	0	0	0	0	+1.000	

(ASCE Table 2A) (continued)

♦	Vertical Edge Load				Horizontal Edge Load				Shear Edge Load				Edge Moment Load			
	T _r (1)	S (2)	T _θ (3)	M _θ (4)	T _r (5)	S (6)	T _θ (7)	M _θ (8)	T _r (9)	S (10)	T _θ (11)	M _θ (12)	T _r (13)	S (14)	T _θ (15)	M _θ (16)
(m) (Continued)																
♦ = 35:																
35	+17.48	0	-1.581	-0.0576	-9.794	0	-1.155	+0.0231	+0.0619	+0.0113	-0.0363	-0.0020	-48.68	-11.31	-0.0433	
30	+13.76	+4.442	+0.932	-0.0648	-8.004	-2.520	-0.794	+0.0279	+0.0294	+0.0112	-0.0381	-0.0020	-40.77	-12.62	-0.0437	
20	-10.37	+6.000	-2.570	-0.0889	+4.010	-3.973	+1.313	+0.0331	+0.0259	+0.0663	-0.0294	+0.0012	+17.11	+0.522	+0.3710	
10	-22.33	-5.090	-3.136	-0.0827	+1.270	-30.32	+1.270	+0.0252	+0.0323	+0.1839	-0.1613	+0.0000	+66.22	+5.83	+0.7039	
0	+68.85	0	+0.574	0	-30.32	0	+0.819	0	+3.204	+0.6000	0	0	+0.0454	0	+1.000	
♦ = 40:																
40	+14.46	0	+2.530	-0.0652	-8.940	0	-1.788	-0.0029	+0.2046	+0.0157	+0.0119	+0.0030	-0.0012	-29.22	0	-0.053
30	+6.70	+6.504	+0.539	-0.0893	-4.810	-4.43	-0.527	+0.0113	+0.0330	+0.3133	-0.0224	-0.0013	-20.21	-1.59	+0.0535	
20	-13.24	+4.992	-3.187	-0.0846	+6.008	-3.889	+2.603	+0.0303	+0.0233	+0.2115	-0.0394	+0.0013	-19.37	+3.59	+0.0538	
10	+65.2	0	-0.643	0	-0.643	0	+6.760	+0.616	+2.331	+0.297	+0.0007	+0.0001	+56.90	+7.36	+0.000	
0	+65.2	0	+0.643	0	-35.15	0	+6.760	+0.616	+2.331	+0.297	+0.0007	+0.0001	+66.2	0	+0.000	
♦ = 45:																
45	+8.00	0	+2.397	+0.0217	-5.729	0	-1.858	-0.0205	+0.2347	0	+0.1924	-0.0004	+0.0286	-0.0005	-7.554	-0.1241
30	+8.05	+2.319	+2.068	+0.0133	-5.622	-1.562	-1.638	-0.0140	+0.1924	+0.1924	-0.0005	+0.0159	-0.0005	-2.49	-7.195	-0.0886
20	+2.68	+5.658	+0.311	-0.0418	-2.980	-4.165	-0.041	+0.0293	+0.0293	-0.1065	-0.0944	-0.0011	+10.35	-10.11	+0.0939	
10	-11.68	+3.500	-3.237	-0.0648	-6.754	-3.438	+2.416	+0.0759	+0.0430	-0.0596	-0.0476	+0.0011	+12.42	+3.667	+0.4113	
0	+58.53	0	-5.641	-0.0772	+2.752	+2.752	+2.752	+0.0696	+0.1906	-0.1895	+0.0361	+0.0011	+12.42	+6.668	+0.7160	
♦ = 50:																
50	+5.09	0	+0.284	+0.0284	-1.816	0	-1.467	-0.0273	+0.1854	+0.0002	+0.0382	+0.0002	+7.18	0	-0.1088	
40	+4.42	+1.981	+1.179	+0.0063	-3.693	-1.374	-1.120	-0.0084	+0.1051	+0.0872	-0.0018	-0.0003	+7.57	+1.40	-0.0572	
30	+2.57	+4.277	-0.638	-0.0476	-3.650	-1.722	-0.325	+0.0406	+0.1854	+0.0872	-0.0826	-0.0012	+10.51	-3.347	+0.1206	
20	-9.53	+2.775	-2.932	-0.0908	+6.372	-4.425	+2.581	+0.0862	+0.3519	-0.0575	-0.0397	+0.0012	+7.53	+3.941	+0.4149	
0	+53.46	0	-5.112	-0.2353	+3.111	+4.935	+6.043	+0.0737	+0.1853	-0.0384	+0.0001	+5.00	+3.85	+0.371	+0.1000	

(ASCE Table 2B) Symmetrical Edge Loads on Simply Supported Cylindrical Shells; Displacements of Edge at $\phi = 0$

Vertical Edge Load		Horizontal Edge Load		Shear Edge Load		Moment Edge Load						
$V_L \frac{P}{r^2 E} \times \text{Col. (1)} \times \sin \frac{\pi x}{l}$		$H_L \frac{P}{r^2 E} \times \text{Col. (4)} \times \sin \frac{\pi x}{l}$		$S_L \frac{P}{r^2 E} \times \text{Col. (7)} \times \sin \frac{\pi x}{l}$		$M_L \times \frac{P}{r^2 E} \times \text{Col. (10)} \times \sin \frac{\pi x}{l}$						
$V_L \frac{P}{r^2 E} \times \text{Col. (2)} \times \sin \frac{\pi x}{l}$		$H_L \frac{P}{r^2 E} \times \text{Col. (5)} \times \sin \frac{\pi x}{l}$		$S_L \frac{P}{r^2 E} \times \text{Col. (8)} \times \sin \frac{\pi x}{l}$		$M_L \times \frac{P}{r^2 E} \times \text{Col. (11)} \times \sin \frac{\pi x}{l}$						
Rotation $\theta -$		Rotation $\theta -$		Rotation $\theta -$		Rotation $\theta -$						
q_8	ΔV (1)	ΔH (2)	θ (3)	ΔV (4)	ΔH (5)	θ (6)	ΔV (7)	ΔH (8)	θ (9)	ΔV (10)	ΔH (11)	θ (12)
(a) $r/l = 100$												
$r/l = 0.1:$		$r/l = 0.2:$		$r/l = 0.3:$		$r/l = 0.4:$						
30	12.535	0.1115	0.1108	-	0.1445	-0.04556	0.3401	0.000480	0.000363	-1.350	0.5469	
35	6.335	0.3338	0.3330	-	0.3711	-0.07108	0.2748	0.001066	0.000544	-1.701	0.8531	
40	3.611	0.1089	0.1082	-	0.2375	-0.03159	0.1630	0.000496	0.000222	-2.052	0.6740	
45	2.501	0.5087	0.5080	-	0.1050	-0.1444	0.0884	0.000271	0.000123	-1.734	0.7542	
50	2.043	0.8434	0.8434	-	0.0559	-0.0702	0.0572	0.000150	0.000075	-2.082	0.8390	
30	17.38	2.031	0.0982	-	2.031	-0.04288	0.6050	0.000726	0.000315	-18.86	0.4893	
35	12.87	3.538	0.1259	-	3.538	-1.794	0.4733	0.02065	0.000178	-24.18	0.5564	
40	12.51	5.514	0.1524	-	5.514	-3.382	-0.09350	0.04590	0.001145	-29.25	0.6150	
45	13.47	7.356	0.1748	-	7.356	-5.417	-0.1243	0.03402	0.00862	-0.01757	-23.07	
50	14.54	10.50	0.1899	-	10.50	-8.270	-0.1546	0.03610	0.15204	0.002478	-29.70	
30	35.24	9.474	0.0891	-	0.474	-4.010	-0.03800	1.187	0.00357	0.000530	-37.88	
35	37.31	15.655	0.1092	-	15.655	-7.860	-0.05800	0.0588	0.1474	-86.04	-0.4499	
40	42.38	32.99	0.1315	-	32.99	-13.350	-0.07256	0.05930	0.2307	-106.2	-54.80	
45	46.00	36.12	0.1317	-	36.12	-25.100	-0.07884	0.05933	0.061613	-121.0	-73.85	
50	45.75	35.11	0.1285	-	35.11	-25.353	-0.07079	0.04229	0.062334	-124.9	-64.14	
30	55.06	26.10 ^f	0.0790	-	26.10 ^f	-11.06	-0.04716	1.040	0.22560	-104.0	-0.4049	
35	87.57	40.75	0.06046	-	40.75	-20.25	-0.03483	0.05921	0.05807	-239.2	-145.2	
40	96.08	55.00	0.06536	-	55.00	-32.68	-0.05921	0.05007	0.000994	-277.7	-181.4	
45	96.10	64.69	0.06326	-	64.69	-44.95	-0.06746	2.490	1.372	-0.01641	-207.1	
50	85.16	67.32	0.08310	-	67.32	-51.74	-0.07210	2.591	1.731	0.001732	-225.7	

(ASCE Table 2B) (continued)

		(b) $r/l = 200$									
r/l	α	0.05	0.14	0.23	0.32	0.41	0.50	0.59	0.68	0.77	0.86
30	0.5	54.14	0.06534	-54.14	-22.98	-0.02900	3.218	0.585	0.00044	-497.6	-216.6
35	142.2	54.14	0.06534	-78.77	-39.97	-0.04811	3.588	1.202	0.00045	-512.0	-285.9
40	163.2	78.77	0.07239	-97.43	-56.47	-0.0484	4.141	1.438	0.00045	-512.3	-376.0
45	167.7	97.43	0.07124	-104.9	-74.31	-0.04855	4.418	2.560	0.00110	-487.5	-366.2
50	152.4	104.9	0.06505	-103.9	-87.21	-0.03166	4.240	2.945	0.00110	-431.0	-356.8
$r/l = 0.6$											-0.3483
30	127.5	103.9	0.05747	-103.9	-88.47	-0.02934	5.112	1.242	0.000620	-861.6	-3247
35	238.5	98.47	0.05550	-126.7	-64.74	-0.02976	5.976	1.242	0.000834	-658.7	-3185
40	252.7	126.7	0.05514	-144.9	-86.10	-0.03296	6.629	3.250	0.000132	-814.6	-525.2
45	216.3	144.9	0.05606	-149.0	-108.3	-0.03700	6.601	3.942	0.000118	-575.4	-301.2
50	175.8	147.9	0.04904	-147.9	-127.9	-0.03967	6.678	4.324	0.000365	-609.4	-3086

		(b) $r/l = 200$									
r/l	α	0.1	0.2	0.3	0.4	0.5	0.6	0.7	0.8	0.9	1.0
30	13.59	0.5508	0.10563	-0.5508	-0.3112	-0.04535	0.3440	0.001423	0.000252	-5.070	-2.186
35	7.732	0.9838	0.13813	-0.9838	-0.4916	-0.07100	0.2228	0.003352	0.000118	-4.020	-2.416
40	5.711	1.576	0.1719	-1.576	-0.9209	-0.1036	0.1579	0.001139	0.000118	-8.255	-6.778
45	5.186	2.354	0.2050	-2.354	-1.462	-0.1484	0.1237	0.001137	0.000118	-6.452	-5.750
50	5.265	3.292	0.2352	-3.292	-2.576	-0.1895	0.1083	0.001300	0.000169	11.25	9.097
$r/l = 0.2$											-0.8195
30	32.02	8.267	0.0986	-8.267	-3.402	-0.02527	0.7716	0.03561	0.000365	-7.070	-37.70
35	33.96	14.07	0.1256	-14.07	-12.602	-0.04422	0.6124	0.08730	0.000700	-95.68	-46.33
40	39.51	21.38	0.1608	-21.38	-23.78	-0.08918	0.6071	0.1815	0.001123	-112.7	-68.34
45	44.27	24.96	0.1660	-24.96	-28.06	-0.1132	0.6094	0.3237	0.001601	-122.0	-86.91
50	45.16	34.63	0.1660	-34.63	-34.63	-0.1321	0.8010	0.4950	0.002014	-122.8	-101.0
$r/l = 0.3$											-0.4298
30	110.9	37.12	0.08556	-37.12	-15.70	-0.03706	1.641	0.2560	0.000532	-34.4	-147.6
35	123.0	55.702	0.08142	-55.702	-58.70	-0.05150	1.782	0.5520	0.000868	-402.2	-200.2
40	136.4	75.62	0.10099	-75.62	-69.62	-0.0707	2.154	0.9824	0.001163	-423.7	-260.8
45	131.1	89.18	0.10274	-89.18	-63.16	-0.07481	2.432	1.410	0.001376	-399.4	-188.4
50	111.5	88.27	0.09013	-89.27	-73.18	-0.07807	2.437	1.005	0.001382	-350.4	-303.5
$r/l = 0.4$											-0.1550
30	247.6	98.82	0.07223	-98.82	-41.89	-0.03237	3.525	0.9471	0.000586	-912.9	-397.6
35	283.3	139.7	0.07495	-139.7	-70.98	-0.04180	4.354	1.701	0.000837	-976.3	-513.6
40	273.8	161.7	0.07471	-161.7	-97.64	-0.04171	4.977	2.518	0.000944	-918.0	-557.1
45	232.0	163.1	0.06551	-163.1	-117.2	-0.04975	4.925	3.016	0.000945	-805.0	-611.3
50	187.9	157.7	0.03768	-157.7	-135.5	-0.05270	4.456	3.239	0.000875	-708.8	-647.5
$r/l = 0.5$											-0.3670
30	473.4	194.4	0.06058	-194.4	-82.77	-0.02060	5.899	2.116	0.000210	-181.7	-890.0
35	486.4	244.3	0.05930	-244.3	-125.5	-0.03167	8.309	3.327	0.000214	-172.2	-950.2
40	442.2	256.6	0.05840	-256.6	-189.6	-0.03414	4.563	0.000207	-157.2	-812.0	
45	349.1	251.2	0.04853	-251.2	-189.1	-0.03071	5.702	4.932	0.000633	-110.1	-811.6
50	285.1	260.4	0.04838	-260.4	-234.5	-0.04713	6.101	5.073	0.000616	-125.2	-832.6
$r/l = 0.6$											-0.3226
30	716.0	315.3	0.04828	-315.3	-135.1	-0.02155	11.82	4.979	0.000510	-309.4	-1341.
35	766.1	360.6	0.04830	-360.6	-88.1	-0.02429	14.15	5.790	0.000535	-2756.	-1511.
40	592.7	367.3	0.03820	-367.3	-242.9	-0.02637	12.46	6.714	0.000519	-2445.	-1640.
45	408.8	374.3	0.03165	-374.3	-287.2	-0.02931	11.18	7.265	0.000480	-2449.	-1623.
50	431.9	389.3	0.03392	-389.3	-357.3	-0.03284	10.21	7.983	0.000481	-2110.	-2043.

Subject Index

Beam-Arch method 74

Buckling of shells

concrete domes 184
concepts 344
circular cylindrical shells 352-366
formulas 360-366, 368, 371
general stability considerations 22
hyperbolic paraboloids 371
shells of revolution 368

Concrete shells

cylindrical roof 63-101
design examples 89-99, 186, 239
domes 169-194
hyperbolic paraboloids 215-247
folded plates 265
liquid retaining 291-341

Conical shells 137

Containment shells 30, 31

Cylindrical shells

axisymmetric loading 53
axisymmetric problems 55
bending analysis 43-61
buckling 353
concrete, see concrete shells
deformation 31, 34
design examples 89-99
displacement equations 50
internal pressure 57
membrane equations 26
membrane behavior 25-42,
membrane displacement 31
liquid retaining, 58
qualitative discussion 36
qualitative behavior 34
roofs, 65-103; also see concrete shells
vaults 28, 31

Domes

- bending analysis 141-167
- design example 186
- dome-ring analysis 171
- dome-ring roof 186
- membrane analysis 103-139
- qualitative behavior 130
- reinforced concrete 169-194
- spherical 111
- with skylight 112

Edge beams

- dimensions 67
- HP shells 223
- vaults 29

Folded plates 249-289

Force method

- general 20
- cylindrical shells, see cylindrical shells
- domes 160, 171, 183
- liquid containers 304

Hyperbolic paraboloids

- design 215-247
- geometrical description 217
- membrane analysis 222

Influence coefficients

- cylindrical shells 54
- shells of revolution 158

Liquid containers 291-341

Membrane behavior

- cylindrical shells 25-42
- general 15
- general shells 197-205
- HP shells 222
- shells of revolution 103-139

Pipes

- external pressure 366
- internal pressure 31, 57

Pressure vessels 120

Reinforcement

- concrete Cylindrical Roofs 70
- domes 186
- HP shells 244
- liquid retaining shells 329

Roofs

- buckling 184, 367, 368
- design examples 89-99, 169-192
- geometric Design of Cylindrical Shell Roofs 66
- analysis of Cylindrical Vaults by ASCE Tables 89

Shells

- classification 4, 8
- codes of practice 23
- cylindrical, see cylindrical shells
- general structural features 8
- geometry 3
- general design considerations 21
- hyperbolic paraboloid, see hyperbolic paraboloids
- Internal Force System in a Shell 12
- liquid containers 291-341
- liquid retaining 58
- qualitative Description of behavior 15, 34, 130, 227
- revolution 103-139
- with arbitrary geometry 195-214
- shallow 212
- Stability, see buckling of shells 22
- theories 19
- thin 12
- uses 2

Shells of revolution

- bending analysis 141-167
- buckling 368
- membrane analysis 105-140

Stability of shells, see buckling of shells

Storage tanks 115, see also liquid containers

Mechanics

From 1990, books on the subject of *mechanics* will be published under two series:

FLUID MECHANICS AND ITS APPLICATIONS

Series Editor: R.J. Moreau

SOLID MECHANICS AND ITS APPLICATIONS

Series Editor: G.M.L. Gladwell

Prior to 1990, the books listed below were published in the respective series indicated below.

MECHANICS: DYNAMICAL SYSTEMS

Editors: L. Meirovitch and G.Æ. Oravas

1. E.H. Dowell: *Aeroelasticity of Plates and Shells*. 1975 ISBN 90-286-0404-9
2. D.G.B. Edelen: *Lagrangian Mechanics of Nonconservative Nonholonomic Systems*. 1977 ISBN 90-286-0077-9
3. J.L. Junkins: *An Introduction to Optimal Estimation of Dynamical Systems*. 1978 ISBN 90-286-0067-1
4. E.H. Dowell (ed.), H.C. Curtiss Jr., R.H. Scanlan and F. Sisto: *A Modern Course in Aeroelasticity*.
Revised and enlarged edition see under Volume 11
5. L. Meirovitch: *Computational Methods in Structural Dynamics*. 1980 ISBN 90-286-0580-0
6. B. Skalmierski and A. Tylikowski: *Stochastic Processes in Dynamics*. Revised and enlarged translation. 1982 ISBN 90-247-2686-7
7. P.C. Müller and W.O. Schiehlen: *Linear Vibrations. A Theoretical Treatment of Multi-degree-of-freedom Vibrating Systems*. 1985 ISBN 90-247-2983-1
8. Gh. Buzdugan, E. Mihăilescu and M. Radeş: *Vibration Measurement*. 1986 ISBN 90-247-3111-9
9. G.M.L. Gladwell: *Inverse Problems in Vibration*. 1987 ISBN 90-247-3408-8
10. G.I. Schuëller and M. Shinozuka: *Stochastic Methods in Structural Dynamics*. 1987 ISBN 90-247-3611-0
11. E.H. Dowell (ed.), H.C. Curtiss Jr., R.H. Scanlan and F. Sisto: *A Modern Course in Aeroelasticity*. Second revised and enlarged edition (of Volume 4). 1989 ISBN Hb 0-7923-0062-9; Pb 0-7923-0185-4
12. W. Szemplińska-Stupnicka: *The Behavior of Nonlinear Vibrating Systems*. Volume I: Fundamental Concepts and Methods: Applications to Single-Degree-of-Freedom Systems. 1990 ISBN 0-7923-0368-7
13. W. Szemplińska-Stupnicka: *The Behavior of Nonlinear Vibrating Systems*. Volume II: Advanced Concepts and Applications to Multi-Degree-of-Freedom Systems. 1990 ISBN 0-7923-0369-5
Set ISBN (Vols. 12–13) 0-7923-0370-9

MECHANICS OF STRUCTURAL SYSTEMS

Editors: J.S. Przemieniecki and G.Æ. Oravas

1. L. Fryba: *Vibration of Solids and Structures under Moving Loads*. 1970 ISBN 90-01-32420-2
2. K. Marguerre and K. Wölfel: *Mechanics of Vibration*. 1979 ISBN 90-286-0086-8

Mechanics

3. E.B. Magrab: *Vibrations of Elastic Structural Members*. 1979 ISBN 90-286-0207-0
 4. R.T. Haftka and M.P. Kamat: *Elements of Structural Optimization*. 1985
Revised and enlarged edition see under Solid Mechanics and Its Applications, Volume 1
 5. J.R. Vinson and R.L. Sierakowski: *The Behavior of Structures Composed of Composite Materials*. 1986 ISBN Hb 90-247-3125-9; Pb 90-247-3578-5
 6. B.E. Gatewood: *Virtual Principles in Aircraft Structures*. Volume 1: Analysis. 1989 ISBN 90-247-3754-0
 7. B.E. Gatewood: *Virtual Principles in Aircraft Structures*. Volume 2: Design, Plates, Finite Elements. 1989 ISBN 90-247-3755-9
Set (Gatewood 1 + 2) ISBN 90-247-3753-2
-

MECHANICS OF ELASTIC AND INELASTIC SOLIDS

Editors: S. Nemat-Nasser and G.Æ. Oravas

1. G.M.L. Gladwell: *Contact Problems in the Classical Theory of Elasticity*. 1980 ISBN Hb 90-286-0440-5; Pb 90-286-0760-9
 2. G. Wempner: *Mechanics of Solids with Applications to Thin Bodies*. 1981 ISBN 90-286-0880-X
 3. T. Mura: *Micromechanics of Defects in Solids*. 2nd revised edition, 1987 ISBN 90-247-3343-X
 4. R.G. Payton: *Elastic Wave Propagation in Transversely Isotropic Media*. 1983 ISBN 90-247-2843-6
 5. S. Nemat-Nasser, H. Abé and S. Hirakawa (eds.): *Hydraulic Fracturing and Geothermal Energy*. 1983 ISBN 90-247-2855-X
 6. S. Nemat-Nasser, R.J. Asaro and G.A. Hegemier (eds.): *Theoretical Foundation for Large-scale Computations of Nonlinear Material Behavior*. 1984 ISBN 90-247-3092-9
 7. N. Cristescu: *Rock Rheology*. 1988 ISBN 90-247-3660-9
 8. G.I.N. Rozvany: *Structural Design via Optimality Criteria. The Prager Approach to Structural Optimization*. 1989 ISBN 90-247-3613-7
-

MECHANICS OF SURFACE STRUCTURES

Editors: W.A. Nash and G.Æ. Oravas

1. P. Seide: *Small Elastic Deformations of Thin Shells*. 1975 ISBN 90-286-0064-7
 2. V. Panc: *Theories of Elastic Plates*. 1975 ISBN 90-286-0104-X
 3. J.L. Nowinski: *Theory of Thermoelasticity with Applications*. 1978 ISBN 90-286-0457-X
 4. S. Łukasiewicz: *Local Loads in Plates and Shells*. 1979 ISBN 90-286-0047-7
 5. C. Firt: *Statics, Formfinding and Dynamics of Air-supported Membrane Structures*. 1983 ISBN 90-247-2672-7
 6. Y. Kai-yuan (ed.): *Progress in Applied Mechanics*. The Chien Wei-zang Anniversary Volume. 1987 ISBN 90-247-3249-2
 7. R. Negruțiu: *Elastic Analysis of Slab Structures*. 1987 ISBN 90-247-3367-7
 8. J.R. Vinson: *The Behavior of Thin Walled Structures. Beams, Plates, and Shells*. 1988 ISBN Hb 90-247-3663-3; Pb 90-247-3664-1
-

Mechanics

MECHANICS OF FLUIDS AND TRANSPORT PROCESSES

Editors: R.J. Moreau and G.Æ. Oravas

1. J. Happel and H. Brenner: *Low Reynolds Number Hydrodynamics*. With Special Applications to Particular Media. 1983 ISBN Hb 90-01-37115-9; Pb 90-247-2877-0
 2. S. Zahorski: *Mechanics of Viscoelastic Fluids*. 1982 ISBN 90-247-2687-5
 3. J.A. Sparensberg: *Elements of Hydrodynamics Propulsion*. 1984 ISBN 90-247-2871-1
 4. B.K. Shivamoggi: *Theoretical Fluid Dynamics*. 1984 ISBN 90-247-2999-8
 5. R. Timman, A.J. Hermans and G.C. Hsiao: *Water Waves and Ship Hydrodynamics. An Introduction*. 1985 ISBN 90-247-3218-2
 6. M. Lesieur: *Turbulence in Fluids. Stochastic and Numerical Modelling*. 1987 ISBN 90-247-3470-3
 7. L.A. Lliboutry: *Very Slow Flows of Solids. Basics of Modeling in Geodynamics and Glaciology*. 1987 ISBN 90-247-3482-7
 8. B.K. Shivamoggi: *Introduction to Nonlinear Fluid-Plasma Waves*. 1988 ISBN 90-247-3662-5
 9. V. Bojarevič, Ya. Freibergs, E.I. Shilova and E.V. Shcherbinin: *Electrically Induced Vortical Flows*. 1989 ISBN 90-247-3712-5
 10. J. Lielpeteris and R. Moreau (eds.): *Liquid Metal Magnetohydrodynamics*. 1989 ISBN 0-7923-0344-X
-

MECHANICS OF ELASTIC STABILITY

Editors: H. Leipholz and G.Æ. Oravas

1. H. Leipholz: *Theory of Elasticity*. 1974 ISBN 90-286-0193-7
 2. L. Librescu: *Elastostatics and Kinetics of Anisotropic and Heterogeneous Shell-type Structures*. 1975 ISBN 90-286-0035-3
 3. C.L. Dym: *Stability Theory and Its Applications to Structural Mechanics*. 1974 ISBN 90-286-0094-9
 4. K. Huseyin: *Nonlinear Theory of Elastic Stability*. 1975 ISBN 90-286-0344-1
 5. H. Leipholz: *Direct Variational Methods and Eigenvalue Problems in Engineering*. 1977 ISBN 90-286-0106-6
 6. K. Huseyin: *Vibrations and Stability of Multiple Parameter Systems*. 1978 ISBN 90-286-0136-8
 7. H. Leipholz: *Stability of Elastic Systems*. 1980 ISBN 90-286-0050-7
 8. V.V. Bolotin: *Random Vibrations of Elastic Systems*. 1984 ISBN 90-247-2981-5
 9. D. Bushnell: *Computerized Buckling Analysis of Shells*. 1985 ISBN 90-247-3099-6
 10. L.M. Kachanov: *Introduction to Continuum Damage Mechanics*. 1986 ISBN 90-247-3319-7
 11. H.H.E. Leipholz and M. Abdel-Rohman: *Control of Structures*. 1986 ISBN 90-247-3321-9
 12. H.E. Lindberg and A.L. Florence: *Dynamic Pulse Buckling. Theory and Experiment*. 1987 ISBN 90-247-3566-1
 13. A. Gajewski and M. Zyczkowski: *Optimal Structural Design under Stability Constraints*. 1988 ISBN 90-247-3612-9
-

Mechanics

MECHANICS: ANALYSIS

Editors: V.J. Mizel and G.Æ. Oravas

1. M.A. Krasnoselskii, P.P. Zabreiko, E.I. Pustylnik and P.E. Sobolevskii: *Integral Operators in Spaces of Summable Functions*. 1976 ISBN 90-286-0294-1
2. V.V. Ivanov: *The Theory of Approximate Methods and Their Application to the Numerical Solution of Singular Integral Equations*. 1976 ISBN 90-286-0036-1
3. A. Kufner, O. John and S. Pučík: *Function Spaces*. 1977 ISBN 90-286-0015-9
4. S.G. Mikhlin: *Approximation on a Rectangular Grid*. With Application to Finite Element Methods and Other Problems. 1979 ISBN 90-286-0008-6
5. D.G.B. Edelen: *Isovector Methods for Equations of Balance*. With Programs for Computer Assistance in Operator Calculations and an Exposition of Practical Topics of the Exterior Calculus. 1980 ISBN 90-286-0420-0
6. R.S. Anderssen, F.R. de Hoog and M.A. Lukas (eds.): *The Application and Numerical Solution of Integral Equations*. 1980 ISBN 90-286-0450-2
7. R.Z. Has'minskii: *Stochastic Stability of Differential Equations*. 1980 ISBN 90-286-0100-7
8. A.I. Vol'pert and S.I. Hudjaev: *Analysis in Classes of Discontinuous Functions and Equations of Mathematical Physics*. 1985 ISBN 90-247-3109-7
9. A. Georgescu: *Hydrodynamic Stability Theory*. 1985 ISBN 90-247-3120-8
10. W. Noll: *Finite-dimensional Spaces*. Algebra, Geometry and Analysis. Volume I. 1987 ISBN Hb 90-247-3581-5; Pb 90-247-3582-3

MECHANICS: COMPUTATIONAL MECHANICS

Editors: M. Stern and G.Æ. Oravas

1. T.A. Cruse: *Boundary Element Analysis in Computational Fracture Mechanics*. 1988 ISBN 90-247-3614-5

MECHANICS: GENESIS AND METHOD

Editor: G.Æ. Oravas

1. P.-M.-M. Duhem: *The Evolution of Mechanics*. 1980 ISBN 90-286-0688-2

MECHANICS OF CONTINUA

Editors: W.O. Williams and G.Æ. Oravas

1. C.-C. Wang and C. Truesdell: *Introduction to Rational Elasticity*. 1973 ISBN 90-01-93710-1
2. P.J. Chen: *Selected Topics in Wave Propagation*. 1976 ISBN 90-286-0515-0
3. P. Villaggio: *Qualitative Methods in Elasticity*. 1977 ISBN 90-286-0007-8

Mechanics

MECHANICS OF FRACTURE

Editors: G.C. Sih

1. G.C. Sih (ed.): *Methods of Analysis and Solutions of Crack Problems*. 1973 ISBN 90-01-79860-8
 2. M.K. Kassir and G.C. Sih (eds.): *Three-dimensional Crack Problems*. A New Solution of Crack Solutions in Three-dimensional Elasticity. 1975 ISBN 90-286-0414-6
 3. G.C. Sih (ed.): *Plates and Shells with Cracks*. 1977 ISBN 90-286-0146-5
 4. G.C. Sih (ed.): *Elastodynamic Crack Problems*. 1977 ISBN 90-286-0156-2
 5. G.C. Sih (ed.): *Stress Analysis of Notch Problems*. Stress Solutions to a Variety of Notch Geometries used in Engineering Design. 1978 ISBN 90-286-0166-X
 6. G.C. Sih and E.P. Chen (eds.): *Cracks in Composite Materials*. A Compilation of Stress Solutions for Composite System with Cracks. 1981 ISBN 90-247-2559-3
 7. G.C. Sih (ed.): *Experimental Evaluation of Stress Concentration and Intensity Factors*. Useful Methods and Solutions to Experimentalists in Fracture Mechanics. 1981 ISBN 90-247-2558-5
-

MECHANICS OF PLASTIC SOLIDS

Editors: J. Schroeder and G.Æ. Oravas

1. A. Sawczuk (ed.): *Foundations of Plasticity*. 1973 ISBN 90-01-77570-5
 2. A. Sawczuk (ed.): *Problems of Plasticity*. 1974 ISBN 90-286-0233-X
 3. W. Szczepiński: *Introduction to the Mechanics of Plastic Forming of Metals*. 1979 ISBN 90-286-0126-0
 4. D.A. Gokfeld and O.F. Cherniavsky: *Limit Analysis of Structures at Thermal Cycling*. 1980 ISBN 90-286-0455-3
 5. N. Cristescu and I. Suliciu: *Viscoplasticity*. 1982 ISBN 90-247-2777-4
-

Kluwer Academic Publishers - Dordrecht / Boston / London

Mechanics

SOLID MECHANICS AND ITS APPLICATIONS

Series Editor: G.M.L. Gladwell

Aims and Scope of the Series

The fundamental questions arising in mechanics are: *Why?*, *How?*, and *How much?* The aim of this series is to provide lucid accounts written by authoritative researchers giving vision and insight in answering these questions on the subject of mechanics as it relates to solids. The scope of the series covers the entire spectrum of solid mechanics. Thus it includes the foundation of mechanics; variational formulations; computational mechanics; statics, kinematics and dynamics of rigid and elastic bodies; vibrations of solids and structures; dynamical systems and chaos; the theories of elasticity, plasticity and viscoelasticity; composite materials; rods, beams, shells and membranes; structural control and stability; soils, rocks and geomechanics; fracture; tribology; experimental mechanics; biomechanics and machine design.

1. R.T. Haftka, Z. Gürdal and M.P. Kamat: *Elements of Structural Optimization*. 2nd rev.ed., 1990 ISBN 0-7923-0608-2
2. J.J. Kalker: *Three-Dimensional Elastic Bodies in Rolling Contact*. 1990 ISBN 0-7923-0712-7
3. P. Karasudhi: *Foundations of Solid Mechanics*. 1991 ISBN 0-7923-0772-0
4. N. Kikuchi: *Computational Methods in Contact Mechanics*. (forthcoming) ISBN 0-7923-0773-9
5. Y.K. Cheung and A.Y.T. Leung: *Finite Element Methods in Dynamics*. 1991 ISBN 0-7923-1313-5
6. J.F. Doyle: *Static and Dynamic Analysis of Structures*. With an Emphasis on Mechanics and Computer Matrix Methods. 1991 ISBN 0-7923-1124-8; Pb 0-7923-1208-2
7. O.O. Ochoa and J.N. Reddy: *Finite Element Modelling of Composite Structures*. (forthcoming) ISBN 0-7923-1125-6
8. M.H. Aliabadi and D.P. Rooke: *Numerical Fracture Mechanics*. ISBN 0-7923-1175-2
9. J. Angeles and C.S. López-Cajún: *Optimization of Cam Mechanisms*. 1991 ISBN 0-7923-1355-0
10. D.E. Grierson, A. Franchi and P. Riva: *Progress in Structural Engineering*. 1991 ISBN 0-7923-1396-8
11. R.T. Haftka and Z. Gürdal: *Elements of Structural Optimization*. 3rd rev. and exp. ed. 1992 ISBN 0-7923-1504-9; Pb 0-7923-1505-7
12. J.R. Barber: *Elasticity*. 1992 ISBN 0-7923-1609-6; Pb 0-7923-1610-X
13. H.S. Tzou and G.L. Anderson (eds.): *Intelligent Structural Systems*. 1992 ISBN 0-7923-1920-6
14. E.E. Gdoutos: *Fracture Mechanics*. An Introduction ISBN 0-7923-1932-X
15. J.P. Ward: *Solid Mechanics*. An Introduction. 1992 ISBN 0-7923-1949-4
16. M. Farshad: *Design and Analysis of Shell Structures*. 1992 ISBN 0-7923-1950-8

Mechanics

FLUID MECHANICS AND ITS APPLICATIONS

Series Editor: R. Moreau

Aims and Scope of the Series

The purpose of this series is to focus on subjects in which fluid mechanics plays a fundamental role. As well as the more traditional applications of aeronautics, hydraulics, heat and mass transfer etc., books will be published dealing with topics which are currently in a state of rapid development, such as turbulence, suspensions and multiphase fluids, super and hypersonic flows and numerical modelling techniques. It is a widely held view that it is the interdisciplinary subjects that will receive intense scientific attention, bringing them to the forefront of technological advancement. Fluids have the ability to transport matter and its properties as well as transmit force, therefore fluid mechanics is a subject that is particularly open to cross fertilisation with other sciences and disciplines of engineering. The subject of fluid mechanics will be highly relevant in domains such as chemical, metallurgical, biological and ecological engineering. This series is particularly open to such new multidisciplinary domains.

1. M. Lesieur: *Turbulence in Fluids*. 2nd rev. ed., 1990 ISBN 0-7923-0645-7
2. O. Métais and M. Lesieur (eds.): *Turbulence and Coherent Structures*. 1991 ISBN 0-7923-0646-5
3. R. Moreau: *Magnetohydrodynamics*. 1990 ISBN 0-7923-0937-5
4. E. Coustols (ed.): *Turbulence Control by Passive Means*. 1990 ISBN 0-7923-1020-9
5. A. A. Borissov (ed.): *Dynamic Structure of Detonation in Gaseous and Dispersed Media*. 1991 ISBN 0-7923-1340-2
6. K.-S. Choi (ed.): *Recent Developments in Turbulence Management*. 1991 ISBN 0-7923-1477-8
7. E.P. Evans and B. Coulbeck (eds.): *Pipeline Systems*. 1992 ISBN 0-7923-1668-1
8. B. Nau (ed.): *Fluid Sealing*. 1992 ISBN 0-7923-1669-X
9. T.K.S. Murthy (ed.): *Computational Methods in Hypersonic Aerodynamics*. 1992 ISBN 0-7923-1673-8
10. R. King (ed.): *Fluid Mechanics of Mixing*. Modelling, Operations and Experimental Techniques. 1992 ISBN 0-7923-1720-3
11. Z. Han & X. Yin: *Shock Dynamics*. 1992 ISBN 0-7923-1746-7
12. L. Svarovsky and M.T. Thew (eds.): *Hydrocyclones*. Analysis and Applications. 1992 ISBN 0-7923-1876-5
13. A. Lichatarowicz (ed.): *Jet Cutting Technology*. 1992 ISBN 0-7923-1979-6

Kluwer Academic Publishers – Dordrecht / Boston / London

 @Seismicisolation